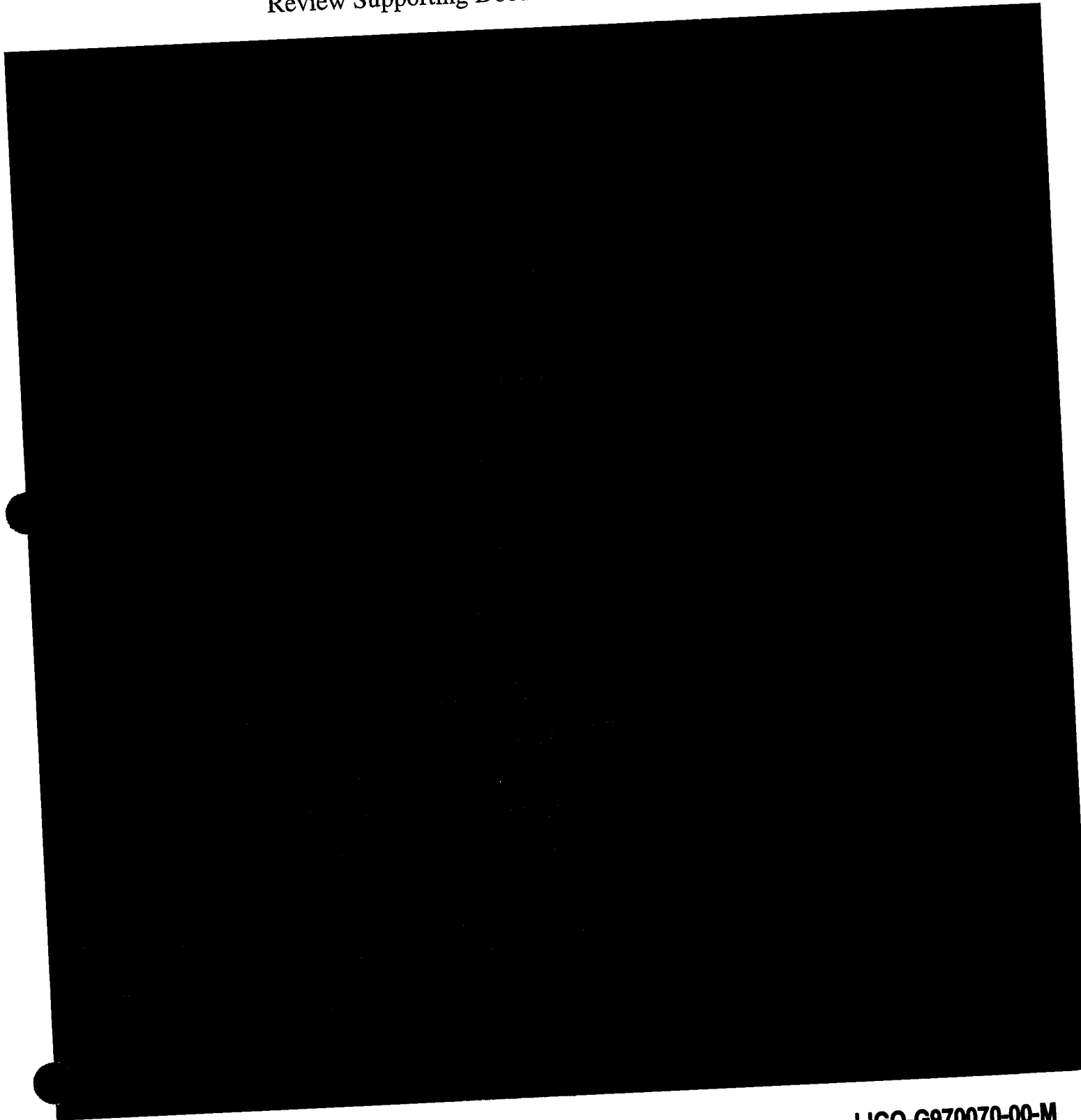


National Science Foundation Technical Review of the LIGO Project
California Institute of Technology
April 15-17, 1997
Review Supporting Documentation Package



National Science Foundation Technical Review of the LIGO Project
California Institute of Technology
April 15-17, 1997

Review Supporting Documentation Package

1) Hanford Site Visit

No supporting documentation.

2) Introduction - Barish

- Response to Review Report of the NSF Review Committee for LIGO October 22-24, 1996 Meeting at Caltech-*LIGO M970153-00-M*
- Revised LIGO FY 1997 Advanced Detector R&D Proposal (PHY97-00601)-*LIGO M970001-00-M*
- The LIGO Laboratory Charter-Draft 2 (March 1997)-*LIGO M970023-02-M*
- LIGO Scientific Collaboration Formation Plan-Draft 2-*LIGO M970022-02-M*
- LIGO Quarterly Report (March 1997)-*LIGO M970034-00-P*
- LIGO Annual Report (January 1997)-*LIGO M970007-00-P*

3) Integration/Acceptance - Stapfer

No supporting documentation.

FACILITIES

4) Civil - Asiri

No supporting documentation

5) Beam Tube - Jones

- CB&I Project Status Review Data Package-*LIGO C970466-00-[]*
- Beam Tube Dynamics-*LIGO T970054-A-E*

6) Baffles - Lazzarini

7) Bakeout - Althouse

- Beam Tube Bakeout Design Requirements Document-*LIGO E960123-01-E*
- Beam Tube Bakeout Conceptual Design-*LIGO T960178-01-E*

8) Vacuum Equipment - Worden

- PSI January 1, 1997-January 31, 1997 Status Report-*LIGO C970498-00-V*

RESEARCH AND DEVELOPMENT

9) PNI - Fritschel

- Noise Analysis of a Suspended High Power Michelson Interferometer-*LIGO P970003-00-D*

10) Recycling - Logan

DETECTOR

11) Overview - Whitcomb

DATA

12) Data Acquisition - Bork

13) Data Processing - Blackburn

- Modeling LIGO Data Analysis-*LIGO P970002-00-E*
- Modeling LIGO Data Analysis-*LIGO G970064-00-E*

14) Networking - Lazzarini

15) Lock Acquisition System - Sievers

- Dynamic Models of Fabry-Perot Cavities-*LIGO T970093-00-R*

16) End-to-End Simulation - Yamamoto

DETECTOR/R&D/DATA

17) Laser - Savage

- NPRO Frequency Stabilization-*LIGO T970051-00-R*

18) Core Optics - Camp

- Optics Development for LIGO-*LIGO P960044-00-D*
- Measurement of Coating Layer Thickness-*LIGO T960168-A-E*

19) Input Optics - Reitze (UFla)

20) Seismic Isolation - Thompson (HYTEC)

- PDR/CDR Design Review Document-*LIGO C970257-00-D*

21) LSC/ASC - Zucker

22) FMI/Alignment - Mavalvala

- Measurement of the Alignment Sensitivity of a Power-Recycled Michelson Interferometer with Fabry-Perot Arm Cavities-*LIGO T970056-00-D*

23) CDS/Electronics - Heefner

- ASC CDS Conceptual Design-*LIGO T970062-00-C*

National Science Foundation Technical Review of the LIGO Project
California Institute of Technology
April 15-17, 1997

Agenda

Tuesday April 15, 1997:

8:00 am - 8:30 am: Coffee (30)

8:30 am - 9:30 am: Review Committee Executive Session (60)
1) Including Report on Hanford Site Visit

2) 9:30 am - 10:00 am: Introduction - Barish (30)

3) 10:00 am - 10:15 am: Integration/Acceptance - Stapfer (15)

10:15 am - 10:30 am: COFFEE BREAK (15)

FACILITIES

4) 10:30 am - 10:50 am: Civil - Asiri (20)

5) 10:50 am - 11:10 am: Beam Tube - Jones (20)

6) 11:10 am - 11:25 am: Baffles - Lazzarini (15)

7) 11:25 am - 11:40 am: Bakeout - Althouse (15)

8) 11:40 am - 12:00 pm: Vacuum Equipment - Worden (20)

12:00 pm - 1:00 pm: LUNCH BREAK (60)

RESEARCH AND DEVELOPMENT

9) 1:00 pm - 1:30 pm: PNI - Fritschel (30)

10) 1:30 pm - 2:00 pm: Recycling - Logan (30)

DETECTOR

11) 2:00 pm - 2:30 pm - Overview - Whitcomb (30)

2:30 pm - 2:45 pm: COFFEE BREAK (15)

Tuesday April 15, 1997 (continued)

FACILITIES

2:45 pm - 5:00 pm: Interactive Session - Engineering Conference Room
(39 Bridge Annex)

DATA

- 12) 2:45 pm - 3:05 pm: Data Acquisition - Bork (20)
- 13) 3:05 pm - 3:25 pm: Data Processing - Blackburn (20)
- 14) 3:25 pm - 3:45 pm: Networking - Lazzarini (20)
- 15) 3:45 pm - 4:05 pm: Lock Acquisition System - Sievers (20)
- 16) 4:05 pm - 4:25 pm: End-to-End Simulation - Yamamoto (20)
- 4:30 pm - 6:00 pm: Executive Session (90)
- 6:00 pm - 8:00 pm: LIGO-hosted Dinner at The Athenaeum

Wednesday April 16, 1997:

FACILITIES

9:00 am - 12:00 pm: Interactive Session - Science Conference Room
(351 West Bridge)

DETECTOR/R&D/DATA

- 9:00 am - 12:00 pm: 112 - 114 East Bridge
- 17) 9:00 am - 9:20 am: Laser - Savage (20)
- 18) 9:20 am - 9:40 am: Core Optics - Camp (20)
- 19) 9:40 am - 10:00 am: Input Optics - Reitze (UFla) (20)

- 10:00 am - 10:20 am: COFFEE BREAK (20)

- 20) 10:20 am - 10:40 am: Seismic Isolation - Thompson (HYTEC) (20)
- 21) 10:40am - 10:55 am: LSC/ASC - Zucker (20)
- 22) 10:55 am - 11:15 am: FMI/Alignment - Mavalvala (15)
- 23) 11:15 am - 11:35 am: CDS/Electronics - Heefner (20)

1:00 pm - 5:00 pm: Committee Executive Session and Writing

LASER INTERFEROMETER GRAVITATIONAL WAVE
OBSERVATORY

- LIGO -

CALIFORNIA INSTITUTE OF TECHNOLOGY
MASSACHUSETTS INSTITUTE OF TECHNOLOGY

Document Type LIGO-970153-00-M 04-02-97

Response to Review Report
of the NSF Review Committee
for the LIGO
October 22-24, 1996
Meeting at Caltech

Barry C. Barish

California Institute of Technology
LIGO Project - MS 51-33
Pasadena CA 91125
Phone (818) 395-2129
Fax (818) 304-9834
E-mail: info@ligo.caltech.edu

Massachusetts Institute of Technology
LIGO Project - MS 20B-145
Cambridge, MA 01239
Phone (617) 253-4824
Fax (617) 253-7014
E-mail: info@ligo.mit.edu

WWW: <http://www.ligo.caltech.edu/>

Response to Review Report of the NSF Review Committee for the LIGO October 22-24, 1996 Meeting at Caltech.

1.0 Facilities

1.1 Facilities

The review committee recommends the use of a safety sling when lifting beam tube enclosure elements. This advice has been implemented. All enclosure elements have been lifted and installed using this sling. (Please see Attachment 1 - photo of safety sling)..

1.2 Beam Tube and Vacuum Equipment

1.3 Systems Integration and Acceptance Testing

Define the methods that LIGO will use to perform its role as General Contractor:

There are three major contract scopes at each site which we act as the General Contractor to integrate. These are the civil construction, vacuum equipment, and beam tube. We have spent considerable effort to keep the interface between these three contracts to a bare minimum. This is done by scheduling their work on a non-interference basis. (We realize that some interference is inevitable; we have a site manager at each site that adjudicates minor interferences that do arise in the course of day-to-day activity.) In the longer term, we continuously update and manage the overall site construction schedules to minimize interference and optimize progress. We have a full time scheduler that supports this work and we hold monthly meetings with the contractors and weekly meetings at the site with the site technical managers, construction superintendents, and relevant technical staff. The nature and status of these activities will be presented at the next NSF review meeting.

Within the existing LIGO Project Integrated Schedule, continue to develop the subsystem schedules:

Interfaces between the Facilities work scope and the Detector workscope are minimized by a schedule which delivers a functioning vacuum system and a commissioned and accepted beam tube within a functioning building on an agreed upon milestone date. This allows the detector development to proceed independently while the Facilities are being built. The bakeout activity is similarly compartmentalized into a self contained activity whose planning and preparation proceeds in parallel with Facilities activities. The bakeout activity interface is primarily the establishment of agreed upon milestone dates where the beam tube is available for this activity.

The project should define bakeout requirements, procedures, testing:

We agree that this is an important list of activities. Substantial effort has been devoted to support the activities listed. Status and progress in this area will be presented and discussed during the next NSF review.

2.0 Detectors

2.1 Overall Findings

2.2 Phase Noise Interferometer

Recommendation: The LIGO program requires that the excess noise be understood and reduced to an insignificant level before final design choices are made. The PNI (and, possibly, the 40 m prototype) should be exercised in order to track down and eliminate excess phase noise as expeditiously as possible. The conversion of the PNI to 1064 nm, currently scheduled for January 97, should not be delayed. However, the committee strongly encourages the vigorous study of the phase noise problem using the 515 nm system until the conversion occurs. Should excess phase noise remain a problem after conversion, then its reduction should receive the highest priority.

LIGO concurs with this recommendation. As the committee suggested, we have not delayed the conversion of the PNI to 1064 nm, beginning the conversion in January 1997 as soon as all key parts became available. Up to that time a vigorous effort was made to establish the causes of the excess noise between 100 and 2000 Hz and substantial progress has been made.

The shot-noise-limited region of the October 96 spectrum shown at the last review began at about 3 kHz, and was at the level of . The level was reduced to by moving the beam on the interferometer optics to a region of lower loss, and the shot noise region was extended down to about 1.5 kHz by improving the optical isolation of the interferometer reflected beam. The improved isolation also lowered the noise in the 600-1 kHz band by roughly a factor of 4 (with some smaller improvement below 600 Hz). The noise in the 100-600 Hz band was further reduced by increasing the effective frequency noise suppression in the interferometer common mode servo loop, leaving the noise lower than the October spectrum by factors of 5-10 in this band. The prominent mechanical resonances of the mirror attachments in the 1-1.5 kHz band remained the same.

2.3 Recycling and Operation of the 40 m Interferometer

Recommendation: The 40 m prototype should be converted to a recycling system as planned and the low-noise rf driver tested and implemented. The possibility of fluctuations in the electro-optic coupling, etc. at frequencies above 100 Hz should be explored and the excess noise on the 40 m systematically reduced as it is operated in an "observatory" mode.

The highest priority for the 40 m interferometer is its conversion to the recycled configuration. Technical problems during the reconfiguration of the vacuum envelop and the input optics chain (required to make room for the recycling mirror) have resulted in approximately one month delay in its expected operation date. The low noise rf source has been acceptance tested and received and will be installed and tested in the 40 m as soon as the interferometer with its reconfigured input optics has been fully checked out. A new data acquisition system is under development which should aid noise studies and permit operation in "observatory" mode.

2.4 Seismic Isolation

Recommendation: LIGO recognizes the seriousness of the seismic isolation problem and the need for a robust solution. A detailed review of the proposed solution will occur at the next meeting.

At the time of the Oct '96 review, the planned date for the Seismic Isolation PDR was mid-Jan '97 with an FDR for the Seismic Isolation structures in late April (4/30) and an FDR for the Seismic Isolation actuators in late-Aug (7/22). The PDR has been delayed by about 6 weeks to allow collection of more complete data concerning the constrained layer damped metal springs. Better definition of the design and improved estimates of fabrication times have made it possible to consider combining the two parts of the FDR and to have a first article test of the seismic system. Costs and schedules for the incorporation of a prototype/first article fabrication and test are being evaluated. The technical solution and program plan will be ready for review by the committee at its next meeting.

2.5 10 Watt Laser at 1064 nm

2.6 Core Optics Coatings

Recommendation: The core optics/pathfinder group should proceed to an equally rigorous test of the SiO₂ films and to tests of full thickness film stacks and coated substrates with known figure.

The uniformity data from the Ta₂O₅ tests were reported to REO and the made changes to their coating chamber to improve the uniformity. Test pieces of both Ta₂O₅ and the SiO₂ sensitive coatings were made and tested, with the result that the uniformity was improved by approximately a factor of 5 for the Ta₂O₅ layer; the SiO₂ layer proved worse than the Ta₂O₅ layer, but still acceptable. A full size HR coating has been made on one of the pathfinder substrates and will be tested soon at NIST. Unless problems develop, results should be available by the next review.

2.7 Alignment and Control System

Recommendation: The program to implement recycling and the new alignment sensors on the 40 m facility is scheduled, with shakedown of the additions to the interferometer set for January 1997, with operation by March 1997. We encourage LIGO to aggressively pursue this part of the program.

The program to implement recycling has been pursued vigorously. The reconfiguration of the input optics to make room for a recycling mirror has been completed and this is being tested now. This effort is approximately one month behind schedule due to some technical problems. Current plans call for the alignment sensors from the fixed mass interferometer at MIT to be transferred to the 40 m for integrated testing.

3.0 Data Analysis

Before addressing the specifics of the findings and recommendations made by the NSF Review Committee in regard to LIGO Data Analysis, LIGO wishes to address a potential misconception appearing in the document provided by the NSF. It is not the case that the challenges inherent in data reduction were only recently recognized. It has always been known out that the potential was being designed into LIGO to acquire data at such rates that they would render the raw volume essentially intractable. It is in this regard that volume of ancillary data channels have been described as being 100X the intrinsic GW data rate.

The LIGO design philosophy which has been pursued is one of flexibility. Thus, the Detector Data Acquisition System (DAQS) has been specified to have a number of signal acquisition and probe points sufficient to ensure that any and all possibly useful signals are accessible, via the DAQS interface, for display, analysis, and recording. This is not to say, however, that all such signals will necessarily always be recorded.

The intent is to utilize the commissioning period of LIGO to identify an efficient, reduced data set which will constitute the LIGO data stream being recorded for archive. LIGO is confident that this rate will be dramatically lower than the potential maximum rate described above.

The LIGO Data Analysis System is presently being defined. The system requirements are determined by the need to ensure a successful and timely delivery of both on-line and off-line facilities providing the needed computational resources to support the initial LIGO science goals data run. Significant progress has been accomplished to date. Specifically, the following activities have taken place since the October NSF Review. They are listed by general category identified in the NSF Review Committee's Report dated 15 November 1996.

3.0a Need For Additional Experienced Staff

LIGO has hired a full time computer systems administrator to relieve scientific staff formerly (but temporarily) burdened with such activities. In addition, we have recently

hired a second individual who will be arriving by 1 April 1997. This individual's responsibilities will be shared between computer systems administration support and code development. This latter activity will be primarily dedicated towards developing on-line diagnostics tools, with a near term goal of supporting the 40m Data Acquisition System prototype development and planned data taking runs once recycling has been demonstrated.

In addition, as part of its 1997 hiring cycle of postdoctoral scientists, LIGO is seeking one, possibly two, scientists with depth of experience in the general area of data manipulation and reduction of large databases. The(se) individual(s) will be specifically tasked with supporting the development of the data analysis design and conceptual implementation.

The recent addition of Prof. Tom Prince to the LIGO Caltech team has also brought with it the experience and resources developed in astrophysical searches for periodic signals. As part of this addition, LIGO has also acquired the services of two computer scientists who are actively developing a prototypical data analysis system for exploring various approaches to providing interfaces into the LIGO database. One of these individuals is associated with the Caltech Center for Advanced Computing research (CACR). In this capacity, he has developed scientific database management and analysis tools for use on parallel machines. The other individual comes from the Caltech Space Radiation Laboratory (SRL) and has worked in developing analysis tools for astrophysical searches of weak periodic signals.

3.0b Need For Standard Data Formats

The LIGO-VIRGO collaboration on a common data format has continued to grow. After our report to the committee last Fall, a series of meetings have served to identify and resolve the concerns raised by LIGO at the last NSF review. With VIRGO's support and feedback, LIGO has successfully implemented the common data format and has been writing data tapes and disc files in this format. We have regular teleconferences and email exchanges with the Ancey group who originated and is maintaining the code. They have agreed to providing needed documentation and standardization. Benoit Mours is planning to visit LIGO for one week in mid-March to continue technical discussions with LIGO personnel.

3.0c Need For Software Standards

As part of the requirements definition for the LIGO Data Analysis System, a Data Analysis System Software Specification is being developed. Among other things, this document identifies supported languages and standards; it identifies the software system architecture at the last NSF Review (i.e., modular, hierarchical, object-oriented where possible, etc.). Another part of this specification will be the definition of LIGO-supported conventions which will be used in all LIGO-developed analysis software.

3.0d Need For Wide Area Networking Among LIGO Laboratory Sites

Since the last review, LIGO has engaged the Louisiana Board of Regents in fruitful discussions which will lead to access for LIGO to state resources (to be resident at LSU) that will enable LIGO Livingston to access the future high bandwidth NSF backbone, vBNS.

LIGO is planning to meet with DOE and PNWL representatives in mid-March to begin similar discussions in support of access for the Hanford Observatory Site.

The MIT/LIGO Group, as part of its relocation to new facilities on campus, has begun discussions at MIT with its University networking services group to gain access to the Center for Space Research (CSR) and Plasma Fusion Center campus backbones. This will provide a natural link to Caltech in support of the WAN topology discussed at the last NSF Review and which is being pursued for LIGO.

3.0e Need For Prototype Activities in Data Acquisition and Analysis

As discussed above, this is moving ahead vigorously. Specifically we are moving the 32 fast channel - plus - 128 -slow channel DAQ prototype built by the Detector CDS Group to the 40m laboratory. This system will be writing LIGO/VIRGO formatted data tapes with up to 160 channels of data (only one channel corresponds to the GW channel). We will also be studying about 45 hours of data taken during in November 1994.

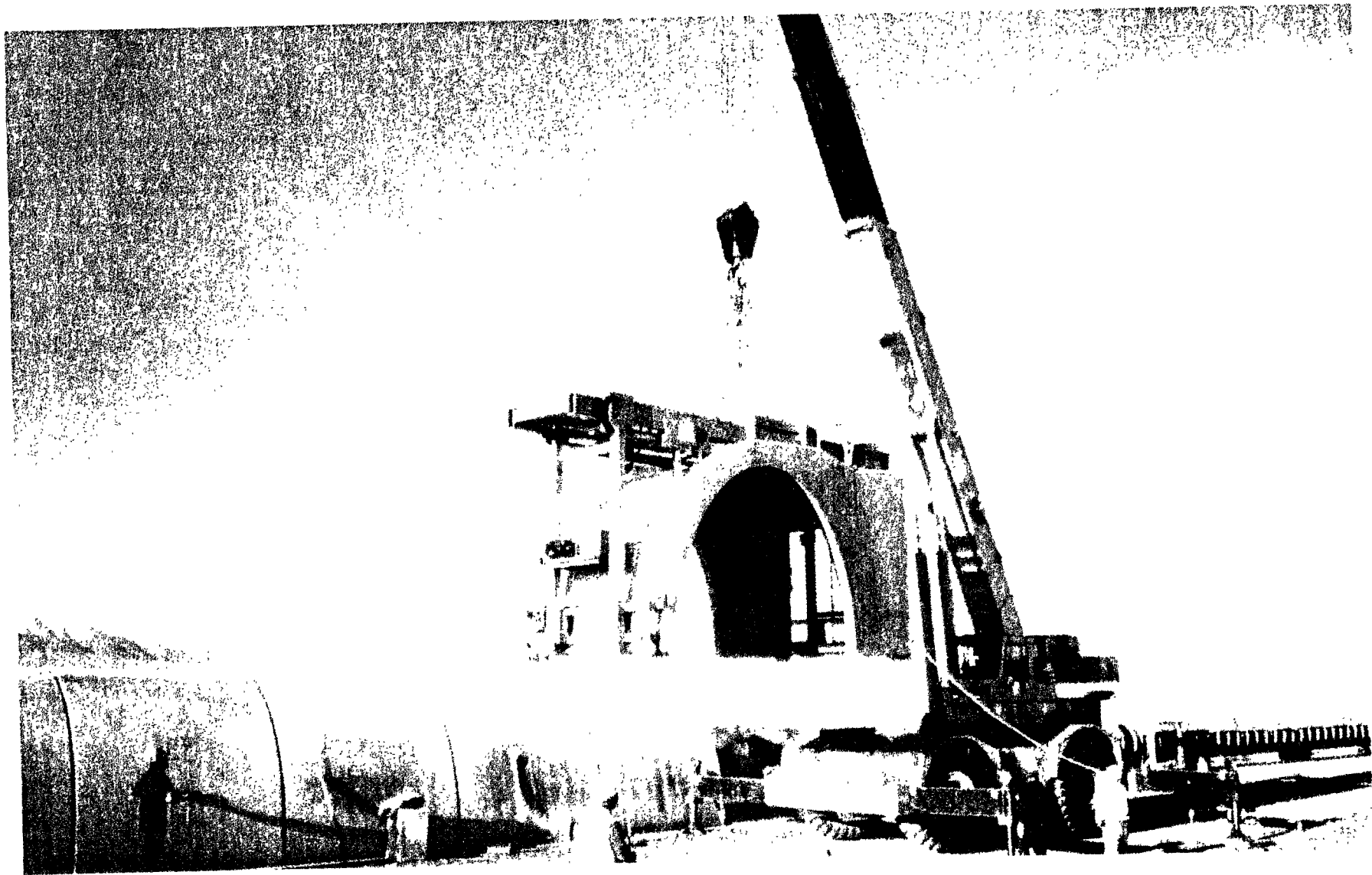
Once data are available, we will be working to prototype analysis tools. These will be for both on-line quick-look and characterization of data and parallelized algorithms for a more automated reduction of data; the Caltech CACR IBM SP2 hardware is the target testbed. The analysis software is being developed in cooperation with Prof. Bruce Allen (Univ. of Wisconsin at Milwaukee). This currently includes a parallelized optimal filtering code which has already demonstrated the ability to keep up with the real-time data stream through a moderate collection of templates (covering the 1.2 to 1.6 solar mass range). These activities are aimed at providing tools to identify instrument behavior and to characterize the instrumental noise floor in real time, as well as to filter the data stream in real time through a set of binary inspiral filters to provide real time feedback on the machines "astrophysics" performance. The off-line prototyping activities involve providing man-machine interfaces to the archive (visualization methods to identify and extract data records from a large volume archive) and parallelized filtering of the data stream.

The prototype will explore using a set of independent modules connected with the data flow paradigm and running on an MPI communications fabric. This approach which can be easily ported to a heterogeneous collection of hardware, from workstations to parallel supercomputers. Perhaps most important is that different collaborators can supply specialized modules without needing to know exactly how the other modules work.

The difficult problem of volume reduction from the raw data to a long term archive will be tackled once experience is gained with these prototypes. It is quite likely, however, that it will require experience gained during the commissioning phase of LIGO, once both sites become operational, before any definitive progress in this area can be made: LIGO will need to know how the interferometers behave before we are able to identify significantly correlated channels and those bearing little, redundant, or no information whatsoever. A significant aspect of this effort is the commitment to bring on experienced scientific staff within the next year to aid in developing conceptual approaches. Also, it is in this area where present and expected future collaborative activities with theorists who are interested in the data analysis challenges will continue.

3.0f White Paper Defining the Initial LIGO Requirements

This document will flow directly from the design and requirements definition activities presently under way within LIGO.



LIGO-970153-00-M Attachment 1: Photo of safety sling for NSF response paper from Mark Coles.

Review Report
of the
NSF Review Committee
for the
Interferometer Gravitational Wave Observatory (LIGO)

Performed for the
Natioanl Science Foundation

Conducted at Caltech
on October 22-24, 1996

Date of this Report
November 15, 1996

LIGO-MS60134 00-M

**Review Report of the
NSF Review Committee
for the Laser
Interferometer Gravitational Wave Observatory (LIGO)**

**October 22-24, 1996
Pasadena, CA**

Table of Contents

Executive Summary	1
1. Facilities	2
1.1 Facilities	
1.2 Beam Tube and Vacuum Equipment	
1.3 Systems Integration and Acceptance Testing	
2. Detectors	5
2.1 Overall Findings	
2.2 Phase Noise Interferometer	
2.3 Recycling and Operation of the 40 m Interferometer	
2.4 Seismic Isolation	
2.5 10 Watt Laser at 1064 nm	
2.6 Core Optics Coatings	
2.7 Alignment and Control System	
3. Data Analysis	9

Appendices

A. Committee Membership	10
B. Charge to the NSF Technical Review Committee	12

Executive Summary

The regular semi-annual review of the Laser Interferometer Gravitational Wave Observatory (LIGO) was conducted by a review committee of experts on behalf of the National Science Foundation on October 22-24, 1996 at the California Institute of Technology in Pasadena, California. The focus of this review was on the technical aspects of the LIGO Project and its supporting R & D. A brief summary of cost and management issues were presented to the committee but not reviewed in detail. Members of the review committee and the observers from the NSF are listed in Appendix A. The NSF charge to the review committee is provided in Appendix B of this report.

Written material provided by LIGO to the committee in advance of the meeting was examined, oral presentations were heard and subgroups of the committee met with appropriate members of the LIGO team to explore details of the project. Based on these evaluations of the technical aspects of the project, the committee discussed its findings in executive session and generated written summary conclusions and observations given below. Details of the assessment of the LIGO technical progress are given in the full text of this report. The Advanced R&D proposal will be treated in a separate report.

The LIGO Review Committee formulated the following summary observations:

- LIGO is making excellent progress. Signed contracts or bids are in hand for all major items and are all within the estimated cost envelopes. Each site includes space for an additional interferometer. The project is 34% complete.
- The PNI phase noise measurement is the world's best.
- The first large pieces of the detector (core optics blanks) have been ordered.
- The Committee notes progress on the formation of the LIGO PAC.

From these observations, it is clear that the committee finds that the LIGO Project is making excellent progress towards its goal of becoming an operational observatory for gravity waves by the end of 2000. Presently, LIGO is 34% complete and all of the major cost items are either under signed contract or firm bids have been received. The costs of these major items have been at or below the estimates. The LIGO team is to be commended on this performance and the committee looks forward to an equally competent performance in completing the design, fabricating, installing and commissioning the detector systems.

1. Facilities

1.1 Facilities

The Facilities Group presented a striking report of excellent accomplishments. Some slippage has occurred at the Louisiana site due to bad weather, but the committee is comfortable with their assurance that with concentrated effort, the facilities can be in place when needed.

The committee notes that:

1. The earth work at Washington for the service roads and the beam pipe slab foundation is complete.

The earth work at Louisiana for the service roads and beam pipe slab foundation is complete except for one lift of fill approximately six hundred feet in length. The contractor should be able to complete it without delay to the project .

Earth compaction tests for the berm at Louisiana indicate 96% which exceeds specification (95%) except for the six hundred feet not yet finished.

2. The precast beam pipe enclosure casting forms and handling fixtures are producing elements beyond the rate required, production is going well, and an adequately flat area is available for storage of finished elements. While lifting these elements, a safety sling is recommended.
3. The contract for beam pipe enclosures and placement is one single contract at Louisiana which furnishes single responsibility and is to be commended. Again, a safety sling is highly recommended.
4. Our discussion with the LIGO team on the quality of the precast sections of the beam pipe enclosure related to shrinkage cracks, level curing slabs, handling stresses, safety slings and concrete ingredients indicated a thorough knowledge of the subjects and a most enthusiastic attitude toward doing the best possible job for the entire project.
5. The building contracts have been awarded in Washington at costs acceptable to LIGO and to the review committee.

The building contracts at the Louisiana site have not been awarded. Bids have been received at reasonable figures which are being evaluated by the LIGO staff.

The LIGO staff clearly demonstrated a most enthusiastic attitude toward their work as well as a high intellectual and technical competence. Keep up the good work.

1.2 Beam Tube and Vacuum Equipment

Significant progress has been made since the April review in both Beam Tube and Vacuum Equipment fabrication.

Chicago Bridge and Iron (CB&I) has set-up a "beam tube factory" at Big Pasco, near the Hanford site and is producing acceptable beam tube sections at the comfortable rate of two per day. Early indications are that all aspects of the fabrication process satisfy LIGO

specifications. To date (10/23/96), 42 beam tube sections have been completed, all passing their final vacuum leak check. CB&I's "beam tube factory" is an impressive facility and reflects a professional, high-quality approach to their job.

CB&I has designed and fabricated a set of portable clean rooms for the on-site installation of the beam tube sections. The first tube section is scheduled to be installed this week. Installation of beam tube sections is scheduled at one section per day per clean room. CB&I's design for this clean room process is well thought out and should support the installation task with no compromise in quality of the completed beam tube assembly.

Baffle fabrication has started with metal forming by Capital Industries, glass coating by West Coast Porcelain, and a final dust removal cleaning by Jet Propulsion Laboratory. The production rate for completed packaged baffles is high. All baffles for Hanford (500) are on hand. Baffle installation techniques have been developed and demonstrated and are consistent with maintaining the high quality demands of the completed beam tube assemblies.

Vacuum equipment is being supplied by Process Systems International (PSI) with sub-contracts by PSI to Raynor, GNB, Varian, and other vacuum equipment suppliers. A prototype Beam Splitter Chamber was successfully fabricated and tested through a vacuum bake to demonstrate fabrication techniques. Fabrication has started on the main chambers - PSI has subcontracted the Beam Splitter Chambers to Raynor. PSI will clean and perform the leak checking of these chambers.

PSI has tested and accepted the first two 48" diameter gate valves from GNB, the first set of 80 °K cryo pumps, the first 10,000 l/s ion pumps from Varian and numerous smaller components needed to build up the required vacuum pumping systems.

Comments:

Early success in both achieving acceptable production rates and high quality are a direct result of LIGO's extensive design analysis, in depth planning, good vendor selection criteria, and close and immediate oversight of vendors by the LIGO staff.

Continued oversight of the various vendors must remain a high priority for the LIGO staff. This will become more difficult as team members move to the LIGO sites.

The better-than-expected results on the heat treating of the stainless steel sheet, the leak-free and clean tube sections, and the baffle coating should now be considered the norm and not the exception. Process changes, such as changing to the 36" wide sheet for the tube mill, must be evaluated and not be allowed to compromise final quality.

Recommendations:

None.

1.3 Systems Integration and Acceptance Testing

Findings

The committee discussed in detail the system integration and acceptance testing of the 2 km beam tube modules with members of the LIGO team responsible for these areas. The

following outline was used to focus the discussion on the principal features of the two areas.

1st Module Performance and Acceptance Test Program

Subtitles or Activities

A) Demonstrate Vacuum Requirements - Including leak checking approach and verification of techniques; leak repair approach and techniques; bake-out and re-bake-out after leak repair performance including approaches and techniques.

B) Activities or Sub-Components - For each item that is a part of this integrated test and for each component(i.e., beam tubes, vacuum equipment, bellows, gate valves, baffles, etc.).

1. Manufacturing and factory acceptance schedules.
2. Final acceptance test at time of installation and schedule requirement.
3. Installation and check-out including any post-installation fabrication, etc.

C) Interface and Inter-connection requirements and installation including contractor responsibilities such as:.

- CBI - Beam Tube System
- PSI - Vacuum Equipment
- LIGO - Furnished by CIT
- Bake-out Equipment
- Conventional Facilities
- Power and other auxiliary systems
- Controls
- Safety
- Special acceptance test equipment and procedures
- etc.

D) Schedule and manpower requirements and associated additional personnel requirements.

E) Special equipment and procedures.

F) Cost impact if any.

G) Management, etc.

H) Acceptance criteria for major contracts and resolution of discrepancies, changes, etc.

1. CBI
2. PSI
3. Conventional Facilities
4. LIGO / CIT Contractors
5. Etc.

Generally speaking, the project staff demonstrated that they have covered most of the essential ingredients of the items in this outline. Obviously they have put a great deal of effort into the work and are ready to proceed with this next phase of activity.

Comment:

LIGO faces a critical path that shows assembly and acceptance of the 2 km beam tube in 10 months and the initiation of bake-out in 20 months. In our discussions with the project staff concerning this challenge, they agreed to the following set of recommendations.

Recommendations:

- 1) Define the methods LIGO will use to perform its role as general contractor at the site to oversee and coordinate the activities of all project participants during execution of the system integration and acceptance testing of the beam module and all subsequent commissioning and operations.
- 2) Within the existing LIGO Project integrated schedule, continue to develop the subsystem schedules especially as they relate to the overall system integration and acceptance tasks at the sites and particularly as they relate to the incorporation of the bake-out system for the beam tubes.
- 3) The project should define bake-out requirements, procedures, testing, schedule, cost, manpower, etc., incorporated into the project effort for the bake-out test of the first beam tube module in Hanford and for the rest of the project.

2. Detectors

2.1 Overall Findings

The committee examined the activities of the LIGO Detector/R&D Group. It was evident that they are making very good progress in meeting target dates, costs and schedules in spite of the planned conversion from 515 nm to 1064 nm wave length which requires new laser systems and optics. The new management structure has brought cohesion and focus to the large LIGO group which is doing an outstanding job of carrying out the difficult and complex task of building the detector system which is the heart of the gravity wave interferometer. The committee notes that LIGO is well into the transitional period from basic R&D to delivery of the actual initial detectors. Several technical issues remain unresolved with regard to the specification of components for the detectors. The group needs to carefully allocate resources to provide the necessary design specifications in a timely way, while simultaneously providing both operating experience and testing of integrated systems on the existing 40-M and PNI facilities.

Actions in Response to April Recommendations

Finding:

The LIGO program has responded appropriately to the recommendations and comments made at the last review in the areas of the detector design and detector R&D.

2.2 Phase Noise Interferometer

Finding:

The committee is impressed and excited by the recent results which demonstrate the world's most accurate measurement of optical phase (3.5×10^{-10} rad/Hz^{1/2}) for

frequencies > 2 kHz. This dramatic improvement in sensitivity was made possible by power recycling and the installation of new accurate wave front sensors for the alignment of the interferometer to get the necessary recycling gain. However, the measurements indicate significant excess noise between 100 and 2000 Hz which increases approximately as $1/f^2$ at lower frequencies. Since this excess noise lies in the gravity wave signal bandwidth for LIGO, it is essential that it be reduced to a negligible level. Although the excess noise may disappear with conversion to 1064 nm, the review committee takes the conservative view that it won't. The committee believes that every effort should be made to identify its source(s) since an understanding of the nature of the excess noise could prove to be vital to the success of LIGO. Possible explanations might include unexpected effects of small amounts of coherently scattered laser light from chamber walls or Rayleigh scattering in the beam splitter.

Comment:

The committee commends the MIT PNI group for their recent rapid progress and their excellent results. We are also encouraged by the recent addition to the MIT-LIGO postdoctoral staff, which at an earlier review was deemed critical to the survival of the LIGO group at MIT.

Recommendation:

The LIGO program requires that the excess noise be understood and reduced to an insignificant level before final design choices are made. The PNI (and, possibly, the 40m prototype) should be exercised in order to track down and eliminate excess phase noise as expeditiously as possible. The conversion of the PNI to 1064 nm, currently scheduled for January 97, should not be delayed. However, the committee strongly encourages the vigorous study of the phase noise problem using the 515 nm system until the conversion occurs. Should excess phase noise remain a problem after conversion, then its reduction should receive the highest priority.

2.3 Recycling and Operation of the 40 m Interferometer

Findings:

The committee looks forward to the initial operation of the 40 m Interferometer with recycling which is currently scheduled for late March 1997. There is good progress toward implementing full beam alignment and control. A low noise rf driver for the probe sidebands at 32 MHz has been purchased and will be evaluated. If there are no major interruptions to the schedule, then the 40 m interferometer, with a recycling cavity, will be operating next spring in time for the next visit by the committee.

Comment:

If this new configuration works (and works well), the committee strongly encourages the LIGO group to operate the 40 m Interferometer (which will then be the world's most sensitive gravity wave detector) to gain an initial experience base for the commissioning of LIGO. This will also provide a significant data sample to begin to exercise the nascent data analysis effort which is at its very earliest stages. The lock acquisition is a major technical concern. Actual lock acquisition and operation is likely to reveal bugs/problems/details that have not been anticipated by the best modeling efforts.

Recommendation:

The 40-m prototype should be converted to a recycling system as planned and the low-noise rf driver tested and implemented. The possibility of fluctuations in the electro-optic coupling, etc. at frequencies above 100 Hz should be explored and the excess noise on the 40 m systematically reduced as it is operated in an "observatory" mode.

2.4 Seismic Isolation

Finding:

Recent seismic data from the sites has indicated that the micro seismic motion with a peak at $\sim 1/6$ Hz driven by ocean waves is greater than anticipated. The relative range of motion between isolation stacks that must be compensated is about ± 40 microns at the micro seismic peak. The common mode component of the earth tide is about three times larger in amplitude but with a twelve hour period. In addition, there is a differential component of the earth tide with approximately 100 micron peak to peak amplitude with the same period. Compensation for this motion poses a serious challenge to the isolation and suspension sub-systems. A determination of the proper means of apportioning the authority and bandwidth of the isolation and servo systems awaits the outcome of a detailed trade study currently underway. The committee understands that by January 1997 a design review will take place, with a complete design by April 1997. The committee also notes the transition of leadership of this activity from Acting Task Leader Raab to Task Leader Fine comes at a critical time for this group.

HYTEC appears to be making good progress in modeling the seismic isolation stacks. A very significant reduction in the stack mass from more than 6000 lbs to 3800 lbs is an important development. With this mass it is now possible to consider active isolation with the existing commercial devices used on the PNI at MIT. This may be an important reserve should unforeseen sources of low frequency seismic noise appear. Progress on the damped springs has proceeded through the finite element analysis modeling stage and prototypes are being prepared. The committee looks forward to the seeing the initial test results at the next meeting.

Comment:

The committee shares LIGO's concern over the seismic noise issues. The dynamic range needed to suppress this noise and extremely rapid decrease in servo loop gain at higher frequencies (to avoid noise pollution in the detection band) make this a difficult problem.

Recommendation:

LIGO recognizes the seriousness of the seismic isolation problem and the need for a robust solution. A detailed review of the proposed solution will occur at the next meeting.

2.5 10 Watt Laser at 1064 nm

Findings:

The acquisition of these new lasers seems to be proceeding well with good contact between the vendor, Lightwave Electronics, and the LIGO group. A flexible relationship that could incorporate the expected future advances in the field seems to be in place and is strongly encouraged.

Comment:

Optical feedback to the master-oscillator needs to be eliminated; even weak back scattering from the optics downstream of the laser will become significant after returning through the power amplifiers.

Schedule

Finding:

The schedule for the detector system as a whole has slipped roughly 2 months behind initial goals.

Comment:

The detector system is not on the critical path at present, and the actual schedule is within acceptable parameters. However, there is little slack available to deal with surprises.

2.6 Core Optics Coatings

Finding:

Coating uniformity of one Ta₂O₅ layer has been measured using a sensitive anti-reflection structure. The observed variation in thickness corresponds to a 1.5 degree phase shift within a 4.5 cm radius for that single layer. Assuming the same level of uniformity for each layer in a 40 layer high-reflectivity stack yields a predicted recycling gain of 36.8, comfortably above the gain of 30 required. The current data on SiO₂ layers is much less sensitive because of the layer design which leads to significantly greater uncertainty in the layer thickness and uniformity.

Comment:

The difficult coating problem seems to be well in hand. The potential for loss and scattering due to rough or non uniform SiO₂ films needs further investigation, as do the interactions between the coating and surface figure.

Recommendation:

The core optics /pathfinder group should proceed to an equally rigorous test of the SiO₂ films and to tests of full thickness film stacks and coated substrates with known figure.

2.7 Alignment and Control System

Finding:

The reorganization of the hierarchy of the alignment sensing servo, partly caused by the difficulty of achieving the required 10⁻⁸ precision using optical levers and partly by the conceptual and rapid technical development of the superior wave front sensors, promises to provide adequate alignment control for the full interferometer. However, three-dimensional control of the full system (Michelson with Fabry-Perot cavities and power recycling cavity) has yet to be carried out. This key technical issue of lock acquisition and control is now being vigorously pursued. The committee notes that the alignment sensing program has slipped in schedule by a few months, but proper effort in this area is certainly being made and there are no apparent show stoppers.

Comment:

The actual systems involve multiple degrees of freedom, which may interact in unexpected ways. Further extensive simulation and the exercise of a multiple-degree-of-freedom hardware system are needed prior to the design review scheduled in January 1997.

Recommendation:

The program to implement recycling and the new alignment sensors on the 40-M facility is scheduled, with shakedown of the additions to the interferometer set for January 1997, with operation by March 1997. We encourage LIGO to aggressively pursue this part of the program.

3. Data Analysis

Finding:

The challenges inherent in collecting, archiving, analyzing and distributing data from an operating LIGO system have just recently been recognized. Information about the state of the detector system may comprise more than 100 times the data volume of the gravity wave detection channel, leading to a total information production of 10^4 computer tapes a year using current tape technology. It is hoped that the LIGO and VIRGO systems will agree on a common data format, but some technical incompatibilities have already arisen. Data processing for some types of event should be done on-line, while others will have to be done off-line. The computational requirements are severe in either case. A white paper on the data processing issues will be available in mid-1997.

Comment:

This is a very important and very complex issue. The formats, paradigms and standards adopted for LIGO may well outlive the first-generation interferometer. While some of the personnel have been working efficiently to explore the possibilities, they have been stretched thin by other responsibilities. The complexity of data acquisition, archiving, formats, links and the possible trade-offs suggests that experienced data managers from outside the program should become involved. Data acquisition and manipulation will only grow in importance and poor choices are likely to have adverse and potentially expensive long-term consequences. Exercising a prototype DAQ system on the 40 m Interferometer should provide insight on these issues and could potentially attract people from other areas of physics with extensive experience in analyzing large data sets.

Appendix A: Members of the LIGO Technical Review Committee and NSF Staff

Consultants

Dr. James C. Berquist
National Institute of Standards and Technology
Div. 847.10, 325 South Broadway
Boulder, CO 80303
Office#: (303) 497-5459
Email: berky@central.bldrdoc.gov
Fax#: (303) 497-7375

Mr. Rudolf Damm
Bldg. 400, ASD/APS
Argonne National Laboratory
9700 South Cass Avenue
Argonne, Illinois 60439
Office#: (708) 252-3129
Email: damm@aps.anl.gov
Fax#: (708) 252-1512

Prof. Roger W. Falcone
Physics Department
366 LeConte Hall
University of California
Berkeley, CA 94720
Office#: (510) 642-3316
Email: rwf@physics.berkeley.edu
Fax#: (510) 643-8497

Prof. Donald L. Hartill (Chair)
234 Newman Laboratory
Cornell University
Ithaca, NY 14853
Office#: (607) 255-8787
Email: dlh@lms62.lms.cornell.edu
Fax#: (607) 255-8062

Dr. Marc Levenson
ECE Dept.
Rice University
P.O. Box 1892
Houston, TX 77251-1892
Home#: (713) 942-8538
Email: MUDDLE@aol.com
Fax#: (713) 524-5237

Dr. Paul Reardon
32 Lochatong Road
West Trenton, NJ 08628
Home#: (609) 883-0843
Email: N/A
Fax#: (609) 406-0114

Mr. E. Parke Rohrer, PE
Box 247 (1934 Hans Herr Drive)
Willow Street, PA 17584
Home#: (717) 464-1085

NSF Staff

Dr. David Berley
Program Manager/LIGO
National Science Foundation
4201 Wilson Blvd., Room 1015
Arlington, VA 22230
Office#: (703) 306-1892
Email: dberley@nsf.gov
Fax#: (703) 306-0566

Dr. Robert A. Eisenstein
Director, Division of Physics
National Science Foundation
4201 Wilson Blvd., Room 1015
Arlington, VA 22230
Office#: (703) 306-1897
Email: reisenst@nsf.gov
Fax#: (703) 306-0566

Dr. Karl Erb
National Science Foundation
4201 Wilson Blvd.
Arlington, VA 22230
Office#: (703) 306-1002
Email: kerb@nsf.gov
Fax#: (703) 306-0109

Mrs. Karen Sandberg
Grants & Agreements Specialist/DGA
National Science Foundation
4201 Wilson Blvd., Room 1015
Arlington, VA 22230
Office#: (703) 306-1212
Email: ksandber@nsf.gov
Fax#: (703) 306-0275

Appendix B: Charge to the LIGO Technical Review Committee

The Technical Review Committee is charged to:

1. Review the technical aspects of the Laser Interferometer Gravitational-Wave Observatory (LIGO). The review should include an assessment of the core optics, the seismic isolation system, the vacuum equipment, the beam tube and the control system. Assess the progress on the R&D program including progress on the 40 m Interferometer and the Phase Noise Interferometer.
2. Provide a review of the proposal from the LIGO Project for Advanced R&D.
3. Assess the actions taken on the recommendations made and the progress on issues raised at the cost review of LIGO held April 9-11, 1996.

The Technical Review Committee is requested to complete its report by November 16, 1996.

CALIFORNIA INSTITUTE OF TECHNOLOGY
LIGO Project, 51-33 East Bridge Laboratory, Pasadena, California 91125
(818) 395-2129, Fax (818) 304-9834

Date: March 3, 1997
Refer to LIGO-L970088-00-P

Dr. David Berley
Program Manager for LIGO
National Science Foundation
4201 Wilson Blvd.
Arlington, VA 22230

Subject: Revised LIGO FY 1997 Advanced Detector R&D Program Proposal (PHY97-00601)

Dear Dr. Berley. *Dave*

The revised proposal for the LIGO Fiscal Year 1997 Research and Development Program for Advanced Detectors (PHY97-00601) is enclosed for your review and approval.

The advanced detector R & D proposal submitted in October 1996 requested \$1,741,000 in FY 1997 (Table 11, page 61 of LIGO-M960089-00-M). This request was for the first of five years of research. Current program guidance from NSF indicates that funds for a 1997 initiation of the program are available at a level of \$880,000. LIGO submits this revised proposal consistent with this funding level.

The LIGO Program Advisory Committee (PAC) met in January 1997. This proposal was reviewed by the PAC, and the PAC concurred with the advanced program for advanced R&D proposed. There was also a meeting of the Advanced R&D Detector Workshop held at Aspen at the end of January. There were several scheduled and impromptu meetings during the Aspen Workshop to facilitate consolidation of the collaborative R&D plans. The enclosed proposal is consistent with the overall programs discussed during these meetings.

We have enclosed a copy of the entire package for the information of Carol Langguth and ask that you forward it to her attention. If there are any questions please contact me at (818) 395-3193.

Sincerely,

Philip E. Lindquist
LIGO Project Controls Manager

Concurrence for
California Institute of Technology:

Richard Seligman
Director, Sponsored Research

PEL:pel
cc:

G. Sanders
Chronological File

B. Barish
Document Control Center

C. Langguth (NSF)

LASER INTERFEROMETER GRAVITATIONAL WAVE OBSERVATORY
- LIGO -

CALIFORNIA INSTITUTE OF TECHNOLOGY
MASSACHUSETTS INSTITUTE OF TECHNOLOGY

Document Type	LIGO-M970001-01-	M	3/3/97
Proposal			
“Revised Proposal for a Research and Development Program For Advanced Detectors by the LIGO MIT/Caltech Groups - FY 1997 Proposal Budget” (LIGO-M960089-00-M)			
LIGO FY1997 Advanced Detector R&D Program			

Distribution of this document:

National Science Foundation

For review and approval of
FY 1997 Advanced R&D Proposal Budget
(PHY97-00601)

California Institute of Technology
LIGO Project - MS 51-33
Pasadena CA 91125
Phone (818) 395-2129
Fax (818) 304-9834
E-mail: info@ligo.caltech.edu

Massachusetts Institute of Technology
LIGO Project - MS 20B-145
Cambridge, MA 01239
Phone (617) 253-4824
Fax (617) 253-7014
E-mail: info@ligo.mit.edu

WWW: <http://www.ligo.caltech.edu/>

1 INTRODUCTION

The LIGO Caltech and MIT groups submitted an advanced detector research and development proposal (LIGO-M960089-00-M) to the National Science Foundation on October 8, 1996. The proposed five year program is intended to underpin future enhancements to the initial LIGO interferometers, and entirely new advanced detector systems. These developments would be part of fulfilling the design assumption in the initial LIGO construction that the LIGO facilities would support future generations of improved detectors.

The proposal was submitted in response to the advice provided to the National Science Foundation in the *Report of the Panel on the Use of the Laser Interferometer Gravitational Wave Observatory*, Boyce McDaniel, Chair, June, 1996. This report called for a vigorous program in advanced detector R&D. It also urged that the R&D be conducted as multi-institution collaborations.

Caltech and MIT proposed a program intended to address each of the limiting noise sources in LIGO detectors. In two phases, advanced subsystems for the initial interferometers and entirely new advanced detectors, the R&D program addresses improvements in the noise floor for seismic noise, thermal noise in suspensions and test masses, and in phase noise limited by the laser power.

In structuring the proposal, we have worked with colleagues in other institutions to define a collaborative approach to the research. The general distribution of responsibilities, and the schedule of research activities in the program is defined in the proposal. The LIGO proposal requests only the resources required by LIGO. Collaborating institutions are responsible to request resources needed by that institution.

The proposed program extends over five years, commencing in 1997. In this document, we provide a simple statement of the first year activities for which we request funding in 1997. The full proposal provides the context within which first year activities are embedded. We request FY1997 funding of \$878K to support activities at MIT and Caltech on implementation of 1064 nm lasers at the 40 Meter Interferometer, on preparation for double pendulum suspension research at the MIT interferometer, thermal noise research at Caltech, and resonant sideband extraction research at Caltech and MIT. It should be noted that the identified 1997 activities are not dependent upon NSF review and support of collaborating institutions.

2 PROGRAM SUMMARY

The advanced detector R&D proposal requested \$1741K in FY1997 (Table 11, page 61 of LIGO-M960089-00-M). This request was for the first of five years of research. Current program guidance from the NSF indicates that funds for a 1997 initiation of the program are available at a level of \$880K. LIGO submits this revised proposal consistent with this funding level.

The LIGO Program Advisory Committee (PAC) met in January 1997. This proposal was reviewed by the PAC, and the PAC concurred with the proposed plan. In addition there was a meeting of the Advanced Detector Workshop held at Aspen at the end of January. There were several scheduled and impromptu meetings during the Aspen Workshop to facilitate consolidation of the collaborative R&D plans.

To meet the reduced funding target, we are deferring expenditures for development of 100 W lasers, core optics research, sapphire test mass research and reducing the hiring and assignment of staff for advanced R&D activities. This will delay several programs into FY1998.

For FY1997, the LIGO advanced R&D will be initiated with the following activities, staff and related equipment costs (including materials and supplies, travel, and the associated indirect costs):

Table 1: FY1997 LIGO Advanced Detector R&D Plan

<i>Task</i>	<i>Equipment (K\$)</i>	<i>Labor (FTE)</i>	<i>Labor (K\$) (Burdened)</i>	<i>Subtotals</i>
40 Meter Interferometer Infrared Conversion	\$151K	0.5 technician, 1.0 postdoc, 0.5 staff scientist	\$211K	\$362K
MIT Interferometer configuration/suspension research	\$92K	1.0 postdoc, 1.0 grad. student	\$131K	\$223K
Resonant Sideband Extraction	\$85K	0.5 grad. student, 0.1 staff scientist	\$38K	\$123K
Thermal noise	\$78K	0.5 postdoc, 0.5 grad. student, faculty summer	\$92K	\$170K
<i>TOTAL</i>	<i>\$406K</i>	<i>0.5 technician, 2.5 postdoc, 0.6 staff scientist, 2 grad. student, plus faculty summer</i>	<i>\$472K</i>	<i>\$878K</i>

3 40 METER INTERFEROMETER INFRARED CONVERSION

LIGO will complete the recycling experiment at the 40 Meter facility during the fourth quarter of FY1997. This is the last deliverable for LIGO construction. It is necessary to upgrade and convert the interferometer for use in the advanced R&D program, and to support operational research. This requires conversion from 514 nm light to the 1064 nm wavelength adopted for LIGO.

During FY1997, a postdoctoral fellow, supervised by a senior staff scientist, will specify and procure the first elements of the new optics system, for installation in FY1998. A technician will

implement LIGO-style controls and electronics for the 40 Meter. This will result in a system capable of stable, quiet operation with a configuration similar to LIGO.

4 MIT INTERFEROMETER CONFIGURATION/DOUBLE PENDULUM RESEARCH

The MIT Phase Noise Interferometer will complete its measurement of LIGO phase sensitivity at 1064 nm at the end of calendar year 1997. This task will provide the last required validation of the LIGO design in the construction project. In order to accommodate the proposed double pendulum suspension research and taking advantage of the relocation at MIT of the interferometer, the MIT group will commence modifications of the interferometer in its new location. In parallel with this, the MIT group will commence advanced R&D activities with prototyping of electrostatic actuators, some revisions of the instrumentation at the MIT interferometer and small scale research with the table-top systems at MIT on suspensions and configurations.

A total of two postdoctoral fellows and two graduate students during the second half of FY1997 will carry out the following activities, together with senior scientific staff:

- Collaborative studies of double pendulum configurations
- Electrostatic actuator development
- Design of suspension tests in MIT interferometer
- Modeling of resonant sideband extraction/signal recycling configurations
- Studies of tunable output coupler/output mode cleaner techniques

5 RESONANT SIDEBAND EXTRACTION

LIGO and the University of Florida have proposed a collaborative program of research in advanced detector configurations. During 1997, Florida will initiate table top research in signal recycling. LIGO will commence parallel work in resonant sideband extraction. These two thrusts will lead to a larger scale test in a LIGO suspended test interferometer of the selected technique.

During FY1997, LIGO proposes to begin this work at Caltech with a graduate student, James Mason, beginning in mid year, supervised by Seiji Kawamura. Modeling and some related effort will take place at MIT. Initial expenditures will provide the laser, and appropriate core optics and active optical elements for use in an existing Caltech laboratory.

6 THERMAL NOISE

Since LIGO submitted the full proposal for advanced detector research, the Caltech LIGO group has been joined by an additional senior faculty member. Professor Ken Libbrecht. He is defining a program of research in thermal noise. For this reason, we are revising our plan to initiate fundamental research in thermal noise in mid-1997, which we had planned to begin in mid-1999. Professor Libbrecht will begin with a postdoctoral fellow and a graduate student in the second half of FY1997, following LIGO review of detailed plans. Table 1 includes initial equipment funding to establish a table top test bed for this research.

REVISED
SUMMARY
PROPOSAL BUDGET

FOR NSF USE ONLY		
ORGANIZATION California Institute of Technology	PROPOSAL NO.	DURATION (MONTHS)
		Proposed Granted
PRINCIPAL INVESTIGATOR/PROJECT DIRECTOR Barish	AWARD NO.	

A. SENIOR PERSONNEL PI/PI, Co-PI's, Faculty and Other Senior Associates (List each separately with title, A.7. show number in brackets)	NSF Funded Person-months			Funds Requested By Proposer	Funds Granted By NSF (If Different)
	CAL	ACAD	SUMR		
1. B. Barish PI/Professor of Physics, CIT				\$	\$
2. G. Sanders Project Manager					
3. K. Libbrecht Assoc. Professor of Astrophysics, CIT	1.5				
4.					
5.					
6. () OTHERS (LIST INDIVIDUALLY ON BUDGET EXPLANATION PAGE)					
7. () TOTAL SENIOR PERSONNEL (1-6)	1.5			13,000	
B. OTHER PERSONNEL (SHOW NUMBERS IN BRACKETS)					
1. (2.5) POST DOCTORAL ASSOCIATES	30			104,000	
2. (1.1) OTHER PROFESSIONALS (TECHNICIAN, PROGRAMMER, ETC.)	13			67,808	
3. (2.0) GRADUATE STUDENTS				41,600	
4. () UNDERGRADUATE STUDENTS					
5. () SECRETARIAL - CLERICAL (IF CHARGED DIRECTLY)					
6. () OTHER TECHNICAL & ADMIN. SUPPORT					
TOTAL SALARIES AND WAGES (A+B)				226,408	
C. FRINGE BENEFITS (IF CHARGED AS DIRECT COSTS) Based on weighted average rate				68,183	
TOTAL SALARIES, WAGES AND FRINGE BENEFITS (A+B+C)				294,591	
D. EQUIPMENT (LIST ITEM AND DOLLAR AMOUNT FOR EACH ITEM EXCEEDING \$5,000.)					
TOTAL EQUIPMENT				333,420	
E. TRAVEL 1. DOMESTIC (INCL. CANADA, MEXICO AND U.S. POSSESSIONS)				19,000	
2. FOREIGN					
F. PARTICIPANT SUPPORT COSTS					
1. STIPENDS \$ _____					
2. TRAVEL _____					
3. SUBSISTENCE _____					
4. OTHER _____					
() TOTAL PARTICIPANT COSTS					
G. OTHER DIRECT COSTS					
1. MATERIALS AND SUPPLIES				27,000	
2. PUBLICATION COSTS/DOCUMENTATION/DISSEMINATION					
3. CONSULTANT SERVICES					
4. COMPUTER SERVICES					
5. SUBCONTRACT AWARDS					
6. OTHER (GRA Benefits)				8,320	
TOTAL OTHER DIRECT COSTS				35,320	
H. TOTAL DIRECT COSTS (A THROUGH G)				682,331	
I. INDIRECT COSTS (SPECIFY DATE AND BASE) 57.45% of T.D.C. excluding equipment, JPL support, subcontracted amounts beyond first \$25,000 of each subcontract, and GRA benefits.					
TOTAL INDIRECT COSTS				195,669	
J. TOTAL DIRECT AND INDIRECT COSTS (H+I)				878,000	
K. RESIDUAL FUNDS (IF FOR FURTHER SUPPORT OF CURRENT PROJECT SEE GPG 11 D 7.1)					
L. AMOUNT OF THIS REQUEST (J) OR (J MINUS K)				\$ 878,000	\$
M. COST-SHARING: PROPOSED LEVEL \$					
					AGREED LEVEL IF DIFFERENT \$

PI/PO TYPED NAME & SIGNATURE*		FOR NSF USE ONLY		
C. Barish		INDIRECT COST RATE VERIFICATION		
REP. TYPED NAME & SIGNATURE*	DATE	Date Checked	Date of Rate	Initials-ORG
Michael Kelly	5-1-97			

Advanced R&D Work Plan
(Proposal Budget Justification Sheet)

Line	Description	FTEs			FY 1997 Dollars					Total	Hourly Rate
		40-m Conversion	MIT Config/ Suspension Research	Resonant Sideband Extraction	Thermal Noise	40-m Conversion	MIT Config/ Suspension Research	Resonant Sideband Extraction	Thermal Noise		
A	Senior Personnel										
B1	Post Doctoral Associates	1.00	1.00		0.13	\$ -	\$ -	\$ -	\$ 13,000	13,000	\$ 50.00
B2	Other Professionals				0.50	\$ 41,600	\$ 41,600	\$ -	\$ 20,800	104,000	\$ 20.00
	Scientists	0.50		0.10		\$ 37,440	\$ -	\$ 7,488	\$ -	44,928	\$ 36.00
	Management					\$ -	\$ -	\$ -	\$ -	-	
	Engineers					\$ -	\$ -	\$ -	\$ -	-	
	Technicians	0.50				\$ 22,880	\$ -	\$ -	\$ -	22,880	\$ 40.00
B3	Graduate Students		1.00	0.50	0.50	\$ -	\$ 20,800	\$ 10,400	\$ 10,400	41,600	\$ 22.00
B4	Undergraduate Students					\$ -	\$ -	\$ -	\$ -	-	
B5	Secretarial - Clerical					\$ -	\$ -	\$ -	\$ -	-	\$ 10.00
B6	Other Technical and Administrative Support					\$ -	\$ -	\$ -	\$ -	-	\$ 20.00
	Total Salaries and Wages	2.00	2.00	0.60	1.13	\$ 101,920	\$ 62,400	\$ 17,888	\$ 44,200	\$ 226,408	
C	Fringe Benefits (based on weighted average)										
	All Except Graduate Students (6 months @ 33.34 percent; 2 months @ 25 percent)					\$ 31,855	\$ 13,002	\$ 2,340	\$ 10,564	\$ 57,762	
	Graduate Students (6 months @ 33.34 percent)					\$ -	\$ 5,210	\$ 2,605	\$ 2,605	\$ 10,421	
	Total Salaries, Wages and Fringe Benefits					\$ 133,775	\$ 80,612	\$ 22,834	\$ 57,369	\$ 294,591	
D	Permanent Equipment					\$ 132,000	\$ 60,500	\$ 69,420	\$ 71,500	\$ 333,420	
E	Travel										
E1	Domestic Travel					\$ 2,000	\$ 10,000	\$ 5,000	\$ 2,000	\$ 19,000	
E2	Foreign Travel										
F	Participant Costs										
G	Other Direct Costs										
G1	Materials and Supplies					\$ 10,000	\$ 10,000	\$ 5,000	\$ 2,000	\$ 27,000	
G2	Publication Costs/Documentation										
G3	Consultant Services										
G4	Computer Services										
G5	Subcontracts										
G6	Other (GRA Benefit, 80 percent of B3 after October 1, 1997 - 2 months)					\$ -	\$ 4,160	\$ 2,080	\$ 2,080	\$ 8,320	
	Total Other Direct Costs					\$ 10,000	\$ 14,160	\$ 7,080	\$ 4,080	\$ 35,320	
H	Total Direct Costs					\$ 277,775	\$ 165,272	\$ 104,334	\$ 134,949	\$ 682,331	
I	Equipment, GRAs)										
J	Total Direct and Indirect					\$ 83,748	\$ 57,802	\$ 18,863	\$ 35,257	\$ 195,669	
						\$ 361,523	\$ 223,074	\$ 123,196	\$ 170,206	\$ 878,000	
	Total Labor (\$K) Burdened					210,629	131,084	38,031	92,408	472,153	
	Total Equipment (\$K) Burdened					150,894	91,990	85,165	77,798	405,847	
	Total (\$K)					361,523	223,074	123,196	170,206	878,000	

Advance R&D Budget Proposal

Budget Justification

Line A. Senior Personnel

B. Barish	Principal Investigator/Laboratory Director/ Professor of Physics, Caltech
G. Sanders	Project Manager/Deputy Laboratory Director
P. Lindquist	Project Controls Manager/Laboratory Administrator
A. Lazzarini	Manager of Integration, Data Analysis, and Computing
R. Weiss	Integration Scientist, Professor of Physics, MIT
K. Libbrecht	Associate Professor of Astrophysics, Caltech

Line C. Fringe Benefits

Benefits (except for Graduate Students) are computed at an average rate of 31.26 percent. This is based on six months at 33.34 percent (April 1, 1997 through September 30, 1997) and two months at 25 percent (October 1, 1997 through November 30, 1997).

Graduate Students receive benefits at 33.34 percent through September 30, 1997. Subsequent to October 1, 1997 Graduate Students are covered under Institute GRA Policy (line G6 below). Benefits for Graduate Students are, therefore, computed using a rate of 25.01 percent (six months at 33.34 percent and two months at 0.0 percent).

Senior Personnel, Post Doctoral Associates, Other Professionals	
33.34 percent for 6 months, 25 percent for 2 months	\$ 57,762
Graduate Students	
33.34 percent for 6 months	<u>\$ 10,421</u>
Total	\$ 68,183

Line G6. GRA Benefits

Graduate Research Assistantship Benefits - Institute Policy is to provide each graduate student employee who meets a required average work week with full tuition and fees. A portion of this cost is requested as a benefit (exempt from indirect costs) equivalent to 80 percent of the graduate research assistant salary effective October 1, 1997.

Line I. Indirect Costs

Computed at a rate of 57.45 percent of total direct costs excluding amounts for individual subcontracts in excess of \$25,000, GRA Benefits, and Equipment



The LIGO Laboratory Charter



Draft 2

March, 1997

LIGO-M970023-02-M

Contents

Mission and Responsibilities
National Science Foundation Cooperative Agreement
Institutional Roles and Responsibilities

Hierarchy
NSF
NSF Program Manager
NSF Division of Grants and Agreements
Caltech
MIT
Caltech Reporting
MIT Reporting
Oversight Committee
Director and Deputy Director

Organization of the LIGO Laboratory:

Directorate
LIGO Scientific Collaboration
LIGO Research Community
LIGO Program Advisory Committee
LIGO Laboratory Executive Committee
LIGO Visitors Program
Science Education Program
Industrial Liaison Program
LIGO Laboratory Functional Groups
Hanford Observatory - Livingston Observatory
Administration
Technical and Engineering Support
Detector Support
Data Analysis and Computing
Research Facilities
Advanced Research and Development

Environment, Safety and Health Protection

Objectives

Responsibilities

Environmental Protection

Safety and Health Protection

Employee Training

Contractors, Collaborators and Visitors

Documentation

Governmental Code Requirements

Procurements and Subcontracts

Policy

Responsibilities

Approach

NSF Reporting and Reviews

Quarterly Reports

Annual Report

Annual Work Plan

Other Reporting

LIGO Oversight Committee

LIGO Program Advisory Committee

NSF Site Visits/Visiting Committee

Workshops

Technical Reports

Mission and Responsibilities

In order to assure the full scientific exploitation of LIGO, it is necessary to provide for the operation and coordination of the LIGO program and for the advocacy and execution of the science. For these reasons, following the guidance of the National Science Foundation (NSF), we establish a LIGO Laboratory to accomplish the first purpose. A LIGO Scientific Collaboration is separately formed to realize the latter purpose.

The LIGO Laboratory will:

- operate the scientific facilities at the observatory sites in Hanford, Washington and in Livingston Parish, Louisiana
- assure the scientific vitality of these detector facilities
- provide the capability for acquisition of the data, and for system modeling and data analysis
- operate LIGO research and test facilities at the observatory sites and on the MIT and Caltech campuses

- support engineering design and fabrication of detector upgrades and of new detector systems
- carry out research and development in support of the future LIGO program
- support the LIGO Scientific Collaboration in its exploitation of the scientific capabilities
- review and coordinate new LIGO research initiatives
- support public education and outreach in areas related to LIGO science and technology
- assure a safe and comfortable working environment for LIGO staff and visitors
- support the educational mission of the participating universities

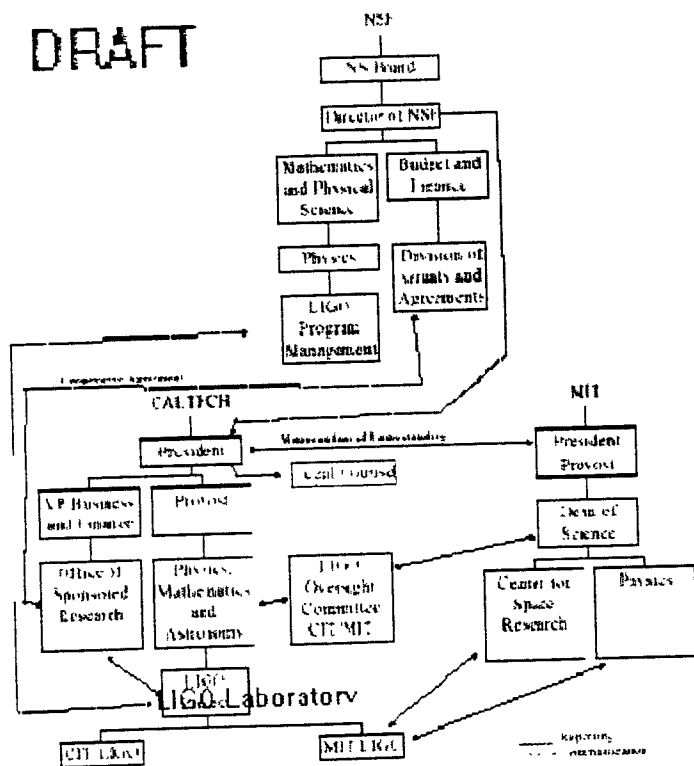
National Science Foundation Cooperative Agreement

The LIGO Laboratory operates under a Cooperative Agreement between the US National Science Foundation (NSF) and the California Institute of Technology (Caltech). The Agreement defines the obligations of Caltech and MIT in carrying out the mission of the Laboratory.

Institutional Roles and Responsibilities

Hierarchy

The LIGO Laboratory reporting and oversight is defined in the organizational hierarchy shown in the figure.



NSF

NSF is responsible for providing funding, general oversight, monitoring, and evaluation to help assure Laboratory performance in accordance with approved workplans. NSF will strive to obtain funding consistent with the Target Funding Levels set forth in the Cooperative Agreement. The actual funding available for LIGO will be negotiated with the Laboratory on the basis of the Annual LIGO Work Plan which, upon approval by NSF, will constitute the official operating plan for the year. Within the framework of the annual operating plan, NSF will undertake to provide the funding in a timely fashion and to provide the

necessary document reviews and approvals as indicated in the Work Plan.

NSF Program Manager

Within the NSF, the LIGO Program Manager is responsible for scientific, technical, cost and schedule review and agency guidance. Review of progress and programmatic review of annual work plans is the responsibility of the LIGO Program Manager. Direct communication between the LIGO Program Manager and the LIGO Laboratory is the method by which this review and guidance will be accomplished. Performance of work under the Cooperative Agreement is subject to the general guidance and monitoring of the NSF Program Manager for LIGO. This NSF involvement includes the following:

- provision of advice;
- review and, where required by the Agreement, approval of required subcontracts, reports, and plans submitted by Caltech;
- assessment of progress by the NSF Program Manager and external reviewers.

NSF Division of Grants and Agreements

The NSF Division of Grants and Agreements is responsible for Cooperative Agreement matters between the NSF and Caltech. Formal communications related to contracts and required Cooperative Agreement designated approvals will be accomplished by the Division of Grants and Agreements and the Caltech Office of Sponsored Research. Annual funding increments and contractual obligations flow from the Division of Grants and Agreements (DGA), National Science Foundation (NSF) to Caltech, under the Cooperative Agreement. Excluding certain contractual arrangements, all subcontracts in excess of \$100,000 issued by Caltech are subject to approval by DGA/NSF.

Caltech

Caltech is accountable, as the awardee, for the performance of the LIGO Laboratory, as described in the LIGO Annual Work Plan. Caltech is responsible for staffing the Laboratory, providing institutional support and ensuring adequate oversight of the execution and performance of the program. Caltech's Office of Sponsored Research is responsible for matters between Caltech and NSF that pertain to the administration of the terms and conditions of the Cooperative Agreement and will accomplish this through formal communications with the NSF Division of Grants and Agreements. Legal review and matters related to real property and property management will be the responsibility of the Caltech Legal Counsel reporting to the President and the Caltech Treasurer, respectively.

MIT

The LIGO Laboratory encompasses a joint effort of Caltech and MIT. The MIT roles and responsibilities are defined through a Memorandum of Understanding and subcontract with Caltech, with details defined in an attachment and updated as necessary. The MIT subcontract is subject to NSF approval. The MIT administration shares responsibility with the Caltech administration for overall oversight of the execution and performance of the LIGO program through representatives on the LIGO Oversight Committee. The MIT administration is also responsible for oversight, staffing and support of the MIT LIGO Group and for insuring that it successfully meets its institutional commitments. It is the policy of the LIGO Laboratory to have a fully integrated MIT participation with institutional boundaries minimized.

Caltech Reporting

LIGO activities at Caltech, like other research programs directed by physics faculty, are part of the Division of Physics, Mathematics and Astronomy (PMA) through which academic appointments and educational matters are administered. The Division also provides administrative and logistical support to LIGO and oversight of the Caltech effort on LIGO.

MIT Reporting

At MIT, academic appointments and educational aspects of LIGO are administered through the Department of Physics; research activities are supported through the Center for Space Research. The Department of Physics and the Center for Space Research provide oversight of the MIT effort on LIGO and they report to the President of MIT through the Dean of Science.

Oversight Committee

The presidents of Caltech and MIT have established a LIGO Oversight Committee, chaired by a member appointed by the Caltech President and composed of two members from each institution appointed by their respective presidents after mutual consultation. The Oversight Committee reports to the presidents through the Chair of Physics, Mathematics and Astronomy at Caltech and the Dean of Science at MIT. It will regularly provide review of LIGO program status and progress as required.

Director and Deputy Director

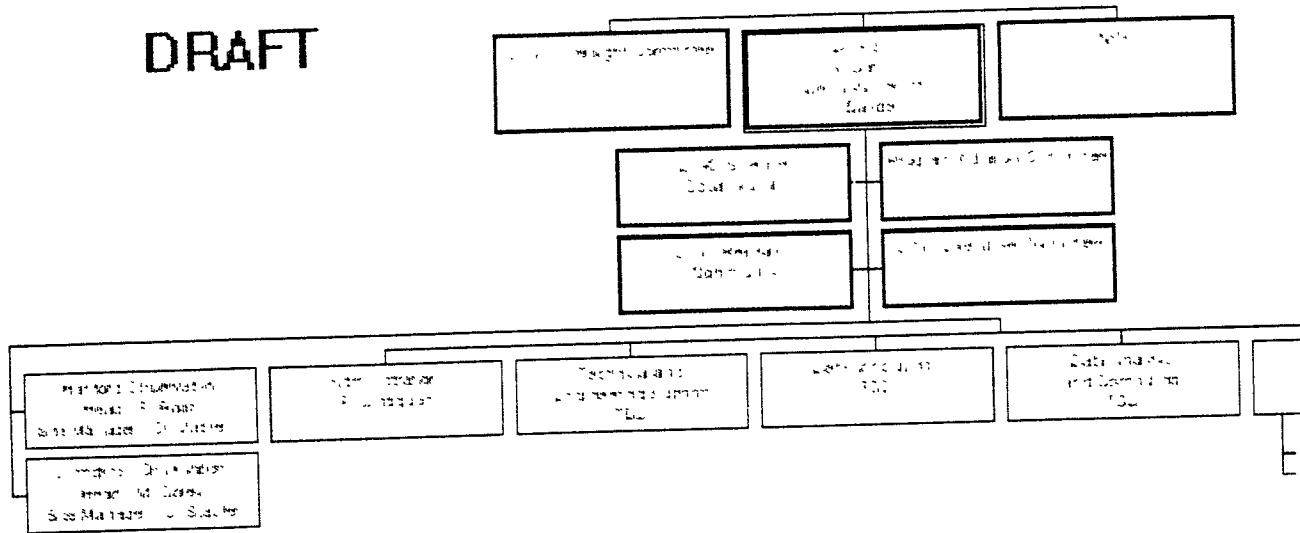
The LIGO Laboratory Director is appointed by the Caltech President in consultation with the MIT President and with the approval of NSF. The Director performs his responsibilities in close association with the LIGO Laboratory Deputy Director, who is appointed by the Director with the approval of the Presidents and the NSF. Other key personnel in the LIGO Laboratory, as defined in the Cooperative Agreement, are appointed by Caltech and MIT with the approval of NSF. The LIGO Laboratory Director, in association with the Deputy Director, reports progress on a quarterly basis to the LIGO Oversight Committee.

Organization of the LIGO Laboratory

The organization of the LIGO Laboratory is shown in the figure. It is a functional organization and has a flat hierarchy.

DRAFT

LIGO LABORATORY ORGANIZATION



Directorate

The LIGO Laboratory Directorate consists of the Director and the Deputy Director. Although each has different well-defined primary responsibilities, the overall Laboratory direction is fully shared and either can speak for the Laboratory. Both the Director and the Deputy Director are fully informed on all major decisions and will be mutually involved in the decision making as appropriate. The LIGO Laboratory Director has overall responsibility for the LIGO Laboratory. The Director's primary responsibility is to ensure the development and implementation of the LIGO Laboratory program in a timely and cost effective manner with the goal of detecting gravitational waves and carrying out a program of gravitational wave astronomy. The Deputy Director is primarily responsible for executing the LIGO program and for organizing and directing the Laboratory team composed of Caltech and MIT staff. The Director is the principal point for communication and interaction with NSF, through its LIGO Program Manager. The Director is also responsible for maintaining interactions and collaboration with the scientific community (both national and international).

LIGO Scientific Collaboration

The LIGO Scientific Collaboration (LSC) will carry out the LIGO research and development program, develop priorities, and enable participation by collaborating groups. It will be organized as a separate entity distinct from the LIGO Laboratory. Through its Spokesperson, the LSC will communicate with the Laboratory through the Laboratory Directorate.

LIGO Research Community

The LIGO Research Community (LRC) consists of all scientists interested in the scientific opportunities offered by LIGO. Membership in the LRC is open to all interested parties and, unlike, the LIGO Scientific Collaboration, requires no formal research commitment and responsibilities. The LRC communicates through its elected Chair with the Laboratory Directorate.

LIGO Program Advisory Committee

The LIGO Program Advisory Committee (PAC) is the principal source of advice to LIGO on scientific policy, technical choices, support of the scientific community and organizational matters. It

provides peer review of scientific and technical proposals for the scientific use of LIGO.

The Committee meets several times per year and will be asked for advice through a written charge provided by the LIGO Laboratory Director. The Committee's advice will be used by the Directorate in making decisions. The National Science Foundation is expected to request that LIGO use the Program Advisory Committee to review proposals to the NSF for R&D and LIGO science proposals.

The Committee is appointed for an initial term of three years after which new members will be appointed with staggered terms to assure renewal of the Committee and continuity.

LIGO Laboratory Executive Committee

The Executive Committee is the principal management body used by the Laboratory Directorate to review Laboratory program execution and status and to develop the basis for management decisions. The Executive Committee will meet regularly and be chaired by the Director, in association with the Deputy Director. It will consist of the managers of each of the LIGO Laboratory functional groups.

LIGO Visitors Program

The LIGO Laboratory operates an NSF-supported Visitors Program intended to provide research opportunities for scientific visitors to the campuses and Observatory sites. Supported visits are expected to be of significant duration and are proposed as research projects to the Laboratory Directorate for review and subsequent support.

Science Education Program

As a national facility based upon an exciting scientific research mission, LIGO can provide a focus for educational programs in science. A Science Education Program will reach beyond the traditional university role of educating undergraduate and graduate students to reaching K-12 grade level students. A Science Education Program Manager will develop and lead programs in educational outreach to the general public, in on-site educational programs at the Observatory sites, as well as the university campuses, and in supporting program development consistent with other NSF educational initiatives.

Industrial Liaison Program

An Industrial Liaison Program will supplement the extensive industrial participation in LIGO construction. LIGO development of enabling technologies promises to provide new capabilities of interest to industry. These include advanced laser and optical technology, and new capabilities in vibration and acoustic isolation. An Industrial Liaison Program Manager will lead direct efforts to inform, collaborate and cooperate with industrial partners.

LIGO Laboratory Functional Groups

Each LIGO Laboratory functional group reports to the Directorate and is led by a Group Leader and a Deputy Group Leader. These positions serve as line management for the respective group. Each group is represented on the Laboratory Executive Committee. Staff assignment to a functional group represents the principal assignment for each staff member. It is expected, however, that scientific and

technical staff will participate significantly in activities of other functional groups.

Hanford Observatory - Livingston Observatory

The Hanford Observatory and the Livingston Observatory are organized as separate functional groups within the LIGO Laboratory. Each is responsible for the effective operation of the facilities and scientific programs at the respective Observatory site. Each Observatory is led by a scientist who serves as the Head of the Observatory. In addition, each group includes a Site Manager who is responsible for the technical and operational effectiveness of the site facilities and staff. The Site Manager serves as the lead Environment, Safety and Health Officer for the Observatory site, reporting to the Head. The staff at each Observatory is structured to support operations, maintenance and the scientific program. The staff is sufficient to assure adequate local human resources for all normal operations including scientific and technical expertise at the site. Each Observatory will work with LIGO staff from the Caltech and MIT groups in executing enhancements, upgrades and new capabilities and in carrying out the scientific program.

Administration

The Administration Group is responsible for program planning support, for all business operations including budgeting, funds management, cost accounting, procurement, property management, personnel actions and effort reporting, for document and records management, for environment, safety and health programs, and for management of Laboratory Policies and Procedures. The Administration Group prepares Laboratory Proposals to the NSF and coordinates all formal communications with the NSF through the Caltech Office of Sponsored Research. The Administration Group provides administrative assistant and secretarial support to the LIGO Laboratory.

Technical and Engineering Support

The Technical and Engineering Support Group is responsible for all engineering design and analysis and design drafting for LIGO scientific programs, facilities, research and development tasks. Members of this group team with LIGO staff and collaborators to support all activities requiring mechanical, optical and electrical engineering. Configuration management, quality assurance and technical standards are provided by this group.

Detector Support

The Detector Support Group is responsible for assuring and improving the performance of the LIGO detector systems used in gravitational wave research. The group supports detector operations and data collection at the Observatory sites, conducts detector research and development with the goal of improving detector system performance and sensitivity, and provides scientific leadership in specifying and introducing detector improvements and upgrades, in association with the staff at the Observatory sites.

Data Analysis and Computing

The Data Analysis and Computing Group is responsible for the hardware and software systems for LIGO modeling and simulation and for data analysis. The primary responsibility for all software standards and software engineering used in LIGO research is carried by this group. Systems for

general computing are implemented and supported in this group.

Research Facilities

Test and research facilities at the universities and Observatory sites not normally used for gravitational wave research are managed by the Research Facilities Group. These include test interferometers at the campuses, as well as special setups used for optics, laser and noise research, metrology and materials research. The group is responsible for the readiness and availability of the research facilities, and for supporting the research and test activities carried out by LIGO Laboratory and collaborator investigators using these facilities. This includes calibration, procedures documentation and training of investigators.

Advanced Research and Development

The Advanced Research and Development Group leads the execution of the R&D program to define future LIGO detector upgrades and to new detectors. The program of this group is primarily supported by NSF Advanced R&D funding which is distinct from Laboratory Operations funding.

Environment, Safety and Health Protection

ES&H is a line management responsibility. The LIGO Laboratory Deputy Director is primarily responsible for ES&H programs throughout LIGO. At each Observatory site, the Site Manager serves as the primary manager responsible for ES&H programs.

Objectives

The LIGO ES&H program has the following specific objectives:

- to prevent personnel injury or loss of life;
- to prevent any environmental contamination;
- to prevent damage to equipment caused by accidents;
- to comply with all federal, state and local laws, rules and regulations.

Responsibilities

The LIGO ES&H program is the responsibility of the Deputy Director. The Deputy Director has responsibility to insure that LIGO staff members and collaborators identify specific ES&H issues and risks, and establish appropriate safeguards and procedures for addressing those risks.

Environmental Protection

The LIGO Laboratory shall follow standards and practices which fully support the NSF environmental protection policies and requirements. The Laboratory will initiate activities necessary to ensure compliance with the Resource Conservation and Recovery Act (RCRA) and the National Environmental Policy Act (NEPA).

Safety and Health Protection

Caltech has an established Safety Office, responsible for the Institute's overall safety and health program, and LIGO management will implement the applicable health and safety program elements as outlined in the Caltech Safety Manual. The Caltech Safety Office policies will be applicable to the Observatory sites, supplemented by additional policies developed by LIGO staff in consultation with the Caltech Safety Office. For work performed at MIT, the safety and health protection measures adopted by MIT will similarly apply.

An order of precedence for resolving safety issues has been adopted by the LIGO Laboratory. Order of precedence shall be as follows:

- **Design for Minimum Risk:** The primary means for mitigation of risk shall be to eliminate the hazard through design.
- **Incorporate Safety Devices:** Fixed, automatic or other protective devices shall be used in conjunction with the design features to attain an acceptable level of risk. Provisions shall be made for periodic functional checks as applicable.
- **Provide Warning Devices:** When neither design nor safety items can effectively eliminate or reduce hazards, devices shall be used to detect the condition, and to produce an adequate warning to alert personnel of a hazard. Devices may include audible or visual alarms, permanent signs or movable placards.
- **Procedures and Training:** Where it is impractical to substantially eliminate or reduce the hazard or where the condition of the hazard indicates additional emphasis, special operating procedures and training shall be used.

Employee Training

Laboratory employees will be provided with procedures, training and information to ensure their safety. Briefings and presentations will be made to managers and supervisors to communicate ES&H policies and procedures.

Contractors, Collaborators and Visitors

Contractors and visitors to the LIGO operational sites will be informed of ES&H rules and procedures applicable to the specific area. Hosts will be responsible for the safety of visitors.

Documentation

The LIGO Laboratory shall provide hazard assessments, safety analyses and evaluations as required. Specific procedures and training documents will be prepared and released.

Governmental Code Requirements

The LIGO Laboratory, including its contractors, will comply with applicable US Federal Codes, laws and regulations, industrial codes and state rules, regulations and codes. The Administration Group, together with the Deputy Director, will be responsible for clarifying compliance requirements and the resolution of safety issues.

Procurements and Subcontracts

Policy

LIGO procurements occur at both Caltech (including the Caltech-managed Observatory sites) and MIT. These are processed according to the procedures established by the Purchasing Department at the host institution and approved by the Office of Naval Research under OMB requirements.

All LIGO facilities and equipment procurements will be processed and administered by the Caltech or MIT Purchasing Department depending upon the institution originating the procurement, assisted by the LIGO Laboratory staff.

Major procurements involving substantive efforts (subcontracts valued in excess of \$100,000) will be submitted to NSF for approval or concurrence, in accordance with the Cooperative Agreement. Subcontract technical and programmatic management is performed by LIGO Laboratory staff. All procurements and subcontracts will be subject to the terms and conditions of the Cooperative Agreement and the requirements of land sale and lease documents pertaining to the LIGO Observatory sites.

Responsibilities

The LIGO Deputy Director is responsible for ensuring that all aspects of LIGO facilities and equipment procurement are managed and planned successfully. A written acquisition plan will support the procurement approach for major procurements in excess of \$500,000. The Deputy Director, in association with the Director, shall approve all major subcontracts. Procurement for the LIGO Laboratory is supported by the Administration Group which is responsible for preparing, facilitating and administering the procurement documentation associated with major LIGO procurements. Subcontracts and procurements will be initiated by the cognizant technical Task Leaders. Working closely with the Administration Group, the Task Leaders will be responsible that all procured components, items, services and construction are produced and delivered as required to support the LIGO Laboratory objectives. The Task Leaders will also provide technical direction and oversight of these contracts and procurements.

Approach

Procurement policies and procedures, embodied in the Caltech Purchasing Policy and Procedure Manual, will be utilized for all facilities and equipment procurement actions originating at Caltech. This manual establishes compliance with NSF and Federal Acquisition Regulations, and ensures the use of competitive procurement techniques and small disadvantaged business subcontracting to the maximum extent. All major procurements which require NSF concurrence will be identified and scheduled in the annual Work Plan. Similarly, LIGO Laboratory procurements originating at MIT may be placed using corresponding policies and procedures at MIT. Both Caltech and MIT have procurement systems approved by the Office of Naval Research under OMB requirements.

NSF Reporting and Reviews

Quarterly Reports

Three LIGO Laboratory Quarterly Reports will be prepared and submitted to NSF annually for the first three quarters of each fiscal year. This report is prepared in accordance with the Cooperative Agreement and shall consist of a summary of work accomplished during the reporting period including major scientific and technical accomplishments, and a status of action items affecting LIGO/NSF responsibilities. This report shall also include management information such as changes to personnel, financial status report and other financial information including actual or anticipated underruns or overruns, and any other action requiring NSF or other Federal Agency notification.

Annual Report

An Annual Report will be prepared and submitted to NSF, in lieu of a fourth Quarterly Report, containing a summary of overall progress, including results to date, and a comparison of actual accomplishments with the proposed goals of the period; indication of any current problems or favorable or unusual developments; and a summary of work to be performed during the succeeding year; and any other pertinent information.

Annual Work Plan

Each year, through the Caltech Office of Sponsored Research, the LIGO Laboratory shall negotiate and submit an annual Work Plan and funding request to the NSF on October 1 for the December 1 annual award date. This Plan shall discuss scientific and program achievements and compare achievements with the projected goals in the currently approved Work Plan. It will summarize the proposed goals for construction, R&D, science and collaborative programs for the program year for which funds are sought. Significant staffing changes, and an organization chart and description of the LIGO organization in the new program year will be presented, together with an explanation of any changes. The Plan shall include a statement of the LIGO annual calendar including proposed dates for meetings of the LIGO Oversight Committee, Program Advisory Committee, scientific workshops and reviews. The Plan shall include an acquisition plan for all procurements in excess of \$100K, including the proposed date of submission to NSF and the type of procurement.

Other Reporting

The Caltech Office of Federal Financial Activities submits to NSF a quarterly reconciliation report against the Letter of Credit covering all NSF sponsored grants at Caltech, including LIGO. This report identifies the incurred expenditures for the quarter, cumulative expenditures effective at the close of the quarter, and the available balance against the allocation for the LIGO Laboratory.

Caltech will submit for approval by NSF all collaborative Memoranda of Understanding.

LIGO Oversight Committee

The LIGO Oversight Committee will hold regular meetings to review progress and to resolve institutional issues. Special meetings may be held to resolve particular issues which must be resolved before the next scheduled meeting.

LIGO Program Advisory Committee

NSF shall be informed of all meetings of the PAC, invited to attend, and shall receive copies of relevant reports. The charge and membership of this Committee will require the concurrence of the NSF Program Manager.

NSF Site Visits/Visiting Committee

The NSF may conduct periodic site visits to review LIGO activities.

The NSF may convene a Visiting Committee to conduct periodic reviews of the LIGO Laboratory, covering technical and management issues. NSF shall provide the Laboratory with a copy of the charge to the Visiting Committee prior to the review, with adequate time to agree on the agenda and to prepare the necessary presentation material.

Workshops

The LIGO Laboratory will sponsor or participate in workshops on specific topics relevant to the development of gravitational-wave interferometers. The frequency of such workshops and the topics they address will be determined in consultation with interested outside scientists, such as LIGO Research Community, the LIGO Scientific Collaboration and the other international groups pursuing laser interferometer gravitational-wave detection.

Technical Reports

To enhance the participation of the general scientific community in gravitational wave research, the LIGO project will continue the publication of research results in refereed journals, and will make unpublished internal technical reports available to the general scientific community on request. A written LIGO Publication Policy will govern this process.

Last modified on March 6, 1997

Please send comments on this draft to Gary Sanders at sanders@ligo.caltech.edu

•



LIGO Scientific Collaboration Formation Plan

LIGO-M970022-02-M DRAFT 2

B. Barish / G. Sanders

March, 1997

Introduction

LIGO construction is proceeding and is presently about 40% complete. The construction project is scheduled to be completed in 1999, at which time a commissioning program will begin. We plan to complete the commissioning, associated engineering tests, and sensitivity studies by the end of 2001.

The first science run (LIGO I) with the initial detectors at design sensitivity ($h \sim 10^{-21}$) is planned to begin in 2002. We propose that the LIGO I run be planned and scheduled for two years of calendar time, to begin once design sensitivity is reached. This will enable a serious search (~ 1 year live time) for binary neutron inspirals (our benchmark design source), and will include an allowance for instrument studies, downtime, etc.

Although this is a notable and exciting milestone, reaching far beyond present or anticipated searches for gravitational waves, the detection of neutron binary inspiral events is likely to require even better sensitivity. The best estimate for the number of such sources corresponds to an event rate in LIGO of a few detections per year at $h \sim 10^{-22}$ (note that the improvement of 10 for sensitivity corresponds to a factor of 10^3 in rate), and conservative estimates require even greater sensitivity. Thus, for detection or for increased event rate, it is crucial that LIGO be able to achieve such sensitivities. This goal has been an integral part of the planning and design philosophy, since the project was first proposed to the NSF.

This has resulted in an approach toward the LIGO design which requires that the constructed facilities (e.g. vacuum, external noise, etc.) will not limit the interferometry, even at levels of sensitivity of the most advanced detectors anticipated. In addition, a conservative plan for the initial detectors has been adopted that is based, as much as is possible, only on technologies that the R&D program has demonstrated; and as much flexibility as possible is being incorporated into the design, in order to anticipate implementation of improved detectors.

Improvements to the sensitivity will be possible both by making incremental enhancements to various subsystems, or by the installation of new "advanced" interferometers. Although the LIGO design anticipates such an evolution to the instruments, the most crucial element in developing these improvements will be a vigorous advanced R&D program to carry out the challenging developmental

work.

As the initial detector design is finalized and construction begins, the supporting R&D for the construction project is beginning to wind down. We propose to continue our R&D effort, but direct it more toward future enhancements and detectors that promise to lead to improved sensitivity. We are developing this program in a fully collaborative mode. A proposal for this advanced R&D by LIGO, along with a set of complementary or collaborative proposals by outside groups, has been submitted to the NSF.

To provide structure and organization for this program, to set priorities, and to enable collaborating groups to participate effectively, we propose to initiate a formal LIGO Scientific Collaboration. This Collaboration will include organized "development groups" involved in LIGO I and in advanced systems development and, thereby, future participation in LIGO science.

Following the initial LIGO I data run, it will be possible and desirable to implement major subsystem enhancements and/or the installation of advanced interferometers. Implementation of advanced subsystems, interferometer tests, and continued science data running will be interleaved, so as to optimize the overall LIGO program. Those participating in these developments will join with continuing LIGO I groups for future data taking and science.

At present, development groups are being formed both for LIGO I, and for the development of advanced subsystems and detectors. These development groups are defined through Memoranda of Understanding (MOUs) with the LIGO management. It is now prudent to form an overall LIGO Scientific Collaboration to organize and coordinate all of these efforts. This document outlines our thoughts and plans to form this Collaboration. It has evolved from our initial draft, following feedback from the LIGO PAC and the community present at the 1997 Aspen Winter Workshop. We are soliciting additional comment by posting this document on the LIGO Web site.

Organizational Issues

The LIGO construction project is organized with a task oriented structure, which is optimized to carry out and meet the milestones, costs, and schedules of LIGO construction. This organization will be replaced with an operational LIGO Laboratory organization (more typical of a research laboratory) as the construction comes to completion. In fact, we plan to create this new Laboratory organization now, in order to operate the LIGO sites as they come into operation, the R&D facilities on campus after they complete their tasks for design of the construction project, and for organizing the creation of computer systems, software and analysis for LIGO.

We define the new organization as the LIGO Laboratory, consisting of the activities supported under LIGO Operations and Advanced R&D support from the NSF. This includes administration of the LIGO detector facilities and the support and test facilities at Caltech, MIT, Hanford and Livingston. The LIGO Laboratory, in its initial phase (through 2001), is to be administered by Caltech and MIT through a Directorate and Groups responsible for the Detector, for Computing/ Analysis, Site Operations, Test Facilities, Engineering Support, etc.

The LIGO Scientific Collaboration will be organized as a separate organization from the LIGO Laboratory. It will include scientists from the LIGO Laboratory, and those from collaborating

institutions, and will have its own leadership and governance. The Collaboration will insure equal scientific opportunity for individual participants and institutions. It will organize the research, publications, and all other scientific activities. The Collaboration will report to the Laboratory Directorate for final approval of its research program, technical work, physics publications, and talks announcing new physics results. This will be done through regular reports to the Directorate and its PAC.

LIGO Scientific Collaboration

Technical and scientific research in LIGO will be organized through the LIGO Scientific Collaboration.

Proposal of Membership

Membership will be formally proposed to the Collaboration. The proposal will define the research and contributions of the group, commitments to the program, resources and competing commitments.

Charter Membership

We propose that an initial period for formation of the charter group of institutions in the LIGO Scientific Collaboration will commence on March 1, 1997 and will end following the first full meeting of the Collaboration at which the Collaboration Council will assume its role. We expect that this transition will occur within six months. Membership in the Collaboration during this charter period will be initiated by proposal to the LIGO Laboratory Directorate.

Following the charter period the proposal will be evaluated through the Collaboration Council. An MOU with the LIGO Laboratory, including Attachments defining specific work will be required for any participating institutions.

Collaboration Council

A representative body with proportionate representation will be the main governing body of the Collaboration. It will consist of representatives at a rate of 1 per multiple of 5 collaborators, with every institution having at least one representative. The representatives will be chosen by their institution and the Spokesperson will be the Chair of the Collaboration Council. The list of active collaborators will be defined in the institutional MOU with the LIGO Laboratory and will be updated every 6 months (in general, a collaborator is someone expected to be included as an author on publications resulting from the research). The chairs of each of the development groups will also be members of the Council regardless of institutional representation. The four LIGO Laboratory sites (Caltech, MIT, Hanford Observatory, Livingston Observatory) will be considered separate institutions on the Collaboration Council.

Collaboration Spokesperson

The Spokesperson will be elected and will serve a three year term. The Spokesperson must be

approved by the Laboratory Directorate, and will coordinate all the activities of the Collaboration and will represent it to the LIGO Laboratory and to the outside community. The Spokesperson's detailed roles and responsibilities will be defined in the Collaboration rules. (We propose that the initial Spokesperson be appointed by the LIGO Directorate, and subsequent Spokespersons be elected.)

Collaboration Deputy Spokesperson

The Spokesperson will choose a Deputy Spokesperson, with the approval of the Collaboration Council and the Laboratory Directorate.

Collaboration Governance

The rules for joining the Collaboration, commitments, guidelines for publishing, presenting at conferences, etc. will be set out by the Collaboration through the Collaboration Council.

Scientific Development Groups

LIGO I Development Group

The LIGO I Development Group will be the scientific collaboration for implementing and exploiting the initial LIGO detector and physics through the initial science data run. Only groups who establish a specific attachment approved by the LIGO Laboratory, which defines a sufficient contribution and participation in LIGO I development, implementation or data analysis will be part of this initial LIGO data run and science. Participation in future data runs and science that follow LIGO I will be possible for other groups, with guidelines to be determined by the LIGO Scientific Collaboration. It is anticipated that LIGO I data will only be made available through formal collaboration within the LIGO I Development Group.

The general guideline for institutional membership in the LIGO I Development Group is that the contribution per collaborator of any new group to the design, construction, and implementation of the initial LIGO detector and to the first data run be comparable to that of the LIGO Laboratory scientists.

Isolation/Suspension/Thermal Noise Development Group

The Isolation/Suspension/Thermal Noise Development Group will be the scientific collaboration for defining and developing future isolation and suspension improvements for use in advanced subsystems for the initial LIGO interferometers or in entirely new advanced interferometers. A specific Attachment will define the roles and responsibilities of groups in this development group. Members of this group will normally be authors on publications reporting the work of the group and will normally be eligible to participate in data runs and science beyond the LIGO I data run.

Lasers/Optics Development Group

The Lasers/Optics Development Group will be the scientific collaboration for defining and developing future high power lasers and required improvements in optics for use in advanced subsystems for the initial LIGO interferometers or in entirely new advanced interferometers. A

specific Attachment will define the roles and responsibilities of groups in this development group. Members of this group will normally be authors on publications reporting the work of the group and will normally be eligible to participate in data runs and science beyond the LIGO I data run.

Advanced Detector Configurations Development Group

The Advanced Detector Configurations Development Group will be the scientific collaboration for defining and developing entirely new advanced interferometers. It is expected that this development group will pursue research in dual recycling, resonant sideband extraction, Sagnac interferometers, systems with non-transmitting optics and other advanced configurations. A specific Attachment will define the roles and responsibilities of groups in this development group. Members of this group will normally be authors on publications reporting the work of the group and will normally be eligible to participate in data runs and science beyond the LIGO I data run.

Other Development Groups

The Collaboration Council may initiate formation of additional Development Groups.

Last Modified: March 6, 1997

Please send comments to Gary Sanders at sanders@ligo.caltech.edu

-
-

Annual Report

(December 1995 through November 1996)

**The Construction, Operation, and Supporting Research
and Development of a Laser Interferometer Gravitational-
Wave Observatory (LIGO)**

NSF Cooperative Agreement No. PHY-9210038

January 1996

CALIFORNIA INSTITUTE OF TECHNOLOGY
MASSACHUSETTS INSTITUTE OF TECHNOLOGY

LIGO  **PROJECT**

Annual Report

(December 1995 through November 1996)

**The Construction, Operation, and Supporting Research
and Development of a Laser Interferometer Gravitational-
Wave Observatory (LIGO)**

NSF Cooperative Agreement No. PHY-9210038

January 1996

Table of Contents

1.0	Introduction.....	1
2.0	Executive Summary	3
2.1	Project Milestones.....	8
2.2	Integrated Schedule.....	9
2.3	Financial Status.....	11
2.4	Performance Status (Comparison to Project Baseline).....	11
2.5	Change Control and Contingency Analysis.....	16
2.6	Staffing.....	18
2.7	Project Organization	19
3.0	Vacuum Equipment (WBS 1.1.1).....	21
4.0	Beam Tube (WBS 1.1.2).....	26
5.0	Beam Tube Enclosure (WBS 1.1.3).....	30
6.0	Civil Construction (WBS 1.1.4)	32
7.0	Detector (WBS 1.2)	35
7.1	Suspensions and Isolation.....	35
7.2	Lasers and Optics.....	36
7.3	Interferometer Sensing/Control	37
7.4	Detector System Engineering/Integration.....	38
7.5	Control and Data Systems (CDS) Activities (WBS 1.2.2)	38
7.6	Physics Environment Monitor (WBS 1.2.3).....	39
7.7	Support Equipment (WBS 1.2.4).....	39
8.0	Research and Development (WBS 1.3)	40
9.0	LIGO Systems Engineering (WBS 1.4.3).....	45
9.1	Integration (WBS 1.4.3.1).....	45
9.2	Modeling and Simulation (WBS 1.4.3.3)	49
10.0	Support Services	56
10.1	Quality Assurance (WBS 1.4.2.1)	56
10.2	Environmental Safety and Health (WBS 1.4.2.2).....	57
11.0	References.....	60

List of Figures

FIGURE 1.	Summary Integrated Schedule	10
FIGURE 2.	Costs and Commitments as a function of time (end of November 1996)..	13
FIGURE 3.	Cost Schedule Status Report (CSSR) for the end of November 1996.....	14
FIGURE 4.	LIGO Project Budget, Earned Value, and Actual Costs as a function of time	15
FIGURE 5.	LIGO staffing history since January 1995	18
FIGURE 6.	LIGO Project Construction Phase Organization.....	20
FIGURE 7.	Prototype Beam Splitter Chamber.	21
FIGURE 8.	Insulated Beam Splitter Chamber.	22
FIGURE 9.	Short 80K pump.	22
FIGURE 10.	80K pump being inserted into the BSC.	23
FIGURE 11.	Vibration tests of the 80K pump.....	23
FIGURE 12.	The first gate valve being installed at the Hanford site.	24
FIGURE 13.	Horizontal Access Module vessel at PSI manufacturing facility.	24
FIGURE 14.	Baffles in field clean room awaiting installation.	28
FIGURE 15.	Tube section shipment	29
FIGURE 16.	Special field enclosures for tube section installation.....	30
FIGURE 17.	Inside the weld enclosure during fit-up	30
FIGURE 18.	Installation of the Beam Tube Enclosures	32
FIGURE 19.	Aerial View of Construction in Hanford, Washington	35
FIGURE 20.	The End-Station on the Southwest Arm at Hanford	35
FIGURE 21.	PNI Performance Improvements in the Recycled Configuration	45
FIGURE 22.	Residual errors from initial slab-flatness survey. Measurements made every 20m. Deviations are relative to design plane.	51
FIGURE 23.	Thermal noise of internal modes	54
FIGURE 24.	40 m displacement sensitivity.....	55
FIGURE 25.	Latest estimate for noise in the initial LIGO	57

List of Tables

TABLE 1.	Status of Significant Facility Milestones	8
TABLE 2.	Status of Significant Detector Milestones	9
TABLE 3.	Costs and Commitments as of the end of November 1996.....	12
TABLE 4.	Approved Change Requests.....	16

Annual Report

(December 1995 - November 1996)

THE CONSTRUCTION, OPERATION, AND SUPPORTING RESEARCH AND DEVELOPMENT OF A LASER INTERFEROMETER GRAVITATIONAL- WAVE OBSERVATORY (LIGO)

NSF COOPERATIVE AGREEMENT No. PHY-9210038

January 1997

CALIFORNIA INSTITUTE OF TECHNOLOGY

This Annual Report is submitted under NSF Cooperative Agreement PHY-9210038¹. The report summarizes Laser Interferometer Gravitational-Wave Observatory (LIGO) Project activities from December 1, 1995 through November 30, 1996.

1.0 Introduction

The Laser Interferometer Gravitational-Wave Observatory (LIGO) Project will open the field of gravitational-wave astrophysics through the direct detection of gravitational waves. LIGO detectors will use laser interferometry to measure the distortions of the space between free masses induced by passing gravitational waves. The design, construction, and operation of LIGO are being carried out by scientists, engineers, and staff at the California Institute of Technology (Caltech) and the Massachusetts Institute of Technology (MIT). Caltech has prime responsibility for the project under the terms of the Cooperative Agreement¹ with the National Science Foundation (NSF). LIGO will become a national facility for gravitational-wave research, providing opportunities for the broader scientific community to participate in detector development, observations and data analysis. LIGO welcomes the participation of outside scientists at any of these levels. The initial LIGO facility will comprise one three-interferometer detector system. The site allows for expansion of the facility to a multiple-detector configuration to enable simultaneous use by several gravitational-wave detectors.

The LIGO Project was described in the LIGO Proposal² submitted to NSF in December 1989, and the Technical Supplement³ submitted to NSF in May 1993. Project organization is described in the LIGO Project Management Plan⁴. The cost of the construction activities for the observatory facilities and the initial detector equipment was presented in the LIGO Cost Book⁵, which was reviewed in September, 1994.

This annual report covers activities accomplished during the fifth year (LIGO fiscal year 1996) and planned during the sixth year (LIGO fiscal year 1997) of the Design and Construction Phase of the LIGO Project, and the related Research and Development. This phase includes facility construction, support equipment acquisition, initial interferometer design and fabrication, and the concurrent research to refine the initial detectors and data algorithms. LIGO Design/Construction began December 1, 1991 as defined in the Cooperative Agreement and will end with the acceptance of the vacuum systems at both sites and completion of the fabrication of the third interferometer.

All planning and budgeting is based on a LIGO Fiscal Year (FY) starting on 1 December and ending on 30 November.

2.0 Executive Summary

The project continues to make excellent progress. The project is 40 percent complete. The rate of accomplishment, as measured by our Performance Measurement tracking systems, has accelerated to reflect the effort in active subcontracts with a total contract value in excess of \$120 million.

Contracts or bids are in hand for all major facility items, and all are within the estimated cost envelope. The bids for the Civil Construction, Beam Tube Enclosure, and Beam Tube Enclosure Installation at Livingston, Louisiana were opened mid-October and were very close to the LIGO cost estimate. The sites at Hanford, Washington and Livingston, Louisiana both include space for an additional interferometer.

The Phase Noise Interferometer at MIT has achieved "world's best" measurements of phase noise. The first significant pieces for the Detector (core optics blanks) have been ordered.

The LIGO Program Advisory Committee (PAC) is being formed with the first meeting scheduled early in January 1997.

A proposal for the Advanced R&D to begin in FY 1997 has been submitted to the NSF.

LIGO staff have begun to relocate to the Hanford site. Otto Matherly, Washington Site Construction Manager, relocated to Hanford during the second quarter. During the third quarter he was joined by John Worden, Cecil Franklin, and Richard Riesen, who will oversee installation of the Beam Tube and Vacuum Systems. In addition, two members of the LIGO team, Alan Sibley and Gerry Stapfer, are in process of relocating to Livingston, Louisiana.

Vacuum Equipment. The contract for the Vacuum Equipment was issued to Process Systems International (PSI) in Massachusetts in September 1995. PSI finalized the Beam Splitter Chamber (BSC) design in December 1995 and initiated the procurement of stainless steel materials and long lead components. PSI hosted a Final Design Review (FDR) in May.

A prototype BSC has now been fabricated, cleaned and tested for leaks. This chamber has been 'baked' to remove potential residual contaminants. The process of baking also provided an opportunity to evaluate the heater blankets and control system which will be used to bake all of the large vacuum vessels. The BSC and the bake equipment both appear to be working well. Evaluation of the ultra-high vacuum (UHV) cleaning process will follow. The first large ion pump has been delivered to PSI for testing. The Horizontal Access Modules (HAMs) and the first six Beam Splitter Chambers (BSCs) are being fabricated.

Vacuum Equipment deliverables required to support the Beam Tube contract are being delivered to the site. Four main turbopump carts, two auxiliary turbo carts, and two main roughing pump carts have been delivered and inspected. The first four large gate valves have been received in Washington and two of the valves have been installed on the beam

tube enclosure slab to terminate the beam tube modules currently being installed. A prototype large ion pump has also been delivered.

Beam Tube. The \$39.5 million contract for fabricating and installing the Beam Tube was issued to Chicago Bridge and Iron (CB&I) in December 1995. The Final Design Review for the Beam Tube was successfully completed in March, 1996. The spiral mill was shipped from Pacific Roller Die (PRD) and received at the Chicago Bridge and Iron (CB&I) Big Pasco facility on July 8. The spiral mill has been commissioned and virtually all of the equipment in the factory is now operational. A successful Fabrication Readiness Review was held on September 18 at the Big Pasco facility, and an Installation Readiness Review was concluded on October 17. One hundred sixty production Beam Tube sections, each 20 meters long, have been welded. One hundred thirty-three have passed the leak tests with no failures. This represents over eight miles of weld. Fifty beam tubes have been cleaned.

Beam Tube Installation. Weld enclosures and air filtration systems have been delivered to the site. The terminating gate valves at the mid-station have been installed. A high precision site survey has been completed to provide reference locations for beam tube installation. Twenty-nine tubes have been installed on the site. Twenty-seven girth welds have been leak tested with no failures.

Beam Tube Baffles. A total of 300 baffles have been fabricated by Capital Industries, shipped to West Coast Porcelain to be coated, cleaned at the Jet Propulsion Laboratory (JPL), and shipped to Hanford during September and October. This is more than sufficient to cover the installation of the first arm of the Beam Tube.

Beam Tube Enclosure. ACME, the Beam Tube Enclosure (BTE) contractor, completed the concrete slabs for both arms at Hanford early in June. Acme has also fabricated approximately 2000 (of 2600 needed) of the precast BTE sections. The enclosure sections are fabricated five miles from the site and are transported to the site for installation as needed. Each weighs nine tons. The installation contract was awarded to Levernier Construction, Incorporated, in September 1996. Approximately 150 enclosures have been installed. The installation contractor works approximately three to five sections behind CB&I on site to avoid interference.

Civil Construction. The bid package for building construction at Hanford (three-interferometer version) was issued, and the bids were opened on June 18. The contract for the construction of the buildings at Hanford was awarded to Levernier Construction, Incorporated, on July 17, 1996. Excavation of the area for the corner station is complete, and the concrete slabs for the mid- and end-stations have been poured.

Parsons completed the bid package for the Beam Tube Enclosure, site work, and precast fabrication of the enclosure segments for the Livingston, LA site during the third quarter. Parsons also completed the bid package for the buildings at Livingston. The designs have been reviewed by a Baton Rouge architectural firm for standard practices and materials, and recommendations have been incorporated into the final design. Architectural approval was obtained from LSU per the site agreement. The bids were opened on October 15,

1996, and contracts were awarded during December 1996. Construction is scheduled to begin in January 1997.

The building planned for the Livingston, Louisiana site will house two interferometers. This configuration preserves the opportunity for one additional interferometer at each site (one complete new detector).

Livingston Rough Grading. The Livingston, Louisiana rough grading task is complete. Approximately 180 work days were lost due to inclement weather and wet soil conditions. The delay has not affected building construction since the grading of the berms to full height was completed in July, and measurements indicate that there has been adequate settling time to allow the beginning of construction in January 1997.

Detector. At the end of FY 1995, LIGO decided to change the baseline laser for the initial interferometers from Argon lasers operating at 515 nm to solid state lasers operating in the near infrared. After careful study of alternative laser strategies, it was concluded that Nd:YAG lasers have reached performance levels, in particular, power and reliability, that makes them suitable for the initial detectors, and that the change will permit us to capitalize on probable future improvements. The change to a longer wavelength has been incorporated into the optics design.

The award of a contract in May to Lightwave Electronics for the development and production of the LIGO 10 W laser represented an important step in the implementation of the solid-state lasers.

Polished substrates have been delivered by the Commonwealth Scientific and Industrial Research Organization (CSIRO) and Hughes-Danbury as a part of the 'Pathfinder' process to develop interferometer test mass optics. The National Institute of Standards and Technology (NIST) has completed all large aperture (15-centimeter diameter) absolute phase-map measurements of the Pathfinder surfaces provided to them. Agreement with the results provided by the polishing vendors is good. The surfaces of some of these optics significantly exceeded very tight LIGO requirements.

Bids have been received for the mirror blanks, and contracts have been awarded to Corning Glass and to Heraeus Amerisil for the different types of material. A total of nearly one-half ton of fused silica has been ordered. Proposals for polishing the Optics were also evaluated, and contracts have been awarded to General Optics (California) and CSIRO (Australia).

A review of the HYTEC, Incorporated, design effort on the Seismic Stack was conducted at Caltech in June 1996. The follow-on contract for design and fabrication of prototypes has been awarded.

Research and Development. Research and Development accomplishments centered on the 40m and 5m interferometers. The Recombination/Recycling of the 40m interferometer continued with an improved understanding of locking the system and integrating the LIGO prototype control hardware and software. There was progress in the development of

techniques for achieving the very high availability planned for LIGO, accomplished by implementing a plan for scheduling and monitoring the 40m interferometer.

The Phase Noise Interferometer at MIT has been converted to a recycled configuration. A wavefront sensor was installed on the output of the interferometer to improve alignment. The total power in the recycling cavity was approximately 90 W. A phase noise sensitivity of roughly 3×10^{-10} rad/ $\sqrt{\text{Hz}}$ has been achieved, in good agreement with calculations. This very encouraging result is, to our knowledge, the highest phase sensitivity measured in any interferometer to date.

Reviews. A semi-annual review of LIGO was conducted by a review committee of experts on behalf of NSF on April 9-11, 1996 at Caltech. The focus of this review was on the cost, schedule, and management aspects of the LIGO Construction Project and the supporting R&D. In preparation for the review, LIGO completed a "replanning" exercise, that incorporated the scheduling information available from major facilities contractors. The new baseline was used to prepare the performance measurement data in Section 2.4 on page 11.

A second meeting of the Pre-Program Advisory Committee was held at MIT in March 1996. The committee having completed its function then self-annihilated. The committee recommended:

- elimination of the External Advisory Committee (this function is to be performed by the Program Advisory Committee),
- expansion of the charter of the Program Advisory Committee,
- how the Program Advisory Committee should start and function,
- membership of the Program Advisory Committee and recommended that the PAC should start by the Fall of 1996.

A second semi-annual review of LIGO was conducted on behalf of NSF on October 22-24, 1996 at Caltech. The focus of this review was on technical progress and plans. Comments received from the committee were favorable. The next semi-annual review, which will also focus on the technical status of the project, is scheduled for April 15-17, 1997.

Aspen Winter Conference. The Aspen Winter Conference on Gravitational Waves and their Detection was held during the week of January 14-20, 1996. This was a very successful meeting. In addition to the many interesting technical presentations, the first meeting of the LIGO Research Community and of its Executive Committee took place. An informal meeting between members of LIGO and VIRGO resulted in a proposed set of near term collaborative actions related to vacuum compatibility testing, optics, thermal noise, beam tube, baffles and data formatting. The next Aspen Winter Conference is scheduled for the week of January 27, 1997.

Visitor's Program. An active visitors program is being developed, roughly equivalent to three full-time equivalents (FTEs) each year (more during later years) with the participants involved in research for periods of six months or longer. Professor Kris Sliwa of

Tufts University completed a 'sabbatical year' at MIT. Dr. Sliwa performed experimental studies of the optical phase noise for the first stage LIGO interferometer and modeled the optical transfer functions of an advanced interferometer using dual recycling.

Dr. Bruce Allen, University of Wisconsin at Milwaukee, has started a one year program at Caltech. Dr. Allen is studying mechanisms by which a stochastic background of gravitational radiation could be produced, and means by which data from the LIGO observatories could be used to detect such a background. He is developing a data-analysis pipeline to use for such analysis.

LIGO Collaboration. Active collaborations are being sought with Stanford and the University of Florida. Stanford can provide good technical input especially in the domain of lasers. The collaboration with the University of Florida has already started. Professor Douglas Tanner and Professor David Reitze visited Caltech to initiate the development of the Input-Output Optics (IOO).

In June 1996 the National Science Foundation convened a Panel to formulate recommendations concerning the future development of the LIGO Project and the relationship between the project and the scientific community. The Panel report⁹ recommends a process for incorporating the outside research community into effective collaboration with the scientific staff of the Laboratory and for making the transition into an organization with two entities: the first is the Laboratory proper, which is responsible for the construction and commissioning of the LIGO facilities and which provides the normal infrastructure and service functions; the second comprises the associated experimental groups or "Collaborations." A broader effort has been initiated to carry out the advanced research and development in the spirit of the recommendation of the Panel. An Advanced R&D Proposal has been submitted to NSF. Collaborators who have contributed in addition to Stanford and the University of Florida include Syracuse University, Eastern Michigan University, JILA, VIRGO, the University of Western Australia, GEO, and Moscow State University.

2.1 Project Milestones

The status of the significant milestones identified in the Project Management Plan (PMP) for the LIGO Facilities is summarized in Table 1. The milestone dates projected in this table have been updated to reflect delivery dates negotiated with Vacuum Equipment, Beam Tube, and Beam Tube Enclosure subcontractors as well as the efforts to integrate these schedules with the plans for constructing the buildings. The projected milestone dates were presented in detail during the NSF review in April and in Revision B to the Project Management Plan submitted to NSF on April 24, 1996.

TABLE 1. Status of Significant Facility Milestones

Milestone Description	Project Management Plan Date ^a		Actual (A)/Projected (P) Completion Date	
	Washington	Louisiana	Washington	Louisiana
Initiate Site Development	03/94	08/95	03/94 (A)	06/95 (A)
Beam Tube Final Design Review	04/94		04/94 (A)	
Select A/E Contractor	11/94		11/94 (A)	
Complete Beam Tube Qualification Test	02/95		04/95 (A)	
Select Vacuum Equipment Contractor	03/95		07/95 (A)	
Complete Performance Measurement Baseline	04/95		04/95 (A)	
Initiate Beam Tube Fabrication	10/95		12/95(A)	
Initiate Slab Construction	10/95	01/97	02/96 (A)	12/96 (P)
Initiate Building Construction	06/96	01/97	07/96 (A)	12/96 (P)
Accept Tubes and Covers	03/98	03/99	03/98 (P)	03/99 (P)
Joint Occupancy	09/97	03/98	09/97 (P)	03/98 (P)
Beneficial Occupancy	03/98	09/98	03/98 (P)	09/98 (P)
Accept Vacuum Equipment	03/98	09/98	03/98 (P)	09/98 (P)
Initiate Facility Shakedown	03/98	03/99	03/98 (P)	03/99 (P)

a. Project Management Plan, Revision B, LIGO-M950001-B-M approved by NSF in October 1996

Table 2 shows the status of the significant milestones for the Detector. This schedule was also presented in detail at the April NSF Review, and was included in the proposed revision to the Project Management Plan. The projected completion date for the *Core Optics Support Final Design Review* is now June 1997 (vs. April 1997). However, the current plan simplifies the subsequent fabrication effort so the overall schedule for installing the interferometers is not affected.

Note that as of the end of November 1996, all significant milestones can be achieved.

TABLE 2. Status of Significant Detector Milestones

Milestone Description	Project Management Plan Date		Actual (A)/Projected (P) Completion Date	
	Washington	Louisiana	Washington	Louisiana
BSC Stack Final Design Review	07/97		07/97 (P)	
Core Optics Support Final Design Review	04/97		06/97 (P)	
HAM Seismic Isolation Final Design Review	07/97		07/97 (P)	
Core Optics Components Final Design Review	07/97		07/97 (P)	
Detector System Preliminary Design Review	12/97		12/97 (P)	
I/O Optics Final Design Review	04/98		04/98 (P)	
Prestabilized Laser Final Design Review	08/98		08/98 (P)	
CDS Networking Systems Ready for Installation	09/97		09/97 (P)	
Alignment (Wavefront) Final Design Review	04/98		04/98 (P)	
CDS DAQ Final Design Review	04/98		04/98 (P)	
Length Sensing/Control Final Design Review	05/98		05/98 (P)	
Physics Environment Monitoring Final Design Review	06/98		06/98 (P)	
Initiate Interferometer Installation	07/98	01/99	07/98 (P)	01/99 (P)
Begin Coincidence Tests	12/00		12/00 (P)	

2.2 Integrated Schedule

A summary of the schedule for all construction and integration activities is shown in Figure 1, based upon data from the detailed schedules as of end of November 1996. The summary schedule displays major activities such as design (through Final Design Review), fabrication or construction, installation at the LIGO sites, and test and acceptance activities for each of the key LIGO systems at each LIGO site. The summary is intended to convey the temporal relationships between major activities, to provide a sense of overall context of the project. Hence, the summary displays current status and estimates-to-completion only; comparisons with baseline estimates are provided in Section 2.4 below.

The summary illustrates several important relationships between activities. Building construction at each site must achieve a minimum degree of completion before Vacuum Equipment installation can begin. Installation of the infrastructure for the Control and Data System can begin at that time also. Beam tube fabrication and installation at the

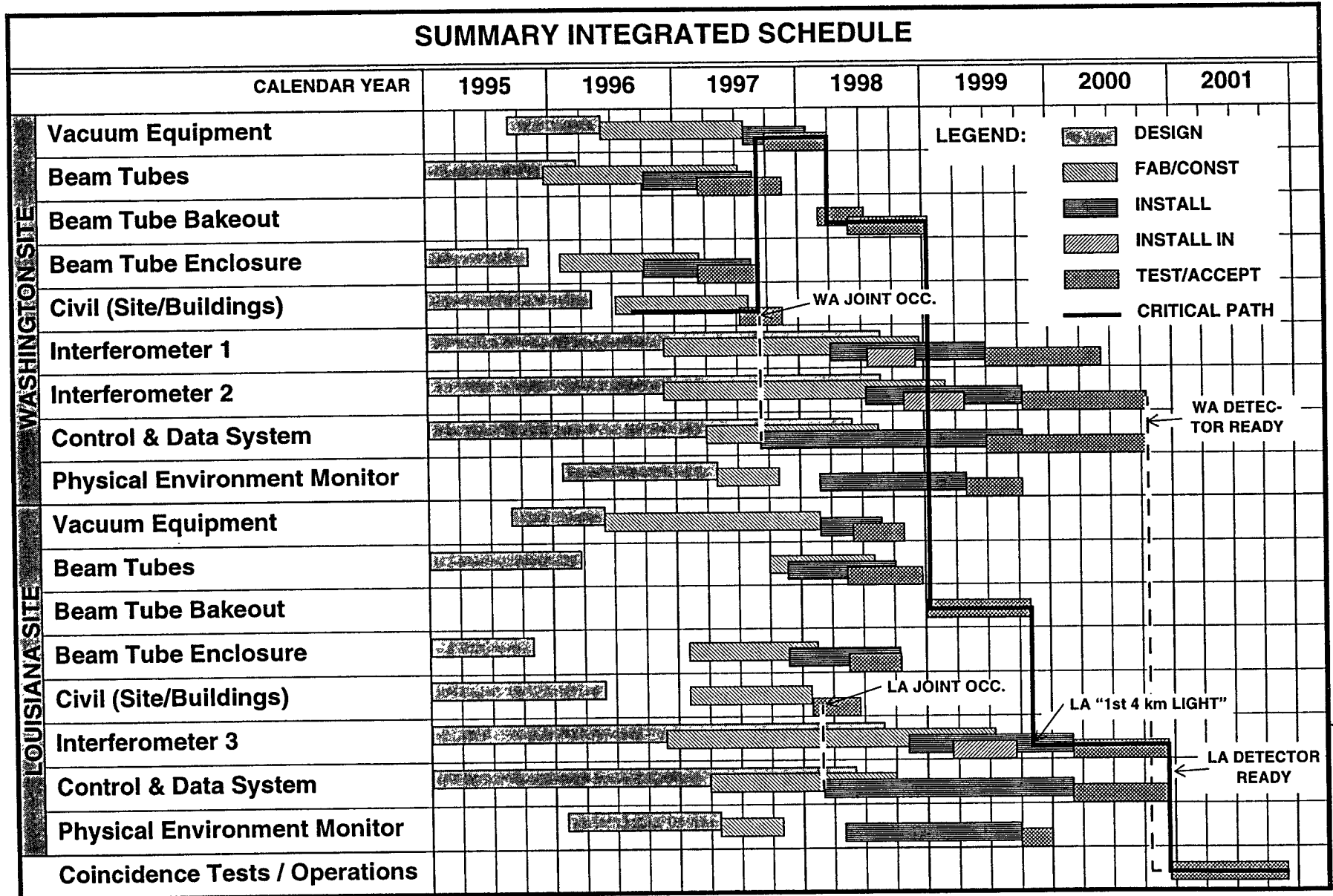


FIGURE 1. Summary Integrated Schedule

Louisiana site is sequentially connected to completion of the corresponding activities in Washington, since the equipment and personnel are shared. Interferometer installation can proceed after the Vacuum Equipment is accepted, but light beams cannot be propagated along the 4 km arms until the bakeout of the beam tubes is completed. (Note that light beams may be used prior to bakeout for alignment.)

The “critical path” (the path through the scheduled activities which connects the end of the project to the present with no gaps, and thus determines the completion date) is illustrated by the dark solid line. Building construction activities at the Washington site determine when the Vacuum Equipment can be installed, which in turn determines when the Beam Tube bakeout (shown as proposed in a recent and still-evolving plan) can proceed to completion. Bakeout at the Louisiana site will be completed just as the detector in Louisiana has reach the point in its installation that it needs to send light beams along the 4 km arms. However, the LIGO project schedule includes several significant near-critical paths, and it is fair to say that vigilance must be maintained in all of the key areas shown in the summary to complete the project on time.

2.3 Financial Status

Table 3 summarizes costs and commitments as of the end of November 1996. Figure 2 on page 13 shows the costs and commitments as a function of time.

2.4 Performance Status (Comparison to Project Baseline)

Figure 3 on page 14 is a Cost Schedule Status Report (CSSR) for the end of November. The CSSR shows the time-phased budget to date, the earned value, and the actual costs through the end of the month for the NSF reporting levels of the WBS. The schedule variance is equal to the difference between the budget-to-date and the earned value and represents a “dollar” measure of the ahead (positive) or behind (negative) schedule position. The cost variance is equal to the difference between the earned value and the actual costs. In this case a negative result indicates an overrun. Figure 4 shows the same information as a function of time for the LIGO Project.

There is an unfavorable schedule variance in the Beam Tube (WBS 1.1.2) as a result of early milestones missed for fabrication and installation. However, ‘learning curve’ improvements in rates are being observed, and LIGO is working with CB&I to develop recovery schedules.

Facility Design and Construction (WBS 1.1.4) was behind schedule at the end of October. Approximately 180 days had been lost due to inclement weather and wet soil conditions in the Livingston, LA rough grading task. However, this work was essentially complete by the end of November. Bids have been received for slab, beam tube enclosure, and building construction, the contracts will be issued in December 1996, and construction is expected to begin in January 1997.

TABLE 3. Costs and Commitments as of the end of November 1996

<i>WBS</i>	<i>Description</i>	<i>Costs Thru Nov 1995</i>	<i>First Quarter LFY 1996</i>	<i>Quarter LFY 1996</i>	<i>Quarter LFY 1996</i>	<i>Quarter LFY 1996</i>	<i>Cumulative Costs</i>	<i>Open Commitments</i>	<i>Total Cost Plus Commit- ments</i>
1.1.1	Vacuum Equipment	4,081	3,242	2,700	8,483	2,748	21,254	22,660	43,914
1.1.2	Beam Tube	2,736	1,620	1,942	3,260	7,704	17,262	36,516	53,778
1.1.3	Beam Tube Enclosure	468	25	1,422	2,477	1,846	6,237	4,197	10,433
1.1.4	Civil Construction	6,677	1,365	1,468	2,148	2,458	14,117	18,854	32,971
1.2	Detector	2,430	789	981	850	1,220	6,270	5,921	12,191
1.3	R&D	13,321	524	1,450	989	532	16,816	1,512	18,328
1.4	Project Management	10,152	1,355	1,911	1,279	1,592	16,288	1,708	17,996
	Unassigned (See Note)	79	(124)	-	1	-	(43)	125	82
TOTAL		39,943	8,795	11,874	19,487	18,101	98,201	91,492	189,693
Cumulative Actual Costs		39,943	48,738	60,613	80,100	98,201			
Open Commitments		44,993	89,934	86,515	88,814	91,492			
Total Costs Plus Commitments		84,936	138,672	147,128	168,914	189,693			
NSF Funding		138,089	149,889	167,089	208,468	208,468			

Note: These costs have not been assigned to specific LIGO Work Breakdown Structure element, but are continually reviewed to assure proper allocation.

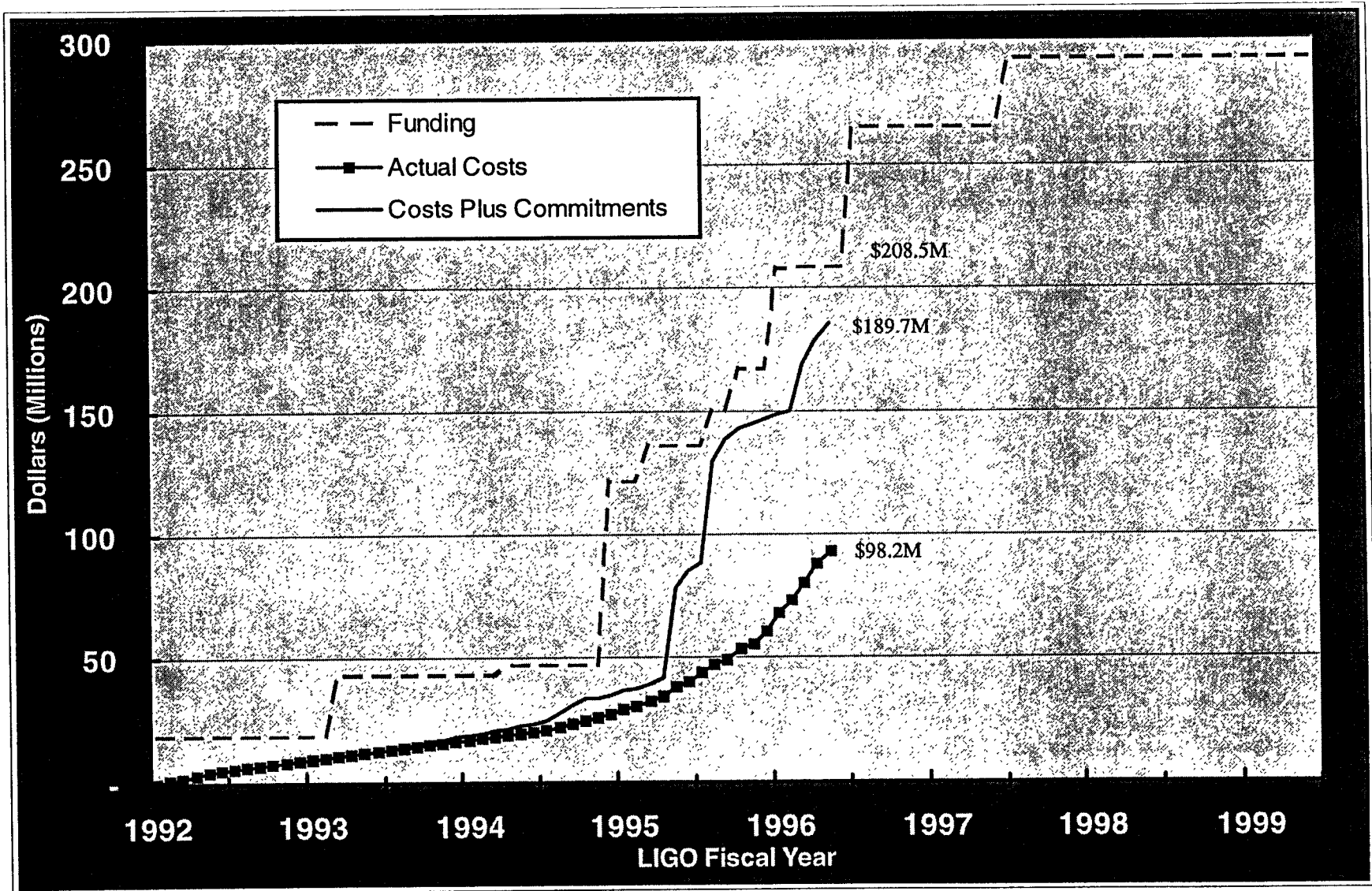












FIGURE 2. Costs and Commitments as a function of time (end of November 1996)

REPORTING LEVEL		CUMULATIVE TO DATE				AT COMPLETION		
MPR LEVEL	BUDGETED COST		ACTUAL COST	VARIANCE		BUDGET (BAC)	ESTIMATE (EAC)	VARIANCE (6-7)
	WORK SCHEDULED	WORK PERFORMED	WORK PERFORMED	SCHEDULE (2-1)	COST (2-3)			
	(1)	(2)	(3)	(4)	(5)	(6)	(7)	(8)
1.1.1 : Vacuum Equipment	22589	22272	21254	(317)	1018	42113	42113	0
1.1.2 : Beam Tubes	17882	16671	17262	(1211)	(591)	47298	47298	0
1.1.3 : Beam Tube Enclosur	6655	6639	6237	(15)	402	19384	19384	0
1.1.4 : Facility Design &	15769	16649	14117	879	2532	48311	48311	0
1.2 : Detector	8396	7486	6232	(910)	1254	52567	53336	(769)
1.3 : Research & Developme	17680	16840	16816	(839)	25	23490	23490	0
1.4 : Project Office	16397	16397	16288	0	109	27074	27074	0
SUBTOTAL	105368	102955	98205	(2414)	4749	260238	261007	(769)
CONTINGENCY						0	31087	(31087)
MANAGEMENT RESERVE						31855	0	31855
TOTAL	105368	102955	98205	(2414)	4749	292093	292094	(1)

COBRA (R) by WST Corp.

FIGURE 3. Cost Schedule Status Report (CSSR) for the end of November 1996

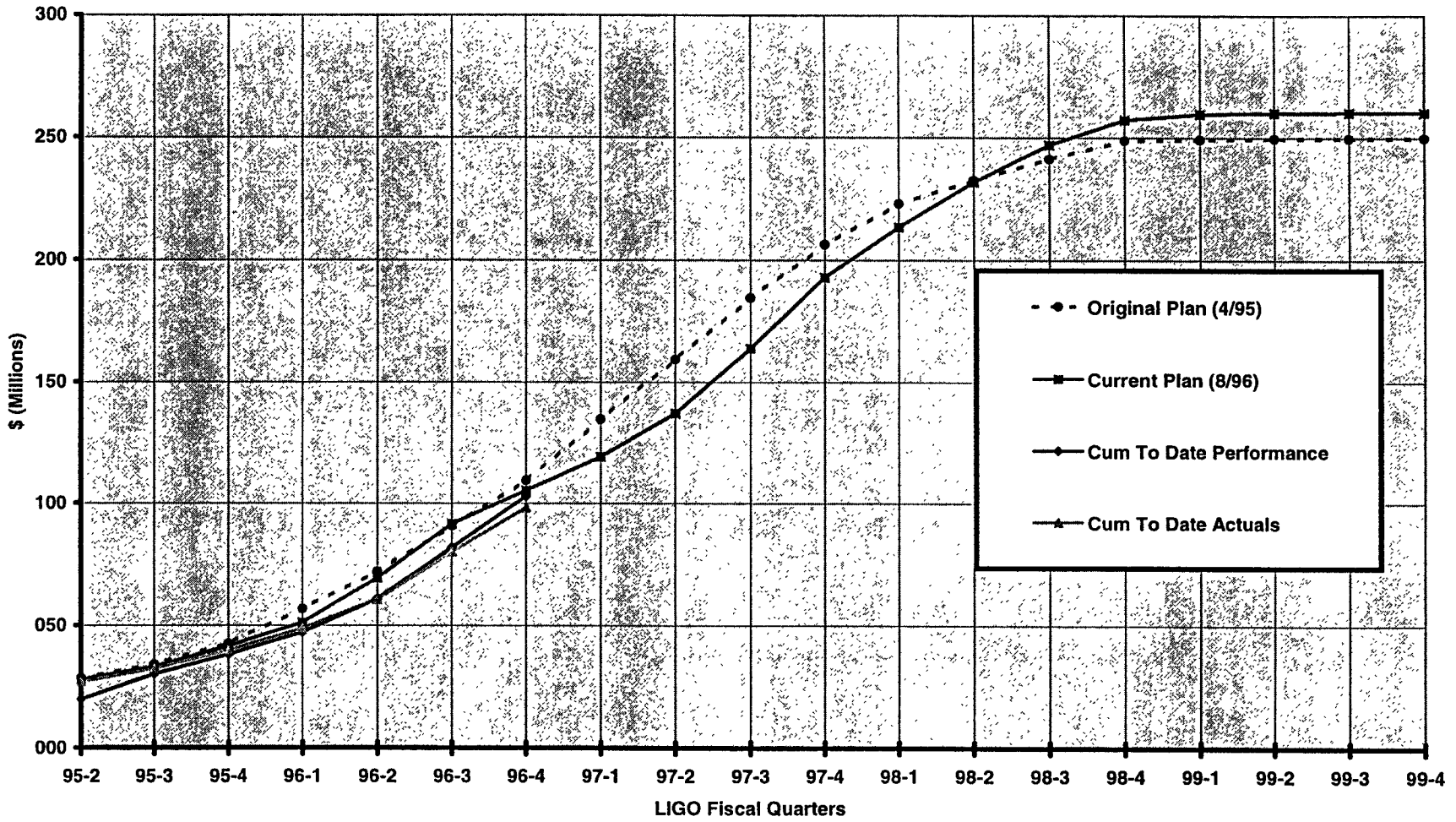


FIGURE 4. LIGO Project Budget, Earned Value, and Actual Costs as a function of time

There is a favorable cost variance in Facilities. This variance is primarily due to the delays in the processes of invoicing and payment and does not translate into a projected underrun at the end of the project. Efforts during FY 1996 to expedite payments have significantly reduced this effect.

The Detector (WBS 1.2) is slightly behind schedule. LIGO has been attempting to hire additional personnel, but this has not been accomplished quickly enough to avoid some delays in the Interferometer Sensing and Control effort, Vibration Isolation, and the Control and Data Systems. Priorities are being set to assure that all critical milestones will be met. Currently there is sufficient float in many of the tasks to avoid an impact on any major project milestones.

The R&D effort (WBS 1.1.3) is six months behind schedule relative to the plan that was presented in September 1994. However, progress has been steady over the last six months as more personnel have become involved. Primary behind-schedule tasks include the Phase Noise Research effort at MIT and the effort in the 40m facility for recombination and recycling.

2.5 Change Control and Contingency Analysis

The Change Requests (CRs) in Table 4 have been approved. These CRs allocated \$6.3 million from the contingency pool and added to the budget baseline that was used for preparing the end of November 1996 reports. The current contingency pool is \$31.9 million.

TABLE 4. Approved Change Requests

Change Request No.	Description	Date Approved	Allocated From/(To) Contingency
CR-950027	1.1.4 - Observation Deck above LVEA (Design Package)	December 1995	\$15,731
CR-950028	1.1.4 - Increase LVEA area at Hanford to accommodate three interferometers (Design Package)	December 1995	\$150,067
CR-960002	1.1.1 - Vacuum Equipment, WA Beam Manifold	January 1996	\$200,557
CR-960003	1.1.1 - Vacuum Equipment, Corner Station Pipe Bridges	January 1996	
CR-960004	1.1.1 - Vacuum Equipment, Roughing Pump Fail-safe Valves	January 1996	
CR-960005	1.1.1 - Vacuum Equipment, Main Ion Pump Auxiliary Ports	January 1996	\$9,854
CR-960006	1.1.2 - Beam Tube and Beam Tube Enclosure Model	February 1996	\$40,600
CR-960007	1.2 - Detector, Increases Due to Conversion to Nd:YAG Laser	February 1996	\$3,390,000

TABLE 4. Approved Change Requests

Change Request No.	Description	Date Approved	Allocated From/(To) Contingency
CR-960008	1.1.1 Vacuum Equipment - Gate Valve Weld Stubs	February 1996	\$17,953
CR-960010A	1.1.1 Vacuum Equipment - BSC Removable Spool Sections	March 11, 1996	\$110,000
CR-960011	1.1.1 Vacuum Equipment - BSC Floors (reduced number, increased loading)	March 4, 1996	\$11,962
CR-960012	1.1.1 Vacuum Equipment - Chillers for Deliverable Pump Carts	March 4, 1996	\$62,145
CR-960013	1.1.1 Vacuum Equipment - Reduce budget for miscellaneous	March 4, 1996	\$(700,000)
CR-960014	1.1.1 Vacuum Equipment - BTM Pump Cart modifications	March 4, 1996	\$40,031
CR-960015	1.1.1 Vacuum Equipment - Annulus Conductance Specification	March 4, 1996	\$(41,427)
CR-960016	WBS 1.1.3 Beam Tube Enclosure, Hanford - shift Access Module centerline	March 4, 1996	\$5,200
CR-960009B	1.4.1.1 Project Office - Allocation of Labor Charges	April 3, 1996	\$1,951,786
CR-960017A	WBS 1.4.1.1 Project Management Plan - NSF Reporting Milestones	April 3, 1996	No Cost
CR-960018	WBS 1.1.2 Beam Tubes - reduced cost beam tube supports	April 3, 1996	\$(206,955)
CR-960019	WBS 1.1.1 Vacuum Equipment - delete 30 inch flanges from Mode Cleaner	April 1, 1996	\$(35,298)
CR-960021	WBS 1.1.2 Beam Tube - Baffle manufacture and coating	April 26, 1996	\$436,200
CR-960022 Rev A	WBS 1.4.3.2 Document Control Center - adds FTEs (5N507)	August 13, 1996	\$624,950
CR-960023 Rev A	WBS 1.4.1.2 Project Controls - add Technical Configuration Manager, address rate variance (5N502)	July 8, 1996	\$1,365,103
CR-960024 Rev A	WBS 1.4.4.1 Administrative Support (5N509) - adds budget to cover additional FTE at MIT, and Supplies and Expenses	August 13, 1996	\$592,622
CR-960026 Rev A	WBS 1.1 Facilities and Vacuum Equipment - adjust budget for cognizant scientist support	July 8, 1996	\$(498,245)
CR-960027	WBS 1.2.1.2 Move IOO and COS fabrication budget into new Suspension Fabrication WBS elements	July 8, 1996	(No cost)
CR-960028 Rev A	WBS 1.2 Detector - increased management costs	July 25, 1996	\$470,000
CR-960029	WBS 1.2.1 Seismic Isolation System	July 25, 1996	\$763,000

TABLE 4. Approved Change Requests

Change Request No.	Description	Date Approved	Allocated From/(To) Contingency
CR-960030 Rev A	WBS 1.2.1 Detector - HTES contract	July 25, 1996	\$140,000
CR-960032	WBS 1.1.1 Beam Tube - Primary adjustment is for Stainless Steel Pricing	September 16, 1996	(\$1,025,530)
CR-960034	WBS 1.1.4 Civil Construction - Adjustment for Negotiated Contract	September 16, 1996	(\$1,544,666)

2.6 Staffing

The LIGO staff currently numbers 93 (full time equivalent). Of these, 16 are contract employees. 76 LIGO staff are located at CIT including four graduate students. Seventeen are located at MIT including five graduate students.

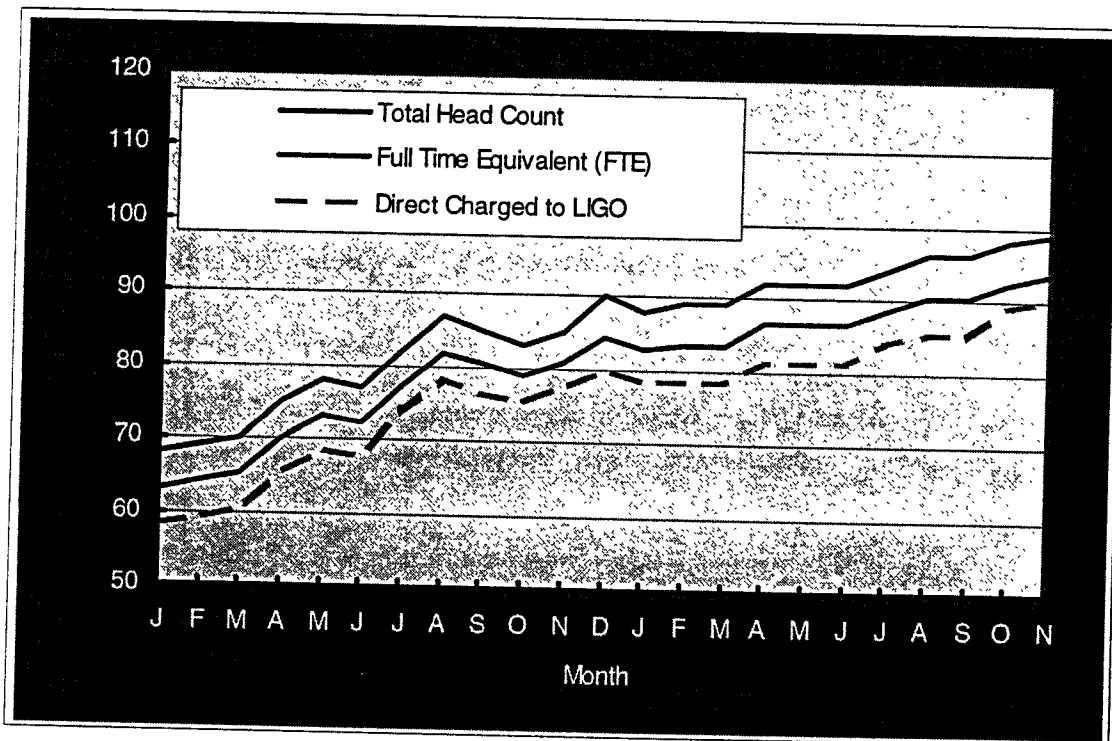


FIGURE 5. LIGO staffing history since January 1995

2.7 Project Organization

To best carry out the next phase of the construction project LIGO has instituted changes in the structure of the LIGO organization. LIGO submitted revisions to sections of the Project Management Plan⁴ to reflect the new organization and responsibilities. This reorganization did not affect project cost or the project reporting milestones identified in the Project Management Plan. Additional organization modifications have been made since the submittal of the Project Management Plan to reflect the following changes:

- D. Coyne has been assigned as the Detector Engineer in the Detector Group and is no longer the Deputy in the Integration Group,
- E. Moniz is no longer in the PI Advisory Group,
- F. Raab and M. Coles have initiated Industrial Liaison and Science Education Programs at Hanford and Livingston respectively,
- D. Tomlinson has been added as a Community Research Coordinator,
- Since the Civil Construction effort has moved from the design phase into construction and subcontract management, the position of Cognizant Scientist for Civil Construction has been deleted,
- Since the Beam Tube effort has moved from the design phase into fabrication and subcontract management, the position of Cognizant Scientist for the Beam Tube has been deleted,
- Since the Vacuum Equipment effort has moved from the design phase into fabrication and subcontract management, the position of Cognizant Scientist for Vacuum Equipment has been deleted,
- J. Camp has been assigned to the position of Task Leader for Laser and Optics.
- M. Fine has been assigned to the position of Task Leader for Suspension and Isolation

These changes are shown in the organization chart in Figure 6 on page 20.

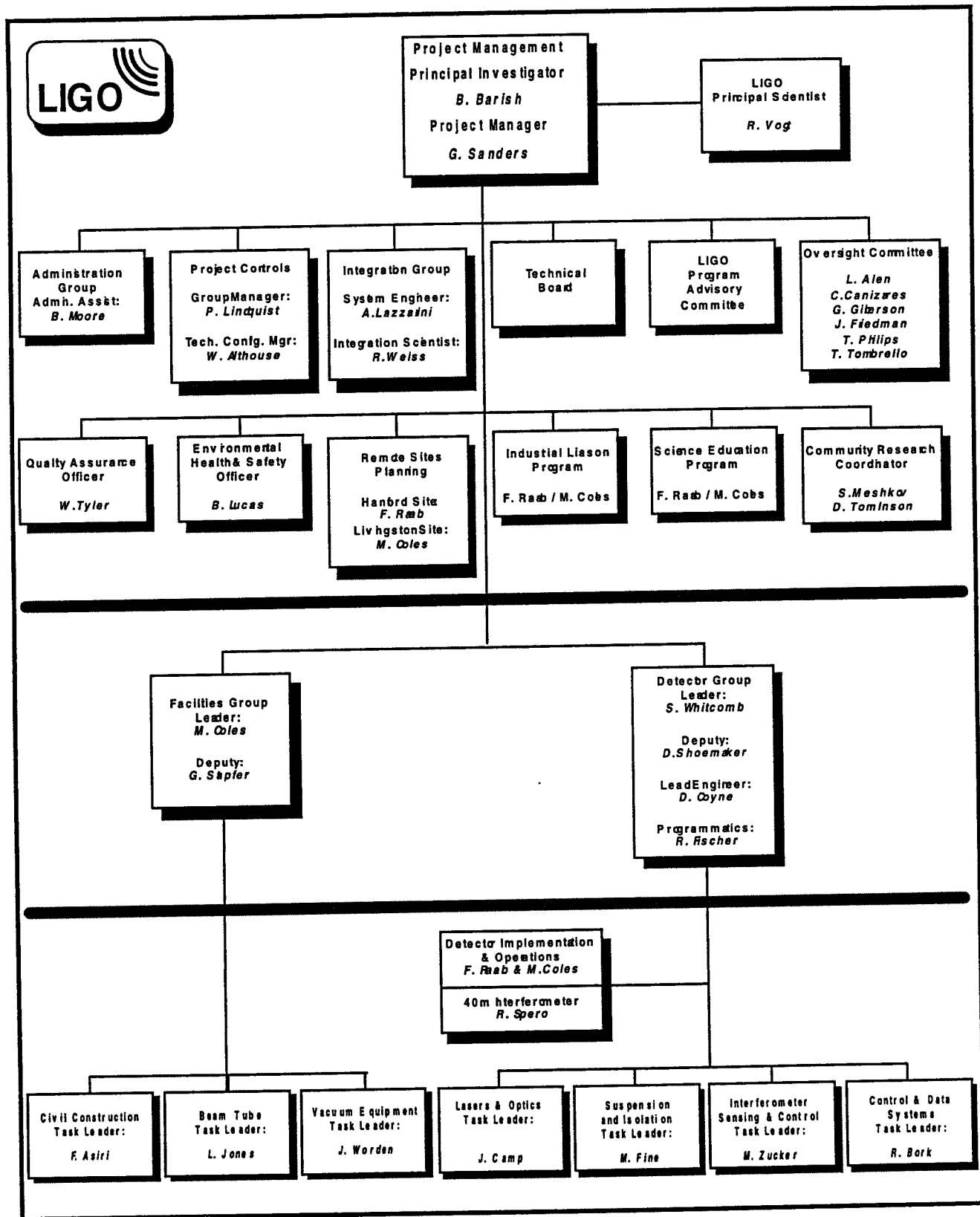


FIGURE 6. LIGO Project Construction Phase Organization

3.0 Vacuum Equipment (WBS 1.1.1)

Significant accomplishments during FY 1996

- Completed the Vacuum System design and completed prototype activities.
- Delivered large gate valves and pump carts to the Hanford, Washington site.
- Began all production work for the Beam Splitter Chambers, the Horizontal Access Modules, the 80K pumps, Spools, the bakeout system, clean rooms.

Discussion of accomplishments and work in progress

During 1996 the Vacuum Equipment design work was completed, the subcontractor, Process Systems International (PSI), initiated a number of large procurements, prototype activities were completed, the vacuum pumps and valves were delivered to the Washington site, and fabrication of production quantities of the chambers and related components was started. Orders for large quantities of stainless steel for the fabrication of the chambers was accomplished immediately following the Final Design Review in May 1996.

In October 1996 PSI completed the prototype Beam Splitter Chamber (BSC) tests. The main purpose of these tests was to perform pumpdown, bakeout and outgassing measurements of a representative sample of the LIGO Vacuum Equipment. Additionally, mechanical conformance of the first BSC was checked and appropriate changes were made to production drawings. The vibration performance of the first 80K pump was also measured at this time. The BSC vessel was a convenient chamber for this test. Figure 7 shows the BSC chamber and Figure 8 shows the chamber after the bakeout insulation has been installed.

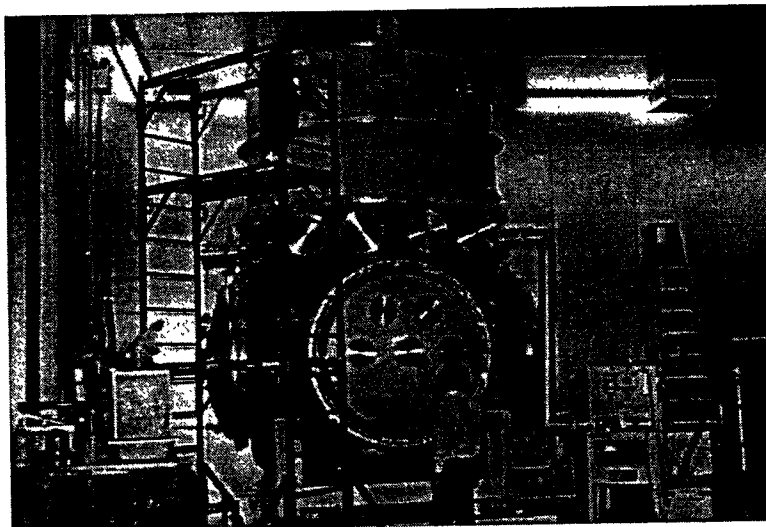


FIGURE 7. Prototype Beam Splitter Chamber.

After the BSC was baked at 150C and pumped for 100 hours the outgassing measurements were taken. Following these tests the chamber was opened up and prepared for insertion of the 80K

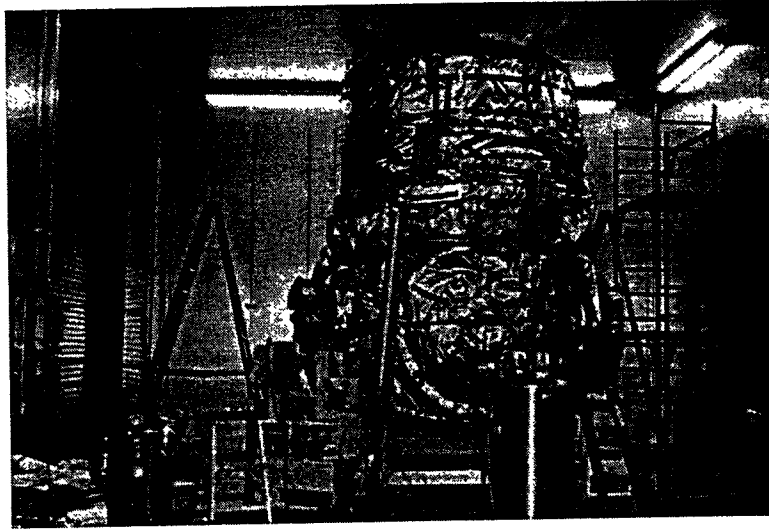


FIGURE 8. Insulated Beam Splitter Chamber.

pump. The cleaning and baking procedures were very effective. There was little evidence of hydrocarbon contamination after the bake. Partial pressures of hydrocarbons were three to four orders of magnitude below that of hydrogen. The principal gas loads after the nitrogen soak are hydrogen, water, and nitrogen.

Figure 9 shows the first short 80K pump at PSI facilities. After wrapping with thermal insulation it was installed (Figure 10) into the prototype BSC for cool down and vibration measurements. In Figure 11 LIGO and PSI personnel are monitoring the vibration tests.

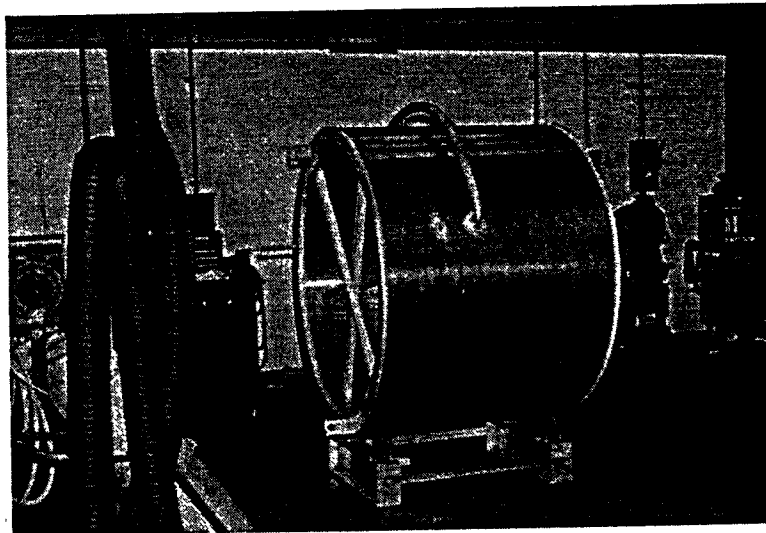


FIGURE 9. Short 80K pump.

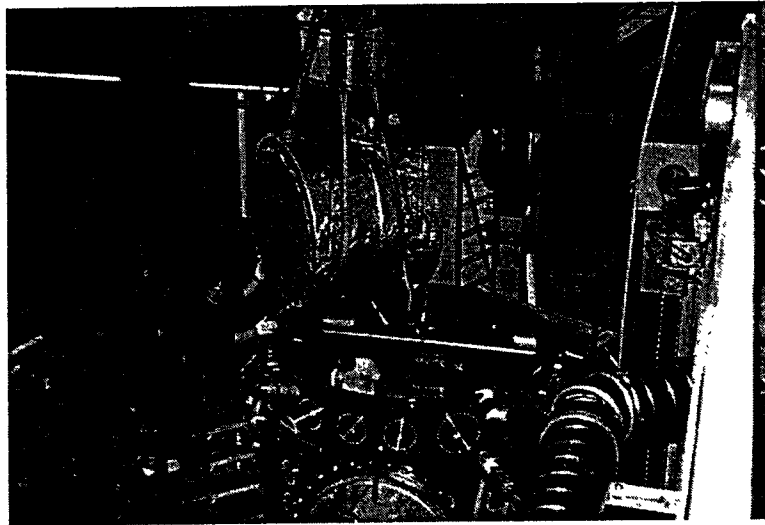


FIGURE 10. 80K pump being inserted into the BSC.

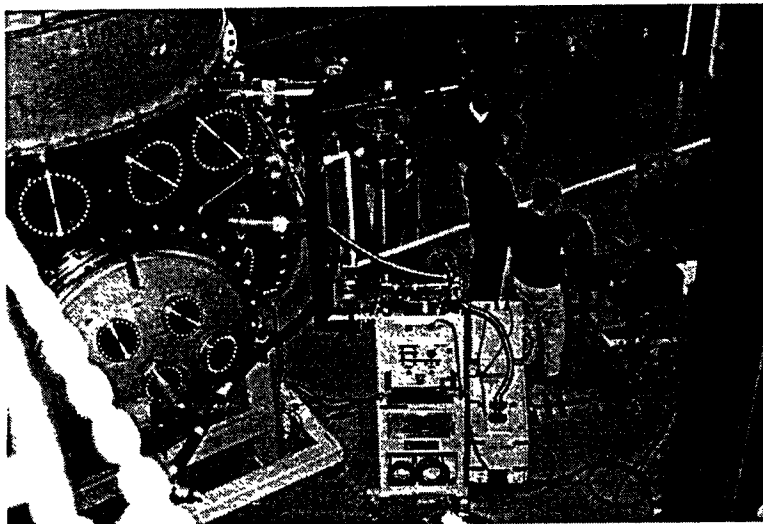


FIGURE 11. Vibration tests of the 80K pump.

While the prototype tests were in progress, pump carts and large gate valves were being delivered to the Washington site. Figure 12 shows the first gate valve being installed on the Washington beam tube slab by Chicago Bridge and Iron (CB&I). The photograph shows the valve mounted on temporary supports which allow the valve to be precision aligned prior to welding to the first beam tube section. After welding, the weight of the valve is shared by a spring loaded support and the weld joint. A temporary shelter is constructed to protect the valve from the weather and to provide a suitable environment for the fit and welding operation.

Production of all vessels is currently underway at PSI facilities and various subcontractors. Figure 13 shows a Horizontal Access Module being fabricated at PSI.

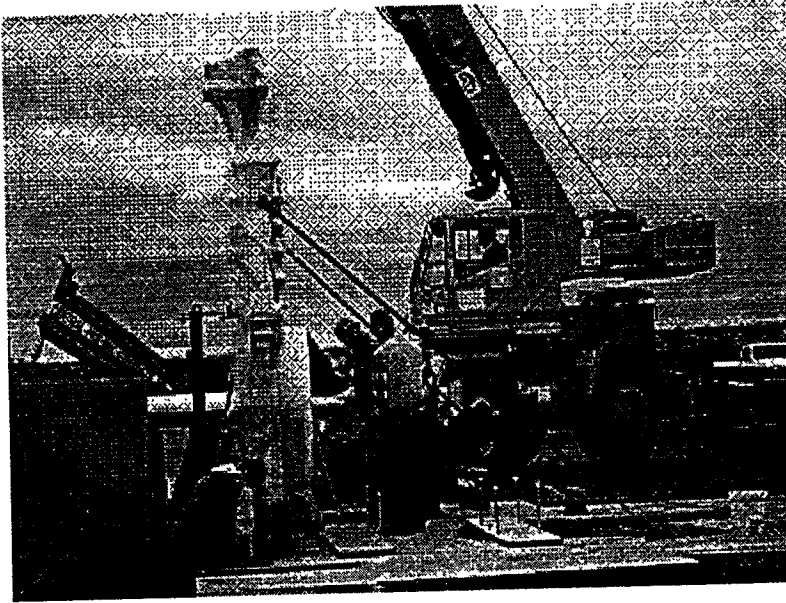


FIGURE 12. The first gate valve being installed at the Hanford site.

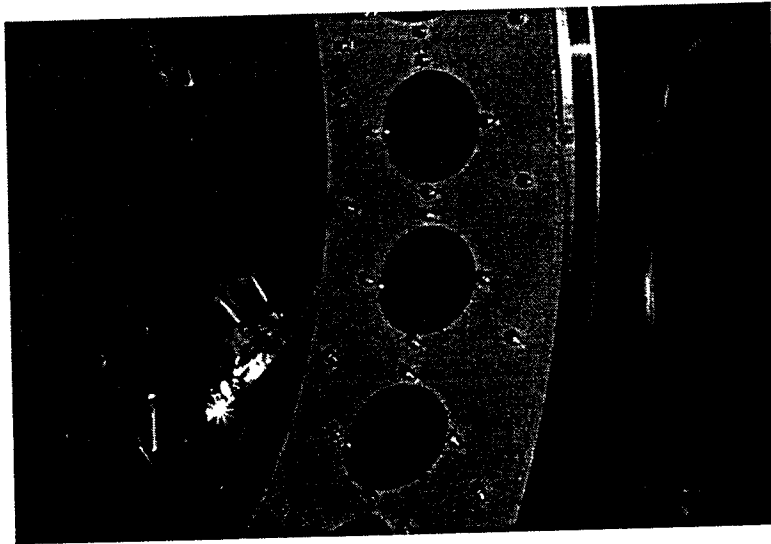


FIGURE 13. Horizontal Access Module vessel at PSI manufacturing facility.

Work planned for FY 1997

- Continue fabrication of chambers and covers, spools and 80K pumps.
- Begin vacuum preparation and pre-ship testing of production chambers.
- Issue contract for Vacuum Equipment Installation.
- Conduct installation readiness review for Washington and begin installation at Washington.

- Begin testing of first vacuum sections at Washington.
- Begin fabrication of the Louisiana vacuum chambers.

4.0 Beam Tube (WBS 1.1.2)

Significant accomplishments during FY 1996

- The fabrication and installation contract was awarded to Chicago Bridge & Iron on December 11, 1995.
- A custom spiral tube mill was designed, built, and qualified
- Stainless steel coil material was ordered and processed for the initial production of tube
- Designs for tube components and fixtures were updated and a design review was held
- Fixtures and equipment were ordered for the fabrication and installation tasks
- A fabrication facility was leased and modified for tube production
- Fabrication equipment was installed and qualified for use
- A successful fabrication readiness review was held
- Fabrication of the first one hundred tube sections was successfully completed
- Installation equipment was received and qualified for use
- A successful installation readiness review was held
- Field installation of tube sections has begun, with eight installed in two modules as of the end of FY 1996
- Science requirements for the beam tube baffles were finalized and the baffle design was completed
- Production baffles were ordered; a quantity of 300 baffles, sufficient for the first two beam tube modules, were received at Hanford by the end of FY 1996
- The first 35 baffles were installed in the beam tube modules at Hanford

Discussion of accomplishments and work in progress

The beam tube design was updated following qualification testing and a design review was conducted to approve the new design features.

Several lots of stainless steel coils were baked in a production mode and the resulting hydrogen outgassing characteristic measured in the Chicago Bridge & Iron (CB&I) coupon test facility. The test results showed the outgassing rates to be an order of magnitude below the maximum allowable level. These favorable readings were confirmed through in-house measurements made by LIGO. To date, a total of 750 tons of stainless steel coils have been processed. The bulk of stainless steel coil needed for fabricating the remaining beam tube sections for both LIGO sites has been ordered by CB&I.

CB&I has been very successful fabricating high quality leak-free beam tube sections meeting the rigorous LIGO specifications. To date, over one hundred fabricated tube sections have been leak tested; all passed without a single failure. Efficient tube section leak testing with helium mass spectrometers was made possible using metal test hoods which also help to achieve high sensitivity.

To fabricate the beam tubes, CB&I designed, assembled and installed a complete factory in a leased facility near the Hanford LIGO site and outfitted it with special hoists and a rail conveyor system. The electric power was upgraded to suit the needs for fabricating beam tube sections, and special rooms were built with separate HVAC systems for leak checking and cleaning tube sections. Special equipment was fabricated for efficient tube production, including a spiral tube mill, stiffening ring welding stations, tube end expander/cutoff machines, tube section leak check hoods, and a spray rig for cleaning. All of this equipment was then qualified for use and a fabrication readiness review was held. Initial spiral mill tube production was made from 24" wide coils, using material remaining from the beam tube qualification tests. This was successfully converted to 36" coil stock, which is currently being used to fabricate all of the remaining tubes.

Production in the fabrication shop has been successful both in terms of quality and schedule. Additional storage space has been leased to accumulate tube sections while tube installation is ramping up.

The cleaning of the completed tubes is performed just prior to shipment to the site for installation. The cleanliness of the tubes, based on Fourier Transform Infrared (FTIR) measurements, are superior to the results achieved during the qualification test.

All of the critical activities which are performed in the fabrication facility by CB&I are monitored on a daily basis by LIGO technical staff. These activities are governed by written procedures and are documented in log books and weekly activity reports.

Baffle science requirements were finalized, and the baffle design was completed. The final configuration involves a truncated cone with a radial height of nine cm, with surfaces porcelain coated for high reflectivity. Two styles are used, with and without inner edge serrations. The design was qualified for acceptable hydrogen outgassing rates. Baffle production is well underway in both fabricating and coating, with 300 completed units at the Hanford site. Thirty-five of these have been installed in the modules to date (See Figure 14).



FIGURE 14. Baffles in field clean room awaiting installation.

Installation of the tube sections has been initiated, starting at the mid station of Arm Two and proceeding simultaneously toward the end and corner stations. A total of 10 tube sections have been installed as of the end of FY 1996.

Figure 15 shows two tube sections being shipped the 30 miles to the Hanford site. Tube ends are capped and double wrapped to maintain cleanliness, and the tube sections are covered to preclude yielding due to solar exposure.

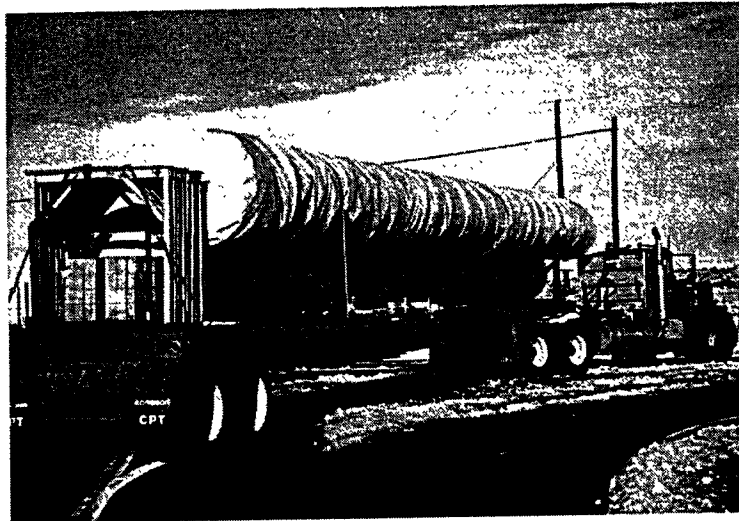


FIGURE 15. Tube section shipment

Tube installation procedures make use of special enclosures (Figure 16) to maintain cleanliness in welding (Figure 17) and to allow sensitive leak checking of the girth seams. A clean room enclosure allows access to the tube interior for installing a purge ring and baffles. A weld enclosure provides a clean environment for fitting and welding the girth seams. A test enclosure provides protection for the helium mass spectrometer and a warm environment to aid sealing of the vacuum box. These units were qualified for the installation process, and an installation readiness review was held. Enclosure sealing is meeting expectations, even in dust-blown conditions.

All of the field installation activities are monitored by the LIGO technical staff.

Work planned for FY 1997

- Fabrication and installation of the remaining beam tube sections at Hanford will be completed
- Work crews will be mobilized at Livingston, Louisiana.
- The acceptance testing of the beam tube modules at Hanford will begin.
- A fabrication facility will be leased in Livingston, and fabrication equipment will be set up.
- A fabrication readiness review will be conducted and tube fabrication at Livingston will be started.

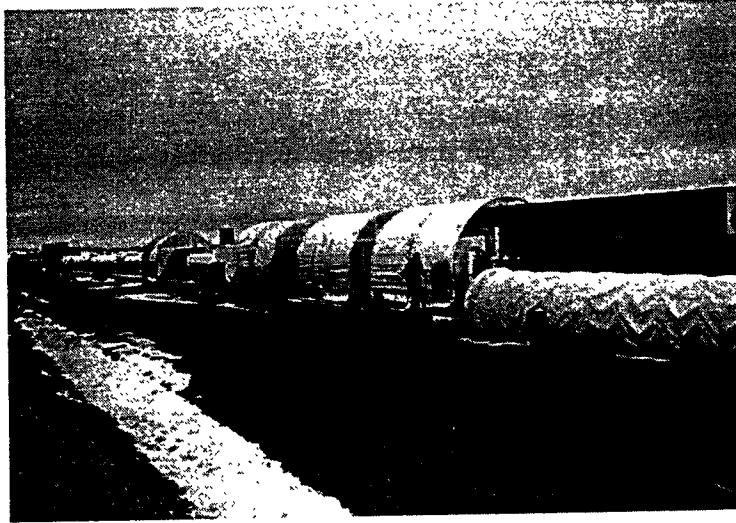


FIGURE 16. Special field enclosures for tube section installation

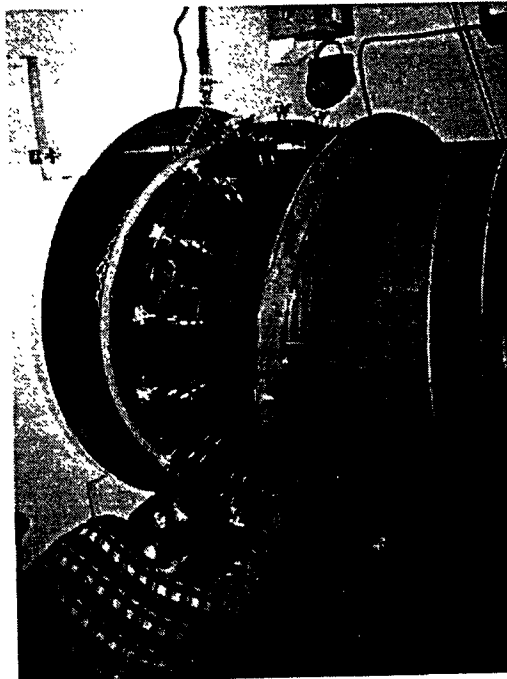


FIGURE 17. Inside the weld enclosure during fit-up

5.0 Beam Tube Enclosure (WBS 1.1.3)

Significant accomplishments during FY 1996

- Signed contract with ACME Material and Construction Company for the site work and precast fabrication of the enclosure for the Hanford site.
- Completed the finish grading and site work for the beam tube enclosure at the Hanford site.
- Completed the slip-forming and placement of concrete for the beam tube enclosure slab at the Hanford site.
- Completed the service road along the both arms at the Hanford site.
- Completed the fabrication of about 2000 concrete segments of the enclosure for the Hanford site.
- Issued a contract with Levernier Construction, Inc., for the installation of the Beam Tube Enclosure.
- Completed the design package for the site work and precast fabrication of the enclosure for the Livingston site.
- Signed a contract with Shannon & Wilson, Inc. to provide quality assurance services for the slab and beam tube enclosure contract at the Hanford site.
- Signed a contract with Rogers Surveying, Inc. to provide surveying audit services for the slab and beam tube enclosure contract at the Hanford site.
- Completed the design and bid package for pre-casting and installation of the beam tube enclosure including the concrete slab and the service road along the arms for the Livingston site. The bids were opened on October 15, 1996.
- Completed the fabrication of the lifting device and successfully demonstrated the mock-up installation of three segments of the enclosure.
- Awarded the contract for the Beam Tube Enclosure fabrication and installation for the Livingston, Louisiana site to Woodrow Wilson Construction Co.

Discussion of accomplishments and work in progress

The contract for the Site Work and Precast Fabrication of the Enclosure for the Hanford site was awarded to ACME Material and Construction Company. The notice to proceed for the above contract was issued on January 25, 1996.

The LIGO and Parsons' construction management office was set up at the Hanford site. Construction of the beam tube enclosure proceeded on schedule and all the major schedule milestones were achieved at the Hanford site.

Levernier Construction Company has begun the installation of the LIGO beam tube enclosure segments (Figures 1). The installation of the enclosure segments is proceeding from both sides of the mid station on the northwest arm towards the corner and end stations. The enclosure is made of precast reinforced concrete segments which are precasted by the

ACME Material and Construction Company at an off-site precast yard in the city of Richland, WA. The typical segment is about ten feet long, with 6 inch thick walls, and weighs approximately ten tons.

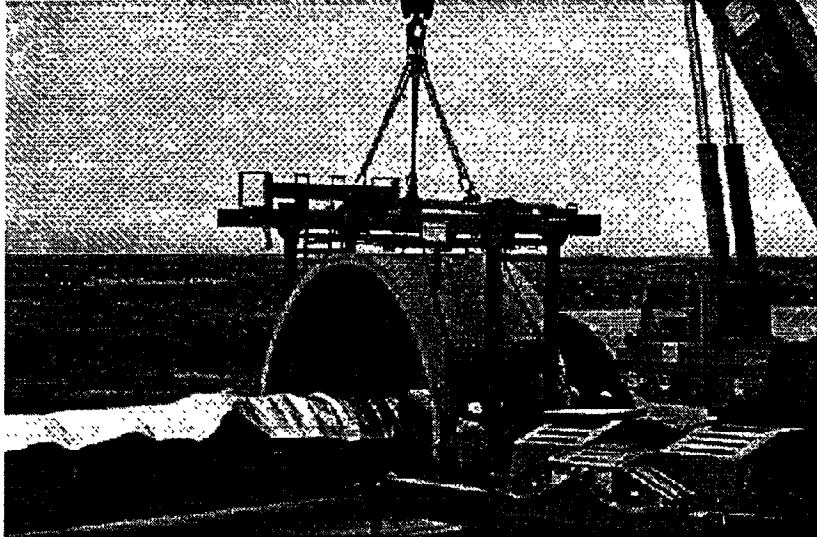


FIGURE 18. Installation of the Beam Tube Enclosures

Parsons I&T, the Architect/Engineering contractor, completed the design and prepared the bid package for fabrication and installation of the beam tube enclosure for the Livingston, Louisiana site. They also prepared the Request for Proposal package for the beam tube enclosure installation the Hanford site.

The Invitation to Bid for the beam tube enclosure fabrication and installation for the Livingston site was issued. The bidders conference/job walk took place at the Livingston, LA on August 28, 1996. The public bid opening was held in Baton Rouge, LA on October 15, 1996, and the contract was issued to the low bidder, Woodrow Wilson Construction Co., in December 1996.

Work Planned for FY 1997

- The fabrication of the precast beam tube enclosure segments and the installation of the enclosure segments over the beam tube are scheduled to be completed at the Hanford site in FY 97.
- The site work and precast fabrication and installation for the beam tube enclosure at the Livingston site will be initiated early in FY 97. It is anticipated that 700 enclosure segments for one arm will be completed by the end of FY 97.

6.0 Civil Construction (WBS 1.1.4)

Significant accomplishments during FY 1996

- Signed a contract with Public Utility District for providing electric power to the Hanford site.
- Signed a contract with Westinghouse Hanford Company for providing the telecommunication services to the Hanford site.
- Completed the final design package for the facility (buildings) for the Hanford site, and conducted the final design review design.
- Installed the electric power line and telecommunication services from Area 400 to the Hanford site.
- Completed the electric distribution system along the both arms at the Hanford site.
- Signed a contract with Stranco Inc. for rough-grading and drainage work for the Livingston site.
- Signed a contract with Dixie Electric Membership Corporation for providing electric power to the Livingston site
- Signed a contract with Professional Service Industries, Inc. for geotechnical field monitoring and testing of the rough grading construction at the Livingston site.
- Signed a contract with ABMB Engineers Incorporated to provide surveying audit services for the rough grading construction at the Livingston site.
- Completed the rough grading at the Livingston site. All activities related to the pipeline crossings at the Livingston site has been completed.
- Selected the general contractor and awarded the contract for construction of facility (buildings) at the Hanford site to Levernier Construction, Inc. Began construction of the facilities (buildings) at the Hanford site.
- Completed the detailed design package for the building and infrastructure at the Livingston site. Conducted the final design review and approval process. The bids were opened on October 15, 1996, and the contract was awarded to Hensel Phelps Construction Co.

Discussion of accomplishments and work in progress

The Parsons I &T, the A-E contractor, completed the final design of the facility (buildings) for the Hanford and the Livingston sites. This design consisted of drawings, specifications, calculations and cost estimates for the two interferometer arrangement at the Hanford site and for two interferometers at the Livingston site.

The Invitation to bid for the facility (buildings) at the Hanford site was issued to about 140 plan holders. The public bid opening took place at Richland, WA on June 18, 1996.

The Invitation to Bid for the facility (buildings) at the Livingston site was issued to about 56 plan holders about 10 of them are general contractors. The bidders conference/job walk

took place at the Livingston, LA on August 28, 1996. The public bid opening was held in Baton Rouge, LA on October 15, 1996.

Hanford Site. The Public Utility District (PUD) was awarded the contract for providing electric power to the Hanford site. PUD has completed installing the 13.8 KV underground power cables from 400 Area to the LIGO site and along the arms. The Westinghouse Hanford Company was contracted for the installation of a 50 pair telephone cable and a 12 fiber single mode fiber optics cable from the 400 Area to the construction site. Underground telephone cable and fiberoptics cable have been installed.

Levernier Construction Inc., was awarded the contract for the Civil Construction-Facilities (Buildings) contract for the Hanford site. The building construction activities are on schedule.

Figure 19 is an aerial view was taken along the Northwest arm of the L-shaped complex at Hanford in December 1996. The corner-station foundation is in the foreground with a vacuum-tube foundation running to the end station at the top of the picture. Vacuum tube installation is proceeding in the middle of the arm, partially obscured by cloud cover. The Southwest arm (running off to the left of photo) points toward Rattlesnake Mountain. Figure is a view of the construction at the end station on the southwest arm.

Livingston Site. The rough-grading and drainage work at the site started by Stranco Inc., at the beginning of this period. Parsons' construction manager has been assigned to the site. The construction of drainage culverts have been completed. The construction of the berm has been completed. Dressing and seeding of the berm will be accomplished by the end of the calendar year.

Work Planned for FY 1997

- Complete construction of the buildings at the corner station, the mid-station, and the end-stations at the Hanford site.
- Complete the infrastructure for the operation of the facility at the Hanford site. Begin operation of the civil facilities.
- Begin beneficial occupancy of the buildings at Hanford.
- Set up the LIGO and Parsons construction management office at the Livingston, Louisiana site prior to the start of construction activities for the Beam Tube Enclosure and the buildings.
- Begin construction of the buildings and infrastructure for the Livingston, Louisiana site.
- Begin construction of the Beam Tube Enclosures for the Livingston site.
- Complete the end-station at the southwest arm at the Livingston site, including all services. The building will be ready for beneficial occupancy.

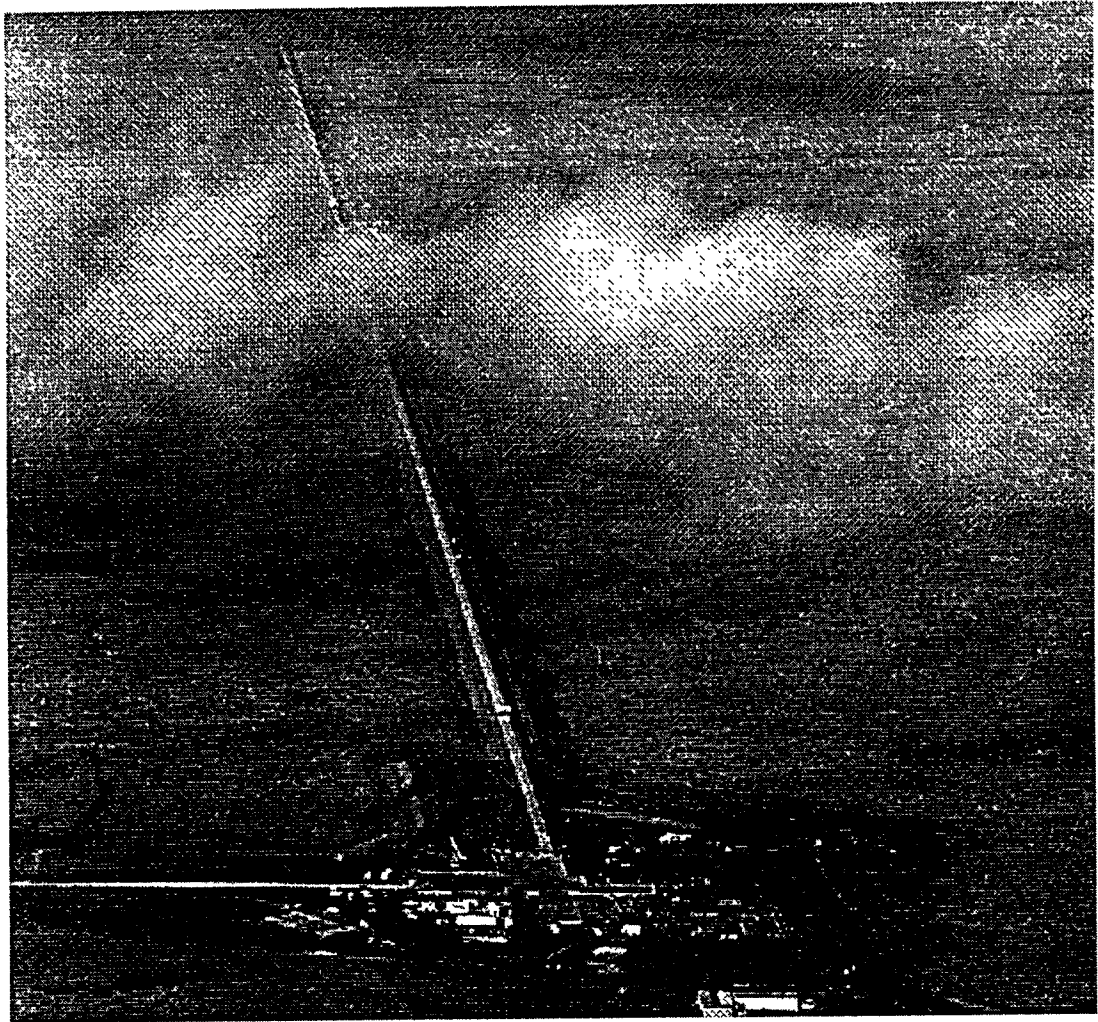


FIGURE 19. Aerial View of Construction in Hanford, Washington

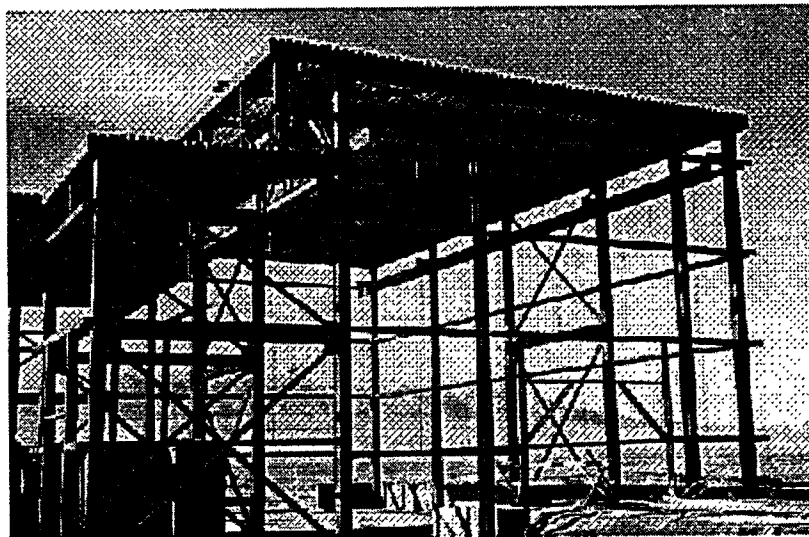


FIGURE 20. The End-Station on the Southwest Arm at Hanford

7.0 Detector (WBS 1.2)

Detector activities are organized according to the LIGO WBS as follows:

- WBS 1.2.1 Interferometer System, organized into three major task groups, each responsible for several Subsystems:
 - Suspensions and Isolation
 - Seismic Isolation
 - Suspension Design
 - Lasers and Optics
 - Prestabilized Laser
 - Input/Output Optics
 - Core Optics Components
 - Core Optics Support
 - Interferometer Sensing/Control
 - Alignment Sensing/Control
 - Length Sensing/Control
- WBS 1.2.1.9 Detector System Engineering/Integration
- WBS 1.2.2 Control and Data Systems
- WBS 1.2.3 Physics Monitoring System
- WBS 1.2.4 Support Equipment

Detector activities started in December 1994. As anticipated in the 1996 Workplan, the switch to a Nd:YAG laser and infrared 1064 nm wavelength has had a significant impact on scheduling of a range of detector activities. In general, we have found that the schedule planned for FY96 was quite aggressive, and we have also had difficulty staffing the activities at the planned rate. As a consequence, it has been necessary to replan several activities, taking advantage of a staged installation schedule. However, we have made considerable progress in particular in several key aspects of the interferometer design, as described below, and the critical path item (the Core Optics Components) is ahead of the baseline schedule.

While we continue to report progress separately for R&D activities and Detector activities, the task groups enumerated above include the relevant R&D (most laboratory activities and exploratory modeling) with the objective of concentrating the activity on a given domain. In addition, the Detector Site Implementation and Operations task group reports activities focussed on these topics and also the activities in the 40m Interferometer facility, which is a primary tool for tests of operations and integration for the Detector group.

7.1 Suspensions and Isolation

Significant accomplishments during FY 1996

- Completed the Design Requirements Review (DRR) of the Seismic Isolation Subsystem.
- Completed the Preliminary Design Review (PDR) of Suspension Subsystem.

Seismic Isolation. The Seismic Isolation subsystem requirements and conceptual design were documented and reviewed, taking into account new ground noise measurements at the Livingston, LA site, and the design constraints imposed by the Suspension design. HYTEC, the subcontractor carrying out the detailed design, presented their trial designs and analysis in a review held on April 4. Prototypes of two alternative spring designs offering improved isolation and vacuum properties are in fabrication, and finite element models of the complete system are complete and in use for design efforts. Activity focused on actuator designs and layout considerations as the year closed.

Suspension Design. A Preliminary Design Review was held on June 6, and the Final Design has started. The mechanical design presented, critical to controlling thermal noise and limiting the effect of mechanical resonances, was found to meet the requirements. The actuator requirements have been refined in a trade with Seismic Isolation, shifting some of the large micro-seismic peak requirement to the Seismic actuators, thus easing the low-noise design at gravitational-wave frequencies. A successful test of a reduced-scale model of the suspension was performed in the 40m interferometer as was a full-scale test of the electronics control and interface system planned for the Small Optics Suspensions.

Work planned for FY 1997

- Seismic Isolation. Complete the preliminary and final mechanical designs for both vacuum chamber configurations (HAM and BSC). Solicit vendors for the fabrication phase.
- Suspension Design. Complete prototype testing. Complete and review the final design in the first quarter of FY 1997; start the fabrication of the LIGO Large and Small Suspensions.

7.2 Lasers and Optics

Significant accomplishments during FY 1996

- Prestabilized Laser. Initiated development of 10W diode-pumped Nd:YAG laser.
- Input Optics. There was significant design activity at the University of Florida.
- Core Optics. Selected substrate materials and polishing vendors for the Core Optics; placed orders. Refined coating procedures.

Prestabilized Laser. A decision was made to switch to a Nd:YAG laser and infrared 1064 nm wavelength. Lightwave Electronics, the subcontractor selected to develop the 10W diode-pumped Nd:YAG laser for LIGO, started the effort by developing an experimental prototype. Long lead-time materials have been received, and the initial prototyping is underway.

Input/Output Optics. A group from the University of Florida developed the Design Requirements Document for the Input Optics during extended visits at LIGO. A design requirements review took place on November 7, and preliminary design is underway.

Core Optics Components. The focus of work has continued in the area of the full size LIGO optics "pathfinder" effort. The three companies selected for polishing trials polished full-size LIGO optics test pieces. A careful examination of the data from the polishers and NIST showed

that all three vendors could meet LIGO requirements, and in fact some test pieces exceed them. Subsequent responses to a Request for Proposals permitted the selection of more than one polishing vendor, with awards being made to General Optics (California) and the Commonwealth Scientific and Industrial Research Organization (Australia).

Collaborative interaction on coating uniformity with Research Electro Optics (REO) continued with in-house testing as well as measurements at REO. In particular, a complete measurement and modeling approach allows us to 'try' out coatings in a numerical interferometer model with encouraging results.

Work planned for FY 1997

- Prestabilized Laser (PSL). Complete the development and fabrication of a first article 10 W Nd:YAG Laser. Complete the preliminary design, and start the final design of the Nd:YAG prestabilized laser.
- Input Optics. Complete the preliminary design, and initiate the final design for all input optics components. Initiate procurement of the first article of the mode-matching telescope.
- Core Optics. Receive blanks and start polishing the initial batch of components. Complete procurement and tooling fabrication for the coating process.
- Core Optics Support. Complete the preliminary and final optical and mechanical design for the support of core optics and begin fabrication.

7.3 Interferometer Sensing/Control

Significant accomplishments during FY 1996

- The Design Requirements Review of the Alignment Sensing/Control Subsystem
- The Design Requirements Review of the Length Sensing/Control Subsystem

Alignment Sensing/Control. During FY 1996 there was significant progress in all aspects of this complex subsystem. A model of the paths for the excitation of the test mass angular motion was developed, and revised estimates for the levels of the environmental input were made. The initial alignment procedure was expanded, and the role of optical levers in both initial and operational modes was refined to ease implementation. The requirements and conceptual design were successfully reviewed on 29 August, enabling Preliminary Design to begin. The Wavefront Sensing prototype has been fabricated in quantity for test in several R&D programs, and the design appears to be quite successful.

Length Sensing/Control. The Design Requirements Review for the Length Sensing/Control system took place on April 30. A change in the baseline design to a single carrier/single modulation sensing system was made as a consequence of detailed design work. The conceptual design presented meets LIGO performance requirements with a realistic servo-system design for operations, and modeling of the dynamics of the cavities and interferometers provided a sequential locking scheme which appears robust. The status of the tools for modeling the acquisition of length control was reviewed on August 26 with the single-spatial-mode model complete. Using this model, a new connection topology was developed which gives an unambiguous path to the operating state.

Preliminary design of the system continued through the end of FY96.

Work planned for FY 1997

- Alignment Sensing/Control. Review the preliminary design for all Alignment subsystems. Complete the final design for the Initial Alignment and Optical Lever subsystems, and complete the prototype fabrication and tests for the Wavefront subsystem. Start fabrication of the Initial Alignment system components.
- Length Sensing/Control. Complete modeling (a time-domain multi-spatial mode acquisition model), final design, and all prototyping. Start programming the control systems.

7.4 Detector System Engineering/Integration

Significant accomplishments during FY 1996

The Detector Systems Engineering/Integration has continued to address the requirements 'flow-down' and the trade studies required to deliver the sensitivity of the initial LIGO detector. Design Requirements and Preliminary Design Reviews for many of the detector systems were held. A draft version of the Detector Subsystems Requirements Document was circulated in August and is in use for assuring consistency between subsystems; the refined document was circulated for review in December 96.

Work planned for FY 1997

- System Design Requirements. Complete documentation of subsystem interfaces.
- Optical Layout. Prepare and review preliminary optical layout.

7.5 Control and Data Systems (CDS) Activities (WBS 1.2.2)

Significant accomplishments during FY 1996

- Documented (in Design Requirements Documents, DRDs) and reviewed the requirements, interfaces, and conceptual design of the Data Acquisition and Interferometer (IFO) Diagnostics System.

Discussion of accomplishments and work in progress

The Core CDS design has been a major focus this year. The requirements, interfaces, and the conceptual design of the Control and Monitoring Systems, Software, Vacuum Cabling, Data Acquisition Systems, Diagnostics Systems, and Vacuum Controls were documented in Design Requirements Documents and reviewed early in the year, and preliminary design reviews for several subsystems have been completed.

The CDS group also prepared prototypes for a number of subsystems this fiscal year, both directly as part of their design effort and also in a role of supporting R&D. The Argon Pre-Stabilized Laser software and hardware at the 40m interferometer has been a rich source of information for human interface and hardware design. Software for data collection on the Alignment Fixed Mass

Interferometer was developed. In addition, the fabrication of the Wavefront Demodulator circuit board was a significant step in support of the R&D related to and the implementation of the wavefront sensor. Additional support was provided the 40m interferometer in the form of electronics development (servo systems, RF modulation/demodulation systems) for the recycling modifications.

Work planned for FY 1997:

- Interferometer Controls. Complete the final design for the Length Control and Suspension controls. Complete prototyping of the Nd:YAG Pre-Stabilized Laser controls, install and start tests, undertake the preliminary design for the Seismic, Alignment and Input Optics controls.
- CDS integration and global systems. Complete and review the Integration and Global Control and Data systems.
- Data acquisition. Complete preliminary design and initiate final design.
- Vacuum system controls. Complete procurement and software fabrication.
- Remote diagnostics. Complete all design, fabrication, and procurement; review installation readiness.

7.6 Physics Environment Monitor (WBS 1.2.3)

The Physics Environment Monitor Design Requirements Review took place on September 12, with preliminary design in progress by the end of FY 1996. The environment at the LIGO sites has been measured and documented, and the requirements and conceptual design for the sensors developed. A staged implementation of the system is planned, with an early presence at the sites in the form of a portable self-contained monitoring system.

Work planned for FY 1997:

- Finish and review the Preliminary Design; perform Final Design and fabrication of the portable components.

7.7 Support Equipment (WBS 1.2.4)

Definition of the required Support Equipment will continue.

8.0 Research and Development (WBS 1.3)

Significant accomplishments during FY 1996

- Demonstrated record level of phase sensitivity in Phase Noise Interferometer (this was a significant step).
- Completed Alignment tests in the Fixed-Mass Interferometer with a successful comparison with Modal Model.
- Concluded work on the non-recycled recombined 40m configuration.
- Installed, tested, and characterized LIGO-like Small Optics Suspension on the 40m Interferometer.

40m Interferometer Investigations. Investigations in support of the R&D and detector program continued on the 40m interferometer.

A major effort on the 40m was the complete characterization of the operation of the interferometer in its optically recombined (but non-recycled) configuration and the development of an understanding of the sources of noise. This configuration introduced several new aspects to the servo-controls which hold the interferometer in lock. The servo loops in the previous configuration were all of the single-input/single-output variety; the recombined loops include multiple inputs and multiple outputs. While trying to understand the noise in this configuration, new versions of diagnostic tests were developed taking into account the interaction of the different loops. This information was incorporated into the design parameters for the recycled system, and the research brought to a close.

The vacuum envelope is being reconfigured as the year closes to accommodate the recycling cavity. This involves the addition of a side chamber, equipped with isolation and mounts to carry the additional optical elements needed for the recycled interferometer. The control system is also being refined based on the latest locking modeling results.

One of the crucial missions of the 40m interferometer is to develop techniques for achieving the very high availability planned for LIGO. This involves making the hardware reliable and also developing work routines which support the continuous operation which LIGO will require. Data were gathered on hardware changes which will be needed for the 40m (and thus LIGO) to maintain high availability. All Caltech scientists are spending some shifts working with the 40m to bring a variety of experience to the research and to train scientists for the installation, commissioning, and operations work at the LIGO sites.

The 40m interferometer is the integration test bed for interferometer subsystems. The Argon Pre-Stabilized Laser, completed and characterized in 1995, was installed on the 40m to allow the training of personnel with the user interface, as a shake-down of the control electronics (much of which will be carried over to the Nd:YAG Pre-Stabilized Laser), and to improve the reliability of the present laser source.

Development of Data Acquisition and Analysis Techniques. Previously acquired 40m data has been analyzed for binary inspirals as a test of data-handling and analysis routines. Improvements in the tape hardware and the template software now support a real-time throughput of five inspiral

templates on a standard workstation. The 40m instrument is being equipped with a prototype LIGO hardware data acquisition system to gain experience and to aid in the development and test of software.

Suspension Development. A new design for test mass suspensions for the 40m interferometer was installed and tested. Fabrication of a first article of this suspension was completed early in the year. The mechanical design was evaluated during the process of developing test-mass hanging techniques. The electronic sensors and actuators, which are of a new design, were characterized and aligned on a test-bed to ensure orthogonality of the translation and angular systems. The new test mass suspension, which incorporates the key features planned for the suspensions on the full-size interferometers, was installed in the 40m at one of the vertex test mass positions. Tests for the control performance, noise, and isolation were performed. The design was found to be satisfactory, and will be replicated to replace all test mass suspensions in FY 1997. The objective is to gain experience with these LIGO-like suspensions. It is also anticipated that the improved control and seismic isolation will allow better low-frequency noise performance in the 40m interferometer.

Phase Noise Research. This effort was undertaken to develop and demonstrate the technology for the shot-noise limited interferometer operation at initial LIGO power levels to achieve the required phase sensitivity using the 5m facility at MIT.

The first phase of the research with the Phase Noise Interferometer (PNI) used a Michelson without recycling, with the objective of getting the newly-commissioned 5m system checked out. This was completed during the first quarter of FY 1996 with incremental improvements resulting from changes in the input optics and the addition of a second Barry Controls, Inc., active isolator. A satisfactory understanding of the spectrum was achieved, and several noise sources were identified and improved with the addition of recycling.

Initial measurements with the recycled Phase Noise Interferometer showed that to achieve the measurement goals a system of automated alignment was needed using the techniques and designs developed for the Fixed-Mass Interferometer test of Alignment and to be used on LIGO. A special-purpose servo-system was developed which optimized the gain in the frequency regime most critical in terms of excitation, and wavefront sensor heads and demodulators were fabricated. The implementation performed as designed and dramatically reduced the fluctuations in circulating power and coupling to laser imperfections.

After shakedown the recycled interferometer was operating with roughly 200 mW of input power (514 nm green light from an Argon laser source). The recycling factor of roughly 450 leads to approximately 90 W of circulating power in the recycling cavity. With this set of parameters, a phase noise sensitivity of roughly 3×10^{-10} rad/ $\sqrt{\text{Hz}}$ has been achieved, in good agreement with calculations. This very encouraging result is, to our knowledge, the highest phase sensitivity of any interferometer to date. Additional effort has uncovered the sources of low frequency excess noise, and steps to reduce the noise have been successful (and are applicable to LIGO). The curve of sensitivity shown in Figure 21 shows this improvement in the performance, due to a reduction of parasitic interferometers between the laser source and the interferometer; the remaining low-frequency noise appears to be dominated by the frequency noise on the laser beam. The research with the Argon laser was completed at the end of the fiscal year. Preparations are underway to

convert to Nd:YAG.

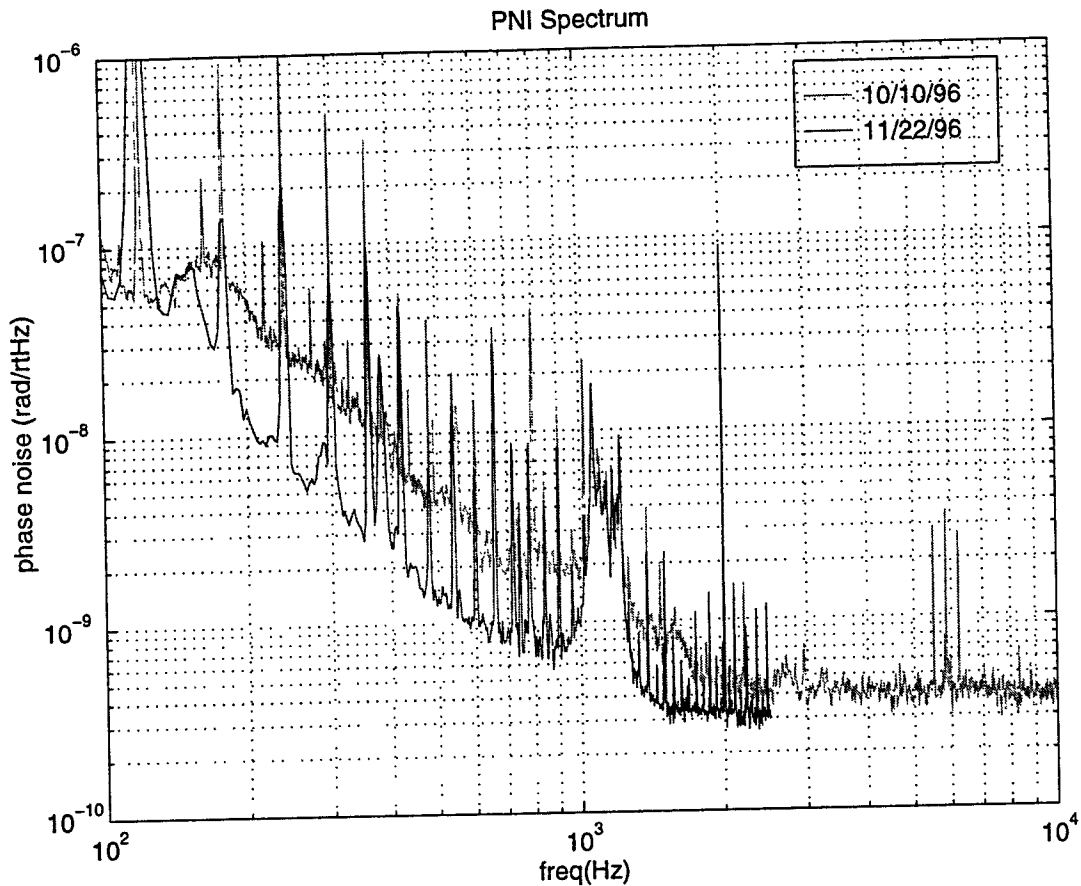


FIGURE 21. PNI Performance Improvements in the Recycled Configuration

Interferometer Alignment Investigations. The purpose of this research effort is to test the operational system of alignment for the initial LIGO interferometer. The effort this fiscal year has been very successful. A test of the target wavefront sensing system was installed on the MIT fixed mass interferometer, with a complete LIGO optical and length sensing system. The discriminants at all interferometer ports were measured and compared with a semi-analytical model. There was good agreement which confirms the model being used to design the LIGO alignment system.

Thermal Noise Investigations. The apparatus used for measurements of the test mass Q has been rebuilt to permit testing of full size LIGO test masses. A larger vacuum system has been designed and built. The electrostatic drive for exciting the internal modes of the test mass has been enlarged and improved. A new suspension tower for safely holding 25 cm diameter test masses has been designed and built. Full size LIGO test masses have been characterized as have various types of suspension fibers and attachments.

Nd:YAG Characterization and Stabilization. To gain familiarity with infrared techniques and

to develop a basis for the LIGO Nd:YAG laser subsystem design, moderate-power (700 mW) commercial lasers are being prepared for use in the campus laboratories. The laser used is very similar to the master laser to be used in LIGO, and so the experience gained is directly applicable. These lasers, with frequency and intensity stabilization, will be used in the Phase Noise Interferometer (where precision tests of the performance of the 700 mW and later the 10W laser will be performed), in mirror contamination testing (where long-term exposure of mirrors to possible contaminants will be evaluated in the presence of high circulating optical powers), and in the 40m interferometer (where systems tests will be performed). The first of these lasers will be delivered to the Phase Noise Interferometer in early FY 1997.

Interferometer Control Modeling. Considerable progress has been made on the length control model for the acquisition of a full LIGO interferometer. Computer code has been completed that describes both the optical response and the feedback controller dynamics. This model is presently being used as a testbed for acquisition controller design. To date LIGO has only built acquisition servos for suspended single Fabry-Perot cavities (LIGO has built acquisition controllers for rigidly mounted coupled cavities but the design is significantly different for a suspended interferometer), so this is the first model for studying the technical challenges of locking an interferometer with coupled degrees of freedom. Presently a straightforward servo design has been shown, in simulation, to lock a coupled cavity interferometer. More investigation is still required to gain a deeper understanding of the important issues in designing feedback controllers for the acquisition of interferometers with coupled degrees of freedom.

R&D FFT Optics Modeling. The effort in Fast Fourier Transform (FFT) optics modeling has been split between refinements of the existing program, and steps toward modeling advanced interferometers. The refinements have been to further automate the optimization procedures, so that all of the parameters which are considered adjustable (lengths, modulation frequencies, and recycling mirror transmission) now can be determined without intervention. Further checks of the consequences of aliasing have led to a more sophisticated filtering procedure. The program is now a useful tool, and has been transferred to the System Integration group for use in the design of the LIGO detector. A model of advanced interferometer configurations, specifically dual-recycled Fabry-Perot Michelsons, has been implemented; modifications to the program to allow the addition of the signal recycling mirror have been developed and debugged.

Work planned for FY 1997

- **40 m Interferometer:**
 - Recombination and Recycling.* Complete the recombination/recycling tests.
 - Suspension Development.* Fabricate and install single-sling suspensions (will take place late in the year) and measure control and noise characteristics (to be completed in parallel with other 40m efforts).
 - Data Acquisition and Analysis.* Continue time-series studies. Address reliability and availability issues for the entire instrument.
- **Phase Noise Demonstration.** Convert the Phase Noise Interferometer to Nd:YAG/1064 nm to be completed early in FY 1997, and characterize the 700 mW prototype laser using the phase-noise testbed.

- Thermal Noise Investigations. Characterize the suspension fibers, attachments, and actuators continuing the close relationship with the suspension tests in the 40m.
- Table-top Interferometer Investigations. Support the Length and Alignment Sensing/Control systems design using table-top techniques on both MIT and Caltech campuses.
- Interferometer Control Modeling. Support the detailed servo design for the Length and Alignment Sensing/Control systems.
- Optical Modeling. Complete the initial round of exploratory optical modeling efforts focusing on how dual recycling can aid in the performance of Fabry-Perot Michelson interferometers.

9.0 LIGO Systems Engineering (WBS 1.4.3)

The LIGO Systems Engineering Group continued to work with the LIGO design groups to ensure that the evolving design and configuration of LIGO is consistent with the scientific requirements of the project. Activities included integration, modeling and simulation. Definition of the LIGO data analysis system requirements has started.

9.1 Integration (WBS 1.4.3.1)

Significant accomplishments during FY 1996

- Identified the requirements for the apertures of the vacuum tube manifold (within the buildings) and gate valve aperture diameter arising from thermal and laser baffling considerations.
- Characterized and selected the BT baffle material and issued a baffle science performance requirements document. The design of the LIGO Beam Tube baffles was completed and responsibility for procurement was transferred to the Facilities Group.
- Designed and completed full-scale mock-ups of the Beam Splitter Chamber (BSC) and the Horizontal Access Module (HAM) chambers to be used for integration planning and assembly jig/fixture design by the detector group.
- Completed the Electromagnetic Interference/Compatibility Plan (EMICP).
- Completed the Beam Tube Bakeout Design Requirements Review. Created the Beam Tube Bakeout Design Requirements Document and Conceptual Design Document
- Completed and released the Reliability Program Plan.
- Developed preliminary drafts of key system-level fault trees. The top level events are the failure to operate in the three LIGO operating modes; single coincidence, double coincidence and triple coincidence. The basic events in the fault tree will identify equipment level failure modes which contribute to the top events. The interferometer fault tree is being developed.
- Completed the Failure Modes, Effects and Criticality Analysis (FMECA) Report for the Vacuum Equipment.
- Completed a draft of the functional FMECA for the Vacuum Control & Monitoring System.
- Prepared and delivered the leak assessment and leak localization software and manuals to CB&I, the beam tube contractor.
- Prepared LIGO global site alignment requirements including the definition of the initial site alignment requirements which in turn included the BT/VE gate valve alignment criteria and the alignment tolerance sensitivity of the LIGO clear aperture.

Discussion of accomplishments and work in progress:

Vacuum tube manifold and gate valve aperture requirements arising from thermal and laser baffling considerations. The current configuration includes 44 inch ID gate valves and allows a two inch (radius) space between the vacuum vessel inside wall and the 1.02 meter clear aperture. Increasing the vessel ID to 48 inch would make a four inch space available to accommodate optical baffling and thermal shielding in the vicinity of the LN₂ pumps and gate valves. The two functions compete with one another, making the space available somewhat more valuable.

The cost of increasing the diameter to 48 inch (both valve and vessel parts) was \$186K. To determine if such an expense is warranted, Systems Engineering studied the integration of the laser light baffling and the infrared shielding in the region around the short cryopumps in the mid- and end-stations (i.e. the locations where it is most difficult to baffle the laser light due to their proximity to the test masses).

The recommendation was to proceed with 44 inch gate valves and vacuum tube. Although this makes it more difficult to implement the integrated baffle-infrared shield design, no serious problems were identified. Responsibility for the detailed implementation of the baffling concept has been transferred to the detector core optics support (COS) task.

Characterization and selection of the BT baffle material. LIGO has completed the specification for the Beam Tube baffles material and is now in the process of procuring baffles. This procurement is a two-step process: mechanical fabrication and surface treatment. This represents the culmination of a year-long trade and design study which was initiated when the decision was made to modify the simpler baseline design for the Beam Tube baffles.

The baffle material is identical to the beamtube: 304L stainless steel (un-oxidized, roughened), approximately one mm in thickness. The baffle form is similar to the VIRGO design: a cylindrical band approximately 15 cm wide which conforms to the inner diameter of the beam tube. To this band, a truncated conical section of material is welded. The conical section protrudes nine cm radially into the beam tube aperture and makes a 35 degree angle with the band. The conical baffle is inclined away from the reflecting surface of the nearest test mass. To mitigate diffraction effects, the inner edge of the conical section is randomly serrated. The conical section surface is roughened (bead blasted) and then glazed with a black glass frit formulation. The optical and vacuum properties appear adequate to meet the LIGO light scattering control requirements.

LIGO global site alignment requirements. Construction is in progress at Hanford, Wa. Each arm has been paved with two concrete slabs approximately 15 cm (six inches) thick and 4.3 m (14 feet) wide, and two km in length. The slabs are segmented by expansion joints. The surfaces of all long slabs are parallel to the top surface of the graded berm and project to a common intersection at the vertex of the "L". The as-built surfaces of these slabs define a plane relative to which the interferometer shall be installed. The long slabs have surface flatness (end-to-end, over four km) of 6.5 mm RMS as measured at intervals of 20 meters along both arms. These results are shown in Figure 22. The precision site surveys and installation of cardinal point benchmarks were completed in the fall, and the results were analyzed using nonlinear regression techniques to find the best fit plane and beam centerlines.

The Beam Tube Modules and Vacuum Equipment chambers are being installed on these slabs and they will be aligned by the contractors fabricating the hardware. LIGO is responsible for providing to the contractors a set of benchmarks along the two arms which will allow them to install and align the hardware.

EMI/EMC Plan Development. The EMI/EMC plan defines an approach to grounding, shielding, bonding and electrical design for the program by calling out relevant design standards and guidelines, as well as defining the basic approach to be taken by LIGO in distributing power and grounds. The EMI/EMC plan scopes the level of activities in design and test; although we used the DOD EMC process as a guide, we tailored it to suit LIGO needs and to ensure that only essential analyses and tests are performed.

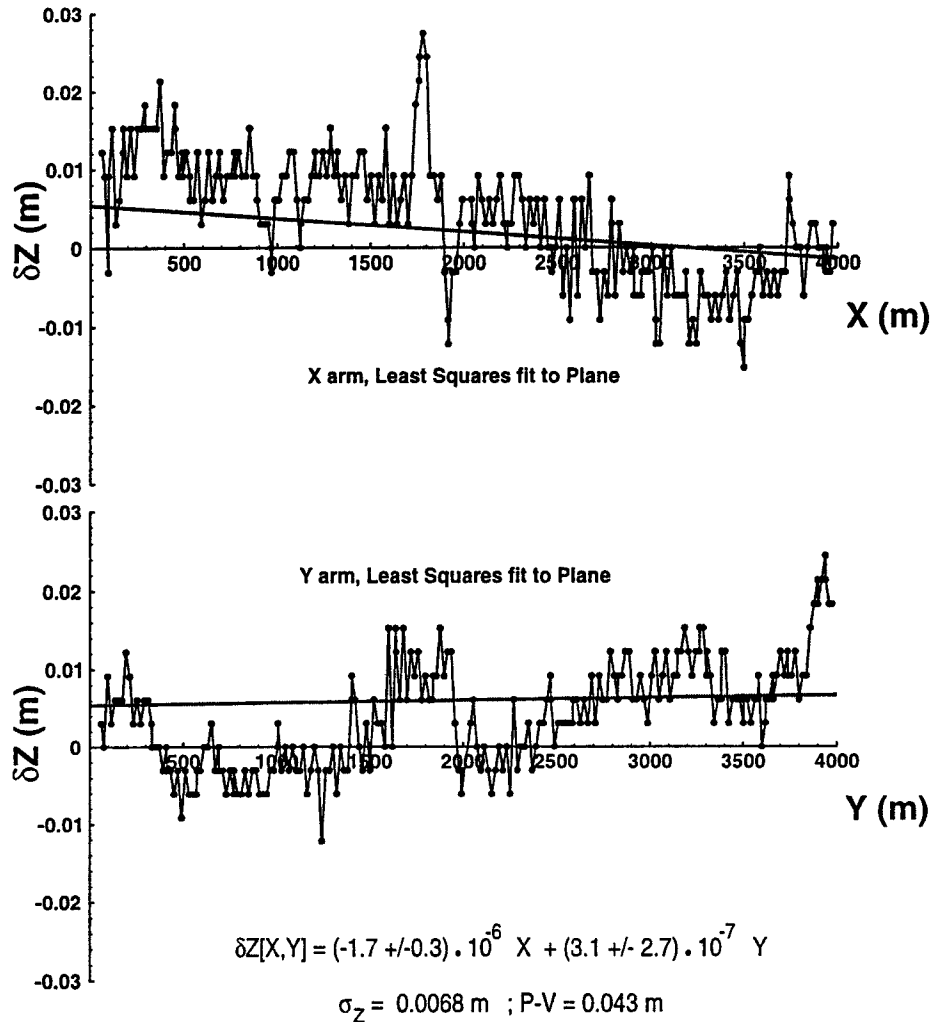


FIGURE 22. Residual errors from initial slab-flatness survey. Measurements made every 20m. Deviations are relative to design plane.

Reliability Plan Development. The Reliability Plan was developed by the Jet Propulsion Laboratory Reliability Group, under the guidance of LIGO System Engineering. The effort began with a review of the LIGO Science Requirements Document as the source of reliability requirements (from a facilities availability perspective).

A draft Reliability Plan has been reviewed by the project and is currently being revised with release scheduled in the next month. Work on the Failure Modes and Effects Criticality Analysis (FMECA) of the Vacuum Equipment System is underway after reviewing the FMECA done by the Vacuum Equipment contractor, PSI. The functional FMECA for the Vacuum Control and Monitoring System has also been started by the Control and Data Systems Group. The top level events in the preliminary system level Fault Tree identified to date are the failure to operate in the three identified operating modes; single coincidence, double coincidence, and triple coincidence. The basic events in the fault tree will identify equipment level failure modes which contribute to the top events

The results of these analyses will be used to develop spares strategies, maintenance strategies, and to perform trade studies on identified weak points of LIGO subsystems to improve their reliability.

Vacuum Compatibility, Cleaning Methods and Procedures for LIGO Instrumentation Materials specification document. Outgassing and contamination potential must be considered and factored into every aspect of interferometer construction, from design and choice of materials through preparation, bakeout, storage and installation procedures as well as during any subsequent handling or adjustment. To insure uniform application of the criteria, a list of vacuum compatibility, cleaning methods and procedures for LIGO instrumentation materials were collected to establish a draft specification. All instrumentation for installation inside LIGO vacuum vessels or tubes must conform to this policy for selection of components and exposed materials and for preparation, handling and storage prior to assembly and during assembly.

The LIGO vacuum compatible materials list has been prepared and approved. This document will be used as a guide by detector system designers. It will be updated as new data become available through planned extensive tests of candidate materials being used by the Detector system. A companion document which defines the procedures and methods to be employed in establishing material compatibility and cleanliness for LIGO is in draft form and is being reviewed by the detector group.

9.2 Modeling and Simulation (WBS 1.4.3.3)

Significant accomplishments during FY 1996

- Performed model comparisons and simulation data exchanges with VIRGO project. During a visit to Europe met with members of the VIRGO project in Annecy, France to discuss modeling and simulation as well as data formats for VIRGO and LIGO data.
- Developed new software for calculating the thermal noise from the internal modes of the test masses. Added four new thermal noise modules to the end-to-end noise modeling software.
- Developed a seismic noise model for LIGO and implemented the model as an end-to-end noise module.
- Performed a detailed analysis of noise propagation in the prestabilized laser system (PSL).
- Defined the top-level optical parameters for the two kilometer interferometer for Hanford, WA.

Discussion of accomplishments and work progress

Noise propagation in the prestabilized laser system. The analytical results of a study on the propagation of frequency, oscillator, and amplitude noise in the prestabilized laser system were refined and incorporated into our dynamic interferometer model. The analytical results and the model agree both in magnitude and in audio frequency dependence.

Support to 40m R&D operations. Three noise modules were developed to calculate contributions from noise sources that play a significant role in the sensitivity of the 40 meter interferometer.

Adjnsn - this module adds the noise contribution due to eddy currents induced in the magnet drive coils to an input amplitude spectral density curve. This eddy current contribution is equivalently thought of as Johnson noise from the magnet drive controller. The model is parameterized by the value of the Johnson noise at 100 Hz.

Adshot - this module adds the noise contribution due to the shot noise equivalent displacement to an input amplitude spectral density curve. The model is parameterized by the noise at 100 Hz and by the corner frequency of the cavity.

Adtmth - this module adds the noise contribution due to elastic vibrational modes in the test mass to an input amplitude spectral density curve. The model is parameterized by the value of the noise due to elastic modes at 100 Hz.

Thermal noise modeling software. An existing Fortran program for calculating the thermal noise associated with the internal modes of the test mass was rewritten in C and made numerically stable by replacing many of the algorithms used to handle calculations of the value of Bessel functions, root solving and the solutions to simultaneous equations of near singular structure. The result was a program that runs to completion without the need for continuous monitoring by the user, and correctly calculates the modal frequencies and the effective mass coefficients used in the determination of the thermal noise. The new code predicts a slightly higher (approximately 10 percent) overall thermal noise from the internal modes of the test masses. Figure 23 is a set of curves for the cumulative contribution to the thermal noise that results from summing up the con-

tributions from each mode. This figure also illustrates the thermal noise sensitivity to the beam spot size and the test mass geometry.

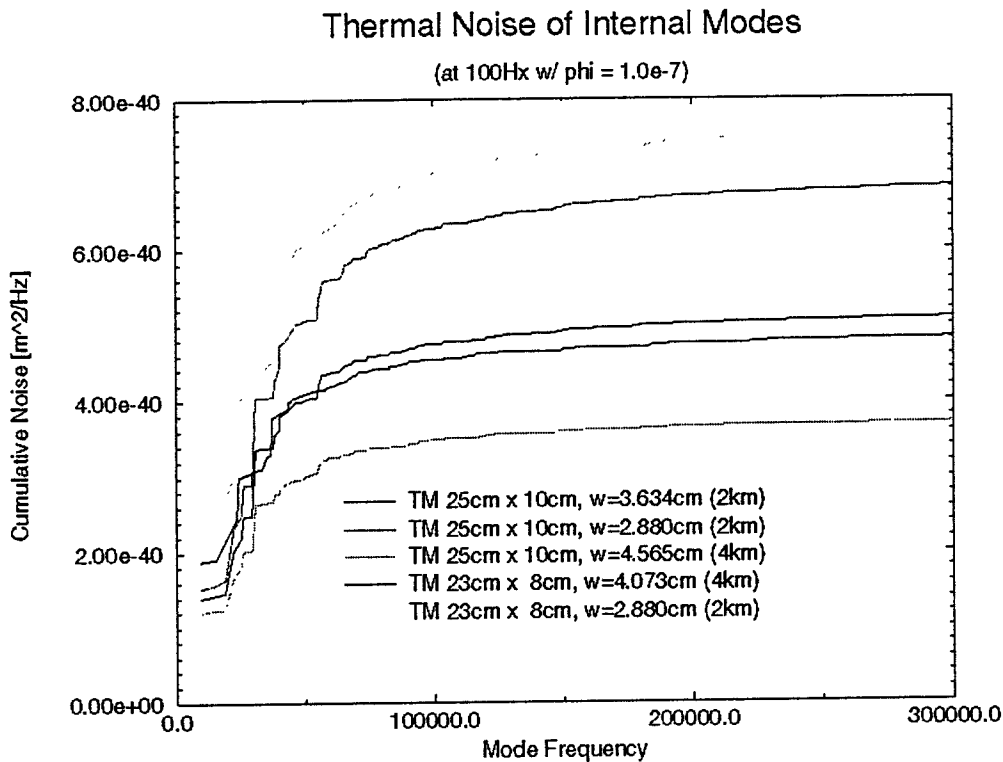


FIGURE 23. Thermal noise of internal modes

End-to-End Noise Module Development. Four new thermal noise source modules were added to the LIGO end-to-end noise model during FY 1996. Three of these modules characterize thermal noise sources found in the suspension system. The fourth is the thermal noise from the internal modes of the test masses discussed above.

Pitch - this module calculates the thermal noise due to the pitch modes of the test masses. Both differential and common modes can be calculated based on the type of suspension model. This allows the module to work equally well for the 40 m interferometer and for the LIGO suspension design.

Yaw - this module calculates the thermal noise due to the yaw modes of the test masses. Both differential and common modes can be calculated based on the type of suspension model. This allows the module to work equally well for the 40 m interferometer and for the LIGO suspension design.

VSpring - this module calculates the thermal noise due to the vertical spring modes of the test mass suspension. The coupling to the displacement noise results from the angle between the local horizon and the beam. By selecting the appropriate parameters the user of this module can model

this contribution to thermal noise in both the 40 m interferometer and in LIGO.

These modules, along with the modules developed specifically for the 40 m noise sources were overlaid with the displacement sensitivity measured in the 40 m interferometer in the fall of 1994 for comparison between measurement and theory. Figure 24 illustrates the agreement between many of these models and their parameters.

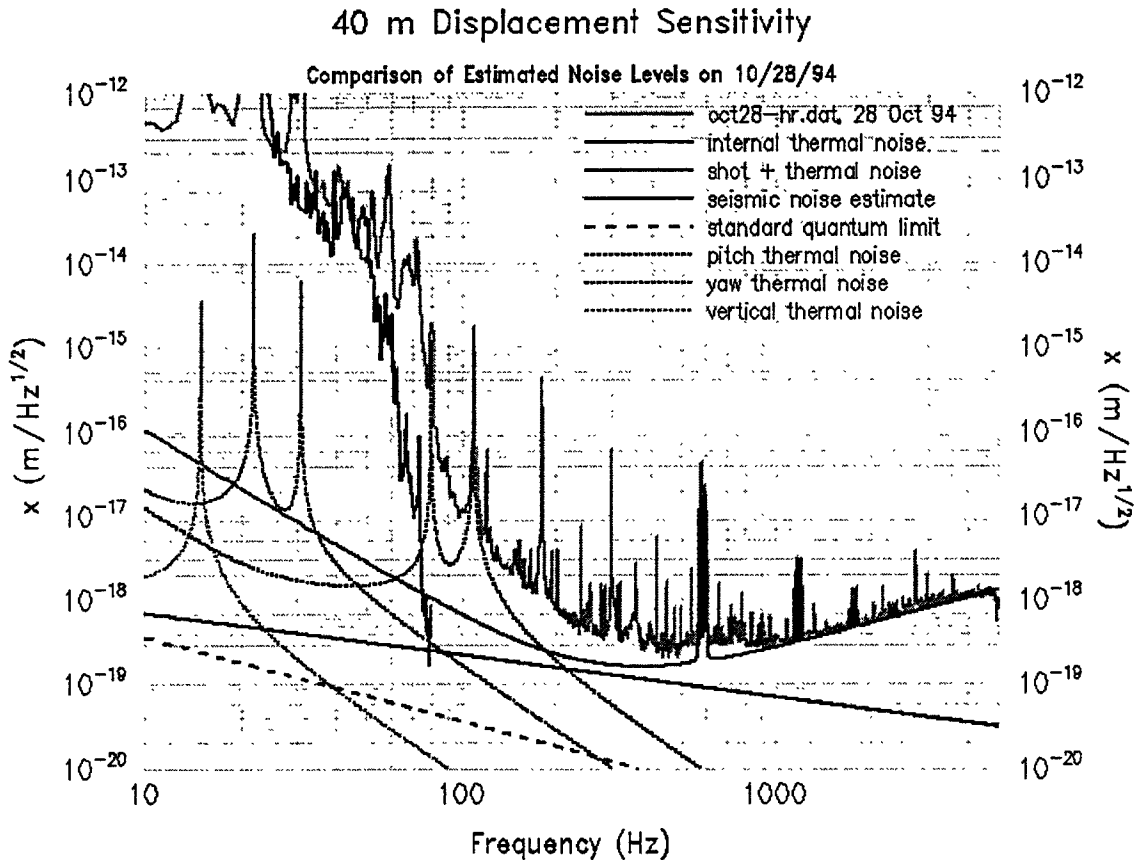


FIGURE 24. 40 m displacement sensitivity

A seismic noise module was developed to calculate the displacement noise sensitivity and was added to the end-to-end noise modeling environment. The model for this noise source utilizes piece-wise continuous fits to the measured ground motion at the Louisiana and Hanford sites, measured two dimensional isolation stack transfer functions and theoretical calculations for the suspension transfer function. The model also includes a transfer for the pitch mode of the stack.

Together these noise models along with the models developed during the past year provide an envelope for the dominant noise sources expected in the LIGO interferometer. These noise sources are statistically combined and shown along with the individual sources in figure WW below. The red curve represents the combined displacement sensitivity from these dominant noise sources. The black curve represents the curve outline from the Science Requirement.

Three noise modules were developed to calculate contributions from noise sources that play a sig-

nificant role in the sensitivity of the initial LIGO detector. They can be used to model 40 m interferometer noise by using appropriate parameter values. By default the values of the parameters in the model correspond to the initial LIGO design. Which has been determined by systems engineering and feed back to the modeling group.

TopPlate - this module calculates the thermal noise associated with the top plate of the isolation stack based on the mass, temperature, resonance frequency and Q of the top plate and the coupling through the suspension to the test masses.

RadPress - this module calculates the displacement noise associated with the radiation pressure force fluctuation on the test masses in a recycled interferometer.

GravGrad - this module calculates the seismic gravity gradient noise based on the theory of Rayleigh and Love waves. Separate transfer functions are used to model the differences in stratification between the Hanford, WA. site and the Livingston LA. site. The user can select the ground spectrum which most closely characterizes the site.

ResidGas - this module calculates the phase induced displacement noise due to the residual gases found in the vacuum of the interferometer. The model calculates contributions from any of H₂, H₂O, N₂, O₂, CO, CO₂, CH₄ and a user specified hydrocarbon based on partial pressures and susceptibility to being polarized for the individual gas species.

Quantum - this module calculates the quantum limited noise due to optimal laser power in the interferometer having test masses of mass m.

These noise models together with the models developed during the past year provide an envelope for the dominant noise sources expected in the LIGO interferometer. These noise sources are statistically combined and shown along with the individual sources in Figure 25.

Core Optics Coating Uniformity Assessment. REO provided an anti-reflective coating (SiO₂ and Ta₂O₅ on the SiO₂ surface) on a nine inch mirror. This coating was designed so that the thickness variation can be determined very accurately. From the first measurement using 12 degree incident angle P and S polarized light, the thicknesses of the two layers turned out to be ten percent different from design values. The phase map variation was calculated from the deduced thicknesses. The phase variation due to the coating turned out to be several times worse than the requirement.

A second run of coatings was obtained from REO. The calculated thicknesses showed large curvature. The high frequency component of the thickness non-uniformity of the Ta₂O₅ was of the order of 0.02 percent, which is the required limit to satisfy the non-uniformity of the phase map with an RMS of $\lambda/800$. The measurement error of the SiO₂ was 0.1 percent, due to the original design, and the roughness was consistent with this uncertainty. The conclusion was that REO will be able to successfully provide the initial LIGO coatings.

Modeling of angular degrees of freedom for interferometers. A consultant to LIGO (Dr. Raymond Beausoleil) is developing a time domain model of the LIGO interferometer, including the length and alignment degrees of freedom. This model is crucial for both the Length Sensing Control and the Alignment Sensing Control systems. In October, Dr. Beausoleil delivered the first

Initial LIGO Noise Curves

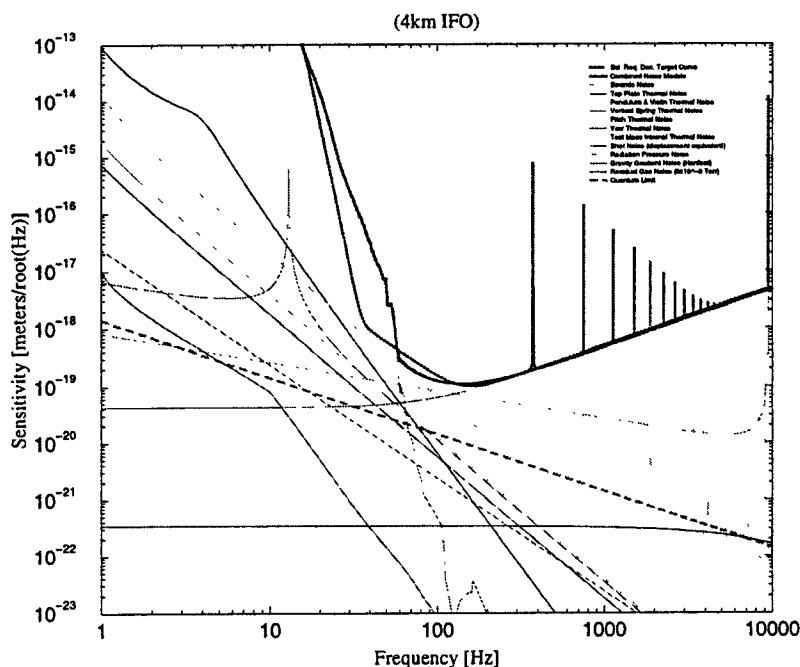


FIGURE 25. Latest estimate for noise in the initial LIGO

code, modeling a single Fabry-Perot cavity with length and angle degrees of freedom. There was a meeting in November to discuss the interface of this code and the LIGO control system. This work will be completed in the spring of 1997.

Data Analysis Activities. Prof. B. Allen (U. of Wisconsin, Milwaukee) is visiting the group this year and has contributed significantly to LIGO data analysis activities.

A review paper describing known mechanisms for stochastic background production and methods of detection was finished and will be published by Cambridge University Press as part of a Les Houches volume. This is the most comprehensive and complete article to date on this subject.

A paper examining the detectability of stochastic background produced by "stringy inflation" (an early universe model) was written in collaboration with Brustein and has just been accepted for publication in Physical Review.

A new paper containing a number of new results is in preparation with Dr. Romano, a post doctoral scholar at Milwaukee. The results include:

- a new Signal/Noise formula obtained without small signal approximations,
- sensitivity limits for LIGO enhanced detector curves,
- detailed results comparing the data-analysis pipeline described below to theoretical expectations (agreement to better than 2% was ultimately obtained),
- sensitivity limit predictions for correlating European and US interferometer sites,

- detailed limits on the correlated noise requirements that would permit useful stochastic background detection experiments using the 2km and 4 km detectors at the Hanford site.

A data analysis pipeline has been completed and is working properly on simulated data. Simulated detector signals (in the presence of a stochastic background) are produced using a new technique that guarantees the correct second-order statistics. The results of the simulation and data-analysis pipeline agree with what is expected theoretically from the optimal signal analysis. The final problem (contamination of the correlation due to side lobes of the windowing function) was recently solved and the data-analysis pipeline now gives results from monte-carlo testing which are in better than two percent agreement with theory.

This signal simulation and data analysis library is now complete, and is being incorporated into the growing software library and documentation.

Work is also ongoing to develop a data analysis package called GRASP (Gravitational Radiation Analysis and Simulation Package). This is a C-language object library of functions, together with documentation and source code. These functions are designed to allow analysis of interferometer data using the standard and specialized techniques described in the literature. The package can be used to compare new data analysis techniques with existing ones, and to study behavior of data analysis algorithms on simulated noise or on real interferometer output. It can also be used to study such practical issues, such as the choice of whitening filters, the effect of non-linear elements in the detector transfer function, effects of quantization noise in the analog to digital conversion, etc.

At the moment, the GRASP package contains libraries of routines to:

- Search for binary inspiral using matched filtering (including routines to optimally place templates in parameter space)
- Search for a stochastic background using detector cross-correlation (including routines to generate/inject a simulated stochastic background, to generate simulated detector noise, and to construct optimal filters for arbitrary detector networks)
- Read, calibrate, and de-whiten data CIT 40-meter data taken in Nov 1994.

Additional libraries that will be added in the future include:

- Time-frequency methods
- Searching for continuous-wave sources
- Matched filtering to look for the quasi-stable modes associated with black-hole formation.
- I/O libraries to allow easy access to data from the new "FRAME" format and from the PEM systems.

The goal for GRASP to provide tools (1) for studying data analysis issues and performing benchmarks with "real world data"; (2) for the comparison of different data analysis techniques, and (3) to serve as a prototype for construction of the full-scale LIGO data analysis system.

Data Analysis System Prototyping Activities. During FY 1996 Caltech submitted a proposal to IBM for a parallel computing equipment hardware grant under the Sponsored University

Research (SUR) program. LIGO personnel visited IBM's Watson Research Center to form several potential collaborations with scientists and engineers where overlap in research offered the most benefit to both groups. The award to Caltech amounted to approximately \$800,000 in SP2 parallel computing equipment. This represents a major success for LIGO and Caltech at a strategic time for the development of a data analysis system to prototype LIGO-like data analysis. Caltech is expecting delivery of the SP2 hardware in the first week of January. At that time LIGO will begin to test the performance of the processors and to determine how the parallel architecture scales to larger systems using the MPI (Message Passing Interface) environment.

The SUR equipment grant will be used to expand an existing SP2 parallel computing system at the CACR (Center for Advanced Computing Research) located on the Caltech campus from its current configuration of seven SP2 nodes to a configuration with 12 nodes.

10.0 Support Services

10.1 Quality Assurance (WBS 1.4.2.1)

Work accomplished during FY 1996

- Preparation of the first draft of the LIGO QA Plan was completed.

Discussion of accomplishments and work in progress

During the 1996 fiscal year, a full time LIGO Quality Assurance Officer was provided by the Jet Propulsion Laboratory [JPL]. In addition, the LIGO QA Officer arranged and coordinated supplementary workforce as needed, from the JPL Quality Assurance and Fabrication Services sections. This workforce was used to assist in QA monitoring of beam tube material processing at various vendors, participation in design and other technical reviews and review/critique of LIGO contract proposals and contractor documentation.

Considerable LIGO QA support was provided to the Facilities Group during this FY year with particular emphasis on the beam tube baffle coating process development and production monitoring. QA monitoring/auditing of the large gate valve and beam tube expansion joint vendors was performed. LIGO QA also prepared process flow charts and monitoring check lists for use by the site personnel.

Preliminary QA planning and implementation discussions were also initiated with the LIGO Detector Optics Group. QA requirements for contractor plans and deliverables, QA receiving inspection and acceptance guidelines/QA procedures were also formulated.

The LIGO QA Plan draft was completed, distributed for comments and prepared for approval and release in FY 1997.

Work planned for FY 1997

During FY 1997, the Jet Propulsion Laboratory (JPL) will continue to support the LIGO project team in the development and implementation of the product assurance and safety programs. This support will be provided by the JPL Office of Engineering and Mission Assurance [OEMA] and includes support from the OEMA Quality Assurance, Reliability Engineering, System Safety, and Mission Assurance organizations. To assure that LIGO mission objectives are met, JPL OEMA QA organization will:

- Continue to provide QA oversight, in the preparation, review, and approval of LIGO and contractor plans and procedures, including workmanship standards, and acceptance processes.
- Release the approved LIGO QA Plan.
- Perform periodic review and audit of contractor and LIGO QA/QC programs.
- Coordinate and arrange for supplemental JPL QA work force as required for QA monitoring and acceptance activities and for other LIGO support.

10.2 Environmental Safety and Health (WBS 1.4.2.2)

Work accomplished during FY 1996

- The Environment Safety & Health office was established and safety program direction was outlined in the LIGO Safety Plan that was accepted during November 1995 providing the project safety parameters with all safety documents identified.
- The Laser Safety Program was established that defined LIGO policies (baseline eye checks - 40 accomplished, laser operation procedures, Laser Safety Officers, etc.) and training. Various training videos and documents were procured to provide a minimum of four safety training classes (50+ personnel trained) for the LIGO laser workers and operators.
- Accomplished a special safety study defining the Beam Tube Enclosure as a confined space thus saving considerable R&D and operational funds that would have been required to meet occupancy space environments.
- Reviewed various LIGO contractors safety programs and work procedures to assure that they are responsible for their workers safety and that they are oriented for prevention of construction injuries and loss of hardware that would translate into schedule variance. All reviewed contractors have established excellent safety programs and their programs have been accepted.
- Started the operational hazard analysis of the LIGO system that will assure that the system will perform without injury, loss of life, or loss of valuable equipment. A special safety review committee was formed to assure that the safety program was on track.

Discussion of accomplishments and work in progress

The Safety Office was established and staffed during September 1995 and has continued to support LIGO through 1996. During 1996 the Laser Safety Plan has been completed along with the procurement of training videos and documents to provide safety information for LIGO laser personnel. The Laser Safety Program conducted five training classes and is currently providing individual training, as required. The training of LIGO personnel, more than 50 to date, along with registration of personnel that will work around LIGO lasers has included a medical clearance (eye check) to verify that the individual may perform duties in the LIGO laser facilities. Parts of the Laser Safety Program are still in the start-up phase i.e. generation of Safety Standard Operating Procedures that will become the basis for the Laser Safety Program at the observatory facilities. Other parts of the program are mature and will continue to monitor laser operations to assure compliance with OSHA safety requirements and the application of optimal approaches for applying the ANSI Z136.1-1993 to LIGO.

A special safety study was completed which defined both the Beam Tube Enclosure and Beam Tube as a confined space with initial entry into this space requiring a Permit Entry Procedure. This area is expected to be entered very few times during the operational year and thus could afford the minimal extra operational costs of confined space permit entry procedure requirements. Assisted Caltech Safety in updating and republishing the Confined Space Safety Plan that LIGO will use as the bases to meet OSHA requirements. This

plan is available to all LIGO personnel on the Internet web and provides all requirements to establish proper training, operational, and permit entry procedures. This procedure requires checks to assure that the area is safe to be down-graded to a non-permit confined space for continuing operations in these areas. This study was coordinated with the U.S. Department of Labor Occupational Safety and Health Administration, regions 10 and 6, which are the two regions responsible for the LIGO observatories. Acceptance for this type of operation has been provided by the OSHA regional safety engineers as meeting the personnel protection requirements. This activity was closed when LIGO Safety accepted the revised Caltech Confined Space Safety Plan. Using this plan as the source document CB&I provided information that ensured that the Beam Tube fabrication and installation on site was compliant with OSHA and LIGO safety requirements.

During the year the Safety Program identified eight top-level hazards that will be monitored and controlled before the observatories can be operational. In addition, PSI, the Vacuum Equipment manufacturer, provided an analysis that identifies and recommends methods to control Vacuum Equipment hazards. These two analyses comprised the initial hazard identification effort that was the subject of a review, accomplished September 25, 1996. The review was conducted at the request of Dr. Gary Sanders (LIGO Project Manager) and Mr. Ben Lucas (LIGO Safety Officer). The review committee members were: Mr. Tom Beat, Lawrence Livermore Laboratory; Mr. Larry Combes, Jet Propulsion Laboratory; and Dr. Rich Orr, former Fermilab Tevatron Project Leader (Chairman). In addition, ten members of the LIGO project team participated in the review. The committee concentrated on the LIGO hazard reports, the PSI vacuum system hazard report, the LIGO Project System Safety Plan, and the LIGO Laser Safety Program. The committee found that the hazard reports reviewed were generally correct and complete. They were particularly impressed with the LIGO Project Safety Plan, the LIGO Laser Safety Program, and the Hazards Analysis for LIGO Vacuum Equipment. The committee suggested additions to the hazard analyses which have been accepted and incorporated into the analysis. The committee was pleased to find that the people interviewed during this review were knowledgeable regarding all aspects of the project. There is clearly excellent communication and little compartmentalization. These are attributes which contribute strongly to safe and successful operation. An additional finding was that the Environmental Safety and Health Officer appears to have sufficient access to the Project Manager as well as the authority to carry out his responsibilities. Although much safety work remains to be done, it is being conducted in a professional manner with direct participation by the LIGO physicists and engineers. A final observation of the committee was that LIGO Safety has made every effort to conform to local, state, and federal regulations. Where more than one regulation covers a situation, the more conservative (usually an OSHA) rule has been followed. The committee did provide a recommendation that as the safety program continues to evolve that a final readiness review be held from the viewpoint of safety before operations begin. The results of this review was presented to the NSF during the Semi-annual Review.

Work planned for FY 1997

During FY 1997, JPL Safety will continue to support the LIGO project team and to assure that LIGO mission objectives are met, JPL OEMA Safety organization will:

- Continue to provide Safety oversight, in the preparation, review and approval of LIGO and contractor safety plans and procedures.
- Continue with Laser Safety training both, initial and recurring. Provide the project with a personnel certification program that will furnish listing and control for approved laser operators and workers. Assist with the establishment of laser operational procedures and follow-up that the procedures are in use or revised for usability.
- Continue safety inspections in support of Caltech safety to assure that Caltech located labs are in compliance with Caltech safety requirements. Establish a safety level of support to assure that Caltech and OSHA safety requirements are met at the observatory sites.
- Continue with the LIGO hazard analysis to include establishing a safety review team (individuals to be external to LIGO project) to evaluate the adequacy of the analysis and assure that any unidentified hazards are not unnoticed.

11.0 REFERENCES

1. Cooperative Agreement No. PHY-9210038 between the National Science Foundation, Washington, DC 20550 and the California Institute of Technology, Pasadena, CA 91125, May 1992.
2. *The Construction, Operation, and Supporting Research and Development of a Laser Interferometer Gravitational-Wave Observatory*, proposal submitted to the National Science Foundation, December 1989.
3. *Technical Supplement to the LIGO Construction Proposal (1989)*, dated May 1993.
4. *LIGO Project Management Plan*, LIGO-M950001, Revision B, April 24, 1996.
5. *LIGO Cost Book*, dated September, 1994.
6. *LIGO Supplement for Installation, Commissioning and Operations*, LIGO-M950039, August 1995.
7. Cooperative Agreement No. PHY-9210038 between the National Science Foundation, Washington, DC 20550 and the California Institute of Technology, Pasadena, CA 91125, Amendment No. 5, April 20, 1995.
8. Cooperative Agreement No. PHY-9210038 between the National Science Foundation, Washington, DC 20550 and the California Institute of Technology, Pasadena, CA 91125, Amendment No. 11, August 23, 1996.
9. Report of the Panel on the Use of the Laser Interferometer Gravitational Wave Observatory, Boyce McDaniel, Chair, United States National Science Foundation, June, 1996.

DRAFT

Quarterly Report
(December 1996 through February 1997)

The Construction, Operation, and Supporting Research
and Development of a Laser Interferometer Gravitational-
Wave Observatory (LIGO)
NSF Cooperative Agreement No. PHY-9210038

March 1997

DRAFT

Table of Contents

1.0	Introduction.....	1
2.0	Executive Summary	3
2.1	Project Milestones	6
2.2	Financial Status	7
2.3	Performance Status (Comparison to Project Baseline)	7
2.4	Change Control and Contingency Analysis	13
2.5	Staffing	13
3.0	Vacuum Equipment (WBS 1.1.1)	14
4.0	Beam Tube (WBS 1.1.2).....	17
5.0	Beam Tube Enclosure (WBS 1.1.3).....	19
6.0	Civil Construction (WBS 1.1.4).....	22
7.0	Detector (WBS 1.2)	26
7.1	Suspensions and Isolation	26
7.2	Lasers and Optics	27
7.3	Interferometer Sensing/Control.....	29
7.4	Detector System Engineering/Integration	30
7.5	Control and Data Systems (CDS) Activities (WBS 1.2.2).....	30
7.6	Physics Environment Monitor (WBS 1.2.3)	31
7.7	Support Equipment (WBS 1.2.4)	32
8.0	Research and Development (WBS 1.3)	33
9.0	Systems Engineering (WBS 1.4.3)	35
9.1	Integration (WBS 1.4.3.1).....	35
9.2	Simulation, Modeling and Data Analysis	37
10.0	Support Services	41
10.1	Quality Assurance (WBS 1.4.2.1).....	41
10.2	Environmental Safety and Health (WBS 1.4.2.2)	42
11.0	LIGO Visitor's Program.....	44
12.0	References.....	46

List of Figures

FIGURE 1.	Costs and Commitments as a Function of Time (End of February 1997)	9
FIGURE 2.	Cost Schedule Status Report (CSSR) for the End of February 1997.....	10
FIGURE 3.	LIGO Project Budget, Earned Value, and Actual Costs as a Function of Time	11
FIGURE 4.	LIGO Staffing History since January 1995.....	13
FIGURE 5.	Horizontal Access Module Chamber.	14
FIGURE 6.	HAM Chamber with Doors.....	15
FIGURE 7.	Production Beam Splitter Chambers at PSI.....	15
FIGURE 8.	80K Pump Reservoirs	16
FIGURE 9.	Welding a Flange onto a Spool.	16
FIGURE 10.	Aerial view of X Arm Beam Tube Installation.....	18
FIGURE 11.	Areas of Glass Shedding near Baffle Serrations.....	18
FIGURE 12.	Delivery and Installation of the Beam Tube Enclosure Segments along the Northwest Arm at Hanford site.....	19
FIGURE 13.	Installation of Beam Tube Enclosure Segments closely following the installation of the Beam Tube.....	20
FIGURE 14.	View of Corner Station at the Hanford Site.	21
FIGURE 15.	View of LVEA at Hanford	22
FIGURE 16.	View of Mid Station on Southwest Arm at the Hanford Site.	23
FIGURE 17.	View of End Station on Southwest Arm at the Hanford Site.....	23
FIGURE 18.	Excavation for the Foundation for the End Station on Southeast Arm at the Livingston Site.	24

List of Tables

TABLE 1. Status of Significant Facility Milestones6
TABLE 2. Status of Significant Detector Milestones.....7
TABLE 3. Costs and Commitments as of the End of February 19978
TABLE 4. Approved Change Requests13

Quarterly Report

(December 1996 - February 1997)

THE CONSTRUCTION, OPERATION, AND SUPPORTING RESEARCH AND DEVELOPMENT OF A LASER INTERFEROMETER GRAVITATIONAL-WAVE OBSERVATORY (LIGO)

NSF COOPERATIVE AGREEMENT No. PHY-9210038

March 1997

CALIFORNIA INSTITUTE OF TECHNOLOGY

This Quarterly Report is submitted under NSF Cooperative Agreement PHY-9210038¹. The report summarizes Laser Interferometer Gravitational-Wave Observatory (LIGO) Project activities from December 1, 1996 through February 28, 1997.

1.0 Introduction

The Laser Interferometer Gravitational-Wave Observatory (LIGO) Project will open the field of gravitational-wave astrophysics through the direct detection of gravitational waves. LIGO detectors will use laser interferometry to measure the distortions of the space between free masses induced by passing gravitational waves. The design, construction, and operation of LIGO is being carried out by scientists, engineers, and staff at the California Institute of Technology (Caltech) and the Massachusetts Institute of Technology (MIT). Caltech has prime responsibility for the project under the terms of the Cooperative Agreement¹ with the National Science Foundation (NSF). LIGO will become a national facility for gravitational-wave research, providing opportunities for the broader scientific community to participate in detector development, observations and data analysis. LIGO welcomes the participation of outside scientists at any of these levels. The initial LIGO facility will comprise one three-interferometer detector system. The site allows for expansion of the facility to a multiple-detector configuration to enable simultaneous use by several gravitational-wave detectors.

The LIGO Project was described in the LIGO Proposal² submitted to NSF in December 1989, and the Technical Supplement³ submitted to NSF in May 1993. Project organization is described in the LIGO Project Management Plan⁴. The cost of the construction activities for the observatory facilities and the initial detector equipment was presented in the LIGO Cost Book⁵, which was reviewed in September, 1994.

This quarterly report covers activities accomplished during the first quarter of the sixth year (LIGO fiscal year 1997) of the Design and Construction Phase of the LIGO Project, and the related Research and Development. This phase includes facility construction, support equipment acquisition, initial interferometer design and fabrication, and the concurrent research to refine the initial detectors and data algorithms. LIGO Design/Construction began December 1, 1991 as defined in the Cooperative Agreement and will end with the acceptance of the vacuum systems at both sites and completion of the fabrication of the third interferometer.

2.0 Executive Summary

The project continues to make excellent progress. The project is 45 percent complete. The rate of accomplishment, as measured by our Performance Measurement tracking systems, has accelerated to reflect the effort in active subcontracts with a total contract value in excess of \$120 million.

The first meeting of the LIGO Program Advisory Committee (PAC) was held at Caltech in January 1997. The LIGO PAC is the principal advisory group to the LIGO Management. The committee will meet approximately twice a year and will give advice on policy, management, and technical issues. The PAC will review all aspects of the program regularly, including LIGO related research by outside groups. Some of this work may be done by subcommittees, which can include outside members. The committee will assist LIGO in giving NSF input on LIGO related issues.

A proposal for the Advanced R&D to begin in FY 1997 has been submitted to the NSF.

Facilities. The activities of the Facilities Group continued to expand during the first quarter of 1997 due to the commencement of building and infrastructure construction on the Louisiana site. Woodrow Wilson Construction Co. (Baton Rouge, LA) began site road work and preparation for placement of the slabs along both arms of the interferometer. Hensel Phelps Construction Co. (Little Rock, AK) has begun excavation of the building foundations in preparation for building erection. Two LIGO personnel (Gerry Stapfer and Allen Sibley) are now resident on the Livingston site along with Parsons Construction Management personnel to oversee this activity. This work is proceeding on schedule.

In Washington, over three quarters of the beam tube sections comprising the northwest arm of the interferometer have been installed and individually leak tested. Fabrication of the beam tubes in the Chicago Bridge and Iron (CB&I) factory in Pasco, WA is running slightly ahead of schedule, with more than 250 beam tubes fabricated out of 400 needed for the entire Hanford site. Field installation work is running 3-4 weeks behind schedule due to start up problems encountered last fall that have since been resolved. CB&I is rapidly recovering schedule. Most recently, they have been installing beam tubes at 140-160% of the anticipated production rate, narrowing the 5-6 week schedule delay that existed at the beginning of the quarter to its present level. It is anticipated that CB&I will complete beam tube fabrication and installation activities on the Hanford site on schedule.

Civil construction at the Washington site has been delayed 28 days relative to the planned schedule due to a series of weather related delays. We expect that this will cause some realignment of the Process Systems International (PSI) schedule for installation of vacuum equipment in the mid- and end-stations of the northwest arm.

PSI began production fabrication of the large vacuum vessels and spool pieces needed for the Hanford site. Three beam splitter chambers and one horizontal access module have been completely assembled and are being readied for bake and final vacuum test. Large gate valves required for termination of the beam tubes (an overdue item last quarter) have been delivered to the site. PSI is proceeding on schedule.

Beam Tube Baffles. A problem with beam tube baffles was recognized early in the installation process when glass particles (from the porcelain coating) were found at the base of the baffles in the beam tube after baffle installation. The source of the problem was traced to a previously unrecognized high-stress region in the porcelain coating near the base of the baffle serrations. The problem was exacerbated by the unseasonably cold weather experienced at Hanford early in the year. Installation of the furfuraeous baffles was suspended and a tiger team was assigned to investigate the cause of the problem and develop corrective action. The investigations cover rework of existing porcelain-coated baffles, design and/or manufacturing process changes to eliminate the problem in future production, and development of a porcelain-free backup solution (with reduced technical performance). In addition, a plan was developed to permit continued installation of beam tube without baffles with baffle installation deferred until Fall '97 or Winter '97/'98 to allow time for the investigations to yield a technically adequate solution.

Detector. The seismic isolation preliminary design (carried out by Hytec, Inc.) was completed, and several prototypes of constrained-layer-damped springs are in testing. The first prototype Small Optics Suspension is in test in the 40-meter interferometer, and tests on a Large Optics Suspension are also underway.

The first blanks for the Core Optics have been delivered to the polishing vendors, and the first coating on a full size optic has been applied to one of the Pathfinder test masses. A pre-stabilized laser for R&D use has been delivered to the Phase Noise Interferometer, and the information is being incorporated into the Pre-Stabilized Laser subsystem design activity. Core Optics Support has made significant strides in the development of requirements and conceptual designs for the relay optics and internal anti-scatter baffling.

The Detector Subsystems Requirements Review was held this quarter, establishing the baseline requirements for the initial detector design. The optical layout advanced to the point of delivering critical wedge angles and distances needed for subsystems designs.

The Control and Data System activities included the start of fabrication of the first deliverable hardware, the racks for the Vacuum Controls, following the Final Design Review held in January. A prototype data acquisition system with LIGO-standard hardware and software has been configured and successfully bench tested; it will be installed in the 40-meter interferometer for further tests. Support for R&D tasks, in particular the 40-meter and Phase Noise Interferometer, continued.

The Phase Noise Interferometer work using the Argon laser source was completed, with a well-understood noise spectrum. The conversion to the Nd:YAG 1064 nm wavelength is underway. The physical re-configuration of the 40-meter interferometer for recycling has been completed as well.

Reviews. A semi-annual review of LIGO was conducted on behalf of NSF on October 22-24, 1996 at Caltech. The focus of this review was on technical progress and plans. Comments received from the committee were favorable. The next semi-annual review, which will also focus on the technical status of the project, is scheduled for April 15-17, 1997. There will be a visit to the Hanford site by a subset of the review committee on April 13 and 14.

Aspen Winter Conference. The Aspen Winter Conference on Gravitational Waves and their Detection, held during the week of January 27-31, 1997 was an Advanced Detector Workshop. There were several scheduled and impromptu meetings during the Workshop to facilitate consolidation of the collaborative R&D plans.

Visitor's Program. An active visitors program is being developed, roughly equivalent to three full-time equivalents (FTEs) each year (more during later years) with the participants involved in research for periods of six months or longer.

LIGO Collaboration. The University of Florida has submitted a proposal that would establish a LIGO Collaboration for the design and fabrication of the Input Optics (part of the Input/Output Optics Subsystem) in support of the initial LIGO Detector development and construction. A subcontract was awarded in November 1996 to initiate the design effort. The University of Florida proposal and modifications to the subcontract for continued effort are currently being considered by NSF.

The Input Optics provide the interface between the laser and the interferometer including mode cleaning and mode matching to the core optics, frequency modulation of the carrier, and additional frequency stabilization of the laser. The Input Optics design effort consists of design requirements definition (completed), conceptual design development (in progress), and experimental and analytical verification of design parameters and preparation of final design documentation for IOO fabrication.

The preliminary designs of the RF Modulation Subsystem, the Mode Cleaner Subsystem, and the Telescope/Beam Steering Optics Subsystem will be completed next quarter.

2.1 Project Milestones

The status of the significant milestones identified in the Project Management Plan (PMP) for the LIGO Facilities is summarized in Table 1. Contracts to begin Slab Construction and Building Construction on the Livingston, Louisiana site were awarded in December 1996 to Woodrow Wilson and Hensel Phelps respectively.

TABLE 1. Status of Significant Facility Milestones

Milestone Description	Project Management Plan Date ^a		Actual (A)/Projected (P) Completion Date	
	Washington	Louisiana	Washington	Louisiana
Initiate Site Development	03/94	08/95	03/94 (A)	06/95 (A)
Beam Tube Final Design Review	04/94		04/94 (A)	
Select A/E Contractor	11/94		11/94 (A)	
Complete Beam Tube Qualification Test	02/95		04/95 (A)	
Select Vacuum Equipment Contractor	03/95		07/95 (A)	
Complete Performance Measurement Baseline	04/95		04/95 (A)	
Initiate Beam Tube Fabrication	10/95		12/95(A)	
Initiate Slab Construction	10/95	01/97	02/96 (A)	12/96 (A)
Initiate Building Construction	06/96	01/97	07/96 (A)	12/96 (A)
Accept Tubes and Covers	03/98	03/99	03/98 (P)	03/99 (P)
Joint Occupancy	09/97	03/98	09/97 (P)	03/98 (P)
Beneficial Occupancy	03/98	09/98	03/98 (P)	09/98 (P)
Accept Vacuum Equipment	03/98	09/98	03/98 (P)	09/98 (P)
Initiate Facility Shakedown	03/98	03/99	03/98 (P)	03/99 (P)

a. Project Management Plan, Revision B, LIGO-M950001-B-M approved by NSF in October 1996

Table 2 shows the status of the significant milestones for the Detector. The projected completion date for the *Core Optics Support Final Design Review* is now June 1997 (vs. April 1997). However, the current plan simplifies the subsequent fabrication effort so the overall schedule for installing the interferometers is not affected.

As of the end of February 1997, all significant project milestones can be achieved.

TABLE 2. Status of Significant Detector Milestones

Milestone Description	Project Management Plan Date		Actual (A)/Projected (P) Completion Date	
	Washington	Louisiana	Washington	Louisiana
BSC Stack Final Design Review	07/97		07/97 (P)	
Core Optics Support Final Design Review	04/97		06/97 (P)	
HAM Seismic Isolation Final Design Review	07/97		07/97 (P)	
Core Optics Components Final Design Review	07/97		07/97 (P)	
Detector System Preliminary Design Review	12/97		12/97 (P)	
I/O Optics Final Design Review	04/98		04/98 (P)	
Prestabilized Laser Final Design Review	08/98		08/98 (P)	
CDS Networking Systems Ready for Installation	09/97		09/97 (P)	
Alignment (Wavefront) Final Design Review	04/98		04/98 (P)	
CDS DAQ Final Design Review	04/98		04/98 (P)	
Length Sensing/Control Final Design Review	05/98		05/98 (P)	
Physics Environment Monitoring Final Design Review	06/98		06/98 (P)	
Initiate Interferometer Installation	07/98	01/99	07/98 (P)	01/99 (P)
Begin Coincidence Tests	12/00		12/00 (P)	

2.2 Financial Status

Table 3 summarizes costs and commitments as of the end of February 1997. Figure 1 on page 9 shows the costs and commitments as a function of time.

2.3 Performance Status (Comparison to Project Baseline)

Figure 2 on page 10 is a Cost Schedule Status Report (CSSR) for the end of February. The CSSR shows the time-phased budget to date, the earned value, and the actual costs through the end of the month for the NSF reporting levels of the WBS. The schedule variance is equal to the difference between the budget-to-date and the earned value and represents a “dollar” measure of the ahead (positive) or behind (negative) schedule position. The cost variance is equal to the difference between the earned value and the actual costs. In this case a negative result indicates an overrun. Figure 3 shows the same information as a function of time for the LIGO Project.

TABLE 3. Costs and Commitments as of the End of February 1997

WBS	Description	Costs				Cumulative Costs	Open Commitments	Total Cost Plus Commit- ments
		Thru Nov 1996	Dec-96	Jan-97	Feb-97			
1.1.1	Vacuum Equipment	21,254	869	43	44	22,210	22,662	44,872
1.1.2	Beam Tube	17,262	107	3,427	1,260	22,057	35,292	57,349
1.1.3	Beam Tube Enclosure	6,237	251	459	247	7,195	12,269	19,465
1.1.4	Civil Construction	14,117	1,665	1,567	1,474	18,822	30,239	49,061
1.2	Detector	6,270	478	281	762	7,791	6,014	13,805
1.3	R&D	16,816	272	153	420	17,661	1,229	18,890
1.4	Project Management	16,288	457	411	583	17,740	1,964	19,704
	Unassigned (See Note)	2	(1)	-	1	2	131	132
TOTAL		98,246	4,098	6,342	4,791	113,477	109,800	223,277
Cumulative Actual Costs		98,246	102,344	108,686	113,477			
Open Commitments		91,492	113,149	112,583	109,800			
Total Costs Plus Commitments		189,738	215,493	221,269	223,277			
NSF Funding		208,468	208,468	265,389	265,389			

Note: "Unassigned costs" have not been assigned to specific LIGO Work Breakdown Structure element, but are continually reviewed to assure proper allocation.

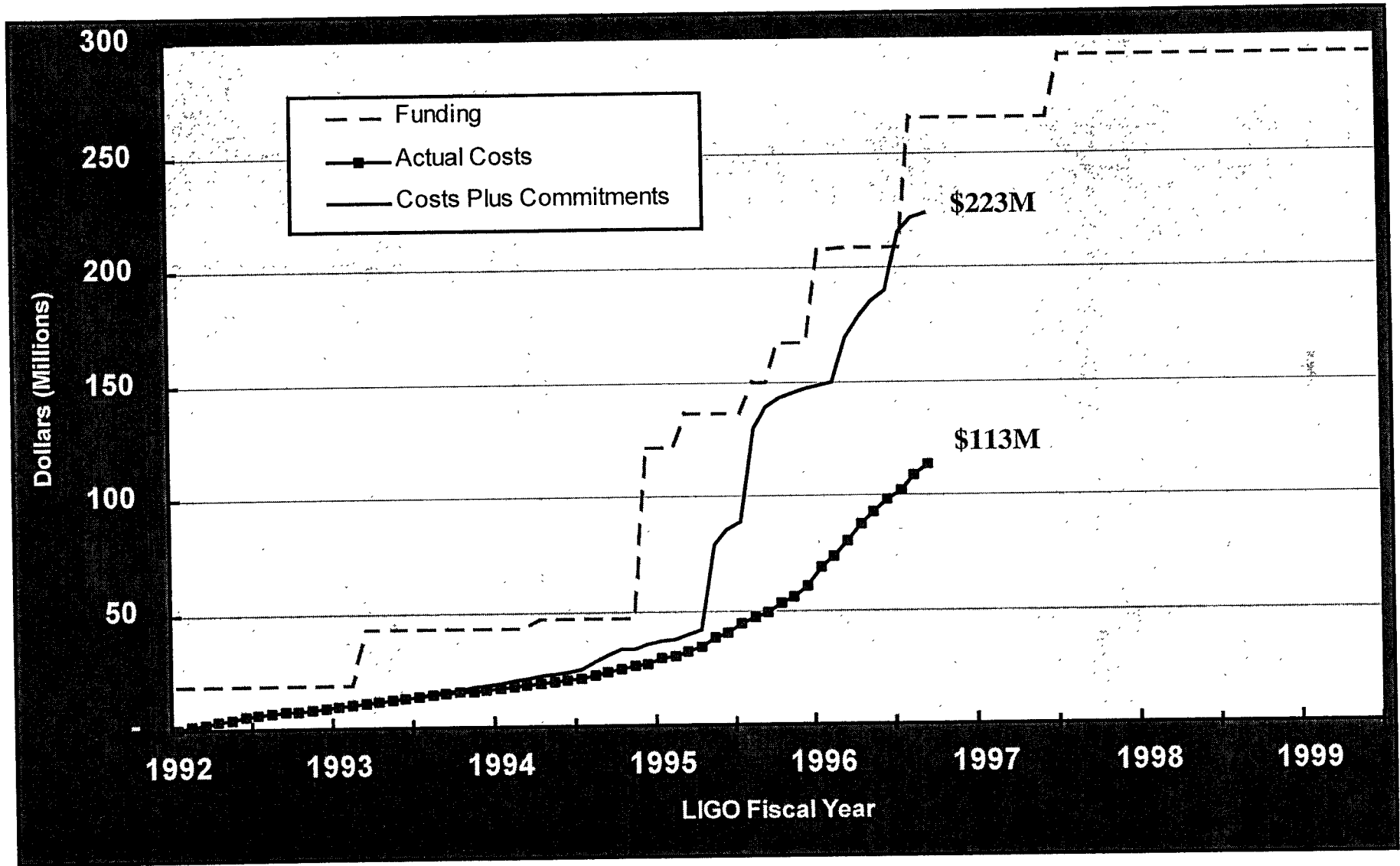












FIGURE 1. Costs and Commitments as a Function of Time (End of February 1997)

Run Date: 26MAR97		COST / SCHEDULE STATUS REPORT (CSSR)				Page 1		
CONTRACTOR: Caltech		CONTRACT NUMBER:	CONTRACT BUDGET	REPORTING PERIOD:	PROJECT FILE NAME:			
LOCATION: Pasadena, CA		PHY-9210038	BASELINE	31JAN97-28FEB97	LIGO Master Merged PMB - WBS 1.0			
PERFORMANCE DATA (K\$s)								
REPORTING LEVEL	CUMULATIVE TO DATE					AT COMPLETION		
MPR LEVEL	BUDGETED COST		ACTUAL COST	VARIANCE		BUDGET (BAC)	ESTIMATE (EAC)	VARIANCE (6-7)
	WORK SCHEDULED	WORK PERFORMED	WORK PERFORMED	SCHEDULE (2-1)	COST (2-3)			
	(1)	(2)	(3)	(4)	(5)	(6)	(7)	(8)
1.1.1 : Vacuum Equipment	23580	23423	22210	(157)	1213	42113	42113	0
1.1.2 : Beam Tubes	20527	22282	22057	1755	226	47298	47298	0
1.1.3 : Beam Tube Enclosur	8641	8151	7195	(490)	956	19384	19384	0
1.1.4 : Facility Design &	18548	19589	18822	1042	767	48311	48311	0
1.2 : Detector	10327	8928	7753	(1399)	1175	52567	53336	(769)
1.3 : Research & Developme	18429	18121	17661	(309)	460	23490	23490	0
1.4 : Project Office	17844	17844	17740	0	104	27074	27074	0
SUBTOTAL	117896	118338	113437	441	4901	260238	261007	(769)
CONTINGENCY						0	31087	(31087)
MANAGEMENT RESERVE						0	0	0
TOTAL	117896	118338	113437	441	4901	260238	292094	(31856)

COBRA (R) by WST Corp.

FIGURE 2. Cost Schedule Status Report (CSSR) for the End of February 1997

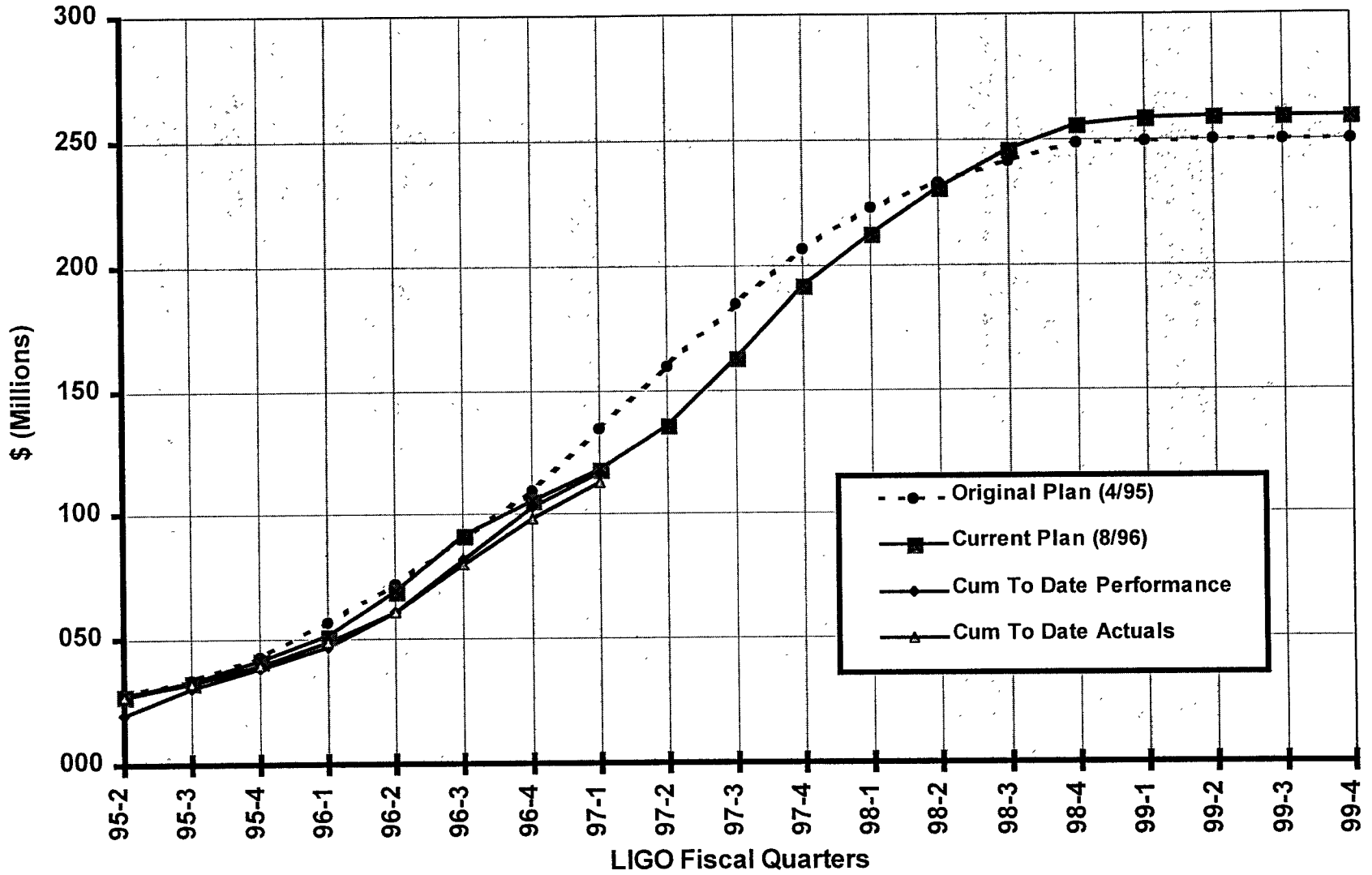


FIGURE 3. LIGO Project Budget, Earned Value, and Actual Costs as a Function of Time

Vacuum Equipment. Vacuum Equipment (WBS 1.1.1) shows a favorable cost variance primarily due to the delays in the processes of invoicing and payment which will not translate into a projected underrun at the end of the project. Efforts during FY 1996 to expedite payments have reduced this effect. Vacuum Equipment is slightly behind schedule. A large number of components have been fabricated but are waiting to be cleaned and tested.

Beam Tube. The favorable schedule variance in the Beam Tube (WBS 1.1.2) reflects purchases of stainless steel that were advanced to take advantage of favorable prices and which offset a behind schedule position in beam tube installation.

Beam Tube Enclosure. The Beam Tube Enclosure (BTE) (WBS 1.1.3) started behind schedule due to a late start by CB&I installing the Beam Tube. In addition there have been weather delays caused by high winds during the winter season that preclude crane operations. However Levernier, the contractor responsible for BTE installation, is installing at rates up to 35 Beam Tube Enclosures per day enabling them to regain schedule.

The favorable cost variance reflects normal delays in processing invoices.

Civil Construction. (WBS 1.1.4) Favorable cost and schedule variances are reported. Actually there have been some delays in Washington on the critical path because the planned supplier for the siding for the buildings is no longer providing the required materials. New suppliers are being sought.

New schedules have been developed based on detailed plans provided by the subcontractors selected in Louisiana, and these new schedules will be incorporated into the LIGO baseline during March.

The favorable cost variance reflects normal delays in processing invoices.

Detector. The Detector (WBS 1.2) is behind schedule and under cost. LIGO has been attempting to hire additional staff, but this has not been accomplished quickly enough to avoid some delays. In addition personnel have been diverted to the R&D tasks. It will be noted that a year ago the R&D effort was approximately six months behind relative to the plan proposed in September 1994, but that during the past year the status of these R&D tasks has improved dramatically. Priorities are being set to assure that all critical milestones will be met.

Specific tasks that are behind schedule include:

- The laser is behind relative to the internal LIGO plan. However, this reflects the fact that the vendor's plan included a longer time for development and a correspondingly shorter time for production.
- A behind schedule position in the Seismic Isolation task is due to explorations of alternative metal springs that are outside of the original scope of work. It is anticipated that schedule will be recovered during fabrication.
- Budget is not adequate for the Length Sensing Control (LSC) effort, and this is being addressed through the change control process.

2.4 Change Control and Contingency Analysis

One Change Requests (CRs) in Table 4 was approved during the first quarter of FY 1997. The change request was approved with a not-to-exceed cost of \$150,000 and will be entered into the baseline when actual costs can be determined. The current contingency pool is \$31.9 million.

TABLE 4. Approved Change Requests

Change Request No.	Description	Date Approved	Allocated From/(To) Contingency
CR-970003	WBS 1.1.4 Civil Construction - Air ducts, manufacturing processes and specifications	February 13, 1997	See text

2.5 Staffing

The LIGO staff currently numbers 104 (full time equivalent). Of these, 21 are contract employees. Eighty-seven LIGO staff are affiliated with CIT including four graduate students. Seventeen are located at MIT including three graduate students. Of these, six are now located at the Hanford, Washington site, and three are located in Livingston, Louisiana.

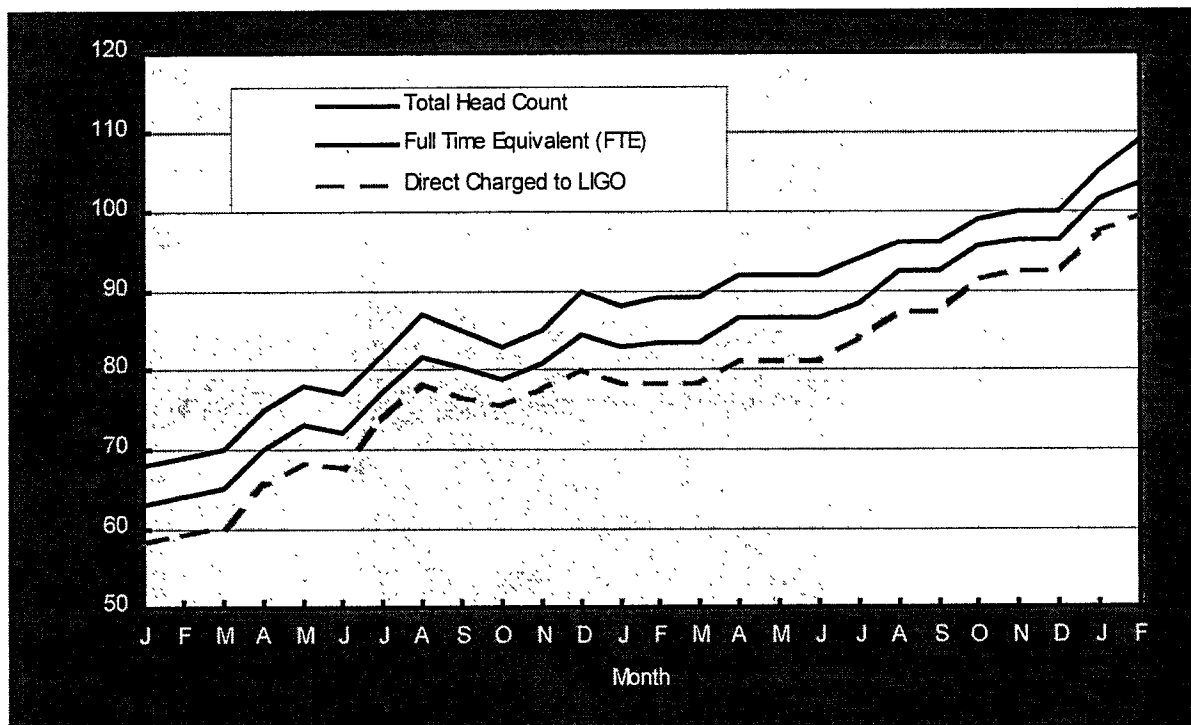


FIGURE 4. LIGO Staffing History since January 1995

3.0 Vacuum Equipment (WBS 1.1.1)

Significant accomplishments during this quarter

- Mechanical completion of first Horizontal Access Modules.
- Receipt of first two production Beam Splitter Chambers from RANOR.
- Completed and tested short 80k pump reservoirs.
- Complete delivery of large GNB gate valves for the Beam Tube contractor.
- Received first bids from potential installation contractors.
- Receipt of first purge air supplies.
- Receipt of all production quantity stainless steel material.
- Receipt of all small ion pumps.
- Start fabrication of small gate valves.

In December 1996 Process Systems International (PSI) issued the Washington installation bid package. A bidders meeting was held in Richland, Washington to answer questions and to allow the bidders to view the site. PSI plans to select a contractor in April 1997.

The first Horizontal Access Module (HAM) chamber was mechanically completed in January and has now been cleaned. The chamber is assembled in the clean room facility at PSI to be baked and vacuum tested. Figure 5 and Figure 6 show the HAM chamber during assembly in the clean room.

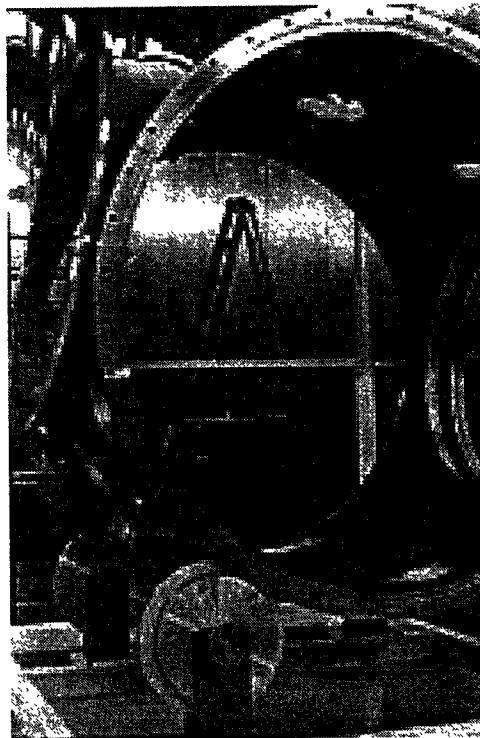


FIGURE 5. Horizontal Access Module Chamber.

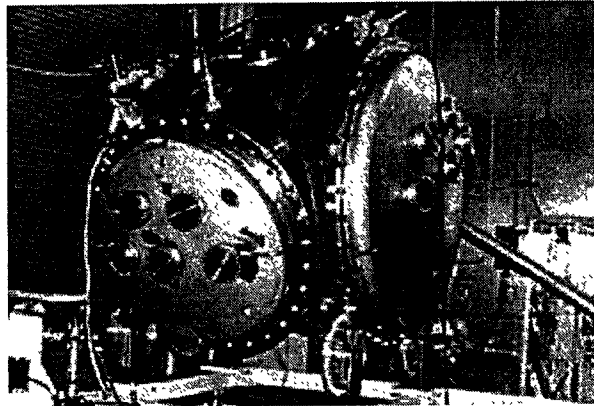


FIGURE 6. HAM Chamber with Doors.

PSI now has on hand three production Beam Splitter Chambers (BSCs). RANOR has recently begun work on the Louisiana BSCs well ahead of the planned start date of June 1997. Figure 7 shows two production BSCs at the PSI facility ready for cleaning and final assembly.

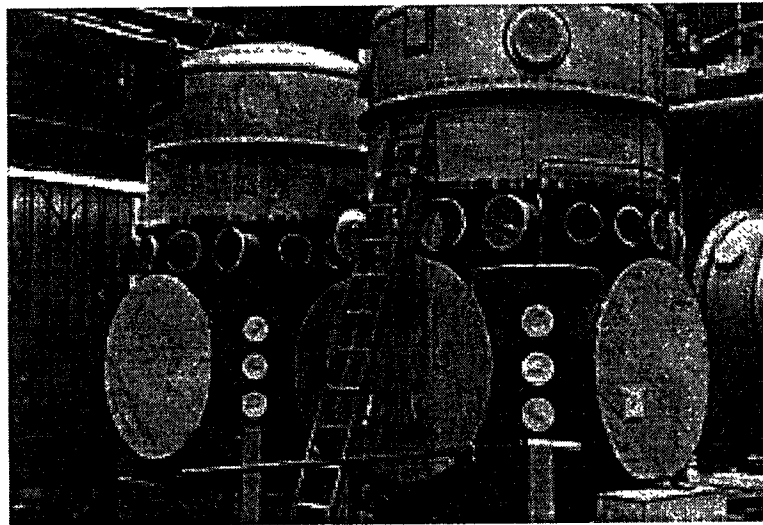


FIGURE 7. Production Beam Splitter Chambers at PSI.

During this quarter PSI has completed and tested three 80K pump reservoirs. Figure 8 shows two of the reservoirs. During this period PSI has also completed fabrication of many spool pieces. Figure 9 shows a flange being welded to a bellows unit in the spool fixture.

The work to be accomplished during the next quarter includes:

- Select the installation contractor for the Washington site.

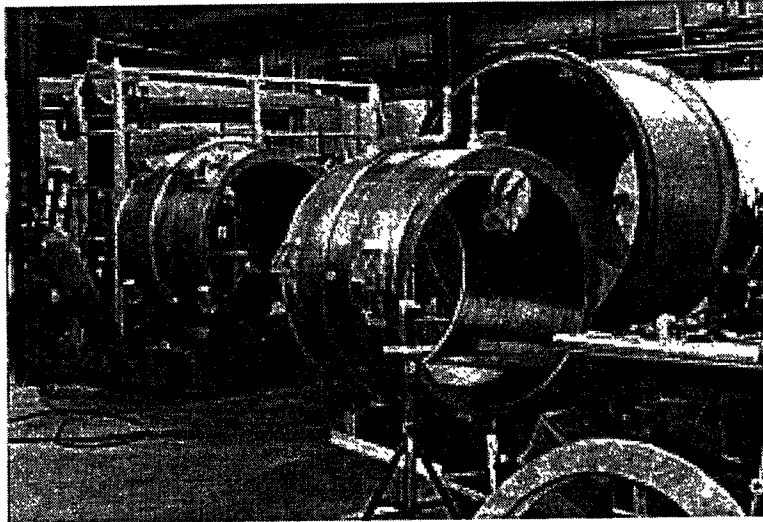


FIGURE 8. 80K Pump Reservoirs

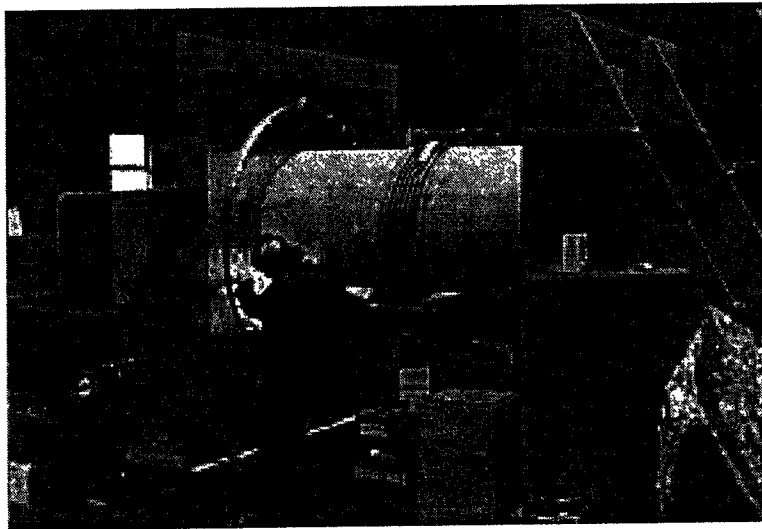


FIGURE 9. Welding a Flange onto a Spool.

- Receive the first production bakeout blankets.
- Commission the PSI hot air bakeout system.
- Perform bakeout and vacuum testing on production chambers.
- Begin fabrication of the large liquid nitrogen dewars for Washington.

4.0 Beam Tube (WBS 1.1.2)

Significant accomplishments during this quarter

- 225 of the 400 tube sections required for the Hanford site were fabricated and leak checked.
- 154 tube sections were installed and leak checked at the Hanford site (as of March 13).
- A facility was leased for fabricating beam tube sections in the Livingston, LA area.

Discussion of accomplishments and work in progress

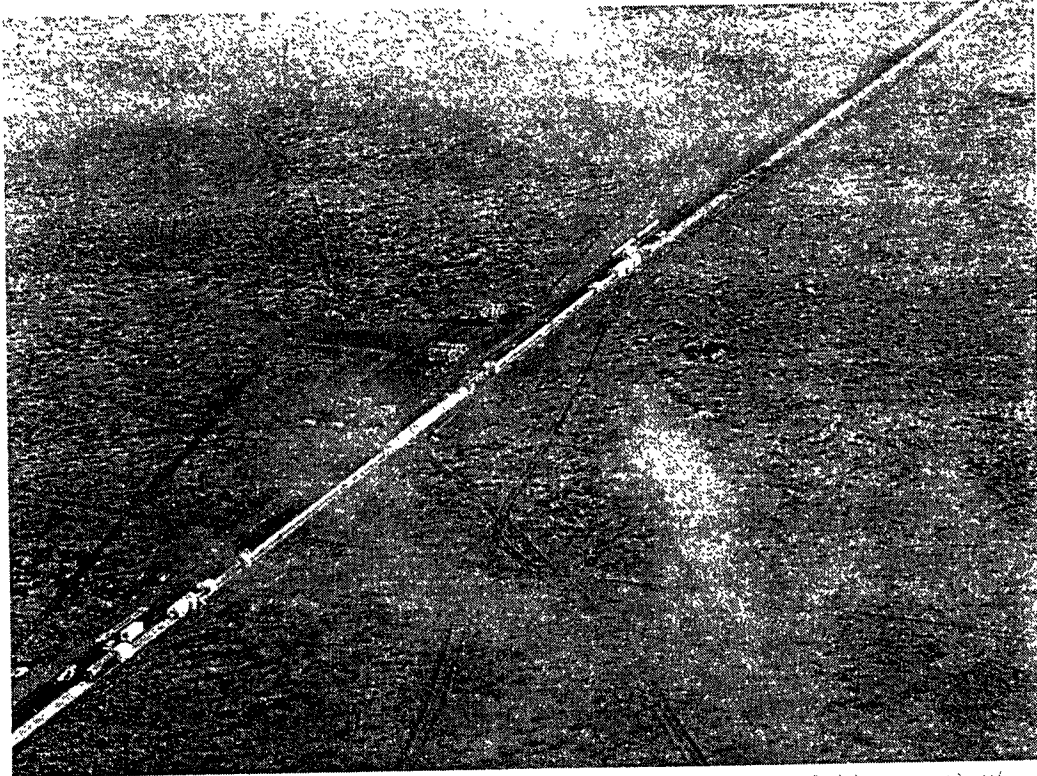
Coil processing continued, with favorable low hydrogen outgassing readings. Both tube section leak checks (fabrication shop) and girth seam leak checks (installation site) have continued to be 100% leak free.

After a slow start due to weather and normal start-up problems, the tube section installation rate has now exceeded plan by 30%, and completion of installation of beam tube modules on the first (X) arm is expected to be one month late. The contractor, Chicago Bridge & Iron (CB&I), expects to finish the Hanford site on schedule.

An inspection of installed tube revealed that some of the installed baffles are shedding glass shards at a rate that would threaten interferometer measurements. Baffle production and installation were placed on hold, and actions were taken to better understand the problem and to develop a solution. Both baffles with improved glass coatings and baffles without glass are being considered, and tests are being developed to give assurance of coating integrity. Currently installed baffles will be replaced, and plans are being formulated for installing baffles deeply into the modules.

Work planned to be accomplished during the next quarter:

- 87% of the beam tube sections for Hanford will be fabricated.
- Installation of beam tube sections for the first arm at Hanford will be completed.
- Acceptance testing of the first module will begin.
- The investigation for understanding baffle glass shedding will be completed. The choices for repair/new manufacture of baffles will be narrowed.



5/16/93 11:11 AM

FIGURE 10. Aerial view of X Arm Beam Tube Installation.

5/16-28374K

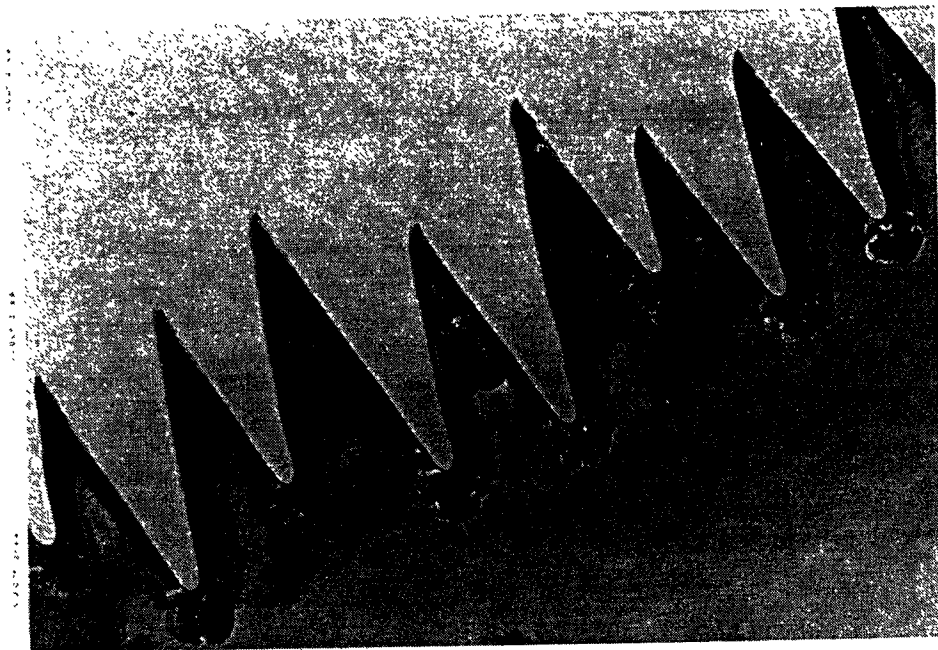


FIGURE 11. Areas of Glass Shedding near Baffle Serrations

5.0 Beam Tube Enclosure (WBS 1.1.3)

Significant accomplishments during this quarter:

- Reached the 90% completion level of precast fabrication of the beam tube enclosure segments for the Hanford site.
- Completed the construction contract documents for the Site Work and Precast Fabrication and Installation of the beam tube enclosure for the Livingston site.
- Started the construction of the service roads, fabrication and installation of the beam tube enclosures at the Livingston site.

Discussion of accomplishments and work in progress

G970040-18-O-P

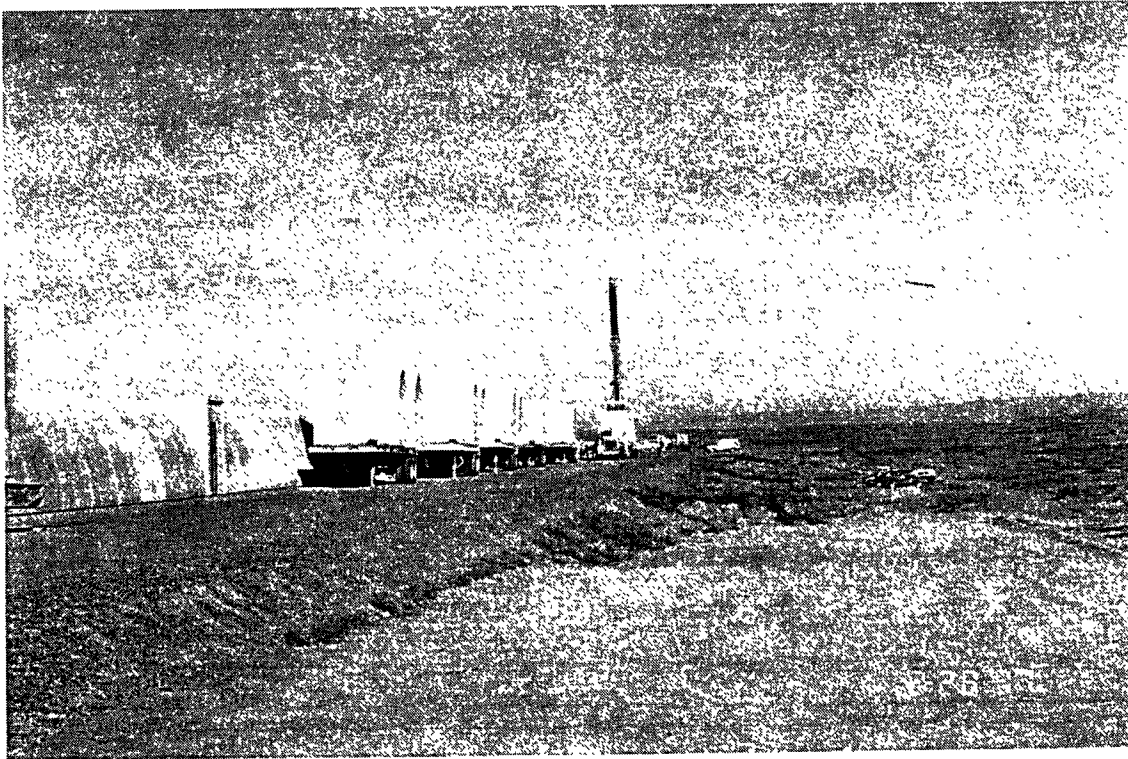


FIGURE 12. Delivery and Installation of the Beam Tube Enclosure Segments along the Northwest Arm at Hanford site.

Hanford Site. Construction of the beam tube enclosures proceeded on schedule and it reached the 90% completion level by the end of this period. This included the completion of both service roads, beam tube enclosure slabs for the both arms and pre-casting of about 2,300 enclosure segments (each 10ft long). Installation of the beam tube segments followed the installation of the beam tube s and about 100 segments were placed successfully during this period (Figure 13).

Livingston Site. The Parsons I &T, the A-E contractor, completed the construction documents for Building and Site Work and Precast Fabrication and Installation for the beam tube enclosure con-

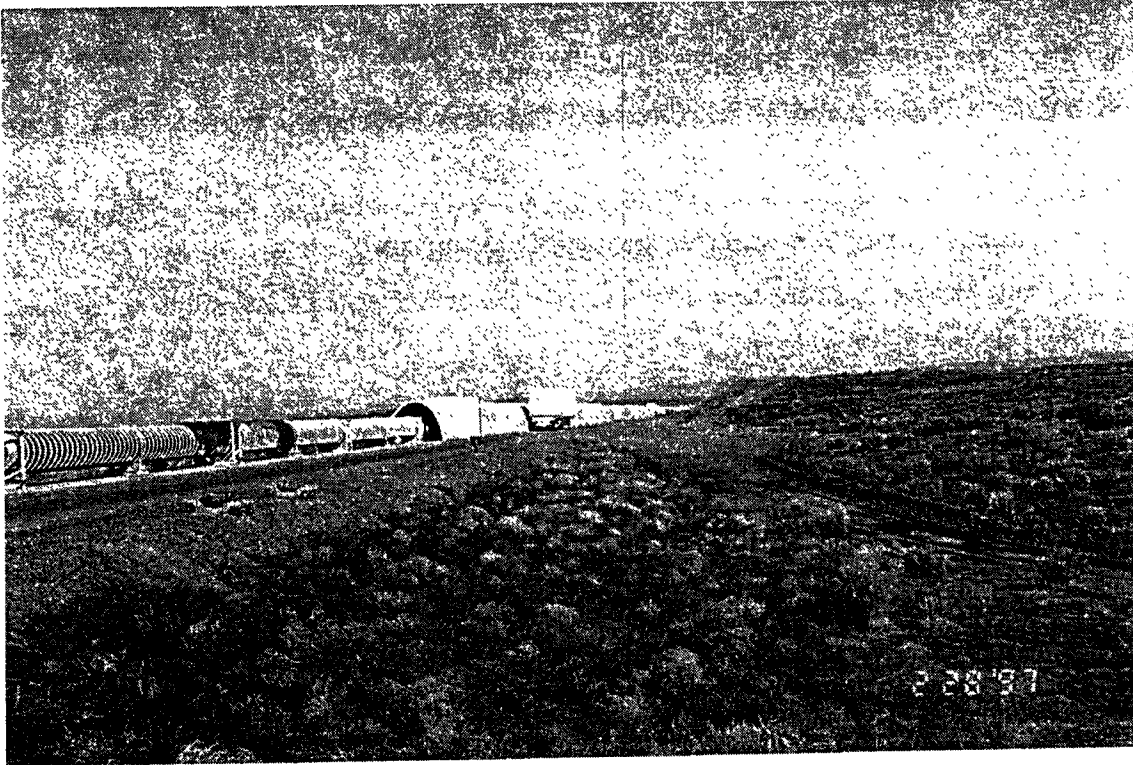


FIGURE 13. Installation of Beam Tube Enclosure Segments closely following the installation of the Beam Tube.

tract. Notice to proceed for this contract was issued to Woodrow Wilson Construction Company. The LIGO and Parsons' construction management office was set up and the construction work began on the service road along southeast arm.

Work planned to be accomplished next quarter

- Complete the precast fabrication of the beam tube enclosure segments for the Hanford site.
- Complete the installation of the beam tube enclosure segments on the northwest arm of the LIGO Hanford site.
- Start the precast fabrication of the beam tube enclosure segments for the Livingston site.
- Submit and obtain the approvals of shop drawings for the beam tube enclosure contract for the Livingston site.
- Complete the finish grading and subbase preparation along both arms at the Livingston site.

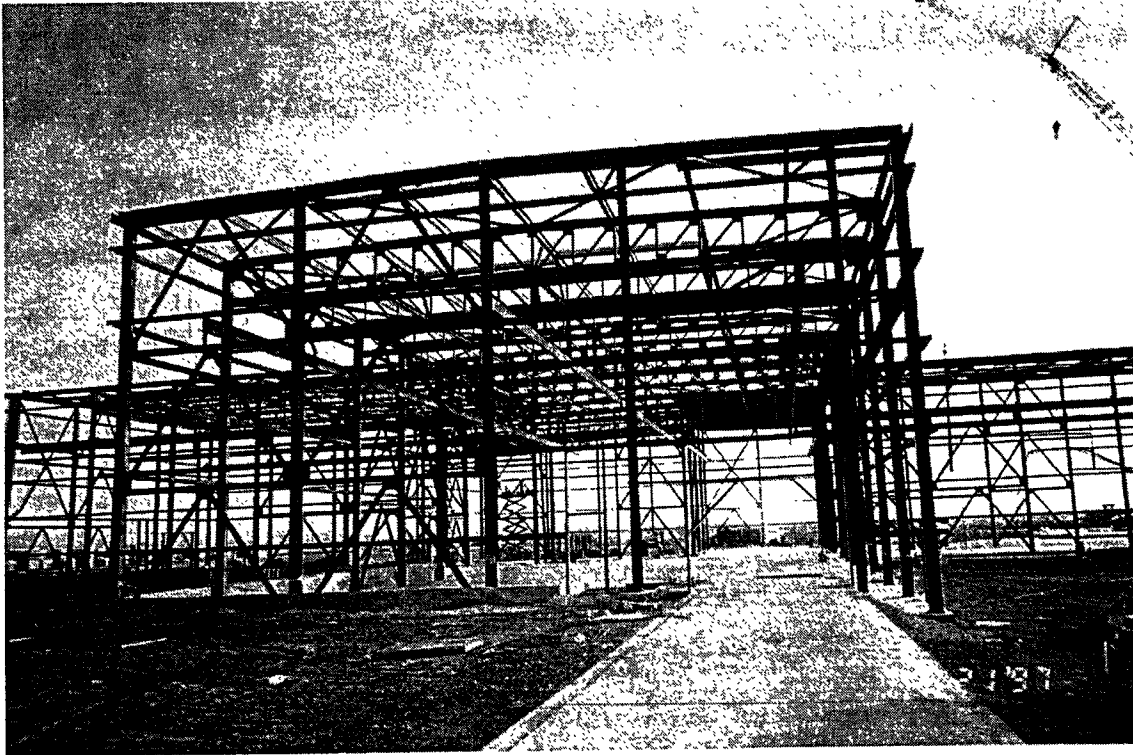


FIGURE 14. View of Corner Station at the Hanford Site.

6.0 Civil Construction (WBS 1.1.4)

Significant accomplishments during this quarter:

- Completed the construction contract documents for the Building and Infrastructure for the Livingston site.
- Started the construction activities for the Buildings and Infrastructure at the Livingston site.
- Reached the 30 percent completion level for construction of the buildings and infrastructure at the Hanford site.
- Awarded the contract for the Surveying Support for the Livingston site to Simmons J. Barry & Associates.
- Awarded the contract for the Quality Assurance, Testing and Reporting for the Livingston site to Delta Testing and Inspection, Inc.

Discussion of accomplishments and work in progress

G970036-01-O-P

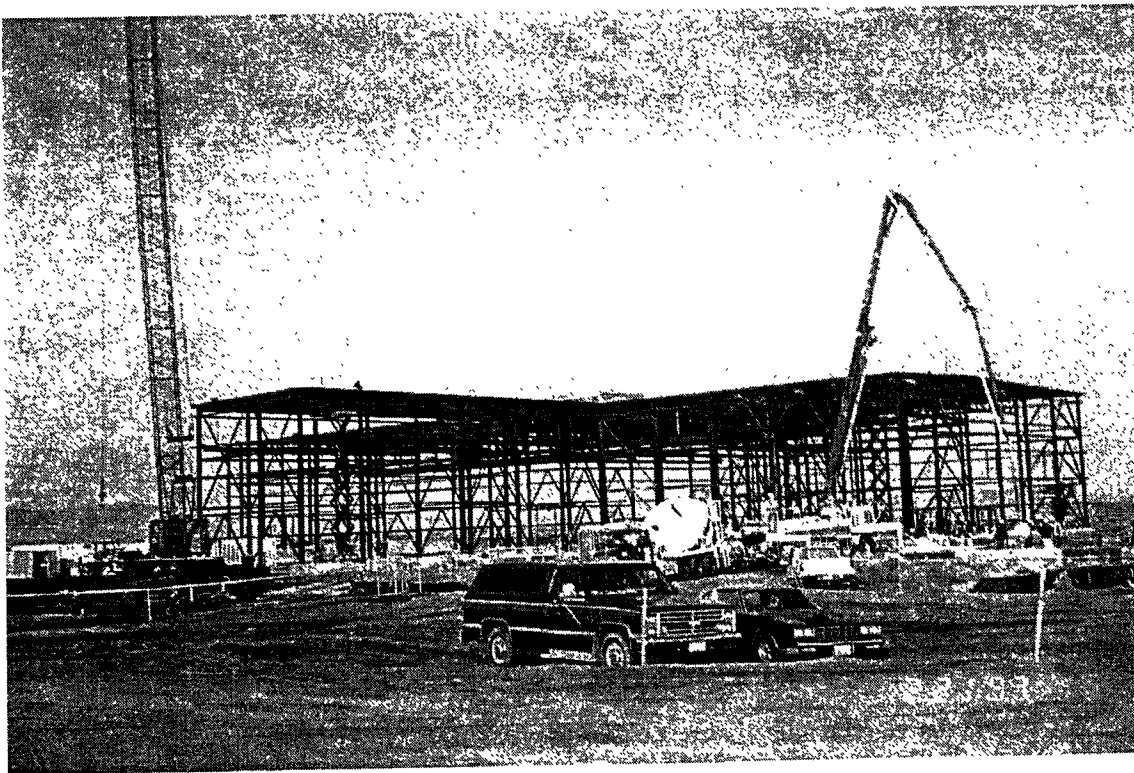


FIGURE 15. View of LVEA at Hanford

Hanford Site. Construction of the buildings and infrastructure continued at the site by Levernier Construction Company. Weather was a problem during this period. Total days lost through the end of this period due to inclement weather is 28 calendar days. However, the construction progress as the end of this period is only a few percent behind the baseline schedule. Construction of the buildings and infrastructure reached the 30 percent completion level at the Hanford site. This included placement of all concrete work for the building and technical foundations for the end and

mid stations on southwest arm as well as the corner stations. Also, completed all structural steel framing for these stations. Siding and roofing of the mid and end stations on southwest arm has been completed and work inside these stations have started (Figure 16 and Figure 17).

G970036-11-O-P

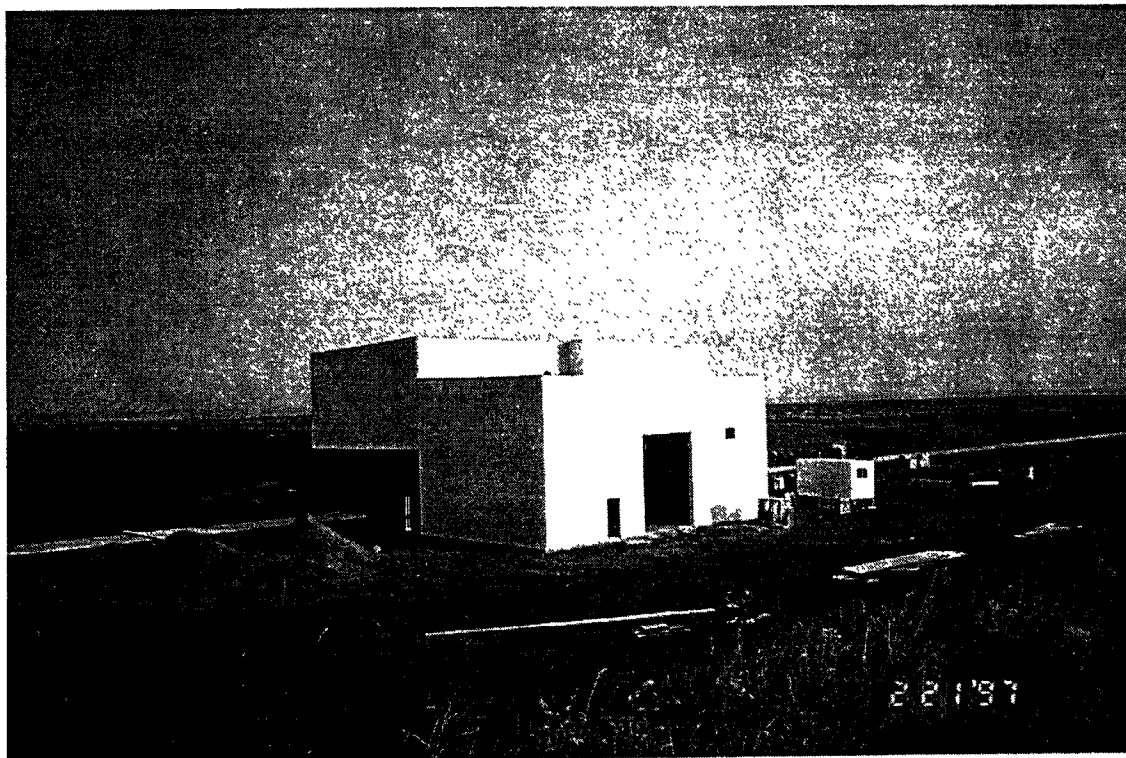


FIGURE 16. View of Mid Station on Southwest Arm at the Hanford Site.

G970040-11-O-P

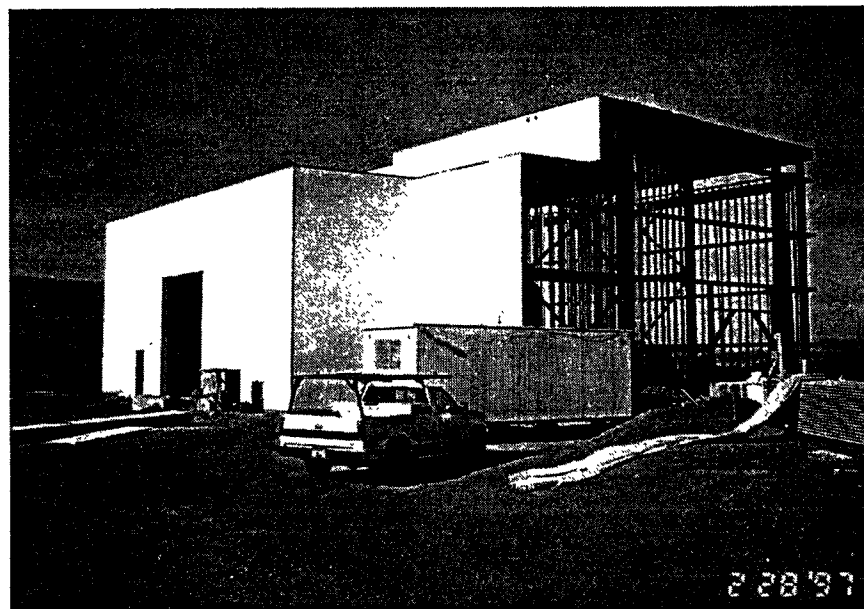


FIGURE 17. View of End Station on Southwest Arm at the Hanford Site.

Livingston Site. The Parsons I & T, the A-E contractor, completed the construction documents for Building and Infrastructure contract design for the Livingston site. This consisted of the signed and stamped technical specification and drawings for the awarded contract. Notice to proceed was issued for this contract to Hensel Phelps Construction Company and construction work started at the end station on northeast arm and corner station (Figure 18).

G970035-01-O-PV



FIGURE 18. Excavation for the Foundation for the End Station on Southeast Arm at the Livingston Site.

Simmon J. Barry & Associates of Baton Rouge, LA was selected and was awarded the contract for performing the surveying support for all construction work at the Livingston site.

Delta Testing and Inspection, Inc. of Baton Rouge, LA was selected and awarded the contract for Quality Assurance and Testing and reporting support for all the construction activities at the Livingston site.

Work planned to be accomplished next quarter:

- Complete the construction work on the mid and end stations on the southwest at the Hanford site.
- Complete placement of concrete for the technical and building foundations for the end station on northwest arm at the Hanford site.
- Complete the siding on the corner station at the Hanford site.
- Complete all submittals and obtain approvals for the shop drawings for the buildings at the Livingston site

- Complete the placement of the concrete for the technical and building foundation for the end station on southeast arm as well as corner station.

7.0 Detector (WBS 1.2)

Detector activities are organized according to the LIGO WBS as follows:

- WBS 1.2.1 Interferometer System, organized into three major task groups, each responsible for several Subsystems:
 - Suspensions and Isolation
 - Seismic Isolation
 - Suspension Design
 - Lasers and Optics
 - Prestabilized Laser
 - Input/Output Optics
 - Core Optics Components
 - Core Optics Support
 - Interferometer Sensing/Control
 - Alignment Sensing/Control
 - Length Sensing/Control
- WBS 1.2.1.9 Detector System Engineering/Integration
- WBS 1.2.2 Control and Data Systems
- WBS 1.2.3 Physics Monitoring System
- WBS 1.2.4 Support Equipment

Detector activities started in December 1994. As noted in the 1996 Annual Report, the schedule planned for FY96 was quite aggressive, and we have also had difficulty staffing the activities at the planned rate. As a consequence, we have replanned a number of activities, taking advantage of the staged installation schedule; no changes in Level 1 Milestones are required.

While we continue to report progress separately for R&D activities and Detector activities, the task groups enumerated above include the relevant R&D (most laboratory activities and exploratory modeling) with the objective of concentrating the activity on a given domain. In addition, the Detector Site Implementation and Operations task group reports activities focussed on these topics and also the activities in the 40-meter Interferometer facility, which is a primary tool for tests of operations and integration for the Detector group.

7.1 Suspensions and Isolation

Significant accomplishments during this quarter

- Produced and characterized (initial) the prototype coil and leaf springs for the seismic isolation system
- Completed the Preliminary Design of the Seismic Isolation System
- Installed and completed the first tests of a LIGO-design Small Optics Suspension prototype in the 40-meter interferometer

Seismic Isolation. The Preliminary Design phase of the Seismic Isolation took place during the first quarter of 1997. Hytec, Inc., performed extensive design and analysis of the isolation 'stack' itself, the structure linking the stack to the optics, the internal and external support structures, and the actuators. The latter present particular design challenges with requirements for moving 12 tons with sub-micron resolution; a combination of air bearings and a piezo-electric transducer (both commercial items) appears to meet the requirements. In addition, prototypes of the two constrained-layer spring designs were fabricated and underwent preliminary testing for stiffness, hysteresis, and damping. The coil spring appears to be satisfactory, and will be produced in larger quantities for further testing and production tuning. Documentation for the design effort was completed and circulated in preparation for the Preliminary Design Review planned for early in the second quarter.

Suspension Design. Work continued on the Final Design for both the Small and Large Optics Suspensions. Initial measurements of prototypes of the suspension cages showed lower than expected internal resonance frequencies (which could lead to thermally driven peaks in the interferometer output). Finite element analysis was performed to find the weak points in the design and small modifications to the design are in process. The Large Optic Suspension prototype underwent testing with a 'dummy' test mass to allow measurements of the controller performance, as well as fit and installation procedure checks. The Small Optic Suspension prototype was installed in the 40-meter interferometer (suspending the beamsplitter), where it will undergo system and noise tests.

Work planned to be accomplished during the next quarter

- Seismic Isolation. Conduct the Preliminary Design Review; start Final Design and prototype/first article activities and conduct tests for static and dynamic performance of the springs.
- Suspension Design. Prototype test reviews will be held for the Large and Small Optics Suspensions; Small optics final design revisions will be carried out.

7.2 Lasers and Optics

Significant accomplishments during this quarter

- Prestabilized Laser. An interim design review was held on December 18 for the Nd:YAG light source.
- Input Optics. Detailed designs for the input coupling telescope were carried out.
- Core Optics. The first substrates have been delivered to polishing vendors, and the first coating performed on a full-scale test optic.

Prestabilized Laser. Lightwave, Inc. continued in their development program for the LIGO 10W Nd:YAG laser, and an interim review was held at Lightwave on December 18. Results from the prototype effort has led to some redesign of the amplifier section of the system, but there are no difficulties anticipated in maintaining the initial schedule. Considerable in-house experience has been obtained with the 700 mW lasers which act as the master oscillator for the Lightwave 10W laser, through the development of a pre-stabilized laser for R&D work (see below) and the characterization of optical components in the infrared. This has allowed the control inputs to the laser to

be exercised and is providing input to the conceptual design for the complete Pre-Stabilized laser. A collaborative effort with Stanford University is investigating the properties of a spatial and temporal filtering cavity which may be needed for the laser subsystem. The prototype has shown encouraging progress, and the optical efficiency is very high. The Design Requirements for the laser subsystem are being refined and documented in preparation for a review in the second quarter.

Input Optics. The University of Florida group responsible for the Input Optics is continuing the Preliminary Design. In addition, the Design Requirements Review last quarter led to a number of action items which are being worked, among them are a requirement for flexibility in the input optics parameters (leading to a challenging coupling telescope design), refinement of control systems, and integrating the design with the overall optical layout (which leads to length and modulation frequency requirements). Visits by both LIGO and University of Florida staff are maintaining the close coupling needed for a good integration of the effort.

Core Optics Components. This time-critical subsystem continues to advance well. The substrates for the recycling mirror, folding mirrors, and end test masses are in production (Corning, Inc.) with some initial deliveries complete. A readiness review for one of our polishing vendors, the Commonwealth Scientific and Industrial Research Organization, took place on 20-21 January, and substrates have been sent to them for the start of production. A Pathfinder polished substrate has been sent to the VIRGO metrology lab for homogeneity tests. A second was sent to General Optics for polishing.

The coating uniformity studies have continued with Research Electro-Optics Inc. (REO). Special-purpose anti-reflective coatings are applied at REO which have a reflectivity with a strong dependence on the coating thickness. A spatial mapping of the reflectivity of the coatings is performed by LIGO, and a complete surface map synthesized from these measurements. These maps are used in the FFT numerical optics model of the complete interferometer to give us an accurate estimate of the performance of these coatings; in addition, recognition of geometric regularities in the coating thickness give indications of how the process can be improved and are shared with REO. This has enabled the first coating runs on full-size LIGO optics at the end of this quarter; these mirrors will be delivered to NIST for measurements.

LIGO plans to perform the final metrology in-house. Requirements for the critical measurement systems were developed this quarter and will be sent to prospective vendors in the next quarter.

Core Optics Support. The core optics support subsystem is responsible for handling the light leaving the interferometer; this includes the principal output beams from which the gravitational-wave will be read out and the other control signals developed, and also the stray light within the and vertex stations and the design of baffling for its control. An initial draft of a Design Requirements Document has been drafted, establishing a paradigm for the system, and the conceptual design has also advanced considerably this quarter.

Work planned to be accomplished during the next quarter

- Prestabilized Laser (PSL). Complete the Preliminary Design Review for the Lightwave 10 watt Nd:YAG lasers. The Design Requirements Review for the laser pre-stabilization subsystem will be held.
- Input Optics. Preliminary design will continue on the expanding optics, modulation system, mode cleaner, and telescope.
- Core Optics. The present fabrication activities will continue. Design/procurement of in-house metrology tools will take place.
- Core Optics Support. The Design Requirements review will be held and preliminary design will commence.

7.3 Interferometer Sensing/Control

Significant accomplishments during this quarter

- The Preliminary Design of the Alignment Sensing/Control Subsystem was completed.
- The Preliminary Design of the Length Sensing/Control Subsystem continued; tests of photo-detectors was carried out.

Alignment Sensing/Control. Preliminary design has dominated the activity this quarter. The information from the very successful R&D demonstration of wavefront sensing was integrated into the design, with a decision to use the prototype hardware as a close-to-final design for the wavefront sensors and demodulators. Several extensions of the models were made: one to allow larger angles to be analyzed (showing that the maximum alignment for lock acquisition is of the order of 10^{-7} radians) and another to allow transfer functions for control signals to be determined (showing that no new concerns lie in this part of the design). The LIGO alignment design team will make the detailed design for the input optics mode cleaner, and a collaborative visit to the group at the University of Florida led to firm plans and resolution of some interface issues. As this quarter closed, the Preliminary Design documentation was completed and sent out; a review will take place early in the next quarter.

Length Sensing/Control. The preliminary design for this subsystem continued, with most of the effort concentrated on the acquisition of the locked state. This work is closely coordinated with the Alignment acquisition studies and uses modeling tools developed for the alignment as well as models developed at JPL under contract for this purpose. The sensitivity of the acquisition sequence to parameter values was explored, with sign changes found for 'under-coupled' (cavity losses larger than input coupling mirror transmission) vs. 'over-coupled'. The modeling is also applied to the configuration of the 40-meter interferometer as this will be where the design is verified (see below). In addition, measurements on InGaAs photodiodes were started to identify the commercial sources which can meet our requirements for power handling, frequency response, and linearity.

Work planned for 2Q FY97:

- Alignment Sensing/Control. Final design will continue; initial alignment and wavefront sensing prototype fabrication will be started.
- Length Sensing/Control. Preliminary Design will continue.

7.4 Detector System Engineering/Integration

Significant accomplishments during this quarter

- The Detector Subsystems Requirements Review was held on December 4, 1996.

The Detector Subsystems Requirements Document was reviewed this quarter, and this document now is the definitive reference for the subsystem requirements. There are elements which need more definition, and that work continues in conjunction with the individual subsystems. The optical layout made significant progress and allowed some specific cross-subsystem design issues to be resolved, including exact lengths of resonant cavities and the wedge angles to be used on the Core Optics.

Work planned for next quarter

- System Design Requirements. The final interferometer subsystems Design Requirements Reviews will be held, and the refined documentation issued for designer reference.
- Optical Layout. The three-dimensional optical and mechanical layouts, integrated with the other project mechanical design tools, will be completed for the LIGO Hanford interferometers.

7.5 Control and Data Systems (CDS) Activities (WBS 1.2.2)

Significant accomplishments during this quarter

- The Final Design Review for the Vacuum Controls was held on January 8
- A prototype data acquisition/frame builder system has been configured and successfully bench tested

The CDS group has placed staff at the LIGO Hanford site to supervise the early activities there; in addition, a strong local group is being built to be ready to take on the principal installation and debugging which will be starting soon.

Support for interferometer subsystems: The CDS group advanced in the design for several of the interferometer subsystems. The Alignment Sensing and Control system, which presents probably the most complicated design problems in the in the interferometer, advanced in parallel with the optics and sensing design reported above, and the CDS Design Requirements Document for this subsystem was circulated at the end of the quarter for review early next quarter. The Pre-stabilized laser system has gone through a prototyping stage in support of R&D activities (see below), and this has allowed the electronics design 'high points' to be identified and a first-cut design developed. The Suspension subsystem has seen the exercise of a LIGO-prototype control system in the

40-meter interferometer, with both electronic performance and in-vacuum wiring concepts tested. The Length Control and Sensing top-level concepts evolved with the modeling, and the states of the system are now identified. In addition, the difficult problem of analog to digital and digital to analog conversion (necessary to pass signals to the 4km-distant end mirrors) has been researched. The Physics Environment Monitor CDS Design Requirements Review was held, with detail in interface and data handling laid out in the associated Requirements and Conceptual Design documents.

Global system and Data acquisition: A full prototype data acquisition system is being developed and will be tested using the data (strain and environmental monitor) from the 40-meter interferometer. During this quarter the software for frame building was adapted from the VIRGO source (with some useful feedback to the VIRGO group on incompatibilities and errors) and is running on the target platform. Tape robot software was installed and configured. Data acquisition hardware was designed and produced, including anti-aliasing filters. As the quarter closes, the complete data system is functional and in test. Networking bandwidth tests using an ATM switch planned for LIGO was performed.

Vacuum Controls: The Final Design Review was held on January 8, enabling the start of hardware production. The wiring of the crates for this control system was half finished at the end of the quarter.

R&D support: Two research efforts received significant support. The 700 mW pre-stabilized laser, to be used on the Phase Noise Interferometer and for other early tests of IR lasers, was completed and shipped to MIT at the end of the quarter; feedback from measurements there will be used for the LIGO laser control design. The 40-meter Recycling experiment has presented a particular challenge, as the locking sequence has required a significant rework of the existing control electronics. This work continues as the quarter closes.

Work planned to be accomplished during the next quarter

- Interferometer Controls. The Pre-Stabilized Laser and Input Optics conceptual design will start. The Preliminary design for the Alignment Sensing/Control, Core Optics Support, and Seismic Isolation will be underway.
- CDS integration and global systems. Final Design activities will continue.
- Data acquisition. Preliminary design will continue.
- Vacuum system controls. Fabrication will continue.
- Interferometer Diagnostics. Refined science input to the design process will be completed and reviewed; Preliminary Design will continue.

7.6 Physics Environment Monitor (WBS 1.2.3)

Significant accomplishments during this quarter

- The Preliminary Design Review was held on February 5.

The Physics Environment Monitor preliminary design was completed during this quarter. Specific

sensors and actuators were identified to meet the requirements, and data acquisition requirements fleshed out. The Preliminary Design Review took place on February 5, enabling the Final Design to begin. Most of the equipment is available commercially, but some sensors and actuators will need in-house development. We plan to make some early measurements at the two LIGO sites to characterize the near-virgin environment, and have thus started to plan a set of measurements using Physics Environmental Monitor hardware but without relying on the (not-yet-installed) CDS backbone but instead a portable PC-based system using commercial software.

Work planned to be accomplished during the next quarter

- The Final Design will continue.
- A system for early on-site measurements will be assembled and employed.

7.7 Support Equipment (WBS 1.2.4)

Definition of the required Support Equipment will continue.

8.0 Research and Development (WBS 1.3)

Significant accomplishments during this quarter

- Completed the physical reconfiguration of the 40-meter interferometer for recycling.
- Concluded work on the Argon-laser Phase Noise Interferometer.

40-meter Interferometer Investigations. The reconfiguration of the 40-meter interferometer as a LIGO-like Fabry-Perot recycled interferometer occupied the installation this quarter. New vacuum chambers were attached and qualified, equipped with seismic isolation systems, and the optical components installed. Some problems with existing 40-meter components were identified and repaired in the process. One important aspect of the reconfiguration is the use of a LIGO Small Optics Suspension for the beamsplitter, and the 40-meter team and the CDS group worked together to test this new system and to work out problems in installation and initial performance. The first light into the system was toward the end of the quarter with precision alignment underway at the close.

Development of Data Acquisition and Analysis Techniques. As reported above, the prototype LIGO data acquisition system is being deployed for use with the 40-meter, and this is a joint effort of the CDS and 40-meter team.

Phase Noise Research. This research effort is designed to develop and demonstrate the technology for the shot-noise limited interferometer operation at initial LIGO power levels to achieve the required phase sensitivity using the 5-meter facility at MIT. The final research with the Argon-laser Phase Noise Interferometer was performed during this quarter. Low-frequency noise sources were specifically targeted. Contributions from parasitic interferometers (formed between the isolated, suspended in-vacuum components and the much seismically noisier input optics) were identified and reduced by improvements in optical surfaces; in addition, measurements were made at night then the ambient seismic noise spectrum was lower. Laser frequency noise was also a contributor and improvements in the control system were carried out to reduce the significance of this noise source. The final spectrum shows a shot noise sensitivity within a factor of three dB of the calculated value and with a well-understood low-frequency spectrum. This phase of the research was completed on January 17.

The reconfiguration of the Phase Noise Interferometer for Nd:YAG Infrared light has commenced. The preparation (attachments, vacuum baking) of the new optics and the installation of the Nd:YAG laser (input optics chain, electronics shakedown) were started. Tests of optical components in the infrared have led to some refinements of the matching scheme. To reduce the parasitic interferometer problems in the new configuration, an active isolation system was installed under the extra-vacuum laser table to reduce its relative motion. As the quarter closed, one of the two initial masses was successfully suspended, and the laser was locked to its reference cavity.

Interferometer Alignment Investigations. This research effort, directed toward testing the operational system of alignment for the LIGO initial interferometer, effectively concluded last quarter. Some final tests of the length control matrix and measurements of signals for very large angles were carried out.

Thermal Noise Investigations. No significant activity this quarter.

Nd:YAG Characterization and Stabilization. To gain familiarity with infrared techniques and to develop a basis for the LIGO Nd:YAG laser subsystem design, moderate-power (700 mW) commercial lasers are being prepared for use in the campus laboratories. The laser used is very similar to the master laser to be used in LIGO, and so the experience gained is directly applicable to the LIGO design. The work this quarter led to a complete tested and document stabilized laser, and it has now been delivered to MIT for use in the Phase Noise Interferometer. The performance of the laser appears to be quite good: The frequency noise, measured at the error point of the servo, was $\sqrt{v(f)} \leq 10^{-2} \text{ Hz}/\sqrt{\text{Hz}}$, and the relative intensity noise, also measured at the error point, was $\delta I(f)/I \leq 4 \times 10^{-8} / \sqrt{\text{Hz}}$. The Phase Noise Interferometer will be used to make independent measurements of these quantities. The work will continue but will be focussed on the LIGO Pre-Stabilized Laser subsystem and will be discussed there in following reports.

Work planned to be accomplished during the next quarter

- 40 m Interferometer:

Recombination and Recycling. The determination of transmission, fabrication, and preparation of the recycling mirror will be done; installation and shakedown of modulation system will take place.

Suspension Development. Interferometer tests of the Small Optics Suspension will be performed.

Data Acquisition and Analysis. Completion of the installation and shakedown of the LIGO-prototype data acquisition system. Test runs of environmental data acquisition and data analysis will be made.

- Phase Noise Demonstration. Installation will be completed of the first phase, which will consist of the prestabilized laser and a suspended two mirror cavity. An automatic alignment system using two wavefront sensors will also be installed. The laser will be characterized using this cavity.
- Thermal Noise Investigations. Tests of wire creep in the LIGO suspension fibers will start.
- Table-top Interferometer Investigations. No activity planned.

9.0 Systems Engineering (WBS 1.4.3)

9.1 Integration (WBS 1.4.3.1)

Significant accomplishments during this quarter

- Completed update of Beam Tube-Civil Construction Interface Control Document (ICD) to reflect as-built information.
- Developed a thermal and mechanical stress model of the Beam Tube system for performing trade-off analyses and defining Beam Tube Bake requirements.
- Completed analysis of the LIGO site survey data to obtain the best fit plane to the LIGO as-built slabs.
- Completed preliminary availability allocations for the LIGO triple coincidence Operating Mode.
- Developed preliminary Interferometer fault tree structure.
- Completed preliminary version of the Vacuum Control and Monitoring System Failure Modes and Effects Analysis.
- Completed drafts of the Suspension System Fault Tree Analysis (FTA) and reliability predictions for components of the Suspension System.
- Issued the LIGO Naming Conventions Standards
- Issued draft LIGO Vacuum Compatibility and Preparations Document.
- Performed field measurement of the BT wall motion at Hanford to provide information for the trade study on identifying acceptable baffle surface preparations.
- Performed an analysis of LIGO Pathfinder Core Optics to determine the surface scatter (BRDF) from similar optics. This was performed in support to provide information for the trade study on identifying acceptable baffle surface preparations.

Discussion of accomplishments and work in progress

Beam Tube Baffles. Late in 1996 it was noticed at Hanford that the installed baffles within the beam tube were apparently shedding glass. This was recognized immediately to be a serious concern potentially limiting LIGO sensitivity to short duration signals. Microscopic glass particles traversing the cavity light beams produce excess phase noise at a level detectable with the interferometers. An analysis indicated that the level of non-Gaussian noise pulses arising from this process could be as large as 100X originally specified levels. This was deemed technically unacceptable. A Technical Review Board was convened to address the issue. A team of individuals from Systems Engineering and Facilities was assembled with the priority goal to identify the causes of the problem, find possible solutions and to recommend adoption of the best solution as soon as possible. It was immediately decided to suspend baffle installation, as it was deemed likely that any baffles installed may need to be removed at some later date. It was also determined that the BT contractor was capable of installing baffles deep into completed sections of BT at a later date.

A subsequent investigation determined that the source of the shedding was principally sharp edges near the serrations on the baffles. Sharp edges cause a concentration of residual stresses in the glass coating, and these stresses cause small particles to separate from the coating near the valleys of the baffle teeth. The glazing material was formulated by the frit manufacturer (Ferro Corp.) for 304SS. Under normal application conditions (i.e., uniform surfaces free of sharp edges) the glazed coating is under slight uniform compression (there is a 10 percent mismatch of the coefficients of thermal expansion between 304SS and the frit). This compression is designed to improve coating robustness. However, the broken symmetry near edges with sharp steep profiles results in unbalanced residual stresses which cause flakes to form. An earlier investigation into coating robustness with non-serrated coupons had not identified this problem.

Several experiments were conducted to search for quantifiable measures for assessing the degree of particle shedding. It was determined that thinning the coating near the sharp edges by either mechanical or chemical means could reduce the shedding to possibly acceptable levels. It has since been determined, however, that large scale application of such techniques for the LIGO baffles is not feasible either due to cost or to environmental concerns from the large quantities of acid that would be required. Another possible mitigation approach was found to be processing the glaze a second time to a its melt temperature in the presence of an O₂-rich gas flame. A local glass blower is presently being explored on a large scale on several baffles. In addition, several new baffles were fabricated with a thinner (1/2X) glaze coating. This, also demonstrated much improved performance with respect to shedding.

An evaluation procedure to identify acceptable baffle performance was developed utilizing repeated thermal cycling between -34C and +50C over the course of 24 hours to screen for shedding baffles. An environmental test oven at a thermal cycling facility (NTS) has been used to cycle test articles every two hours (12 cycles per day). The amount of shedding was measured and particle size distributions estimated using a microscope to survey the residues. To date, none of the identified fixes has been deemed acceptable. We are presently waiting to evaluate the O₂-rich flame process.

As a parallel effort in order to establish a backup approach, we resumed developing an oxidation process to produce blued 304SS baffles. The substrate is cold rolled, bright annealed sheet material with a low backscatter (BRDF). Oxidation produces an absorbing oxide layer on the steel which reduces the forward reflected light. The net contribution to LIGO residual phase noise from scattered light using oxidized baffles is estimated to be three times worse than expected from the best glazed baffle performance. An increase in the level of scatter of this amount is undetectable by the initial LIGO instruments. Accounting for the expected continued improvement of high quality optical surfaces and coatings, it is expected that advanced interferometers utilizing better mirrors will be able to regain this factor three times in phase noise.

Beam Tube Bake. Late in the previous quarter we held a Design Readiness Review (DRR) for the Beam Tube Bake. We are presently involved in performing a detailed design of the bake procedure, including developing procurement specifications for major purchased components. The Facilities Group identified a GFE source for high current power supplies that will be used for the bake. These are surplus magnet power supplies from FNAL which can be loaned to LIGO for the duration of the Beam Tube Bake activity at both LIGO sites.

Major Interface Definition and Control Documents (ICD). We are performing a final audit of

the major LIGO Interface Control Documents. This audit involves capturing final as-built and as-designed interface details which were red-lined in earlier revisions. In addition, major previously undetermined details have been resolved and these are being updated. The first completely revised document has been the BT-CC ICD.

Integrated Layout Drawings. We are continuing to update the integrated layouts drawings of the LIGO systems. The LVEA and VEA drawings are being used to develop installation plans for the Detector subsystems.

Reliability Plan Development. A draft reliability plan has been released. It is presently awaiting incorporation of top-level allocation of reliability among major LIGO systems.

Vacuum Compatibility, Cleaning Methods and Procedures for LIGO Instrumentation Materials Specification Document. An initial draft is being revised for the standards and procedures by which major detector components will be deemed vacuum compatible and how they shall be prepared for installation into the LIGO vacuum chambers. A significant effort to develop vacuum compatibility evaluation facilities (cavity ring down measurements, surface absorption tests, optical contamination tests, outgassing accumulation chambers) has been resumed, motivated by the need for acceptance criteria for vacuum compatibility.

Work planned to be accomplished during the next quarter:

- Continue development of subsystem fault trees as PDR information becomes available.
- Initiate effort to obtain reliability data on various off the shelf equipments by contacting suppliers.
- Expand the Beam Splitter Chamber (BSC) and Horizontal Access Module (HAM) chamber mock-ups with a Seismic Stack representation and a clean room enclosure; plan and begin to exploit the BSC and HAM mock-ups.
- Continue developing the relation database for the Hardware Configuration Items list.
- Complete revision of the Interface Control Documents
- Continue work on the Beam Tube Bake design.
- Complete baffle redesign task.

9.2 Simulation, Modeling and Data Analysis

Significant accomplishments during this quarter

- Completed an analysis of core optics mirror coatings to determine their uniformity. This information was gathered as part of the Pathfinder detector task.
- Completed a time domain model with length and alignment degree of freedom. the next phase will be a validation of the model.
- Completed framework for the time domain end-to-end model work using 40-meter as the prototype.
- Reviewed the GRID modeling and simulation package from the GEO 600 collaboration.
- Made a prototype of a new object-oriented class library paradigm for the LIGO noise models.

- Integrated the GRASP (gravitational radiation analysis simulation package) onto the LIGO computer network.
- Drafted a document addressing LIGO Data Analysis Software Specifications Issues.
- Initiated discussions with LSU (Louisiana) and PNNL (Hanford) to establish LIGO WAN access for the Observatory sites.

Discussion of accomplishments and work in progress

The analysis of four mirrors with two kinds of AR coatings, one sensitive to Ta₂O₅ thickness and the other sensitive SiO₂ thickness, delivered from REO last December has been finished and the result was fed back to REO for the next round of improvements.

This coating incorporates the result of the previous analysis and the uniformity was improved by factor of 5. The thickness of SiO₂ layer increases by 0.5 percent in the peripheral region ($r \sim 3$ inch) and that of Ta₂O₅ by 0.2 percent. In the peripheral region, a periodical structure was observed at every 60 degree. The size of the variation is around 0.1 percent P-V. Due to the correlation, it is difficult to resolve if the variation exists only in SiO₂ layer or in both layers (it is very unlikely that the variation is only in Ta₂O₅ layer). REO has improved the bearing to remove this periodical structure.

Four mirrors were coated under the same specification to see the planet-to-planet variation. Although the measured reflectance of those mirrors showed variation from one to another, the measurements (15P and 15S) were not enough to quantify the dependence.

Dr. Ray Beausoleil held a meeting at Caltech summarizing his work on the time domain IFO simulation code development. He continued the work and delivered the final code for the full LIGO configuration with length and alignment degree of freedom (this still needs some change, which will be done along with the model validation period).

The next tasks to be completed include how to do the model validation, and how to interface the code to the existing control system framework (today's and future version of SMAC). Dr. Beausoleil will work on these two tasks. For the model validation, Daniel Sigg of MIT will work with him, and for the integration with the control system, Lisa Sievers and Dave redding will help him to write the interface code to MatLab.

The framework of the end-to-end model work for the 40-meter has been completed by M. Evans, M. Rakhmanov and H. Yamamoto based on the digital filter model designed by M.Evans. Within this frame, the configuration of the detector - complete system or partial system - can be easily setup. Several of the basic building blocks have been written, tested and improved, including optics elements, pendulum system, digital servo and so on. Time domain noise models are being developed.

A study of the GEO 600 modeling environment know as GRID was carried out by staff. GRID has a very similar look and feel to that of AVS. However, it is based on JAVA and requires development of modules using the JAVA language as a base. A JAVA module to simulate a binary inspiral chirp was developed to gain familiarity with the package. It was found to be very simple in its interfaces but had substantial bugs which routinely caused it to fail.

The existing noise models for LIGO were developed using AVS5. This product line has been discontinued on the Caltech LIGO computers in favor of AVS/Express and AVS/Viz product lines. This will require the noise models to be recast (AVS5 APIs were highly embedded) as a stand-alone package. A model for this based on a C++ class library was drafted and one of the noise models was rewritten as a Unix stand-alone in C++ based on this paradigm.

The GRASP (gravitational radiation analysis simulation package) was integrated onto the LIGO computer network. This package was developed by Prof. Bruce Allen, a LIGO visiting scientist. Using this package, the 40-meter data from November of 1994 has been reanalyzed for chirp signals. The package includes functionality for template generation, optimal filtering, stochastic background detection, and a collection of general purpose utilities. It also runs on a network of computers using MPI.

The LIGO Data Analysis System is currently being specified. Documentation describing the science goals, system specifications, requirements and software standards are currently being written. One of these documents, LIGO Data Analysis Software Specification Issues was drafted. A final version of the document will be available in the next quarter.

A proceedings paper for the Computers in High Energy Physics conference was submitted to the proceedings editors. The paper details the efforts within LIGO to model the scope and scale of the data analysis system based on the science goals expected for initial LIGO.

A kickoff meeting was held in Baton Rouge with LSU Administration officials to identify options for LIGO to gain access to Louisiana State University resources for Internet connectivity. The meeting identified several areas of mutual interest that will be explored further. These include participating in the state's LAsernet consortium to bring vBNS (NSF-funded very High Bandwidth Network Services) service to LSU and the Baton Rouge area. We generated a letter of intent to use such facilities and support for the state in its proposal to NSF for this development.

A second kickoff meeting was held with computer systems and networking systems administrators at Battelle Pacific Northwest National Laboratory (PNNL). The intent of the meeting was to identify options for LIGO to gain access to high bandwidth communications infrastructure in the Pacific Northwest. It was agreed that LIGO and PNNL would work together to explore how to develop an interagency MOU to allow LIGO to gain access to ESNNet in the northwest. It was determined that mutual interest and need existed in this regard because of Battelle's need for reliable access to Caltech's CACR Supercomputers, which they routinely utilize for DOE work.

Work planned to be accomplished during the next quarter

- Now the latest 4 mirrors have been delivered using new bearings and incorporating the analysis. The analysis of these mirrors will be continued, and will be compared with the NIST measurement of the 40 layer HR coating. Also, more through analysis will be done for the 4 mirrors to quantify the planet to planet dependence.
- The end-to-end model for the 40-meter will be developed further so that it includes the minimal components so that the model can be used. The major tasks to be done include (1) finish the integration of the IFO code - fast enough to generate long time period, (2) time domain noise models (thermal noise, mainly, plus the seismic motion data to be combined with the suspension module), and (3) complete control loops with realistic parameters.

- Twiddle code will be ported to C++ class library. This will be used to investigate the possibility to write a very fast near-lock state time domain model by the FT of the frequency domain model.
- A SURF student will work to find the speed improvements of the full featured (time domain IFO model with length and alignment DOF) model. Preliminary study will be done by the SURF program starts.
- The LIGO Data Analysis System will be characterized and reviewed by the project in the next quarter. In preparation for this review, documentation covering the science specifications, design requirements and software specifications and standards will be completed.
- A research project involving Caltech SURF (summer undergraduate research fellowship) students is planned which will involve recasting the LIGO noise models into an object oriented class library paradigm. The concept will be developed and finalized over the next quarter in preparation for the summer project.
- The GRASP package will be brought under software configuration management in the next quarter. This will most likely involve using the RCS and CVS version control systems. It will also act as a test bed for software configuration management for all LIGO software.

10.0 Support Services

10.1 Quality Assurance (WBS 1.4.2.1)

Work accomplished during this quarter

- Completed rewrite and revision of the LIGO Quality Assurance (QA) Plan
- Arranged and coordinated JPL QA engineering and other technical support
- Performed QA monitoring/oversight of annealing and pickling of beam tube coils
- Completed receiving and pre-ship inspection of over 600 porcelain coated baffles
- Completed QA surveillance visits and reports for the large gate valve and expansion joint vendors
- Prepared Quality Assurance Instruction (QAI) and data check list for core optic blank receiving inspection
- Completed review and provided comments for core optic blank grinding vendor's QA Manual
- Performed QA survey of core optic carrier component fabrication shops
- Provided technical and other support for the baffle shedding tests
- Performed vendor source inspection and coordination/QA monitoring of the baffle steam cleaning and high temperature oxidation of prototype/pre-production Bright Anneal baffles

Discussion of accomplishments and work in progress

During this quarter LIGO Quality Assurance (QA) has increased the QA engineering support to the Detector core optic blank activities. A receiving inspection QA instruction for the incoming blanks was prepared and has been implemented with LIGO QA assistance/input for creating the as-built data base. LIGO QA has also provided support to the core optic blank carrier fabrication work and helped arrange for the assistance of a JPL manufacturing/liaison engineer in support of the fabrication and assembly work. Another part of this fabrication task included verifying the presence/implementation of adequate QA systems at the component fabrication vendors.

LIGO QA personnel performed receiving inspection, in-process and final coating inspection/process monitoring for in excess of 600 beam tube baffles. This QA task included visual pre and post coating inspections for damage and coating quality. Spot checks/inspections of coating thickness and surveillance of the final cleaning and bagging of the baffles performed at JPL. LIGO QA has created a spread sheet database of this baffle inspection data for future reference.

Several visits and discussions were held with QA personnel at the vendors supplying the large gate valves and the expansion joints. The large gate valve vendor has now implemented what appears to be an effective QA tracking and NCR status reporting system where there was none before. For the expansion joint vendor there were test data errors, and it was not obvious whether the vendor was using or had available approved test procedures. Resolution of this concern is still pending the outcome of a CB&I QA audit report and the identification of QA issues/problems and

vendor actions required. LIGO QA is continuing surveillance of this situation to assure acceptable closure.

Work planned to be accomplished during the next quarter

- Establish QA processes/procedures for fabrication and surface optical treatment for the Bright Anneal baffles
- Establish QA plan and procedures/processes for the Detector Control and Data Systems (CDS)
- Provide QA guidance for delivery of Vacuum Equipment Pump Carts and associated documentation
- Establish QA monitoring of Process Systems International (PSI) acceptance testing

10.2 Environmental Safety and Health (WBS 1.4.2.2)

Work accomplished during this quarter

- Provided Safety oversight in the preparation, review, and approval of LIGO contractor safety plans and procedures.
- Continued to provide Laser Safety training, initial and recurring.
- Continued with safety inspections of LIGO campus facilities in support of Caltech Safety to assure that Caltech located labs are in compliance with the University safety requirements.
- Continued with the LIGO hazard analysis.

Discussion of accomplishments and work in progress

The primary focus for Safety oversight has been with Chicago Bridge and Iron and Hensel Phelps Construction Company. Both companies have been excellent in outlining their safety approach and CB&I has been able to demonstrate compliance with OSHA, LIGO, and their own requirements at Hanford.

The project personnel certification program provides reporting and control for approved laser operators and workers. The Safety Officer has begun to assist with the establishment of laser operational procedures, and is performing reviews to assure that the procedures are being used or are revised for usability.

The LIGO Safety Officer is supporting Caltech Safety to assure that Caltech labs are in compliance with the University safety requirements. The Safety Officer also provided on-site support to assure that OSHA safety requirements are met at the observatory sites.

LIGO Safety is continuing with the development of the LIGO hazard analysis to include operational hazard analysis. The goal is to establish a capability to evaluate the adequacy of the safety of the system and assure that any unidentified hazards are not unnoticed or properly controlled.

Work planned to be accomplished during next quarter

- Continue to provide Safety oversight in the preparation, review, and approval of LIGO and contractor safety plans and procedures.
- Continue with Laser Safety training both, initial and recurring. Provide the project with a personnel certification program that will furnish listing and control for approved laser operators and workers. Assist with the establishment of laser operational procedures and follow-up that the procedures are in use or revised for usability.
- Continue safety inspections in support of Caltech safety to assure that Caltech located labs are in compliance with Caltech safety requirements. Establish a safety level of support to assure that Caltech and OSHA safety requirements are met at the observatory sites.
- Continue with the LIGO hazard analysis with the previously established safety review team (individuals external to the LIGO project) to evaluate the adequacy of the analysis and assure that any unidentified hazards are not unnoticed.

11.0 LIGO Visitor's Program

Bruce Allen - University of Wisconsin, Milwaukee. Dr. Allen has been at LIGO as a visitor/collaborator since August 1996, and plans to stay through July 1997. He also visited LIGO for five months at the end of 1995. Dr. Allen's work is in data analysis. This work is important for the timely development of a LIGO data-analysis infrastructure. The techniques which he is developing are being tested on data from the 40-meter prototype.

During Dr. Allen's visit, he has developed a data analysis package called GRASP (Gravitational Radiation Analysis and Simulation Package). This is a C-language object library of functions, together with documentation and source code. These functions are designed to allow analysis of interferometer data using the standard and specialized techniques described in the literature. The package can be used to compare new data analysis techniques with existing ones, and to study the behavior of data analysis algorithms on simulated noise or on real interferometer output. It can also be used to study such practical issues, such as the choice of whitening filters, the effect of non-linearities in the detector transfer function, effects of quantization noise in the analog to digital conversion, etc.

Dr. Allen's goal is that the GRASP package be used by LIGO to:

- study data analysis issues and perform benchmarking with "real world data",
- compare different data analysis techniques, and
- serve as a prototype for construction of the full-scale LIGO data analysis system.

In collaboration with LIGO the GRASP package will be distributed in the public domain and can be used and further developed by other groups and researchers.

Discussion of accomplishments and work in progress

A long review paper describing known mechanisms for stochastic background production and methods of detection was finished and will be published by Cambridge University Press as part of a Les Houches volume. This is the most comprehensive and complete article to date on this subject.

A paper examining the detectability of stochastic background produced by "stringy inflation" (an early universe model) was written in collaboration with Brustein and has just been accepted for publication in Physical Review.

A paper containing a number of new results is being prepared with Dr. Romano, a postdoc at Milwaukee. These include:

- a new Signal-to-Noise formula obtained without small signal approximations,
- sensitivity limits for the LIGO enhanced detector curves,
- detailed results comparing the data-analysis pipeline described below to theoretical expectations (agreement to better than two percent was ultimately obtained),
- sensitivity limit predictions for correlating European and US IFO sites,

- detailed limits on the correlated noise requirements that would permit useful stochastic background detection experiments using the two kilometer and four kilometer detectors at the Hanford site.

A data analysis pipeline for stochastic background searching has been under development for approximately two years. This data analysis pipeline is now finished and working properly on simulated data. The data-analysis pipeline gives results from Monte-Carlo testing which are in better than two percent agreement with theory.

The stochastic background signal simulation and data analysis library is now complete, and has been incorporated into the GRASP library and documentation. We are currently using these routines to analyze real 40-meter data now that the performance of the pipeline on simulated Gaussian noise is completely understood.

Dr. Allen has also developed techniques that could be used to determine (or place limits on) the multipole moments that characterize any anisotropy in the stochastic gravity wave background. A paper just completed in collaboration with Dr. Ottewill (faculty at University College, Dublin) and submitted to Physical Review describes one such technique in great detail. Dr. Otte will is currently visiting Caltech to work on related issues.

The binary-inspiral detection routines in GRASP have been tested on 40-meter data and a pair of different vetoing techniques have been developed. The binary inspiral filtering code has been parallelized and run both on workstation networks and on a dedicated parallel processor (the Intel Paragon) at the Center for Advanced Computing Research.

A users manual (about 210 pages, at present) has been completed for GRASP.

Work planned to be accomplished during next quarter

- Finish binary inspiral analysis of 45 hours of 40-meter data.
- Shepherd GRASP through installation at the first half-dozen sites.
- Test and optimize the binary inspiral code on the IBM SP2 and Intel Paragon machines.
- Generalize the parallel inspiral analysis code for dynamic allocation of template lists.
- Implement/test multi-taper analysis of correlations and removal of line features.
- Modify GRASP to deal in real time with arriving data in the FRAME format.

Richard Gustafson, Keith Riles - University of Michigan. Dr. Gustafson has been resident at the LIGO 40-meter facility since October 96. He has focused on learning the 40-meter systems and exploring operational realities directed towards making lock robust, running the system, and reducing the most egregious noise sources and processes. The larger goal is to make operation routine and to identify and address actual noise sources and limits. A physics interest is the gravitational wave detection of hums, clicks and chirps, and studying inertia ideas as expressed in binary coalescence signals. Riles plans a sabbatical at LIGO during the winter of 1998 working on Data Acquisition and analysis.

12.0 REFERENCES

1. Cooperative Agreement No. PHY-9210038 between the National Science Foundation, Washington, DC 20550 and the California Institute of Technology, Pasadena, CA 91125, May 1992.
2. *The Construction, Operation, and Supporting Research and Development of a Laser Interferometer Gravitational-Wave Observatory*, proposal submitted to the National Science Foundation, December 1989.
3. *Technical Supplement to the LIGO Construction Proposal (1989)*, dated May 1993.
4. *LIGO Project Management Plan*, LIGO-M950001, Revision B, April 24, 1996.
5. *LIGO Cost Book*, dated September, 1994.
6. *LIGO Supplement for Installation, Commissioning and Operations*, LIGO-M950039, August 1995.
7. Cooperative Agreement No. PHY-9210038 between the National Science Foundation, Washington, DC 20550 and the California Institute of Technology, Pasadena, CA 91125, Amendment No. 5, April 20, 1995.
8. Cooperative Agreement No. PHY-9210038 between the National Science Foundation, Washington, DC 20550 and the California Institute of Technology, Pasadena, CA 91125, Amendment No. 11, August 23, 1996.
9. Report of the Panel on the Use of the Laser Interferometer Gravitational Wave Observatory, Boyce McDaniel, Chair, United States National Science Foundation, June, 1996.

LASER INTERFEROMETER GRAVITATIONAL WAVE OBSERVATORY
 - LIGO -
 CALIFORNIA INSTITUTE OF TECHNOLOGY
 MASSACHUSETTS INSTITUTE OF TECHNOLOGY

Document Type	LIGO-T970054-A - E	03/18/97
Beam Tube Dynamics		
S. Chatterji and R. Weiss		

Distribution of this draft:
 LIGO Project

This is an internal working note
 of the LIGO Project.

California Institute of Technology
LIGO Project - MS 51-33
Pasadena, CA 91125
 Phone (818) 395-2129
 Fax (818) 304-9834
 E-mail: info@ligo.caltech.edu

Massachusetts Institute of Technology
LIGO Project - MS 20B-145
Cambridge, MA 02139
 Phone (617) 253-4824
 Fax (617) 253-7014
 E-mail: info@ligo.mit.edu

WWW: <http://www.ligo.caltech.edu/>

SUMMARY

Measurements of the motion of the beam tube at the Washington site were made to refine the estimates of the phase noise due to scattering. The measurements indicate:

- 1) The beam tube is primarily driven by acoustic excitation rather than seismic noise.
- 2) Both measurements and finite element modeling show the beam tube to be a complex multi-mode mechanical oscillator with closely spaced (3 to 5 Hz) normal modes. The system is more simply described as an acoustic transmission line than as a lumped element mechanical system.
- 3) Under quiet conditions (winds less than 5 mph and all rotating machinery at the site turned off), the broad band displacement spectrum ($f < 100$ Hz) of the covered beam tube at a fixed support exceeds the LIGO standard spectrum by a factor of 3 to 10 and by factors of 30 to 100 in high Q transmission modes of the beam tube. The motions are correlated with acoustic pressure fluctuations and not seismic motions.
- 4) The beam tube motions at a point halfway between the fixed and compliant support is larger by factors of 2 to 3 than motion at a fixed support.
- 5) The prior estimates of beam tube motion used in the initial calculations for the scattering noise power in the beam tube need to be multiplied by factors of 3 to 10 for quiet conditions at the site and, furthermore, by an additional factor of the square of the wind velocity ratio for average conditions at the site (another factor of 2 to 4). The assumption is that the dominant acoustic noise on the beam tube comes from wind induced acoustic excitations transmitted through the beam tube enclosure.
- 6) The acoustic coupling to the beam tube will be reduced by the thermal insulation applied for the bakeout. The insulation will provide acoustic isolation at frequencies above 200 Hz but is not expected to provide attenuation at frequencies below 100 Hz.
- 7) It would be useful to directly measure the 10 to 200 Hz acoustic noise spectrum in the beam tube enclosure over a range of wind conditions at the site.

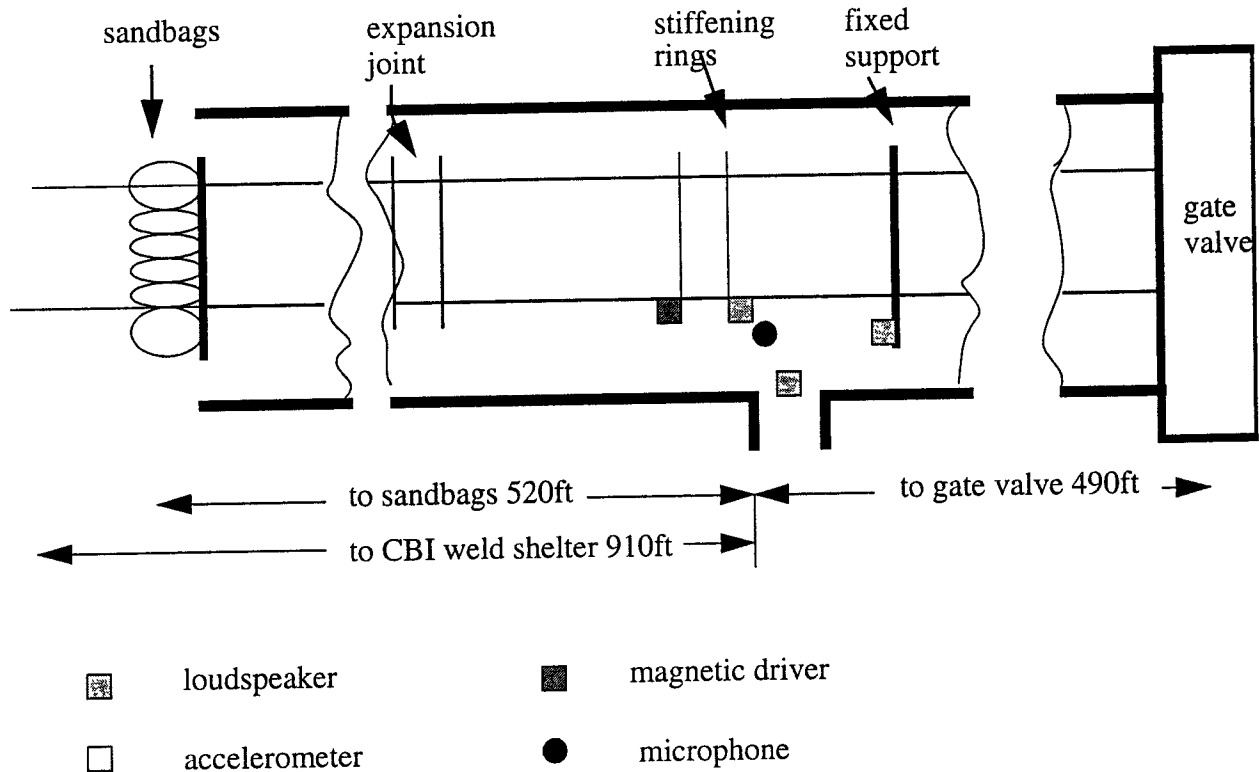


Figure 1 Schematic of the experimental arrangement

INTRODUCTION. The measurements, made between January 30 through February 1, 1997, included:

- 1) A sampling of the acceleration power spectrum in the vertical, horizontal, and longitudinal directions of the tube at a fixed support ring, at a stiffening ring 10 meters from the fixed support and at the base of the fixed support where it attaches to the concrete slab. These measurements were made after dark with all CB&I rotating machinery off, under low wind conditions and with the instruments powered by batteries.
- 2) A measurement of the acoustic transfer function of vertical, horizontal and longitudinal acceleration response to acoustic excitation derived from a loudspeaker monitored by a microphone in proximity to the accelerometer. The loudspeaker was mounted in one of the doors of the beam tube enclosure. The excitation was a chirped sinusoid.
- 3) Measurement of the transient response of the tube at a stiffening ring 10m from the fixed support. The measurements consisted of the horizontal spectrum after a horizontal impulse at the fixed support, the vertical spectrum after a vertical impulse and the longitudinal spectrum after a longitudinal impulse.
- 4) Measurement of the acceleration to applied force transfer function for horizontal acceleration from horizontal excitation, and longitudinal acceleration from longitudinal excitation. The excita-

tion was derived from a magnet attached to the beam tube driven by an oscillating current in a coil mounted to the ground. The excitation was a chirped sinusoid.

The experimental arrangement is schematized in figure 1. The beam tube cover extends from the gate valve to the sandbags placed on the tube, a distance of about 1000 ft. The sandbags were intended to attenuate the propagation of wind induced excitations on the uncovered part of the tube to the measurement region. The gaps in the beam tube enclosure between sections as well as at their join to the slab were filled by flexible polyethane rope to reduce wind induced acoustic coupling to the tube. The sealing was done for approximately 180 ft on either side of the measurement area. The instrumentation was setup near one of the safety escape doors in the beam tube enclosure approximately in the middle of the covered section. The door could be covered by a plywood sheet.

Measurements were carried out after CB&I had stopped construction for the day. Critical low noise measurements were taken with all CB&I rotating equipment turned off (pumps and air conditioning fans, beam tube air distribution system), the measurement equipment was battery powered and during conditions with winds under 5 mph. The power to the CB&I equipment (lighting, heaters, instrumentation, etc.) was not turned off since the perturbation to the measurements was manageable and would have caused delays in construction activities on the crew's return in the morning. The spectral features at 60 Hz and multiples in the high sensitivity acceleration power spectra are due to mechanical excitation of the slab and tube by vibrating transformers 1000 ft from the measurement region. The less critical measurements were made with AC power provided by a portable generator placed 100 ft from the door outside the beam tube enclosure.

The instrumentation consisted of high sensitivity PZT accelerometers coupled to low noise preamplifiers operating at the thermal noise limit, Stanford Instrument bandpass intermediate amplifiers, a storage oscilloscope and a portable (battery operable) Hewlett Packard dynamic signal analyzer. The data was observed during the measurements and recorded for analysis on floppy disks. (The use of the Stanford Instrument amplifiers, storage oscilloscope and the loan of the HP dynamic signal analyzer were arranged by Rick Savage.) Additional instrumentation consisted of a PZT microphone and various acoustic and mechanical drivers to stimulate the tube.

Acceleration spectra on the beam tube. Figures 2, 3 and 4 show the acceleration noise in $\frac{g}{\sqrt{\text{Hz}}}$ on the beam tube under quiet conditions at the site. The legend in all the figures is the same. The dashed curve at the bottom is the instrument noise which begins to encroach on the measurement below 10 Hz. The next higher curve shows the noise on the fixed support at the intersection with the concrete slab. The 60, 120, 180 and 300 Hz peaks come from mechanical motions imparted to the beam tube and slab by magnetostriction in the transformers in the CB&I buildings. The broadband noise agrees with Rohay's seismic measurements for quiet conditions below 100 Hz. Above 30 Hz the seismic noise is about a factor 10 to 20 lower in amplitude than the LIGO standard spectrum (shown as a dashed line in the figures). The spectrum using a solid line is from an

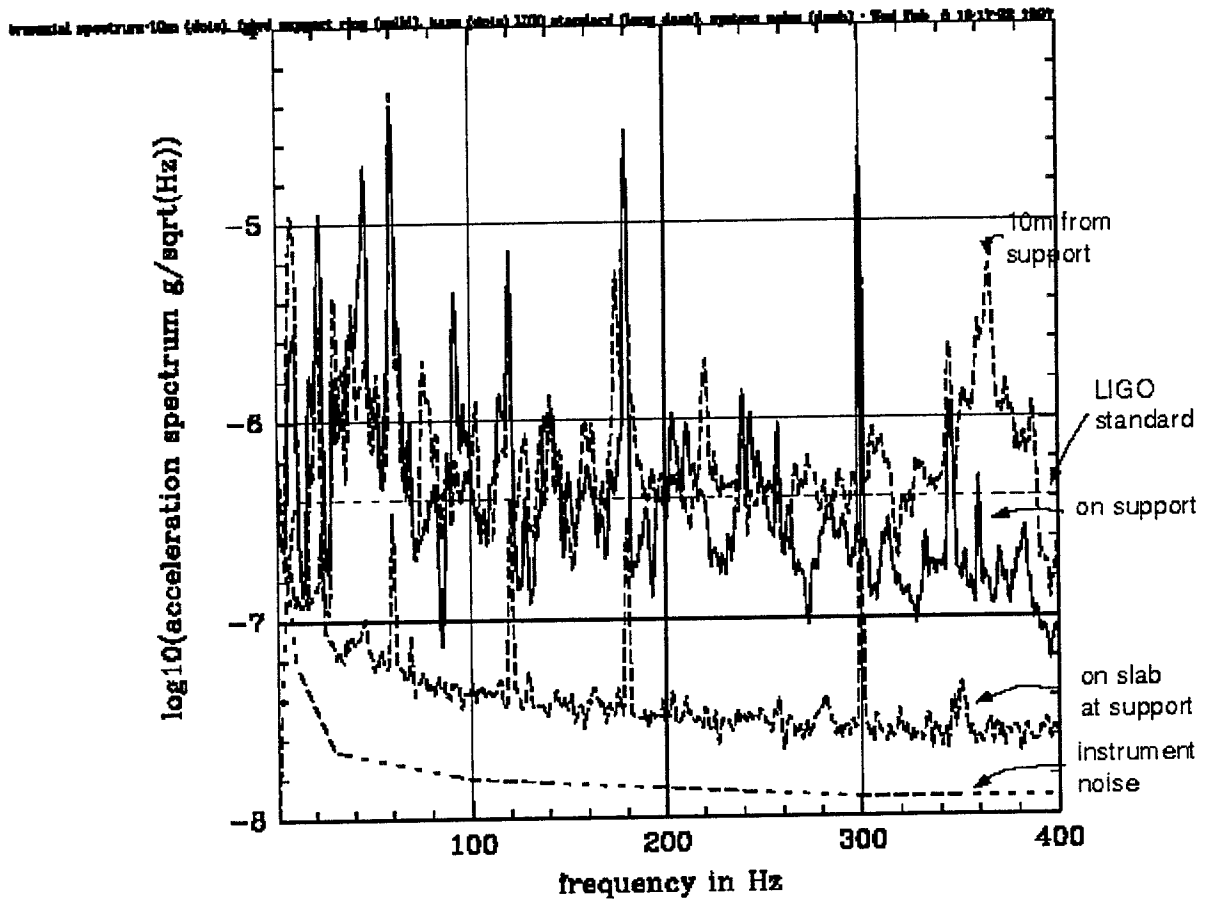


Figure 2 Horizontal acceleration spectrum

accelerometer mounted on the support ring associated with the fixed support. This is the location for most of the baffles, especially those near the middle of the tube. The spectrum is dominated by closely spaced narrow spectral lines with Q larger than 100 but generally less than 600. The same lines are seen in driven and transient spectra shown in subsequent figures and in table 1. The spectrum plotted in dots is taken at a stiffening ring 10 meters from the fixed support, about halfway between the fixed and flexible support. This shows larger motions at some of the normal modes and a general tendency to be more easily excited than the region at the support in the 300 to 400 Hz band which includes the radial stiffening ring modes.

The horizontal motions were always measured on a horizontal diameter of the tube, the vertical measurements at the top of the tube and longitudinal measurements at a point on the horizontal diameter. The apparatus cross coupling of the three directions due to accelerometer imperfections and mounting block errors was less than 0.5%.

The tube motions are largest in the horizontal direction where the broadband motion is between 3 to 10 times larger than the standard LIGO spectrum and the amplitude in several normal modes 30 to 100 times larger.

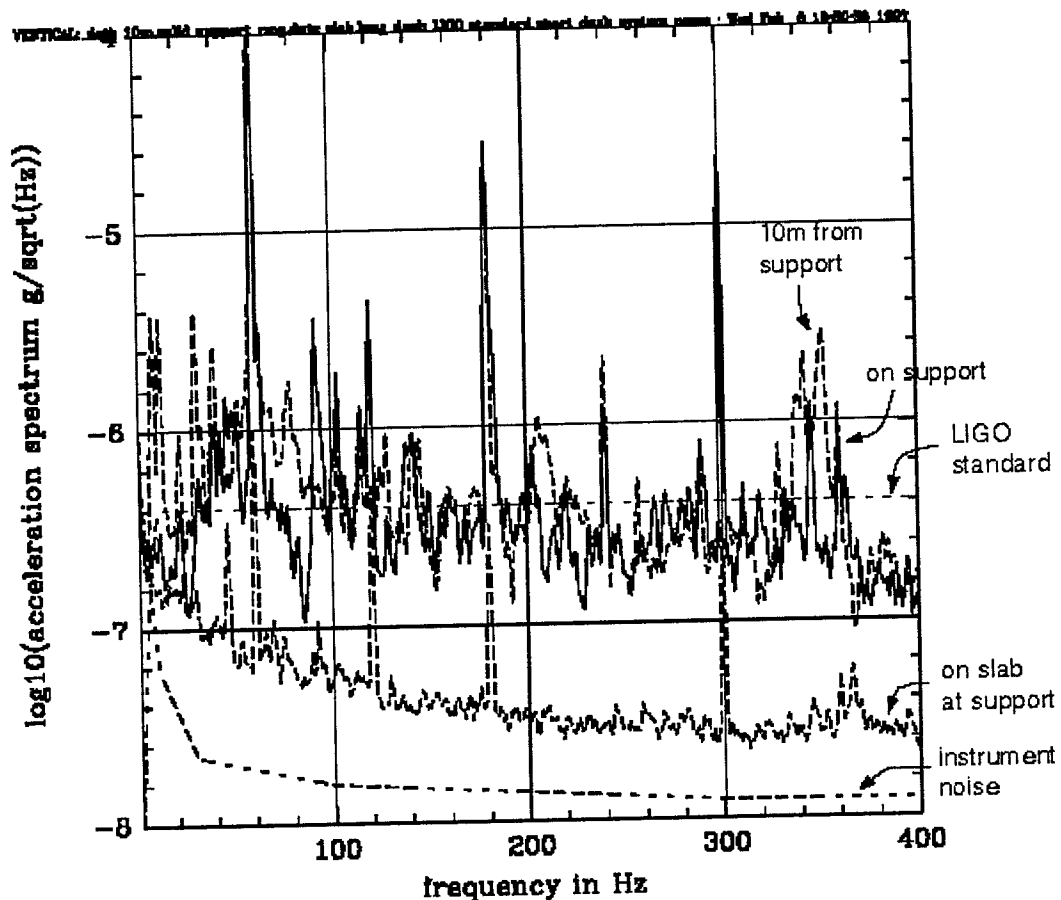


Figure 3 Vertical acceleration spectrum

All the spectra taken on the tube are poorly correlated with the acceleration spectra taken near the slab and (as was discovered later) are well correlated with the acoustic pressure spectra measured on a microphone placed near the accelerometer on the tube. The motion of the tube implies a driving sound field of 25 to 30 db (3 to 6×10^{-3} dynes/cm² rms), just below audible in the 100 Hz band, which is consistent with our observations that it was really quiet (as quiet as the proverbial church crypt) while taking the measurements. The acoustic noise is expected to vary as the square of the wind velocity so that under more typical conditions of 10 mph wind velocities, the acceleration noise may increase by a factor of 4. This factor is consistent with daytime measurements but not well defined since besides increased wind there was increased activity on the road to the Hanford facilities as well as CB&I construction.

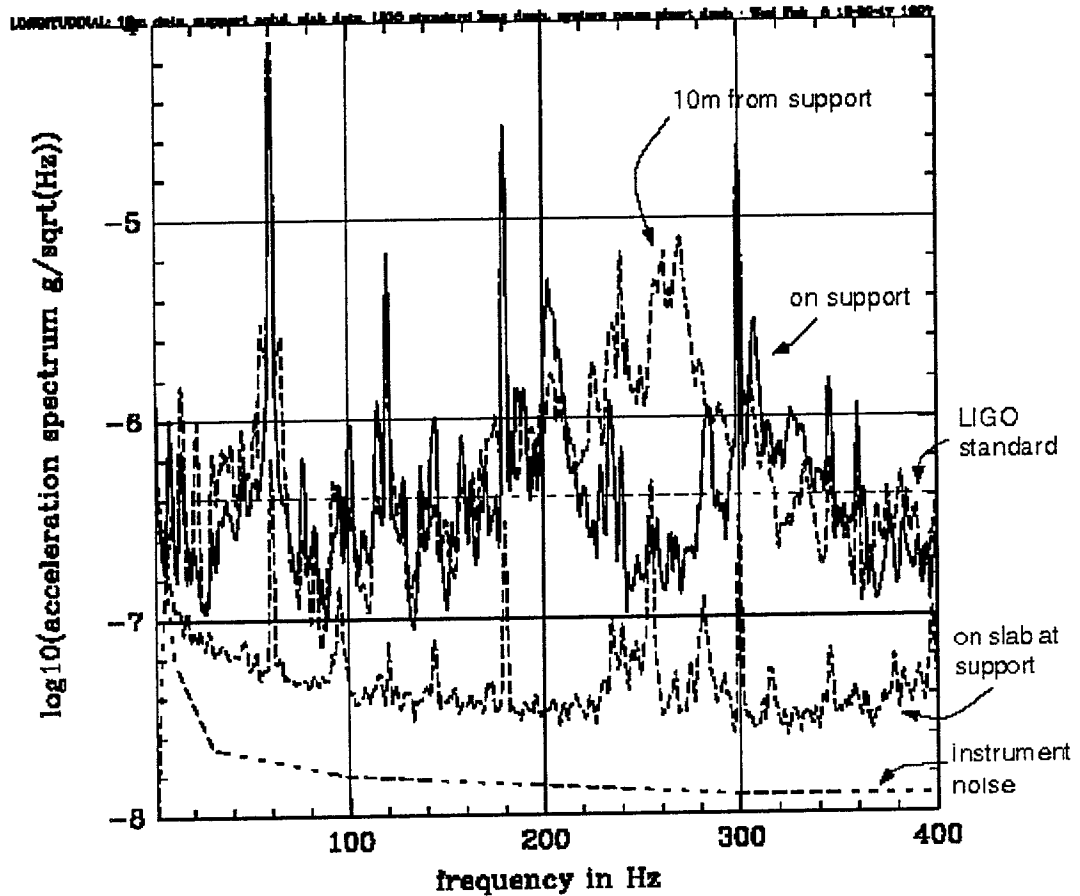


Figure 4 Longitudinal acceleration spectrum

Acoustic transfer functions. Figures 5, 6 and 7 show the calibrated transfer functions of beam tube acceleration in g for acoustic pressure in dynes /cm² measured next to the accelerometer by a microphone (calibrated after the fact). The accelerometer was located mid tube 10 meters from the fixed support and oriented for horizontal, vertical and longitudinal motions sequentially. The sound source was a loudspeaker mounted at the beam tube enclosure door (the outside world acting as an infinite baffle). There is little random noise in the figures since the excitation was made large enough to override the ambient background. The scruffy appearance of the data is due to the complexity of the beam tube normal mode structure.

The large scale interaction of the beam tube with the acoustic field is described by P.M. Morse in *Vibration and Sound* McGraw Hill (1948) p 352. The scale parameter for the process is the ratio

$$\mu = \frac{2\pi a}{\lambda} = \frac{2\pi a f}{c}$$

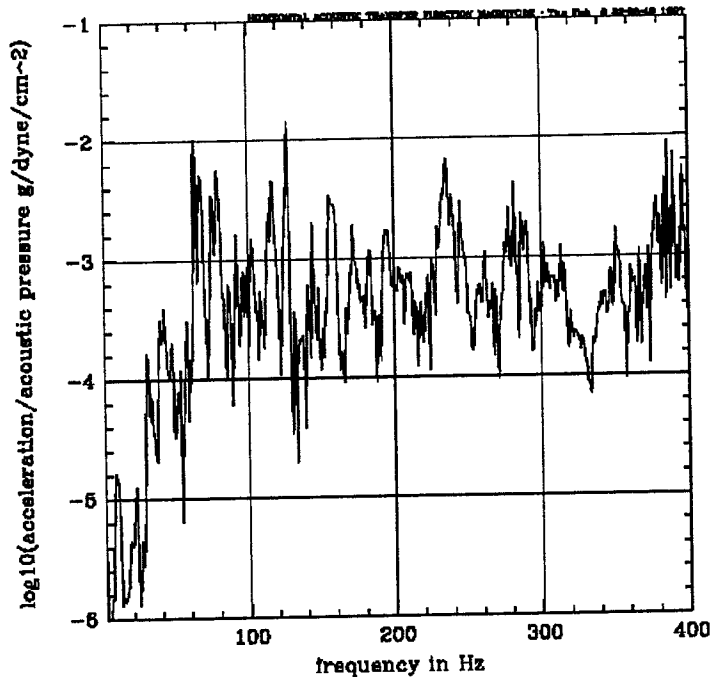


Figure 5 Acoustically driven horizontal acceleration

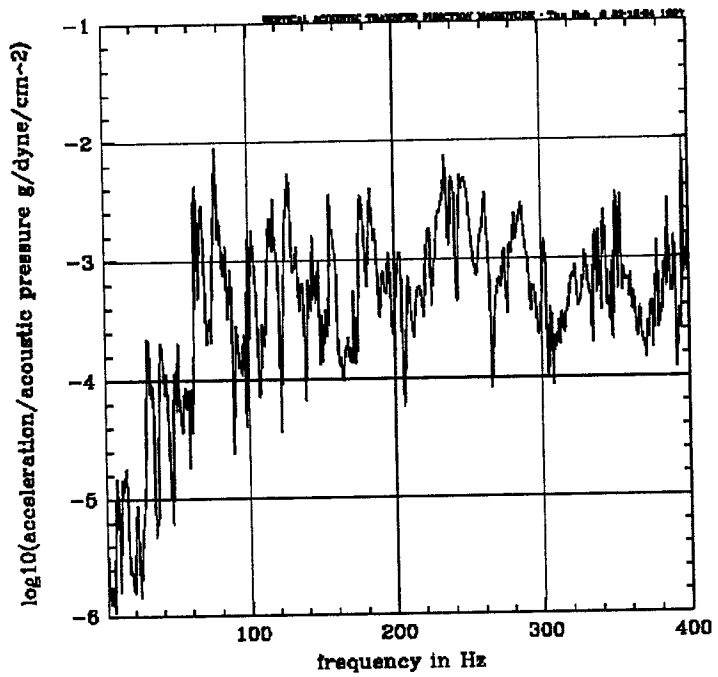


Figure 6 Acoustically driven vertical acceleration

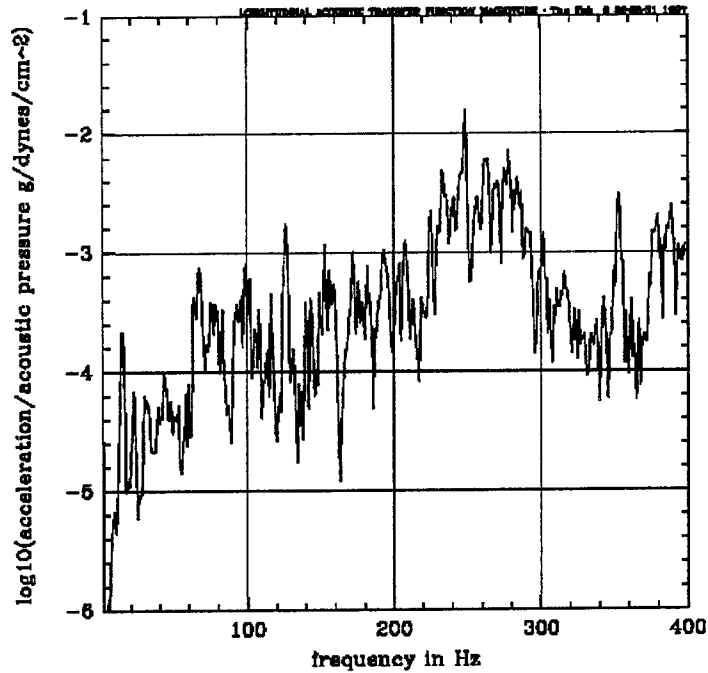


Figure 7 Acoustically driven longitudinal acceleration

where a is the tube radius, c the speed of sound in air and f the acoustic frequency. The scale factor becomes unity at about 85 Hz. At lower frequencies the tube acceleration in units of g per acoustic pressure grows linearly with frequency and is given by

$$\frac{(acc)/g}{p} = \frac{2\pi af}{c\rho_{ss}tg}$$

where ρ_{ss} is the density of the stainless steel, t the thickness of the tube wall modified for the stiffening rings. At frequencies above 85 Hz the sound diffraction is less important and the acceleration of the tube per acoustic pressure decreases slowly with frequency as

$$\frac{(acc)/g}{p} = \frac{1}{\pi g t \rho_{ss}} \sqrt{\frac{c}{2af}}$$

The crude model gives $3 \times 10^{-4} \text{ g/dyne/cm}^2$ at a 100 Hz possibly fortuitous in its good agreement with the data.

We failed in our measurement of the acoustic transmission of the beam tube enclosure and in subsequent measurements at the site it would be useful to measure this quantity as a function of frequency. An approximate relation for the acoustic transmission loss of a sheet of material between 125 to 4000 Hz is given in the American Institute of Physics Handbook (p 3-150) as a function of the material mass per unit area $\sigma = \rho_{mat}t$,

$$db_{\text{att}} = 12.7 + 14.7 \log \sigma (\text{kg/m}^2)$$

Using the above expression the 6 inch thick beam tube enclosure would provide about 50 db of acoustic noise reduction. The 6 inches of insulation to be placed on the tube for the bake is expected to provide about 20 db of isolation at frequencies above 200 Hz but be ineffective at frequencies below 100Hz.

The simple geometry of the beam tube enclosure is amenable to active acoustic noise reduction (closed loop nulling systems of microphones and loudspeakers) that have been developed for noise reduction in ducts. This may be a promising direction to take if advanced interferometer systems require further reduction in the beam tube motions.

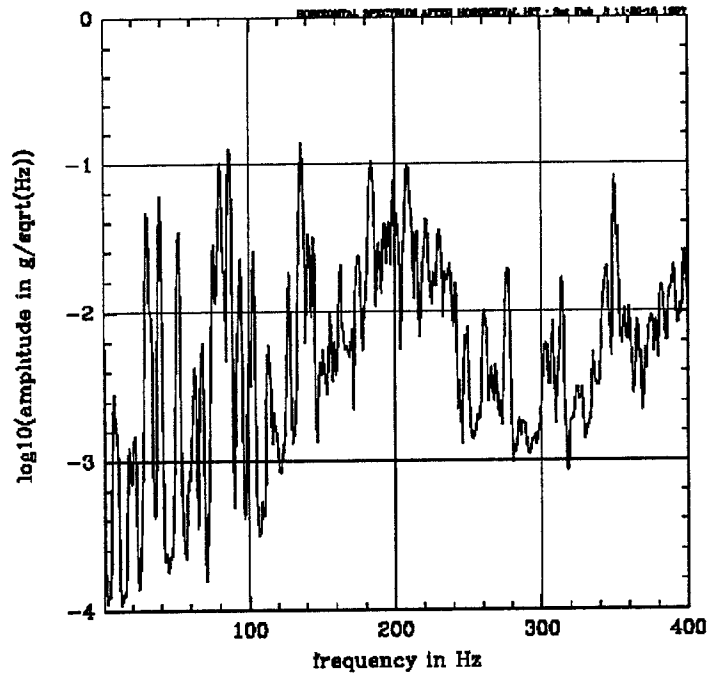


Figure 8 Horizontal transient spectrum after horizontal impulse

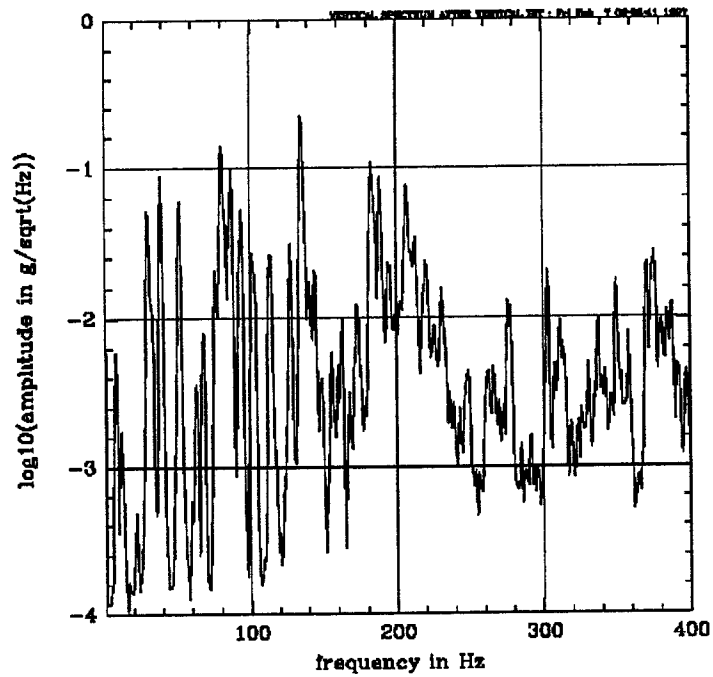


Figure 9 Vertical transient spectrum after vertical impulse

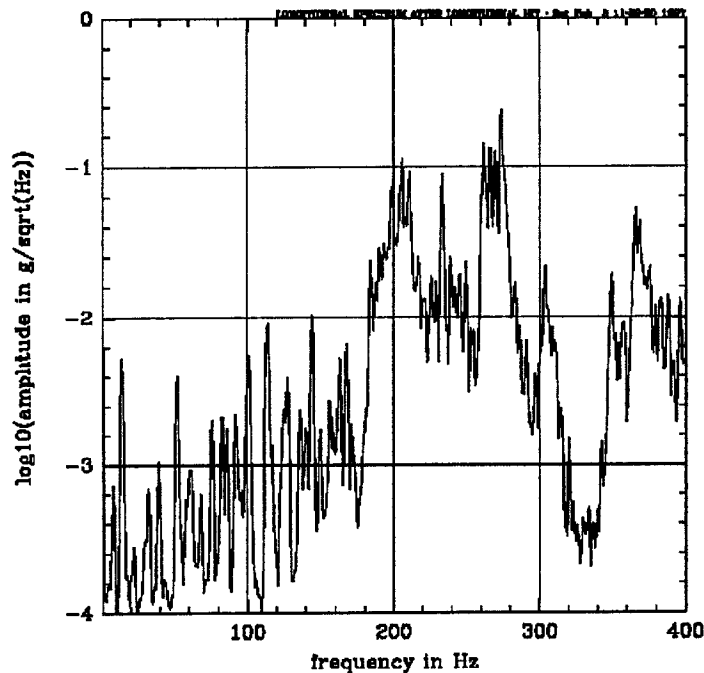


Figure 10 Longitudinal transient spectrum after longitudinal impulse

Transient measurements The ringdown spectrum after an impulse to the beamtube by a wooden hammer is shown in Figures 8, 9 and 10. A compilation of the normal mode frequencies for the three orthogonal directions of motion is given in table 1. All the measurements were made by mounting the accelerometer on a stiffening ring at the midpoint of the tube. The impulse was given at the fixed support in the direction indicated in the figure caption. The normal mode peak widths in the figures are determined by the observation time rather than the intrinsic normal mode losses. All resonances are narrower than 1 Hz. The ringdown time of several of the higher frequency modes was measured directly. The several of the modes between 300 to 400 Hz (stiffening ring radial modes coupled by the beam tube shell) have a ringdown time of 2 seconds, the Q of some of these modes is over 1000. The Q of the 87 Hz transverse mode is about 400. The thermal insulation needed for the bakeout should provide enough damping to reduce the Q to below 100 for all the modes with frequency higher than 50 Hz.

We should have taken high resolution spectra commensurate with line widths equal to the normal mode widths when evaluating the noise. The error in the peak heights will at most be a factor of 2 while the area (the broad band excitation) is correctly described. The insulation will bring the peak heights to the values in figures 2, 3 and 4.

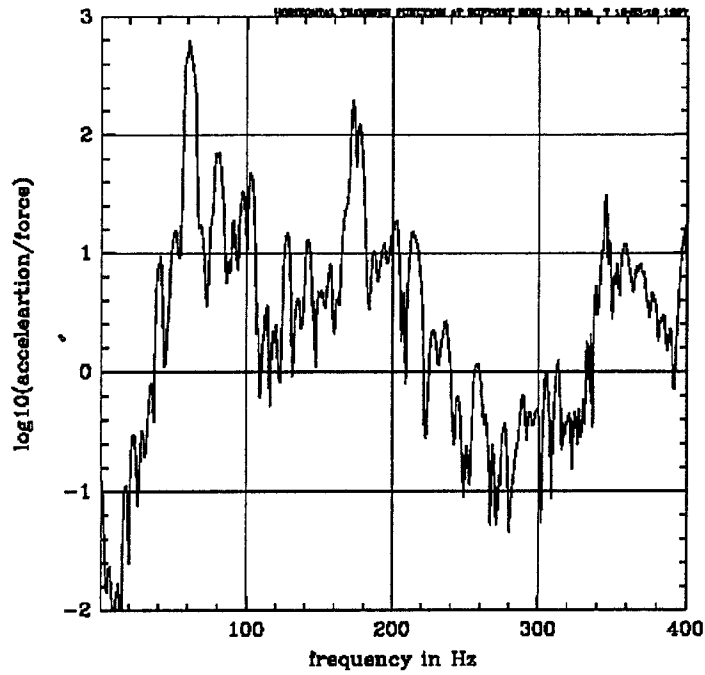


Figure 11 Horizontal acceleration for horizontal excitation

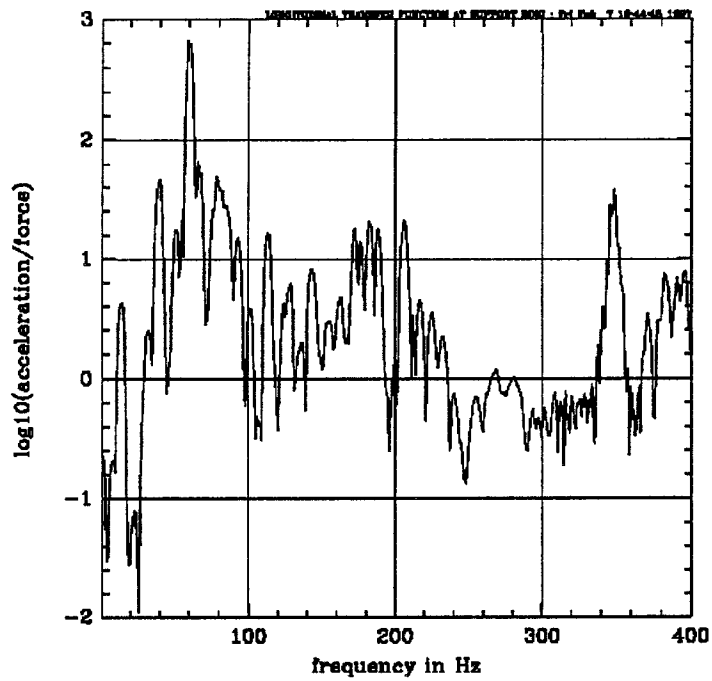


Figure 12 Longitudinal acceleration for longitudinal excitation

Driven measurements Figures 11 and 12 show the transfer functions of acceleration to force with a swept sine excitation. The force was applied to the beam tube by a magnet attached to the tube driven by the current in a coil which was held to the ground. The curves have been corrected for the inductance of the coil since the system was driven from a voltage source. The accelerometer was placed at the fixed support and the driver on a stiffening ring. The data has been included in the report for completeness but has not been used in the analysis.

Table 1: Normal mode frequencies in Hz

vert freq	strength	horiz freq	strength	long freq	strength
8	st	8		8	
12		18		14	
17		22		22	
22		30	st	32	
30	st	39	st	39	
39	st	52	st	52	
52	st	63		61	
60		68		68	
63		76	st	76	
68		80	st	83	
76	st	82	st	92	
80	st	86	st	101	
87	st	94	st	114	st
94	st	100		128	
101	st	103	st	136	
113	st	109		140	
128	st	113		144	st
135	st	127	st	150	
141	st	136	st	156	
144	st	141	st	163	
156		144	st	168	
163		149		184	st

Table 1: Normal mode frequencies in Hz

vert freq	strength	horiz freq	strength	long freq	strength
168		156	st	188	st
173	st	159		190	st
183	st	163	st	193	st
189	st	175	st	199	st
194	st	184	st	206	st
196	st	189	st	211	st
200	st	193	st	217	st
207	st	196	st	222	st
213	st	199	st	226	st
220	st	208	st	234	st
226		221	st	239	st
231	st	230	st	246	st
236		234	st	250	st
243		238	st	253	
249		241	st	262	st
254		250		267	st
263		261	st	270	st
270		266		274	st
276	st	269		284	st
278	st	278	st	291	
285		303		297	
292		308		301	
303	st	314	st	304	st
312		324		320	
319		325		330	
324		345	st	334	
331		350	st	343	

Table 1: Normal mode frequencies in Hz

vert freq	strength	horiz freq	strength	long freq	strength
335		357	st	350	st
338	st	360		354	
342		365		358	st
350	st	371		366	st
358		375		369	st
371	st	378		376	st
376	st	382	st	380	st
381		390	st	383	st
384	st	395	st	388	st
388	st	398	st	396	st
398					



P.O.Box 160
Richland, WA
99352

March 25, 1997

Phone: 509 376-0606
Fax: 509 372-1582

California Institute of Technology
LIGO Project
Ms. Linda Turner, Mail Stop 51-33
391 So. Holliston Ave.
Pasadena, California 91125

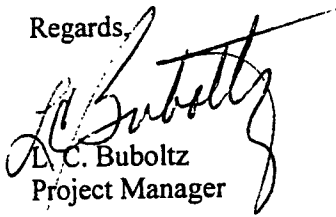
Reference: Caltech Contract No. PC181520
LIGO Beam Tube Modules
Fabrication and Installation

Subject: Project Status Review Data Package - CDRL # 25 O
CBI-CT-2.2 / 0216

Attached is a copy of the data package that was transmitted to Caltech during the March 25 Project Status Review Meeting at LIGO site Hanford, WA. Five copies of CDRL # 25O were provided to the LIGO representatives at the meeting. This copy is being sent for your convenience.

This data package is submitted for information and no response from Caltech is required.

Regards,


L.C. Buboltz
Project Manager



Project Status Review Data Package

CBI Services, Inc.
953570

Contract No. PC181520
LIGO Beam Tube Modules

DRD No. 04
CDRL No. 25 O

Date of Issue: March 25, 1997

Document No. LIGO-C970466-00-1

Submitted for: Caltech's Information
Caltech's Approval

If Submitted for Approval:

Submitted By : _____ Date _____
CBI Signature

This Document has been reviewed and is: A - Approved
(Reviewer to circle appropriate code) C - Approved with Comments
D - Disapproved

By : _____ Date _____
Caltech Signature

DRD No. 04 - Project Status Review Data Package
CDRL # 25o - March 25, 1997 Meeting
Data Package Index

A)	Monthly Up-date Schedule	4 pages
B)	Review Active Tasks	4 pages
	Attachment: Procurement Schedule/Plan	5 pages
C)	CDRL # 1 Through 24 Status	2 pages
D)	CBI RFI Status Report	1 page
E)	Action Item Log	1 page

LIGO - 1.1.2 Beam Tube Modules

California Institute of Technology
CBI Services, Inc.
Monthly Schedule Update - DRD#4-b

Planned 
Critical 
Float 
Milestone 
Baseline 

Project: L-NOW
Time Now: 21Mar97
Start: 11Dec95
Finish: 03Feb99
Run: 24Mar97
Page: 1 of 4

Activity ID	Activity Desc.	FI	Start	Finish	% Cp.	1996												1997												1998												1999			
						01	02	03	04	05	06	07	08	09	10	11	12	01	02	03	04	05	06	07	08	09	10	11	12	01	02	03	04	05	06	07	08	09	10	11	12	01	02	03	04
0	Contract Award	0	11Dec95	12Dec95	100	.S. #1																																							
1.01	Prepare DRD # 1 for Review	0	11Dec95	07Mar96	100	Time Now																																							
1.02	Prepare DRD # 2 for Review	0	11Dec95	09Mar96	100																																								
1.03	Prepare DRD # 3 for Review	0	11Dec95	09Mar96	100																																								
1.05	Prepare DRD #5 - Presentations	0	27Feb96	27Mar96	100																																								
1.09	Presentation Practice	0	20Mar96	27Mar96	100																																								
1.10	Submit Draft Documents for Review	0	11Mar96	14Mar96	100																																								
1.11	Caltech Review	0	13Mar96	27Mar96	100																																								
1.12	Design Review Meeting	0	27Mar96	28Mar96	100	ΔMS.#2																																							
1.13	Caltech Comments and Design Approv	0	28Mar96	26Oct96	100																																								
1.14	Final Design / Details	0	22Apr96	12Nov96	100																																								
1.20	Purchase Mill	0	21Dec95	22Dec95	100																																								
1.21	Fabricate Tube Mill and Qualify in Sho	0	26Dec95	30Jun96	100																																								
1.22	Mill Qualification in Shop Complete	0	29Jun96	30Jun96	100	ΔMS.#3																																							
1.24	Commence Ordering Material	0	19Feb96	20Feb96	100	Δ																																							
2.01	Washington On-Site Project Team	0	25Mar96	26Mar96	100	Δ																																							
2.02.7	Mob On Site Tube Spiral Welding Shop	0	03Jun96	27Jul96	100																																								
2.06.10	Complete Batch #1 to Ship (at Mill)	0	28Mar96	29Mar96	100	ΔMS.#4																																							
2.06.20	Complete Batch #2 to Ship (at Mill)	0	21May96	22May96	100	ΔMS.#4a																																							
2.06.30	Complete Batch #3 to Ship (at Mill)	0	31Jul96	01Aug96	100	ΔMS.#5																																							
2.06.40	Complete Batch #4 to Ship (at Mill)	0	07Oct96	08Oct96	100	ΔMS.#6																																							
2.07	Purchasing	0	29May96	02Nov96	100																																								
2.08.00	Equipment Qualification Tests	0	13Aug96	30Aug96	100																																								
2.08.01	Fabrication Readiness Review at WA	0	18Sep96	19Sep96	100																																								
2.08.02	Fab Tube Number 0-50	0	14Aug96	26Oct96	100																																								
2.08.03	Complete Tube Number 0-50	0	25Oct96	26Oct96	100	ΔMS.#8																																							
2.08.04	Fab Tube Number 51-100	0	22Oct96	27Nov96	100	ΔMS.#9																																							
2.08.05	Complete Tube Number 51-100	0	26Nov96	27Nov96	100	ΔMS.#10																																							
2.08.06	Fab Tube Number 101-150	0	13Nov96	15Jan97	100																																								
2.08.07	Complete Tube Number 101-150	0	14Jan97	15Jan97	100																																								
2.08.08	Fab Tube Number 151-200	0	14Dec96	14Feb97	100																																								

Section B

Design

Final Design and Details

(Activity ID 1.14)

Changes to the engineering documentation have been made in response to site activities. The "Accept" procedure and the "Leak-Loc" procedure of CDRL's 21 and 22 have been revised by CBI and a preliminary copy has been sent to Caltech. CBI and LIGO project personnel are involved in ongoing discussions regarding the module leak test activities. CBI will formally submit revised procedures for CDRL's #21 and 22 on or before April 4th. Record drawings have been prepared for each specific module at Hanford and Livingston.

The following CDRL's were submitted since the last Project Review Meeting held on February 20th:

CDRL #10 Termination Support

The termination support drawings were revised to incorporate a bolted connection in the termination support. The bolted connection allows placement of the termination support after the beam tube has been welded to the valve in the final location. The calculations for the bolted connection were included with this submittal.

CDRL #13 Pump Port Hardware

The drawing for the Type B Pump Port Hardware were revised to include an LN2 level controller and to incorporate minor changes in the equipment mounting locations.

CDRL #17 Cleanliness Monitor

The procedures have been revised to reflect current practices.

CDRL #24-4 Alternative Guided Support

The guided support drawings were revised to allow the use of an anchor bolt coupling and to include the cable spacers for the horizontal cables at the Hanford site. A thermal analysis was also submitted which shows that the horizontal cables do not slacken and slide downward during module bake out.

CDRL #24-5 Installation Sequence

The procedures have been revised to reflect current practices.

CDRL #24-13 Fitting and Purging Procedures

The procedures for fitting and purging in the shop and field have been revised to reflect sequencing modifications.

Coupon Testing

Coupon testing continued with the tenth batch of coupons from coils 5B which were designated "J" coupons. The hydrogen outgassing rate was measured on March 20th. The hydrogen outgassing rate of this batch of material was calculated to be between -3.1×10^{-15} and -3.9×10^{-15} TL/s cm². Although the results are negative, the results were very repeatable and the combined chamber and coupon average outgassing rate was 3.6×10^{-14} TL/s cm² which is well below the acceptance rate of 1×10^{-13} TL/s cm².

Major Purchases

SS Material for WA Site

(Activity ID 2.06)

The final shipment of batch #5A has been received at the Pasco Facility. Batch # 5B coupons have been tested for hydrogen outgassing. Batch #5D is scheduled for loading in the bake oven in two weeks. Batch # 5C will complete coil needs for the Hanford site. The procurement schedule/plan for coil batches #5 and, #6 is attached at the end of this section.

Other Beam Tube Parts and Components

Material deliveries continue at the Pasco shop. Additional material requirements are being quantified for fabrication of the remainder of Hanford tubes.

Module Testing Equipment

The assembly and testing of the Pump Port Hardware has been completed by Meyer Tool and Manufacturing of Oak Lawn, Illinois. The type B pump port hardware assemblies are currently in transit from Oak Lawn to the Hanford site and are scheduled for delivery to site by March 31.

The transformers have been procured through Benton County PUD. Purchase orders for associated electrical equipment have been issued for delivery on or before April 18

Hanford Production

Fabrication

As of Friday March 21,

- 276 tubes have been produced by the spiral mill.
- 255 tube assemblies have been manufactured.
- 252 tube assemblies have passed leak testing.
- 191 tube assemblies have been cleaned and sealed.
- 172 tube assemblies have been transported to the site.

An improved spider assembly is being installed on the tube mill. The ball transfers with machined shafts allow increased movement without binding. A WeldLogic technician is scheduled to visit Pasco on 3-31-97 to perform maintenance.

The shop is fabricating the short tube assemblies required at the terminations.

Installation

As of Friday March 21,

170 tube assemblies have been fit-up and welded in place.

168 field weld seams have passed leak testing.

29 tube assemblies have baffles installed and final inspected.

161 supports have been installed.

7 supports have been final aligned.

The crew continues to work four 10 hour shifts as the regular work hours, plus selective overtime some evenings and Fridays.

Tube installation is progressing smoothly and is slightly ahead of the rate needed to achieve the completion of the X-arm tube installation and removal of the BDF units from the mid-station area prior to April 25.

Some "new" baffles were received, and CBI began installing these. Putting the baffles in place went as expected, however, CBI did encounter more problems getting the baffles in the beam tube than anticipated. Changes are being made to the method of transporting the baffles (transport carts) prior to installing additional baffles.

The BDF particulate monitor has been installed and is functioning.

The X-arm alignment is proceeding concurrently with beam tube installation. Final position of beam tube supports and reference nail locations are pacing the installation of supports. Alignment of beam tube supports under the covers is proceeding. Seven(7) are complete, inspected and painted. CBI will continue the adjustments under the concrete covers using the GPS layout and reference nail positions. The check of fixed support positions is also proceeding using an alignment scope for vertical inspection and a string line for lateral checks.

CBI has begun the layout of the -Y- arm coordinates. Initial points will be located at the end station, corner station and both sides of the mid-station for an optical verification of GPS calibration.

Livingston Mobilization

Fabrication Facility Mobilization

300' of the floor slab was poured as of 3/20/97. The metal building is scheduled for delivery 3/28/97. Structural design is complete. Facility drawings will be completed by 3/25/97. Power City Electric is prepared to support the shop demobilization and re-mobilization efforts. V. Gervais and K. Drake have schedule a trip to Louisiana for 3/31/97 through 4/4/97.

Procurement Schedule/Plan - Batch #5 (18 @ 36" Wide Coils)

Start Date	Duration (Days)	Complete Date	Description of Operation	Surveillance by CBI	
Manufacture Batch #5 - Sixty (60) Coils					
Completed	56		Armco produces eighteen (18) hot rolled coils		
Completed	7		Anneal & Pickle the eighteen (18) coils at NAS	W1	
Bake, Level, Test & Slit - Six (6) Coils (Batch #5A)					
Completed	7		Ship six (6) of the coils to Metlab		
Completed	14		Bake six (6) coils @ Metlab		
Completed	7		Ship six (6) coils to Leveltek		
Completed	7		Level six (6) coils and cut coupons at Leveltek		
Completed	7		Ship & Clean Coupons		
Completed	14		Perform Hydrogen Outgas Test at CBI		
Completed	7		Ship six (6) coils to Washington Specialty		
Completed	7		Slit six (6) coils to 36" width	W2	
Completed	14		Ship six (6) coils to site		
Completed	7		Receive and Inspect six coils at site	W3	
Bake, Level, Test & Slit - Six (6) Coils (Batch #5B)					
Completed	7		Ship six (6) coils to Metlab		
Completed	14		Bake six coils @ Metlab	W2	
Completed	7		Ship coils to Leveltek		
Completed	7		Level coil and cut coupons		
Completed	7		Ship & Clean Coupons		
Completed	14		Perform Hydrogen Outgas Test at CBI		
Completed	7		Ship coils from Leveltek to Washington Specialty		
In Process	7	4/2/97	Slit coils to 36" width	W2	
	4/2/97	14	4/16/97	Ship six (6) coils to site	
	4/16/97	3	4/19/97	Receive and Inspect six coils at site	W3
Bake, Level, Test & Slit - Six (6) Coils (Batch #5C)					
Completed	7		Ship six (6) coils to Metlab		
Completed	11		Bake six coils @ Metlab	W2	
Completed	7		Ship coils to Leveltek		
In Process	7	3/28/97	Level coil and cut coupons		
	3/28/97	4	4/1/97	Ship & Clean Coupons	
	4/1/97	10	4/11/97	Perform Hydrogen Outgas Test at CBI	
	4/11/97	7	4/18/97	Ship coils from Leveltek to Washington Specialty	
	4/18/97	7	4/25/97	Slit coils to 36" width	W2
	4/25/97	14	5/9/97	Ship six (6) coils to site	
	5/9/97	3	5/12/97	Receive and Inspect six coils at site	W3

Procurement Schedule/Plan - Batch #5 (18 @ 36" Wide Coils)

Start Date	Duration (Days)	Complete Date	Description of Operation	Surveillance by CBI
Bake, Level, Test & Slit - Six (6) Coils (Batch #5D)				
Completed	7		Ship six (6) coils to Metlab	
4/7/97	14	4/21/97	Bake six coils @ Metlab	W2
4/21/97	7	4/28/97	Ship coils to Leveltek	
4/28/97	7	5/5/97	Level coil and cut coupons	
5/5/97	7	5/12/97	Ship & Clean Coupons	
5/12/97	14	5/26/97	Perform Hydrogen Outgas Test at CBI	
5/26/97	7	6/2/97	Ship coils from Leveltek to Washington Specialty	
6/2/97	7	6/9/97	Slit coils to 36" width	W2
6/9/97	77	8/25/97	Store Material for use at Livingston	
8/25/97	7	9/1/97	Ship six (6) coils to site	
9/1/97	3	9/4/97	Receive and Inspect six coils at site	W3
Bake, Level, Test & Slit - Six (6) Coils (Batch #5E)				
4/21/97	7	4/28/97	Ship six (6) coils to Metlab	
4/28/97	14	5/12/97	Bake six coils @ Metlab	W2
5/12/97	7	5/19/97	Ship coils to Leveltek	
5/19/97	7	5/26/97	Level coil and cut coupons	
5/26/97	7	6/2/97	Ship & Clean Coupons	
6/2/97	14	6/16/97	Perform Hydrogen Outgas Test at CBI	
6/16/97	7	6/23/97	Ship coils from Leveltek to Washington Specialty	
6/23/97	7	6/30/97	Slit coils to 36" width	W2
6/30/97	77	9/15/97	Store Material for use at Livingston	
9/15/97	7	9/22/97	Ship six (6) coils to site	
9/22/97	3	9/25/97	Receive and Inspect six coils at site	W3
Bake, Level, Test & Slit - Six (6) Coils (Batch #5F)				
5/12/97	7	5/19/97	Ship six (6) coils to Metlab	
5/19/97	14	6/2/97	Bake six coils @ Metlab	W2
6/2/97	7	6/9/97	Ship coils to Leveltek	
6/9/97	7	6/16/97	Level coil and cut coupons	
6/16/97	7	6/23/97	Ship & Clean Coupons	
6/23/97	14	7/7/97	Perform Hydrogen Outgas Test at CBI	
7/7/97	7	7/14/97	Ship coils from Leveltek to Washington Specialty	
7/14/97	7	7/21/97	Slit coils to 36" width	W2
7/21/97	77	10/6/97	Store Material for use at Livingston	
10/6/97	7	10/13/97	Ship six (6) coils to site	
10/13/97	3	10/16/97	Receive and Inspect six coils at site	W3

Procurement Schedule/Plan - Batch #5 (18 @ 36" Wide Coils)

Start Date	Duration (Days)	Complete Date	Description of Operation	Surveillance by CBI
Bake, Level, Test & Slit - Six (6) Coils (Batch #5G)				
6/2/97	7	6/9/97	Ship six (6) coils to Metlab	
6/9/97	14	6/23/97	Bake six coils @ Metlab	W2
6/23/97	7	6/30/97	Ship coils to Leveltek	
6/30/97	7	7/7/97	Level coil and cut coupons	
7/7/97	7	7/14/97	Ship & Clean Coupons	
7/14/97	14	7/28/97	Perform Hydrogen Outgas Test at CBI	
7/28/97	7	8/4/97	Ship coils from Leveltek to Washington Specialty	
8/4/97	7	8/11/97	Slit coils to 36" width	W2
8/11/97	77	10/27/97	Store Material for use at Livingston	
10/27/97	7	11/3/97	Ship six (6) coils to site	
11/3/97	3	11/6/97	Receive and Inspect six coils at site	W3
Bake, Level, Test & Slit - Six (6) Coils (Batch #5H)				
6/23/97	7	6/30/97	Ship six (6) coils to Metlab	
6/30/97	14	7/14/97	Bake six coils @ Metlab	W2
7/14/97	7	7/21/97	Ship coils to Leveltek	
7/21/97	7	7/28/97	Level coil and cut coupons	
7/28/97	7	8/4/97	Ship & Clean Coupons	
8/4/97	14	8/18/97	Perform Hydrogen Outgas Test at CBI	
8/18/97	7	8/25/97	Ship coils from Leveltek to Washington Specialty	
8/25/97	7	9/1/97	Slit coils to 36" width	W2
9/1/97	77	11/17/97	Store Material for use at Livingston	
11/17/97	7	11/24/97	Ship six (6) coils to site	
11/24/97	3	11/27/97	Receive and Inspect six coils at site	W3
Bake, Level, Test & Slit - Six (6) Coils (Batch #5I)				
7/14/97	7	7/21/97	Ship six (6) coils to Metlab	
7/21/97	14	8/4/97	Bake six coils @ Metlab	W2
8/4/97	7	8/11/97	Ship coils to Leveltek	
8/11/97	7	8/18/97	Level coil and cut coupons	
8/18/97	7	8/25/97	Ship & Clean Coupons	
8/25/97	14	9/8/97	Perform Hydrogen Outgas Test at CBI	
9/8/97	7	9/15/97	Ship coils from Leveltek to Washington Specialty	
9/15/97	7	9/22/97	Slit coils to 36" width	W2
9/22/97	77	12/8/97	Store Material for use at Livingston	
12/8/97	7	12/15/97	Ship six (6) coils to site	
12/15/97	3	12/18/97	Receive and Inspect six coils at site	W3

Procurement Schedule/Plan - Batch #5 (18 @ 36" Wide Coils)

Start Date	Duration (Days)	Complete Date	Description of Operation	Surveillance by CBI
Bake, Level, Test & Slit - Six (6) Coils (Batch #5J)				
8/4/97	7	8/11/97	Ship six (6) coils to Metlab	
8/11/97	14	8/25/97	Bake six coils @ Metlab	W2
8/25/97	7	9/1/97	Ship coils to Leveltek	
9/1/97	7	9/8/97	Level coil and cut coupons	
9/8/97	7	9/15/97	Ship & Clean Coupons	
9/15/97	14	9/29/97	Perform Hydrogen Outgas Test at CBI	
9/29/97	7	10/6/97	Ship coils from Leveltek to Washington Specialty	
10/6/97	7	10/13/97	Slit coils to 36" width	W2
10/13/97	77	12/29/97	Store Material for use at Livingston	
12/29/97	7	1/5/98	Ship six (6) coils to site	
1/5/98	3	1/8/98	Receive and Inspect six coils at site	W3

- W1 Witness the first operation
- W2 Witness first operation and others as needed
- W3 Witness all operations

Procurement Schedule/Plan - Batch #6 (12 @ 36" Wide Coils)				
Start Date	Duration (Days)	Complete Date	Description of Operation	Surveillance by CBI
Manufacture Batch #6 - Twelve (12) Coils				
9/8/97	42	10/20/97	Armco produces eighteen (12) hot rolled coils	
10/20/97	14	11/3/97	Anneal & Pickle the eighteen (18) coils at NAS	W1
Bake, Level, Test & Slit - Six (6) Coils (Batch #6A)				
11/3/97	7	11/10/97	Ship six (6) of the coils to Metlab	
11/10/97	14	11/24/97	Bake six (6) coils @ Metlab	
11/24/97	7	12/1/97	Ship six (6) coils to Leveltek	
12/1/97	7	12/8/97	Level six (6) coils and cut coupons at Leveltek	
12/8/97	7	12/15/97	Ship & Clean Coupons	
12/15/97	14	12/29/97	Perform Hydrogen Outgas Test at CBI	
12/29/97	7	1/5/98	Ship six (6) coils to Washington Specialty	
1/5/98	7	1/12/98	Slit six (6) coils to 36" width	W2
1/12/98	7	1/19/98	Ship six (6) coils to site	
1/19/98	7	1/26/98	Receive and Inspect six coils at site	W3
Bake, Level, Test & Slit - Six (6) Coils (Batch #6B)				
11/17/97	7	11/24/97	Ship six (6) of the coils to Metlab	
11/24/97	14	12/8/97	Bake six (6) coils @ Metlab	
12/8/97	7	12/15/97	Ship six (6) coils to Leveltek	
12/15/97	7	12/22/97	Level six (6) coils and cut coupons at Leveltek	
12/22/97	7	12/29/97	Ship & Clean Coupons	
12/29/97	14	1/12/98	Perform Hydrogen Outgas Test at CBI	
1/12/98	7	1/19/98	Ship six (6) coils to Washington Specialty	
1/19/98	7	1/26/98	Slit six (6) coils to 36" width	W2
1/26/98	7	2/2/98	Ship six (6) coils to site	
2/2/98	7	2/9/98	Receive and Inspect six coils at site	W3



LIGO PROJECT
 CDRL # 1 THROUGH 24 STATUS
 PROJECT REVIEW MEETING
 JANUARY 16, 1997

cdrl	DESCRIPTION	CT DOC	STATUS	CB&I
1.	Schedule	TDM 96-003	Submitted & approved.	MLT
2.	Configurations Mgmt	TDM 96-003	Submitted & approved.	MLT
3.	QA Plan	TDM 96-003 & 96-007	Survey plan & record dwgs revision required per 96-007.	RAJ
4.	Resource Plan	TDM 96-003	Submitted & approved.	MLT
5.	Safety Plan	TDM 96-003	Submitted & approved.	GPB
6.	Subcontract Plan	TDM 96-003	Submitted & approved.	RAJ
7.	Fabrication Plan	TDM 96-004	Submitted & approved.	SWP
8.	Installation Plan	TDM 96-004	Preliminary reviewed by Caltech. Rev required for spring rate / temp adjust.	KSD
9.	Acceptance Test Plan	TDM 96-003	Submitted & approved.	VFG
10.	Terminations	TDMs 96-003 & 006	Revised per TDM-006 & submitted for approval 9/13/96. Rev req'd for bolting.	WAC
11.	Termination ICD	TDM 96-003	ICD-BTT approved. ICD-BTSLAB rev req'd.	MLT
12.	Module Length	TDMs 96-003 & 006	Rev 1 per 96-003 & rev 2 per 96-006 approved. Rev for additional bake T submitted on 12/11/96.	MLT
13.	Pump Port Hardware	TDM 96-003	Revised drawings #101 & 104 submitted for approval on 12/11/96.	WAC
14.	Pump Port Hard ICD	TDM 96-020 TDM 96-003 & 96-008A	Revision required per PSI drawings in 96-008A.	MLT
15.	Spiral Weld Quality	TDM 96-004	Submitted & approved.	RAJ
16.	Cleaning Equipment	TDM 96-003	Submitted & approved.	DWD
17.	Cleanliness Monitor	TDM 96-004	Revised & submitted 3/18/97	SWP
18.	Field Enclosures	TDM 96-003	Revision required.	VFG
19.	Vacuum Box	TDMs 96-003, 008, & 020	HMST2N revision required per TDM 96-020.	PBS
20.	Baffles	TDM 96-003 & 96-005.	ICD & procedure partially revised. Position documentation req'd.	WAC
21.	Leak Localization		Draft submitted on 9/24. Caltech comments required.	WAC
22.	Acceptance Test Pro.		Draft submitted on 9/24. Caltech comments required.	WAC
23.	Alignment Alternate	TDM 96-003 TDM 96-018	Submitted and approved except for aperture budget.	SDH
24-1	Fabrication Sequence	TDM 96-004	Submitted and approved.	KSD
24-2	Section Leak Test	TDM 96-003 & 96-009	Submitted and approved.	PBS
				WAC



LIGO PROJECT
CDRL # 1 THROUGH 24 STATUS
PROJECT REVIEW MEETING
JANUARY 16, 1997

24-3	Alternative Fixed	TDMs 96-003 & 006	Submitted and approved.	MLT
24-4	Alternative Guided	TDMs 96-003 & 006	Thermal analysis provided to Caltech for review.	MLT
24-5	Installation Sequence	TDM 96-004	Revised & submitted 3/18/97.	VFG
24-6	WPS & PQR		Submitted & approved.	RAJ
24-7	Expansion Joint Spec		Submitted & approved. Rev req'd for range in motion due to higher bake T.	MLT
24-8	Stiffener Dwgs & Specs	TDM 96-006	Submitted and approved.	DTR
24-9	Soft Support Drawing	TIM 17A & RFI #22	Submitted and approved.	DTR
24-10	Coil Material Bake Spec	RFI #21	Submitted and approved.	MLT
24-11	Pump Port Dwg & Specs		Submitted and approved.	MLT
24-12	Pump Port Leak Test		HMST3N revision required per 96-020.	MLT
24-13	Fitting & Purging Procedures		Revised & submitted 3/18/97.	RAJ

CBI RFI STATUS REPORT

Notebook 1 Page 1

RFI 1 - RFI 29

21-Mar-97

CBI rfi#	CBI-CT TRANS #	DESCRIPTION	Dwg or Spec	RESPONSE TRANSMIT #	REPLY	O/C
1	2.2-0023	Valve To Tube Interface	NA	LJ Fax 12/8/95	Interface discussions with Caltech required.	O
2	2.2-0023	Air Signature and Leak Localization	NA	LJ Fax 2/16/96	DRD No.03 j & k sent to Caltech for review.	C
3	2.2-0023	Request for 100% Baffle Design Submittal	NA	Change Oder 3	Baffles detail dwgs provided, locations & wps required.	C
4	2.3-0024	Expansion Joint Material Surface Finish	C-EJ-CO	LJ Fax 1/19/96	Cold rolled material is allowed.	C
5	2.3-0024	Ex Joint Factory Leak Test Sensitivity	C-EJ-CO	LJ Fax 1/19/96	Retain leak criterion & cleaning req., change spec C-EJ-CO	C
6	2.3-0029	BT Valve Soft Support	NA	LJ Fax 1/26/96	Employing a custom unit per valve (see Change 9504)	C
7	2.3/0036	Expansion Joint Spec Revision	C-EJ-CO	LJ Fax 2/2/96	Requested revisions to C-EJ-CO approved	C
8	2.2/0037	PSI 48 inch Gate Valve Leak Potential	NA	LJ Fax 2/21/96	Leak check at acceptance test w/HMS	C
9	2.2/0037	GPS Altnernate Alignment, DRD #3 item l	ALM-B	TDM 96-02	Draft DRD No. 3I submitted on 3/12/96 per verbal	C
10	2.2/0037	112 cm & 122 cm Gate Valve Dimensions	NA	Ltr4/29&TIM017	Dwgs for 112 provided, dwgs for122 req'd. Final dwgs req'd.	O
11	2.2/0041	P P Hardware Interface Requirements	NA	TDM 96-02	CBI to prep. COR for xformer delection & interface per TIM 20	C
12	2.3/0038	B T Guided Support Configuration	CBI 17,18	LJ Fax 2/22/96	Approved alternative supports.	C
13	2.3/0040	Termination Support Foundation Dimen	NA	LJ Fax 3/1/96	Dimensions from end of BT to termination block	C
14	2.2/0049	Pump Port Hardware	NA	LJ Fax 3/1/96	Approved replacement of valves (see Change 9607)	C
15	2.3/0043	Pump Port Locations at Terminations	NA	LJ Fax 3/1/96	Approved change in length	C
16	2.3/0043	Fixed Support Bracket Modification	CBI 6,7	LF Fac4/8/96	Approved alternative supports subject to \$ negotiations.	C
17	2.2/0079	Fixed Support Base Plate Modification	CBI 8		Subject to acceptance of CBI value engineering proposal.	C
18	2.3/0064	Gate Valve Soft Support Review	D-960051	TIM-014, 5/23	Caltech response provided.	C
19	2.2/0093	Pump Port Hardware Clarification	NA		Verbal response provided.	C
20	2.2/0093	Ex Jt Cleaning & Leak Testing Sequence	C-EJ-CO	TIM-016,6/28	Hold for 24 hours after cleaning before leak testing.	C
21	2.2/0128	Higher Baked Temperature	C-CMBS1		Bake temperature range increased to 444 C +/- 12 C	C
22	2.3/0069	Soft Support Interference	CBI 22		Verbal response received to modify support & reduce adjust.	C
23	2.3/0178	Pump Port Hardware Configuration	D-950027	TDM-021	Caltech response provided.	C
24	2.3/0087	Building Status at module terminations		CBI-CT2.2/210	LCB/L Jones, 2.2/210 Mtg. Notes are Response	C
25	2.3/0088	Power for Module Leak Testing		CBI-CT2.2/210	LCB/L Jones, 2.2/210 Mtg. Notes are Response	C
26	2.2/0207	Cover Cond./P.P.Access at Mod. Lk. Test				O
27	2.3/0089	Y-Arm Monument Coordinates		TDM 96-014C		C
28	2.3/0090	Ambient Air Monitor Req.		TIM-028	CT-CBI-2.8/0032	C
29	2.3/0092	Use of Support Stiffener		TIM-029	CT-CBI-2.8/0034	C

LIGO Beam Tube Module Contract # PC181520

Action Item List

Item #	Description of Issue	Initiation Date	Doc./ Ltr #	Resp.	Response Date	Comments / Closing Action	Open / Closed
CBI Action Items							
						Incorporated in CO # 6	C
CBI-31	Provide proposal for supplemental particulate monitor	11/15/96	Verbal	LCB	11/27/96	Incorporated in CO # 6	C
CBI-36	Formally proposal S-001 Tube Cleaning	12/10/96	PSRM	LCB	1/23/96	Incorporated in CO # 6	C
CBI-38	Develop Plan to Ensure Balanced BDF air flow	1/16/97	PSRM	SDH	2/7/97	Periodic monitoring and rebalancing	O
CBI-39	Provide COR 13 & 14	2/20/97	PSRM	LCB	2/25/97		O
CBI-40	RFI for module end conditions	2/20/97	PSRM	VFG	2/25/97	RFI 24 and 25 issued	C
CBI-41	Advise Caltech regarding Start of Cover Grouting	2/20/97	PSRM	VFG	2/25/97		O
CBI-42							
CBI-43							
CBI-44							
CBI-45							
CBI-46							
Caltech Action Items							
		2/13/96	CM	OM	9/4/96	Preliminary information provided, add'l discuss req'd	O
CAL-10	Provide information on end of slab building conditions.	6/19/96	PSRM	BA	2/20/97		O
CAL-19	Provide controlled drawing list with current rev levels.	11/13/96	PSRM	LJ	11/15/96	LeVernier is working at end station	C
CAL-34	LeVernier access to the X arm	1/16/97	PSRM	LJ	2/7/97		O
CAL-40	Provide response to CDRL 21 and 22	1/16/97	PSRM	EJ	2/7/97	Incorporated in CO # 6	C
CAL-41	Modify GP's to include CBI as Agent in LA	2/20/97	PSRM	EJ	2/28/97	CO # 6 received	C
CAL-42	Prepare CO #6	2/20/97	PSRM	LJ	2/28/97	TIM # 027	O
CAL-43	Prepare TIM regarding use of sunscreen	2/20/97	PSRM	LJ	2/25/97	NCR's being resolved	O
CAL-44	Response on Weld Seam Alignment and related NCR's	2/20/97	PSRM	LJ	3/7/97		O
CAL-45	Provide Y arm monument positions in WGS-84 coordinates						
CAL-46							
CAL-47							
CAL-48							
CAL-49							

LASER INTERFEROMETER GRAVITATIONAL WAVE OBSERVATORY
- LIGO -

CALIFORNIA INSTITUTE OF TECHNOLOGY
MASSACHUSETTS INSTITUTE OF TECHNOLOGY

Technical Note LIGO-T960178-01 - E 12/9/96
Beam Tube Bakeout Conceptual Design
W. Young

Distribution of this draft:

This is an internal working note
of the LIGO Project.

California Institute of Technology
LIGO Project - MS 51-33
Pasadena CA 91125
Phone (818) 395-2129
Fax (818) 304-9834
E-mail: info@ligo.caltech.edu

Massachusetts Institute of Technology
LIGO Project - MS 20B-145
Cambridge, MA 01239
Phone (617) 253-4824
Fax (617) 253-7014
E-mail: info@ligo.mit.edu

WWW: <http://www.ligo.caltech.edu/>

1 INTRODUCTION

1.1. Purpose and Scope

The purpose of this document is to outline a conceptual design for the thermal insulation, heating power and control, pumping, instrumentation, and data acquisition and logging equipment to be used for the bakeout of the LIGO Beam Tube Modules. The conceptual design is used to illustrate a design approach which meets the requirements defined in the draft Beam Tube Bakeout Design Requirements Document (LIGO-E960123-01-E). During the preliminary design phase, analytical and trade-off studies will be performed to optimize the design approach. Once the design has been completed and approved, the equipment and processes developed will be used by the on-site LIGO staff to perform the bakeout.

1.2. Acronyms

AC	Alternating Current
AP	Blanked Port for Auxiliary Turbo Pump
BT	Beam Tube
BTE	Beam Tube Enclosure
CBI	Chicago Bridge and Iron, Inc. (Beam Tube fabrication and installation contractor)
CC	Cold Cathode Gauge
CH ₄	Methane
CL	Blanked Port for Calibrated Leaks
CO	Carbon Monoxide
CO ₂	Carbon Dioxide
DAS	Data Acquisition System
DC	Direct Current
DRD	Design Requirements Document
L	Variable Leak Valve
LIGO	Laser Interferometer Gravitational Wave Observatory
LN ₂	Liquid Nitrogen Trap
M	Metal Sealed Valve
P	Pirani Gauge
PCF	Pound/Cubic-Foot
PSI	Process Systems International
PLC	Programmable Logic Controller
RGA	Residual Gas Analyzer
RP	Blanked Port for Roots and Turbo Pumps
TBS	To Be Supply
V	Viton Sealed Valve

1.3. Applicable Documents

1.3.1. LIGO Documents

- M950001 Project Management Plan, latest revision
- E950018 Science Requirements Document, latest revision
- E950020 Beam Tube Module Requirements-Fabrication & Installation Contract, latest revision
- E960123 Beam Tube Bakeout Design Requirements Document, latest revision
- E940002 Vacuum Equipment Specification, latest revision
- E94xxxx Beam Tube Module Specification (formerly Specification No. 1100004)
- E94xxxx Process Specification for Low Hydrogen, Type 304L Stainless Steel Vacuum Products (formerly Specification No. 1100007)
- M96xxxx Configuration Management Plan, latest revision
- M950046 Project System Safety Plan, latest revision
- E950089 Interface Control Document (ICD): Beam Tube (BT) - Civil Construction (CC), latest revision
- D950027 Beam Tube Pump Port Hardware, latest revision

1.3.2. Non-LIGO Documents

TBD

2 OVERVIEW

The salient features of the LIGO beam tubes which affect the design of the bakeout are summarized here. The beam tube will be baked out in increments of 2 kilometer modules. The LIGO beam tube modules are stainless steel vacuum vessels, 1.2 m diameter by 2 km long. There are four such modules at each of two sites (8 total). Each vessel consists of 50 sections of stainless steel thin-wall (3.2 mm wall thickness) tubing, each 40 m long, separated by a stainless steel expansion joint designed to accommodate the thermal expansion of the 40 m sections during a bakeout. The tube sections are supported by structures designed to accommodate the thermal expansion and to minimize heat loss through the mechanical connections. The tube sections and expansion joints are welded together to form a continuous leak-tight tube. The ends of the 2 km long modules are terminated by 122 cm gate valves. There are nine 250 mm diameter pumping ports distributed at 250 m intervals along the module. The beam tube is enclosed in a concrete protective cover with access doors at each pump port location (there are also emergency accesses between the pump ports).

The beam tube bakeout design must meet the requirements given in the Beam Tube Bakeout Design Requirements Document, LIGO-E960123. The basic plan is to heat each beam tube module to ~ 150 °C under high vacuum for ~ 30 days, with sufficient pumping speed to remove adsorbed water and contaminants. The key elements of the conceptual design to do this are illustrated in schematic form in Figure 1 (here, to aid visualization, the beam tube is regarded simply as a vacuum vessel, stripped of its unusual geometry). The eight beam tube modules are baked sequentially, with equipment moved from one module to the next.¹ The elements are:

- **Insulation**, which reduces heat loss during bakeout from the hot vacuum vessel to an economical level and increases the thermal time constant of the vacuum vessel, reducing temperature dependence (both during bake and afterwards) on the ambient environment. Insulation will be wrapped around the entire length, ends and ports of a beam tube module.
- A **heater**, which dissipates energy from the local power company to raise the temperature of the vacuum vessel. The proposed bakeout system will heat the beam tube module with direct current flowing through the shell of the beam tube. Heating is by power loss in the resistance of the stainless steel shell (I^2R).
- The **heater power source**, which consists of the local power company which provides the electrical energy, AC transformers and wiring to deliver the power to DC power supplies which in turn convert the power to voltages and currents suitable for the heater, and attendant electrical wiring.
- A **heater controller**, which receives a signal from the **control temperature sensor** and adjusts the power delivered to the heater to maintain a constant temperature of the vacuum vessel.
- The **bake pumps**, which remove gases evolved during the bakeout and maintain a vacuum in the vacuum vessel.
- A **residual gas analyzer (RGA)**, a mass spectrometer which measures the partial pressures of residual gas in the vacuum vessel.

1. Currently it is assumed that it is most economical to leave the insulation and temperature sensors in place on each beam tube module, but this assumption is not crucial to the conceptual design.

- A **monitor system** which includes sensors (temperature of vacuum vessel, power supply currents and voltages, environmental parameters such as outside temperature and wind speed, and other engineering parameters as needed), data acquisition and display, and data recording. Data display and recording for the RGA will be separate from the monitor system, since these features can be purchased as options with the RGA controller, and data can be merged after-the-fact.

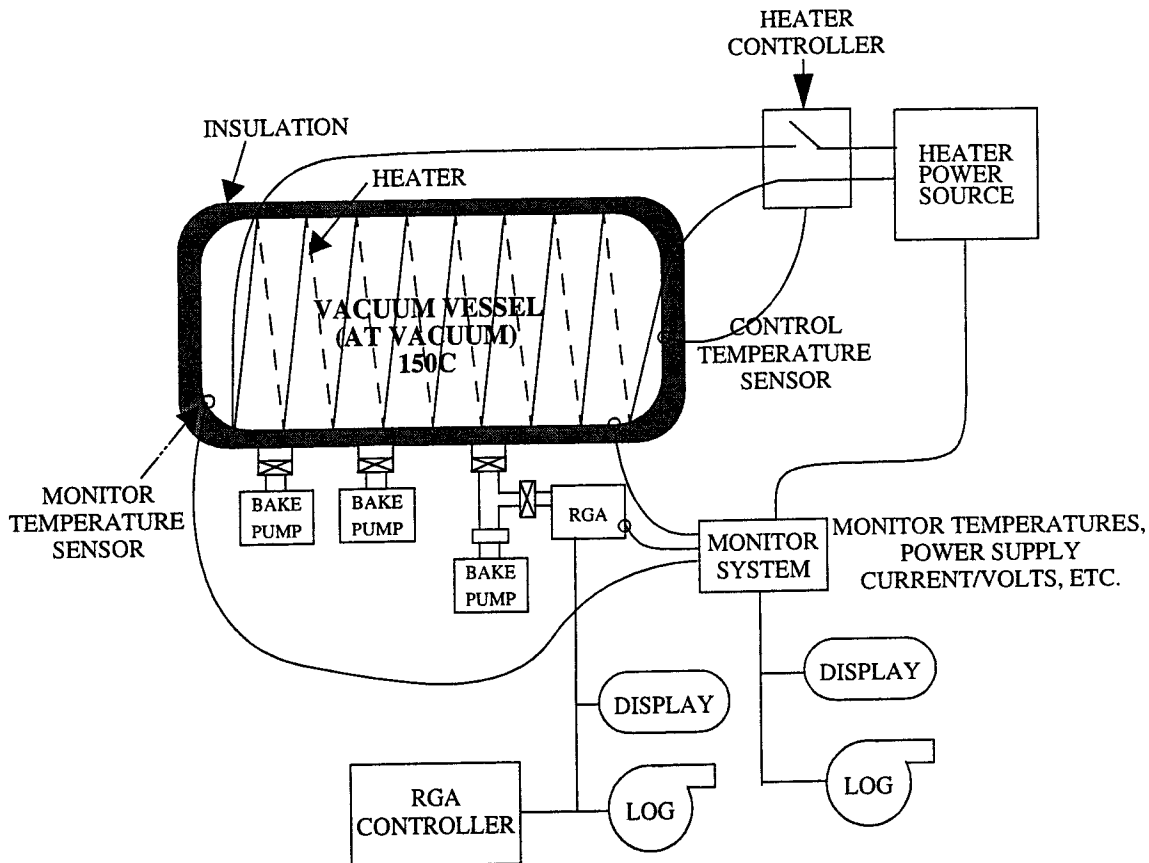


Figure 1: Schematic diagram of equipment during bakeout and cooldown

After the beam tube has been baked sufficiently, it is allowed to cool down (by shutting down the heater power) while continuing to pump. The heating equipment (heater power source and controller) can be immediately moved to the next beam tube module to be baked. After reaching ambient temperature, measurements are made of the residual gases in the beam tube to verify the success of the bakeout and to determine with maximum sensitivity whether any air leaks are present. The pumping speed needed is much lower than during the bake, and the RGA sensitivity needed is higher. To maximize equipment usage, the plan is to remove the pumps and RGA used during the bakeout and install them on the next beam tube module to be baked. A pump and RGA dedicated to post-bake measurements are then installed. This simplified equipment arrangement is illustrated schematically in Figure 2, where the nomenclature is the same as that defined above.

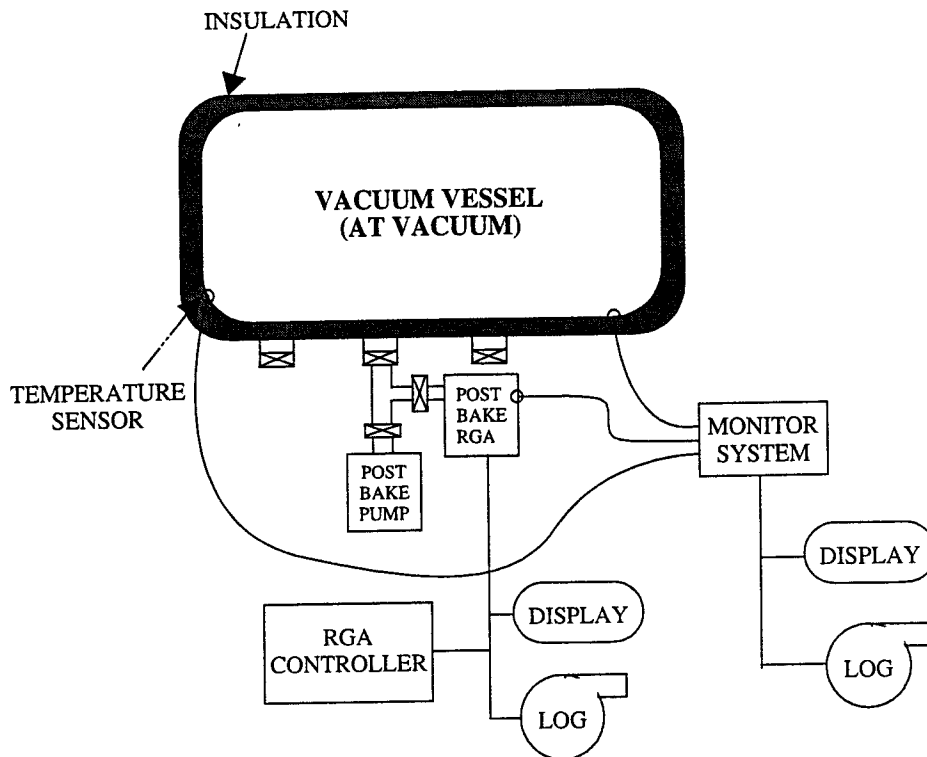


Figure 2: Schematic diagram of equipment during post-bake measurements

3 TECHNICAL DESCRIPTION

3.1. INSULATION

3.1.1. Tube Walls

The insulation consists of two layers of thermal insulation materials (see Figure 3). The first (inner) blanket layer is a 1.1 lb/ft³, 4 inch thick inorganic glass fiber blanket material bonded together by a high-temperature thermosetting resin. The inner blanket material is rated for 500°C. The second (outer) layer is a 0.75 lb/ft³, 2 inch thick inorganic glass fiber duct wrap rated for 120°C. The inside layer will be installed in wraps which match the stiffener ring spacing (~30 inch wide) and secured in place with aluminum bands. The outer layer will be installed over the inner layer with staggered seams, and also secured by bands. The outer layer has an aluminum foil scrim facing on the outside to block moisture penetration and reduce radiation losses; the joints will be sealed with aluminum foil scrim adhesive tape.

The two layers, a total of 6 inches thick, provide a combined thermal conductivity of 5.5 mW/cm^2 of beam tube surface area (220 W/m of beam tube length) at a beam tube temperature of 150°C and a thermal time constant of about 9 hours.

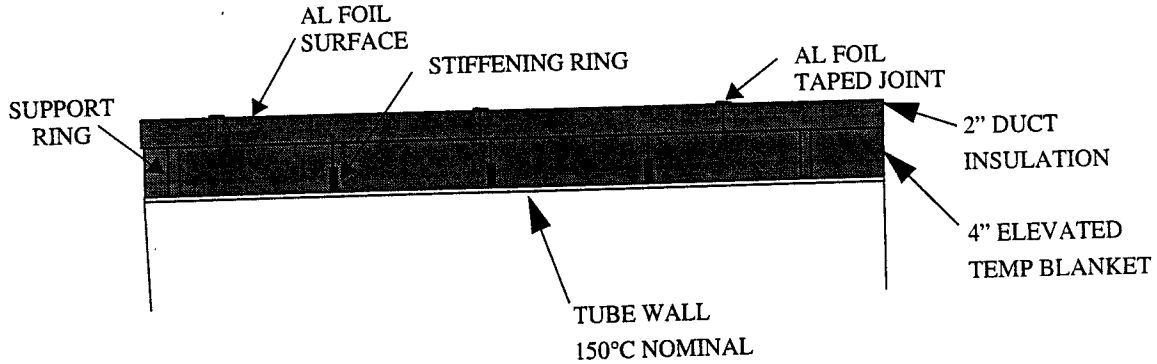


Figure 3: Tube wall insulation (section view)

3.1.2. Bellows

The bellows convolutions and thinner (2.7 mm) wall thickness lead to increased heat loss per unit length. To compensate for the higher heat dissipation per unit length, the insulation thickness at the bellows will be reduced by omitting the inner 4 inch layer (Figure 4).

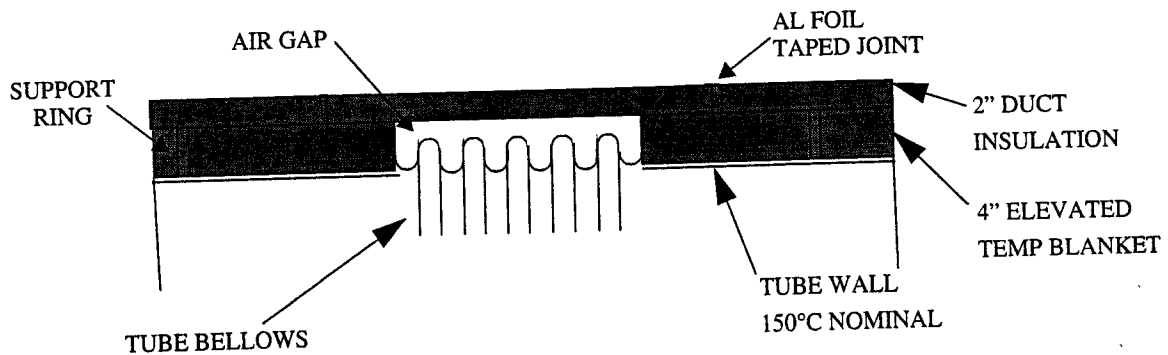


Figure 4: Bellows insulation (section view)

3.1.3. Supports

An additional wrap of one layer insulation will be installed at support points to account for increased conductive losses through supports.

3.1.4. Ends and Pump Ports

The ends of the beam tube module are connected to the 122 cm gate valves. The 122 cm gate valves and the nine pump ports will be insulated with custom fitted thermal heater jackets similar to those designed by PSI for the bakeout of the LIGO Vacuum Equipment. The thermal jackets will be purchased directly by LIGO for the beam tube bakeout.

3.2. Heating Power and Control

3.2.1. AC Source/Distribution

The power to be used for the bakeout will be supplied by the 13.8 kV (WA, 13.2 kV in LA) AC power available along the beam tube every 250m and provided by the local site public utility. The 13.8 kV, 1300 kVA power line (WA) (13.2 kV, 1300 kVA in LA) is housed in subsurface electrical vaults along the arms and across the service road from the beam tube service entrances.

The 13.8 kV power will be converted down to 480 VAC, 3Ø and brought to the beam tube module stub-ups near the service entrances by the local public utility (Figures 5 and 6). Power transformers for the high power DC heating will be provided at four locations along the beam tube module (see Figure 5). These transformers will be moved with the DC power supplies to each beam tube module. Separate (because they are moved at a different time) transformers and power distribution panels with 480 VAC, 3Ø and 120VAC, 1Ø power for pumps, instrumentation and smaller equipment will be supplied and installed at seven locations along the beam tube module (see Figure 6).

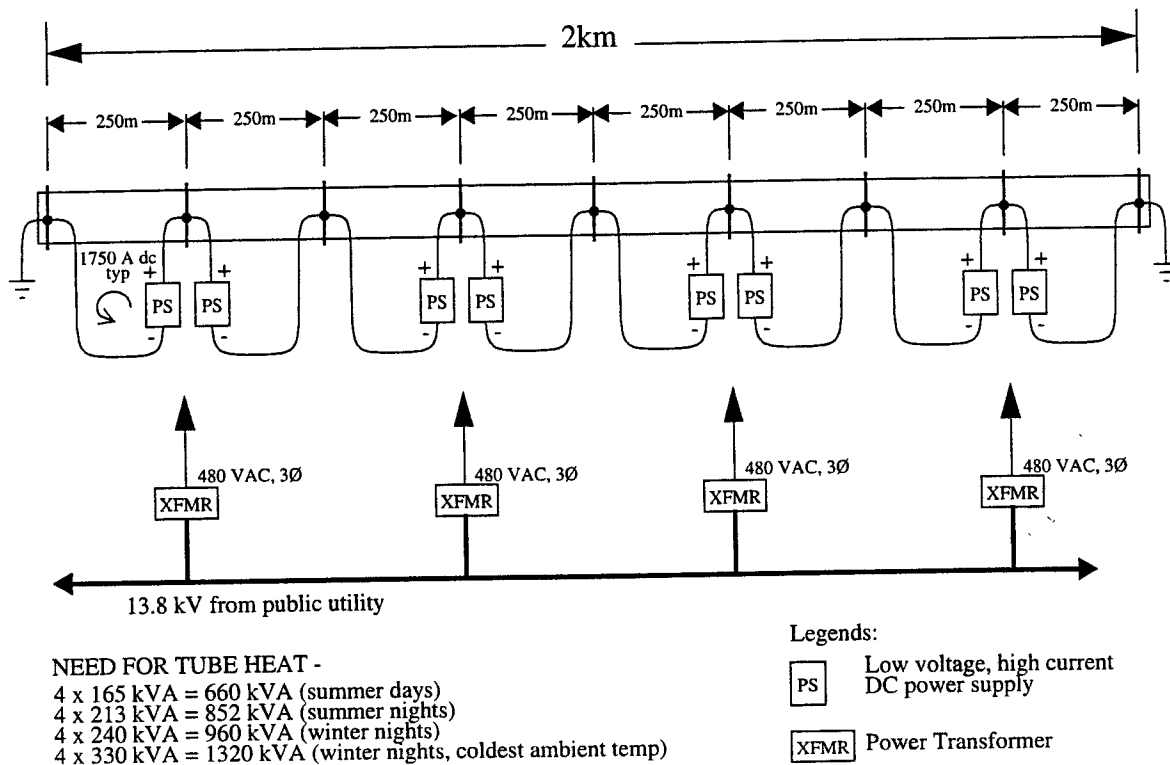


Figure 5: Heating power source layout

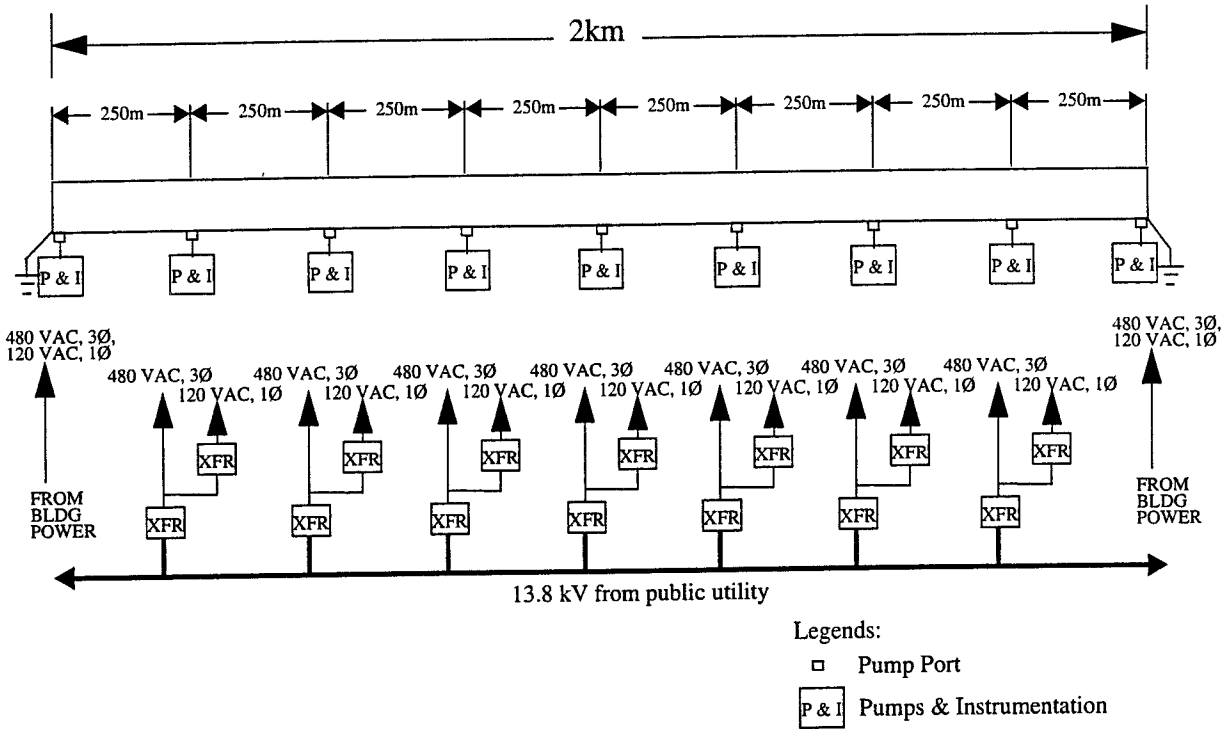


Figure 6: Power distribution for pumps and instrumentation

3.2.2. DC Power Supplies

Each of the eight 250m sections will have two 1000 A power supplies connected in parallel (Figure 7). A total of 16 power supplies are required for the bakeout of a module. The power supplies will be grouped into four clusters of four units each at 500m intervals along the beam tube (see Figure 5). The DC power supplies will be operating nominally at 35 V and at 1750 A. One of the two DC power supplies will be adjusted to provide a constant current of 1000 A. The second DC power supply will be controlled using temperature feedback (see next section).

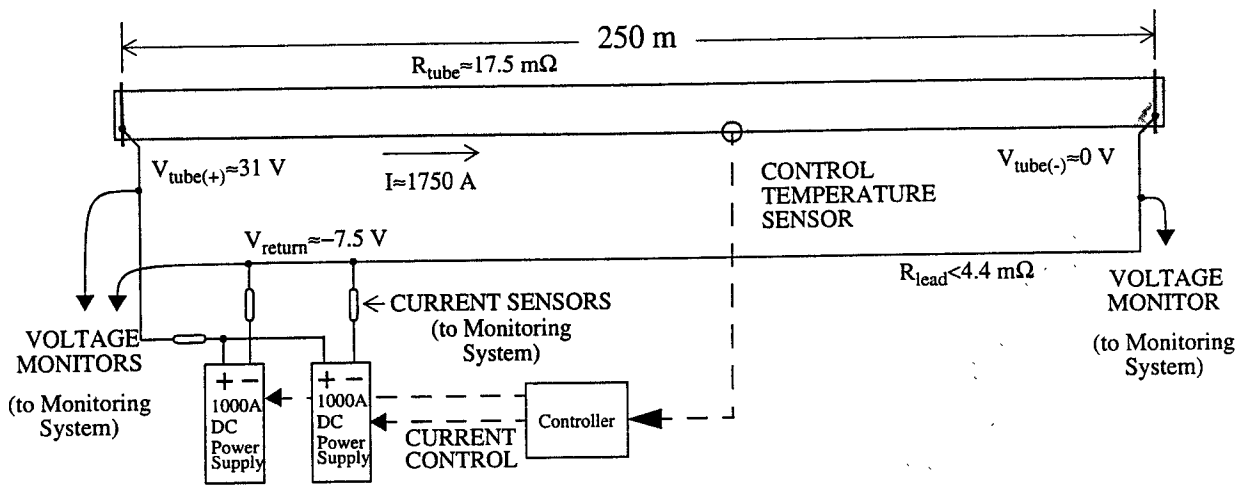


Figure 7: DC power supply control and connections to beam tube

The 1000 A DC power supplies to be used for the beam tube module heating will be commercial grade arc welding power sources with acceptable characteristics on both constant voltage and constant current usage. They have a power factor of 0.74 and power efficiency of 79% at an operating load of 1200 A. The power supplies will be able to operating continuously at 100% duty cycle for more than 30 days. The power supplies can be controlled by an external voltage (0 to 10 V) to adjust the output current.

3.2.3. Temperature Control of Tube Wall

The beam tube bakeout temperatures will be ramped up in 10 °C steps to a nominal bakeout temperature of 150 °C. The temperature is controlled by adjusting the current output of the DC power supplies which in turn are controlled by four I/O modules located at the power supply clusters, connected to the monitoring system I/O bus (see Section 3.4). The control function will be implemented in the monitoring system computer (a PC running a commercial data acquisition and control software program). Temperature feedback information from designated beam tube temperature sensors as well as DC current and voltage information from the current sensors will be used to adjust the currents in each of the eight 250 m loops to maintain a temperature set by the operator (see Figure 7).

3.2.4. Heating and Temperature Control of Ends/Ports

The gate valves at the ends of the module and the pump port hardware along the module will be heated to bake temperature with custom thermal heater jackets fit tightly over the gate valves, termination anchor supports and pump inlets. The jacketed elements will be maintained at the bake temperature with standalone, manually operated temperature controllers and dedicated temperature sensors, separate from the monitoring system. Power for the gate valve and pump port hardware bakeout heaters and controllers will be provided from the power distribution panels.

3.3. VACUUM PUMPS AND VACUUM INSTRUMENTATION

3.3.1. Vacuum Pumping and Monitoring During Bakeout

Pumping during bakeout will be provided by one 500 liter/second(l/s) turbomolecular pump for pumping H₂ and other non-condensable gases and nine 10 inch He cryo (refrigerating) pumps for pumping of H₂O and other condensable gases. The arrangement of shown schematically in Figure 8. The cryo pumps will be commercially available single stage refrigeration units, cooled by refrigeration compressors located near the pump ports. The pumping surface temperature is adjustable and will be set to 100 K. The cryo pumps will provide about 2,500 l/s pumping speed for H₂O at each port, which yields the same pump speed per unit of beam tube surface area as used during the earlier beam tube qualification test (QT). Power for the vacuum pump hardware will be provided from the power distribution panels.

Partial pressures will be monitored during the bakeout and cool down by a single RGA located at the module mid-point (see Figure 8). The RGA output will be displayed and recorded remotely at the location of the monitoring system display and operator's controls for the bake temperature. A cold cathode gauge to measure total pressure and a Pirani gauge to measure turbo pump back-pressure will be connected to the monitoring system (Section 3.4).

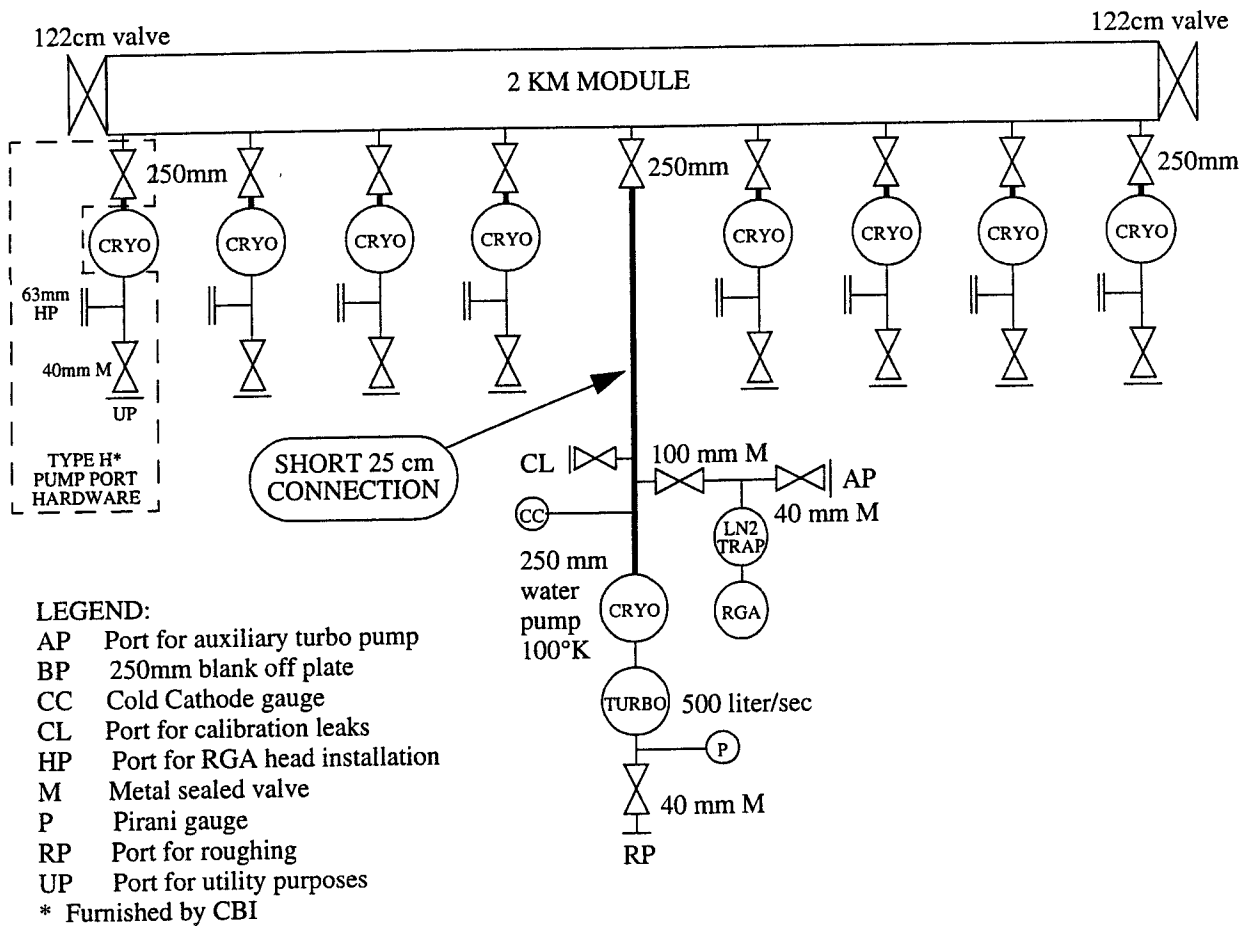


Figure 8: Schematic of vacuum pumps and RGA during bakeout

3.3.2. Vacuum Pumping and Measurement After Bakeout

Pumping during post-bake measurements will be provided by a single 500 l/s turbo pump. After the beam tube module has cooled to ambient temperature, the 250 mm gate valves will be closed and the bakeout pumps, RGA and associated hardware will be removed. A separate, clean turbo pump will be installed, along with a clean, pre-baked, high-sensitivity RGA, cold cathode and Pirani gauges. The RGA and gauges will have only local control and display (at the module mid-point). The equipment arrangement is shown in Figure 9. The expected partial pressures are shown in Table 1. A portable calibration module (Figure 10) will be used to verify RGA partial pressure measurements.

Table 1: Estimated Partial Pressures at 23 °C After Bakeout

	Mid-point Pressure (torr)
H ₂	$< 7 \times 10^{-9}$
CO	$< 8 \times 10^{-11}$
CO ₂	$< 3 \times 10^{-11}$
H ₂ O	$< 1.4 \times 10^{-12}$
Hydrocarbons Σ 41,43,55,57	$< 1.8 \times 10^{-12}$

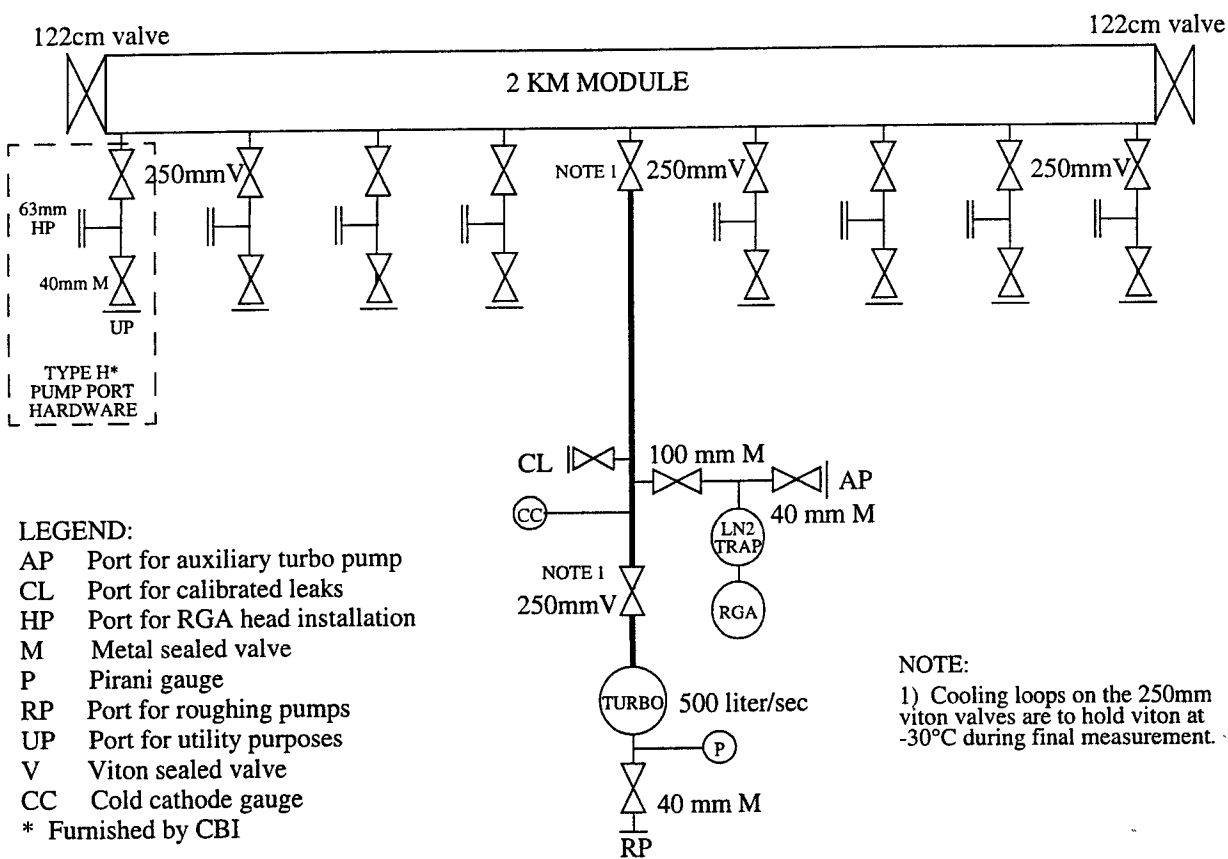


Figure 9: Final (post-bake) test configuration

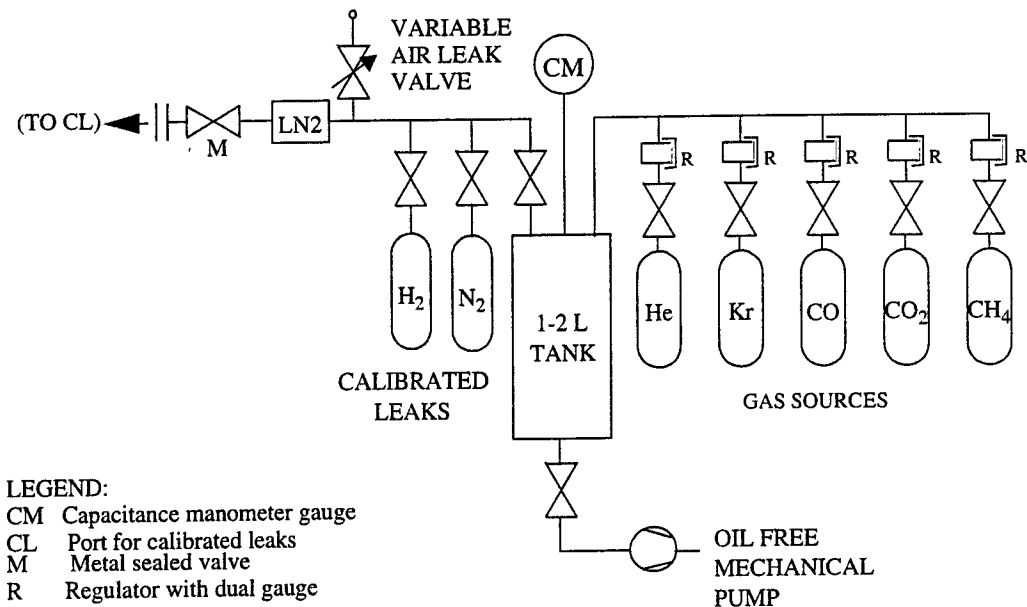


Figure 10: Portable Calibration Module

3.4. MONITORING SYSTEM

The monitoring system will consist of a standard PC computer running a commercial data acquisition and control software program. Commercially available I/O modules operating on a proprietary I/O bus with a range of 7,500 ft will be distributed along the beam tube module to measure temperatures, power supply electrical parameters, pressures, and equipment status and provide analog outputs to control the DC power supplies. The layout is shown schematically in Figure 11.

Table 2 provides a sample list of measurement channels. Temperature measurements will be taken at representative locations, mostly concentrated around the tube ends and pump ports, to ensure that the temperature behavior of the entire beam tube module is understood. Selected temperature channels will be used to set the current outputs of the power supplies to maintain all sections of the beam tube at a temperature set by the operator.

From the computer operator interface terminal, the operator will be able to access, record and alarm all DC current and voltage data and all temperature data. A complete sample of all data (< 256 channels) will take about 1 Kbyte, so if samples are logged once per minute, a 30 day bakeout will need about 50 Mbyte, which can easily fit onto the PC's hard disk drive. An ethernet connection to the corner station's networking facilities will allow the data to be downloaded over the Internet for permanent archiving and remote analysis.

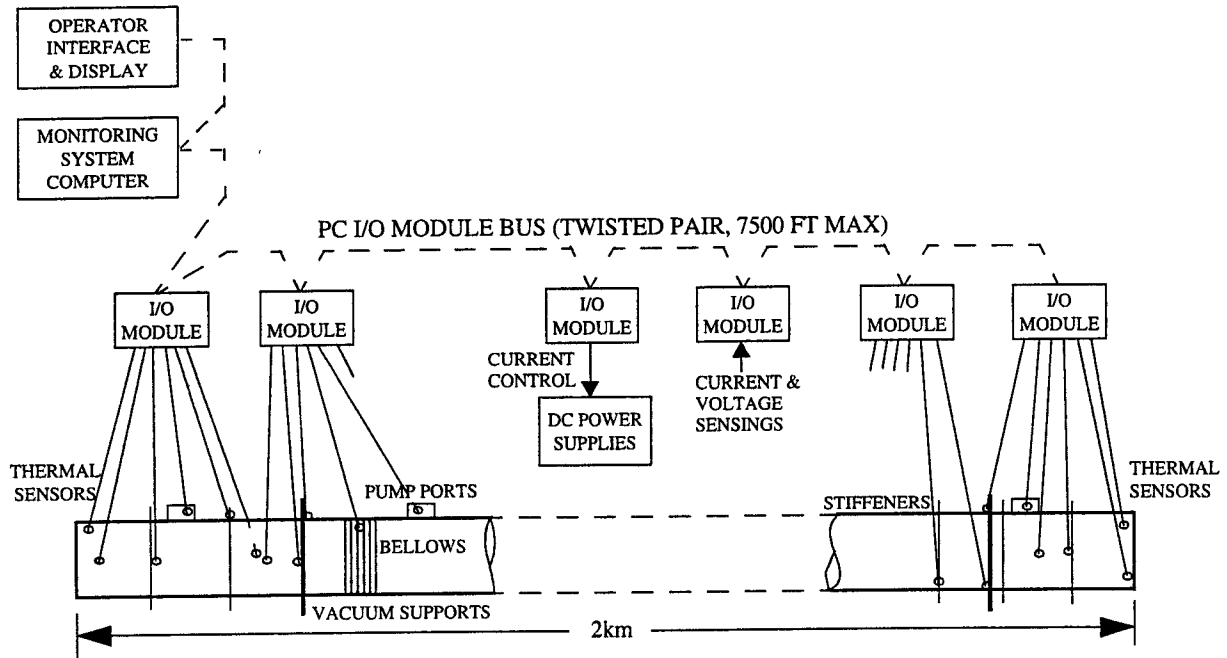


Figure 11: Monitoring system layout

Table 2: Monitoring System Channels

Signal Name	Station (m)	Description
Temperatures:		
T1-T32		Temperatures at near end beam tube gate valve, pump port, and tube wall in representative locations along the first 100 m of beam tube
T33-T64		Temperatures at far end beam tube gate valve, pump port, and tube wall in representative locations along the last 100 m of beam tube
T65-T106		Six representative temperatures at each pump port location (7 places)
T107		Ambient air temperature (outside)
T108		Ambient air temperature inside enclosure
T109-T128		Spare channels
Bakeout power supply electrical:		
V1-V4		Voltages on tube and at power supply for first heater section
V5-V32		Voltages on tube/power supplies for remaining 7 heater sections
I1-I3		Currents in + and - power supply legs for first heater section
I4-I24		Currents for remaining 7 power supplies

Table 2: Monitoring System Channels

Vacuum gauges:			
P1-P3		Pressures at cold cathode, Pirani and capacitance manometer (Calibration Module) gauges	
RGA1		RGA analog output	
Miscellaneous channels and status indicators:			
W1		Digital output from weather station (wind speed, temperature, humidity)	
CR1-CR9		Status of cryo pumps	
TP1		Status of turbo pump	
CT1-CT9		Cold trap stations	
LN1		Status of LN2 trap at RGA	
ETC1		Etc.	
Output channels:			
PS1-PS16		Set current outputs of the 16 DC power supplies for heating	

LASER INTERFEROMETER GRAVITATIONAL WAVE OBSERVATORY
- LIGO -

CALIFORNIA INSTITUTE OF TECHNOLOGY
MASSACHUSETTS INSTITUTE OF TECHNOLOGY

Specification	LIGO-E960123-01 - E	12/02/96
Beam Tube Bakeout Design Requirements Document		
W. Young		

Distribution of this draft:

This is an internal working note
of the LIGO Project.

California Institute of Technology
LIGO Project - MS 51-33
Pasadena CA 91125
Phone (818) 395-2129
Fax (818) 304-9834
E-mail: info@ligo.caltech.edu

Massachusetts Institute of Technology
LIGO Project - MS 20B-145
Cambridge, MA 01239
Phone (617) 253-4824
Fax (617) 253-7014
E-mail: info@ligo.mit.edu

WWW: <http://www.ligo.caltech.edu/>

Abstract

This document specifies the design requirements for the Beam Tube Bakeout to be used at the LIGO sites. It covers the heating power and control, thermal insulation, pumping and instrumentation, data acquisition, and electrical requirements to execute the beam tube bake.

1 INTRODUCTION

1.1. Purpose

The purpose of this document is to define the requirements for the bakeout of the LIGO Beam Tube Modules. These requirements will be used to guide the design and testing of bakeout equipment and procedures.

1.2. Scope

This document provides requirements for the bakeout equipment (heating power and controls, thermal insulation, pumping, instrumentation, data acquisition and logging), processes (equipment setup and conduct of the bakeout, and post-bakeout data analysis) and electrical requirements to be used for the beam tube bakeout.

1.3. Definitions

1.4. Acronyms

AC	Alternating Current
AMU	Atomic Mass Unit
BT	Beam Tube
BTD	Beam Tube Demonstration
BTE	Beam Tube Enclosure
CH ₄	Methane
CO	Carbon Monoxide
CO ₂	Carbon Dioxide
DAS	Data Acquisition System
DC	Direct Current
DRD	Design Requirements Document
LIGO	Laser Interferometer Gravitational Wave Observatory
LN ₂	Liquid Nitrogen
PLC	Programmable Logic Controller
QT	Qualification Test
RGA	Residual Gas Analyzer
TBS	To Be Supplied

1.5. Applicable Documents

1.5.1. LIGO Documents

M950001	Project Management Plan, latest revision
E950018	Science Requirements Document, latest revision
E950020	Beam Tube Module Requirements-Fabrication & Installation Contract, latest revision
E940002	Vacuum Equipment Specification, latest revision
E94xxxx	Beam Tube Module Specification (formerly Specification No. 1100004)
E94xxxx	Process Specification for Low Hydrogen, Type 304L Stainless Steel Vacuum Products (formerly Specification No. 1100007)
M96xxxx	Configuration Management Plan, latest revision
M950046	Project System Safety Plan, latest revision
D950027	Beam Tube Pump Port Hardware, latest revision
E950089	Interface Control Document (ICD): Beam Tube (BT) - Civil Construction (CC), latest revision

1.5.2. Non-LIGO Documents

2 GENERAL DESCRIPTION

2.1. Product Perspective

The LIGO Beam Tube Modules will be fabricated and installed by a contractor, CBI, Inc. Current plans call for conducting a bakeout (the subject of this document) of each beam tube module before integration with the rest of the LIGO vacuum system.

2.2. Product Functions

The beam tube modules will be unbaked when accepted from the contractor. At that point, partial pressures for H₂O and hydrocarbon gas species will exceed LIGO partial pressure goals. The beam tube bakeout is intended to reduce these partial pressures to the goal levels.

2.3. General Constraints

The beam tube is already designed and is under construction. The bakeout must meet its objectives without modification to the beam tube design, and must not subject the beam tube, attached

components (such as gate valves), foundations or enclosure to stresses beyond the capabilities of the existing design.

Some beam tube bakeout requirements are derived from empirical results obtained during earlier test programs.

To reduce significant capital costs, the equipment required for the bakeout will be used sequentially on each 2 km beam tube module, first at the Hanford, Washington site and then at the Livingston, Louisiana site.

2.4. Assumptions and Dependencies

The following factors affect the scope of the bakeout task and, if these change, then the scope may have to be changed accordingly:

- The beam tube will be baked out in increments of 2 kilometer modules.
- Adequate AC power (13.8 kV, 1300 kVA) will be available along the beam tubes.
- Safe access to beam tube enclosures during installation and bake (if needed) will be allowed.
- The beam tube will have been accepted from the beam tube fabrication and installation contractor and will meet its performance requirements (E950020).
- The beam tube is left under rough vacuum up to the time of the bakeout.
- Leaks larger than the LIGO specification which are present after the bakeout will be identified and localized, but repair/recovery procedures are not within the scope of this document.
- Insulation and thermal sensors will be left in place after each beam tube module is baked.

3 REQUIREMENTS

The allowable residual gas pressure in the beam tubes is set by the anticipated sensitivity of the detectors in the LIGO. The LIGO Science Requirements Document (referenced in 1.5.1 above) sets the goal for residual gas pressure "...at a level at or below an equivalent strain noise of $2 \times 10^{-25} \text{ Hz}^{-1/2}$ ". The beam tube bakeout is intended to reduce the rate of outgassing of adsorbed gases (principally H_2O , but also CO , CO_2 , CH_4 and heavier hydrocarbons) to a level which meets the residual gas pressure goal when the beam tube modules are pumped from their ends only (2 km points).

The bakeout requirements are derived from the above primary consideration and the empirical results achieved during the successful Qualification Test (QT) and earlier Beam Tube Demonstration (BTD) bakeouts.

3.1. Characteristics

3.1.1. Performance Characteristics

3.1.1.1 Components to be Baked

All vacuum surfaces of the bake volume, including beam tube wall material, expansion joints, pump ports, pump port hardware, 122 cm gate valves, and terminations shall be maintained within temperature limits specified below during the module bake.

3.1.1.2 Partial Pressures During the Bakeout

Partial pressures during the bake shall be controlled (by suitable choice of pumping speeds and control of temperature rate-of-rise) to maintain attached RGA(s) in their linear range to ensure proper operation throughout the bake.

Partial pressures of condensible gases shall be sufficiently low at the end of the bakeout and during cool down to avoid re-adsorption. The partial pressure for water vapor at an average bake temperature of 150°C at the end of the bakeout interval shall be $P(\text{H}_2\text{O}) < 2 \times 10^{-8}$ torr.

3.1.1.3 Bake Temperature

3.1.1.3.1 Minimum Temperature

The temperature of any point along the surface of beam tube bakeout volume shall be greater than 130°C.

3.1.1.3.2 Maximum Temperature of Beam Tube Wall

In order to avoid mechanical overstress of the beam tube wall structure, the maximum temperature at any point on the spiral welded beam tube wall shall be less than TBD(170°C).

3.1.1.3.3 Maximum Temperature of Beam Tube Bellows

The temperature at any point on any beam tube bellows shall be less than TBD°C (presently assumed to be quite high -- looking for the limiting driver).

3.1.1.3.4 Maximum Difference in Temperatures of the Beam Tube Wall

In order to avoid mechanical overstress (axial) of the beam tube support structures, the average temperature of any individual 20 m-long section of the beam tube wall shall not differ from the average temperature of any other section by more than 25°C.

In order to avoid mechanical overstress (transverse) of the beam tube support structures due to thermally-induced “banana mode” distortions, the average temperature of any semicylindrical half of any individual 20 m-long section shall not differ from the average temperature of its other semicylindrical half by more than 6°C.

3.1.1.3.5 Maximum Temperature of 122 cm Gate Valves

In order to avoid over heating of the 122 cm gate valve O-rings, the maximum temperature at any point on the gate or gate valve body shall not exceed 170°C. Valve motor and electronics shall be removed during the bakeout.

3.1.1.3.6 Maximum Temperature of Other (TBD) Components

TBD.

3.1.1.4 Beam Tube Insulation

Beam tube walls shall be insulated as required to achieve the above temperature limits.

3.1.1.5 Bake Duration

The coldest spot of the beam tube module under bakeout shall be maintained above the minimum temperature (3.1.1.3.1) for the earlier of either an elapsed time of 30 days, or until the water (H₂O) outgassing rate has decreased to $J(\text{H}_2\text{O}) < 1 \times 10^{-11}$ torr l/s cm² at 150°C. If the temperature of any sensor monitoring the vacuum wall surfaces falls below the minimum bake temperature, the bake time shall be extended as needed to ensure that the minimum time requirement is met.

3.1.1.6 Data Acquisition, Display, Monitoring and Recording

The beam tube module shall be instrumented to measure the wall temperatures at representative positions, including anticipated hot or cold spots, interfaces with pump port hardware, 122 cm gate valves and terminations. The beam tube module shall also be instrumented with at least one RGA to measure partial pressures of H₂ and H₂O during the bakeout (10⁻⁹ torr instrument sensitivity), and partial pressures through AMU 100 during post-bake (10⁻¹⁵ torr sensitivity) measurements. Instrumentation shall also be provided to measure DC power supply currents and voltages, operating status of equipment (such as vacuum pumps), and such other engineering data, including ambient environmental conditions (temperature, humidity, wind speed and direction), which determine the state of bakeout equipment.

During the initial bakeout, the equipment shall include provisions for measuring representative strains on the beam tube structure. During post-bake measurements, the equipment shall include provisions for measuring pumping speeds and outgassing rates.

All needed data shall be available at a single location for the purposes of display, monitoring and recording.

All acquired data shall be time stamped and recorded as needed (at approximately 15 minute intervals during bake) and the accumulated data file shall be archived periodically.

3.1.1.7 Vacuum Components

All vacuum components attached to the beam tube module shall comply with the requirements given in the LIGO Vacuum Equipment Specification, section 5, for similar components.

3.1.2. Physical Characteristics

The bakeout equipment, excluding beam tube insulation and temperature sensors, shall be installed and de-installed from module to module during the bake of subsequent modules. In addition, this equipment shall be transportable from site to site.

3.1.3. Interface Definitions

3.1.3.1 Interfaces to other LIGO systems

3.1.3.1.1 Mechanical Interfaces

The vacuum hardware shall be compatible with the BT module pump ports hardware, Type H, as called out in drawing D950027.

Electrical connections for delivering DC heating power to the beam tube module shall use bolted attachments via holes drilled through beam tube Support Rings near each pump port (these holes are not part of the present beam tube fabrication).

Temperature sensors shall be attached to the beam tube wall using TBD technique.

3.1.3.1.2 Electrical Interfaces

Step-down transformers shall be used to provide needed AC power (480VAC, 120VAC) from the site power (13.8 kV, WA; 13.2 kV, LA). Up to 1300 kVA is required.

The beam tube module shall be grounded at the ends only during the bake.

The beam tube modules shall have electrical connections to DC power supplies for heating.

Monitoring and recording devices shall use AC power (110-120VAC), also derived from site utilities power.

The bakeout equipment shall have adequate protection from lightning.

3.1.3.1.3 Optical Interfaces

There are no optical interfaces.

3.1.3.1.4 Thermal Interfaces

No special provisions other than insulation and heating of the beam tube walls will be made to influence the thermal behavior of the beam tube or Beam Tube Enclosure during the bakeout.

3.1.3.1.5 Stay Clear Zones

Access to beam tube enclosure shall be restricted during bake. Access to all service and emergency entrances to module under bake shall be kept clear during the duration of the bake activities.

3.1.4. Reliability/Maintainability

As a minimum, system design shall be such to provide a 30 day bake period with 90% confidence that the bakeout performance requirements are met (reference 3.1.1).

The insulation blanket shall have a minimum usable lifetime of 1 bake cycle. As a goal, a 10 year lifetime is desired.

The thermal sensors shall have a minimum usable life of 20 years installed.

The insulation blanket shall be constructed of materials which do not pose a threat to long-term corrosion of the stainless steel tube wall or reinforcing rings.

3.1.5. Environmental Conditions

The beam tube bakeout equipment shall be able to achieve and maintain design bake temperatures under anticipated temperature extremes at either site. The equipment must be safe to other equipment and personnel during exceptional circumstances such as a power failure, earthquake, lightning, etc.

3.1.5.1 Natural Environment

3.1.5.1.1 Temperature and Humidity

Table 1: Environmental Performance Characteristics

	<i>Operating</i>	<i>Non-operating (storage)</i>	<i>Transport</i>
Equipment in contact with beam tube wall	0°C to +200°C, 0-90%RH	-40°C to +70°C, 0-100% RH	-40°C to +70°C, 0-90% RH
Equipment located inside the BTE	0°C to +70°C, 0-90%RH	-40°C to +70°C, 0-100% RH	-40°C to +70°C, 0-90% RH
Equipment located outside the BTE	-30°C to +40°C, 0-100%RH	-40°C to +70°C, 0-100% RH	-40°C to +70°C, 0-90% RH
Equipment located inside buildings	20°C to 30°C, 20-70%RH	-40°C to +70°C, 0-100% RH	-40°C to +70°C, 0-90% RH

3.1.5.1.2 Atmospheric Pressure

TBD

3.1.5.1.3 Seismic Disturbance

TBD

3.1.5.2 Induced Environment

3.1.5.2.1 Electromagnetic Radiation

TBD

3.1.5.2.2 Acoustic

TBD

3.1.5.2.3 Mechanical Vibration

TBD

3.1.6. Transportability

All removable bakeout equipment shall be packaged to be transported between beam tube modules with minimum labor required for transportation and setup. All equipment shall be transportable across the country by commercial carrier without degradation in performance. If necessary, provisions shall be made for measuring and controlling environmental conditions (temperature and accelerations) during transport and handling. Special shipping containers, shipping and handling mechanical restraints, and shock isolation shall be utilized to prevent damage. All containers shall be movable by forklift. All items over 100 lbs. which must be moved into place within LIGO buildings shall have appropriate lifting eyes and mechanical strength to be lifted by cranes.

3.2. Design and Construction**3.2.1. Materials and Processes****3.2.1.1 Finishes**

TBD

3.2.1.2 Materials

Surface-to-surface contact between dissimilar metals shall be controlled in accordance with the best available practices for corrosion prevention and control.

Insulation shall be constructed of materials which do not pose a threat to long-term corrosion of the stainless steel tube wall or reinforcing rings.

Insulation shall not emit toxic gasses when the beam tube is heated to bake temperature.

3.2.1.3 Processes

TBD

3.2.2. Component Naming

TBD

3.2.3. Workmanship

TBD

3.2.4. Interchangeability

TBD

3.2.5. Safety

Equipment and procedures associated with executing bakeout task shall meet all applicable Federal safety regulations, plus applicable State, Local and LIGO safety requirements. A hazard/risk analysis shall be conducted in accordance with guidelines set forth in the LIGO Project System Safety Plan. Special issues expected to be addressed includes:

- working in confined space (controlled access to beam tube enclosure)
- high power (up to 1.3 MW)
- high current (2000 A)
- high voltage (13.8 kV)
- high temperature (150°C)
- lightning protection

3.2.6. Human Engineering

TBD

3.3. Documentation

3.3.1. Specifications

TBD

3.3.2. Design Documents

T960124 Issues and Consideration on the Beam Tube Bake, Nov. 30, 1995.
 T96xxxx Information for the Bakeout Design, Aug. 12, 1996.
 T960178 Beam Tube Bakeout Conceptual Design

3.3.3. Engineering Drawings and Associated Lists

3.3.4. Technical Manuals and Procedures

3.3.4.1 Procedures

Procedures shall be provided for, at minimum,

- Initial installation and setup of equipment
- Normal operation of equipment
- Normal and emergency shut down
- Normal and/or preventive maintenance
- Troubleshooting guide for anticipated potential malfunctions

3.3.4.2 Manuals

TBD

3.3.5. Documentation Numbering

All documents shall be numbered and identified in accordance with the LIGO documentation numbering system LIGO document TBD

3.3.6. Test Plans and Procedures

All test plans and procedures shall be developed in accordance with the LIGO Test Plan Guidelines, LIGO document TBD.

3.4. Logistics

The design shall include a list of all recommended spare parts and special test equipment required.

3.5. Precedence

TBD

3.6. Qualification

TBD

4 QUALITY ASSURANCE PROVISIONS

4.1. General

4.1.1. Responsibility for Tests

TBD

4.1.2. Special Tests

4.1.2.1 Engineering Tests

TBD

4.1.2.2 Reliability Testing

Reliability evaluation/development tests shall be conducted on items with limited reliability history that will have a significant impact upon the operational availability of the system.

4.1.3. Configuration Management

Configuration control of specifications and designs shall be in accordance with the LIGO Configuration Management Plan.

4.2. Quality conformance inspections

Design and performance requirements identified in this specification and referenced specifications shall be verified by analysis, demonstration, or test. Verification method selection shall be specified by individual specifications, and documented by appropriate test and evaluation plans and procedures. Verification of compliance to the requirements of this and subsequent specifications may be accomplished by the following methods or combination of methods:

4.2.1. Inspections

TBD

4.2.2. Analysis

TBD

4.2.3. Demonstration

TBD

4.2.4. Test

TBD

APPENDIX A DETERMINATION OF MAXIMUM ALLOWABLE AXIAL AND TRANSVERSE (RADIAL) THERMAL GRADIENTS.

A model was developed to determine the maximum allowable thermal gradients during bake out. The components of the model were:

[1] Maximum allowable forces on BT fixed supports. These included axial forces ($F < 7300$ lb) and transverse/vertical forces ($F < 1300$ lb). The values are from the Beam Tube (BT)-Civil Construction (CC) Interface Control Document (ICD) and correspond to design values provided by CB&I and Parsons for the BT design and associated slab interfaces.

[2] Thermal expansion characteristics for the BT material (304L SS).

[3] Axial loads at the module ends caused by atmospheric pressure on the evacuated beam tube.

[4] Transverse force-displacement relation associated with the “banana mode” bending of the tube (in both horizontal & vertical planes) caused by the presence of thermal gradients across the BT.

[5] The distribution function of expansion joint spring constants. The statistical representation was derived from CB&I empirical data for the first 42 joints, which have mean and standard deviations of 7800 lb/in and 232 lb/in, respectively (Figure A-1). The model incorporated the 42 data points and random samples of the distribution for the remaining expansion joints.

Using these parameters as inputs, the model was used to generate representative chains of 50 x 40 m long tube sections (length between fixed supports). The distribution of three dimensional forces at the fixed supports was determined and maximum axial and transverse thermal gradients were determined which could satisfy the maximum load limits from [1] above (see Figures A-2 and A-3).

Distribution of Hyspan expansion joints spring constants, first 42 articles

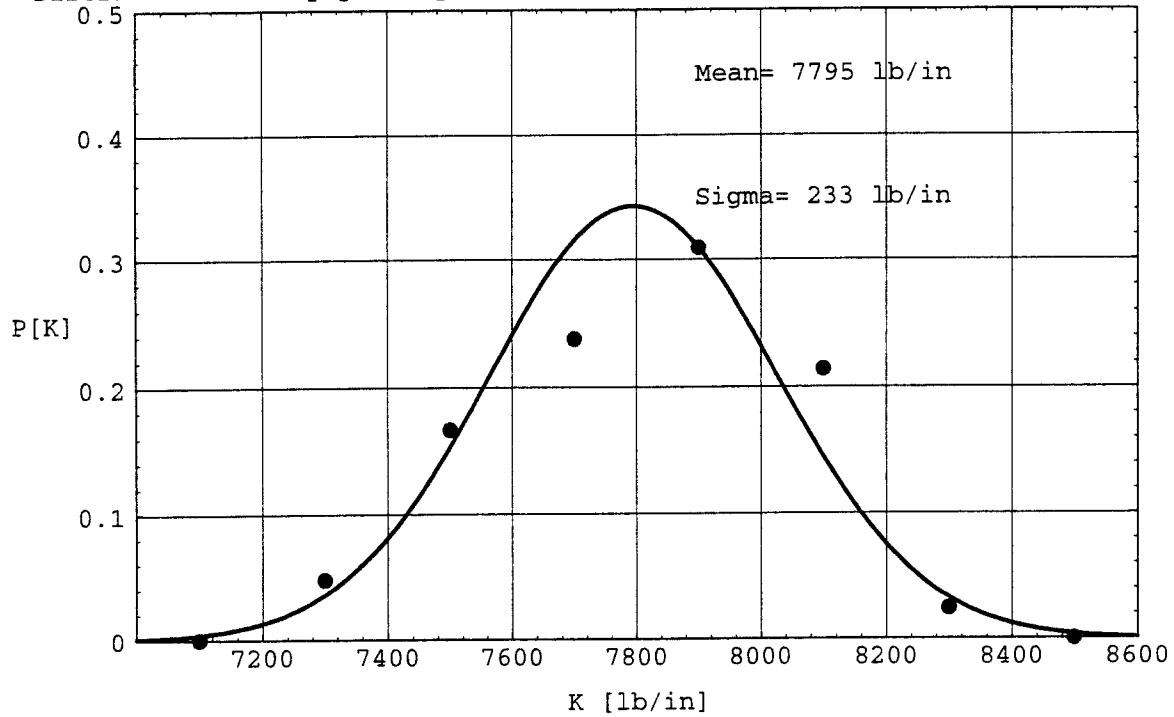


Figure A-1: Distribution of Hyspan expansion joints spring constants, first 42 articles

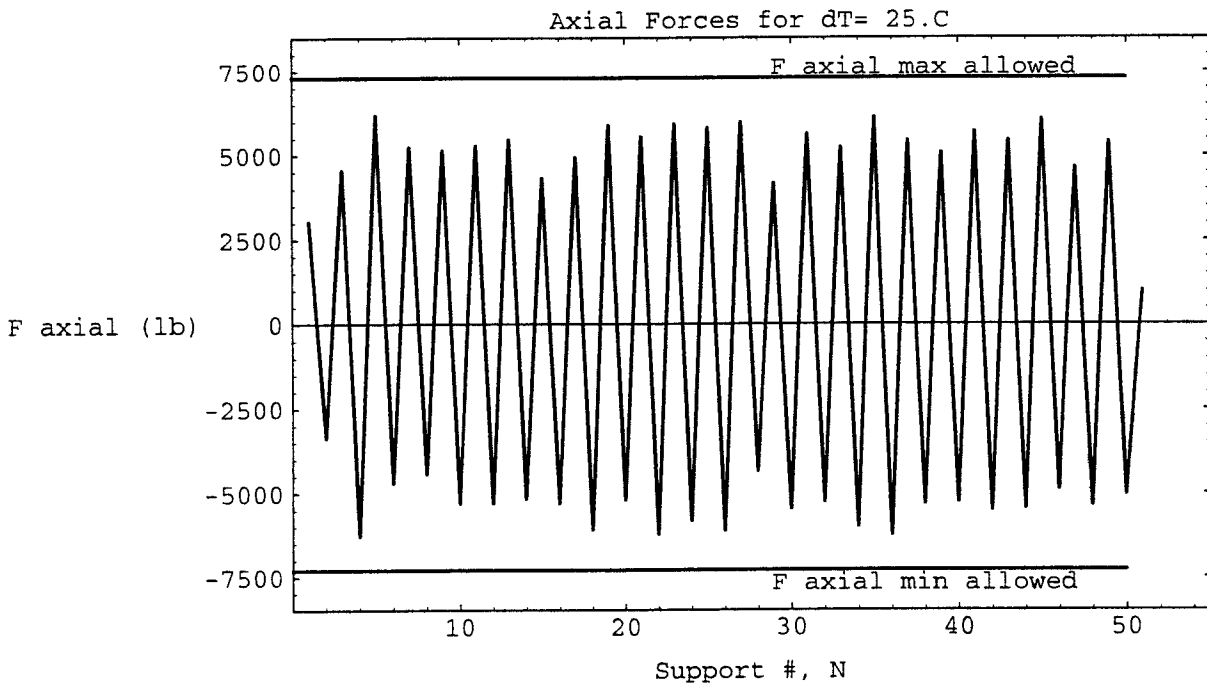


Figure A-2: Axial force at fixed supports with tube sections between adjacent pairs of supports at alternating temperatures (for temperature difference $dT=25^{\circ}C$)

Figure A-3: To be supplied

Vacuum Equipment

The attached document is a monthly status report issued by PSI. This document is one of the tools used by LIGO management to track the performance of the contractor. This monthly report is discussed at monthly status meetings held at the contractor's facilities.



PROCESS SYSTEMS INTERNATIONAL, INC.

STATUS REPORT

PERIOD: JANUARY 1, 1997 THROUGH JANUARY 31, 1997
PSI DOCUMENT NO: PC175730
PROGRAM I.D. LIGO VACUUM EQUIPMENT
ISSUE DATE: MARCH 5, 1997
CDRL NO: 09-15
APPROVAL STATUS: X

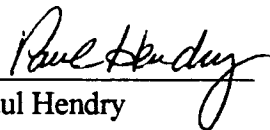
SUBMITTED TO:

California Institute Of Technology
 391 South Holliston Avenue
 Pasadena, CA 91125

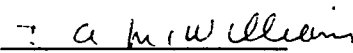
SUBMITTED BY:

Process Systems International, Inc.
 20 Walkup Drive
 Westborough, MA 01581

Cost/Schedule Mgr:


 Paul Hendry

Technical Director:


 David McWilliams

Project Director:


 Richard Bagley, P.E.



PROCESS SYSTEMS INTERNATIONAL, INC.

CALIFORNIA INSTITUTE OF TECHNOLOGY

MASSACHUSETTS INSTITUTE OF TECHNOLOGY



LIGO VACUUM EQUIPMENT

STATUS REPORT

Table of Contents

1. Management Summary
2. Areas of Concern
3. Information and Decisions Required
4. Engineering and Design Status
5. Procurement Status
6. Manufacturing Status
7. Quality Assurance Status
8. Installation Status
9. Schedule Status
10. Change Order Status
11. Contract Price



SECTION 1 MANAGEMENT SUMMARY

PROJECT STATUS SUMMARY

Through the end of January 1997, the engineering, design, and fabrication activities for the LIGO project is proceeding essentially on schedule. PSI has received approximately 95% of all raw materials for vessel fabrication, and fabrication is well underway on HAM's, BSC's, 80K cryopumps, and spools/adapters. PSI has purchased all major materials and contracted for all major outside fabrication services required for the project. Critical outside purchases remain the BSC weldments, large gate valves, and bakeout blankets. Deliveries of remaining major equipment and components currently support the LIGO schedule requirements.

Section 2 lists PSI concerns which must be addressed to ensure a successful project.

Section 3 contains the current Project Needs List (#24). The Needs List continues to be a valuable tool for promoting intercompany communication.

Sections 4 to 8 contain updates on the current status of various segments of the project.

Section 9 contains detailed project schedules which highlight current and planned activities.

Section 10 and 11 detail the current status of change orders and the contract price. The contract price has increased by \$15,974 for this period due to approval of a change order for all metal o-ring testing by LIGO. Change order activity is currently negligible with no potential changes in process which will have significant schedule impact

PERIOD HIGHLIGHTS

Completed fabrication of the first article HAM vessel

Received four responsive bids for the Washington installation

Received two BSC weldments from Ranor

Continued receiving flange forgings, stainless steel plate, vessel heads, and conflat flanges for Washington vessels. These orders will complete in early February

Continued fabrication of spools/adapters with welding of long seams, stiffener rings, bellows assemblies, conflat flanges, end flanges, and girth seams



PROCESS SYSTEMS INTERNATIONAL, INC.

CONCERN 6: FINAL LIGO STATION BUILDING DRAWINGS

The LIGO Station building drawings have continued to change during the final design period. The PSI schedule has been affected by the building design changes, new equipment studies, and requested for new layouts.

SUGGESTED ACTION:

PSI received the final design of the Washington buildings on April 22, 1996, which was too late for incorporation into our final design for the vacuum equipment. The drawings were sent for information only, because they had not yet been reviewed/approved by LIGO. PSI issued the final design for the vacuum equipment based on the preliminary building drawings (dated 10/31/95). PSI will incorporate any changes when the final design package is reissued. PSI received the final Washington building drawings on July 29, 1996, and the final Louisiana building drawings on August 19, 1996. PSI is currently in the process of reissuing the Washington and Louisiana final design packages based on these drawings. Any significant changes that PSI's discovers will be brought to LIGO's immediate attention.

STATUS: OPEN

CONCERN 7: DECISION ON THE NUMBER AND LOCATION OF THE REMOVABLE SPOOL SECTIONS - CHANGE ORDER NO. 16

STATUS: CLOSED



PROCESS SYSTEMS INTERNATIONAL, INC.

**CONCERN 8: LARGE GATE VALVE DELIVERY TO SUPPORT
WASHINGTON BEAM TUBE DELIVERABLE DATE**

ACTION REQUIRED:

The delivery of the large gate valves required for the Washington Beam Tube installation will complete at the end of February 1997, which is approximately six months late. Fortunately, the valve deliveries have supported the field installation schedule. PSI and LIGO have spent much time and money in addressing this serious problem. GNB is required to deliver 18 more valves in the third quarter of 1997. PSI has seen dramatic positive changes in GNB's execution approach for the 1997 valve deliveries. Much of the materials required to fabricate the valves is currently in stock at GNB. PSI is visiting GNB bi-monthly to insure that the proper resources are applied and the valves get fabricated and tested as planned. GNB schedule updates will be sent to LIGO when received.

STATUS: CLOSED WITH FOLLOW-UP ON 1997 DELIVERIES

CONCERN 9: TECHNICAL ISSUES WITH THE MAIN ION PUMPS

STATUS: CLOSED



SECTION 3 INFORMATION AND DECISIONS REQUIRED

Attached to this section is the latest copy of the project needs list. Two lists are included which indicate items needed by PSI from LIGO, and items needed by LIGO from PSI.

Below is a summary of Needs List No. 24 which is attached to this report.

	<u>NEEDED BY LIGO</u>	<u>NEEDED BY PSI</u>
New Items Added	1	0
Items Closed	2	4
Total Open Items	3	3
Overdue Items	2	0

Information needs are critical to the success of the project, and this list receives weekly attention by the respective project management teams to minimize delays to the project caused by lack of timely information.

PROJECT NEEDS LIST - Needed by LIGO - Action by PSI

03/05/97

Project: LIGO Vacuum Equipment - Contract PC 175730

V049-NL-24

Proj. No.: V59049

Item No. V049-NL-LP-	Description of Request	Requested By /Date Requested	Action By	Date Required	Date Closed	Closure Document
80	Perform an air backfill test to complete the data set for the o-rings.	J. Worden 10/30/96	D. McWilliams	01/30/97		
81	After prototype and 10" data analysis, meet with LIGO to discuss adjustment of the acceptance criteria defined in the contract.	J. Worden 10/30/96	R. Bagley	01/15/97	02/07/97	TIM 50
84	Provide better definitions for payment milestones.	E. Jasnow 10/30/96	P. Hendry	02/07/97	02/20/97	V049-PL-366
85	Provide further definition of prototype mechanical measurements	J. Worden 11/21/96	R. Bagley	01/10/97		
87	Provide a drawing showing PSI proposed survey monument locations in Washington building	J. Worden 1/30/97	R. Curtis	03/14/97		

PROJECT NEEDS LIST - Needed by PSI - Action by LIGO

03/05/97

Project: LIGO Vacuum Equipment - Contract PC 175730

V049-NL-24

Proj. No.: V59049

Item No. V049-NL-PL-	Description of Request	Requested By /Date Requested	Action By	Date Required	Date Closed	Closure Doc.
69	Provide PSI a status update of Louisiana tax issues.	R. Bagley 4/16/96	E. Jasnow	03/31/97		
83	Provide an updated site building joint occupancy schedule for both sites.	R. Bagley 9/27/96	G. Stapfer	01/30/97	02/17/97	TIM 52
84	Provide response on site surveying monument issue. (after V049-NL-LP87)	R. Bagley 9/27/96	J. Worden	01/30/97		
90	After prototype and 10" data analysis, meet with PSI to discuss adjustment of the acceptance criteria defined in the contract.	R. Bagley 10/30/96	J. Worden	01/15/97	02/07/97	TIM 50
92	Provide as-builts drawings of the embedded conduit stub-up locations for both sites after the floor slabs have been poured.	R. Bagley 11/21/96	J. Worden	By Building		
93	Provide response for Change Order No. 22 for metal o-ring testing	R. Bagley 1/16/97	J. Worden	02/18/97	02/14/97	TIM 51
94	Provide response for Change Order No. 20 for using the prototype BSC as production unit, and deleting one production BSC weldment	R. Bagley	J. Worden	02/28/97	02/14/97	TIM 51



SECTION 4 ENGINEERING AND DESIGN

ACTIVITIES FOR THE CURRENT PERIOD:

Continued work on finalizing drawings for the reissue of the Final Design Package with LIGO's comments. The Washington drawing package was reissued on 1/3/97. The Louisiana package will be issued at the end of February.

Attended a review of the bakeout blanket status in England, and reviewed the first plastic mold of a HAM vessel which will be used for blanket fabrication

Designed a large component bakeout oven and prepared a bill of materials

Continued work on wash cart modifications for the wide variety of components to be washed

Commenced work on shipping skids and shipping supports

Finalized design of test covers and shipping covers

Completed all design details for the 80K cryopump assembly

ACTIVITIES PLANNED FOR NEXT PERIOD:

Continue work on the reissue of the final design package for the Louisiana site

Continue to optimize designs based on the value engineering program and lessons learned from ongoing fabrication of first article components

Continue specifying and purchasing miscellaneous instrumentation and small manual valves

Continue work on finalizing design details for the lifting jacks, regen heater vessel, bakeout cart, and miscellaneous wash carts



SECTION 5 PROCUREMENT STATUS

ACTIVITIES FOR THE CURRENT PERIOD:

Continued to receive stainless steel vessel heads from Trinity Industries Inc , stainless steel plate from Avesta Sheffield, flange forgings from Standard Steel, and conflat flanges from A&N and Varian. All of these orders are scheduled to complete early February

Shipped 95% of the Washington site bellows type expansion joint assemblies from Hyspan to PSI

Received four more Auxiliary Turbomolecular Pump Carts from Edward's High Vacuum

Continued to expedite the early delivery of much of the raw materials for the project to minimize project schedule risk and maximize possible manufacturing efficiencies

Received all viton o-rings required for the project (unbaked)

Complete work with Varian on the Main Ion Pump and released them to fabricate and ship

Received 100% of the order for rolled stainless steel stiffeners for the spools and adapters

Received another 50 scfm clean air compressor from JPL Consulting

Shipped two more electric 44" gate valves from GNB to the Hanford site

ACTIVITIES PLANNED FOR NEXT PERIOD:

Continue to monitor the status of the outstanding Washington beam tube deliverables (GNB gate valves)

Continue vendor surveillance activities, and expediting to purchase order commitments

Continue to purchase miscellaneous materials, as all major materials required for the entire project have been purchased



SECTION 6 MANUFACTURING STATUS

ACTIVITIES FOR THE CURRENT PERIOD:

Continued work on wash carts and the drive assemblies for rotating the components in the large component wash station.

Continued weekly status meetings for the outside machining, cutting, beveling, rolling, and carbon steel fabrication purchase orders

Continued to update the detail manufacturing schedules for all components. These schedules are transmitted to LIGO monthly

Continued fabrication of 84 inch and 60 inch port covers for HAM's and BSC's, which is well ahead of schedule. Most are complete and await final machining

Continued HAM fabrication with 15 vessels in fabrication as of the end of January. Eight HAM's have been through stress relieving and final machining. Fabrication of the first article HAM was completed at the end of January, and is ready for cleaning, baking, and testing. Shell and nozzle material for all HAM's has been received. All HAM bellows have been received.

Spool fabrication continued in January with the welding of long seams, stiffener rings, bellows assemblies, conflat flanges, end flanges and girth welding of sections. PSI has a large inventory of rolled shells on which to work

Three LN2 reservoirs for short cryopumps are completed, with a fourth currently in test. Outer shell fabrication is complete on the first cryopump and a trial fit-up of the entire assembly was completed in January. Work on outer shells for the two more short 80K pumps also continues. Several material shortages have been holding up progress, primarily due to late release of drawings

Beam splitter weldment fabrication continued at Ranor with nine BSC's currently in progress. The two BSC weldments were completed and delivered to PSI in January. PSI is pre-fabricating annulus tubing, as practical, and will expedite final assembly. Shell and nozzle material for all BSC's has been received.



PROCESS SYSTEMS INTERNATIONAL, INC.

ACTIVITIES FOR THE CURRENT PERIOD: (Continued)

PSI completed final assembly of two HAM cleanrooms in January. These cleanrooms will be used in the PSI clean area for component leak checking, bakeout, and testing

Completed the set-up a vacuum oven for the bakeout of o-rings, and started production baking of o-rings.

ACTIVITIES PLANNED FOR NEXT PERIOD:

Continue the fabrication of HAM's, BSC's, cryopumps, and spools/adapters

Commence wash station operations for production components

Complete the fabrication of the miscellaneous fixtures, as required

Continue work on port covers for HAM's and BSC's, with the delivery of additional head and flange forgings

Continue weekly meetings at Ranor, and Arland Tool

ATTACHMENT

PSI fabrication status summary as of the end of January 1997

Beam Splitter Chambers			
Item	Serial Number	Tag #	Status
BSC Weldment	V0494003-01	WA	Annulus tubing to complete on 2/3. Ready for cleaning.
	V0494003-02	WA	Arrived from Ranor on 1/31. Start annulus tubing this week.
	V0494003-03	WA	Dimensional inspection at Ranor on 2/5. Ship to PSI on 2/7.
	V0494003-04	WA	60" nozzle machining complete. 60" flanges being fit/welded. Upper shell machining complete.
	V0494003-05	WA	Lower shell is being machined. Upper shell has been welded and is ready for machining.
	V0494003-06	WA	Lower head is being fit/tacked. Upper head has been tacked and is ready for welding.
	V0494003-07	WA	Long seam has been welded. 60" ports have been stitch cut.
	V0494003-08	WA	Long seam has been welded. 60" ports have been stitch cut.
	V0494003-09	WA	Long seam has been welded. 60" ports have been stitch cut.
	V0494003-10	WA	Long seam has been welded. 60" ports have been stitch cut.
	V0494003-11	LA	Long seam has been welded. 60" ports have been stitch cut.
	V0494003-12	LA	All heads, shell & nozzle material received - start rolling in late June 1997
	V0494003-13	LA	All heads, shell & nozzle material received - start rolling in late June 1997
	V0494003-14	LA	All heads, shell & nozzle material received - start rolling in late June 1997
	V0494003-15	LA	All heads, shell & nozzle material received - start rolling in late June 1997

Item	Serial Number	Tag #	Status
BSC 60" Port Covers	V0494014-01		Complete
	V0494014-02		at machine shop for final machining with conflat welded
	V0494014-03		at machine shop for final machining with conflat welded
	V0494014-04		Complete
	V0494014-05		Complete
	V0494014-06		at machine shop for final machining with conflat welded
	V0494014-07		at machine shop for final machining with conflat welded
	V0494014-08		at machine shop for final machining with conflat welded
	V0494014-09		at machine shop for final machining with conflat welded
	V0494014-10		at machine shop for final machining with conflat welded
	V0494014-11		at machine shop for final machining with conflat welded
	V0494014-12		at machine shop for final machining with conflat welded
	V0494014-13		at machine shop for final machining with conflat welded
	V0494014-14		Complete
	V0494014-15		at machine shop for final machining with conflat welded
	V0494014-16		at machine shop for final machining with conflat welded
	V0494014-17		awaiting forging
	V0494014-18		awaiting forging
	V0494014-19		Complete
	V0494014-20		Complete
	V0494014-21		Complete
	V0494014-22		Complete
BSC 60" Port Covers	V049A11-01		at machine shop for final machining with conflat welded
	V049A11-02		at machine shop for final machining with conflat welded
	V049A11-03		at machine shop for final machining with conflat welded
	V049A11-04		at machine shop for final machining with conflat welded

Horizontal Access Modules			
Item	Serial Number	Tag #	Status
			All Washington HAM bellows have been received
HAM Weldment	V0494128-01	WA	Complete, dimension check with new fixture on 2/3. Ready for cleaning.
	V0494128-02	WA	Final machining is complete. Ready for pickup at Ranor.
	V0494128-03	WA	Ready for "E" nozzle fit-up. Completed slotted 60" flange and tie rod welding.
	V0494128-04	WA	DR on 60" flange being repaired. "E" nozzle fit-up ongoing. Annulus tubing pre-fab complete.
	V0494128-05	WA	Ready for "E" nozzle fit-up. Completed slotted 60" flange and tie rod welding.
	V0494128-06	WA	Ready for large flange welding.
	V0494128-07	WA	Ready for large flange welding.
	V0494128-08	WA	Ready for large flange welding.
	V0494128-09	WA	Complete shell layout and cutting. Welding on 60" nozzles.
	V0494128-10	WA	Completed cutting out penetrations on shell. Ready to fit-up 60" nozzles.
	V0494128-11	WA	Long seam welded and shell penetrations laid out. Starting to cut out shell.
	V0494128-12	WA	Roll-up of shell and nozzles received by PSI; no long seams welded as yet
	V0494128-13	WA	Roll-up of shell and nozzles received by PSI; no long seams welded as yet
	V0494128-14	LA	Roll-up of shell and nozzles received by PSI; no long seams welded as yet
	V0494128-15	LA	Roll-up of shell and nozzles received by PSI; no long seams welded as yet
	V0494128-16	LA	All shell and nozzle material is at Ranor; ready for rolling
	V0494128-17	LA	All shell and nozzle material is at Ranor; ready for rolling
	V0494128-18	LA	All shell and nozzle material is at Ranor; ready for rolling
	V0494128-19	LA	All shell and nozzle material is at Ranor; ready for rolling

Item	Serial Number	Tag #	Status
HAM 84" Port Covers	V0494127-01		Complete
	V0494127-02		Complete
	V0494127-03		at machine shop for final machining; needs conflats welded in
	V0494127-04		Complete
	V0494127-05		at machine shop for final machining; needs conflats welded in
	V0494127-06		Complete
	V0494127-07		at machine shop with conflats welded in
	V0494127-08		at machine shop with conflats welded in
	V0494127-09		at machine shop with conflats welded in
	V0494127-10		at machine shop with conflats welded in
	V0494127-11		at machine shop with conflats welded in
	V0494127-12		at machine shop with conflats welded in
	V0494127-13		at machine shop with conflats welded in
	V0494127-14		at machine shop with conflats welded in
	V0494127-15		at machine shop with conflats welded in
	V0494127-16		at machine shop with conflats welded in
	V0494127-17		holes cut in head; await forging
	V0494127-18		at machine shop with conflats welded in
	V0494127-19		at machine shop with conflats welded in
	V0494127-20		at machine shop with conflats welded in
	V0494127-21		holes cut in head; await forging
	V0494127-22		at machine shop with conflats welded in
	V0494127-23		holes cut in head; await forging
	V0494127-24		holes cut in head; await forging
	V0494127-25		holes cut in head; await forging
	V0494127-26		awaiting flange forging
	V0494127-27		awaiting flange forging
	V0494127-28		awaiting flange forging
	V0494127-29		awaiting flange forging
	V0494127-30		awaiting flange forging
	V0494127-31		awaiting flange forging
	V0494127-32		awaiting flange forging
	V0494127-33		awaiting flange forging
	V0494127-34		awaiting flange forging
	V0494127-35		awaiting flange forging

Item	Serial Number	Tag #	Status
	V0494127-36		awaiting flange forging
	V0494127-37		awaiting flange forging
	V0494127-38		awaiting flange forging
HAM 60" Port Covers	V0494A4-01		at machine shop with con flats welded in
	V0494A4-02		at machine shop with con flats welded in
	V0494A4-03		complete
	V0494A4-04		complete
	V0494A4-05		complete
	V0494A4-06		complete

80K Cryopumps			
Item	Serial #	Tag #	Status
Short 80K Pump Righthand Weldment	V0494121-01	WA	Bayonets received. Complete fit-up of assy this week and start initial cleaning.
Short 80K Pump Righthand AL Reservoir	V0494090-01	WA	Complete and tested; ready for final assembly
Short 80K Pump Righthand Weldment	V0494121-02	WA	Outer shell assy and heads being worked. Long seam welded & layout ongoing.
Short 80K Pump Righthand AL Reservoir	V0494090-02	WA	Complete and tested; ready for final assembly
Short 80K Pump Righthand Weldment	V0494121-03	WA	Outer shell long seam welded & penetrations being laid out. Starting heads.
Short 80K Pump Righthand AL Reservoir	V0494090-03	WA	Complete and tested; ready for final assembly
Short 80K Pump Righthand Weldment	V0494121-04	LA	material at Ranor for rolling
Short 80K Pump Righthand AL Reservoir	V0494090-04	LA	roll-up received by PSI
Short 80K Pump Lefthand Weldment	V0494120-01	WA	Outer shell rollup received
Short 80K Pump Lefthand AL Reservoir	V0494091-01	WA	Cold shock completed. He leak test ongoing.
Short 80K Pump Lefthand Weldment	V0494120-02	WA	roll-up received by PSI
Short 80K Pump Lefthand AL Reservoir	V0494091-02	WA	roll-up received by PSI
Short 80K Pump Lefthand Weldment	V0494120-03	WA	material at Ranor for rolling
Short 80K Pump Lefthand AL Reservoir	V0494091-03	WA	roll-up received by PSI
Short 80K Pump Lefthand Weldment	V0494120-04	LA	material at Ranor for rolling
Short 80K Pump Lefthand AL Reservoir	V0494091-04	LA	roll-up received by PSI
Long 80K Pump Lefthand Weldment	V0494118-01	WA	roll-up received by PSI
Long 80K Pump Lefthand AL Reservoir	V0494092-01	WA	partial roll-up received
Long 80K Pump Lefthand Weldment	V0494118-02	LA	roll-up received by PSI
Long 80K Pump Lefthand AL Reservoir	V0494092-02	LA	material at Ranor for rolling

Item	Serial #	Tag #	Status
Long 80K Pump Righthand Weldment	V0494119-01	WA	roll-up received by PSI
Long 80K Pump Righthand AL Reservoir	V0494093-01	WA	material at Ranor for rolling
Long 80K Pump Righthand Weldment	V0494119-02	LA	material at Ranor for rolling
Long 80K Pump Righthand AL Reservoir	V0494093-02	LA	material at Ranor for rolling

Spools and Adapters			
Item	Serial Number	Tag #	Status
Adapter A1	V0494A1-01	WA	Hyspan bellows assembly received by PSI & checking on finish machined flange status
	V0494A1-02	WA	Hyspan bellows assembly received by PSI & checking on finish machined flange status
	V0494A1-03	WA	Hyspan bellows assembly received by PSI & checking on finish machined flange status
	V0494A1-04	WA	Hyspan bellows assembly received by PSI & checking on finish machined flange status
	V0494A1-05	WA	Hyspan bellows assembly received by PSI & checking on finish machined flange status
	V0494A1-06	WA	Hyspan bellows assembly received by PSI & checking on finish machined flange status
	V0494A1-07	LA	await bellows assembly (mat'l at Hyspan) & finish machined flanges
	V0494A1-08	LA	await bellows assembly (mat'l at Hyspan) & finish machined flanges
	V0494A1-09	LA	await bellows assembly (mat'l at Hyspan) & finish machined flanges
	V0494A1-10	LA	await bellows assembly (mat'l at Hyspan) & finish machined flanges
Adapter A2	V0494A2-01	LA	await roll-up from Ranor; all shell material at Ranor
	V0494A2-02	LA	await roll-up from Ranor; all shell material at Ranor
Adapter A3	V0494A3-01	WA	Hyspan bellows assembly received by PSI & checking on finish machined flange status
	V0494A3-02	WA	Hyspan bellows assembly received by PSI & checking on finish machined flange status
	V0494A3-03	LA	await bellows assembly (mat'l at Hyspan) & finish machined flanges
	V0494A3-04	LA	await bellows assembly (mat'l at Hyspan) & finish machined flanges
	V0494A6-01	WA	Hyspan bellows assembly received by PSI & checking on finish machined flange status
	V0494A6-02	WA	Hyspan bellows assembly received by PSI & checking on finish machined flange status
Adapter A7A	V0494A7A-01	WA	Penetrations cut, stiffener rings installed, fit-up of girth welds on 2 sections complete. Need flanges.
	V0494A7A-02	WA	All roll-ups rec'd. Ready for long seam welding.
	V0494A7A-03	LA	72" roll-up rec'd from Ranor, need 60" roll-up
Adapter A7B	V0494A7B-01	WA	Penetrations cut, stiffener rings installed, fit-up of girth welds on 2 sections complete. Need flanges.
	V0494A7B-02	WA	All roll-ups rec'd. Ready for long seam welding.
	V0494A7B-03	LA	72" roll-up rec'd from Ranor, need 60" roll-up
Adapter A12	V0494A12-01		Hyspan bellows assembly received by PSI & checking on finish machined flange status
	V0494A12-02		Hyspan bellows assembly received by PSI & checking on finish machined flange status

Item	Serial Number	Tag #	Status
Adapter A13	V0494A13-01	WA	await bellows assembly (mat'l at Hyspan) & finish machined flanges
	V0494A13-02	WA	await bellows assembly (mat'l at Hyspan) & finish machined flanges
Adapter A14	V0494A14-01	WA	Hyspan bellows assembly received by PSI & checking on finish machined flange status
	V0494A14-02	WA	Hyspan bellows assembly received by PSI & checking on finish machined flange status
Adapter A15	V0494A15-01	WA	Spool complete except for annulus piping connection (rec'd 2/4). Ready for clean/bake/test.
	V0494A15-02	WA	Spool complete except for annulus piping connection (rec'd 2/4). Ready for clean/bake/test.
Spool B1	V0494B1-01	WA	Long seam welded. One flange rec'd, awaiting second.
	V0494B1-02	WA	Long seam welded. One flange rec'd, awaiting second.
	V0494B1-03	LA	roll-up received from Ranor
	V0494B1-04	LA	await roll-up from Ranor; all shell material at Ranor
	V0494B1-05	LA	await roll-up from Ranor; all shell material at Ranor
	V0494B1-06	LA	await roll-up from Ranor; all shell material at Ranor
Spool B2A	V0494B2A-01	WA	Need flanges. Girth welds fit-up for 2 of 3 sections. Bellows rec'd.
Spool B2B	V0494B2B-01	WA	Need flanges. Girth welds fit-up for 2 of 3 sections. Bellows rec'd.
Spool B3A	V0494B3A-01	WA	Long seam welded; awaiting flanges.
	V0494B3A-02	LA	Roll-up & bellows rec'd. Ready for welding.
Spool B4	V0494B4-01	WA	Spool complete except for annulus piping connection (rec'd 2/4); ready for clean & test
	V0494B4-02	WA	await roll-up from Ranor; most shell material at Ranor
Spool B5A	V0494B5A-01	WA	Long seam welded; awaiting flanges.
	V0494B5A-02	LA	Roll-up rec'd from Ranor; await bellows assy from Hyspan.
Spool B6	V0494B6-01	WA	Welding of stiffener rings complete. Starting flange fit-up.
Spool B7	V0494B7-01	WA	Long seam welding complete; welding on stiffener rings (some on DR). Laying out penetrations.
Spool B8	V0494B8-01	WA	Long seam being welded.
	V0494B8-02	WA	Roll-up rec'd from Ranor; ready to start long seam welding.

Item	Serial Number	Tag #	Status
Spool B9	V0494B9-01	WA	Stiffener rings installed. Girth welds fit-up for 2 of 3 sections.
	V0494B9-02	WA	Stiffener rings installed. Girth welds fit-up for 2 of 3 sections.
	V0494B9-03	LA	await roll-up from Ranor; all shell material at Ranor
	V0494B9-04	LA	await roll-up from Ranor; all shell material at Ranor
Spool BE1	V0494BE1-01	LA	await bellows assy from Hyspan, all material at Hyspan
	V0494BE1-02	LA	await bellows assy from Hyspan, all material at Hyspan
Spool BE2	V0494BE2-01	WA	Hyspan bellows assembly received by PSI & checking on finish machined flange status
	V0494BE2-02	WA	Hyspan bellows assembly received by PSI & checking on finish machined flange status
	V0494BE2-03	LA	await bellows assy from Hyspan, most material at Hyspan
	V0494BE2-04	LA	await bellows assy from Hyspan, most material at Hyspan
Spool BE3	V0494BE3-01	WA	await roll-up from Ranor; all shell material at Ranor. Bellows assy received from Hyspan.
	V0494BE3-02	WA	await roll-up from Ranor; all shell material at Ranor. Bellows assy received from Hyspan.
	V0494BE3-03	LA	await roll-up from Ranor; all shell material at Ranor. Bellows assy received from Hyspan.
Spool BE3A	V0494BE3A-01	WA	await roll-up from Ranor; bellows assy received from Hyspan
	V0494BE3A-02	WA	await roll-up from Ranor; bellows assy received from Hyspan
	V0494BE3A-03	LA	await roll-up from Ranor; and bellows assy from Hyspan
Spool BE4	V0494BE4-01	WA	Hyspan bellows assembly received by PSI & checking on finish machined flange status
	V0494BE4-02	WA	Hyspan bellows assembly received by PSI & checking on finish machined flange status
	V0494BE4-03	WA	Hyspan bellows assembly received by PSI & checking on finish machined flange status
	V0494BE4-04	WA	Hyspan bellows assembly received by PSI & checking on finish machined flange status
	V0494BE4-05	WA	Hyspan bellows assembly received by PSI & checking on finish machined flange status
	V0494BE4-06	WA	Hyspan bellows assembly received by PSI & checking on finish machined flange status
	V0494BE4-07	WA	Hyspan bellows assembly received by PSI & checking on finish machined flange status
	V0494BE4-08	WA	Hyspan bellows assembly received by PSI & checking on finish machined flange status
	V0494BE4-09	LA	await bellows assy from Hyspan, all material at Hyspan
	V0494BE4-10	LA	await bellows assy from Hyspan, all material at Hyspan
	V0494BE4-11	LA	await bellows assy from Hyspan, all material at Hyspan
	V0494BE4-12	LA	await bellows assy from Hyspan, all material at Hyspan

Item	Serial Number	Tag #	Status
Spool BE5	V0494BE5-01	WA	await roll-up from Ranor; bellows assy received from Hyspan
	V0494BE5-02	LA	await roll-up from Ranor; and bellows assy from Hyspan
Spool BE6	V0494BE6-01	WA	await roll-up from Ranor; bellows assy received from Hyspan
	V0494BE6-02	LA	await roll-up from Ranor; and bellows assy from Hyspan



SECTION 7 QUALITY ASSURANCE STATUS

ACTIVITIES FOR THE CURRENT PERIOD:

Continued incoming inspection activities on materials being received such as flange forgings, stainless steel plate, vessel heads, clean air compressor system, ultra high vacuum valves, instrumentation, ion pumps, and conflat flanges. Materials are being inspected at PSI's facility, Ranor, Arland Tool, and Hyspan, as materials are being directly drop shipped from vendors.

Continued in-process inspections at Ranor for BSC fabrication, rolling, and machining; Arland Tool for flange machining; Atlas Metal Products for carbon steel assemblies; and Hyspan for bellows type expansion joint fabrication.

The following non-conformance reports generated during the period (January):

1. Various discrepancies were noted on an inspection of stainless steel plate at Ranor ranging from incorrect size to possible laminations. Disposition: Incorrect sizes will be returned to the vendor, laminations will be ultrasonic tested, and damaged plate will be used if localized damaged area is not used.
2. Installation problems occurred with the cleanroom lights and curtains. Disposition: Installation procedures were modified to install the cleanroom lights, and the curtain was modified so as not to interfere with the leg extensions.
3. Machined flange surface contained burrs and minor scratches. Disposition: Repair at PSI and notify vendor to prevent reoccurrence.
4. List of minor discrepancies generated from the inspection of the first BSC weldment at Ranor. Disposition: Ranor to make necessary repairs prior to receiving PSI release to ship.
5. Lockwashers were received and the material did not conform to the specification. Disposition: Use as is and an RFC will be generated to change the part description to match what was delivered.
6. Stainless steel stiffener ring received not in conformance with the drawing. Disposition: Return to vendor for correct part.
7. Stainless steel stiffener ring received with improper diameter. Disposition: Return to vendor to correct.
8. Two more stainless stiffener rings received which were not in conformance to the drawing. Disposition: Return to vendor to correct.
9. A lamination was discovered on a rolled up HAM shell. Disposition: Part was tested to confirm to the lamination and returned to the vendor for a replacement part.
10. Hangers were provided with 304 stainless steel material versus 304L stainless specified on the drawing. Disposition: Use as is. Location of the material was examined and it was determined 304 stainless steel was acceptable.



PROCESS SYSTEMS INTERNATIONAL, INC.

11. 10" gate valve had damage on the conflat knife edges and the flange hardware was metric.
Disposition: Return to vendor for correct part.
12. 80K pump low emissivity liner not in conformance with the drawing. Disposition: PSI to repair the discrepancy and notify vendor to prevent reoccurrence.
13. HAM bellows bought for the first articles had two convolutions and the production bellows had four convolutions: Disposition: Order replacement four convolution bellows and change out bellows on S/N 001 and S/N 004 with four convolution bellows.
14. Damaged a 8" conflat flange on a loaned valve from Varian. Disposition: Return to vendor.
15. Expansion bellows tie rod assemblies in the wrong location and shipping damage evident.
Disposition: Repair tie rods at PSI and backcharge vendor. Vendor to be notified of shipping damage to prevent reoccurrence.

ACTIVITIES PLANNED FOR THE NEXT PERIOD:

Continue weekly in-process inspection at Ranor, Arland Tool, and Atlas Metal Products based on established witness/hold points

Continue review of vendor quality plans, and equipment specifications, as required

Continue to participate in the manufacturing / inspection cycle with vendors, as required

Continue in-process inspection of vessels and components being fabricated at PSI



SECTION 8 INSTALLATION STATUS

Installation is not scheduled to commence until mid-1997.

PSI issued the Washington installation for bid in early December, and bids were received in mid January. Four bids were received and bid review meetings will be held in early to mid February. Interest in the project is very positive, and PSI received very responsive bids. A bid clarification will be sent out in late February to those who submitted bids.

The installation subcontract will be awarded after an additional bid review meeting with the two low bidders to reconfirm an understanding of the scope of work, and commitment to the project schedule. The installation contract will be awarded well in advance of the site mobilization date. The target date is currently early April to choose a contractor and commit to a contract.

Installation scope activity currently consists of detail planning input and preparation of required installation documentation. PSI is also starting to make plans to relocate the construction management team to the Hanford site.



PROCESS SYSTEMS INTERNATIONAL, INC.

SECTION 9 SCHEDULE STATUS

SELECT/NEAR TERM MILESTONES

<u>Milestone</u>	<u>Planned Date</u>	<u>Current Forecast</u>	<u>Actual Date</u>
Contract Award	09/12/95	09/12/95	09/12/95
Issue Updated Preliminary Design	10/12/95	09/27/95	09/27/95
Complete Final Design	04/12/96	05/07/96	05/07/96
Final Design Review	05/17/96	05/22/96	05/22/96
LIGO Approval of Final Design	05/12/96	06/07/96	06/07/96
Complete Prototype Testing Program	06/05/96	10/08/96	10/08/96
Conduct Prototype Vessel Data Review	07/12/96	10/30/96	10/30/96
Start WA Vessel Fabrication	07/22/96	08/01/96	08/01/96
Reissue Final Design Package - WA	08/01/96	01/03/97	01/03/97
- LA	08/01/96	03/07/97	
Complete 1st HAM Fabrication	12/27/96	12/30/96	01/07/97
Complete 1st BSC Fabrication (Ranor)	11/27/96	01/10/97	01/14/97
Issue Installation Bid Pkg for Washington	12/31/96	12/31/96	12/04/96
Award Washington Installation Contract	05/01/97	04/01/97	
Readiness Review - Washington	07/01/97	07/01/97	
Joint Occupancy - Washington	08/01/97	08/01/97	
Readiness Review - Louisiana	02/01/98	02/01/98	
Joint Occupancy - Louisiana	03/01/98	03/01/98	



SUMMARY

The project continues to be essentially on schedule as of January 31, 1997, with an existing slippage in one major project milestone (Large Gate Valve Delivery for the Washington Beam Tube Contractor), which does not impact field installation, at this time. This milestone will be achieved in February. Major raw materials for all components continue to be delivered to PSI with over 95% of the project raw materials having been delivered. Fabrication is underway for cryopumps, BSC's, HAM's, and spools/adapters. Fabrication of the BSC weldments at Ranor continues to be only slightly behind their initial schedule, and they are adhering to their recovery plan and supporting PSI's schedule. The schedule for HAM fabrication is approximately three weeks behind last month's schedule due to delays in receiving fixtures for "E" nozzle dimensional checks, getting wash station / test area completely operational. The first article cryopump is approximately three weeks behind last month's forecast due to delays in design and late receipt of the low emissivity liners. The delivery of the last Washington cryopump has improved by six weeks due to a rescheduling of PSI resources, and good progress on other cryopumps. Overall spool fabrication is approximately two months behind last month's forecast due to reprioritizing shop floor and field priorities. PSI is currently analyzing the spool schedule with a four week target improvement. All changes from last month's forecast are being mitigated through a recovery plan (i.e. Ranor) or being absorbed by the float associated with these items in the schedule (i.e. HAM's, cryopumps). The critical path continues to run through the completion of fabrication and testing of BSC's required for the Washington site, then through the Washington installation, and then through installation at the Louisiana site.

A secondary critical path is through the delivery of the large gate valves which are a beam tube deliverable for the Washington site in August 1996. Six of eight valves have shipped to the Washington site, and the balance will ship on February 24, 1997. All technical issues have been resolved. The large gate valves are behind schedule due to vendor delays. Field needs for the valves have been satisfied.

PROJECT SCHEDULE

The detailed project schedule continues to be updated on monthly basis, and schedule status is reviewed weekly with project team members in weekly progress meetings. Detail fabrication schedules have been developed for all manufactured components, and are being transmitted to LIGO under separate cover. The detail manufacturing schedules are currently being updated on a weekly basis. A component fabrication schedule is being transmitted to LIGO weekly for information. It is important to note the manufacturing sequence directly supports the installation sequence for HAM's, BSC's, and 80K cryopumps.

Attached to this section is the following reports: Detail Project Schedule



PROCESS SYSTEMS INTERNATIONAL, INC.

CORRECTIVE ACTIONS

An overtime program continues in design, and manufacturing to maintain schedule on critical path items, and to complete the reissue of the final design package.

Ranor continues work on a 5 day a week, two shift basis for weekdays; and single shifts on Saturdays and Sundays to support PSI's material needs for rolled and machined products, as well as BSC weldments. Arland Machine also continues on a two shift basis to supply PSI with finish machined flanges and port covers.

PSI is maintaining close surveillance on GNB (large gate valve vendor), and GNB is working overtime and hiring new personnel in order to attain the best possible schedule for the balance of the Washington Beam Tube Deliverables, and the 1997 valve deliveries. PSI project management is making bimonthly visits to GNB to assure that schedule commitments are being carried out for the balance of the order.



PROCESS SYSTEMS INTERNATIONAL, INC.

**DETAILED PROJECT SCHEDULE
(SORTED BY SYSTEM AND ACTIVITY ID)**

Act ID	Description	Orig Dür	Early Start	Early Finish	Percent Complete	Year											
						1995	1996	1997	1998	1999							
Contractual Schedule Milestones - Acticle II																	
30	Complete Updated Preliminary Design (Phase B)	0		27SEP95 A	100	◆											
31	Submit & Implement Updated Proj Mgmt Plan	0		27SEP95 A	100	◆											
32	Deliverables to the Beam Tube Contractor - WA	80	16AUG96 A	26FEB97	79												
33	Deliverables to the Beam Tube Contractor - LA	0		05SEP97	0												
34	Complete Final Design	0		07MAY96 A	100		◆										
35	Begin fabrication and procurement	0	07JUN96 A		100		◆										
36	Begin Installation - Washington Site	0	04AUG97		0												
37	Begin Installation - Louisiana Site	0	03MAR98		0												
38	Complete Acceptance Testing - Washington Site	0		24FEB98	0												
39	Complete Acceptance Testing - Louisiana Site	0		02NOV98	0												
40	Updated Preliminary Design Review	1	03OCT95 A	03OCT95 A	100	△											
41	Deliverables to the Beam Tube Final Design Rvw	0		07NOV95 A	100	◆											
42	Final Design Review	0	22MAY96 A		100		◆										
43	Final Prototype Vessel Design Review	2	30OCT96 A	30OCT96 A	100			△									
44	Installation Readiness Review - Washington	0		01JUL97	0												
45	Installation Readiness Review - Louisiana	0		02FEB98	0												
46	Acceptance Test Review - Washington	0		11MAR98	0												
47	Acceptance Test Review - Louisiana	0		01DEC98	0												
Common Engineering / Design Activities																	
1	Phase B Award	0		12SEP95 A	100	◆											
2	Submit Ph B Updated PDR for approval (CDRL 01)	0		27SEP95 A	100	◆											
3	Approval of Updated PDR (CDRL 01) by LIGO	0		10NOV95 A	100	◆											
4	Submit Proj Mgmt Plan for Approval (CDRL 02)	0		27SEP95 A	100	◆											
5	Approval of Proj Mgmt Plan by LIGO (CDRL 02)	0		06DEC95 A	100	◆											
6	Submit Final Design for Approval (CDRL 03)	0		07MAY96 A	100		◆										
7	Approval of Final Design by LIGO (CDRL 03)	0		07JUN96 A	100		◆										
8	Full Release for Fabrication and Procurement	0		07JUN96 A	100		◆										
000	Contract Award	1	12SEP95 A	12SEP95 A	100	△											
100	Phase B Update of PDR & Proj Mgmt Plan	1	12SEP95 A	27SEP95 A	100	△											
101	P&ID's - Initial Issue	10	13SEP95 A	22SEP95 A	100	△											
102	P&ID's - Issue for Design	30	16OCT95 A	03JAN96 A	100	△											
103	P&ID's - Issue As-Built	15	01SEP98 *	22SEP98	0												
104	PFD's - Issue for Design	10	01FEB96 A	03JAN96 A	100	△											
105	Receive LIGO comments on updated prelim design	10	03OCT95 A	10NOV95 A	100	△											
106	Final issue of Ph B update of prelim design pkg	30	13NOV95 A	01DEC95 A	100	△											



- △ Early start point
- ▽ Early finish point
- ▬ Early bar
- ▬ Progress bar
- ▬ Critical bar
- ▬ Summary bar
- ▲ Progress point
- ▼ Critical point
- ◆ Summary point
- ◆ Start milestone point
- ◆ Finish milestone point

Process Systems International, Inc.

LIGO Vacuum System Project

Project Schedule

1Aof18A

Data date 01FEB97

Run date 04MAR97

Filter All Activities

Layout System

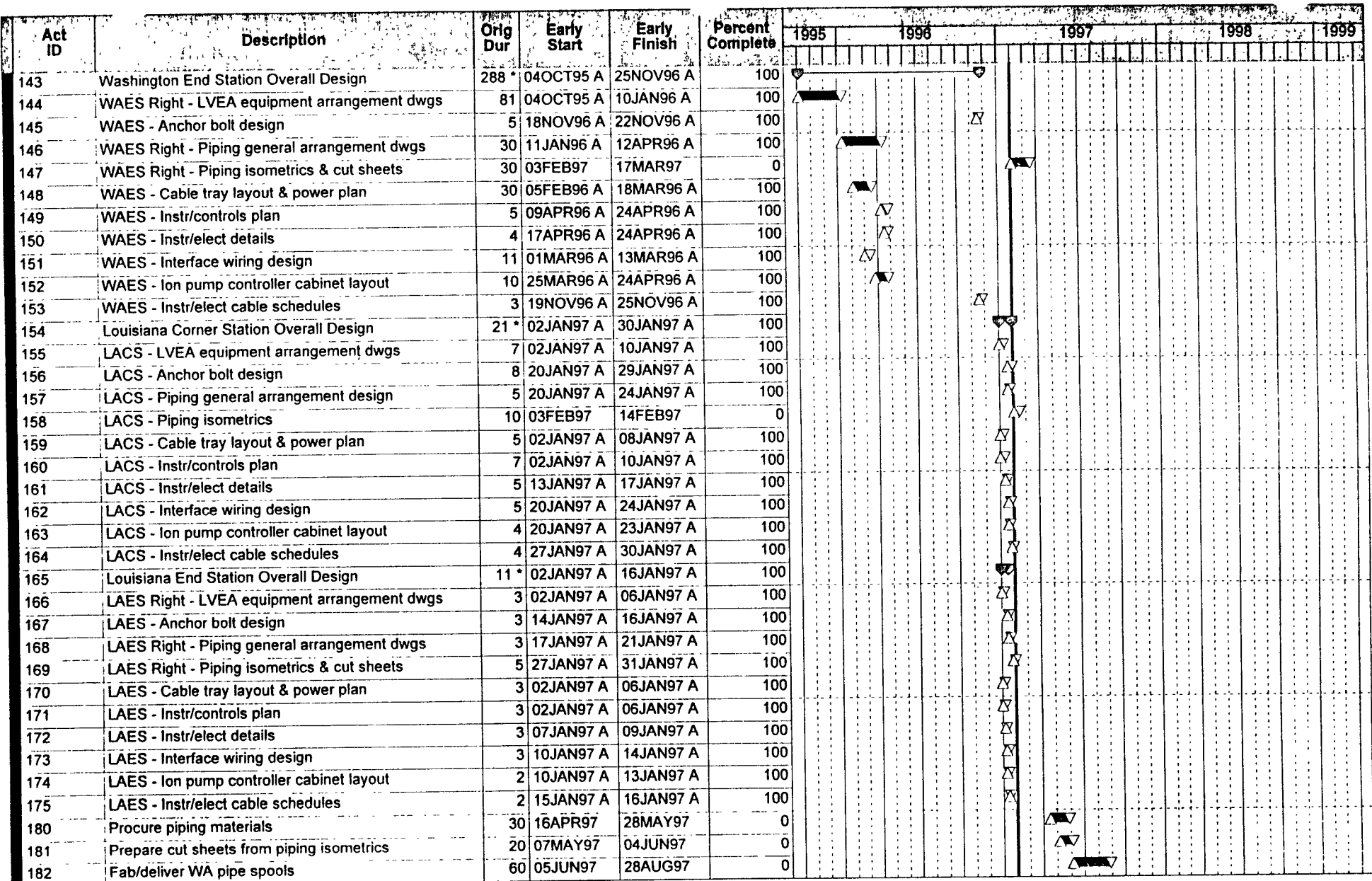
© Primavera Systems, Inc.

Date
05MAR97

Revision
Status Rpt No 15

Checked
PFH

Approved
REB



- △ Early start point
- ▽ Early finish point
- ▬ Early bar
- ▬ Progress bar
- ▬ Critical bar
- ▬ Summary bar
- ▲ Progress point
- ▼ Critical point
- ◆ Summary point
- ◆ Start milestone point
- ◆ Finish milestone point

Process Systems International, Inc.

LIGO Vacuum System Project

Project Schedule

3Aof18A

Date date 01FEB97

Run date 04MAR97

Filter All Activities

Layout System

© Primavera Systems, Inc.

Date 05MAR97

Revision Status Rpt No 15

Checked PFH

Approved REB

Act ID	Description	Orig Dur	Early Start	Early Finish	Percent Complete	1995												1996												1997												1998												1999											
183	Fab/deliver LA pipe spools	50	29AUG97	07NOV97	0																																																												
184	Update the 3D model	10	25MAR96 A	05APR96 A	100																																																												
185	C.O #5 - Add cw supply to roots & turbo pumps	20	24OCT95 A	12JAN96 A	100																																																												
186	CO #11 - WACS beam manifold spool changes	25	21DEC95 A	26JAN96 A	100																																																												
188	CO #14 - LVEA changes to mid/end mech rooms	1	09JAN96 A	02FEB96 A	100																																																												
190	CO #16 - BSC removable spools due to space limit	15	16JAN96 A	14MAR96 A	100																																																												
192	CO #18 - Reduce annulus pumping speed	15	14FEB96 A	06MAR96 A	100																																																												
194	CO #19 - 30" Mode Cleaner Tube Changes	15	14MAR96 A	01APR96 A	100																																																												
196	Conduct final design review with LIGO	2	22MAY96 A	23MAY96 A	100																																																												
197	Prepare & Issue Final Design Package Draft	15	10APR96 A	07MAY96 A	100																																																												
198	Receive LIGO Approval of Final Design Package	1	07JUN96 A	07JUN96 A	100																																																												
199	Final Issue of Final Design Package	24	03FEB97	07MAR97	0																																																												
105A	LIGO approval of the Project Mgmt Plan	15	03OCT95 A	06DEC95 A	100																																																												
118A	PSI to receive revised WA bldg dwgs for comments	1	22APR96 A	22APR96 A	100																																																												
118AA	PSI to receive revised WA bldg dwgs for constrct	1	29JUL96 A	29JUL96 A	100																																																												
118B	PSI to receive LA bldg dwgs for comments	1	26AUG96 A	26AUG96 A	100																																																												
120D	WACS - Equipment detail dwgs	40	26FEB96 A	19APR96 A	100																																																												
133D	WAMS Right - Equipment detail dwgs	40	12FEB96 A	12APR96 A	100																																																												
133DL	WAMS Left - Equipment detail dwgs	3	16APR96 A	18APR96 A	100																																																												
133L	WAMS Left - LVEA equipment arrangement dwg	2	16APR96 A	17APR96 A	100																																																												
135L	WAMS Left - Piping general arrangement dwgs	5	18APR96 A	24APR96 A	100																																																												
136L	WAMS Left - Piping isometrics & cut sheets	15	18MAR97	07APR97	0																																																												
144D	WAES Right - Equipment detail dwgs	27	11JAN96 A	12APR96 A	100																																																												
144DL	WAES Left - Equipment detail dwgs	3	16APR96 A	18APR96 A	100																																																												
144L	WAES Left - LVEA equipment arrangement dwg	2	16APR96 A	17APR96 A	100																																																												
146L	WAES Left - Piping general arrangement dwgs	5	16APR96 A	22APR96 A	100																																																												
147L	WAES Left - Piping isometrics & cut sheets	20	18MAR97	15APR97	0																																																												
155D	LACS - Equipment detail dwgs	5	13JAN97 A	17JAN97 A	100																																																												
166D	LAES Right - Equipment detail dwgs	3	09JAN97 A	13JAN97 A	100																																																												
166DL	LAES Left - Equipment detail dwgs	3	14JAN97 A	16JAN97 A	100																																																												
166L	LAES Left - LVEA equipment arrangement dwgs	2	07JAN97 A	08JAN97 A	100																																																												
168L	LAES Left - Piping general arrangement dwgs	3	22JAN97 A	24JAN97 A	100																																																												
169L	LAES Left - Piping isometrics & cut sheets	5	03FEB97	07FEB97	0																																																												
Vacuum Envelope																																																																	
10	Begin Vessel Fabrication - Washington	0	01AUG96 A		100																																																												
11	Begin Vessel Fabrication - Louisiana	0	10FEB97		0																																																												



- ▲ Early start point
- ▼ Early finish point
- Early bar
- ▨ Progress bar
- Critical bar
- ▨ Summary bar
- ▲ Progress point
- ▲ Critical point
- ◆ Summary point
- ◆ Start milestone point
- ◆ Finish milestone point

Process Systems International, Inc.

LIGO Vacuum System Project

Project Schedule

4Aof18A

Data date 01FEB97

Run date 04MAR97

Filter All Activities

Layout System

© Primavera Systems, Inc.

Date
05MAR97

Revision
Status Rpt No 15

Checked
PFH

Approved
REB

Act ID	Description	Orig Dur	Early Start	Early Finish	Percent Complete	1995	1996	1997	1998	1999
16	Order First Article Material	0		14DEC95 A	100					
19	Complete Prototype Vessel Tests	0		08OCT96 A	100					
201	Design HAM Vessels	96	13SEP95 A	04APR96 A	100					
202	Design BSC Vessels	45	13SEP95 A	05DEC95 A	100					
203	Design BSC chamber fab fixtures	15	26FEB96 A	15MAR96 A	100					
204	Design long 80K cryopump vessels	30	13NOV95 A	30APR96 A	100					
205	Design adapters and spool pieces	256 *	11JAN96 A	16JAN97 A	100					
206	WACS - Prepare skid/pre-assy details	20	03FEB97	03MAR97	0					
207	WAMS - Prepare skid/pre-assy details	10	03FEB97	14FEB97	0					
208	WAES - Prepare skid/pre-assy details	10	03FEB97	14FEB97	0					
209	LACS - Prepare skid/pre-assy details	5	03FEB97	07FEB97	0					
210	LAES - Prepare skid/pre-assy details	5	03FEB97	07FEB97	0					
214	Prepare a vessel fabrication specification	20	30OCT95 A	15DEC95 A	100					
215	Prepare a final cleaning procedure	10	16APR96 A	29APR96 A	100					
217	Develop a leak test procedure	20	19FEB96 A	29APR96 A	100					
219	Develop a bakeout procedure	15	01APR96 A	22APR96 A	100					
222	Develop welding procedures	10	15JAN96 A	22FEB96 A	100					
223	Design and specify test/shipping covers	25	01DEC95 A	22APR96 A	100					
224	Bellows expansion joints - Prepare Purchase Spec	10	01FEB96 A	09FEB96 A	100					
225	Bellows expansion joints - Bid/Purchase 69 items	20	12FEB96 A	28AUG96 A	100					
226	Bellows expansion joints - receive/review v/dwgs	20	29AUG96 A	25SEP96 A	100					
227	Bellows expansion joints - Fab & ship 74 items	108 *	26SEP96 A	03MAR97	82					
228	Fabrication Fixtures - Detail design & BOM's	20	28MAY96 A	11JUL96 A	100					
229	Order mat'l & fab test/shipping covers	80	18JUN96 A	12MAR97	66					
235	SS Vessel Mat'l - Bid & purchase total quantity	20	31JAN96 A	24MAY96 A	100					
237	SS Vessel Mat'l - Fab & deliver 1st shipment	40	27MAY96 A	30AUG96 A	100					
239	Vessel Heads - Bid & purchase total quantity	30	05APR96 A	28MAY96 A	100					
240	Flange Forgings - Bid & purchase total quantity	25	05APR96 A	10JUN96 A	100					
241	Flange Forgings - Fab & deliver 1st shipment	50	11JUN96 A	30AUG96 A	100					
242	Release vessel material for shipment	3	10JUN96 A	12JUN96 A	100					
243	Vessel Heads - Fab & deliver 1st shipment	38	29MAY96 A	23AUG96 A	100					
244	BSC's - Fab and test WA vessels (10)	259 *	23SEP96 A	01OCT97	35					
245	BSC's - Fab and test LA vessels (5)	267 *	10FEB97	03MAR98	0					
246	HAM's - Fab and test WA vessels (12)	218 *	22AUG96 A	03JUL97	51					
247	HAM's - Fab and test LA vessels (6)	111 *	02JUN97	05NOV97	0					
248	WA Beam Tube Manifolds / Spools / Adapters - Fab	228	26SEP96 A	21AUG97	39					

Data date	01FEB97	Date	05MAR97	Revision	Status Rpt No 15	Checked	Approved
Run date	04MAR97					PFH	REB
Filter	All Activities						
Layout	System						
© Primavera Systems, Inc.							

Process Systems International, Inc.

LIGO Vacuum System Project

Project Schedule

5Aof18A



- △ Early start point
- ▽ Early finish point
- ▬ Early bar
- ▬ Progress bar
- ▬ Critical bar
- ▬ Summary bar
- ▲ Progress point
- ▲ Critical point
- ▲ Summary point
- ◆ Start milestone point
- ◆ Finish milestone point

Act ID	Description	Orig Dur	Early Start	Early Finish	Percent Complete	1995												1996												1997												1998												1999											
						1995												1996												1997												1998												1999											
249	WA BTM/Spools/Adapters - Clean/test/prep to ship	128	17MAR97 *	16SEP97	0																																																												
250	Long 80K Cryopumps - Fab & test WA pumps (2)	101 *	01FEB97	26JUN97	0																																																												
251	Long 80K Cryopumps - Fab & test LA pumps (2)	64 *	14JUL97	10OCT97	0																																																												
252	Short 80K Cryopumps - Fab & test WA pumps (6)	162 *	09OCT96 A	02JUN97	49																																																												
253	Short 80K Cryopumps - Fab & test LA pumps (2)	62 *	19AUG97	13NOV97	0																																																												
254	LA Beam Tube Manifolds / Spools / Adapters - Fab	110	22AUG97	30JAN98	0																																																												
255	LA BTM/Spools/Adapters - Clean/test/prep to ship	110	22SEP97	27FEB98	0																																																												
257	CO # 6 - Additional bracing on BSC chamber	15	21NOV95 A	21DEC95 A	100																																																												
258	CO #10 -Increase pumping surface clear aperature	9	12DEC95 A	21DEC95 A	100																																																												
260	10" Benchscale Vessel Program	149 *	04DEC95 A	08JUL96 A	100																																																												
262	CO #13 - BSC internal floor loading requirements	20	19OCT95 A	06MAR96 A	100																																																												
265	1st Article HAM - Procure fab materials	50	05APR96 A	06JUN96 A	100																																																												
266	1st Article HAM - Evaluate outside fabrication	30	05APR96 A	14AUG96 A	100																																																												
267	Lifting Jacks - Design & requisition materials	15	22JUL96 A	08NOV96 A	100																																																												
268	Lifting Jacks - Procure materials	20	03FEB97	03MAR97	0																																																												
269	Lifting Jacks - Fabricate one set of jacks	20	04MAR97	31MAR97	0																																																												
272	Design long 80K cryopump shroud	20	27NOV95 A	26APR96 A	100																																																												
273	Design short 80K cryopump vessel	50	13NOV95 A	26APR96 A	100																																																												
274	Design short 80K cryopump shroud	60	01NOV95 A	26APR96 A	100																																																												
279	Conduct a plasma welding investigation	10	13OCT95 A	31OCT95 A	100																																																												
280	Procure a plasma welding machine	20	20NOV95 A	15DEC95 A	100																																																												
281	Qualify Welding Procedure for Plasma Welding	10	02JAN96 A	22FEB96 A	100																																																												
284	Procure cleaning equipment	20	24JAN96 A	16FEB96 A	100																																																												
285	Conduct materials testing program	10	01APR96 A	12APR96 A	100																																																												
286	Conduct a viton investigation	15	22APR96 A	08JUL96 A	100																																																												
289	Short 80K Cryopump - Procure shroud mat'l (1)	10	03JUL96 A	10JUL96 A	100																																																												
290	Short 80K Cryopump - Fab shroud for prototype	25	11JUL96 A	16SEP96 A	100																																																												
291	Order Prototype BSC Flange Forgings	5	06DEC95 A	13DEC95 A	100																																																												
292	Fab and deliver Prototype BSC flange forgings	53	14DEC95 A	13MAR96 A	100																																																												
293	Order Prototype BSC shell, head, & nozzle mat'l	5	06DEC95 A	14DEC95 A	100																																																												
294	Fab & del Prototype BSC head, shell, nozzle matl	50	15DEC95 A	12MAR96 A	100																																																												
295	Fabricate Prototype BSC Vessel	71 *	01MAY96 A	12AUG96 A	100																																																												
296	Test program for Prototype vessel	40 *	13AUG96 A	08OCT96 A	100																																																												
297	Fabricate chamber fab fixtures	15	08APR96 A	24MAY96 A	100																																																												
298	Order mat'l for test/ship covers for prototype	40	15DEC95 A	13MAR96 A	100																																																												
12A	Receipt of 1/3 of SS vessel material	0		30AUG96 A	100																																																												



- ▲ Early start point
- ▼ Early finish point
- ▬ Early bar
- ▬ Progress bar
- ▬ Critical bar
- ▬ Summary bar
- ▲ Progress point
- ▲ Critical point
- ▲ Summary point
- ◆ Start milestone point
- ◆ Finish milestone point

Process Systems International, Inc.

LIGO Vacuum System Project

Project Schedule

6Aof18A

Data date 01FEB97

Run date 04MAR97

Filter All Activities

Layout System

© Primavera Systems, Inc.

Date 05MAR97

Revision Status Rpt No 15

Checked PFH

Approved REB

Act ID	Description	Orig Dur	Early Start	Early Finish	Percent Complete	1995												1996												1997												1998												1999											
12B	Receipt of 2/3 of SS vessel material	0		18NOV96 A	100																																																												
12C	Receipt of All SS vessel material	0		21FEB97	0																																																												
13A	Complete fab on 1/3 of WA vessels	0		24MAR97	0																																																												
13B	Complete fab on 2/3 of WA vessels	0		28APR97	0																																																												
13C	Complete fab of all WA vessels	0		01AUG97	0																																																												
14A	Complete fab on 1/3 of LA vessels	0		04AUG97	0																																																												
14B	Complete fab on 2/3 of LA vessels	0		10SEP97	0																																																												
14C	Complete fab of all LA vessels	0		02JAN98	0																																																												
227A	Bellows Expansion Joints - Fab & ship 1st lot	40	26SEP96 A	11DEC96 A	100																																																												
227B	Bellows Expansion Joints - Fab & ship 2nd lot	20	12DEC96 A	15JAN97 A	100																																																												
227C	Bellows Expansion Joints - Fab & ship last lot	30	16JAN97 A	03MAR97	33																																																												
260A	10" Benchscale Vessel - System Engineering	20	04DEC95 A	08JAN96 A	100																																																												
260B	10" Benchscale Vessel - Procure materials	30	09JAN96 A	01MAR96 A	100																																																												
260C	10" Benchscale Vessel - Fabricate vessel	10	11MAR96 A	22MAR96 A	100																																																												
260D	10" Benchscale Vessel - Conduct test program	60	01APR96 A	08JUL96 A	100																																																												
260E	10" Benchscale Vessel - Order mat/fab new sectn	15	25MAR96 A	30APR96 A	100																																																												
260F	10" Benchscale Vessel - Viton Offgassing Test	15	09OCT96 A	04NOV96 A	100																																																												
295A	Prototype BSC Fab - Roll/weld shell	4	01MAY96 A	24MAY96 A	100																																																												
295B	Prototype BSC Fab - Weld on heads	4	24MAY96 A	29MAY96 A	100																																																												
295C	Prototype BSC Fab - Cut/weld nozzle necks	5	14MAY96 A	13JUN96 A	100																																																												
295D	Prototype BSC Fab - Machine flanges/blinds	5	14JUN96 A	26JUN96 A	100																																																												
295E	Prototype BSC Fab - Stress relieve - final	5	14JUN96 A	17JUN96 A	100																																																												
295F	Prototype BSC Fab - Square off nozzles	2	18JUN96 A	21JUN96 A	100																																																												
295G	Prototype BSC Fab - Weld on flanges	8	24JUN96 A	08JUL96 A	100																																																												
295H	Prototype BSC Fab - Install welded attachments	3	09JUL96 A	10JUL96 A	100																																																												
295I	Prototype BSC Fab - Install internal floor suppt	1	11JUL96 A	11JUL96 A	100																																																												
295J	Prototype BSC Fab - Install annulus tubing & pmp	3	15JUL96 A	24JUL96 A	100																																																												
295K	Prototype BSC Fab - Clean chamber to spec	6	05AUG96 A	12AUG96 A	100																																																												
296A	Start prototype testing program	2	13AUG96 A	14AUG96 A	100																																																												
296B	Prototype Test - Rough leak check	4	15AUG96 A	30AUG96 A	100																																																												
296C	Prototype Test - Bakeout	10	03SEP96 A	16SEP96 A	100																																																												
296D	Prototype Test - Perform dimensional check	1	17SEP96 A	17SEP96 A	100																																																												
296E	Prototype Test - Final leak check	2	18SEP96 A	19SEP96 A	100																																																												
296F	Prototype Test - Ultimate pressure test	4	20SEP96 A	25SEP96 A	100																																																												
296G	Prototype Test - Install cryopump shroud	7	26SEP96 A	04OCT96 A	100																																																												
296H	Prototype Test - Vibration/boiloff test	2	07OCT96 A	08OCT96 A	100																																																												



- △ Early start point
- ▽ Early finish point
- ▬ Early bar
- ▬ Progress bar
- ▬ Critical bar
- ▬ Summary bar
- ▲ Progress point
- ▲ Critical point
- ▲ Summary point
- ◆ Start milestone point
- ◆ Finish milestone point

Process Systems International, Inc.

LIGO Vacuum System Project

Project Schedule

7Aof18A

Data date 01FEB97

Run date 04MAR97

Filter All Activities

Layout System

© Primavera Systems, Inc.

Date 05MAR97

Revision Status Rpt No 15

Checked PFH

Approved REB

Act ID	Description	Orig Dur	Early Start	Early Finish	Percent Complete	1995												1996												1997												1998												1999											
296I	Prototype BSC - Prep final data review pkg	15	09OCT96 A	29OCT96 A	100																																																												
9C	Place PO for SS vessel material (main release)	0		24MAY96 A	100																																																												
LBSC01F	LBSC1 - Outside fabrication	142	10FEB97 *	02SEP97	0																																																												
LBSC01T	LBSC1 - Final fab/clean/test/prep for ship	42	03SEP97	30OCT97	0																																																												
LBSC02F	LBSC2 - Outside fabrication	186	10FEB97 *	03NOV97	0																																																												
LBSC02T	LBSC2 - Final fab/clean/test/prep for ship	42	04NOV97	07JAN98	0																																																												
LBSC03F	LBSC3 - Outside fabrication	163	10FEB97 *	01OCT97	0																																																												
LBSC03T	LBSC3 - Final fab/clean/test/prep for ship	42	02OCT97	02DEC97	0																																																												
LBSC04F	LBSC4 - Outside fabrication	225	10FEB97	02JAN98	0																																																												
LBSC04T	LBSC4 - Final fab/clean/test/prep for ship	42	05JAN98	03MAR98	0																																																												
LBSC05F	LBSC5 - Outside fabrication	204	10FEB97	01DEC97	0																																																												
LBSC05T	LBSC5 - Final fab/clean/test/prep for ship	41	02DEC97	30JAN98	0																																																												
LCP1F	LCP1 - Fabricate long 80K cryopump	31	14JUL97 *	25AUG97	0																																																												
LCP1T	LCP1 - Final clean/test/prep to ship long pump	15	26AUG97	16SEP97	0																																																												
LCP2F	LCP2 - Fabricate long 80K cryopump	31	07AUG97	19SEP97	0																																																												
LCP2T	LCP2 - Final clean/test/prep to ship long pump	15	22SEP97	10OCT97	0																																																												
LCP3F	LCP3 - Fabricate short 80K cryopump	31	19AUG97	01OCT97	0																																																												
LCP3T	LCP3 - Final clean/test/prep to ship short pump	15	02OCT97	22OCT97	0																																																												
LCP4F	LCP4 - Fabricate short 80K cryopump	31	11SEP97	23OCT97	0																																																												
LCP4T	LCP4 - Final clean/test/prep to ship short pump	15	24OCT97	13NOV97	0																																																												
LHAM01F	LHAM1 - Fabricate weldment	42	02JUN97 *	30JUL97	0																																																												
LHAM01T	LHAM1 - Final fab/clean/test/prep for ship	37	31JUL97	22SEP97	0																																																												
LHAM02F	LHAM2 - Fabricate weldment	43	04JUN97	04AUG97	0																																																												
LHAM02T	LHAM2 - Final fab/clean/test/prep for ship	37	05AUG97	25SEP97	0																																																												
LHAM03F	LHAM3 - Fabricate weldment	49	12JUN97	20AUG97	0																																																												
LHAM03T	LHAM3 - Final fab/clean/test/prep for ship	37	21AUG97	13OCT97	0																																																												
LHAM04F	LHAM4 - Fabricate weldment	66	12JUN97	15SEP97	0																																																												
LHAM04T	LHAM4 - Final fab/clean/test/prep for ship	37	16SEP97	05NOV97	0																																																												
LHAM05F	LHAM5 - Fabricate weldment	63	12JUN97	10SEP97	0																																																												
LHAM05T	LHAM5 - Final fab/clean/test/prep for ship	37	11SEP97	31OCT97	0																																																												
LHAM06F	LHAM6 - Fabricate weldment	52	12JUN97	25AUG97	0																																																												
LHAM06T	LHAM6 - Final fab/clean/test/prep for ship	37	26AUG97	16OCT97	0																																																												
WBSC01F	WBSC1 - Outside fabrication	75	15JAN97 A	01MAY97	17																																																												
WBSC01T	WBSC1 - Final fab/clean/test/prep for ship	42	02MAY97	01JUL97	0																																																												
WBSC02F	WBSC2 - Outside fabrication	95	16JAN97 A	02JUN97	13																																																												
WBSC02T	WBSC2 - Final fab/clean/test/prep for ship	42	03JUN97	31JUL97	0																																																												



- ▲ Early start point
- ▼ Early finish point
- ▬ Early bar
- ▬ Progress bar
- ▬ Critical bar
- ▬ Summary bar
- ▲ Progress point
- ▲ Critical point
- ▼ Summary point
- ◆ Start milestone point
- ◆ Finish milestone point

Process Systems International, Inc.

LIGO Vacuum System Project

Project Schedule

8Aof18A

Data date 01FEB97

Run date 04MAR97

Filter All Activities

Layout System

© Primavera Systems, Inc

Date 05MAR97

Revision Status Rpt No 15

Checked PFH

Approved REB

Act ID	Description	Orig Dur	Early Start	Early Finish	Percent Complete	1995												1996												1997												1998												1999											
WBSC03F	WBSC3 - Outside fabrication	86	15JAN97 A	16MAY97	15																																																												
WBSC03T	WBSC3 - Final fab/clean/test/prep for ship	42	19MAY97	17JUL97	0																																																												
WBSC04F	WBSC4 - Outside fabrication	109	23SEP96 A	27FEB97	84																																																												
WBSC04T	WBSC4 - Final fab/clean/test/prep for ship	39	28FEB97	24APR97	0																																																												
WBSC05F	WBSC5 - Outside fabrication	114	16JAN97 A	27JUN97	11																																																												
WBSC05T	WBSC5 - Final fab/clean/test/prep for ship	42	30JUN97	27AUG97	0																																																												
WBSC06F	WBSC6 - Outside fabrication	83	16SEP96 A	14JAN97 A	100																																																												
WBSC06T	WBSC6 - Final fab/clean/test/prep for ship	74	30DEC96 A	15APR97	32																																																												
WBSC07F	WBSC7 - Outside fabrication	122	23SEP96 A	18MAR97	75																																																												
WBSC07T	WBSC7 - Final fab/clean/test/prep for ship	47	19MAR97	23MAY97	0																																																												
WBSC08F	WBSC8 - Outside fabrication	132	23SEP96 A	01APR97	69																																																												
WBSC08T	WBSC8 - Final fab/clean/test/prep for ship	41	02APR97	30MAY97	0																																																												
WBSC09F	WBSC9 - Outside fabrication	138	16JAN97 A	01AUG97	9																																																												
WBSC09T	WBSC9 - Final fab/clean/test/prep for ship	42	04AUG97	01OCT97	0																																																												
WBSC10F	WBSC10 - Outside fabrication	94	16SEP96 A	31JAN97 A	100																																																												
WBSC10T	WBSC10 - Final fab/clean/test/prep for ship	56	30JAN97 A	21APR97	4																																																												
WCP1F	WCP1 - Fabricate long 80k cryopump	47	19MAR97 *	23MAY97	0																																																												
WCP1T	WCP1 - Final clean/test/prep for ship long pump	15	27MAY97	16JUN97	0																																																												
WCP2F	WCP2 - Fabricate long 80K cryopump	36	15APR97 *	04JUN97	0																																																												
WCP2T	WCP2 - Final clean/test/prep to ship long pump	16	05JUN97	26JUN97	0																																																												
WCP3F	WCP3F - Fabricate short 80K cryopump	118	09OCT96 A	28MAR97	67																																																												
WCP3T	WCP3 - Final clean/test/prep to ship short pump	15	31MAR97	21APR97	0																																																												
WCP4F	WCP4 - Fabricate short 80K cryopump	130	25SEP96 A	01APR97	69																																																												
WCP4T	WCP4 - Final clean/test/prep to ship short pump	15	02APR97	23APR97	0																																																												
WCP5F	WCP5 - Fabricate short 80K cryopump	72	07JAN97 A	18APR97	26																																																												
WCP5T	WCP5 - Final clean/test/prep to ship short pump	15	21APR97	09MAY97	0																																																												
WCP6F	WCP6 - Fabricate short 80K cryopump	53	10FEB97 *	25APR97	0																																																												
WCP6T	WCP6 - Final clean/test/prep to ship short pump	15	28APR97	16MAY97	0																																																												
WCP7F	WCP7 - Fabricate short 80K cryopump	91	03DEC96 A	11APR97	46																																																												
WCP7T	WCP7 - Final clean/test/prep to ship short pump	15	15APR97	05MAY97	0																																																												
WCP8F	WCP8 - Fabricate short 80K cryopump	44	10MAR97 *	09MAY97	0																																																												
WCP8T	WCP8 - Final clean/test/prep to ship short pump	15	12MAY97	02JUN97	0																																																												
WHAM01F	WHAM1 - Fabricate weldment	69	22AUG96 A	27DEC96 A	100																																																												
WHAM01T	WHAM01 - Final fab/clean/test/prep for ship	67	30DEC96 A	03APR97	36																																																												
WHAM02F	WHAM2 - Fabricate weldment	142	22AUG96 A	17MAR97	79																																																												
WHAM02T	WHAM2 - Final fab/clean/test/prep for ship	37	18MAR97	08MAY97	0																																																												



- ▲ Early start point
- ▼ Early finish point
- ▬ Early bar
- ▬ Progress bar
- ▬ Critical bar
- ▬ Summary bar
- ▲ Progress point
- ▼ Critical point
- ◆ Summary point
- ◆ Start milestone point
- ◆ Finish milestone point

Process Systems International, Inc.

LIGO Vacuum System Project

Project Schedule

9Aof18A

Data date 01FEB97

Run date 04MAR97

Filter All Activities

Layout System

© Primavera Systems, Inc

Date

05MAR97

Revision

Status Rpt No 15

Checked

PFH

Approved

REB

Act ID	Description	Orig Dur	Early Start	Early Finish	Percent Complete	1995												1996												1997												1998												1999											
WHAM03F	WHAM3 - Fabricate weldment	97	21NOV96 A	15APR97	49																																																												
WHAM03T	WHAM3 - Final fab/clean/test/prep for ship	37	15APR97	06JUN97	0																																																												
WHAM04F	WHAM4 - Fabricate weldment	76	16JAN97 A	05MAY97	16																																																												
WHAM04T	WHAM4 - Final fab/clean/test/prep for ship	37	06MAY97	26JUN97	0																																																												
WHAM05F	WHAM5 - Fabricate weldment	74	13JAN97 A	28APR97	20																																																												
WHAM05T	WHAM5 - Final fab/clean/test/prep for ship	37	29APR97	19JUN97	0																																																												
WHAM06F	WHAM6 - Fabricate weldment	92	09DEC96 A	21APR97	41																																																												
WHAM06T	WHAM6 - Final fab/clean/test/prep for ship	37	22APR97	12JUN97	0																																																												
WHAM07F	WHAM7 - Fabricate weldment	101	28OCT96 A	24MAR97	65																																																												
WHAM07T	WHAM7 - Final fab/clean/test/prep for ship	37	25MAR97	15MAY97	0																																																												
WHAM08F	WHAM8 - Fabricate weldment	101	04NOV96 A	31MAR97	60																																																												
WHAM08T	WHAM8 - Final fab/clean/test/prep for ship	37	01APR97	22MAY97	0																																																												
WHAM09F	WHAM9 - Fabricate weldment	105	05NOV96 A	07APR97	57																																																												
WHAM09T	WHAM9 - Final fab/clean/test/prep for ship	37	08APR97	30MAY97	0																																																												
WHAM10F	WHAM10 - Fabricate weldment	90	28OCT96 A	07MAR97	73																																																												
WHAM10T	WHAM10 - Final fab/clean/test/prep for ship	37	10MAR97	30APR97	0																																																												
WHAM11F	WHAM11 - Fabricate weldment	92	10OCT96 A	21FEB97	85																																																												
WHAM11T	WHAM11 - Final fab/clean/test/prep for ship	33	24FEB97	09APR97	0																																																												
WHAM12F	WHAM12 - Fabricate weldment	122	22AUG96 A	14FEB97	92																																																												
WHAM12T	WHAM12 - Final fab/clean/test/prep for ship	36	18FEB97	08APR97	0																																																												
WHAM13F	WHAM13 - Fabricate weldment	78	21JAN97 A	12MAY97	12																																																												
WHAM13T	WHAM13 - Final fab/clean/test/prep for ship	37	13MAY97	03JUL97	0																																																												
Pumping System																																																																	
301	Perform vacuum/backfill calculations	10	23OCT95 A	03NOV95 A	100																																																												
302	Develop line list and line sizing	30	06DEC95 A	03JAN96 A	100																																																												
303	Develop piping specifications	13	27NOV95 A	22JAN96 A	100																																																												
305	Prepare special material specifications	20	08JAN96 A	26APR96 A	100																																																												
306	Main Roughing Pump - Issue specification	10	16OCT95 A	27OCT95 A	100																																																												
307	Main Roughing Pumps - Finalize bid & purchase (4)	15	06NOV95 A	12DEC95 A	100																																																												
308	Main Roughing Pumps - Receive/review v/dwgs	30	13DEC95 A	12JUN96 A	100																																																												
309	Main Roughing Pumps - Fab/deliver to WA BTC (2)	75	13JUN96 A	16AUG96 A	100																																																												
310	Main Roughing Pumps - Fab LA BTC (2); del to PSI	271	13JUN96 A	26DEC96 A	100																																																												
311	Main Turbo Pumps - Issue specification	10	16OCT95 A	27OCT95 A	100																																																												
312	Main Turbo Pumps - Finalize bid & purchase (10)	15	06NOV95 A	12DEC95 A	100																																																												
313	Main Turbo Pumps - Recieve/review v/dwgs	30	13DEC95 A	13FEB96 A	100																																																												
314	Main Turbo Pumps - Fab/deliver to WA BTC (4)	95	14FEB96 A	16AUG96 A	100																																																												



- ▲ Early start point
- ▼ Early finish point
- ▬ Early bar
- ▬ Progress bar
- ▬ Critical bar
- ▬ Summary bar
- ▲ Progress point
- ▲ Critical point
- ▲ Summary point
- ◆ Start milestone point
- ◆ Finish milestone point

Process Systems International, Inc.

LIGO Vacuum System Project

Project Schedule

10Aof18A

Data date 01FEB97

Run date 04MAR97

Filter All Activities

Layout System

© Primavera Systems, Inc.

Date 05MAR97

Revision Status Rpt No 15

Checked PFH

Approved REB

Act ID	Description	Orig Dur	Early Start	Early Finish	Percent Complete	Year																
						1995	1996	1997	1998	1999	1995	1996	1997	1998	1999	1995	1996	1997	1998	1999		
315	Main Turbo Pumps - Fab LA BTC (4), del to PSI	330	14FEB96 A	26DEC96 A	100																	
316	Main Turbo Pumps - Fab/deliver to Westboro (2)	40	14FEB96 A	10JUL96 A	100																	
318	Aux Turbo Pumps - Issue specifications	5	16OCT95 A	27OCT95 A	100																	
319	Aux Turbo Pumps - Finalize bid & purchase (10)	15	06NOV95 A	12DEC95 A	100																	
320	Aux Turbo Pumps - Receive/review v/dwgs	30	13DEC95 A	13FEB96 A	100																	
321	Aux Turbo Pumps - Fab/deliver to WA BTC (2)	110	14FEB96 A	16AUG96 A	100																	
322	Aux Turbo Pumps - Fab/del to LA BTC (2)(PSI)	330	14FEB96 A	06MAR97	93																	
323	Aux Turbo Pumps - Fab/deliver to Westboro (2)	40	14FEB96 A	24JUN96 A	100																	
325	Aux Turbo Pumps - Fab/del to WA site (3)(PSI)	340	14FEB96 A	31JAN97 A	100																	
326	Aux Turbo Pumps - Fab/del to LA site (1)(PSI)	465	14FEB96 A	31JAN97 A	100																	
327	All Ion Pumps - Issue specification	20	06NOV95 A	17NOV95 A	100																	
328	Main Ion Pumps - Bid and purchase (18)	7	20NOV95 A	22FEB96 A	100																	
329	Main Ion Pumps - Recieve/review v/dwgs	40	23FEB96 A	30APR96 A	100																	
330	Main Ion Pumps - Fab/deliver to Westboro (1)	43	01MAY96 A	03SEP96 A	100																	
331	Main Ion Pumps - Fab/deliver to WA site (12)	100	03FEB97 *	25JUN97	0																	
332	Main Ion Pumps - Fab/deliver to LA site (5)	100	26JUN97	14NOV97	0																	
333	Annuli Ion Pumps - Bid & purchase (43lg & 32sm)	4	20NOV95 A	22FEB96 A	100																	
334	Annuli Ion Pumps - Receive and review v/dwgs	40	23FEB96 A	30APR96 A	100																	
335	Annuli Ion Pumps - Fab/deliver to Westboro (2)	8	01MAY96 A	08MAY96 A	100																	
336	Annuli Ion Pumps - Fab/del WA site (48)(PSI)	318	01MAY96 A	10DEC96 A	100																	
337	Annuli Ion Pumps - Fab/del LA site (25)(PSI)	444	01MAY96 A	10DEC96 A	100																	
338	Gather turbomolecular pump vibration data (CAA)	3	30SEP96 A	02OCT96 A	100																	
339	Gather Main Ion Pmp controls vibration data (CAA)	2	08OCT96 A	09OCT96 A	100																	
340	Design main turbo pump cart vib dampeners	10	14FEB96 A	23FEB96 A	100																	
341	Design Main Ion Pump supports	20	26FEB96 A	01MAR96 A	100																	
342	Perform cryopump process calculations	10	02OCT95 A	13OCT95 A	100																	
343	LN2 System - Perform detail design	25	22JAN96 A	02FEB96 A	100																	
344	LN2 System Components - Issue specifications	10	05FEB96 A	29FEB96 A	100																	
345	LN2 System Components - Bid and purchase	60	01MAR96 A	16AUG96 A	100																	
346	LN2 System Components - Rec/rvw v/dwgs	40	05AUG96 A	05NOV96 A	100																	
347	LN2 System Components - Fab/deliver to WA site	80	03MAR97 *	24JUN97	0																	
348	LN2 System Components - Fab/deliver to LA site	80	25JUN97	16OCT97	0																	
350	LN2 Dewars - Prepare specification	5	01MAR96 A	13MAR96 A	100																	
351	LN2 Dewars - Bid and purchase (12)	40	14MAR96 A	17MAY96 A	100																	
352	LN2 Dewars - Receive & review vendor drawings	40	20MAY96 A	26AUG96 A	100																	
353	LN2 Dewars - Fab/deliver to WA site (8)	44	01APR97 *	03JUN97	0																	

- △ Early start point
- ▽ Early finish point
- ▬ Early bar
- ▬ Progress bar
- ▬ Critical bar
- ▬ Summary bar
- ▲ Progress point
- Critical point
- ◆ Summary point
- ◆ Start milestone point
- ◆ Finish milestone point

Process Systems International, Inc.

LIGO Vacuum System Project

Project Schedule

11Aof18A

Data date 01FEB97

Run date 04MAR97

Filter All Activities

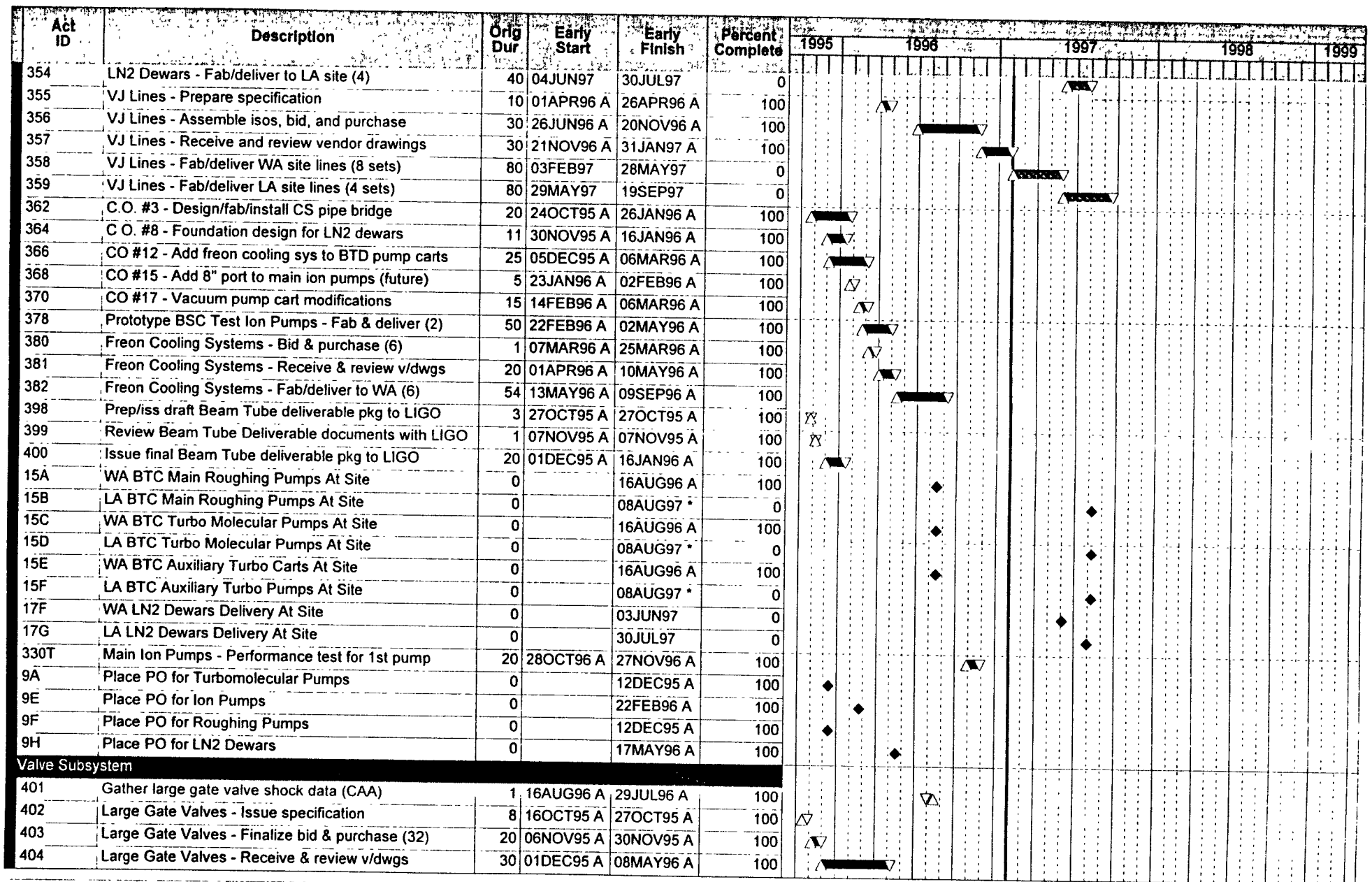
Layout System
© Primavera Systems, Inc.

Date 05MAR97

Revision
Status Rpt No 15

Checked
PFH

Approved
REB



- ▲ Early start point
- ▼ Early finish point
- ▬ Progress bar
- ▬ Critical bar
- ▬ Summary bar
- ▲ Progress point
- ▼ Critical point
- ▲ Summary point
- ◆ Start milestone point
- ◆ Finish milestone point

Process Systems International, Inc.

LIGO Vacuum System Project

Project Schedule

12Aof18A

Data date 01FEB97

Run date 04MAR97

Filter All Activities

Layout System

© Primavera Systems, Inc.

Date 05MAR97

Revision Status Rpt No 15

Checked PFH

Approved REB

Act ID	Description	Orig Dur	Early Start	Early Finish	Percent Complete	Schedule																
						1995	1996	1997	1998	1999	1995		1996		1997		1998		1999			
405	Large Gate Valves - Fab/deliver to WA BTC (8)	161	21MAY96 A	26FEB97	89																	
406	Large Gate Valves - Fab/deliver to LA BTC (6)	45	03JUL97	05SEP97	0																	
407	Large Gate Valves - Fab/deliver to WA site (12)	88	27FEB97	02JUL97	0																	
408	Large Gate Valves - Fab/deliver to LA site (6)	113	08SEP97	18FEB98	0																	
409	6/10/14" Gate Valves - Issue specification	8	25OCT95 A	03NOV95 A	100	△																
410	6/10/14" Gate Valves - Final bid & purchase (37)	20	06NOV95 A	07MAR96 A	100		▬															
411	6/10/14" Gate Valves - Receive & review v/dwgs	30	08MAR96 A	30MAY96 A	100			▬														
412	6/10/14" Gate Valves - Fab/deliver to Wbro (5)	25	31MAY96 A	30AUG96 A	100				▬													
413	6/10/14" Gate Valves - Fab/deliver WA site (27)	100	03FEB97 *	25JUN97	0																	
414	6/10/14" Gate Valves - Fab/deliver LA site (18)	100	26JUN97	14NOV97	0																	
415	Control Valves - Issue specifications	8	01MAR96 A	12MAR96 A	100			△														
416	Control Valves - Bid & purchase	40	13MAR96 A	29JUL96 A	100				▬													
417	Control Valves - Receive & review vendor dwgs	30	30JUL96 A	15NOV96 A	100					▬												
418	Control Valves - Fab/deliver to WA site	20	18NOV96 A	25NOV96 A	100						△											
419	Control Valves - Fab/deliver to LA site	20	18NOV96 A	25NOV96 A	100							△										
421	Relief Valves - Issue specification	15	30AUG96 A	18OCT96 A	100																	
422	Relief Valves - Bid & purchase	20	21OCT96 A	23JAN97 A	100																	
423	Relief Valves - Receive & review vendor dwgs	50	24JAN97 A	04APR97	12																	
424	Relief Valves - Fab/deliver to WA site	40	07APR97	03JUN97	0																	
425	Relief Valves - Fab/deliver to LA site	40	07APR97	03JUN97	0																	
427	Small Valves - Issue specifications	30	12FEB96 A	08MAR96 A	100																	
428	Small Valves - Bid and purchase	50	11MAR96 A	30JUL96 A	100																	
429	Small Valves - Receive & review vendor dwgs	40	31JUL96 A	30AUG96 A	100																	
430	Small Valves - Fab/deliver to WA site	30	16SEP96 A	06JAN97 A	100																	
431	Small Valves - Fab/deliver to LA site	30	16SEP96 A	06JAN97 A	100																	
433	Design supports for gate valves	20	26FEB96 A	25APR96 A	100																	
434	Large Gate Valves - Fab prototype large valve	80	12MAR96 A	15JUL96 A	100																	
435	Large Gate Valves - Test/prep to ship prototype	16	16JUL96 A	13SEP96 A	100																	
450	C.O. #1 - Change lg gate valve actuation	20	24OCT95 A	21DEC95 A	100																	
452	C.O. #2 - Change LA midpoint valves from 48 to 44	20	24OCT95 A	21DEC95 A	100																	
454	C.O. #4 - Add fail safe gates to roughing pumps	20	24OCT95 A	26JAN96 A	100																	
456	C.O. #7 - 304L weld stubs for lg gate valves	1	30NOV95 A	21DEC95 A	100																	
458	C.O. No. 9 - Change all lg gates to 48" electric	10	12DEC95 A	21DEC95 A	100																	
15G	WA BTC Large Gate Valves At Site	0		26FEB97	0																	
15H	LA BTC Large Gate Valves At Site	0		05SEP97	0																	
9B	Place PO for Beam Tube Large Gate Valves	0		30NOV95 A	100																	



- △ Early start point
- ▽ Early finish point
- ▬ Early bar
- ▬ Progress bar
- ▬ Critical bar
- ▬ Summary bar
- ▬ Progress point
- ▲ Critical point
- ▼ Summary point
- ◆ Start milestone point
- ◆ Finish milestone point

Process Systems International, Inc.

LIGO Vacuum System Project

Project Schedule 13Aof18A

Data date 01FEB97

Run date 04MAR97

Filter All Activities

Layout System
© Primavera Systems, Inc.

Date 05MAR97

Revision Status Rpt No 15

Checked PFH

Approved REB

Act ID	Description	Orig Dur	Early Start	Early Finish	Percent Complete	1995												1996												1997												1998												1999											
9D	Release for Remaining Large Gate Valves (Main)	0		10JUN96 A	100																																																												
Instrumentation and Controls																																																																	
501	Vacuum Gauges/Tees - Issue specification	5	22JAN96 A	01FEB96 A	100																																																												
502	Vacuum Gauges/Tees - Bid & purchase (39)	40	02FEB96 A	25SEP96 A	100																																																												
503	Vacuum Gauges/Tees - Receive/ review vendor dwgs	30	26SEP96 A	03DEC96 A	100																																																												
504	Vacuum Gauges - Fab/deliver to WA site (28)	19	02JUN97 *	26JUN97	0																																																												
505	Vacuum Gauges - Fab/deliver to LA site (15)	19	02JUN97 *	26JUN97	0																																																												
506	Misc Instrumentation - Issue specifications	3	24APR96 A	30APR96 A	100																																																												
507	Misc Instrumentation - Bid & purchase	50	01AUG96 A	01OCT96 A	100																																																												
508	Misc Instrumentation - Receive & review v/dwgs	30	02OCT96 A	11OCT96 A	100																																																												
509	Misc Instrumentation - Fab/deliver to WA site	70	14OCT96 A	30DEC96 A	100																																																												
510	Misc Instrumentation - Fab/deliver to LA site	70	14OCT96 A	30DEC96 A	100																																																												
511	Develop logic lists	5	29APR96 A	03MAY96 A	100																																																												
512	Establish control interface definitions	5	12FEB96 A	29FEB96 A	100																																																												
513	I/E Cabinets - Determine size reqmts	10	29JAN96 A	14FEB96 A	100																																																												
515	Ion Pump Controller Cabinets - Size and specify	20	26FEB96 A	24APR96 A	100																																																												
519	Cabinets/Racks - Bid and purchase	40	04NOV96 A	04DEC96 A	100																																																												
520	Cabinets/Racks - Fab/deliver to WA site	100	05DEC96 A	09MAY97	32																																																												
521	Cabinets/Racks - Fab/deliver to LA site	80	12MAY97	03SEP97	0																																																												
522	Residual Gas Analyzer - Prepare specification	10	01DEC95 A	07DEC95 A	100																																																												
523	Residual Gas Analyzer - Bid & purchase (2)	30	11DEC95 A	23FEB96 A	100																																																												
524	Residual Gas Analyzer - Receive & review v/dwgs	10	26FEB96 A	26FEB96 A	100																																																												
525	RGA's - Fab/deliver to Westboro/Prototype (2)	20	27FEB96 A	28FEB96 A	100																																																												
599	LIGO Test Eqt & Cleanroom Training	80	18MAR96 A	09AUG96 A	100																																																												
Vent and Purge Subsystem																																																																	
601	Air Supply Skids - Issue specification	12	02JAN96 A	10JAN96 A	100																																																												
602	Air Supply Skids - Bid and purchase (8)	30	12JAN96 A	22MAR96 A	100																																																												
603	Air Supply Skids - Receive & review vendor dwgs	50	25MAR96 A	30MAY96 A	100																																																												
604	Air Supply Skids - Fab/deliver to Westboro (2)	97	31MAY96 A	14JAN97 A	100																																																												
605	Air Supply Skids - Fab/deliver to WA site (5)	100	01APR97 *	21AUG97	0																																																												
606	Air Supply Skids - Fab/deliver to LA site (1)	40	22AUG97	17OCT97	0																																																												
608	Portable Cleanrooms - Issue specification	18	02JAN96 A	10JAN96 A	100																																																												
609	Portable Cleanrooms - Perform make/buy analysis	20	12JAN96 A	29JUL96 A	100																																																												
610	Gowning Rooms - Bid and purchase (8)	30	25OCT96 A	10MAR97	17																																																												
612	Gowning Rooms - Fab/deliver to WA site (5)	50	11MAR97	20MAY97	0																																																												
613	Gowning Rooms - Fab/deliver to LA site (3)	50	21MAY97	31JUL97	0																																																												



- ▲ Early start point
- ▼ Early finish point
- ▬ Progress bar
- ▬ Critical bar
- ▬ Summary bar
- ▲ Progress point
- ▼ Critical point
- ◆ Summary point
- ◆ Start milestone point
- ◆ Finish milestone point

Process Systems International, Inc.

LIGO Vacuum System Project

Project Schedule 14Aof18A

Date data 01FEB97

Run date 04MAR97

Filter All Activities

Layout System

© Primavera Systems, Inc.

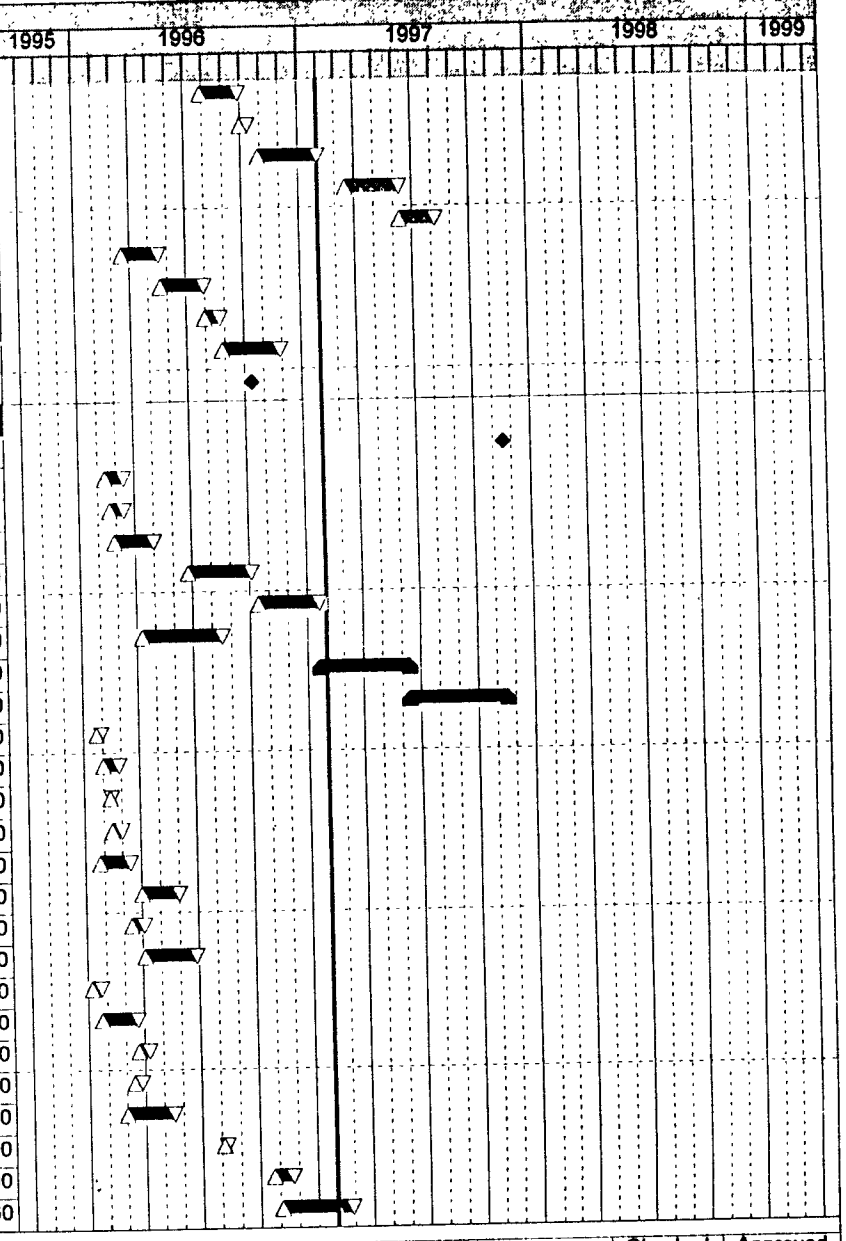
Date 05MAR97

Revision Status Rpt No 15

Checked PFH

Approved REB

Act ID	Description	Orig Dur	Early Start	Early Finish	Percent Complete
620	Portable Cleanrooms - Perform detail design	40	29JUL96 A	27SEP96 A	100
622	Portable Cleanrooms - Procure materials	10	30SEP96 A	11OCT96 A	100
624	Portable Cleanrooms - Fab 1st lot (2 HAM)	40	28OCT96 A	31JAN97 A	100
625	Portable Cleanrooms - Fab 2nd lot (6 BSC)	60	17MAR97 *	10JUN97	0
626	Portable Cleanrooms - Fab 3rd lot (4 BSC)	40	11JUN97	06AUG97	0
630	Large Component Wash Station - Conceptual design	60	18MAR96 A	17MAY96 A	100
632	Large Component Wash Station - Detail design	20	20MAY96 A	29JUL96 A	100
634	Large Component Wash Station - Procure materials	20	30JUL96 A	23AUG96 A	100
636	Large Component Wash Station - Fabricate / Test	30	26AUG96 A	27NOV96 A	100
9G	Place PO for Clean Rooms	0		11OCT96 A	100
Bakeout Subsystem					
18	Delivery of Bakeout System to WA Site	0		17NOV97	0
701	Prepare a bakeout system schematic	15	12FEB96 A	13MAR96 A	100
702	Perform bakeout system calculations	30	19FEB96 A	13MAR96 A	100
703	Bakeout Blankets - Issue specification	20	26FEB96 A	30APR96 A	100
704	Bakeout Blankets - Bid and purchase system	30	24JUN96 A	03OCT96 A	100
705	Bakeout Blankets - Receive & review vendor dwgs	40	14OCT96 A	20JAN97 A	100
706	Bakeout Blankets - Fab/deliver Prototype BSC	20	09APR96 A	16AUG96 A	100
707	Bakeout Blankets - Fab/deliver to Westboro (21)	100	21JAN97 A	12JUN97	9
708	Bakeout Blankets - Fab/deliver to WA site (28)	110	13JUN97	17NOV97	0
709	Bakeout System Controls - Issue specs	10	22JAN96 A	29JAN96 A	100
710	Bakeout System Controls - Bid and purchase	20	01FEB96 A	26FEB96 A	100
711	Bakeout System Controls - Receive/review v/dwgs	10	12FEB96 A	13FEB96 A	100
712	Bakeout System Controls - Fab/deliver to PSI	20	14FEB96 A	29FEB96 A	100
717	Design bakeout cart(s) - Preliminary design	5	24JAN96 A	13MAR96 A	100
718	Program PLC's for bakeout system	40	01APR96 A	31MAY96 A	100
719	Bakeout Carts - Bid & award assembly of carts	15	14MAR96 A	03APR96 A	100
720	Bakeout Carts - Assemble 1st cart	31	04APR96 A	26JUN96 A	100
721	Prototype Bakeout Blankets - Issue specification	21	08JAN96 A	22JAN96 A	100
722	Prototype Bakeout Blankets - Bid & purchase (6)	20	23JAN96 A	21MAR96 A	100
723	Prototype Bakeout Blankets - Receive/rvw v/dwgs	15	22MAR96 A	08APR96 A	100
726	Final design of bakeout carts	15	14MAR96 A	26MAR96 A	100
727	Program PC's for Bakeout System	70	01MAR96 A	17MAY96 A	100
730	Bakeout Carts - Test 1st bakeout cart	5	05AUG96 A	09AUG96 A	100
731	Bakeout Carts - Procure materials for 3 carts	30	23OCT96 A	22NOV96 A	100
732	Bakeout Carts - Assemble 3 carts	40	04NOV96 A	25FEB97	60



PSI

- ▲ Early start point
- ▼ Early finish point
- ▬ Early bar
- ▬ Progress bar
- ▬ Critical bar
- ▬ Summary bar
- ▲ Progress point
- ▼ Critical point
- ▲ Summary point
- ◆ Start milestone point
- ◆ Finish milestone point

Process Systems International, Inc.

LIGO Vacuum System Project

Project Schedule 15Aof18A

Data date 01FEB97

Run date 04MAR97

Filter All Activities

Layout System

© Primavera Systems, Inc.

Date	Revision	Checked	Approved
05MAR97	Status Rpt No 15	PFH	REB

Act ID	Description	Orig Dur	Early Start	Early Finish	Percent Complete	1995												1996												1997												1998												1999											
733	Bakeout Carts - Test 3 carts	15	26FEB97	18MAR97	0																																																												
734	Bakeout Carts - Procure materials for last cart	30	19MAR97	30APR97	0																																																												
735	Bakeout Carts - Assemble last cart	40	01MAY97	26JUN97	0																																																												
736	Bakeout Carts - Test last cart	5	27JUN97	03JUL97	0																																																												
750	PSI Bakeout Oven - Design & order material	30	25NOV96 A	31JAN97 A	100																																																												
751	PSI Bakeout Oven - Procure materials	30	03FEB97	17MAR97	0																																																												
752	PSI Bakeout Oven - Erect & test oven	12	18MAR97	02APR97	0																																																												
91	Place PO for Bakeout System/Blankets	0		03OCT96 A	100																																																												
Systems Installation																																																																	
20	Begin Installation At Washington Site	0	05AUG97		0																																																												
21	Begin Installation At Louisiana Site	0	03MAR98		0																																																												
22	Mechanical Completion At Washington Site	0		24NOV97	0																																																												
23	Mechanical Completion At Louisiana Site	0		03AUG98	0																																																												
798	Bid & award Washington installation subcontract	80	04DEC96 A	27MAR97	53																																																												
799	WA Site - Installation subcontractor mobilize	15	02JUL97	23JUL97	0																																																												
801	Conduct installation readiness review - WA site	1	01JUL97 *	01JUL97	0																																																												
802	Verify interfaces & as-built site conditions -WA	21	02JUL97	31JUL97	0																																																												
803	Joint occupancy of WA site	1	01AUG97 *	01AUG97	0																																																												
804	WA Site - Receive/store/set eqt in all stations	50	04AUG97	13OCT97	0																																																												
810	WACS installation	80 *	05AUG97	25NOV97	0																																																												
811	WACS - Offload, clean, & position all components	30	05AUG97	16SEP97	0																																																												
812	WACS - Install vertex components	20	17SEP97	14OCT97	0																																																												
814	WACS - Install right beam manifold components	10	15OCT97	28OCT97	0																																																												
816	WACS - Install diagonal components	10	29OCT97	11NOV97	0																																																												
817	WACS - Install left beam manifold components	10	12NOV97	25NOV97	0																																																												
818	WACS - Install mechanical room eqt/piping/wiring	20	04AUG97	29AUG97	0																																																												
819	WACS - LN2 supply systems installation	20	04AUG97	29AUG97	0																																																												
820	WA Arm 1 (left) - Install mid/end station eqt	40 *	04AUG97	29SEP97	0																																																												
821	Left WAMS - Offload, clean, position components	3	04AUG97	06AUG97	0																																																												
822	Left WAMS - Install components	17	07AUG97	29AUG97	0																																																												
824	Left WAMS - Install mechanical room eqt/wiring	20	04AUG97	29AUG97	0																																																												
825	Left WAMS - LN2 supply systems installation	20	04AUG97	29AUG97	0																																																												
826	Left WAES - Offload, clean, position components	3	04AUG97	06AUG97	0																																																												
827	Left WAES - Install components	20	02SEP97	29SEP97	0																																																												
828	Left WAES - Install mechanical room eqt/wiring	20	02SEP97	29SEP97	0																																																												
829	Left WAES - LN2 supply system installation	20	02SEP97	29SEP97	0																																																												



- ▲ Early start point
- ▼ Early finish point
- Early bar
- ▬ Progress bar
- ▬ Critical bar
- ▬ Summary bar
- ▲ Progress point
- ▼ Critical point
- ◆ Summary point
- ◆ Start milestone point
- ◆ Finish milestone point

Process Systems International, Inc.

LIGO Vacuum System Project

Project Schedule 16Aof18A

Data date 01FEB97

Run date 04MAR97

Filter All Activities

Layout System
© Primavera Systems, Inc.

Date

05MAR97

Revision
Status Rpt No 15

Checked
PFH

Approved
REB

Act ID	Description	Orig Dur	Early Start	Early Finish	Percent Complete	1995												1996												1997												1998												1999											
830	WA Arm 2 (right) - Install mid/end station eqt	62 *	28AUG97	24NOV97	0																																																												
831	Right WAMS - Offload, clean, position components	3	28AUG97	02SEP97	0																																																												
832	Right WAMS - Install components	20	30SEP97	27OCT97	0																																																												
834	Right WAMS - Install mechanical room eqt/wiring	20	30SEP97	27OCT97	0																																																												
835	Right WAMS - LN2 supply systems installation	20	30SEP97	27OCT97	0																																																												
836	Right WAES - Offload, clean, position components	3	02OCT97	06OCT97	0																																																												
837	Right WAES - Install components	20	28OCT97	24NOV97	0																																																												
838	Right WAES - Install mechanical room eqt/wiring	20	28OCT97	24NOV97	0																																																												
839	Right WAES - LN2 supply system installation	20	28OCT97	24NOV97	0																																																												
848	Bid & award Louisiana installation subcontract	40	26NOV97	27JAN98	0																																																												
849	LA Site - Installation subcontractor mobilize	15	03FEB98	23FEB98	0																																																												
851	Conduct installation readiness review - LA site	1	02FEB98 *	02FEB98	0																																																												
852	Verify interfaces & as-built site conditions -LA	19	03FEB98	27FEB98	0																																																												
853	Joint occupancy of LA site	1	02MAR98	02MAR98	0																																																												
854	LA Site - Receive/store/set eqt in all stations	105	03MAR98	29JUL98	0																																																												
860	LACS installation	85	03MAR98	30JUN98	0																																																												
870	LA Arm 3 (left) - Install end station eqt	23	01JUL98	03AUG98	0																																																												
872	LA Arm 4 (right) - Install end station eqt	20	04AUG98	31AUG98	0																																																												
17A	WA Corner Station Major Vessel Delivery	0		31JUL97	0																																																												
17B	LA Corner Station Major Vessel Delivery	0		07JAN98	0																																																												
17C	WA End Station Major Vessel Delivery	0		01OCT97	0																																																												
17D	LA End Station Major Vessel Delivery	0		03MAR98	0																																																												
17E	WA Mid Station Major Vessel Delivery	0		27AUG97	0																																																												
Commissioning and Acceptance Testing																																																																	
25	Complete WA Acceptance Test Review Package	0		10MAR98	0																																																												
26	Complete LA Acceptance Test Review	0		30NOV98	0																																																												
910	WACS - Test/commission station	121 *	02SEP97	24FEB98	0																																																												
911	WACS - Complete station commissioning	10	11FEB98	24FEB98	0																																																												
912	WACS - Test/commission vertex section	20	15OCT97	11NOV97	0																																																												
914	WACS - Test/commission right beam manifold	20	12NOV97	11DEC97	0																																																												
916	WACS - Test/commission diagonal section	20	12DEC97	13JAN98	0																																																												
917	WACS - Test/commission left beam manifold	20	14JAN98	10FEB98	0																																																												
918	WACS - Test/commission mechanical room equipment	15	02SEP97	22SEP97	0																																																												
919	WACS - Test/commission LN2 supply systems	15	02SEP97	22SEP97	0																																																												
920	WA Arm 1 (left) - Test/commission mid/end sta's	60 *	02SEP97	24NOV97	0																																																												
922	Left WAMS - Test/commission station components	30	16SEP97	27OCT97	0																																																												



- △ Early start point
- ▽ Early finish point
- ▬ Early bar
- ▬ Progress bar
- ▬ Critical bar
- ▬ Summary bar
- ▲ Progress point
- ▲ Critical point
- ▲ Summary point
- ◆ Start milestone point
- ◆ Finish milestone point

Process Systems International, Inc.

LIGO Vacuum System Project

Project Schedule 17Aof18A

Data date 01FEB97
 Run date 04MAR97
 Filter All Activities
 Layout System
 © Primavera Systems, Inc.

Date	05MAR97	Revision	Status Rpt No 15	Checked	Approved
				PFH	REB

Act ID	Description	Orig Dur	Early Start	Early Finish	Percent Complete	1995												1996												1997												1998												1999											
924	Left WAMS - Test/commission mechanical room eqt	10	02SEP97	15SEP97	0																																																												
925	Left WAMS - Test/commission LN2 supply systems	10	02SEP97	15SEP97	0																																																												
927	Left WAES - Test/commission station components	30	14OCT97	24NOV97	0																																																												
928	Left WAES - Test/commission mechanical room eqt	10	30SEP97	13OCT97	0																																																												
929	Left WAES - Test/commission LN2 supply system	10	30SEP97	13OCT97	0																																																												
930	WA Arm 2 (right) - Test/commission mid/end sta's	43	25NOV97	29JAN98	0																																																												
932	Right WAMS - Test/commission station components	30	11DEC97	26JAN98	0																																																												
934	Right WAMS - Test/commission mechanical room eqt	10	25NOV97	10DEC97	0																																																												
935	Right WAMS - Test/commission LN2 supply systems	10	28OCT97	10NOV97	0																																																												
937	Right WAES - Test/commission station components	33	11DEC97	29JAN98	0																																																												
938	Right WAES - Test/commission mechanical room eqt	10	25NOV97	10DEC97	0																																																												
939	Right WAES - Test/commission LN2 supply system	10	25NOV97	10DEC97	0																																																												
940	Complete acceptance testing - WA site	0		10FEB98	0																																																												
945	Prepare acceptance test report for WA site	20	11FEB98	10MAR98	0																																																												
946	Conduct acceptance review meeting - WA site	1	11MAR98	11MAR98	0																																																												
960	LACS - Test/commission station	64	01JUL98	30SEP98	0																																																												
970	LA Arm 3 (left) - Test/commission end station	22	01SEP98	01OCT98	0																																																												
972	LA Arm 4 (right) - Test/commission end station	22	02OCT98	02NOV98	0																																																												
980	Complete acceptance testing - LA site	0		02NOV98	0																																																												
985	Prepare acceptance test report for LA site	19	03NOV98	30NOV98	0																																																												
986	Conduct acceptance review meeting - LA site	1	01DEC98	01DEC98	0																																																												
24A	Start Acceptance Testing At Washington Site	0	02SEP97		0																																																												
24B	Start Acceptance Testing At Louisiana Site	0	01JUL98		0																																																												
24C	Complete Acceptance Test - WA Corner Station	0		24FEB98	0																																																												
24D	Complete Acceptance Test - LA Corner Station	0		30SEP98	0																																																												
24E	Complete Acceptance Test - WA Mid Stations	0		26JAN98	0																																																												
24F	Complete Acceptance Test - WA End Stations	0		29JAN98	0																																																												
24G	Complete Acceptance Test - LA End Stations	0		02NOV98	0																																																												



- △ Early start point
- ▽ Early finish point
- Early bar
- ▬ Progress bar
- ▬ Critical bar
- ▬ Summary bar
- ▲ Progress point
- Critical point
- ◆ Summary point
- ◆ Start milestone point
- ◆ Finish milestone point

Process Systems International, Inc.

LIGO Vacuum System Project

Project Schedule 18Aof18A

Data date 01FEB97
 Run date 04MAR97
 Filter All Activities
 Layout System
 © Primavera Systems, Inc

Date 05MAR97

Revision Status Rpt No 15

Checked PFH
 Approved REB



PROCESS SYSTEMS INTERNATIONAL, INC.

SECTION 10 CHANGE ORDER STATUS

SUMMARY

Number Of Change Order Requests To Date:	22
Change Order Requests Submitted To Date:	22
Change Order Requests In Process:	0
Change Order Requests Approved To Date:	12
Change Order Requests Rejected To Date:	10
Change Order Requests Pending With LIGO:	0

Please refer to the latest issue of the attached change order log.



PROCESS SYSTEMS INTERNATIONAL, INC.

SECTION 11 CONTRACT PRICE

There was one change order approved during the reporting period. The change order approved during the period was Change Order Number 22 for All Metal O-ring Testing (Option 1), in the amount of \$15,974.00. To date, twelve (12) change orders have been approved by LIGO.

<u>Original Contract Value</u>	<u>Approved Change Orders</u>	<u>Current Contract Value</u>
\$39,100,000	\$52,799	\$39,152,799

There are no change orders currently in process.

LIGO-P970003-00-D

NOISE ANALYSIS OF A SUSPENDED HIGH POWER MICHELSON INTERFEROMETER

by

Partha Saha

S.B. (Physics with Electrical Engineering)

Massachusetts Institute of Technology (1989)

S.B. (Mathematics)

Massachusetts Institute of Technology (1992)

*submitted in partial fulfillment
of the requirements for the degree of*

DOCTOR OF PHILOSOPHY

at the

MASSACHUSETTS INSTITUTE OF TECHNOLOGY

February, 1997

©Massachusetts Institute of Technology 1997

Signature of Author _____ Department of Physics
February, 1997

Certified by _____ Rainer Weiss
Thesis Supervisor

Accepted by _____ George Kostel
Chairman, Department Committee

NOISE ANALYSIS OF A SUSPENDED HIGH POWER MICHELSON INTERFEROMETER

by

Partha Saha

Submitted to the Department of Physics

on February, 1997 in partial

fulfillment of the requirements for the Degree of

DOCTOR OF PHILOSOPHY

Abstract

The Laser Interferometer Gravitational Wave Observatory (LIGO Project) will search for gravitational waves by observing shifts in the interference of a Michelson interferometer. To start detecting gravitational waves with any measure of confidence, current estimates require the interferometer to be sensitive to differences of at least 10^{-9} radians in the phase of light. Ground-based LIGO will offer this sensitivity in a band around 100 Hz. The sensitivity of LIGO is limited at frequencies below 200 Hz by random (mainly seismic and thermal) forces acting on its optical elements. Around and above 200 Hz — where this “displacement noise” is no longer significant — the sensitivity is determined by how well the interference shift can be determined at the detector. The quantum nature of coherent laser light in the interferometer imply a power fluctuation at the detector that scales as \sqrt{I} , where I is the light intensity at the Michelson beam-splitter. With the signal power scaling as I , a fundamental sensitivity limit is thus set for detection. To obtain the desired sensitivity given this limit, LIGO will have close to 100 watts of laser light incident on the beam-splitter. No laboratory in the world, to the best of our knowledge, has had experience with interferometry at these high power levels prior to this thesis. This thesis experimentally tests an important assumption used in the noise estimates — that the noise above 200 Hz will be quantum limited.

To investigate the noise in interference detection at high power levels, a team at MIT (to which the author belongs)¹ has constructed a suspended Michelson interferometer. The noise in the detection of the differential phase of this interferometer was investigated at two stages. At the first stage, several hundreds of milliwatts from a frequency stabilized Ar^+ gas laser was incident directly on the beam-splitter. At the second stage, the input light was constructively built (recycled) to above 30 watts at the beam-splitter using an optical cavity — this cavity was formed by placing a partially transmitting mirror in the input light as the front (power recycling) mirror and the Michelson interferometer as the back mirror. Our experience showed that above 1 kHz, the noise indeed was quantum limited consistent with the incident power. This led to

¹Prof. R. Weiss and Dr. D. Shoemaker gave birth to the Phase Noise Interferometer (PNI) project after they wrote the proposal in 1992, the actual work started in full swing around mid 1994. The team at MIT consisted of Brian Lantz and Partha Saha as graduate students, Drs. Peter Fritschel (in charge), Gabriela Gonzalez (from April 1995), and Mike Zucker (actively from September 1994 to early 1995, in an advisory role thereafter) as research scientists. Mr. Tom Evans, Mr. Ed Kruezel, and Mr. Ralph Burgess offered technical help, while Prof. R. Weiss and Dr. D. Shoemaker offered advice and guidance. The project drew support and technical help from the entire LIGO team in many ways — especially Dr. Sigg and Ms. Mavalvala, who gave the project its first working wavefront sensor.

the measurement of a phase noise sensitivity of about 3×10^{-10} radian/ $\sqrt{\text{Hz}}$ in the recycled interferometer, better than any known measurement to date. Below 1 kHz, we examined the “technical” noise sources that caused the noise to be above the quantum limit. We concluded that back scattering of light, input beam jitter, and residual frequency noise need to be controlled to get down to the fundamental limit required by LIGO at these frequencies.

This thesis discusses the construction of the interferometer, the noise models and experiments used to analyze the measured phase noise at the two stages, and the implications of the experimental results to LIGO.

Thesis Supervisor: Rainer Weiss

Title: Professor of Physics

Contents

Abstract	i
1 Gravitational Wave Detection Through Interferometry	2
1.1 Gravitational waves and their detection	2
1.2 Sources of gravitational waves	4
1.3 History of gravitational wave detection and LIGO	5
1.4 The LIGO noise budget	7
2 A Suspended High Power Michelson Interferometer	10
2.1 Interferometry techniques used in the PNI	10
2.1.1 A simple Michelson interferometer	10
2.1.2 A phase modulated Michelson interferometer with asymmetry	11
2.1.3 A recycled Michelson interferometer	14
2.2 Sources of phase noise in the PNI	16
2.2.1 Noise in the input light	16
2.2.2 Noise sources in the interferometer	17
2.3 Construction of the PNI	18
2.3.1 PNI in the first stage	18
2.3.2 Laser stabilization subsystems	18
2.3.3 Suspensions	20
2.3.4 Seismic isolation	23
2.3.5 Optics	22
2.3.6 Michelson length control	24
2.3.7 PNI in the second stage	25
2.3.8 The recycled Michelson length control	26
2.3.9 The common mode servo	27
2.3.10 The active differential alignment system	29
2.4 Performance of the PNI	31
3 Noise Sources in the Light	33
3.1 Fundamental or quantum Noise in light	33

3.2	Frequency noise	37
3.3	Amplitude Noise	39
3.4	Beam jitter noise	41
4	Noise Sources in the Interferometer	48
4.1	Displacement noise	48
4.1.1	Seismic noise	48
4.1.2	Thermal noise	49
4.1.3	Radiation pressure	50
4.2	Interferometer misalignment	51
4.3	Parasitic Interferometry	52
4.4	Instrumentation noise	57
4.4.1	Amplitude modulation by Pockels cell	57
4.4.2	Noise in the differential length sensing and control loop	57
5	Final Remarks	59
5.1	The PNI spectra	59
5.2	Implications for LIGO	62
	Appendices	63
A	The Michelson Interferometer as an Optical Element	64
B	The Fabry Perot Cavity: Optical Parameters and Resonance	66
C	Feedback Control Systems	70
	Bibliography	71

Chapter 1

Gravitational Wave Detection Through Interferometry

This chapter will offer a brief and simple introduction to the physics of gravitational waves and their detection. The aim will be to motivate the focus of this thesis, that the phase difference measured by a Michelson interferometer can achieve a sensitivity of 10^{-10} radian/ $\sqrt{\text{Hz}}$ in a bandwidth around several hundreds of Hertz.

1.1 Gravitational waves and their detection

The theory of special relativity relates events across inertial frames of reference through Lorentz transformations. It gives us the metric $g_{\mu\nu}$ which, acting on a space-time interval, gives us an invariant across all inertial frames of reference.

General theory of relativity introduces non-inertial effects to $g_{\mu\nu}$. The motion of massive objects causes changes in $g_{\mu\nu}$ to propagate away at the speed of light. In the coordinate frame of an observation point far away from a massive object in motion, small perturbations $h_{\mu\nu}$ to the special relativistic metric $\eta_{\mu\nu}$ can be sensed:

$$g_{\mu\nu} = \eta_{\mu\nu} + h_{\mu\nu}. \quad (1.1)$$

It is this $h_{\mu\nu}$ that gets referred to as gravitational waves.

Einstein's equation, assuming small variations in $g_{\mu\nu}$ and excluding the source, reduces to a wave equation for $h_{\mu\nu}$ — a transverse variation of $\eta_{\mu\nu}$ with respect to the direction of propagation can then be assumed. The freedom to choose a coordinate frame allows us to select one where $h_{\mu\nu}$ is traceless (the transverse traceless or TT gauge). If the propagation direction be z the non-zero elements of $h_{\mu\nu}$ correspond to those that multiply the x and y coordinates, and get symmetrically located within a matrix representation (metric property). Thus the most general TT h_{ij} can be written as

$$h_{\perp} \begin{bmatrix} 1 & 0 \\ 0 & -1 \end{bmatrix} + h_{\times} \begin{bmatrix} 0 & 1 \\ 1 & 0 \end{bmatrix}, \quad (1.2)$$

where the first piece is referred to as the '+' (h_{\perp}) polarization, and the second one the ' \times ' (h_{\times}) polarization.

The effect of a gravitational wave can be demonstrated if a measurement of time interval with light is attempted in some coordinate frame of reference. Arbitrarily, we choose an h_+ wave, the h_x wave has exactly the same effect in a coordinate frame rotated 45° with the one we will use for our calculations. We send a light pulse from the origin along each of the transverse orthogonal axes of the coordinate frame given to us by the h_+ wave. These light pulses are retro-reflected by mirrors back to the origin after traveling the same coordinate length l in the two orthogonal directions, and we compare the two round trip times in the presence of an h_+ wave. For the light ray sent along the x axis,

$$\begin{aligned} -(cdt)^2 + (1+h_+)(dx)^2 &= 0 \\ \Rightarrow \int_{\text{round trip}} dt &= \int_{\text{round trip}} \sqrt{1+h_+} \frac{dx}{c} \\ \Rightarrow \int_{\text{round trip}} dt &= \int_{\text{round trip}} \frac{dx}{c} + \int_{\text{round trip}} \frac{1}{2} h_+ dt + O(|h_+|^2). \end{aligned} \quad (13)$$

For the other pulse launched at the same time in the other orthogonal direction y , its round-trip time differs by $\int_{\text{round trip}} h_+ dt$ from the one along x . Thus the phase difference between two phase-fronts starting at the same time via a beam splitter at the origin and then combined after retro-reflection at the two mirrors is

$$\delta\phi(t) = \omega_0 \int_{t-\frac{l}{c}}^t h_+ dt' \quad (14)$$

where ω_0 is the frequency of light. Let us now assume that $h_+ = h_0 \cos(\omega_g t)$ in our coordinate frame, where ω_g is the frequency of the gravitational wave reaching us. Carrying out the integration in Equation 14, we finally obtain,

$$\delta\phi(t) \approx h_0 \frac{2l}{c} \frac{\omega_0 \sin(\omega_g l/c)}{\omega_g(l/c)} \cdot \cos[\omega_g(t-l/c)]. \quad (15)$$

If $\omega_g l/c$ is much less than 1, we get

$$|\delta\phi(t)| \approx h_0 \omega_0 (2l/c) \quad (16)$$

Thus we are naturally led to the concept of interferometry for detection of gravitational waves, the phase difference measured by a Michelson interferometer can be attributed to passing gravitational waves in absence of other sources of such phase change. We also notice from Equation 16 that the longer the arms of this Michelson interferometer, the larger is the measured phase difference owing to gravitational waves.

In the example we just described, the two masses were aligned along the principal axes of h_+ , to understand what happens when the two masses lie along two arbitrarily chosen orthogonal axes, we refer to Figure 11. We show masses distributed in a ring and their relative separations, as a gravitational wave propagates normally through the ring. Any two masses at the end of lines intersecting at 90° can be used as mirrors to define a Michelson interferometer with a beam-splitter at the origin, as the arm lengths from the origin to these two masses show any relative change, so will the phase difference measured at the beam-splitter. We thus observe that even if the wave may not be properly aligned with the two arms of the interferometer, we will measure some phase difference owing to the passing gravitational wave —

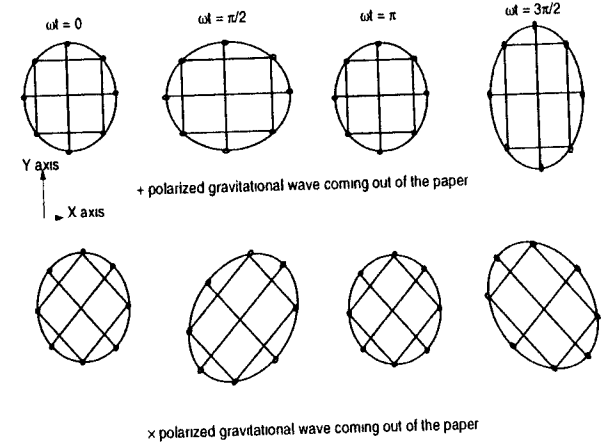


Figure 11 A ring of free masses in some coordinate frame as the gravitational wave propagates normally through it, the relative separation of the masses change as indicated for the two different polarizations

this phase difference, however, may not be as large as that in the aligned case. Let $\delta\phi_{+,x}(t)$ refer to the maximum possible phase difference that can be measured by properly aligning the interferometer for the corresponding polarization. The phase difference, measured by an interferometer with its arms defining the x and y axes of an arbitrary coordinate frame in which the gravitational wave is incident at a zenith angle of θ_{gw} , and an azimuth angle of ϕ_{gw} , is then given by

$$\delta\phi(t) = \frac{1}{2} (1 + \cos^2 \theta_{gw}) \cos(2\phi_{gw}) \phi_+(t) + \cos \theta_{gw} \sin(2\phi_{gw}) \phi_x(t) \quad (17)$$

1.2 Sources of gravitational waves

We can try to estimate the magnitude of h_0 by drawing analogs with electro-magnetic radiation. Mass and momentum conservation rule out radiation from the monopole and dipole parts of a system of moving masses, the quadrupole is then the first term that radiates, and this happens to be the \dot{Q} term. To have the energy propagating out, we must have this term associated with an $1/r$ spatial dependence. We form a dimensionless h_0 with the fundamental constants G and c and the radiating Q/\dot{r} (the radiation, being in the classical limit, cannot involve \hbar) as

$$h_0 \sim \frac{G}{c^4} \cdot \frac{Q}{r}. \quad (18)$$

Defining E^Q to be the kinetic energy in quadrupolar form, and putting the relevant numbers in Equation 18 above, we find:

$$\begin{aligned} h_0 &\sim 10^{-20} \frac{E^Q}{M_\odot c^2} \cdot \frac{10 \text{ Mpc}}{r} \text{ where} \\ 1 M_\odot &= 1.99 \times 10^{30} \text{ kg} = 1 \text{ Solar Mass, and} \\ 10 \text{ Mpc} &= 3.09 \times 10^{20} \text{ kilometers} = \text{distance to Virgo Cluster} \end{aligned} \quad (19)$$

The numbers quickly establish that gravitational wave sources cannot be terrestrial, they must be generated by objects that are of interest in astrophysics.

Some estimates of gravitational wave strength are offered in [1] for different kinds of astrophysical sources. Bursts of gravitational waves immediately precede a collision of compact binaries or a supernova collapse, these bursts produce radiation at frequencies that are very low initially, but increase to about 10 kHz as the impending catastrophe draws near. Thorne [2, 1] calculates the strength for gravitational waves from a supernova collapse to be

$$h_{rms} \approx 3 \times 10^{-20} \left(\frac{\Delta E}{M_{\odot} c^2} \right)^{1/2} \left(\frac{1 \text{ kHz}}{f} \right)^{1/2} \left(\frac{10 \text{ Mpc}}{r} \right), \quad (1.10)$$

where ΔE represents the energy lost to gravitational waves. In fact, energy lost to gravitational waves (extremely slowly over years of observation) have been shown to be consistent with the decay of the orbital period of the binary system PSR 1913+16 (this is the famous binary pulsar system that obtained a nobel prize for Hulse and Taylor in 1993).

Gravitational waves of well defined periodicity are supposed to be generated by rotating stars. Thorne [1] calculates the gravitational wave strength generated by a rotating neutron star of ellipticity ϵ to be ($\epsilon \leq 10^{-6}$)

$$h_{rms} \approx 8 \times 10^{-20} \cdot \epsilon \cdot \left(\frac{f}{1 \text{ kHz}} \right)^2 \left(\frac{10 \text{ kpc}}{r} \right), \quad (1.11)$$

where f is the frequency of rotation.

Another source of gravitational radiation may well be a stochastic background which, because of its lack of any fixed direction of propagation, allows for easier data analysis — however, its strength cannot be predicted very well.

1.3 History of gravitational wave detection and LIGO

Attempts to detect gravitational waves started with the work of Joe Weber in the sixties, when he searched for coincident excitations of normal modes in two massive Aluminum cylinders separated by a large distance. In 1970, Weber claimed that two such cylinders indeed were registering vibrations owing to passing gravitational waves. This attracted a lot of experimenters. Weiss [3] conceived of an interferometric detection of the waves, and performed a detailed study of an instrument that could achieve this goal. Most of Weber's claims were later disputed, but the work on gravitational wave detection that had been initiated still continues unabated. The original idea of Weber has been developed by many groups, and the resonant "bar" technology — operated at low temperatures with better sensors — now claims detections at the level of $h \approx 10^{-18}$ in a bandwidth of few Hz around a resonance of approximately 1 kHz [4].

The idea of Weiss has undergone many modifications, and groups around the world have seriously pursued the idea of gravitational wave detection through interferometry. In the first section, we showed how a passing gravitational wave could be demonstrated by a change in the differential phase of a Michelson interferometer.

$$\delta\phi \approx h_0 \omega_0 (2l/c) \quad (1.12)$$

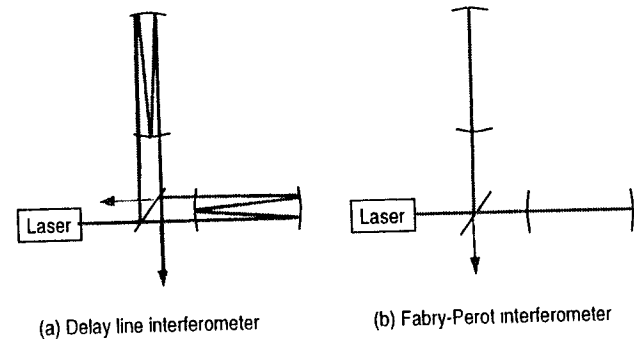


Figure 1.2: Two methods for amplifying the differential phase

We notice that we can amplify the phase difference caused by a gravitational wave at low frequencies, if we can make the light traverse a long distance l . The original instrument constructed by Weiss [5], and a German group at Garching [6], involved a delay line in which the light bounced back and forth many times between two mirrors to build up the phase-shift before making its way out for interference. A French group [7], a Scottish group [8] and a group at Caltech [9] pursued the idea of using Fabry-Perot cavities as the arms of the Michelson interferometer — in this scheme, a partially transmitting mirror allowed the incident light to enter an optical cavity while letting a part of the light inside the cavity to escape out. Figure 1.2 illustrates the difference between a delay line and a Fabry-Perot interferometer.

The work with proto-types [6, 5, 9] quickly established that the gravitational waves reaching us could not have amplitudes larger than $h_{rms} \approx 10^{-16}$ – 10^{-17} , and that the dominant ones most probably have frequencies below 1 kHz. Given this uncertain description of the waves, interferometric methods offer more advantages than the resonant "bar" technology as they allow a wider bandwidth search around low frequencies. A number of groups therefore have pooled their resources to develop the interferometer technology for direct detection and monitoring of gravitational waves. The Fabry Perot scheme of Figure 1.2 has become the preferred overall design, as optical cavities allow high and spatially pure light intensities which then lead to better signal to noise ratios. The LIGO project of United States, a joint collaboration between MIT and Caltech, aims at building two interferometers with 4 km long arms — one in Hanford, Washington and another in Livingston Parish, Louisiana. The VIRGO project, a joint collaboration between a group in Italy and another in France, plans to build one interferometer with arm lengths of 3 km. GEO-600, a project pursued by a British and a German group, wishes to build one interferometer with arms 600 meters long, while TAMA-300, a Japanese effort, wants to construct its interferometer with 300 meter arms.

The work that is documented in this thesis was undertaken under the auspices of the LIGO project. This project [10] builds on the experience of Caltech and MIT with laser interferometers, and has two primary tasks: to build two 4 km long interferometers as stated before, and to understand and reduce the noise in these interferometers so that their sensitivity can be enhanced to where continual monitoring

of gravitational waves is possible. While construction of the two interferometers are vigorously under way, scientists at the two institutions are also trying to understand the noise in laser interferometers by constructing proto-types. The 40 meter proto-type at Caltech recently achieved a (potential) sensitivity to gravitational waves of $h \approx 3 \times 10^{-19}$ around 450 Hz [11]. To understand what is needed to make this sensitivity even better and motivate the work documented in this thesis, we need to present the LIGO noise estimates. We do this in the next section.

1.4 The LIGO noise budget

The approximate form of Equation 1.5, given in Equation 1.6, holds true for a Fabry-Perot interferometer at very low (gravitational wave) frequencies: if the transit time $2l/c$ is replaced by the equivalent “storage time”, τ_s , of an optical cavity. The storage time of an optical cavity represents approximately the time spent by light inside the cavity before it escapes back out again; for a cavity with low loss (of light power in a round trip), we can approximate $\tau_s \approx (2l/c) \cdot (1/T)$ where T is the transmission of the input mirror and l is the length of the cavity. The measured phase difference spectrum gets related to a gravitational wave amplitude in a Fabry-Perot cavity as [2]

$$\delta\phi(\omega) = 4\omega_0\tau_s \cdot h(\omega) \cdot \frac{1}{\sqrt{1 + 4\omega^2\tau_s^2}}, \quad (1.13)$$

where ω_0 corresponds to the frequency of the laser used. If we use the parameters for the optical cavities used in LIGO [12] we obtain a τ_s equal to 0.87 mill-seconds, assuming a wavelength of 0.5 microns, we can thus write

$$\delta\phi(f) = 2 \times 10^{12} \cdot h(f) \cdot \frac{1}{\sqrt{1 + (f/91.57)^2}}. \quad (1.14)$$

LIGO has recently decided to switch to the Nd YAG laser with a wavelength of 1.06 microns, if we used this laser, the factor on the right hand side of Equation 1.14 (2×10^{12}) will be halved.

How small a $\delta\phi$ can LIGO hope to measure? Light used for interferometry introduces quantum noise in detection of phase by an interferometer, and this noise scales up as \sqrt{P} as P , the power inside the interferometer, is increased, the differential phase signal, on the other hand, is also amplified as it gets multiplied by the power P . The equivalent phase noise thus scales as $1/\sqrt{P}$ — in Chapter 2 we show how a power level of about 80 watts at a wavelength of 514.5×10^{-9} meter inside the interferometer can get the equivalent phase noise down to 1×10^{-10} radian/ $\sqrt{\text{Hz}}$.

However, quantum noise is not the only noise present in the detection of phase — numerous other noise sources, described extensively elsewhere [3, 10] and reviewed recently [12], can appear as $\delta\phi$ at the output of the interferometer. We present the most dominant ones in the different frequency bands in the LIGO interferometer in Figure 1.3. Below about 60 Hz, seismic noise causes the interferometer mirrors to shake, thus compromising the sensitivity of the interferometer to phase shifts from gravitational waves. The ground seismic noise can be approximated to be about $10^{-7}/f^2$ m/ $\sqrt{\text{Hz}}$ above 10 Hz; the passive vibration isolation system of LIGO limits the transfer of the ground noise to the interferometer table to about 10^{-6} around 100 Hz. There is additional vibration isolation of the mirrors from the interferometer table as the

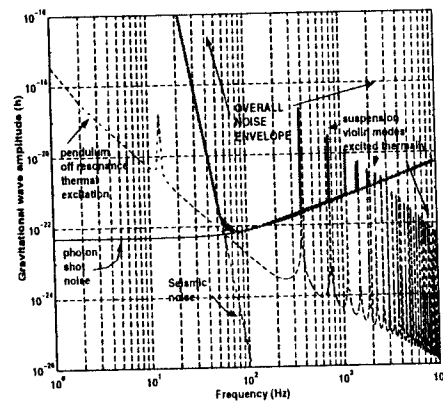


Figure 1.3. Noise in the LIGO interferometer that limits its sensitivity; the vertical axis is in terms of h , the equivalent gravitational wave amplitude.

mirrors are hung as pendulums with a resonant frequency of 0.74 Hz — the seismic noise contribution therefore falls off sharply as shown in Figure 1.3. Above 70 Hz, the off-resonance thermal excitations of the pendulum motion and the transverse violin modes of the suspension wire dominate the spectrum. The exact models used to estimate the off-resonance contributions from thermal excitation are presented in Chapter 4. The Q of the pendulum designed for LIGO is assumed to be about 3.33×10^5 , the Q for the violin modes is taken to be 1.7×10^5 with the fundamental frequency at 376 Hz. Where the seismic and thermal noise estimates intersect, we achieve a sensitivity to gravitational waves of strengths $h \approx 6 \times 10^{-23}$, if we try to ensure that the quantum noise in light does not undermine this sensitivity, we see from Equation 1.14 that the quantum noise should be no more than 1×10^{-10} radian/ $\sqrt{\text{Hz}}$ as used in Figure 1.3. We also see why the choice of an optical storage time of about 1 millisecond — as shown in Figure 1.3, was made for LIGO — any larger does not give us any more sensitivity, and a smaller storage time compromises the sensitivity that the seismic and thermal noise estimates allow.

Given the overall noise envelope shown in Figure 1.3, we may wonder what kind of gravitational waves LIGO might detect. Theoretical work predicts that the most promising source of gravitational waves are binaries in coalescence, and that these occur at the rate of three per year if one can look upto 100 Mpc [2]. These coalescences produce a gravitational wave chirp that sweeps up from tens of Hertz to about 1 kHz in a few minutes, and have strengths of about $h_0 \approx 10^{-21}$. LIGO will be able to detect these waves with a signal to noise ratio of about 5 if the sources are located within 30 Mpc, optimally oriented, and produce a signal that lies in a bandwidth of about 100 Hz.

We observed before that we need a light level of about 80 watts inside the interferometer, to get the quantum noise down to 1×10^{-10} radian/ $\sqrt{\text{Hz}}$ with a Argon gas laser at 0.5 microns. At the time LIGO was conceived, there was no experience with interferometry at these high power levels — the best phase

noise sensitivity known at that time was about 1.5×10^{-9} radian/ $\sqrt{\text{Hz}}$ [6] with a power level of 730 milliwatts. Though no new fundamental source of noise was expected at these high power levels, a sense of uncertainty existed in the project over this lack of experience. A proposal to build an interferometer to study the problems of phase detection at these high power levels was therefore presented to the LIGO project by Weiss and Shoemaker [13]. The idea was to build a Michelson interferometer with several tens of watts of light incident on the beam-splitter, and compare the measured phase noise to that predicted by quantum noise. The Fabry-Perot cavities were avoided in the arms of the Michelson interferometer to make the interferometer as insensitive to “displacement” noise as possible. While there were research efforts undertaken to understand and reduce displacement noise in the 40 meter interferometer caused by seismic and thermal excitations [11], the task at MIT was to build a simple high power Michelson interferometer with 50 cm arms and investigate the “readout” problems with light. This thesis documents the construction of this interferometer at MIT, the measured phase noise, and its analysis into contributions from the different noise sources.

Chapter 2

A Suspended High Power Michelson Interferometer

The last chapter showed why it was considered necessary to construct an interferometer and study the noise in optical phase detection at the level of 10^{-10} radian/ $\sqrt{\text{Hz}}$ in a bandwidth around 200 Hz. In this chapter, we develop the background required to understand the noise spectral density of such an interferometer. The interferometer, given its purpose, is henceforth referred to as the Phase Noise Interferometer, or PNI.

An outline of the contents of this rather long chapter is appropriate before we begin. The fundamental noise in phase detection is given by the quantum noise in light, and this determines the smallest phase difference that can be resolved in interferometers using non-squeezed light. In the first section, we address signal to noise issues given this fundamental noise. In the next section, we itemize the other noise sources in interferometry, and present estimates that influenced the design of the PNI. These noise sources are revisited in chapters 3 and 4, where we develop models to understand their coupling to optical phase, and describe experiments that carefully determine their contributions to the PNI noise spectra. The actual construction and layout of the PNI through its two stages form the subsequent section. Finally, we present the performance of the PNI through noise spectra measured in its two stages of construction, as a prelude to detailed noise analyses undertaken in chapters 3 and 4.

2.1 Interferometry techniques used in the PNI

2.1.1 A simple Michelson interferometer

To motivate the signal extraction technique used, we start with a simple Michelson interferometer whose optical layout appears in Figure 2.1. A laser beam with incident power, P_i , is split by a 50-50 beam-splitter and sent along two orthogonal paths to be retro-reflected back to the splitter. The returned beams are combined; a portion then makes its way to the laser, and the remainder to a photo-detector as shown in the figure. The side of the beam-splitter from where light is incident is often labeled the symmetric port if most of the light is returned that way, while the (dark) side the photo-detector then sees gets referred to as the anti-symmetric port. The light at the anti-symmetric port, P_{out} , is termed the output of the interferometer because it carries information (signal) about the phase difference between the two orthogonal optical paths.

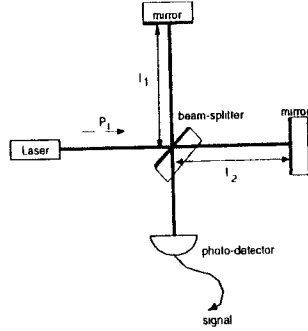


Figure 2.1 A simple Michelson interferometer

$\phi = 2k(l_1 - l_2)$, as measured by light

$$P_{out} = \frac{P_1}{2}(1 - \cos \phi). \quad (2.1)$$

Equation 2.1 is non-linear, however, if the Michelson interferometer is held at a fixed ϕ_d away from where P_{out} attains an extremum, and our signal $\Delta\phi$ causes small and therefore linear changes in P_{out} , then a measurable quantity proportional to the signal is obtained. Usually, a feedback control system is required to “lock” ϕ because of the noise in the environment, and this is usually chosen — to maximize the signal — where $\frac{dP_{out}}{d\phi}$ is maximum. $\phi_d = \frac{\pi}{2}$. The quantity P_1 is not constant, and if we assume its variation to be given by ΔP_1 , then — at our optimal operating point — we measure

$$P_{out} = \frac{P_1}{2} + \frac{\Delta P_1}{2} + \frac{P_1}{2} \Delta\phi. \quad (2.2)$$

Since the noise owing to ΔP_1 competes with the signal $\Delta\phi$, it is desirable to measure the signal where ΔP_1 is smallest — this happens at radio-frequencies where the laser intensity noise reaches its quantum (lower) limit. Thus the phase difference at the output of the interferometer is modulated at a fixed radio-frequency, and the signal is upconverted to sideband frequencies using the non-linearity of Equation 2.1. The next sub-section discusses this method.

2.1.2 A phase modulated Michelson interferometer with asymmetry

If ϕ in Equation 2.1 is modulated by $\Gamma \cos(\omega_m t)$, then we can write the equation as,

$$P_{out} = \frac{P_1}{2}(1 - \cos \phi - \cos(\Gamma \cos(\omega_m t)) + \sin \phi - \sin(\Gamma \cos(\omega_m t))). \quad (2.3)$$

With $\Gamma \ll 1$, the signal that multiplies $\Gamma \cos(\omega_m t)$ is maximized if our operating $\phi_d = 0$ or a multiple of π . The output of the interferometer then reads:

$$P_{out} = \frac{P_1}{4} (\Delta\phi)^2 + \frac{P_1}{2} \Delta\phi - \Gamma \cos(\omega_m t) + \frac{P_1}{4} (\Gamma \cos(\omega_m t))^2. \quad (2.4)$$

ΔP_1 disappears in first order — however, since it still comes multiplied by the slow components of $(\Delta\phi)^2$, or $\frac{t^2}{2}$ from the third term, modulation at radio-frequencies remains necessary for rejection of intensity noise

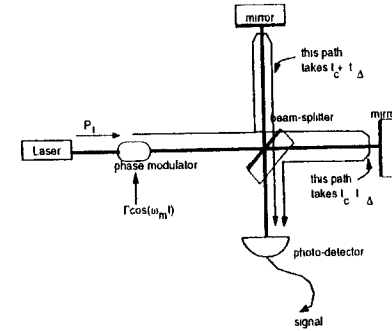


Figure 2.2. A phase modulated Michelson interferometer with asymmetry

As the anti-symmetric port is held at a dark fringe — i.e., since $l_1 \approx l_2$, the properties of light that vary (like power, frequency, etc.) exactly cancel out in first order. Most of the incident light is now reflected (at the symmetric port), and this naturally leads to “recycling of light” as will be shown in the next sub-section. We may wonder why $(\Delta\phi)^2$ is shown in Equation 2.4 — this is because the two mirrors’ surfaces may not be perfectly alike, causing the two wavefronts reaching the splitter to have an average phase difference of $\Delta\phi = 0$, but the rms $(\Delta\phi)^2$ to be non-zero. We will return to this shortly.

Though a modulation of ϕ is desirable, it requires the use of phase modulators in the two arms of the Michelson interferometer. This leads to problems at high laser powers, because phase modulators tend to corrupt the spatial quality of the beams and thus degrade the cancellation that is important for good recycling. More discussion about the problems with this “in-line modulation” appears in [2].

A different technique uses a phase modulator in the input light. We still wish to hold the anti-symmetric port at a dark fringe for recycling of light, however, if we do so, there is no signal derived at that port synchronous with the phase modulation. Therefore, we decide to put an intentional asymmetry between the two arms of the interferometer, i.e., we have $l_1 - l_2 = \delta l$ of macroscopic size. Referring to Figure 2.2, we notice that this implies that Equation 2.1 has to be rewritten — with the intentional phase difference caused by the modulation separated from that caused by noise or signal — as

$$P_{out} = \frac{P_1}{2}(1 - \cos(\phi + \Gamma \cos[\omega_m(t - t_c - t_\Delta)]) - \Gamma \cos[\omega_m(t - t_c + t_\Delta)]). \quad (2.5)$$

Here we have introduced two time intervals for light that are important: t_c refers to a time interval “common” to both paths and $t_\Delta = \frac{\delta l}{c}$ captures the asymmetry in the intervals. Notice how the asymmetry prevents the phase modulation from canceling out. A trigonometric identity simplifies Equation 2.5:

$$P_{out} = \frac{P_1}{2}(1 - \cos(\phi + 2\Gamma \sin[\omega_m t_\Delta] \sin[\omega_m(t - t_c)])) \quad (2.6)$$

If we define $\Gamma_c = 2\Gamma \sin[\omega_m t_\Delta]$, then we can write Equation 2.6 as,

$$P_{out} = \frac{P_1}{2}(1 - \cos(\phi + \Gamma_c \sin[\omega_m(t - t_c)])) \quad (2.7)$$

Expanding the above equation now gives us a form similar to Equation 2.3. Though we have a phase modulator in the path before the beam-splitter and thus common to both beams, we still get differential phase modulation through the asymmetry.

The first part of the PNI work involved the construction of an asymmetric Michelson interferometer with phase modulation at 25 MHz. The asymmetry was set at $\delta l = 20.8$ cm. With Γ chosen to be 1, the asymmetry fixed Γ_c to be 0.22. When we expand Equation 2.7 to second order in both ϕ and Γ_c , we obtain (similar to Equation 2.1)

$$P_{out} = \frac{1}{4}P_i(\Delta\phi)^2 + \frac{1}{8}P_i\Gamma_c^2 + \frac{1}{2}P_i\Gamma_c \sin(\omega_m(t-t_c))\Delta\phi - \frac{1}{8}P_i\Gamma_c^2 \cos(2\omega_m(t-t_c)) \quad (2.8)$$

The above equation captures all the elements that we need for our first signal to noise calculation. The first term, $\frac{1}{4}P_i(\Delta\phi)^2$, is a measure of the defect in contrast of the interferometer, a term which we will now define. We must understand that laser light in our experiment is not a plane wave with a fixed phase across its (infinite) planar front — it is better represented by a superposition of Hermite-Gaussian functions [11] whose variation in field amplitude and phase in a transverse cross-section is given by:

$$E(x) = \Sigma_n C_n \cdot H_n\left(\frac{\sqrt{2}r}{w}\right) \exp\left[-\frac{r^2}{w^2} - i\frac{kx^2}{2R}\right] = \Sigma_n U_n \quad (2.9)$$

where C_n is a normalization constant, and H_n is a Hermite polynomial of order n . Two parameters in the above equation, the spot size w , and the radius of curvature, R , determine how the amplitude and phase of the field change across the transverse axis. As the beam propagates in space, these parameters also change owing to diffraction [15], the wavefront, in addition, picks up an overall phase — a longitudinal part (kz), and another part (the Guoy phase) that comes from the finite transverse extent of the beam. Thus, when we write the phase difference as $\Delta\phi$, we imply $\iint \Delta\phi(x, y) dA$ and, in a similar manner, $(\Delta\phi)^2 \equiv \iint (\Delta\phi(x, y))^2 dA$. Clearly, $\Delta\phi$ averages over the transverse variation but keeps the overall phase, while $(\Delta\phi)^2$ adds the square of the transverse variation to that of the overall phase. If the two end mirrors of the Michelson interferometer have surfaces that are not exactly alike or are misaligned with respect to each other, we can force $\Delta\phi$ to zero, but not $(\Delta\phi)^2$ necessarily. Referring to Equation 2.1, we hence notice that the minimum P_{out} possible is $\frac{1}{4}P_i(\Delta\phi)^2$. One figure of merit of a Michelson interferometer is how close the contrast is to unity where

$$\text{contrast} = \frac{P_{out}^{max} - P_{out}^{min}}{P_{out}^{max} + P_{out}^{min}} \quad (2.10)$$

or, equivalently, how small the defect in contrast, (c.d.) $\equiv 1 - \text{contrast}$ is measured to be. Some amount of algebra shows that the c.d. of a simple Michelson interferometer is $(\Delta\phi)^2/2$, an expression that also shows up in the first term of Equation 2.8 multiplied by $P_i/2$.

The second term in Equation 2.8 shows that phase modulation causes additional light to leak out at the dark port. The first two terms have sizeable dc components and some low frequency variation as the alignment of the interferometer or the level of incident light changes. Apart from the direct amplitude noise that they then create, they also constitute a source of broadband quantum noise, the power spectral

density of which, in watts/ $\sqrt{\text{Hz}}$ [2], is

$$\sqrt{2h\nu\left(\frac{1}{4}P_i(\Delta\phi)^2 + \frac{1}{8}P_i\Gamma_c^2\right)}. \quad (2.11)$$

The signal $\Delta\phi$ occurs at frequencies much lower than the radio-frequency ω_m — thus the third term oscillating at ω_m shows the effect of $\Delta\phi$ through a modulation of its amplitude. If a mixer multiplied P_{out} with $\sin[\omega_m(t-t_c)]$, and a low pass filter removed from the product all frequencies above some fraction of the modulation frequency, ω_m ,

$$\frac{1}{2}P_i\Gamma_c(\Delta\phi) \quad (2.12)$$

is obtained. This quantity — in watts of power — is what is measured and gives our signal $\Delta\phi$ in radians when divided by the calibration, $\frac{1}{2}P_i\Gamma_c$, in watts per unit radian change in phase. The broadband quantum noise also enters through the process just described — at any non-zero frequency of $\Delta\phi$ there are 2 sidebands at a level given by (2.11) that add in quadrature. Thus, given the calibration just derived, the fundamental noise power spectral density in radian/ $\sqrt{\text{Hz}}$ is

$$\sqrt{\frac{2h\nu}{P_i} \cdot \left(1 + \frac{2(\Delta\phi)^2}{\Gamma_c^2}\right)^{1/2}}, \quad (2.13)$$

where h is the Planck's constant, and ν is the frequency of light. This is also our fundamental noise limited sensitivity. If the contrast were perfect (i.e., 1), we can calculate what P_i implies a quantum noise limited sensitivity of 10^{-10} radian/ $\sqrt{\text{Hz}}$, we thus find that we need $P_i = 77.4$ watts with a wavelength of 514.5 nm. This is beyond a conventional single mode laser — hence, a new technique of "Recycling", which we introduce in the next sub-section, becomes imperative.

Though all our quantities have been in laser power so far, the more convenient unit is the photocurrent I (in Amperes) in the photo-detector — as that is what gets measured. The conversion is given by $I_{out} = (\eta e)/(h\nu) \cdot P_{out}$ where e is the electronic charge, and η the quantum efficiency (of the conversion of photon to electron). For the wavelength of our choice (5.14×10^{-7} m), the conversion factor $(\eta e)/(h\nu)$ is about 0.3 Ampere/Watt for the Silicon photo-detectors used in our experiment with light incident near Brewster's angle. In units of current, the expression 2.13 can be written as:

$$\sqrt{\frac{2e}{I_i} \cdot \left(1 + \frac{4 \text{ c.d.}}{\Gamma_c^2}\right)^{1/2}}, \quad (2.14)$$

where I_i is the "bright fringe" current (or the power incident on the beam-splitter converted to a current).

2.1.3 A recycled Michelson interferometer

Figure 2.3 shows the optical layout of the PNI in its second stage, where the light lost at the symmetric port is reflected (or "recycled") back by a mirror placed in the path of the input light. This mirror forms an optical cavity with the Michelson interferometer as its other (back) mirror.

Phase modulation produces sideband frequencies on the light,

$$\mathcal{E}e^{i(\omega t + \Gamma \cos(\omega_m t) + \phi)} = \mathcal{E}e^{i(\omega t - \phi)} \left[J_0(\Gamma) + iJ_1(\Gamma)(e^{i\omega_m t} + e^{-i\omega_m t}) + \dots \right] \quad (2.15)$$

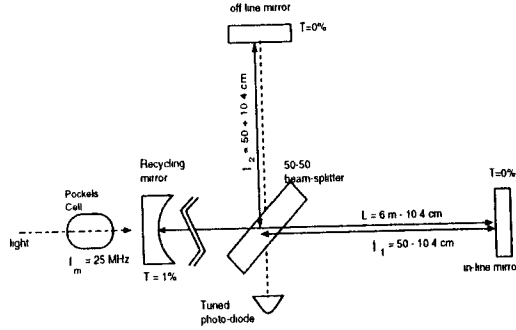


Figure 2.3 The optical configuration of PNI in its second stage

Using the field transmission and reflectivity derived for the Michelson interferometer in Appendix A, we can rewrite Equation 2.8 in terms of $J_0(\Gamma) \equiv J_0$ and $J_1(\Gamma) \equiv J_1$ (ignoring the term at twice the modulation frequency)

$$P_{out} = \frac{1}{4}P_i J_0^2(\Delta\phi)^2 + 2P_i J_1(\Gamma)^2 [\sin^2(\omega_m t_\Delta) + \frac{(\Delta\phi)^2}{4}] + 2P_i J_0 J_1 \sin(\omega_m t_\Delta) \sin[\omega_m(t - t_c)] \Delta\phi, \quad (2.16)$$

where all the parameters, P_i , J_0 and J_1 are for light at the beam-splitter. With a simple Michelson interferometer these parameters are the same as that for the input light. With recycling, these parameters get modified — as discussed in Appendix B, the recycling optical cavity provides internal field gain (an increased P_i) that then gives us the high phase sensitivity we desire. However, an asymmetric Michelson interferometer causes the “back” mirror of the recycling optical cavity to have different “transmissions” at different frequencies — hence the field gain as seen at the carrier frequency is not necessarily the same as that seen at the sidebands caused by phase modulation. The proportion of carrier to sideband fields at the beam-splitter is then different from that in the input light. There are thus two effects of recycling on the light incident at the beam-splitter (which decides the fundamental noise limited sensitivity) — an increased light level, and a modified carrier to sideband field ratio.

Before we calculate the revised parameters, we should note that our recycling method assumes that both the carrier and the sideband fields are resonant in the cavity. In Appendix B, we notice that if the frequency of the light is changed by a full spectral range (fsr) ($c/2L$ where L is the length of the cavity), the light is resonant again — thus to get the sideband field resonant we should have the modulation frequency at least at the first fsr (this fixes the length of the cavity to be $c/(2 \cdot (f_m = 25 \text{ MHz})) = 6$ meters. In the actual experiment, the resonant frequency was found to be 25.33 MHz, so the length of the cavity was actually 5.92 meters. From Appendix A, we find that the field reflection coefficient at the beam-splitter of the Michelson interferometer is $e^{-i\alpha_k} \cos \delta_k$ where α_k involves the sum of the lengths of the two Michelson arms — hence, the recycling mirror was placed about 5.5 meters from the beam-splitter (thus, $2 \times$ beam-splitter to recycling mirror distance + sum of two Michelson arm lengths = $2 \times$ length of common mode path = 12 meters).

Since the Michelson interferometer is held at a dark fringe for the carrier frequency, the loss (or transmission) of the field at this frequency through the “back mirror” can be assumed to be much smaller than the transmission of the input mirror. The loss comes from an imperfect contrast, from Appendix A, the power transmission through a Michelson interferometer was derived as $\delta_0^2 = (1/2)$ (c.d.). Given the typical c.d.s for the PNI of around 1000 ppm, the power transmission could be estimated to be 500 ppm. The transmission of the input mirror, on the other hand, was about 8200 ppm. The field gain at the carrier frequency could thus be approximated as $2/\sqrt{T_1}$ for the PNI (Appendix B), or the recycling power gain as $R_G = 4/T_1$.

For the sidebands, the transmission through the Michelson interferometer to the dark port is $\sin^2(\delta_1 \equiv \omega_m t_\Delta)$, equal to about 12 000 ppm for the PNI. Since this transmission through the “back mirror” is larger than the transmission of the input mirror that we used (8200 ppm), the recycling cavity was slightly undercoupled for the sidebands. The field gain is $(2\sqrt{T_1})/(\sin^2(\delta_1) + T_1 + L)$ where L lumps all the other losses seen by light inside the cavity distinct from the transmissions at the two end mirrors. If we divide the sideband field gain by the carrier field gain, we obtain $g_r = L_{common}/(\sin^2(\delta_1) + L_{common})$ where $L_{common} = T_1 + (1/2) \cdot (\text{c.d.}) + L$. Since we are working where the approximation $J_1 \approx \Gamma/2$ holds true, we thus notice that if we revise $\Gamma \rightarrow g_r \Gamma$, and $P_i \rightarrow R_G P_i$ for all our unrecycled formulas, we get the corresponding relationships that hold for the recycled case. For example, the fundamental noise power spectral density, Equation 2.13, for the recycled interferometer is

$$\sqrt{\frac{2h\nu}{R_G P_i}} \cdot \left(1 + \frac{2(\Delta\phi)^2}{g_r^2 \Gamma^2}\right)^{1/2}, \quad (2.17)$$

where P_i is the input power before the recycling mirror. Given that R_G is about 500, we thus see that recycling requires only 200 milli-watts of input power to get the required 80 watts at the beam-splitter for a quantum noise spectral density of 10^{-10} rad/ $\sqrt{\text{Hz}}$.

2.2 Sources of phase noise in the PNI

In the last section, we presented techniques that help in reducing quantum noise to the level of the required detection sensitivity of 10^{-10} radian/ $\sqrt{\text{Hz}}$. However, quantum noise is not the only noise that shows up in the detected phase — and the goal of the construction of PNI, as indicated in Chapter 1, was to investigate which of the other sources (if any at all) showed up as limiting “sensing” noise in the bandwidth of interest around several hundreds of Hertz. At the time the construction of PNI was proposed [13], several of these noise sources influenced the construction and design of the PNI. In this section, we will briefly introduce these sources — with an eye to explaining the construction of the PNI that occupies the next section — and then return to them again for a detailed look in chapters 3 and 4.

2.2.1 Noise in the input light

Frequency noise: The measurement of $\phi = 2k(l_1 - l_2)$ is affected by both a change of Δk as much as $\Delta(l_1 - l_2)$ — thus a fixed asymmetry (i.e. a fixed $(l_1 - l_2)$), causes sensitivity to Δk . Given our $\delta l = 20.8$

cm, the PNI thus had a sensitivity of $(4\pi\delta l)/c = 8.71 \times 10^{-9}$ radian/Hz. To achieve a phase noise of 10^{-10} radian/ $\sqrt{\text{Hz}}$, we thus required a frequency stability of about 10^{-2} Hz/ $\sqrt{\text{Hz}}$ in our bandwidth of interest.

Scattered light can interfere at the photo-detector after traveling through a path different than the main beam. If this path differs in length by a large extent from the main one, and the element reflecting the scattered light back to the photo-detector is more or less stationary, the spurious interference is another way of adding frequency noise coherently to the detected phase. If the element shakes, it causes additional spurious interference to appear at the dark port — we discuss this kind of “parasitic interferometry” in detail in chapter 4.

Amplitude noise: There is no first order dependence of the phase noise in Equation (2.16) on amplitude noise — except that imperfections in the construction of the interferometer, like an offset from the minimum possible null at the dark port, can give rise to such a dependence. If the phase modulation process gives rise to some amplitude modulation (AM), then we again get a contribution from amplitude noise in the phase noise spectrum through the AM in the light leaking out at the dark port. Otherwise, the amplitude noise contribution is through its bilinear coupling with the most dominant features in the noise in ϕ . An amplitude stabilization system was kept ready, but the main strategy planned was to get rid of the imperfections that cause the amplitude noise to influence the measured phase noise.

Beam pointing noise: Light varies in direction at the input of the interferometer, and this gets converted to a varying phase-difference through a differential misalignment of the Michelson mirrors. Once again, the emphasis was to align the Michelson mirrors as best as possible and keep them aligned through active feedback, rather than trying to fix the input beam direction.

2.2.2 Noise sources in the interferometer

Seismic noise causes the optical elements in the interferometer to shake — leading to a differential **displacement** of the Michelson mirrors that gets converted to an optical phase noise, and then also to **misalignment** of the elements with respect to each other which disturbs the operating point of the interferometer. Great pains were therefore taken to isolate the optical elements from seismic noise — the elements were suspended as pendulums from structures that in turn rested on passive and active isolation stages. These isolation systems will be discussed in the section on construction of the PNI. Thermal excitation of the mirror surface and the suspending wires can also be a source of phase noise — this influenced the dimensions of the mirrors used, while modeling of the thermal noise in the suspension wires was carried out to see the effect on the phase noise sensitivity. We will return to these issues later.

Instrumentation noise in the electro-optic and electronic components (e.g., the dark noise in the photo-detector, or the amplitude modulation accompanying the phase modulation in the modulators) was carefully measured, and care was taken to ensure that it did not affect our noise sensitivity. At the time the PNI was constructed, we did not anticipate the extent of **parasitic** or unintended **interferometry** caused by scattered light sent back to the dark port photo-detector by a reflector in motion — so no special precautions, apart from the inclusion of a Faraday isolator along with the input optics, were taken in the

design.

2.3 Construction of the PNI

The PNI was constructed in two stages — first, a phase-modulated asymmetric Michelson interferometer was assembled to undertake a preliminary study of noise in phase detection consistent with low operating power levels. Steps to exclude the noise sources discovered were then implemented, and the interferometer recycled in power. At this second (recycled) stage, sources that could cause deviation from the fundamental noise limited sensitivity were again investigated.

Given the construction process described, we organize this section accordingly in two parts, the first part presents the construction of the unrecycled Michelson interferometer, while the second part points out the changes carried out before recycling of light.

2.3.1 PNI in the first stage

Figure 2.4 shows an overview of the PNI in its first stage of construction. Laser light was stabilized in frequency and amplitude in one room; it was then steered into a clean vacuum envelope in the other room. The vacuum envelope housed a near tank, a bigger central tank, and a 5 meter long tube that connected the two tanks. The main purpose of the vacuum (about a few μtorr s) was to keep the mirror and beam-splitter surfaces free from hydro-carbon contaminants (that can introduce significant optical loss). There were other benefits — e.g., the elimination of air drafts that can excite the suspended optical elements, and phase noise via refractive index fluctuations of air. The Michelson interferometer with 50 cm nominal arm lengths was located on a table inside the bigger tank. The near tank had steering mirrors on the table inside it in the first stage; the second stage added a recycling mirror as shown outlined in Figure 2.4.

We now discuss each subsystem separately.

2.3.2 Laser stabilization subsystems

An Ar⁺ laser from Spectra Physics (model 2080) was used for the experiment. The frequency and amplitude of the laser were stabilized before the light was used for interferometry — Figure 2.5 shows the optical layout for the stabilization subsystems.

Although not obvious in Figure 2.5, the laser plasma tube had to be put on a stack made of alternating layers of lead and rubber elements to isolate the vibration of (pumped) cooling water from the optical table. The resonator mirrors were put on the optical table, and not in physical contact with the plasma tube so that the laser resonator cavity length and alignment did not fluctuate with the cooling water flow.

The Ar⁺ laser (wavelength = 5.14×10^{-7} m) had significant frequency noise, about 10 kHz/ $\sqrt{\text{Hz}}$ at about 100 Hz and falling roughly as $1/f^2$. Thus stabilization of its frequency was essential for reaching a level of 10^{-10} radian/ $\sqrt{\text{Hz}}$. The required noise suppression of 10^6 at 100 Hz was carried out in two stages: first by stabilizing the frequency with respect to a passive quartz cavity (the reference cavity in Figure 2.5), and then by using the recycling cavity as an additional reference in the second part of the

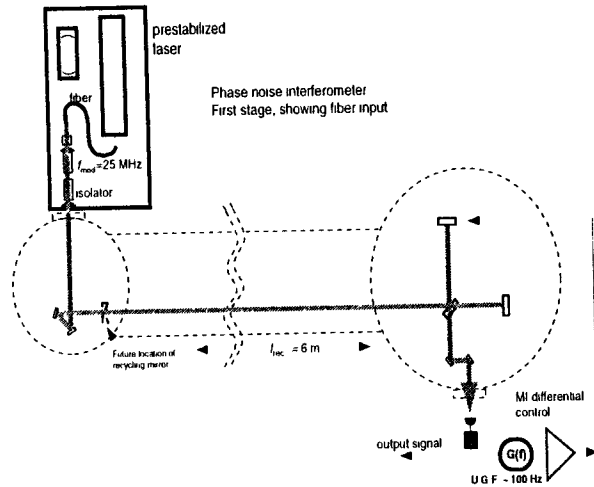


Figure 2.4. Overview of the PNI subsystems in the first stage

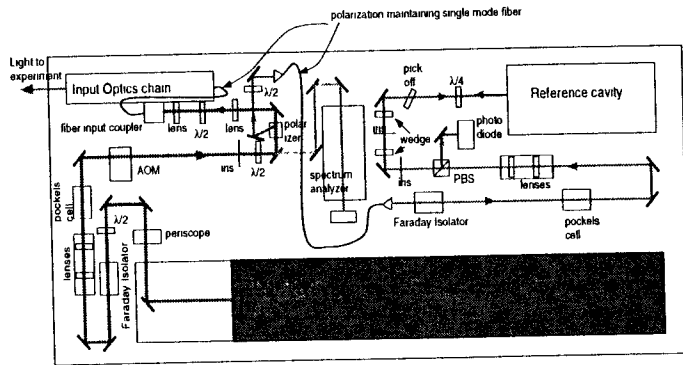


Figure 2.5. Optical layout of the laser stabilization subsystems (first stage) Error signal obtained from the photo-diode in the figure was used to stabilize the frequency of the laser by electronic feedback to PZTs on the laser cavity mirrors

experiment. Stabilization with respect to a passive cavity has been shown to achieve about $1 \text{ Hz}/\sqrt{\text{Hz}}$ at several hundreds of Hertz and to keep roughly that level until 10 kHz [16]. Thus the frequency noise at the first stage of our experiment provided a lower limit to the best phase noise sensitivity.

To get the requisite frequency noise suppression with the reference cavity, the first stage stabilization system had a unity gain frequency of close to 1 MHz. A number of different actuators were used to get this bandwidth. The mirrors that were used to define the laser resonator cavity (of length 2.16 meters) were put on PZT actuators — the high reflector (flat) mirror assembly reached its first resonance at about 230 kHz with a maximum dynamic range of 80 nanometers, while the output coupler (with a mirror of radius of curvature 8 meters) end resonated at about 8 kHz but had a maximum dynamic range of 8 micrometers. A Pockels cell phase corrector extended the bandwidth of the servo to 1 MHz. The laser was observed to be multi-mode above 2.5 watts of output power, thus establishing an upper-bound to the power that we could use for our experiment.

About 25 milliwatts of phase modulated (frequency of modulation — 12.33 MHz) light (with 40% of the power in the sideband fields, i.e. $J_0^2/J_1^2 \approx 3$) was incident on the reference cavity, and the Pound-Drever technique described in Appendix B was used to obtain the error signal for frequency stabilization. The control signal was applied to the actuators described in the last paragraph. The reference cavity was made of two mirrors separated by a quartz spacer of length 35 cm ($f_{sa} = 428.6 \text{ MHz}$), the input mirror was flat while the other mirror had a radius of curvature of 1 meter. Both the mirrors had the same nominal transmission of 700 ppm. A ring-down experiment (explained in Chapter 3) with the passive cavity yielded a total loss of 1600 ppm — thus the finesse of the cavity was about 2000.

An Acousto-optic modulator appears in Figure 2.4 which deflected about 20% of the incident power into the first diffraction order. It was intended to keep the amplitude of light constant by adding or taking out light in the first diffracted order. A photo-detector was included in the Input Optics chain for monitoring the amplitude fluctuations.

2.3.3 Suspensions

A mass suspended as a pendulum from a tower is free in an inertial space at frequencies above the pendulum resonance — its displacement, d , in the inertial space at frequency ω much above the pendulum resonance ω_0 can be approximated by $d = (\omega_0^2/\omega^2) d_t$, where d_t is the displacement of the tower in the same space. This is the idea behind suspending a mirror to isolate it from ambient vibration, the pendulum frequency in our experiment was about 1 Hz, thus there was vibration isolation of about 10^{-4} starting at around 100 Hz, our bandwidth of interest. Figure 2.6 shows the structure from which we suspended our mirror as a pendulum. The tower had a height of 15.7 inches, and it was about 5.4 inches wide and 2.5 inches deep, the mirror was suspended 9.8 inches below the top plate to get the pendulum resonance at about 1 Hz. The tower had its first resonance at about 157 Hz. The mirror also had resonances in its yaw (ϕ or side to side motion) and pitch (θ or up and down motion) motions at about 0.5 Hz. Steel wire, 2×10^{-3} inches thick, was used to suspend the mirror with a single loop as shown in Figure 2.6 in dotted lines. The wire took

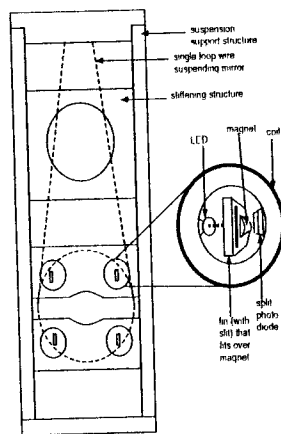


Figure 2.6. The structure for suspension of mirror and an expanded view of an OSEM

off tangentially at about 0.017 inches above the center of mass of the mirror. The mass of the mirror was about 0.25 kg, this caused a vertical “bounce” resonance at about 18.7 Hz. The wire could also be excited transversely like a violin string — the first such “violin” resonance was found to be at 550 Hz

The Q of the pendulum was high ($\approx 10^6$), hence the mirror needed damping at its low frequency resonances to hold it steady for interferometry. With this purpose in mind, four magnets (2.2 mm in length and 1.5 mm in diameter) were glued on top of Aluminum stand-offs (1/16 inches in diameter and 1/8 inches long) at four points on the mirror as shown in Figure 2.6. A fin with a slit in it was slipped on top of each magnet and then brought inside an OSEM (Optical Sensor Electric motor) unit. Each OSEM unit had an LED that was made to shine through the slit on to a split photo-detector — when the two photo-detectors saw equal light there was no signal; however, when the fin moved along with the mirror, one photo-detector saw more light than the other and a signal was produced by subtraction. The four signals from the four OSEM units were brought inside an OSEM processor box where they were linearly combined and then corrected for the corresponding resonance frequencies to form the longitudinal shift, and the pitch and yaw displacements of the mirror. Next, a derivative was taken electronically to get the velocity and a proportionate force applied, via coils around the OSEM units, on the magnets glued to the mirror to counter the mirror motion. Velocity damping was obtained in this manner and used to hold the mirror stationary at low frequencies.

Since electronic noise making its way onto the coils is a source of displacement noise, the velocity damping feedback was filtered by a 7 pole filter at 22 Hz. The final displacement noise owing to electronics was due to the thermal noise in the resistor used to convert a voltage to current in the coils. There was concern about thermal noise in the mechanical structures causing displacement in the measurement bandwidth — this happens through off resonance excitation of the pendulum, the violin modes of the suspending wire,

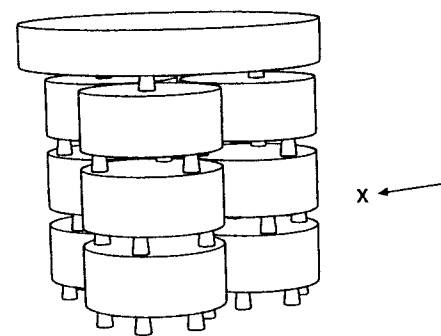


Figure 2.7. Passive vibration isolation stack

or the mirror structure modes [17]. Great care was therefore taken to keep the Q of these resonances high, so that the off resonance contribution was small. For example, the suspension tower was made of stainless steel to prevent the reduction of the pendulum Q through eddy current damping of the magnets glued to the mirror (as well as being compatible with a clean vacuum system). The residual contributions to phase noise from the sources just described are calculated in Chapter 4.

When we set up the suspensions in our experiment, we found that the mirrors were disturbed by tens of μ radian in alignment over time scales of tens of seconds. The cause of these alignment fluctuations was not completely understood. To counter the alignment changes, position feedback was introduced in the damping loops with a single pole filter at 0.06 Hz (there was negligible gain at 2 Hz to avoid coupling the mirror to the stack resonance).

2.3.4 Seismic isolation

The suspension towers rested on tables that were seismically isolated by active and passive methods. Passive isolation was provided by a cascade (or stack) of steel mass and viton spring elements as laid out in Figure 2.7. This stack, which has been extensively studied elsewhere [18], has been shown to transmit less than 10^{-4} of ground noise at 100 Hz from the base to the top. However, it does amplify motion by a roughly a factor of 5 at its resonances between 2 and 10 Hz in the horizontal and vertical directions.

The base of the stack rested on three legs that provided active isolation — these legs were commercial units available from Barry controls and their performance has been described in a recent technical report [19]. Each of these units has a central mass whose velocity is sensed in the three orthogonal directions by geophones and damped using PZTs that can withstand a payload of about 2500 lbs per foot. As shown in Figure 2.8, the system eliminated amplification of ground noise from the stack resonances at the interferometer table, and offered about 20 dB of isolation from 2 to 100 Hz in the horizontal direction. In the vertical direction, it gave 20 dB of isolation at about 1 Hz, rose to about 40 dB of isolation at 10 Hz and then started to fall again from 20 Hz upwards.

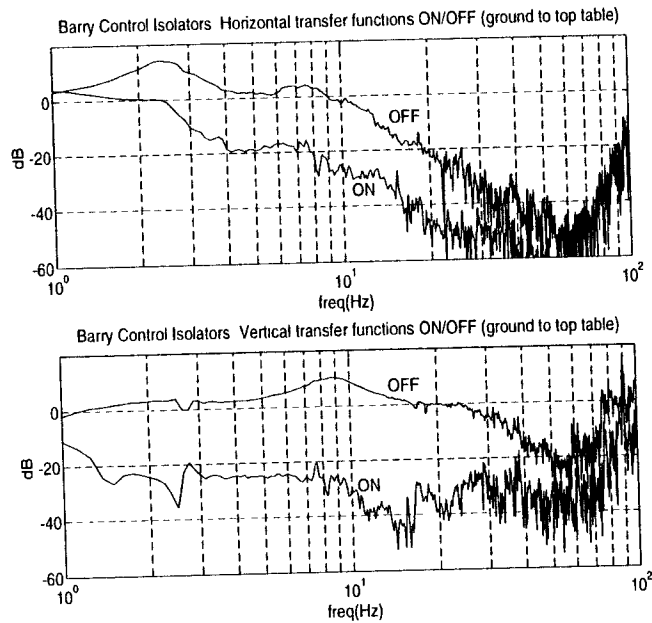


Figure 2.8: Performance of the Barry isolators, from [19]

Of more relevance to interferometry were impulsive seismic events that reached up to 80 microns in amplitude, and had characteristic frequencies between 5 and 10 Hz. Events up to 40 microns (the dynamic range limit of the Barry Control PZTs) were suppressed by factors between 20 to 30 at the top of the stack by the active isolation units.

2.3.5 Optics

The interferometer mirrors, as described before, were suspended as pendulums and placed within a vacuum envelope. There were additional optical elements, referred to collectively as the “input optics” which, as shown in Figure 2.9, prepared the light for interferometry and steered it into the vacuum envelope. The optical fiber stabilized the beam pointing. The Pockels cell phase-modulated the light at 25 MHz with a modulation index of $\Gamma \approx 1$. care was taken to orient the Brewster windows and the crystal so that the associated AM (peak) depth at 25 MHz was less than 5×10^{-5} . The $\lambda/2$ was oriented along with the Faraday rotator to get p-polarized light incident on the beam-splitter. The Faraday isolator provided 40 dB of isolation (in power) from light reflected back. The lenses were used to mode-match the light from the output characteristics of the fiber to a waist radius of about 0.9 mm at the end of the common mode path, however, without the recycling mirror which acts as a diverging lens with its radius of curvature of 10

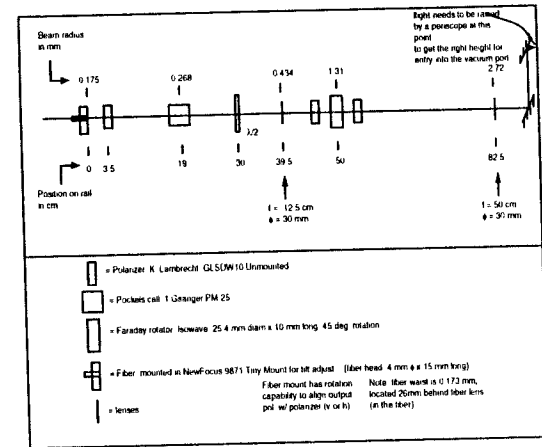


Figure 2.9. Input Optics in the first stage of the PNI

meters, the spot radius was about 1.2 mm. The entire optical train, except the steering mirrors at the end, was mounted on rails that were damped from resonances. The first steering mirror transmitted some light so that the amplitude noise in the input light could be monitored, thus allowing for necessary corrective signals to be sent to the AOM on the laser stabilization table.

The Michelson interferometer was made of optical elements that were 3 inches in diameter and 1 inch thick; the two end mirrors were coated for high reflectivity (with transmission at about 10 ppm), and the beam splitter had a (power) transmission of 49.75% and a reflectivity of 50.25% for p-polarized light (with AR reflectivity of 130 ppm). The Michelson asymmetry ($l_1 - l_2$) was measured to be 20.8 cm.

2.3.6 Michelson length control

Figure 2.10 shows the layout of the feedback system that was used to hold the Michelson interferometer at the dark fringe (a description of this system in the traditional language of feedback control systems appears in Appendix C). We present here the details of the different settings as used in the first stage of the experiment. The oscillator output was at 2.00 volts pp and set at a frequency of 25 MHz. This output was then split 50-50 in power; half of which was amplified 40 dB before coupling it to a Gsanger PM-25 Pockels cell through a tuned transformer. The other half was phase-shifted and boosted to 23 dBm before being fed as the LO to a Mini-Circuits ZAY-1B mixer. The photo-detector at the dark port used the capacity of the photo-diode and an external inductor to amplify its signal at 25 MHz through a low Q resonance. The signal was further amplified by a ZFL-500 amplifier from Mini-Circuits, before being low-pass filtered at 30 MHz to remove all harmonics of the modulation frequency. Next, the signal was down-converted by the mixer, and the 1F signal low-pass filtered at 5 MHz. Filter 3 in Figure 2.10 received the signal through a buffer and set the servo gain at low frequencies. At its low gain setting, Filter 3 had unity gain until 1

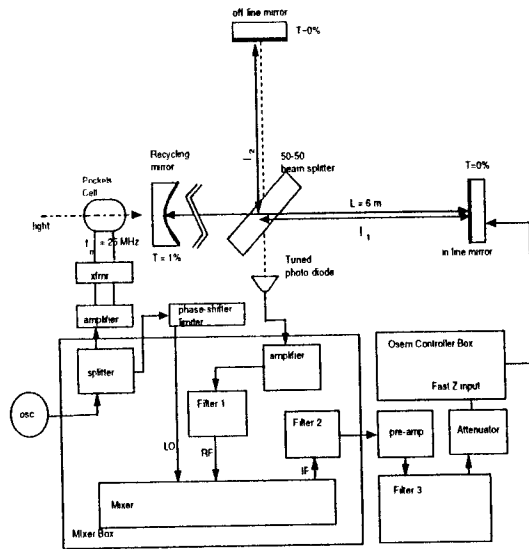


Figure 2 10 Block diagram of PNI differential length control servo

Hz, a zero at 1 Hz, and finally a pole at 1 kHz. In the high gain setting, there was gain of about 36 dB upto 63 Hz, and the first zero occurred there (the pole frequency was left at its previous value). A variable resistor (usually set at 2.5 k Ω) offered gain control by varying the current given a fixed voltage (each coil presented 500 Ω looking into the Fast Z input as shown in Figure 2 10). The overall loop gain varied with input light power — the u g f of the servo varied from 50 to 250 Hz in the different data runs (with a phase modulation index, Γ , equal to 1).

2.3.7 PNI in the second stage

Based on the experience in the first stage, the PNI underwent some changes in the second recycled stage. As the phase noise spectrum in the first stage suffered from beam pointing fluctuations, the entire input optics chain was moved to a separate table, closer to the vacuum envelope, and covered with acoustic shielding. The mode-matching of light to the recycling cavity had to be redone. The recycling mirror was suspended inside the near vacuum tank to reduce the seismic excitations of the mirror, active Barry isolation feet were now added under the passive stack inside the tank. The light retro-reflected off the recycling mirror was steered out onto the input optics table by the Faraday isolator, and received on a photo-detector. This photo-detector — exactly like the one at the dark port, was tuned to the phase-modulation frequency with a resonant circuit. Signals at the phase modulation frequency were thus obtained for frequency and common mode length correction, and used in a servo loop to keep the recycling cavity resonant. This “common mode” servo, as pointed out before, was also designed to obtain the necessary frequency noise suppression.

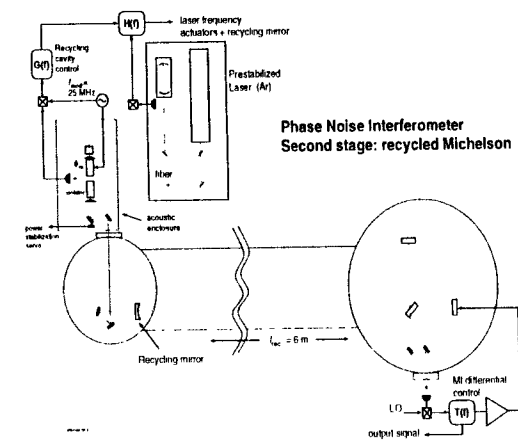


Figure 2 11 Overview of the PNI subsystems at the second stage

Changes were also made in the differential length control servo, and a wavefront sensor was used for active control of the differential misalignment. On the laser stabilization table, the light going to the reference cavity was sampled before the AOM — the laser frequency stabilization was now thus isolated from the effects of the amplitude stabilization system. An overview of the different subsystems in the second stage appears in Figure 2 11.

We discuss below the changes in the differential length control servo, and the two new additions in the second stage: the common mode servo and the wavefront sensing system.

2.3.8 The recycled Michelson length control

Recycling built up light power at the beam splitter on resonance from 1% (recycling mirror power transmission) of the input light intensity to a factor of 500 — this required careful tailoring of the differential length control servo so that the increased gain from the recycling cavity power build-up did not lead to saturation. Given the earlier (Michelson) length control servo design as discussed in section 2.3.6 and shown in Figure 2.10, we cut the signal going into Filter 3 by a factor of 10. Filter 3 was changed drastically — it could now provide gain increments of 2 dB from 2 dB upto 22 dB (with its highest setting gain comparable to that obtained with the earlier Michelson servo); also, the filter now had a zero at around 2 Hz but the pole was shifted to around 12 kHz. Thus a wide-band servo was now possible. Mirror structure resonance at around 23 kHz forced us to put a 4 pole Chebyshev filter at around 14 kHz in Filter 2 along with the 5 MHz low pass filter. Instead of the attenuator after Filter 3, the impedance seen in the Fast Z path varied from 10 k Ω to 2k Ω from 3 kHz to 15 kHz respectively — this helped in extending the bandwidth of the servo without high voltage gain. At the operating parameters of the recycled Michelson, the lowest gain setting of Filter 3 set the u g f to be around 400 Hz. The phase modulation index was reduced to 1/2 —

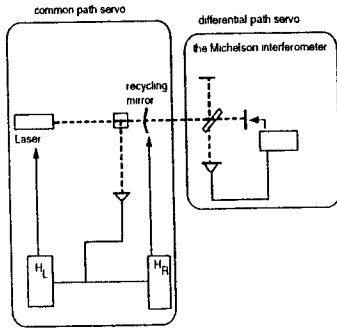


Figure 2 12 The length control servos

this was done to prevent the dark port photo-detector from seeing too much light.

Filter 3 also had a bypass stage that increased the gain upto 2 Hz by about 100, and then in decreasing amounts upto 120 Hz — this helped in reducing the measured phase noise at these frequencies and thus the contribution from the bilnear coupling with amplitude noise. We will discuss this more in the next chapter.

2.3.9 The common mode servo

The common mode servo, shown schematically in Figure 2 12 served two purposes: it had to keep the recycling cavity on resonance, and it had to provide an additional frequency noise suppression of 10^2 over that obtained from frequency comparison with a reference quartz cavity. The recycling cavity deviates from resonance for two reasons, at low frequencies upto about 100 Hz, the length changes of the cavity dominate, while — at higher frequencies — the frequency noise of the laser becomes important. Thus the error signal had to be sent to one of the two actuators shown in Figure 2 12 depending on its frequency. If the deviation from resonance be u (in radians), then the application of a servo as shown in Figure 2 12 reduces it to $u/(1 + H_R + H_L)$. At the point where H_R equals H_L in gain (the cross-over point), the phase difference between H_R and H_L is important — a π phase-shift can reduce the servo gain to unity.

Given the constraints described, the two paths, H_R and H_L , were designed as shown in Figure 2 13. The feedback path (H_L in Figures 2 12 and 2 13) to the laser cavity actuators was made to see a 6 dB/octave high pass filter with a corner frequency of 100 Hz, a flat portion from 100 Hz until 1 kHz whence it dropped 12 dB/octave to 10 kHz, and then, finally, a 6 dB/octave fall after 10 kHz. The feedback path to the recycling cavity (H_R) mirror followed the $1/f^2$ response of the mirror after its resonance at around 1 Hz until 80 Hz when an electronic “zero” caused a slower $1/f$ fall to 1 kHz — from that point onwards a 5 pole Butterworth filter caused a precipitous $1/f^6$ drop. Configured in this manner, the cross-over between the two paths happened around 150 Hz depending on operating conditons, and the n g f of the servo was around 30 kHz. This implied that though the H_L path had a gain of 300 from 100 Hz to 1 kHz, it only corrected

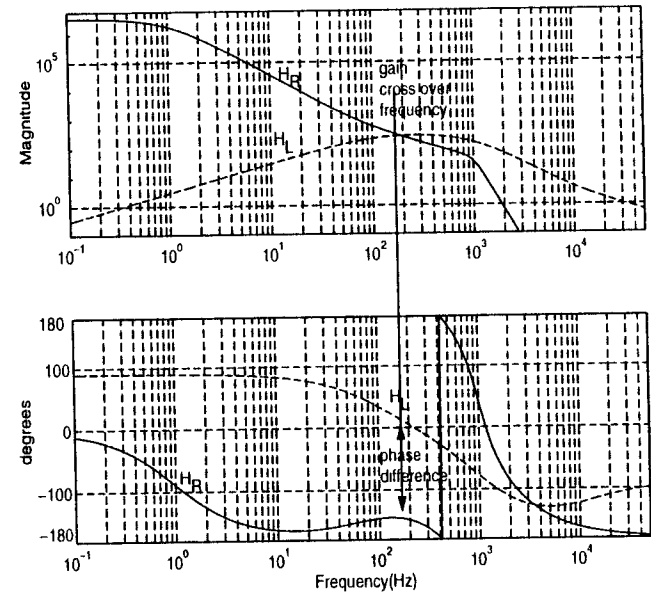


Figure 2 13 Relative gain and phase of the two actuator paths used in the common mode servo (bypass stage turned off).

for 50% of the deviation from resonance at 150 Hz and about 90% at 1 kHz. Thus, if frequency noise of $1 \text{ Hz}/\sqrt{\text{Hz}}$ caused the deviation from resonance, we could expect the common mode servo to suppress the frequency noise to only $0.5 \text{ Hz}/\sqrt{\text{Hz}}$ at 150 Hz, and to $0.1 \text{ Hz}/\sqrt{\text{Hz}}$ at 1 kHz. However, the Butterworth helped the H_L path to account for about 99% of the resonance deviation at about 1.7 kHz where the gain in that path dropped to about 100 — hence, we could expect to obtain our best phase noise around that frequency.

A bypass stage was tuned on after the recycling cavity was resonant that increased the servo gain as f^1 from 13 Hz until 1 Hz and as f from 1 to 0.5 Hz. The increased low frequency gain decreased the fluctuations from resonance owing to the large excitations at these frequencies.

Appendix B describes the Pound-Drever scheme of holding an optical cavity resonant at a carrier frequency with non-resonant side band frequencies. We used a variant of this technique, where the carrier and sidebands were both resonant with different couplings; while the carrier was over-coupled, the sidebands were slightly under-coupled. We can write the real (R) and imaginary (Im) reflectivities for the carrier field as $(r_R^c + \epsilon \cdot r_{Im}^c \cdot \psi)$, and for the sideband field as $(r_R^s + \epsilon \cdot r_{Im}^s \cdot \psi)$, where ψ is the deviation in the phase of the carrier field from resonance (Appendix B discusses why the reflectivities may be written this way). We then notice that the term at radio-frequency ω_m in Equation B 17 can be written as $4J_1 J_0 (r_{Im}^c r_R^s - r_{Im}^s r_R^c) \cos(\omega_m t) \psi$. Thus, if the carrier and sidebands are both resonant, their reflectivities have to be different (through different couplings as in our experiment) for an error signal to be obtained to hold the optical cavity resonant.

2.3.10 The active differential alignment system

If we put the signal wavefront at the modulation radio-frequency, as shown in Equation 2.12, on a split photo-diode face and subtract the two signals from the two photo-detectors, we reject the phase information common to both parts but pick up that information which is anti-symmetric in the two. Differential misalignments create such anti-symmetric phase patterns (refer Figure 2.14) — e.g., a small differential mirror tilt ϕ about the vertical axis z creates a phase pattern $(2k \cdot \phi \cdot y)$ if x be the path along which light travels — this phase pattern is anti-symmetric about $y = 0$. In this way, a quad photo-detector can be used to extract information about the differential pitch and yaw displacements of the Michelson mirrors. Once the information is obtained, active feedback can be used to stabilize the differential alignment of the mirrors (after the necessary down-conversion using a mixer and appropriate compensation filters) through the OSEM actuators. Extensive literature [20, 21] already exists in the LIGO project about the details of this technique.

A quad wavefront sensor was installed at the dark port. There were substantial differential pitch and yaw displacements between 2 and 10 Hz because of stack resonances, and some at sub Hertz frequencies as discussed before. A feedback loop was designed with high gain around 2 Hz — thus, with position feedback discussed before, was instrumental in stabilizing the power inside the recycling cavity to within a few percent.

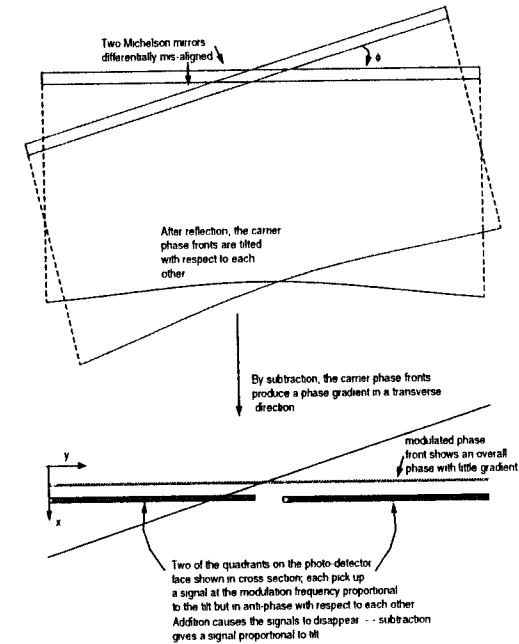


Figure 2.14: A simplified schematic to illustrate the principle behind the wavefront sensor

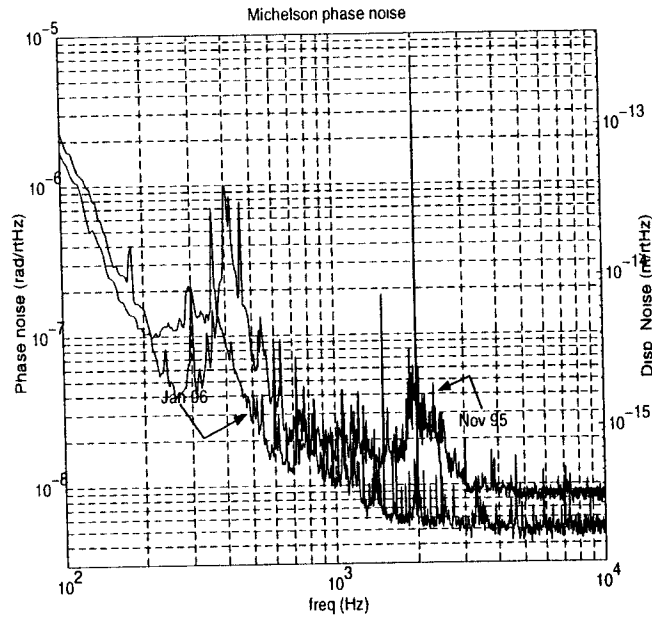


Figure 2 15 P s d in radian/ $\sqrt{\text{Hz}}$ of the PNI in its first stage

2.4 Performance of the PNI

The performance of the PNI was gauged by the phase noise spectrum that was measured from the signal at the dark port. The measured spectrum was corrected by the feedback gain and then converted to a power spectral density in radian/ $\sqrt{\text{Hz}}$. It was then compared to what would be obtained from the fundamental noise alone. In this section, we present two spectra that were obtained with an unrecycled Michelson in the first stage of PNI, and then the spectrum obtained with the recycled Michelson during the second stage of PNI. In the next two chapters, we undertake a study of these spectra.

Figure 2 15 shows the power spectral density of the unrecycled Michelson interferometer, the lower phase noise was obtained with three times more input light than the upper one, and with acoustic shielding around the input optics after it was moved to a new table.

Figure 2 16 shows the p s d of the PNI in its second recycled stage. We notice that the high frequency end reached 3.5×10^{-10} radian/ $\sqrt{\text{Hz}}$, about 15% above what is expected for the quantum noise level. This plot shows a phase sensitivity in interferometers that seems not to have been achieved before.

We turn now to a detailed study of phase noise in the next two chapters.

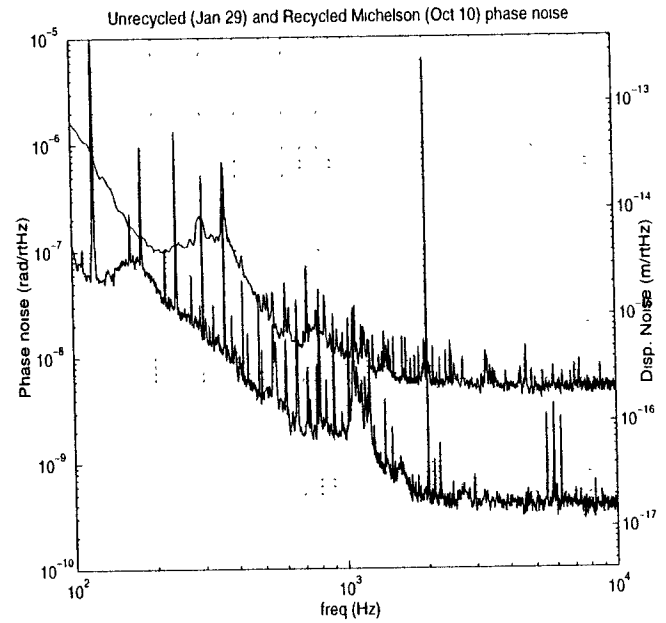


Figure 2 16 P s d in radian/ $\sqrt{\text{Hz}}$ of the PNI in its first and second stage

Chapter 3

Noise Sources in the Light

In this chapter, we look at the noise sources present in light used for interferometry and estimate their contributions to the dark port phase noise of the PNI (Phase Noise Interferometer). These noise sources are inherent in light, independent of the interferometer — we investigated which parameters of the interferometer were most influential in determining their contributions. There are other sources of noise that exist only when an interferometer interacts with light, and cease to have meaning without an interferometer — we reserve these sources for Chapter 4.

To analyze the dark port noise into elements from the different (classical) noise sources in light, we usually started by measuring the noise source directly. Then we simulated the noise source we were investigating with a calibrated stimulus, and measured the corresponding change in the phase noise spectrum. The observed change in the spectrum highlighted the particular mechanisms that were at work in the interferometer, to form a contribution from the noise source to the dark port detected phase. Once the mechanisms were identified, we could predict, given the measured level of the noise source, how much of the detected phase noise was due to that particular source.

3.1 Fundamental or quantum Noise in light

In section 2.1, we obtained the quantum noise (referred to usually as “shot noise”) psd in the detection of phase for the unrecycled and recycled Michelson interferometers. For the Michelson interferometer, the parameters required for this estimate were the input light power at the beam-splitter (the bright fringe photo-current), the c/d , and the additional photo-current that is measured owing to phase modulation. Recasting expression (2.11) in the quantities measured with the dark port photo-detector, we obtain

$$\sqrt{\frac{2c}{I_{max}}} \cdot \left(1 + \frac{I_{min}}{I_1}\right)^{1/2}, \quad (3.1)$$

where I_{max} is the current measured when the unlocked interferometer swings through a bright fringe, I_{min} is the photo-current when the interferometer is locked with a very small modulation index, and I_1 is the increase in this current after the modulation index is brought to its desired level. The expression (3.1) assumes that the modulation index is sufficiently small so that the J_2 and higher order Bessel expansion terms (Appendix A) may be neglected.

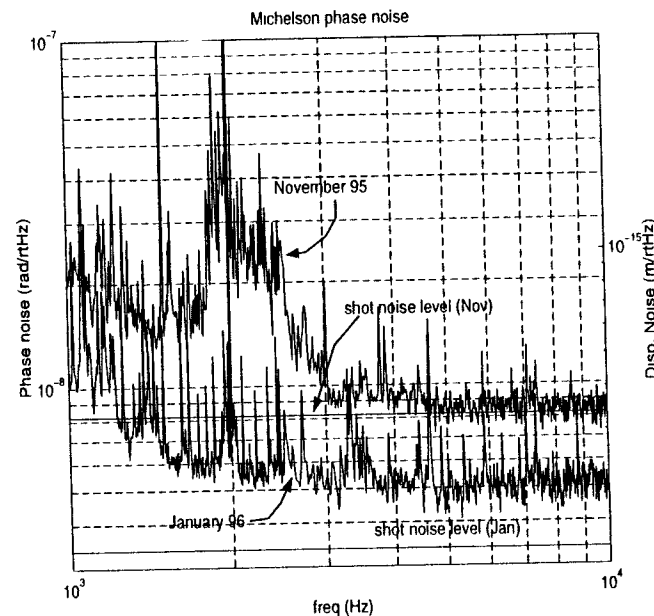


Figure 3.1: Shot noise level comparisons with measured unrecycled PNI spectra

The quantum noise in light is added in quadrature with the dark noise of the photo-detector (this includes the thermal noise from the photo-diode and some contribution from the transimpedance pre-amplifier) — to express the dark noise in units of phase power spectral density, we need to multiply it by the calibration of the measured quantity in radians of phase difference. This calibration constant is obtained experimentally by injecting a known sinusoidal current (at a frequency where the driven mirror behaves as a free mass) into the OSEM coils of one of the Michelson mirrors. With the known force constant of the OSEM coils (in Newtons per ampere) and the mass of the mirror, we can calculate the phase difference in radians produced by this motion. The phase noise spectrum would show this signal in volts/ $\sqrt{\text{Hz}}$ and thus give us the calibration constant. Figures 2.15 and 2.16 show the calibration signal as peaks at 2 kHz.

The November 95 spectrum in Figure 3.1 was taken for an I_{max} of 21.2 ma, an I_{min} of 60 μa , and an I_1 of 0.2 ma — with these values, 4.43×10^{-9} radian/ $\sqrt{\text{Hz}}$ is obtained from expression 3.1. The dark noise floor was at 6.9×10^{-9} radian/ $\sqrt{\text{Hz}}$; together with the quantum noise in quadrature, we get 8.2×10^{-9} radian/ $\sqrt{\text{Hz}}$, the level that we see from 5 kHz onwards.

The January 96 spectrum in Figure 3.1 was taken for an I_{max} of 64 ma, an I_{min} of 124 μa , and an I_1 of 0.6 ma — these values establish a quantum noise limited sensitivity of 2.46×10^{-9} radian/ $\sqrt{\text{Hz}}$. The dark noise floor now was at 2.3×10^{-9} radian/ $\sqrt{\text{Hz}}$ — thus we expect 3.37×10^{-9} radian/ $\sqrt{\text{Hz}}$ if the phase

noise is quantum noise limited. However, the measured spectrum noise asymptotes to between 4.5×10^{-9} and 5×10^{-9} radian/ $\sqrt{\text{Hz}}$ above 2 kHz — obviously, some other source of noise was more dominant.

The measurements of the recycled interferometer parameters needed for the quantum noise estimate requires a somewhat different approach. The value of Γ cannot be reduced to determine the contrast defect of the interferometer, as the modulation index influences the gain in two length control loops and one alignment control loop — also, a change in Γ causes a slight change in the beam direction which then affects the recycling cavity alignment [22]. With recycling, it is not possible to directly measure the bright fringe current at the dark port as well.

The round trip power loss of the light inside the recycling cavity can be measured by modulating the input light in amplitude with a square wave, and monitoring the light intensity variation transmitted through one of the Michelson end mirrors (which approximately had 10 ppm of power transmission). The recycling cavity of the PNI contained light at different frequencies (the carrier and its sidebands), each of which saw a different (transmissive) loss through the Michelson interferometer. However, as the sideband field was only about 1/8 of the carrier field in amplitude, and the (transmissive power) loss for each sideband was more than twice that for the carrier — after the first half-life interval¹, the monitored time decay in the light intensity could be expected to be entirely due to the carrier field. Since our modulation did not exceed more than 10% of the existing light level, we measured half-lives that captured field decay times [23]. These measured half-lives were averaged and converted to a power decay time (t_e) by dividing by $2\ln(2)$, the measured round trip power loss for the carrier could then be calculated as $t_{\text{roundtrip}}/t_e$ given the high finesse. We thus obtained about 9730 ppm for L_{common} , defined as in Section 2.1.3, for our recycling cavity.

An optical spectrum analyzer was used to look at the carrier to sideband power ratios in the light at several places — at the input to the interferometer ($(\frac{J_0^2}{J_1^2})_{\text{input}}$), at the dark port of the interferometer ($(\frac{J_0^2}{J_1^2})_{\text{dark}}$), and in the light inside the recycling cavity seen transmitted through one of the Michelson mirrors ($(\frac{J_0^2}{J_1^2})_{\text{inside}}$). From Section 2.1.3,

$$g_r^2 = \left(\frac{J_0^2}{J_1^2}\right)_{\text{input}} \div \left(\frac{J_0^2}{J_1^2}\right)_{\text{inside}}. \quad (3.2)$$

We measured g_r^2 to be 12.8/65 = 0.197, and given the L_{common} measured before, we calculated $\sin^2(\delta_1)$ to be about 12192 ppm. With 20.8 cm of asymmetry as measured, and our actual modulation frequency of 25.33 MHz, we get $\sin^2(\delta_1) = 12176$ ppm — thus the two numbers agreed within 5%.

The carrier to sideband power ratio at the beam-splitter is altered at the anti-symmetric port as the two frequencies see different transmissions through the Michelson interferometer — the carrier transmission is through the contrast defect only, while the sideband transmission gets dominated by a term that involves the asymmetry as well. Writing $\epsilon/d = 2 \times \delta_0^2$, the change in ratio can be expressed as

$$\left(\frac{J_0^2}{J_1^2}\right)_{\text{inside}} = \frac{\delta_0^2}{\delta_0^2 + \sin^2(\delta_1)} = \left(\frac{J_0^2}{J_1^2}\right)_{\text{dark}}. \quad (3.3)$$

We thus could solve for δ_0^2 given our measured carrier-sideband power ratio of 3.7 at the dark port, and found this to be 736 ppm (the contrast defect was thus about 1.4×10^{-4}).

¹This is the time in which the monitored light intensity decays to half its value.

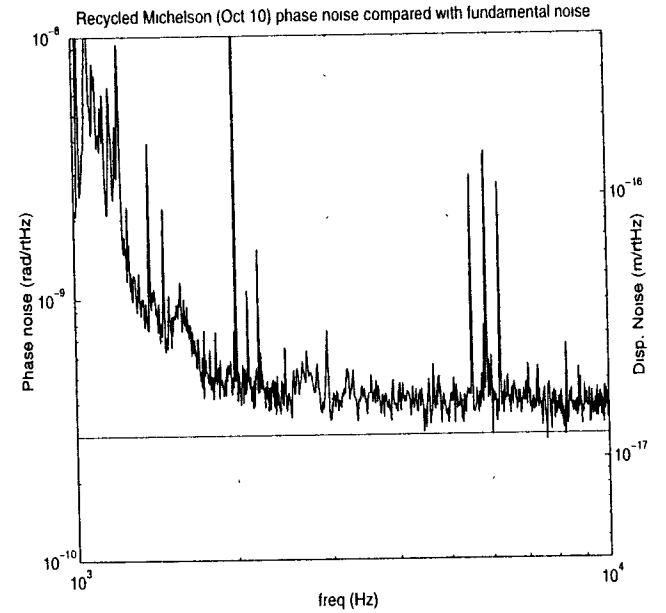


Figure 3.2. Comparison of recycled PNI phase noise with quantum noise

The relationship (3.3) also allows us to deduce what the photo-current (as measured by the anti-symmetric photo-detector) at the beam-splitter must be, given the measured dark port current. If the light power (measured in photo-current) in the carrier at the beam-splitter be pJ_0^2 and that of one of the sidebands be pJ_1^2 — we can write,

$$pJ_1^2 \left[\left(\frac{J_0^2}{J_1^2}\right)_{\text{inside}} \delta_0^2 + 2 \cdot (\delta_0^2 + \sin^2 \delta_1) \right] = \text{dark port current} \quad (3.4)$$

The measured dark port current for Figure 3.2 was 11 ma; given this value, pJ_1^2 is about 149 ma and $pJ_0^2 = 0.149 \times 65 = 9.7$ amperes. The photo-current at the beam-splitter J_{max} , is then equivalent to 10 amperes, and we can recast Equation 2.14 for the parameters of the recycled Michelson interferometer as

$$\sqrt{\frac{2r}{J_{\text{max}}}} \cdot \left[1 + \frac{1}{2} \cdot \left(\frac{J_0^2}{J_1^2}\right)_{\text{dark}} \right]^{1/2}. \quad (3.5)$$

If we use the numbers as measured when the plot of Figure 3.2 was recorded, we get a quantum noise limited sensitivity of 3×10^{-10} radian/ $\sqrt{\text{Hz}}$ — we can see that the measured high frequency noise in the figure asymptotes to this level within less than 25%.

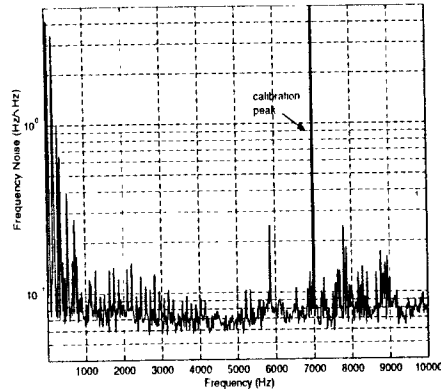


Figure 3.3 Error signal in the reference cavity stabilization loop

3.2 Frequency noise

As discussed before, frequency noise shows up in the phase noise of the PNI primarily because of the asymmetry in the two arms of the Michelson interferometer — given the asymmetry of $\delta l = 20.8$ cm in the PNI, we could thus expect a coupling of 8.7×10^{-9} radian/Hz. With the unrecycled Michelson interferometer, the spectrum that we show for January 96 in Figure 3.1 asymptotes to about 4.5×10^{-9} radian/ $\sqrt{\text{Hz}}$, at a level above that expected for the quantum and dark noise, if we assume that this excess is all due to the frequency noise added in quadrature, we find that our frequency noise was no greater than $0.34 \text{ Hz}/\sqrt{\text{Hz}}$ from 2 kHz onwards (this frequency noise sets a phase noise of 2.98×10^{-9} radian/ $\sqrt{\text{Hz}}$ which was overwhelmed by the dark noise in the November 95 spectrum). The level of stability is slightly better than the expected $1 \text{ Hz}/\sqrt{\text{Hz}}$ as reported before from the use of a quartz cavity longitudinal mode as a reference [16]. We did not have another analyzer cavity in the first stage of PNI, so we did not have an independent measure of the frequency noise — however, a spectrum of the error signal in the frequency stabilization feedback loop as shown in Figure 3.3 provided a lower limit of about $0.06 \text{ Hz}/\sqrt{\text{Hz}}$ to the frequency noise above 2 kHz. To calibrate the measured spectrum in frequency units, we wiggled one of the laser cavity mirrors with a known displacement and observed the peak in the spectrum — a modulation δL of the laser cavity length L produces a frequency modulation of $f (\delta L/L)$ where f is the frequency of light.

Where the recycling cavity does not deviate from resonance from its length fluctuations, the error signal obtained for holding it resonant is proportional to the residual frequency noise after the light has been stabilized in frequency with the quartz reference cavity. The length changes of the recycling cavity are mainly seismically driven and seismic excitation drops off fast above some 10s of Hz — however, the cross-over between actuators must happen gradually to avoid phase-shifts between the two paths that

can then compromise the servo gain. If we change the laser resonator cavity length to correct for the measured residual frequency noise, we cannot allow for any large corrections that would cause a shift from the frequency at which the reference quartz cavity is resonant. All these considerations had to be taken into account at the second stage of the PNI as we tried to achieve the required frequency noise suppression to reach a phase noise level of 10^{-10} radian/ $\sqrt{\text{Hz}}$.

The design of the common mode servo has been discussed in Chapter 2. The common mode error signal shown in Figure 3.4 was first converted to frequency units using the calibration method described before and then converted to phase noise using the asymmetry. The error signal captures the lower limit

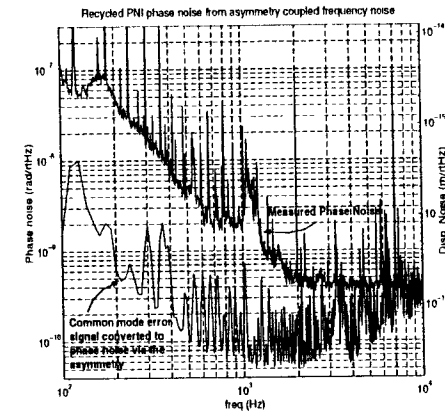


Figure 3.4 Common mode error signal converted to phase noise in the recycled PNI

to frequency noise; the upper limit is set by the measured phase noise of the PNI. Thus, where the two traces meet — as around 10 kHz — the phase noise could be attributed to the residual frequency noise coupled through the asymmetry. We measured the phase coherence between the measured dark port phase noise and the common mode error signal in the bandwidth shown in Figure 3.4. Since seismic noise drops off within few tens of Hertz, the deviation of the recycling cavity from resonance should be dominated by frequency noise above 100 Hz. However, as discussed in Chapter 2, frequency noise correction did not take full effect until beyond 1 kHz (the deviation from resonance was corrected by a corresponding change in the length of the recycling cavity) — hence we could expect phase noise owing to the residual frequency noise, phase coherent with the common mode error signal, from 100 Hz to around 1 kHz. At first no such phase coherence was detected, later experiments (by Dr. Gonzalez and Mr. Lantz) which put an extra Faraday isolator in the input optics chain brought down the phase noise in these frequencies by a factor between 3 and 5 and showed phase coherence with the common mode error signal from 400 Hz downwards. We will return to back scattered light in the section on parasitic interferometry.

Light scattered from the main beam and then recombined back at the dark port photo-detector after

reflecting off a surface can be a source of frequency noise. We noticed a strong dependence of the dark port noise at frequencies above 2 kHz to the setting of the phase-shifter used with the local oscillator — the noise increased if the setting was disturbed slightly from the optimal, and became coherent with the common mode error signal. Since the noise came roughly at quadrature, this scattered path must have had a reflector about 1.5 meters away from the recycling mirror, most possibly at the vacuum entry port (the reflector could also have been half way in the vacuum tube connecting the tanks though this was unlikely). Efforts to locate this scatterer did not succeed — however, the scatterer was also not important as its noise came at quadrature to the phase signal.

3.3 Amplitude Noise

Amplitude noise in light and its coupling to the phase noise was extensively investigated during both stages of the PNI work, the noise was found to not have any significant influence at either of the two stages. As shown in Chapter 2, radio-frequency phase modulation does isolate the phase noise from amplitude noise in the bandwidth of interest; however, phase modulation with a Pockels cell leads to a slight amplitude modulation that can re-introduce the amplitude noise. We will look at this amplitude modulation under the section on instrumentation noise in the next chapter and show how it can be avoided.

The Relative Intensity Noise (RIN) of the free running laser — defined as $(\Delta I)/I$ where I is the dc power level — had a measured spectral density of $1 \times 10^{-3}/\sqrt{\text{Hz}}$ at around 10 Hz, falling off roughly as $1/f$ upto 10 kHz. We had an active stabilization system which achieved a suppression of the amplitude noise by a factor of 100 at 100 Hz, dropping to around 30 at 1 kHz and unity around 16 kHz. With the stabilization system in operation, we thus had an RIN of about 1×10^{-6} around 1 kHz.

Expression 2.12, which captures the signal from which the phase-difference is inferred, shows how the RIN can contribute to the dark port phase noise. Recasting this expression in terms of the Bessel functions used in Equation 2.16, we obtain

$$2P_1 \cdot (1 + \text{RIN}) [J_0 J_1 \sin(\omega_m t_\Delta)] \sin[\omega_m(t - t_c)] \cdot \Delta\phi. \quad (3.6)$$

We notice that if the Michelson interferometer has a fixed offset from its null, there is phase noise coherent with the RIN, if there are larger residual $\Delta\phi$ changes at say frequency f_ϕ , the RIN at frequencies $f \pm f_\phi$ would be the main sources of phase noise at frequency f . Thus — to ascertain how much phase noise is contributed by the RIN — we need to identify the largest features in $\Delta\phi$ and find their frequencies. This is easily obtained by injecting a sizeable RIN at some frequency where the phase noise is at its minimum and identifying the resulting (most dominant) peaks that then appear as sidebands of this frequency. For example, Figure 3.5 shows the phase noise spectrum of the recycled PNI when an RIN of 7.7×10^{-3} was introduced in the input light — a number of sidebands which can be identified with mechanical resonances were obtained. From the measured phase noise at the peaks and the known RIN, the $\Delta\phi_{\text{peak}}$ at the resonant frequencies can be determined. We can also determine the most dominant peak — the one that would cause phase noise coupled with the RIN. Figure 3.6 shows what happened when a high gain (at low frequencies)

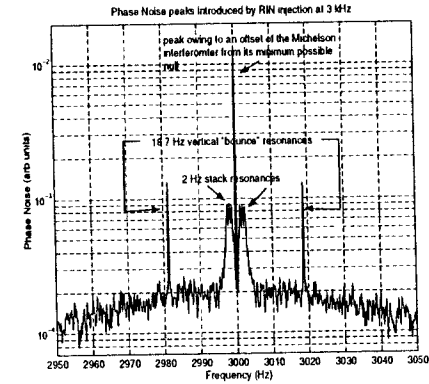


Figure 3.5 Phase noise peaks produced by RIN injection at 3 kHz

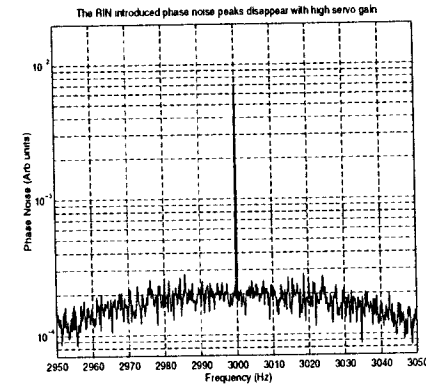


Figure 3.6 Phase noise owing to RIN injection at 3 kHz with high bypass gain at low frequencies

bypass stage was turned on in the Michelson length control servo — the sideband peaks disappeared and the one that was left was due to the offset of the Michelson interferometer from the minimum possible null. Again, from the known RIN and phase noise at the RIN peak, we determined this offset to be 3.7×10^{-5} radian in the recycled PNI. From Equation 3.6, it is clear that the relevant RIN for the recycled PNI is that of the light at the beam-splitter, this was obtained by measuring the RIN of the light transmitted through one of the Michelson end mirrors. As shown in Figure 3.7, we noticed that this RIN, with the active differential alignment system installed, was not much different from that of the input light (shown with an $1/f$ line in Figure 3.7). Thus, given the recycled phase noise spectrum of October 10 (shown in Figure 2.16), the unstabilized RIN multiplied by 3.7×10^{-5} radian — the dc offset, gave rise to a phase noise

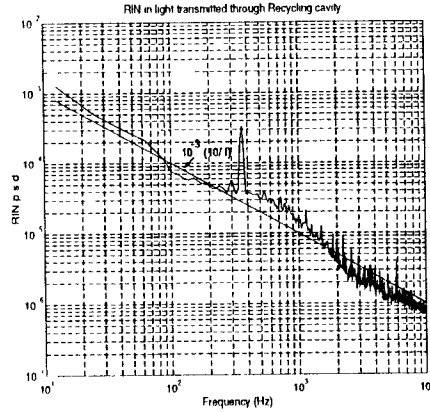


Figure 3.7 RIN of the light transmitted through the recycling cavity

that was below the measured p.s.d

During the first stage of the PNI, the unrecycled interferometer suffered from large $\Delta\phi$ variations at around 19 Hz, the vertical bounce resonance of the suspensions. Our recorded spectrum rejected any (peak) excursions beyond 1 milli-radian — with the amplitude stabilization in operation, an RIN of $1 \times 10^{-6}/\sqrt{\text{Hz}}$ in the input light resulted in a phase noise of 1×10^{-9} radian/ $\sqrt{\text{Hz}}$, below the phase noise shown in Figure 2.15.

From Equation 3.6, we notice that variations in the term $J_0 J_1 \sin(\omega_m t_\Delta)$ will have the same effect on the phase noise as RIN — this noise can be measured by injecting a $\Delta\phi$ at some frequency where the phase noise has reached a minimum and measuring the increased phase noise that result at side band frequencies of the excitation. However, this requires that the excitation be more stable than the RIN or the fractional noise in the calibration terms, $J_0 J_1 \sin(\omega_m t_\Delta)$. When we did this experiment we measured the RIN until our oscillator (excitation) noise dominated at a level of $10^{-5}/\sqrt{\text{Hz}}$ from 400 Hz onwards. The oscillator noise level of 10^{-5} converted to a phase reached the noise level of our measured spectrum from 2.5 kHz onwards — this implied that the noise in the elements that set the phase calibration, and the RIN, did not dominate in our phase noise spectrum.

3.4 Beam jitter noise

In this section we look at how fluctuations of the beam pointing at the interferometer input results in phase noise. We first present the formulation that describes this noise in an unrecycled Michelson interferometer, and then an experiment that was carried out to verify our result. We next show which parts of our Michelson spectra in the first stage were dominated by beam pointing jitter. Finally, we show how we need to revise our formulation to address the recycled interferometer, and present experiments that established

the contribution of beam jitter to the recycled PNI phase noise spectrum

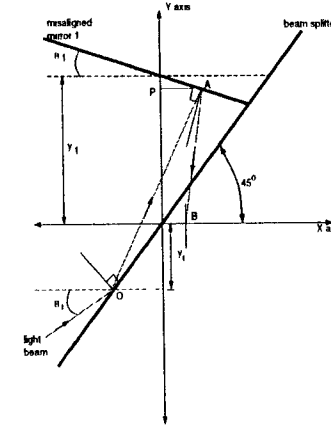


Figure 3.8 Definition of variables in the geometry of a beam varying in direction on a misaligned mirror

Referring to Figure 3.8, we set up a coordinate frame on the beam-splitter, in which the beam-splitter itself lies diagonally at 45° to the positive X axis. In this coordinate frame, the input light beam comes and strikes the splitter at a point whose y coordinate is given by y_1 , the beam also makes a counter-clockwise angle θ_1 with the negative X axis. The aligned situation thus assumes that θ_1 and y_1 are 0.

After the beam hits the splitter, half the power is transmitted while the other half is reflected. The reflected beam makes its way to one of the mirrors — which we henceforth refer as mirror 1 — and reaches the point A to be reflected back again. Mirror 1 is misaligned with (clockwise) angle θ_1 to the negative X axis, it also intersects the Y axis at the point $(0, y_1)$. The beam, after reflection from the mirror and transmission through the splitter, meets the X axis at B.

The distance y_1 is given by the corresponding arm length of the Michelson interferometer. To determine the interference detected at the anti-symmetric port, we need to follow the path of the other beam transmitted through the splitter to the X axis also. We simplify the calculation by assuming that the second beam follows the path of the first (reflected) beam — i.e. it reflects off the beam-splitter like the first and then off the second mirror which is now placed to intersect the Y axis at $(0, y_2)$. The beam reflected off this second mirror is then transmitted through the splitter to the X axis, exactly like the first one, for interference. The asymmetry in the two arms is captured in $y_2 - y_1$. When the two phase-fronts are brought to the X axis for interference, they differ in their

- (1) gaussian parameters;
- (2) positions of centers on the X axis,
- (3) tilts, given the angle between each beam and the vertical where it crosses the X axis,
- (4) extra distances they had to travel over their nominal ones ($2y_1$ or $2y_2$)

The gaussian parameters are set by how the beams are shaped by lenses and other optical elements. Expressions for the terms in (2), (3), and (4) for the beam reflected off mirror 1 can be formulated with the parameters θ_1 , y_1 , θ_1 , and y_1 , the subscript 2 substituted for 1 gives us corresponding expressions for the beam reflected off mirror 2. We need to first define AP , the length of the perpendicular on the Y axis in Figure 3.8

$$AP = \frac{\tan(\theta_1) \cdot (y_1 - y_1) + y_1}{1 + \tan(\theta_1) \cdot \tan(\theta_1)}. \quad (3.7)$$

The point B then has an x coordinate of

$$AP - (y_1 - AP \cdot \tan(\theta_1)) \cdot \tan(2\theta_1 - \theta_1), \quad (3.8)$$

while the angle the reflected beam makes with the vertical at B is $2 \cdot \theta_1 - \theta_1$.

The extra distance that each of the beams has to travel given a misaligned mirror and a mis-pointed beam contributes most significantly to the phase noise. This is

$$\frac{y_1 - y_1 - AP \cdot \tan(\theta_1)}{\cos(\theta_1)} + \frac{y_1 - AP \cdot \tan(\theta_1)}{\cos(2\theta_1 - \theta_1)} - 2 \cdot y_1 \quad (3.9)$$

for mirror 1. The extra distances, converted to an extra optical phase for each of the beams, need to be subtracted to form the phase difference between the two beams at the anti-symmetric port. Accordingly, we define

$$\begin{aligned} y_1 + y_2 &= L \\ y_1 - y_2 &= \Delta, \end{aligned} \quad (3.10)$$

and enumerate terms upto second order (in misalignment and beam pointing angle) in the phase difference:

$$\begin{aligned} &k \cdot (\theta_2 - \theta_1) \cdot (2y_1 + 2L\theta_1 - 2y_1\theta_1) \\ &+ k \cdot (\theta_2 + \theta_1) \cdot (2\Delta\theta_1) \\ &+ k \cdot L \cdot (\theta_2 + \theta_1)(\theta_1 - \theta_2) \\ &+ k \cdot \Delta \cdot (\theta_1^2 + \theta_2^2 + 2\theta_1^2), \end{aligned} \quad (3.11)$$

where $k = \frac{2\pi}{\lambda}$

Not all terms in the expression above contribute equally to the longitudinal phase difference, given our asymmetry (Δ) of 20.8 cm, the term that dominates is

$$k \cdot (\theta_2 - \theta_1) \cdot (2y_1 + 2L\theta_1) \quad (3.12)$$

To verify that this term dominates, we wiggled one of the steering mirrors that sent the light over a distance of 10 meters to the beam-splitter of the unrecycled Michelson interferometer. Figure 3.9 shows two time traces — the error signal of the Michelson length control loop and the simultaneous low frequency variation of the Michelson dark port photo-current. As can be seen clearly, the modulation of the error signal at our wiggle frequency followed the variation in the low frequency photo-current quite closely. In the last

chapter, we discussed how the low frequency changes were dominated by differential misalignment in the unrecycled PNI, i.e., a variation in $(\theta_2 - \theta_1)$. A comparison is thus possible between the modulation of the error signal and the low frequency change in photo-current. Working out the values for the dip in the middle of the trace, $\theta_1 = (\text{Calibration of } 0.4 \mu\text{rad/Volt}) \times (50 \text{ mV peak input}) = 2 \times 10^{-8} \text{ rad pk}$; phase modulation amplitude $= 2 \times 10^{-4} \text{ rad/Volt calibration} \times 0.75 \text{ volt amplitude on trace} = 1.5 \times 10^{-4} \text{ rad}$ — we thus find that expression 3.12 establishes $(\theta_2 - \theta_1)$ to be about $30 \mu\text{rad}$.

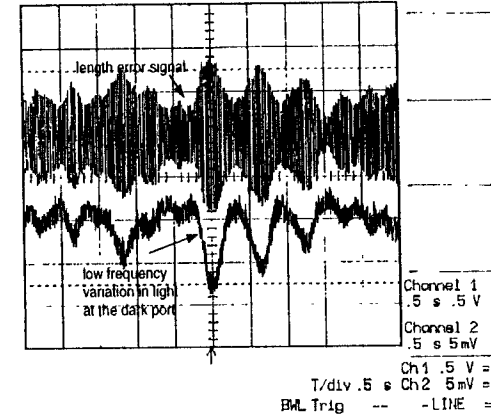


Figure 3.9 Time traces of the length error signal and the low frequency light variation at the dark port of the unrecycled PNI, as the input beam is wiggled in direction.

The fluctuation in the low frequency trace corresponded to roughly 3% in contrast variation. Integrating the interference pattern that results at the dark port of a Michelson interferometer (with equal arms) when the two end mirrors are misaligned, we get a contrast variation of

$$\frac{1}{4} k^2 (\theta_1 - \theta_2)^2 w^2, \quad (3.13)$$

where w is the waist radius of the two beams. Using $w = 1 \text{ mm}$ at the beam-splitter for the unrecycled PNI, we find $(\theta_1 - \theta_2) \approx 30 \mu\text{rad}$ as obtained in the last paragraph.

Figure 3.10 shows the influence of beam jitter on the phase noise of the unrecycled PNI. As shown in the figure, the November 95 spectrum was dominated by mechanical resonances of the elements in the input optics chain, care was taken to therefore damp these resonances and an acoustic shield was used to isolate the input optics from ambient excitation. This resulted in elimination of the phase noise owing to input beam jitter above 1 kHz as the spectrum from Jan 96 clearly shows, the beam jitter peaks between 400 and 500 Hz were also substantially reduced. The signal from a quad photo-detector looking at the light reflected from the unrecycled PNI showed phase-coherence with the phase noise between 400 Hz and 2 kHz — thus the phase noise in this region could be attributed to variation in input beam pointing.

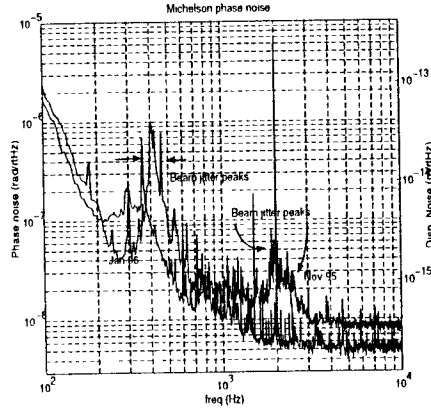


Figure 3 10 Effects of input beam jitter in the unrecycled PNI

The recycled PNI requires some modification of the above formulation. We rewrite the expression in 3 12 for the unrecycled PNI slightly differently,

$$k \cdot (\theta_2 - \theta_1) \cdot (2d_t) \tag{3 14}$$

where d_t is the displacement of the beam from its axis (the path it would follow if it were properly aligned). If the source of the beam jitter is a steering mirror that shakes (with angle θ_1) at a distance s from where the common mode path terminates, then $d_t = s \cdot \theta_1$. When we introduce the recycling mirror (but not recycling of light, e.g. by misaligning the recycling mirror), we introduce the effects of a diverging lens via the 10 meter radius of curvature of the mirror — the source of the wiggle appears to move closer to the beam splitter, and thus the effective d_t is less than before. For example, if the source is at a distance p from the recycling mirror $s = 6 + (5p)/(5 + p)$, instead of $6 + p$. With the recycling mirror in place, the beam forms a waist at the end of its common mode path — at this location, given the wiggle θ_1 and the displacement d_t , we can write a modal (field) description of beam as [24]

$$\psi(r) = A[U_0(r) + \frac{d_t}{w_0} U_1(r)], \tag{3 15}$$

where w_0 is the waist radius, and $U_{0,1}$ represent the Hermite Gaussian functions of order 0 and 1. When we begin to recycle light, the field U_1 does not build up as much as U_0 — if light sees a round trip power loss of L , we can write the following (approximate) expression for the recycled light:

$$\psi(r) = A[U_0(r) + \frac{L}{4} \cdot \frac{d_t}{w_0} U_1(r)] \tag{3 16}$$

The carrier and the sidebands thus see different “effective” displacements at the end of the common mode path inside the recycling cavity, as then losses are different. These fields next see the differentially misaligned

Michelson interferometer which give rise to further U_1 fields; the sideband and the carrier U_1 fields next interfere to form a signal at our phase modulation frequency which add noise to the detected phase. Using the model discussed in [20] and the parameters of the recycled PNI, we obtain about 2.2 radian of optical phase for 1 μ radian of $(\theta_2 - \theta_1)$, 1 radian of θ_1 , and $s = 8$ meters. An experiment performed with a steering mirror located at this value of s (≈ 8 meters) yielded about 7 radian of optical phase per radian of θ_1 — this seemed to indicate that the static differential misalignment was about 3 μ radian.

Looking at the light reflected off the PNI with a quad photo-detector, and calibrating the signal by dithering the recycling mirror in angle, we can obtain the power spectral density of θ_1 . Using the coupling measured by a calibrated input beam jitter as described in the last paragraph, the contribution of beam jitter to optical phase noise can be determined. Figure 3 11 shows exactly such a comparison. The phase

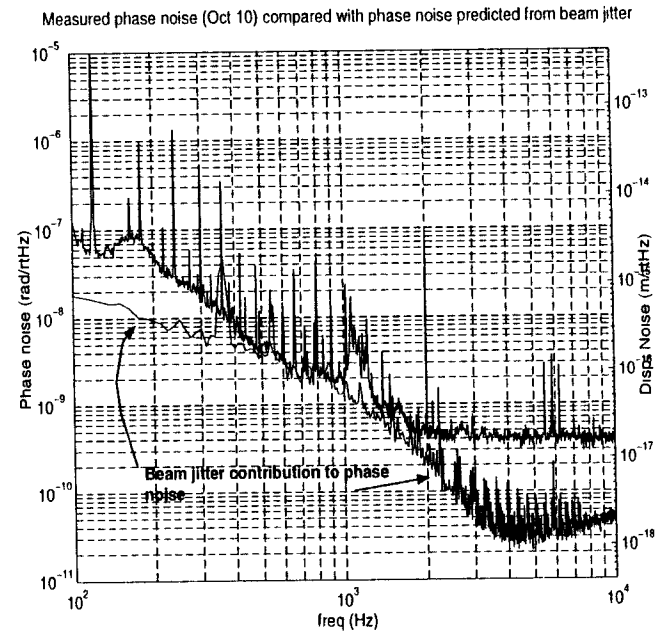


Figure 3 11: Phase noise from input beam jitter compared with the Oct 10 spectrum of the PNI

noise predicted from input beam pointing comes close to explaining the measured phase noise on October 10 from 400 Hz to about 2 kHz — however, at the time the beam pointing noise was measured, the phase noise in this bandwidth was higher by roughly a factor of 3 than the noise measured on Oct 10. The plot serves to illustrate that the noise in beam pointing, unless actively controlled, can become the limiting noise from several hundreds of Hertz to a few kHz. The PNI spectrum in this bandwidth clearly had many sources of noise — the residual frequency noise in laser, some back scattering, and definitely beam pointing

noise. A lot of effort thus needs to be concentrated on controlling these sources of noise to stretch the level of 10^{-10} radian phase noise into this bandwidth.

We now turn to the sources of noise that come from the interaction of light with the elements that make up the interferometer.

Chapter 4

Noise Sources in the Interferometer

The elements that comprise the interferometer introduce noise in the detected optical phase — e.g., the mirrors are disturbed from their positions by random forces which can have seismic or thermal origin, the sensing and active control systems are limited by noise from the electronics used to implement them; and, finally, light scattered off the intended path of travel can find its way to the photo-detector used at the dark port and interfere with the light carrying the phase signal. The purpose of this chapter is to look at these sources of noise and estimate their levels in the detected phase noise.

4.1 Displacement noise

The goal of the PNI (Phase Noise Interferometer) was to minimize the conversion of differential displacement in two orthogonal directions (required for the detection of gravitational waves) to optical phase; hence, our interferometer constructed a Michelson interferometer with 50 cm arms without optical cavities in them. However, displacement noise still played a role in the detected phase noise and we discuss the sources of this noise in this section.

4.1.1 Seismic noise

The ground shakes at low frequencies to produce differential displacements between the two Michelson arms; this seismic noise has a stationary part that usually rises from 0.1 Hz to 1 Hz, reaches a flat level between 1 and 10 Hz, and, finally, falls off as $1/f^{-2}$ from 10 Hz upwards. The stationary ground noise at MIT (where we built the PNI) was approximately 3×10^{-10} m/ $\sqrt{\text{Hz}}$ at around 80 Hz and isotropic — given the attenuation (of around 10^{-4}) of the stack, and (of around 3×10^{-4}) of the pendulum — we expected the differential motion of the Michelson mirrors to not exceed 3×10^{-18} m/ $\sqrt{\text{Hz}}$. This level of ground noise produces less than 1×10^{-10} radian/ $\sqrt{\text{Hz}}$ of optical phase noise.

The site of the PNI was affected by impulsive seismic events which lasted several seconds at frequencies between 5 and 10 Hz, and reached amplitudes as large as 80 microns. Most of this ground noise excited the vertical bounce resonance of the pendulums in the first stage of the PNI, in the second stage, a servo with high gain at around 20 Hz (the bounce resonance) was implemented to avoid the bilinear coupling of this low frequency phase noise to the phase noise above 100 Hz.

4.1.2 Thermal noise

Apart from the longitudinal resonance at about 1 Hz of the pendulum, the mirror position can also be disturbed by transverse excitations of the wire used for suspension, or the excitations of the “internal mirror” modes that are defined by the mirror material and geometry. These resonances are damped out by mechanisms internal to the excited element — and, by the Fluctuation Dissipation Theorem (see [17] for example) — are also therefore excited thermally. Internal damping is modeled by adding an imaginary part to the usual spring constant k , i.e. the force F in Hooke’s law is written as:

$$F = -k[1 + i\phi(\omega)]x, \quad (4.1)$$

where x is the corresponding change in the quantity of interest with the application of force. The Fluctuation Dissipation Theorem then establishes the thermal power spectral density for x [17].

$$r^2(\omega) = \frac{4k_B T k \phi(\omega)}{\omega[(k - m\omega^2)^2 + k^2 \phi^2]}, \quad (4.2)$$

where k_B is the Boltzmann constant, T the absolute temperature, and m the mass of the object in motion. It is clear that knowledge of the frequency dependence of ϕ is important in predicting how the excitation would affect the optical phase noise — given the resonances we are usually concerned with and our frequencies of interest (several hundreds of Hz to a kHz), it seems that ϕ can be assumed to be a constant (the “structure damping hypothesis” [17, 25, 26]). It is clear from Equation 4.2 that the Q of the resonance (defined to be $\omega_0/\delta\omega$, where ω_0 is the resonant frequency and $\delta\omega$ the full width of the resonance at the half power points) is then $1/\phi(\omega_0) = 1/\phi$. We present here some thermal noise estimates given the parameters of the PNI.

The longitudinal pendulum mode is the first ($n = 0$) of a series of modes called the violin modes (the term is usually reserved for the $n > 0$ modes) — the displacement of the mirror owing to these modes may be written as [17, 25]

$$x^2(\omega) = \sum_n \frac{4k_B T}{\omega \mu_n} \cdot \frac{\omega_n^2 \phi_n}{(\omega_n^2 - \omega^2)^2 + \omega_n^4 \phi_n^2}, \quad (4.3)$$

where $\mu_n = m$, the mass of the pendulum for the longitudinal mode (with frequency ω_p), and $\mu_n = (m\omega_n^2)/(2\omega_p^2)$ for the violin modes with a resonant frequency of $\omega_n = 2\pi f_n$ for the n th mode. The first violin frequency was measured to be at 550 Hz with a Q of 1.7×10^5 — at this resonant frequency, we find,

$$x^2(550 \text{ Hz}) = \frac{8k_B T Q \omega_p^2}{m \omega_n^5} = 1.81 \times 10^{-30} \cdot \left(\frac{550}{f_n}\right)^5 \cdot \left(\frac{Q}{1.7 \times 10^5}\right) \text{ m}^2/\sqrt{\text{Hz}}. \quad (4.4)$$

The above displacement noise corresponds to about 3×10^{-8} radian/ $\sqrt{\text{Hz}}$ in the optical phase which we should have been able to detect in the second stage (the first stage noise was approximately at this level); however, no peaked structure at this level was apparent in the spectrum around 550 Hz. In the bandwidth where we show the optical phase noise power spectral density in Figures 2.15 and 2.16, the longitudinal mode of the pendulum introduces its off resonant thermal noise, from Equation 4.3 we find this to be

$$x^2(f) = \frac{4k_B T (2\pi f_p)^2}{m(2\pi f)^5 Q} \text{ m}^2/\sqrt{\text{Hz}} \quad (4.5)$$

The Q of the pendulum is hard to measure; however, the work of Gillespie and Raab [25] shows how this can be approximated to roughly two times the Q of the violin resonance. We thus approximate Q to be of the order of 3×10^5 , and can approximate Equation 4.5 to be

$$x^2(f) = 1.34 \times 10^{-38} \cdot \left(\frac{100}{f}\right)^5 \text{ m}^2/\sqrt{\text{Hz}} \quad (4.6)$$

The expected phase noise is then about 4×10^{-12} radian/ $\sqrt{\text{Hz}}$ at 100 Hz, and below our measured phase noise.

Gillespie and Raab [26] have studied the physical deformation modes of the mirror modeled as a right solid cylinder. They have looked at the change in overall phase of a Gaussian beam reflected off a mirror whose modes have been excited thermally, and have added the (off resonance) contributions from these mechanical modes in the bandwidth of our interest until the sum converged to a specific value. Their modeling has shown that given the dimensions of our mirrors (3 inches in diameter and 1 inch in thickness), and summing the first 20 modes, the thermal displacement power spectral density can be given by

$$x_{th} = 2.4 \times 10^{-18} \cdot \left(\frac{100 \text{ Hz}}{f}\right)^{1/2} \cdot \left(\frac{\phi}{10^{-4}}\right)^{1/2} \text{ m}/\sqrt{\text{Hz}}. \quad (4.7)$$

A differential displacement of 4×10^{-18} m/ $\sqrt{\text{Hz}}$ corresponds to a phase difference of 1×10^{-10} radian/ $\sqrt{\text{Hz}}$.

The first mirror structure resonance seems to be between 23 and 29 kHz in the mirrors, where an attempt at the measurement of Q gave a low value of around 1000 (fused silica is expected to have Q values of around 10^6); this may be because the first resonance sees more loss owing to the attachments to the mirror. If we assume this low value of Q for all the modes, we get a phase noise spectral density of around 2×10^{-10} radian/ $\sqrt{\text{Hz}}$ which is still below the measured phase noise.

4.1.3 Radiation pressure

The force exerted on an object by light is given by P/c where P is the incident power, and c the speed of light [27]. The incident power has quantum fluctuations whose PSD is given by $\sqrt{2h\nu P}$, where h is the Planck’s constant and ν the frequency of light. These fluctuations then correspond to fluctuating forces on the mirrors which result in their displacement. Adding the displacements in the two arms in quadrature, we obtain a measured phase noise density at frequency ω (much larger than the pendulum resonant frequency) of

$$\phi_{ns} = \frac{4k}{m\omega^2 c} \sqrt{\eta} \cdot \left(\frac{h\nu}{\eta c}\right) \sqrt{\frac{c I_{max}}{2}}, \quad (4.8)$$

where k is the wave number, m the mass of the mirrors, η the quantum efficiency of the photo-detector used, e the electronic charge, and I_{max} the photo-current at the beam-splitter. Given 10 amperes of current at the beam splitter in the recycled stage (Chapter 3), we thus obtain,

$$\phi_{ns} = 3 \times 10^{-15} \cdot \left(\frac{I_{max}}{10 \text{ amp}}\right)^{1/2} \cdot \left(\frac{100}{f}\right)^2 \cdot \left(\frac{0.25 \text{ kg}}{m}\right) \text{ radian}/\sqrt{\text{Hz}}. \quad (4.9)$$

This shows us that the radiation pressure from the quantum fluctuations in light did not play a major role in the detected phase noise — however, if the beam-splitter is not exactly 50-50, or, if the masses of the

two mirrors are not exactly equal, we can obtain a differential displacement owing to the intensity noise in light (RIN). If τ represents the fractional difference in the two masses (i.e., $2(m_1 - m_2)/(m_1 + m_2)$), or the difference in the power reflected off the beam-splitter from that transmitted, then

$$\phi_{ms} = \frac{kP}{m\omega^2 c} (\tau \cdot RIN) = 1.23 \times 10^{-5} \cdot \left(\frac{I_{max}}{10 \text{ amp}}\right) \left(\frac{100}{f}\right)^2 (\tau \cdot RIN) \left(\frac{0.25 \text{ kg}}{m}\right) \text{ radian}/\sqrt{\text{Hz}} \quad (4.10)$$

Given that the RIN was roughly at 1×10^{-6} , and τ definitely not greater than 10 %, we thus find that the displacement noise owing to the radiation pressure in light could not have contributed to the phase noise of the recycled PNI.

The feedback system that damped the pendulums could also convert its electronic noise to a displacement signal — we will look at this in the section on instrumentation noise.

4.2 Interferometer misalignment

As the suspended mirrors get disturbed from their equilibrium positions, they produce a misalignment of the optical elements used for interferometry, in addition to a change in the distances between mirrors (longitudinal displacement). We can distinguish between two kinds of misalignments in the PNI — a common mode misalignment, where the input beam in a round trip to its starting point sees optical elements that are not in their intended alignments; a differential misalignment, where the two beams interfered at the anti-symmetric port see their wavefronts rotated or shifted with respect to each other.

As discussed in the section on beam jitter in Chapter 2, the primary cause of differential misalignment is the difference, $(\theta_2 - \theta_1)$, of the two Michelson mirrors. We have already seen how this difference in angle, coupled with beam jitter, gives rise to a longitudinal phase. This difference also can cause light to leak out of the dark port and cause a poor contrast. In the first stage of the PNI, the c.d. owing to differential misalignment was sometimes as high as 3 % (see Figure 3.9 for example) — this corresponded to a “transmissive” loss of about 15,000 ppm through the Michelson interferometer. During the unrecycled stage, apart from the phase noise through the bilinear coupling with beam jitter, this differential misalignment was of not much consequence — causing only about 1.5 % change in the quantum noise level at its worst. However, this was a serious impediment to recycling, given that the input transmission to the recycling cavity was only 8200 ppm; this level of loss could cause the carrier to be undercoupled and hence not build up the light power to the desired extent at the beam-splitter. Some position feedback in the damping control of the mirrors, along with the wavefront sensor described in Chapter 2, had to be therefore implemented to stabilize the differential misalignment of the Michelson mirrors at the second stage of the PNI.

The recycling cavity can be thought to be made of the recycling mirror as the front mirror, and the Michelson interferometer as the “back” mirror. While the differential misalignment influences the reflectivity and transmission of this back mirror, the alignment of the back mirror is determined by the angle $\theta = (\theta_1 + \theta_2)$ of the two Michelson mirrors with respect to a perpendicular on the path of the input laser beam. When the two mirrors of the recycling cavity are disturbed from their correctly aligned positions, the input beam projects onto the first order Hermite-Gaussian modes at the expense of the zeroth order mode — this

causes a reduction in power at the beam-splitter inside the recycling cavity. If the angle of the recycling mirror from its correctly aligned orientation be given by α , then the power lost can be expressed as a reduction in transmission of the input light power of [2]

$$\left(\frac{R}{w} \cdot \alpha - \frac{(R-L)}{w} \cdot \theta\right)^2 + \left(\frac{kw\theta}{2}\right)^2, \quad (4.11)$$

where R is the radius of curvature of the recycling mirror (10 meters), and w is the waist radius at the end of the common mode path (0.9 mm). Thus while a 10 μ radian change in the recycling mirror orientation produces about an 1 % drop in power at the beam-splitter, the same change in θ results in only a 0.4 % reduction in power.

It may seem that during the first stage of PNI, common mode alignment — i.e., the adjustment of θ , the input beam angle as defined in the section on beam jitter in Chapter 3, or $\theta = (\theta_1 + \theta_2)$ of the two Michelson mirrors — was not as important as differential alignment for a good contrast at the output of the interferometer. This is not true — the asymmetry in the Michelson interferometer makes the common mode alignment just as important. From Equation 3.8 expanded to second order in the terms $\theta_{1,2}$, and y , we obtain the separation of the centers of the two Gaussian beams interfering at the dark port to be

$$\Delta \cdot [2\theta_1 - \theta] + L \cdot (\theta_2 - \theta_1), \quad (4.12)$$

where Δ and L are as defined in Chapter 3. The angle between the two Gaussian beam cross-sections is $2(\theta_2 - \theta_1)$; thus given any arbitrary θ_1 and θ_2 , it is hard to have the centers coincident and the profiles aligned, as are necessary for a good contrast. Only when the input beam is retro-reflected are we able to satisfy both these criteria.

4.3 Parasitic Interferometry

The light incident on the interferometer is primarily made of fields at three frequencies — the carrier frequency, ω , and the two sideband frequencies, $\omega \pm \omega_m$. We can combine the two fields at the two sideband frequencies, and obtain an expression for the (time dependent) field amplitude at the input of the interferometer as,

$$J_0 E_m + 2iJ_1 E_m \cos(\omega_m t), \quad (4.13)$$

where J_0 and J_1 are the zero and first order Bessel functions with the modulation index Γ as their arguments. A photo-detector looking at this light (as shown in Figure 4.1) does not see any signal at the modulation radio-frequency — thus, if we down-converted the photo-detector output from a bandwidth around the modulation frequency, we expect to see shot noise consistent with the light level. In practice, we may see some intensity noise owing to the slight amplitude modulation that accompanies the phase modulation process. When we blocked the light going to the interferometer at the point shown in Figure 4.1, we found that the input light was in fact shot noise limited as shown in Figure 4.2. When the light was allowed to be incident on the interferometer, the signal on the photo-detector would periodically rise sharply above

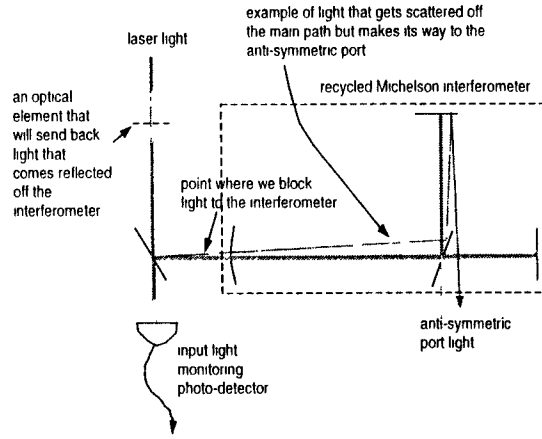


Figure 4-1: Figure showing where we put a photo-detector to monitor back-scattered light, an extra beam scattered off the main beam to interfere with the phase signal is also shown

the shot noise level, as shown in Figure 4.3, usually around the time of increased seismic activity. This is because a small portion of the light reflected off the interferometer is sent back along with the input light by a reflector in the input optics chain. The amplitude of this additional field can be written as,

$$[r' J_0' E_m + 2v' J_1' E_m \cos(\omega_m t + \phi_s)] \cdot e^{i\phi_c}, \quad (4.14)$$

where r' equals the products of the reflectivities of the interferometer and the back-scatterer, J_0' represents the changed modulation index in the reflected light, and ϕ_c , are the extra carrier and sideband phases respectively that this light acquires with respect to the input light owing to its extra path of travel. The modulation index is unchanged in the case of the unrecycled PNI unless the light travels through the phase modulator; however, in the case of the recycled PNI, the modulation index is affected by the differing reflectivities of the carrier and the sidebands. This light then interferes with the input light to produce a signal at the modulation frequency of

$$4r' |E_m|^2 \cdot [J_0' J_1 \cos(\omega_m t) - J_1' J_0 \cos(\omega_m t + \phi_s)] \cdot \sin \phi_c, \quad (4.15)$$

The quantity ϕ_c contains the effect of the changes in the extra travel path — this path is modulated as the reflecting surface of the interferometer or the reflector in the input optics chain shakes. If either of these is excited as $A \cos(\omega_r t)$, then we obtain $\sin \phi_c = \sin(\phi_0 + 2kA \cos(\omega_r t))$; hence, the frequency of the signal in expression (4.15) drops to a maximum of $(2A/\lambda)$ where λ is the wavelength of light. Thus the spectrum shows a sudden drop at a maximum frequency as evident in Figure 4.3. The level of the spectrum is set by the expression multiplying $\sin \phi_c$ — as can be seen from expression (4.15), if the modulation index is unchanged as in the unrecycled PNI, a modulation frequency can be chosen so that ϕ_s is a multiple of 2π and the signal forced to disappear. If there are more than one scatterer, we will obtain a sum of expressions

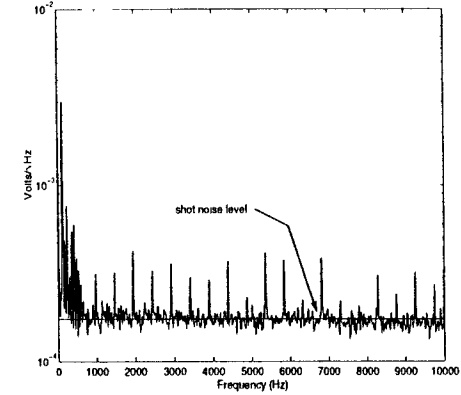


Figure 4-2: Input light intensity noise around the phase modulation frequency — as shown, it is quantum noise limited to about 100 Hz

of the form of 4.15 for each scatterer. It is clear that this “parasitic” interference can be diminished by reducing the reflectivity r' , or, alternatively, restricted to low frequencies by lowering the amplitude of vibration of the reflectors with respect to each other.

The input light amplitude given by 4.13 converts to that of

$$iJ_0 E_{b_s} \delta_0 + 2iJ_1 E_{b_s} \sin(\delta_1) \sin(\omega_m t + \phi_D) + 2J_1 \delta_0 E_{b_s} \cos(\omega_m t + \phi_D) \quad (4.16)$$

at the anti-symmetric port, where δ_0 is determined by the Michelson differential phase ($\delta_0 = (1/2) \cdot \Delta\phi$) and the contrast defect ($2\delta_0^2 = \epsilon/d$), and $\delta_1 = (\omega_m/c) \cdot (l_2 - l_1)$, while ϕ_D contains the time delay owing to travel to the dark port from the input to the interferometer. As discussed before, E_{b_s} is the same as the input field E_m in the unrecycled PNI, but amplified by the recycling field gain at the second stage of the PNI. The modulation index also needs to be multiplied by g_r at the second stage. The extra field owing to back scattering shows up with amplitude

$$r' E_{b_s} [iJ_0' \delta_0 + 2iJ_1' \sin(\delta_1) \sin(\omega_m t + \phi_s + \phi_D) + 2J_1' \delta_0 \cos(\omega_m t + \phi_s + \phi_D)] \cdot e^{i\phi_c}. \quad (4.17)$$

Thus a spurious signal is obtained at the modulation frequency, equal to

$$2r' (\Delta\phi) \sin(\delta_1) |E_{b_s}|^2 [J_0' J_1 \sin(\omega_m t + \phi_D) + J_0 J_1' \sin(\omega_m t + \phi_D + \phi_s)] \cos(\phi_c) \\ + 4r' \delta_0^2 |E_{b_s}|^2 [J_0' J_1 \cos(\phi_c) \cos(\omega_m t + \phi_D) + J_1' J_0 \sin(\phi_c) \cos(\omega_m t + \phi_D + \phi_s)]. \quad (4.18)$$

With a big excitation of the path making up ϕ_c , we obtain a spectrum similar to the one discussed before with respect to the input light monitoring photo-detector; Figure 4.4 shows such a spectrum obtained for

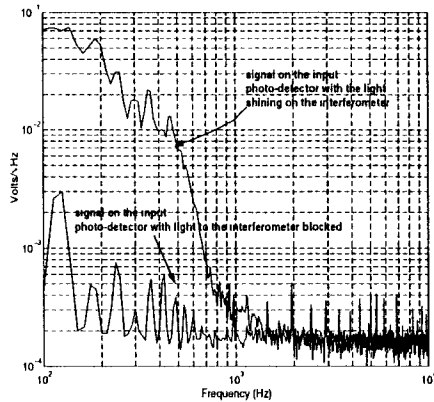


Figure 13 Signal on the input light monitoring photo-detector

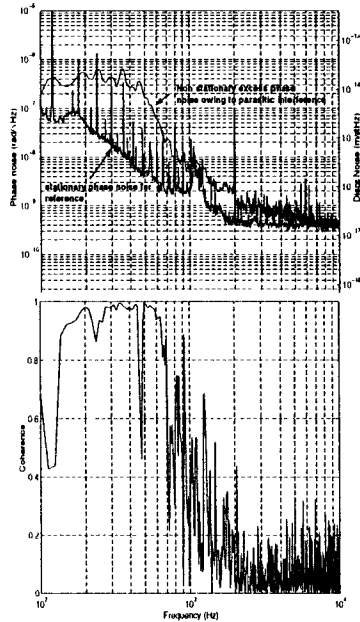


Figure 44 Effect of a large excitation of a back scatterer on the phase noise of the recycled PNI; the coherence shown is the one obtained with the signal picked up by an input light monitoring photo-detector

the increased phase noise at the anti-symmetric port for the recycled PNI. The lower figure shows the phase coherence of the anti-symmetric signal with the signal obtained at the input light photo-detector (this quantity is the projection of one signal on the other — if one is entirely due to the other, then we obtain a value of 1, otherwise, a value less than 1 is obtained), we observe that the additional light making its way to the anti-symmetric port can account for the increased noise upto 2 kHz. This kind of coherence was non-stationary, however, and required big excitations which would cause the scatterer to vibrate through many wavelengths. We can see some influence of this noise in the spectra of the unrecycled PNI also, as indicated in Figure 4 5

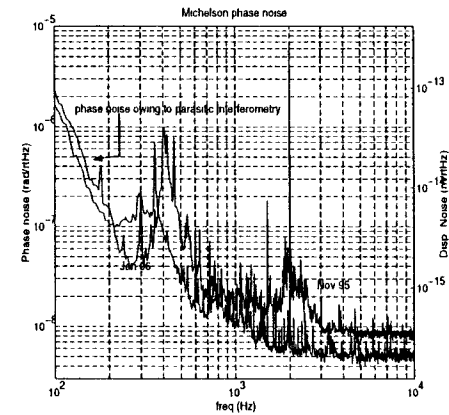


Figure 4 5 Influence of back scattering on the phase noise of the unrecycled PNI

The path ϕ_i , when disturbed by big excitations, led to signals that were coherent in both the input light and the anti-symmetric output as shown in Figure 4 4. When the excitations were less and probably via stationary sources like ambient acoustics, the modulation of ϕ_i could still cause phase noise, but coherence with the input light signal would not necessarily be obtained (since one is proportional to $\sin \phi_i$ and the other to a complicated superposition of $\sin \phi_i$ and $\cos \phi_i$). Thus, when ϕ_i excitations were small and no coherence was observed with the signal at the input light photo-detector, back scattering as a way of adding stationary phase noise to the detected signal at the anti-symmetric port could not be ruled out — in fact, addition of an extra Faraday isolator (reported by Mr. Lantz and Dr. Gonzalez) in later experiments seemed to have reduced the phase noise in the stationary spectrum shown in Figure 2 16 by a factor of about 3 from 400 Hz to a kHz.

In Figure 4 1 we show a beam that is scattered off the main path at an angle to recombine back at the dark port photo-detector. The noise owing to this beam is added to the phase noise exactly the way we have just described, with necessary adjustments of J'_0 , J'_1 , r' , and E . If the length of the path taken by the beam is quite different from the main one, ϕ_c can be dominated by frequency noise — especially, if

the surface scattering back the light onto the photo-detector is not subject to large vibrations. Also, from Equation 1.18, we notice that this noise can come at the modulation frequency with a different phase than the signal we are trying to measure, hence, we can reject this noise by properly adjusting the phase of the local oscillator. We indeed observed such increased phase noise above 2 kHz, coherent with the common mode error signal, if the local oscillator was not optimally set for the anti-symmetric output.

4.4 Instrumentation noise

4.4.1 Amplitude modulation by Pockels cell

The polarization of the laser beam needs to be aligned with the birefringent axis of the electro-optic crystal for pure phase modulation — misalignment leads to amplitude modulation at that frequency. The Pockels cell that we used for the PNI had Brewster entry and exit windows (a PM-25 from Gsänger) — these windows also needed alignment with the crystal. For a phase modulation index of $\Gamma = 1$, we measured an AM depth of 4×10^{-6} at the modulation frequency.

Referring to Equation 2.8, we notice that the amplitude modulation at radio-frequency comes multiplied with P_i in every term, however, the amplitude modulation comes as $RIN \cdot \cos(\omega_m(t - t_c))$ which is in quadrature to the term carrying the phase signal ($\Delta\phi$). This helps us reject the low frequency terms in Equation 2.8 that would have otherwise come at the modulation radio-frequency multiplied by the AM, and competed with the measured phase.

4.4.2 Noise in the differential length sensing and control loop

The photo-detector used at the dark port of the PNI produced current noise (primarily owing to the thermal noise of its real impedance, and pre-amplifier input noise) with a flat power spectral density of 1.06×10^{-11} amp/ $\sqrt{\text{Hz}}$ — this is equivalent to the quantum noise produced by 0.35 ma of photo-current. The photo-current at the dark port during the unrecycled stage of the PNI was measured to be 0.26 ma for the November 95 spectrum and 0.66 ma for the January 96 spectrum (Figure 3.1); thus, during the unrecycled stage, the quantum noise in the photo-current measured was quite close to the dark noise in the photo-detector. In the second recycled stage of PNI, the dark port photo-current was 11 ma, producing quantum noise significantly above that owing to the photo-detector.

The coils of each of the OSEM units produced a force of 0.05 N/amp — if we used a resistor R to convert a voltage to current in these coils, we could expect a Johnson noise of $\sqrt{(4kT)/R}$ amp/ $\sqrt{\text{Hz}}$ which then would produce a displacement noise in the mirror of

$$x(f) = \frac{1}{(2\pi f)^2 m} \sqrt{\frac{4kT}{R}} (0.05 \text{ N/amp}) \text{ m}/\sqrt{\text{Hz}}. \quad (4.19)$$

Efforts were taken to make sure that the feedback control loop did not produce noise above that produced by the Johnson noise of a 2k resistor: with the displacement noise in the two Michelson mirrors added in quadrature, we obtained a phase noise power spectral density of

$$5 \times 10^{-11} \cdot \left(\frac{100 \text{ Hz}}{f}\right)^2 \text{ radian}/\sqrt{\text{Hz}} \quad (4.20)$$

which then was below the sensitivity we attempted to measure.

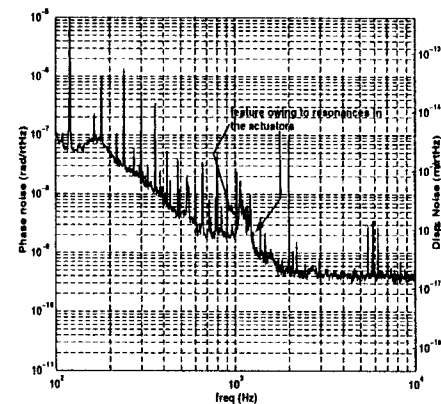


Figure 4.6: A feature in the phase noise measured with the recycled PNI that could be attributed to resonances in the actuators.

Though attempts were made to make the coil and magnet actuator have a constant current to force conversion at all frequencies of interest, the actuator did end up having resonances that caused displacement noise in the measured bandwidth. In Figure 4.6, we show a feature in the measured phase noise spectrum that could be attributed to this kind of resonance. The resonant system was defined by the magnet pieces and the glue with which they were attached to the mirror. As this system was thermally excited, the measured phase noise was consistent with the recoil motion of the mirror.

Chapter 5

Final Remarks

This chapter will attempt to summarize the results of this thesis and their implications. The aim of the work was to investigate the noise sources that come along with the use of light to read the phase difference of a Michelson interferometer. The phase difference is caused by the change of one arm length of the interferometer with respect to the other. The change in length is converted to an optical phase, which then gets measured as a light level at the output of the interferometer. Chapter 1 showed that the change attributed to gravitational waves can be monitored if the changes caused by other sources are kept small — thermal and seismic excitations cause the arm lengths to vary, and constitute “displacement” noise that directly competes with the signal from gravitational waves. The use of light for “readout” causes additional noise — as the measured phase may not be owing to a change in arm lengths but because of change in frequency, or the varying light level at the interferometer output may be due to the fluctuations of light intensity or because light adds its own quantum noise in its detection. Scattered light recombined with the interferometer output at the dark port will also cause spurious signals that compete with the phase to be detected. We will look at the PNI spectrum in its two stages in this chapter and discuss what we learnt about this “readout” noise. Next, we will revisit the LIGO noise estimate discussed in Chapter 1, and show what our experimental results imply.

5.1 The PNI spectra

Figure 5.1 shows the different noise sources at different frequencies in the unrecycled Michelson interferometer. Above 3 kHz, the noise asymptotes to a level that is given by three noise sources added in quadrature: the quantum noise in light, the residual frequency noise, and the dark noise in the photo-detector (which refers to the thermal noise of the photo-diode and the pre-amplifier noise added in quadrature). These three noise sources, converted to an equivalent phase noise power spectral density, show different scalings with the input light power P — while the frequency noise contribution is a constant, the photo-detector dark noise gets reduced as $1/P$, and the quantum noise as $1/\sqrt{P}$. The two spectra show the low and high power limits, at low powers (I_{max} of about 20 mA), the photo-detector dark noise dominates while at high powers (I_{max} of about 65 mA), the frequency noise contribution becomes the limiting noise.

Between 300 Hz and 1.5 kHz in the Jan 96 spectrum, and upto 3 kHz in the Nov 95 spectrum, input beam jitter, through a bilinear coupling with the differential misalignment of the Michelson mirrors, was

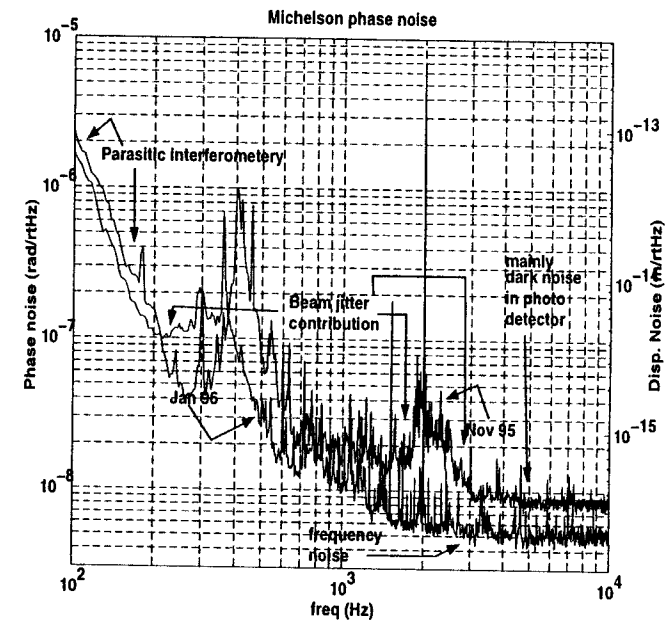


Figure 5.1 Unrecycled Michelson interferometer spectra showing the dominant noise sources at different frequencies

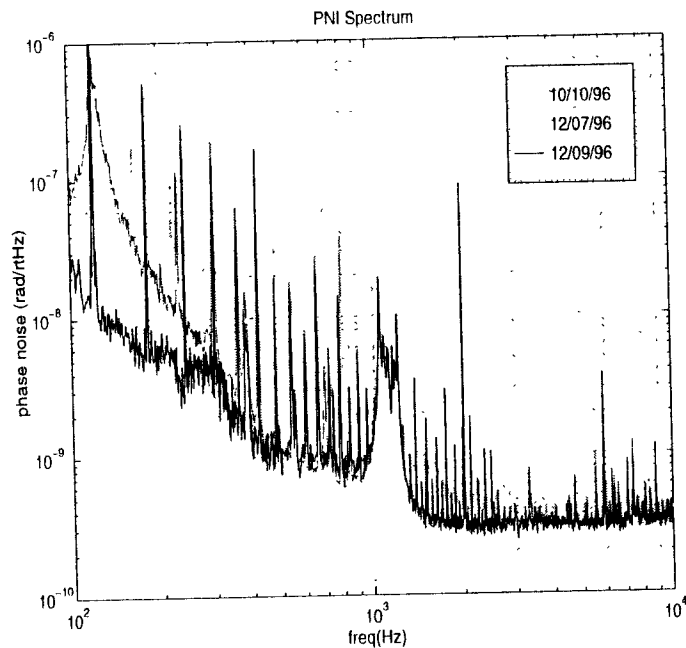


Figure 5-2: Two recent and improved recycled PNI spectra compared with the one analyzed for this thesis

the main contributor of phase noise. Acoustic shielding and damping of the resonances of the optical elements at the input to the interferometer helped in reducing the beam jitter above 1.5 kHz and between 300 and 500 Hz — this caused the improvement in the Jan 96 spectrum over the one of Nov 95. Parasitic interferometry, as discussed in Chapter 4, caused by back scattering of the light returned to the symmetric port, brought the phase noise up sharply below 200 Hz.

Analysis of the noise below 2 kHz detected at the dark port of the recycled PNI was more complicated because a number of noise sources were involved at the same time. The spectrum that was analyzed for this thesis, taken on Oct 10 96, did not clearly show any dominant noise source as discussed; however, subsequent work by Lantz and Gonzales improved the spectrum and elucidated which noise sources must have been at work. We show two recent and improved spectra in Figure 5-2 along with the one analyzed for the thesis. The improvement shown in the spectrum of 12/07/96 (a factor of 3 reduction in the phase noise between 200 Hz and 1 kHz) followed from a lower contrast defect (most probably from better alignment of the interferometer), and an extra Faraday isolator included in the input optics chain. At this stage, the spectrum showed coherence with the common mode error signal below 400 Hz. This spectrum also shows quantum limited noise from around 1.1 kHz at a level slightly lower than the spectrum of Oct 10 because of a better contrast. Thus back scattering of light must have contributed significantly to the phase noise

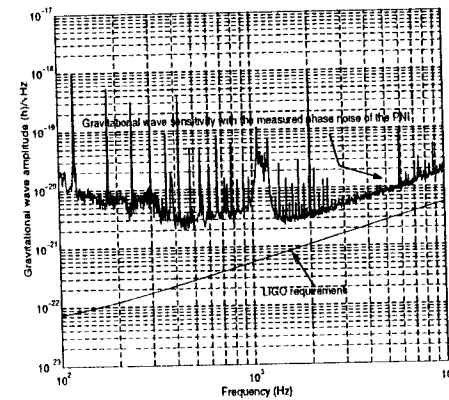


Figure 5-3: The PNI phase noise compared to the LIGO requirement

of Oct 10 below 2 kHz. No detailed analysis of the spectrum of 12/07 has been carried out — however, apart from the resonant feature from the actuators around 1 kHz (as discussed in Chapter 4), the excess noise from 400 Hz to 1.1 kHz can be suspected to be mainly from input beam jitter. The limiting noise, ultimately, will be the contribution from residual frequency noise. The improvement in the spectrum of 12/09/96 followed from an extra 10 dB of frequency noise suppression (implemented by Lantz) from 100 Hz to 400 Hz.

5.2 Implications for LIGO

Figure 5-3 shows the sensitivity of the LIGO interferometer if its dark port noise was limited to the noise measured with the recycled PNI, in the bandwidth where “readout” noise is expected to dominate (the spectrum of 12/09 has been used). At frequencies above 1.1 kHz, the phase noise is about 3×10^{-10} radian/ $\sqrt{\text{Hz}}$ instead of the 1×10^{-10} required by LIGO; below 1.1 kHz, the deviation is explained by technical noise sources as described in the last section. Though not exactly according to the LIGO requirement, the phase noise measured — consistent with above 30 watts of light incident on the beam-splitter — is better than any known measurement known until now. The Garching group [6] showed a phase noise consistent with 730 milliwatts at the beam-splitter, and the 40 meter prototype — at its best sensitivity [11] — only had 150 milliwatts at the splitter. A better contrast (through the use of mirrors with better surface figure than the ones used in the PNI), or a higher modulation index will allow the high frequency spectrum to approach the LIGO goal. If higher modulation index is preferred, a photo-detector capable of handling high light powers (without saturating or becoming non-linear) must be used — also, more power at the input should be available. LIGO is currently developing photo-detectors capable of handling high light powers (the recycled PNI dark port photo-detector had to handle somewhere between 7 to 11 ma of photo-current,

close to the limits of linearity in the detector used)

LIGO has recently decided to use Nd YAG lasers instead of the green Ar⁺ laser used for the PNI. To achieve the required phase noise sensitivity above 1 kHz, LIGO then needs twice the input power. It seems that such high powers are indeed possible with the solid state lasers — but photo-detectors capable of handling higher light levels become imperative. Below 1 kHz, the excess noise, as we discovered, was mostly due to back scattering, residual frequency noise, and input beam jitter. The problem of back scattering will require high quality Faraday isolators with wedged surfaces. The frequency noise of Nd YAG lasers seems to be a factor of 100 better than the Ar⁺ gas lasers [28], hence the required frequency noise suppression will be easily obtained. The input beam direction will also be actively controlled with the wavefront sensors described before, hence the input beam jitter should not be a problem for LIGO.

In summary, the recycled PNI results are encouraging for LIGO. The required phase noise sensitivity will be obtained if — as planned — a photo-detector capable of handling high powers is developed, better Faraday isolators are used to reduce back scattered light, and a switch to the new laser is carried out so that control of frequency noise does not require a complicated servo design.

Appendix A

The Michelson Interferometer as an Optical Element

The purpose of this Appendix is to present the Michelson interferometer as an optical element with frequency dependent field reflectivity and transmission. This approach is useful because phase modulation by a Pockels cell results in a number of fields at (sideband) frequencies spaced by harmonics of the modulation frequency from the main (carrier) frequency of laser light. The Michelson interferometer then reflects and transmits these fields with its corresponding (frequency dependent) field coefficients. The measurement of power at the dark port leads to mixing of the transmitted fields, producing signal at different beat frequencies. A slightly different approach than that taken in the text is thus presented — one that easily ties in with the frequency selective nature of optical cavities.

Referring to Figure A, we assume that the field E_i has been phase-modulated by a Pockels cell, if we have light $\mathcal{E}e^{i(\omega t)}$ incident on the Pockels cell, the light that exits the Pockels cell (and is phase modulated by it) may be written as

$$\begin{aligned} \mathcal{E}e^{i(\omega t + \Gamma \cos(\omega_m t))} &= \mathcal{E}e^{i(\omega t)} \left[J_0(\Gamma) + 2 \sum_{k=1}^{\infty} (-)^k J_{2k}(\Gamma) \cos[2k\omega_m t] \right. \\ &\quad \left. + 2i \sum_{k=0}^{\infty} J_{2k+1}(\Gamma) \cos[(2k+1)\omega_m t] \right] \end{aligned}$$

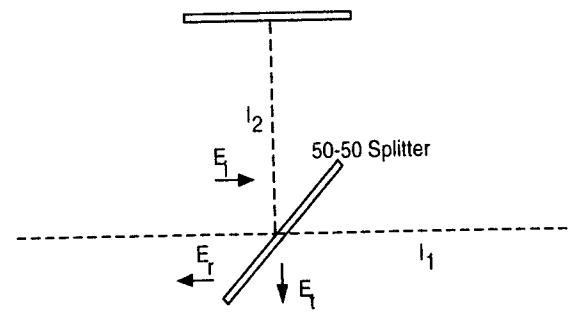


Figure A 1 The Electric fields relevant to a Michelson Interferometer

$$= \mathcal{E}e^{i(\omega t)} \{ J_0(\Gamma) + iJ_1(\Gamma)(e^{i\omega_m t} + e^{-i\omega_m t}) - J_2(\Gamma)(e^{2i\omega_m t} + e^{-2i\omega_m t}) + \dots \},$$

where we have kept terms upto twice the modulation frequency. The above expression clearly shows how various frequencies are created by phase modulation. We will index the displayed five frequencies in E_i as E_i^k where k is one of $-2, -1, 0, 1, 2$; e.g., $E_i^{-2} = -J_2(\Gamma)e^{-2i\omega_m(t-t_{tr})}\mathcal{E}$, where t_{tr} refers to the time of transit to the beam-splitter. Note that we have omitted $e^{i(\omega t)}$ as this is common to all fields, and drops out when the field expressions are converted to an expression for light power, the quantity that is actually measured.

Consider the reflected and transmitted fields of the Michelson interferometer — E_r^k and E_t^k respectively, as shown in Figure A. If k also indexed the frequency of the fields (i.e., $\omega_0 = \omega$, $\omega_{\pm 1} = \omega \pm \omega_m$, etc.), we may write the following relation between the fields

$$E_r^k = \frac{1}{2}E_i^k \left(e^{-\frac{2i\omega_k t_1}{c}} + e^{-\frac{2i\omega_k t_2}{c}} \right), \tag{A.1}$$

and

$$E_t^k = \frac{1}{2}E_i^k \left(e^{-\frac{2i\omega_k t_1}{c}} - e^{-\frac{2i\omega_k t_2}{c}} \right). \tag{A.2}$$

Let us define $\alpha_k = \frac{\omega_k(t_1+t_2)}{c}$, and $\delta_k = \frac{\omega_k(t_1-t_2)}{c}$. Then the above equations can be recast as

$$E_r^k = E_i^k e^{-i\alpha_k} \cos(\delta_k), \tag{A.3}$$

$$E_t^k = -iE_i^k e^{-i\alpha_k} \sin(\delta_k) \tag{A.4}$$

Thus the Michelson after the beam splitter can be considered to have a field reflection coefficient of $e^{-i\alpha_k} \cos(\delta_k)$ and a field transmission coefficient of $-ie^{-i\alpha_k} \sin(\delta_k)$. We see that the ϕ in Equation 2.1 corresponds to $2\delta_0$. To derive Equation 2.1 we have to observe that $P_{out} = (E_t^0)^* E_i^0$. To obtain Equation 2.8, we have to assume that δ_0 is small (and equal to $(\Delta\phi)/2$) and hence $\delta_{\pm 1,2}$ are dominated by terms involving ω_m and the asymmetry. We next have to add the $k = 0$ and $k = 1$ fields and multiply by the complex conjugate of the sum, we would then notice that Equation 2.12 is given by

$$2P_i J_0(\Gamma) J_1(\Gamma) \sin[\omega_m t_{\Delta}] (\Delta\phi) \tag{A.5}$$

For $\Gamma \ll 1$, $J_0(\Gamma) \approx 1$ and $J_1(\Gamma) \approx \frac{\Gamma}{2}$; substituting these values, we retrieve the form of Equation 2.12

Appendix B

The Fabry Perot Cavity: Optical Parameters and Resonance

We will derive expressions for optical cavity parameters in this appendix: the reflectivity, the transmission, and the gain in field strength inside the cavity compared to the incident external field that illuminates it. We will introduce the concept of resonance, and show how these expressions simplify in resonant low loss cavities. Finally, we will discuss the Pound-Drever technique for holding optical cavities on resonance.

We will use the geometry of the optical cavity as shown in Figure B.1 for our discussion. Examining the left ‘input’ mirror and choosing the sign for the field reflectivity of the interface between air and mirror coating to be negative, the incident fields, E_x and E_b , and the ones leaving it, E_r and E_f , must obey:

$$E_r = t_1 E_b + r_1 E_x, \tag{B.1}$$

$$E_f = t_1 E_x - r_1 E_b$$

Here t_1 and r_1 are the transmission and reflectivity of the mirror for the electric field. For mirrors with no loss, $|r|^2 + |t|^2 = 1$. The right hand ‘back’ mirror in Figure B.1 similarly stipulates

$$E_r' = t_2 E_f' + r_2 E_x', \tag{B.2}$$

$$E_b' = t_2 E_x' - r_2 E_f'$$

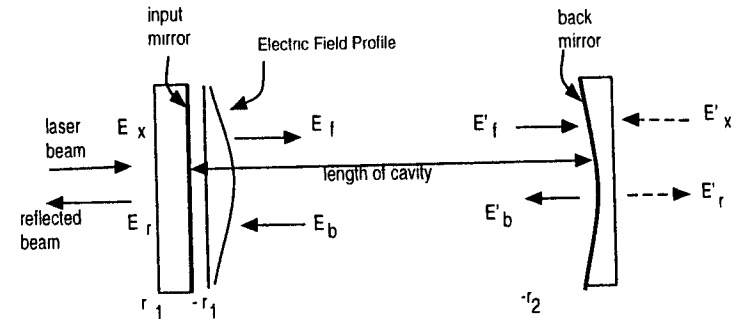


Figure B.1 A Fabry-Perot cavity and the relationship among its fields

For this formulation, let us assume that E'_x is non-existent. Then Equations B 2 simplify to $E'_b = -r_2 E'_f$. For the curved back mirror, r_2 is a complex function in x and y capturing the change in amplitude and phase of the field reflecting off the mirror surface.

The field E'_f as shown in Figure B 1, is E_f after propagation in space over the length L of the cavity. This may be expressed, assuming paraxial propagation, as ¹

$$E'_f(x, y) = \mathbf{FT}^{-1}_{[x, y]} \left[\exp(-ikL + i \frac{(k_x^2 + k_y^2)L}{2k}) \times \mathbf{FT}_{[k_x, k_y]}[E_f(x, y)] \right] \quad (\text{B } 3)$$

In the above equation, λ is the wavelength of light, $\mathbf{FT}_{[k_x, k_y]}[\mathcal{E}]$ represents the 2-dimensional Fourier Transform of the field \mathcal{E} resulting in a function in k_x and k_y , and $k = 2\pi/\lambda$. We notice that free space propagation mainly involves the change in phase of the Fourier amplitudes at the different spatial frequencies (k_x, k_y).

We will represent free space propagation over a length L by the action of an operator $\mathbf{K}(z = L)$ or simply \mathbf{K} , $E'_f = \mathbf{K}E_f$. It should be clear from Figure B 1 that E_b is related to E'_b in exactly the same way — via a free space propagation over distance L . $E_b = \mathbf{K}E'_b$. Since $E'_b = -r_2 E'_f$, we have $E_b = -\mathbf{K}r_2 \mathbf{K}E_f$. Now Equations B 1 give us

$$E_f = t_1 E_x + r_1 \mathbf{K}r_2 \mathbf{K}E_f \quad (\text{B } 4)$$

This is the steady-state field equation. Now $U \equiv (r_1/r_1) \mathbf{K}(r_2/r_2) \mathbf{K}$ is a unitary operator with eigenmodes and eigenvalues which, if the field E_f is resolved into, simplifies the above problem considerably. If the mirrors are spherical, then the eigenmodes are the Hermite-Gaussian modes which find extensive description in all laser textbooks [29]. In that case, the eigen-value of the operator U happens to be $e^{-2ikL + i\psi_G}$, where ψ_G refers to the Guoy phase that depends on the particular mode chosen. Writing $\psi \equiv -2kL + \psi_G$ and assuming that r_1 and r_2 stand for the amplitudes of the corresponding quantities, we thus can solve for E_f

$$E_f = \frac{t_1 E_x}{1 - r_1 r_2 e^{i\psi}}. \quad (\text{B } 5)$$

The reflected and transmitted fields are E_r and E'_r respectively and these are — from Equations B 1 and B 2 before —

$$E_r = \frac{r_1 - (r_1^2 + t_1^2) \cdot r_2 e^{i\psi}}{1 - r_1 r_2 e^{i\psi}} E_x, \quad (\text{B } 6)$$

and

$$E'_r = \frac{t_1 t_2 e^{i\psi/2}}{1 - r_1 r_2 e^{i\psi}} E_x. \quad (\text{B } 7)$$

By dividing out the expressions (B 6) and (B 7) by E_x , we get the field reflectivity and transmittance for an optical cavity. By dividing out E_x in Equation (B 5), we obtain the field gain inside the cavity. The denominators of these expressions depend on the values of r_1 and r_2 — if these values are close to 1, then for ψ equal to a multiple of 2π , the denominators get very small while the expressions for (B 5), (B 6), and (B 7) become quite large, a condition termed resonance.

In ψ , we capture the source of change in reflectivity, transmittance, and (internal field) gain with the change in the length of the optical cavity, or the change in frequency of the laser. For example, if the optical

cavity is resonant, every change of $\lambda/2$ in the length of the cavity or, equivalently, every change of $c/(2L)$ (the full spectral range, or fsr) in the frequency of laser will make it resonant again. Let us write the light intensity transmission of an optical cavity in terms of the maximum transmission ($T_{\max} = (t_1^2 t_2^2)/(1 - r_1 r_2)^2$) and the detuning of ψ from resonance.

$$T = \frac{T_{\max}}{1 + (2\mathcal{F}/\pi)^2 \sin^2(\psi/2)} \quad (\text{B } 8)$$

The expression, \mathcal{F} is thus defined as,

$$\mathcal{F} = \frac{\pi \sqrt{r_1 r_2}}{1 - r_1 r_2}. \quad (\text{B } 9)$$

What finesse signifies is easy to understand as the value it takes becomes much larger than 1 — in that case the denominator of Equation B 8 reaches a value of 2 for very small values of $\sin(\psi/2) \approx \psi/2$. If we plotted the intensity transmission as a function of the frequency of light, we would see that it drops from a maximum to half that value when the frequency changes Δf — half of the Full Width at Half Maximum (FWHM) value. From the relationship between ψ and the frequency of light, we can easily show that,

$$\mathcal{F} = \frac{\text{fsr}}{2\Delta f}. \quad (\text{B } 10)$$

Thus, given a fixed length of the cavity, the higher the finesse, the narrower the line-width Δf is also referred to as the pole frequency of the cavity in the same approximation (i.e. when $\mathcal{F} \gg 1$), and the storage time of the cavity is defined as $\tau_s = 1/(4\pi\Delta f)$.

When we assume high finesse optical cavities at resonance, a number of simplifications are possible in the formulas given so far. The smaller the fraction of power lost in one round trip of light inside the cavity, the more accurate are these simplified formulas. We assume the delta notation of Siegman [30] in somewhat different way. $T_1 \equiv t_1^2 \equiv \delta_1$, $T_2 \equiv t_2^2 \equiv \delta_2$, and we also assume a fraction of power scattered off the beam inside the cavity, δ_0 , in any kind of optical pick-off, etc. It is then easily shown that, our expressions for (B 5), (B 6), and (B 7) become:

$$\frac{E_r}{E_x} = \frac{\delta_2 + \delta_0 - \delta_1}{\delta_2 + \delta_0 + \delta_1} \quad (\text{B } 11)$$

$$\left| \frac{E_f}{E_x} \right| = \frac{2\sqrt{\delta_1}}{\delta_2 + \delta_0 + \delta_1} \quad (\text{B } 12)$$

$$\left| \frac{E'_r}{E_x} \right| = \frac{2\sqrt{\delta_1 \delta_2}}{\delta_2 + \delta_0 + \delta_1} \quad (\text{B } 13)$$

There is distinction made between the input mirror indexed 1 and facing the incident external light and the output mirror indexed 2 which transmits the light inside the cavity. If $\delta_2 + \delta_0 \gg \delta_1$ the cavity is called undercoupled because the internal field strength is (most probably) smaller than that of the incident field strength, as is obvious from Equation B 12. If $\delta_2 + \delta_0 = \delta_1$, we have a critically coupled optical cavity, since the reflectivity drops to 0 while transmission is maximized. Finally, when $\delta_2 + \delta_0 \ll \delta_1$, we have an overcoupled cavity where the field reflectivity becomes negative but reaches unity again and the internal field builds up to high levels (the power gain = $4/\delta_1$). It is clear that the formulas for finesse and storage time also simplifies accordingly.

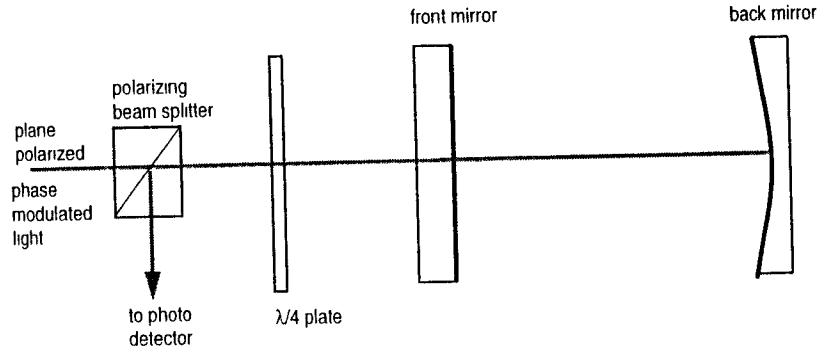


Figure B 2 Optical layout for The Pound Drever reflection lock of optical cavities

The Pound Drever Scheme of ‘locking’ optical cavities on resonance will now be briefly introduced. The optical layout for the implementation of this scheme appears in Figure B 2

A phase modulator is used to modulate light before illuminating the optical cavity. As derived before (Equation A.1) phase modulated light at the input of the optical cavity may be written as:

$$\mathcal{E}_e^{i(\omega t + \Gamma \cos(\omega_m t) + \phi)} = \mathcal{E}_e^{i(\omega t + \phi)} [J_0(\Gamma) + 2iJ_1(\Gamma)\cos(\omega_m t) + \dots], \quad (B 14)$$

where we have kept only the terms first order in Γ (small Γ approximation). Using the expression that we derived for the reflected field (Equation B 6), and assuming the delta notation can be used, the (field) reflection coefficient of an optical cavity on resonance varies with small changes of ψ as

$$r = \frac{\delta_0 + \delta_2 - \delta_1}{\delta_0 + \delta_2 + \delta_1} - \frac{4\delta_1}{(\delta_0 + \delta_2 + \delta_1)^2} (i\psi), \quad (B 15)$$

or simply $r = r_R + r_{Im}\psi$. The frequency ω_m is selected to be a radio-frequency outside the line FWHM of the optical cavity so that — if the carrier is resonant — the side band frequencies are not. Thus the field reflected off the optical cavity may be written as,

$$\mathcal{E}_r^{i(\omega t + \phi)} [r_R J_0(\Gamma) + i(2J_1(\Gamma)\cos(\omega_m t) + r_{Im} J_0\psi)] \quad (B 16)$$

A photo-detector as shown in Figure B 2 is used to look at the intensity of the reflected light, thus, taking the amplitude square of the field expression (B 16), we obtain

$$|\mathcal{E}|^2 [r_R J_0]^2 + 2J_1^2 + 2J_1^2 \cos(2\omega_m t) + 4J_1 J_0 r_{Im} \cos(\omega_m t)\psi]. \quad (B 17)$$

We notice that the term at radio-frequency ω_m is modulated by ψ that can be extracted by a down conversion process as explained in the text before with respect to a Michelson interferometer. The slowly varying terms in the above terms give rise to shot noise — thus, given the calibration $4\mathcal{E}^2 J_0 J_1 r_{Im}$, we can find out the fundamental noise limited detection sensitivity of deviation ψ from resonance

Appendix C Feedback Control Systems

It is hard to describe feedback control systems with all their subtleties in a few pages. The purpose of this short description will therefore be to introduce the jargon that goes with these systems since it appears sprinkled through the text of the thesis.

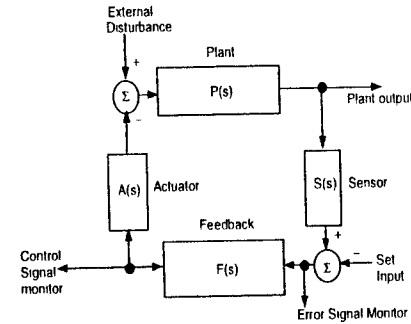


Figure C 1 A Block diagram of a Feedback Control System

The purpose of the feedback control systems used in our work was primarily to hold a interferometric system at some desired operating point — e.g., the Michelson interferometer at a dark fringe or a Fabry-Perot cavity on resonance. Let us take an interferometric system therefore — the Michelson interferometer for example — to illustrate the correspondence between what happens in the interferometer and where it fits in the block diagram in Figure C 1. The mirrors, and the beam-splitter of the interferometer (refer Figure 2.3) are disturbed from their positions by seismic activity and the resulting displacement noise, labeled “External Disturbance”, then enters a summing junction indicated by Σ on the top left corner of the block diagram. The “Plant” is our Michelson interferometer which converts the length disturbance into a phase difference, and then into a power fluctuation at the dark port of the interferometer (details of this process have already been presented in Chapter 2). The photo-detector at the dark port is our “Sensor” which picks-up the power fluctuation and converts it into a measured voltage. We can decide to hold the Michelson interferometer at a dark fringe, or any fraction of the bright fringe, this is set by an external input at the summing junction, Σ , in the bottom right corner of Figure C 1. Finally, the difference between

our set input and the actual state of interference (the error signal) is amplified and filtered by additional electronics forming the "Feedback" path to an actuator — where actuator refers to a device that converts an electric signal to physical motion, like the coils that exert force on the little magnets glued on the mirrors in our actual experiment. The actuator thus pushes one of the mirrors to counter the phase difference caused by the "External Disturbance". We now arrive at the summing junction where we started. The signal that feeds the actuator is known as the control signal.

The different boxes, $P(s)$, $S(s)$, $F(s)$, and $A(s)$ represent the filtering and change of units that happen at each stage described in the paragraph above. Let us define $G(s) = P(s) \cdot S(s) \cdot F(s) \cdot A(s)$. Assume that the seismic disturbance correspond to a length change of l_d , which, through the plant and sensor, appears as voltage, v_d . If our set voltage is v_s , we can show easily that the error signal monitor will show:

$$\text{Error monitor} = \frac{v_d - v_s}{1 + G}, \quad (C.1)$$

while the output of the Actuator $A(s)$ will be $G \cdot l_d / (1 + G)$ and the control monitor will read:

$$\text{Control monitor} = \frac{G(l_d/A)}{1 + G}, \quad (C.2)$$

where l_d/A is the measure of the displacement in terms of the actuator's electrical input. From the above two equations we notice that higher the Gain G , the less is the error and more faithfully does the actuator follow the disturbance. However, it is impossible to have high gain at all frequencies — mechanical and electronic constraints roll off the gain at high frequencies — thus G equals unity at some frequency, the so called unity gain frequency (u.g.f.). This frequency then gives us a measure of frequencies (bandwidth) over which there is active feedback (servo). It is desirable that G not have a phase of 180° at this frequency — the vanishing denominator of Equation C.1 leads to undesirable instability which often manifests itself in (unity gain) oscillation.

Bibliography

- [1] K. S. Thorne, *300 Years of Gravitation*, p. 330, Cambridge University Press, 1987.
- [2] P. K. Fritschel, *Techniques for Laser Interferometer Gravitational Wave Detectors*, PhD thesis, Massachusetts Institute of Technology, 1991.
- [3] R. Weiss, "Electromagnetically coupled broadband gravitational antenna," *MIT RLE Quarterly Progress Report*, no. 105, pp. 54-72, 1972.
- [4] P. F. Michelson *et al.*, "Ultralow Temperature Resonant-mass Gravitational Radiation Detectors: Current Status and Future Prospects," in *Gravitational Astronomy: Instrument Design and Astrophysical Prospects* (D. E. McClelland and H. A. Bachor, eds.), pp. 11-56, World Scientific, 1991.
- [5] R. Weiss *et al.*, "The MIT Prototype Gravitational Wave Detector," in *Proceedings of Fourth Marcel Grossman Meeting on General Relativity* (R. Ruffini, ed.), p. 591, 1985.
- [6] K. Mäuschberger, A. Rudiger, R. Schilling, L. Schnupp, W. Winkler, and G. Lenchis, "Status of the Garching 30 meter prototype for a large gravitational wave detector," in *International Symposium on Experimental Gravitational Physics* (P. F. Michelson, ed.), pp. 316-321, World Scientific, 1988.
- [7] A. Giazotto *et al.*, "Interferometric detection of gravitational waves: the VIRGO project," in *Gravitational Astronomy: Instrument Design and Astrophysical Prospects* (D. E. McClelland and H. A. Bachor, eds.), pp. 110-135, World Scientific, 1991.
- [8] R. Drever, "Interferometric Detectors For Gravitational Radiation," in *Gravitational Radiation* (N. Deruelle and T. Piran, eds.), pp. 321-338, 1982.
- [9] R. Drever *et al.*, "The Caltech Gravitational-Wave Detector," in *Proceedings of the 10th International Conference on General Relativity and Gravitation* (B. Bertotti, F. de Felice, and A. Pascolunghi, eds.), pp. 930-932, 1984.
- [10] Caltech and MIT, "A Laser Interferometer Gravitational-wave Observatory (LIGO)," Proposal to the National Science Foundation, Dec. 1989.
- [11] A. Abramovici *et al.*, "Improved sensitivity in a gravitational wave interferometer and implications for LIGO," *Physics Letters A*, no. 218, pp. 157-163, 1996.

- [12] J. K. Blackburn, "The Laser Interferometer Gravitational Wave Observatory Project" *Submitted to Proceedings of the Banach semester on Mathematical Aspects of Gravitational Waves*, Warsaw, Poland, Mar. 1996.
- [13] D. Shoemaker and R. Weiss, "Experimental Study of Phase Noise for the Initial Ligo Interferometer" Draft Proposal, Nov. 1992.
- [14] A. E. Siegman, *Lasers*, ch. 17, p. 686. University Science Books, 1986.
- [15] A. E. Siegman, *Lasers*, ch. 17, p. 665. University Science Books, 1986.
- [16] D. G. Blair, ed., *The detection of gravitation waves*, ch. 13, pp. 329-352. Cambridge University Press, 1991.
- [17] P. R. Saulson, "Thermal noise in mechanical experiments," *Phys. Rev. D*, vol. 42, pp. 2437-2445, Oct. 1990.
- [18] J. Graine, P. Saha, D. Shoemaker, and L. Sievers, "A passive vibration isolation stack for LIGO: Design, modeling, and testing," *Rev. Sci. Instrum.*, vol. 67(1), pp. 208-214, Jan. 1996.
- [19] P. Fritschel and G. Gonzalez, "Performance of the Barry Controls, Inc. STACIS active isolation system," tech. rep., LIGO Project, Massachusetts Institute of Technology, July 1995.
- [20] Y. Hefetz, N. Mavalala, and D. Sigg, "Principles of Calculating Alignment Signals in Complex Resonant Optical Interferometers." Submitted to JOSA B.
- [21] D. Sigg, "Wavefront Sensor," tech. rep., LIGO Project, Massachusetts Institute of Technology, July 1996.
- [22] P. Fritschel, P. Saha, and I. Bena, "Optical distortion in Gsanger Pockels cells," tech. rep., LIGO Project, Massachusetts Institute of Technology, Feb. 1994.
- [23] M. E. Zucker, "Transmission of Optical Power Transients by Fabry-Perot Cavities: Laser Power Stabilization and Ringdown Measurement Applications." LIGO Technical Memorandum, Oct. 1990.
- [24] D. Z. Anderson, "Alignment of resonant optical cavities," *Applied Optics*, vol. 23 (17), pp. 2944-2949, Sept. 1984.
- [25] A. Gillespie and F. Raab, "Thermal Noise in the Test Mass Suspensions of a Laser Interferometer Gravitational-wave Detector Prototype," *Phys. Lett. A*, vol. 178, pp. 357-363, 1993.
- [26] A. Gillespie and F. Raab, "Thermally excited vibrations of the mirrors of laser interferometer gravitational-wave detectors," *Phys. Rev. D*, vol. 52(2), pp. 577-585, July 1995.

- [27] P. R. Saulson, ed., *Fundamentals of Interferometric Gravitational Wave Detectors*, ch. 5, p. 77. World Scientific, 1994.
- [28] A. Abramovici and D. S. Shoemaker, "Impact of Replacing Argon Lasers with Nd:YAG Lasers," tech. rep., LIGO Project, Caltech and MIT, Aug. 1995.
- [29] A. E. Siegman, *Lasers*, ch. 16, pp. 642-652. University Science Books, 1986.
- [30] A. E. Siegman, *Lasers*, ch. 11, pp. 428-432. University Science Books, 1986.

LASER INTERFEROMETER GRAVITATIONAL WAVE OBSERVATORY
 - LIGO -
 CALIFORNIA INSTITUTE OF TECHNOLOGY
 MASSACHUSETTS INSTITUTE OF TECHNOLOGY

Document Type	LIGO-P970002-00 - E	2/14/97
Modeling LIGO Data Analysis		
James Kent Blackburn		

Submitted to the
 Proceedings of Computers in High Energy Physics
 April 1997, Berlin, Germany

California Institute of Technology
LIGO Project - MS 51-33
Pasadena CA 91125
 Phone (818) 395-2129
 Fax (818) 304-9834
 E-mail: info@ligo.caltech.edu

Massachusetts Institute of Technology
LIGO Project - MS 20B-145
Cambridge, MA 01239
 Phone (617) 253-4824
 Fax (617) 253-7014
 E-mail: info@ligo.mit.edu

WWW: <http://www.ligo.caltech.edu/>

CHANGE RECORD			
REVISION	DATE	PAGES AFFECTED	ITEM(S) AFFECTED
0	2/14/97	Original Publication	--

Modeling LIGO Data Analysis

James Kent Blackburn^{a,1}

^a *California Institute of Technology
Physics, Math and Astronomy Division
LIGO Project, Mail Code 51-33
Pasadena, CA 91125 U.S.A.*²

The Laser Interferometer Gravitational Wave Observatory (LIGO) will search for direct evidence of gravitational waves emitted by astrophysical sources in accord with Einstein's general theory of relativity. State of the art laser interferometers located in Hanford, Washington and Livingston Parish, Louisiana will unambiguously measure the infinitesimal displacements of inertially isolated test masses which convey the signature of these gravitational waves. The initial commissioning of LIGO will consist of three interferometers operating in coincidence to remove spurious terrestrial sources of noise. These initial LIGO interferometers will search for gravitational wave signatures with very low event rates and low detection signal to noise ratios out to distances as great as 300 million light years. Data will be collected continuously from the three interferometers at rates as high as 16 megabytes per second. Data analysis for LIGO ranges from the extremely simple for the case of intense short duration supernova bursts which will rely on site to site communications to share data used in coincidence, to state of the art parallel and distributed computing utilizing several hundred nodes to detect the chirp signals from neutron star/black hole binary systems, to petaflop computers of the future needed by the all-sky periodic source surveys.

Key words: LIGO; interferometer; gravitational radiation; astrophysics; data analysis; modeling; distributed computing; wide area network

¹ Electronic Address: kent@ligo.caltech.edu

² URL: <http://www.ligo.caltech.edu>

1 Introduction

The Laser Interferometer Gravitational Wave Observatory (LIGO) is presently under joint development by the California Institute of Technology and the Massachusetts Institute of Technology and funded by the National Science Foundation. LIGO's scientific goal is the broadband detection and analysis of gravitational waves of cosmic origin in the tens of hertz to tens of kilohertz region. Understood sources of these waves include coalescing binary systems of neutron stars and black holes, black hole quasi-normal modes, supernovae, pulsars and a stochastic background (the gravitational analog to the microwave background). Beyond these sources await many great surprises as this new class of instrument opens a never before viewed window on the cosmos.

Initially LIGO will be configured as a Michelson interferometers with Fabry-Perot arm cavities and a recycling cavity [1]. The interferometers are being designed to detect RMS motions between the perpendicular arms as small as 10^{-18} meters [2]. To achieve this level of sensitivity, a high power stabilized Nd:YAG laser will provide input to each recycling mirror. All optical components contributing to the sensitivity of the instrument will be suspended as pendula and isolated seismically to reduce coupling to sources of thermal noise and ground motion. The optical path lengths of the interferometer will be maintained by a servo-system, keeping the interferometer phase locked on a particular dark fringe at the gravitational wave port.

LIGO data will be collect from roughly 3600 channels at sampling rates ranging from 2 to 16K samples per second. These channels will compliment the gravitational wave channel with environmental, and housekeeping information. The total data collected from each interferometer is estimated at over 5 megabytes per second. The data will be packed into units called frames which carry a complete representation of the data for one or two seconds. This frame data is archived to tape and directed to the data analysis system, where detection challenges begin.

2 LIGO Data Analysis

Gravitational waves couple to the differential length of the interferometer arms. The signal observed at the gravitational wave port is proportional to this length difference. The amplitude of the signal will depend on the characteristics of the source and its relative orientation to the arms of the interferometer. Gravitational waves from a distribution of matter are dominated by the quadrupole moment. The gravitational strain from a source in the Virgo cluster with a distribution of mass on the order of M_{\odot} (one solar mass), moving

at a few tenths of the speed of light would at most produce a strain amplitude of $\sim 10^{-20}$. As a result, LIGO data will typically have very low signal to noise ratios.

The most promising source for gravitational waves for LIGO comes from the inspiral of binary systems composed of neutron stars and black holes. The waveforms for such systems are well described by post-Newtonian approximations [3]. This allows for the application of optimal Wiener filtering on the data. This method involves a weighted matching of the known waveforms to the data. The inspiral will have frequency content observable to LIGO from tens of hertz to a few kilohertz. The number of templates needed to carry out the inspiral search is given by

$$\mathcal{N} \simeq 2.4 \times 10^5 \left(\frac{\mathcal{L}}{0.1}\right)^{-1} \left(\frac{M_{min}}{0.2M_{\odot}}\right)^{-2.7} \left(\frac{\hat{f}}{200Hz}\right)^{-2.5} \quad (1)$$

where \mathcal{L} is the expected fraction of signals lost in the analysis, M_{min} is the mass of the smaller of the binary companions, M_{\odot} is one solar mass, and \hat{f} is the frequency at which the interferometer is most sensitive (roughly 140 Hz for the initial LIGO interferometers) The computing resources required for this search are dominated by Fourier transforms and roughly scale as

$$\mathcal{P} \simeq 90 \times 10^9 \text{ FLOPS} \left(\frac{\mathcal{L}}{0.1}\right)^{-1} \left(\frac{M_{min}}{0.2M_{\odot}}\right)^{-2.7} \left(\frac{\hat{f}}{200Hz}\right)^{-1.5}. \quad (2)$$

A search for such objects with component masses as low as $0.2M_{\odot}$ would require an estimated 6.1×10^5 templates with an associated computing performance of 150 GFLOPS to keep up with the data from a single LIGO interferometer.

Rotating neutron stars having asymmetries about their axis of rotation will emit weak quasi-periodic gravitational waves. The method of detection for these sources involves re-sampling several days of data to correct for Doppler and source spin-down effects and then Fourier transforming the data and performing peak detection on frequency bins below a few kilohertz. A complete search involves dividing the sky into roughly 10^6 patches to correct for the Doppler shift at a high enough accuracy to limit the signal power to a single frequency bin associated with a data stretch of order 10 days. This would require computing performance at the teraflop level. Including spin-down effects in the search is expected to increase this into a petaflop class computing problem [5].

Other sources of gravitational waves such as supernovae and stochastic background do not require the same scale of computers. The detection technique

with these sources involves a coincidence measurement of data collected from both LIGO sites. These will only require a communication of the gravitational wave port data and a composite data quality channel. The data will be time tagged using Global Positioning System (GPS) to guarantee proper coincidence. Since the frequency bandwidths of interest for these sources is typically a few kilohertz, the demands on communication are minimal.

Sources of gravitational radiation that have not been characterized will require robust techniques that provide detection of waveforms that are poorly understood. Candidate techniques currently being studied include multi-taper and wavelet methods.

3 Conclusions

LIGO data analysis of expected sources of gravitational waves is being characterized and the magnitude of the computing requirements needed to carry out searches for these sources has been modeled. The predictions made by these models indicate that LIGO data analysis will require several hundred gigaflops of compute power for the binary inspiral searches and similar performance for a targeted pulsar search. The all sky survey for periodic sources requires compute power in the petaflop regime when spin-down effect are included on integrations times of order ten days. This could be scaled back to teraflops by reducing the integration time to roughly a day, but at the expense of signal strength. Proto-type analysis systems designed to test the fundamental algorithms to be utilized in the analysis are currently being implemented on parallel computing platforms at Caltech. The proto-type analysis will enhance the understanding and allow scaling of the data analysis specifications to the level required to reach LIGO's scientific goals.

References

- [1] A. Abramovici *et al.*, *Science*, **256**, 325,(1992).
- [2] J. K. Blackburn in *Mathematics of Gravitation, Part II, Gravitational Wave Detection*, edited by A. Królak, Banach Center Publications, **41**, (1997).
- [3] Luc Blanchet, Bala R. Iyer, Clifford M. Will and Alan G. Wiseman, *Class. and Quantum Grav.* **13** 575 (1996)
- [4] Benjamin J. Owen, *Phys. Rev. D* **53** 6749 (1996).
- [5] P. R. Brady, T. Creighton, C. Cutler and B.F. Schultz, submitted to *Phys. Rev. D* (1997).

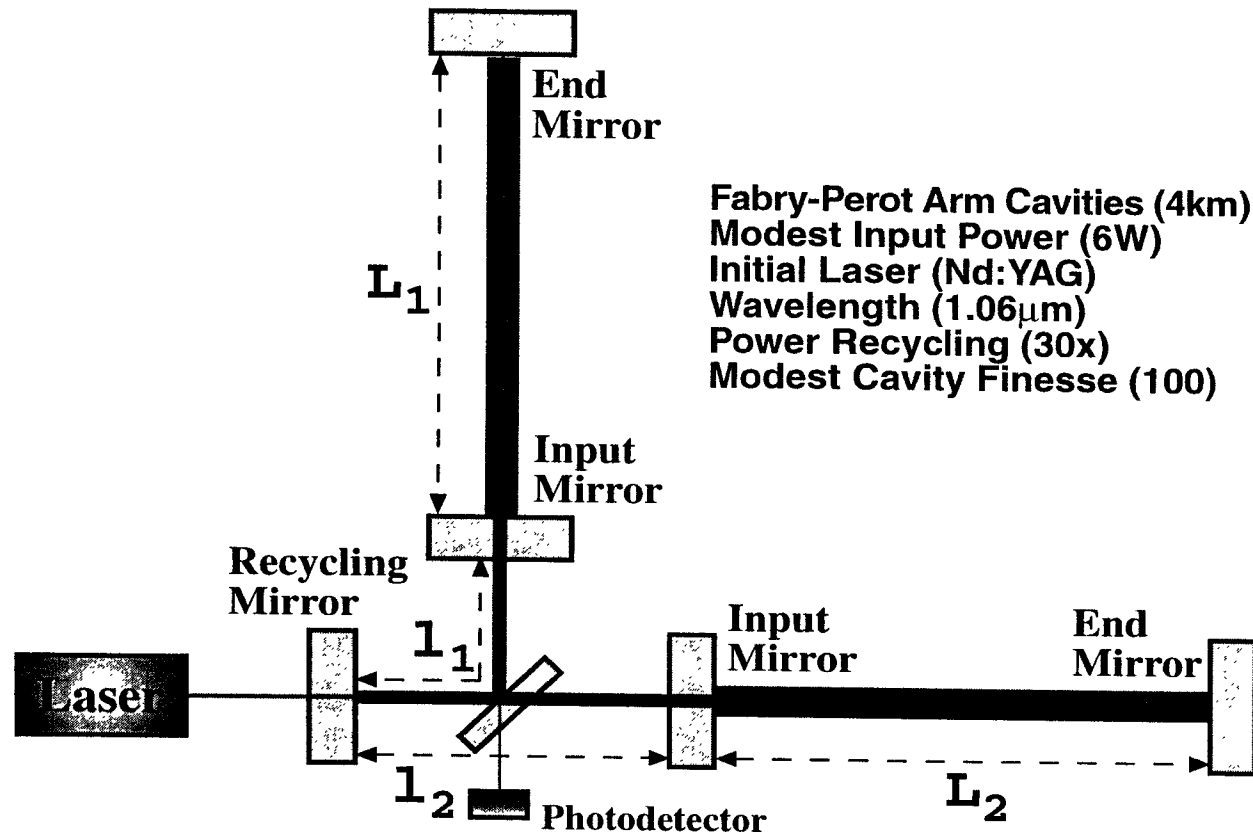
Modeling LIGO Data Analysis

James Kent Blackburn

*California Institute of Technology
Physics, Math, Astronomy Division
LIGO Project, Mail Code 51-33
Pasadena, CA 91125 U.S.A.*

The Laser Interferometer Gravitational Wave Observatory (LIGO) will search for direct evidence of gravitational waves emitted by astrophysical sources in accord with Einstein's general theory of relativity. State of the art laser interferometers located in Hanford, Washington and Livingston Parish, Louisiana will unambiguously measure the infinitesimal displacements of inertially isolated test masses which convey the signature of these gravitational waves. The initial commissioning of LIGO will consist of three interferometers operating in coincidence to remove spurious terrestrial sources of noise. These initial LIGO interferometers will search for gravitational wave signatures with very low event rates and low detection signal to noise ratios out to distances as great as 300 million light years. Data will be collected continuously from the three interferometers at rates as high as 16 megabytes per second. Data analysis for LIGO ranges from the extremely simple for the case of intense short duration supernova bursts which will rely on site to site communications to share data used in coincidence, to state of the art parallel and distributed computing utilizing several hundred nodes to detect the chirp signals from neutron star/black hole binary systems, to petaflop computers of the future needed by the all-sky periodic source surveys.

Initial LIGO Interferometer Configuration



Initially LIGO will be configured as a Michelson interferometer with Fabry-Perot arm cavities and a recycling cavity. The interferometers are being designed to detect RMS displacement motions on the order of 10^{-18} meters. To achieve this level of sensitivity, high power stabilized Nd:YAG lasers will provide input to each recycling mirror. All optical components contributing the sensitivity of the instrument will be suspended as pendula and isolated seismically to reduce coupling to sources of thermal noise and ground motion. The optical path lengths of the interferometer will be maintained by a servo-system, keeping the interferometer phase locked on a particular dark fringe at the output port.

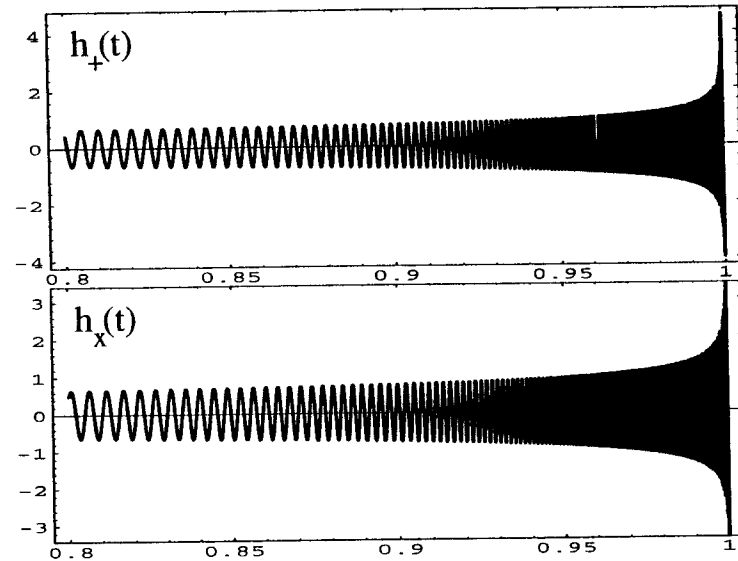
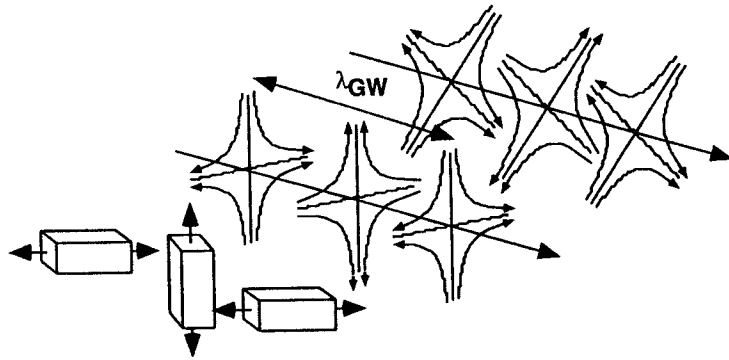
LIGO Data Channels and Rates

Estimates of LIGO IFO and PEM channel counts and sampling rates

System	2 Hz	256 Hz	2048 KHz	16384 KHz	Total (KHz)
Suspension	120	90	30	60	300
Prestablized Laser	20	10	5	8	43
Mode Cleaner	30	20	10	20	80
Injection Optics	20	15	5	10	50
IFO Readout	20	15	0	30	65
Auto Alignment	20	15	0	0	35
Channels/IFO	230	165	50	128	573
KBytes/sec/IFO	0.9	84.5	204.8	4194.3	4484.5
Auxiliary	0	200	10	30	240
Housekeeping	300	50	20	0	370
Channels/site	300	250	30	30	610
KBytes/sec/site	1.2	128	122.9	983.0	1235.1

LIGO data will be collected from roughly 3600 channels at sampling rates ranging from 2 to 16384 samples per second. These channels will compliment the gravitational wave output channel with physical environmental monitoring, housekeeping information and controls monitors. The total data collected from each interferometer is estimated at over 5 megabytes per second. LIGO will collect data continuously throughout the year in order to record the raw gravitational events. This results in a yearly data rate of 5.02×10^{14} bytes for all three interferometers. If 50 gigabyte tapes were used to store the data, ten thousand tapes would be needed to record the raw data from the three interferometers. The data will be packed into units called frames which carry a complete representation of the data for one second. These frames will be the bases for data archival, processing and analysis.

Gravitational Waves



When compact massive objects such as neutron stars and black holes experience an acceleration as in the case of a supernova or the inspiral of a compact binary system, the geometry of space-time experiences a dynamic change which propagates at the speed of light in the form of gravitational waves. The gravitational waves transverse space-time producing a cyclic elongation and contraction of the bodies in the plane perpendicular to the propagation direction (figure on left). Like electromagnetic waves, the gravitational waves can be represented by two orthogonal polarizations, h_x (h-cross) and h_+ (h-plus). The figure on the right shows the waveforms for these two polarizations for the final 200 milliseconds of a binary system of two 10 solar mass black holes with an inclination angle of 30° and at a distance of 10 megaparsecs is shown above. The vertical axis is the strain on space-time in units of 10^{-20} .

Binary Inspiral Data Analysis

The inspiral and coalescence of compact binary systems composed of neutron stars and black holes are among the most promising sources of gravitational waves for LIGO to detect. The sensitivity of the initial LIGO interferometers will allow an inspiral of 1.4 solar mass neutron stars to be detected out to 20 megaparsecs. A pair of 10 solar mass black holes could be detected at roughly 100 megaparsecs. Detection of this type of source is greatly enhanced by the fact that the waveforms are known to a very high precision from the second order post-Newtonian approximation (2PN). This allows for the use of Wiener optimal filtering (*matched filtering*) techniques on the frequency representation of the interferometer data $h_{obs}(f)$ using the equation

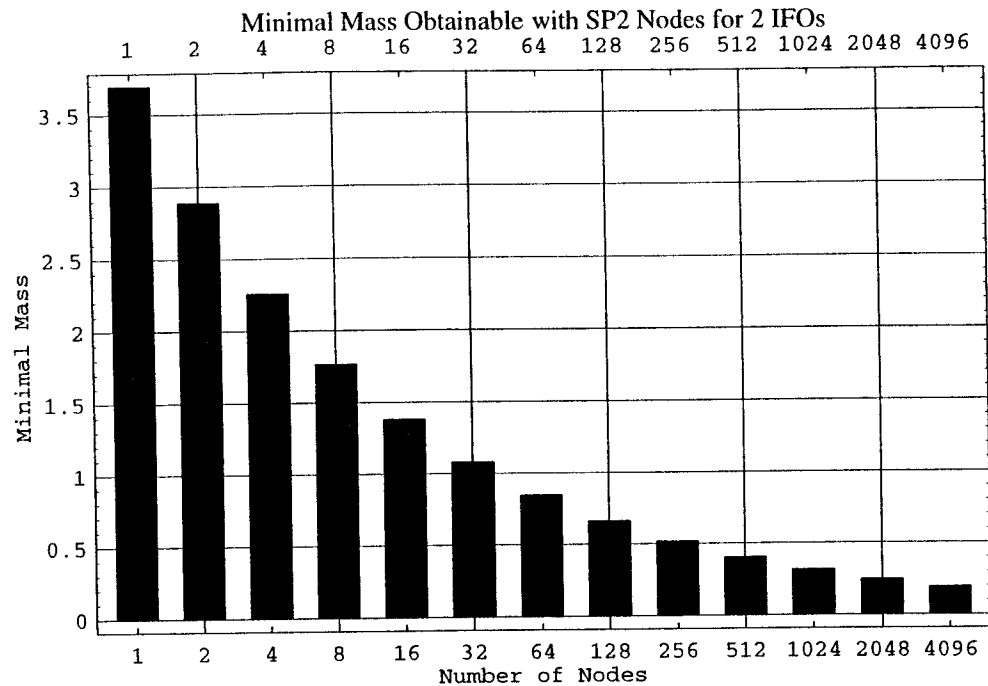
$$S = \int_{-\infty}^{\infty} \frac{h_{obs}(f) \cdot T^*(f) \cdot e^{-i2\pi f t_0}}{S_h(f)} df$$

Templates ($T(f)$) parameterized by the two masses in the system are constructed using the 2PN waveforms (spin is currently neglected). Because of the detector's noise ($S_h(f)$), it is not possible to say with absolute certainty that a particular inspiral event was seen in the data using the matching parameters. However, it is statistically possible to state that an inspiral of sufficiently large amplitude occurs, it will be seen with a sufficiently high probability (say 90%) if the template used to detect it lies in a sufficiently nearby region of the parameter space for the masses. The spacing of these templates in the parameter space of masses is a function of the interferometer noise floor. For the initial LIGO interferometers the number of templates (N) needed for detection with specific statistical probability for event *loss* is approximately given by

$$N = 7592 \cdot \left(\frac{loss}{0.1}\right)^{-1} \cdot (Mmin)^{-2.7}$$

where $Mmin$ is the mass of the smaller member of the binary system in solar mass units.

Compute Model for Binary Inspiral Analysis



Computer Configuration:

- 70% of 235 Megaflops/Node
- 256 MB Ram/Node
- 2 GB disks/Node
- 14 MB/sec I/O Xfer Rate
- FFT $\sim 5N\log_2(N)$ “complex”
- \$90K/Node for IBM SP2

Model Predictions:

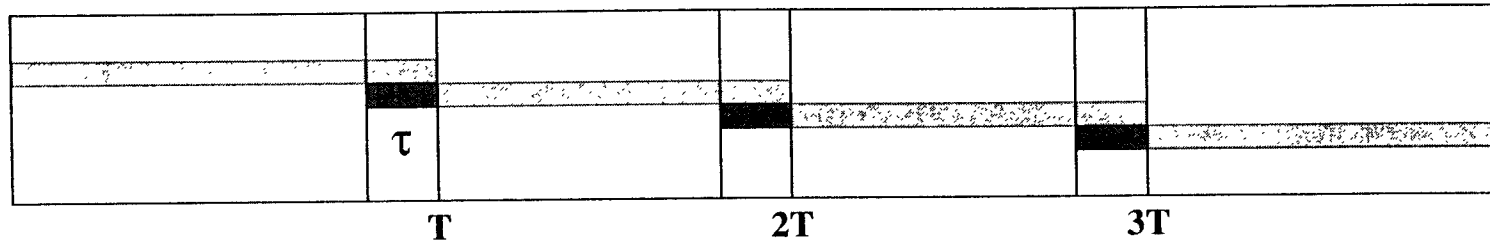
- CPU Limited Analysis
- Dominated by FFT & IFFT

The detailed computational needs for the two interferometers at the Hanford, Washington Site have been modeled. The model is based using an Excel spreadsheet program which takes into account all floating point operations associated with the flow diagram. It calculates the total number of template swaps carried out at in each node based on the available memory and includes the time to move templates and data between the nodes and out of storage. The megaflops (P) needed to reach a given

$$P = 7186 \cdot (Mmin)^{-2.806}$$

$Mmin$ from the model fits the equation shown above. A total of 16 nodes are needed to carry out analysis down to the Chandrasekhar limit of 1.4 solar masses at an estimated cost of \$1.4 million using IBM SP2 hardware. To reach a minimum mass of 1 solar mass would require nearly 40 nodes.

Marching through the Binary Inspiral Data



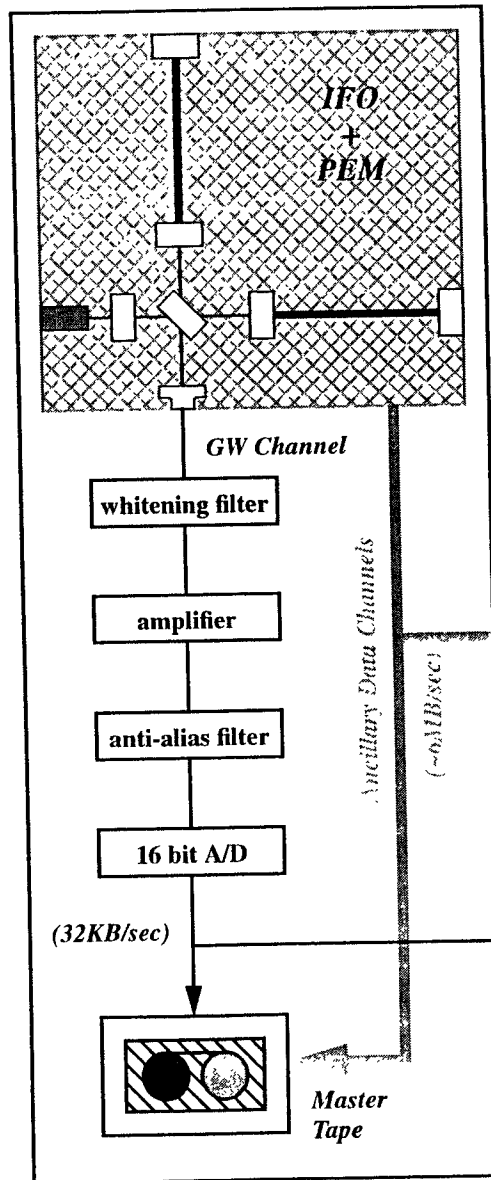
τ - optimal template length; amount of data reused in each pass

T - amount of data analyzed in each pass; 36 times longer than τ

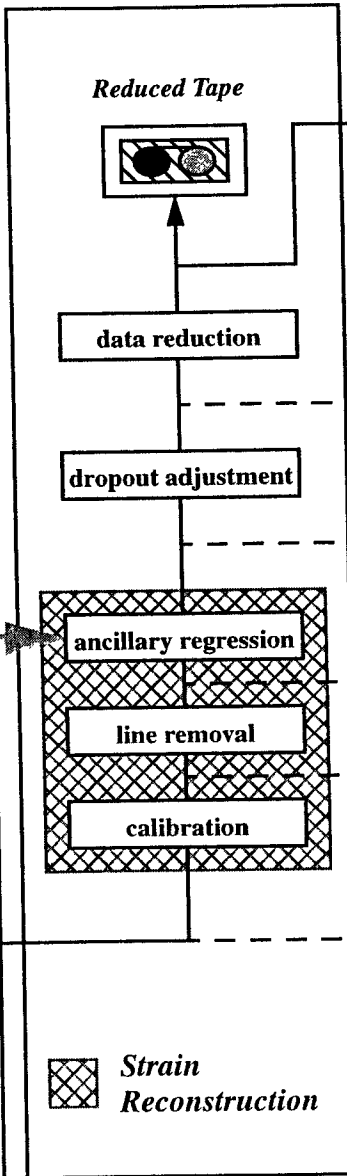
The underlying principle to the binary inspiral analysis shown in the flow diagram is the correlation of the gravitational wave data channel with the templates. This is carried out by using the correlation theorem, appropriately weighed for instrument noise, i.e., matched filtering. The correlation of two discretely sampled functions, one of which goes on indefinitely and the other which is of fixed length is dealt with by zero padding of the shorter function (the templates in this case). To be able to see a binary inspiral event that begins at one of the edges, that data must be reused. Taking these two effects together introduces a competition between doing long inverse FFTs and analyzing the most data in a single pass. The lowest order approach to how to optimize these competing processes suggests a ratio between T and t of somewhere between 5 and 15. Using the data analysis model for the binary inspiral, this ratio is actually optimized to give the largest data throughput on the parallel hardware and the result suggests that the actual ratio is **36**. The minimum in this optimization is very shallow and the actual value is sensitive to the hardware configuration but has little impact on the performance for ratios within 10 to 15 of this value.

Data Flow Diagram for Binary Inspirals

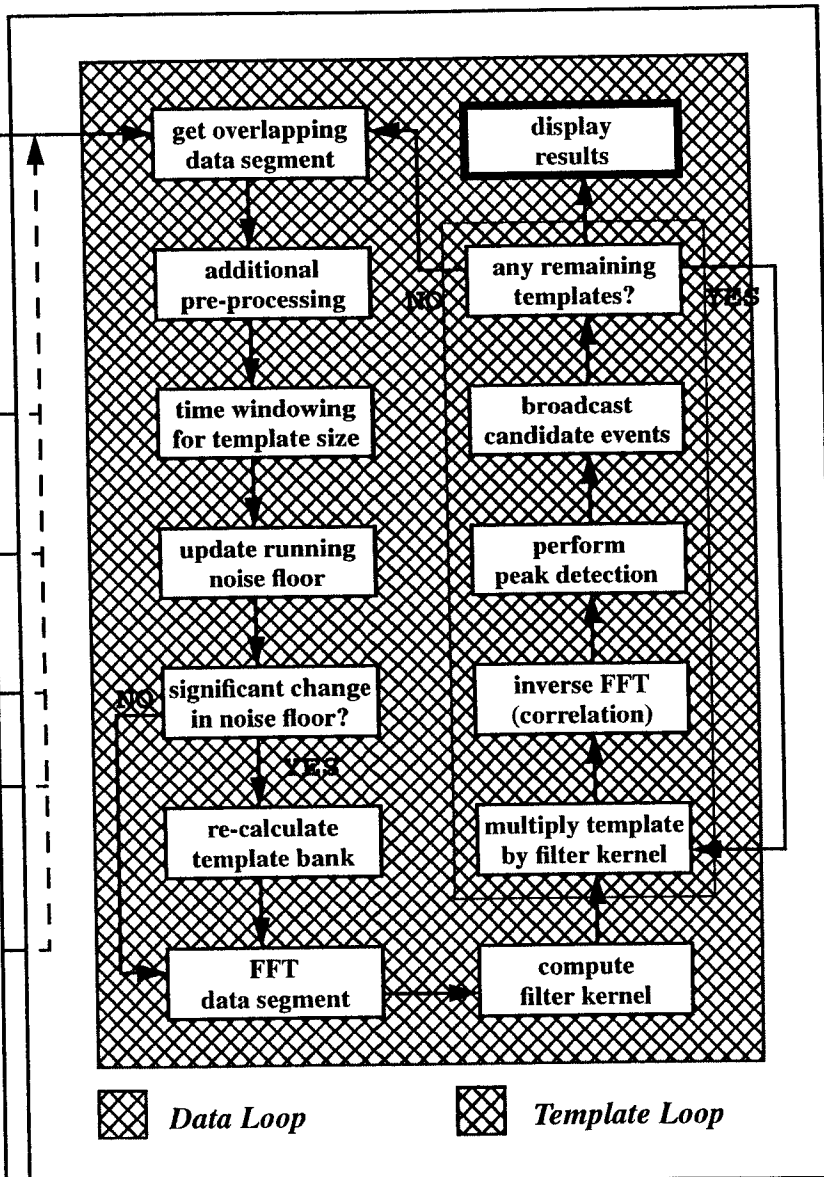
Data Acquisition



Data Processing



Binary Inspirals Data Analysis



Periodic Source Data Analysis

The LIGO frequency band will open a window into periodic sources of gravitational waves from rapidly rotating neutron stars (pulsars). Currently there are more than 700 known pulsars, all within the galactic distances. Using sensitivity arguments for radio astronomy observations this implies that the galaxy is populated with more than 100,000 active pulsars. Gravitational wave emission from pulsars is expected to be very weak, but not out of the question for detection by LIGO.

The detection strategy for pulsars or any other periodic source of gravitational waves consists of building up power in frequency bins by Fourier transforming long stretches of data. By doing such, the power in monochromatic signals will grow as the square root of the integration time. Expected signal strengths suggest that weeks to months of data may need to be analyzed to bring the signal out of the noise. This would require FFTs of 10^{10} data points for source frequencies of order 1000 Hz. A single such FFT would require about 1 second on a teraflops computer.

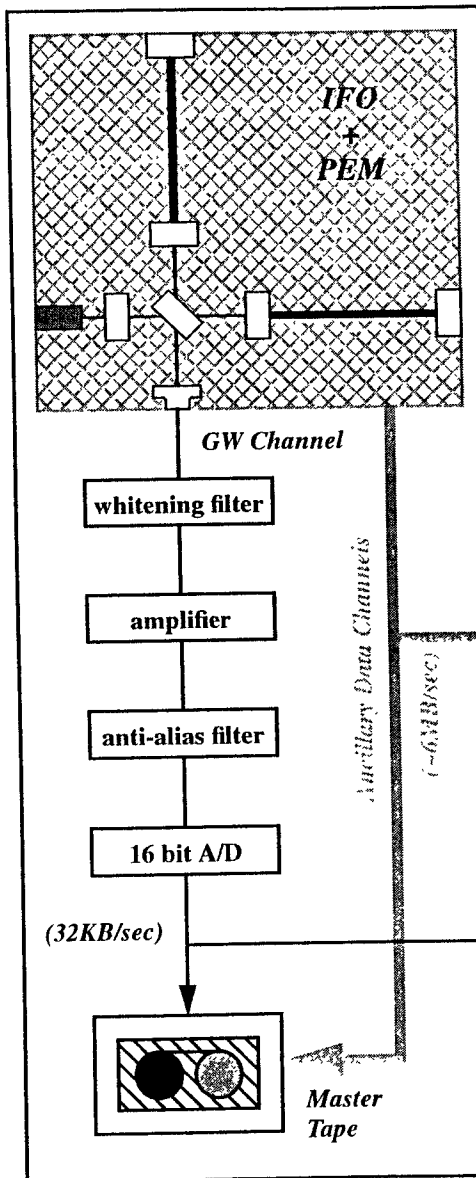
The detection problem is complicated by several factors related to the way the signal is received:

- Complex motions of Earth bound detectors lead to significant Doppler shifts in frequency
- Energy loss through radiation mechanisms result in frequency spindown of the sources
- Pulsars may be members of a binary system having rapidly changing proper motion
- Large proper velocities may carry pulsars across more than one resolution element, “~arcsecond”
- Frequency glitches triggered by instabilities in the internal structure of the pulsar routinely occur.

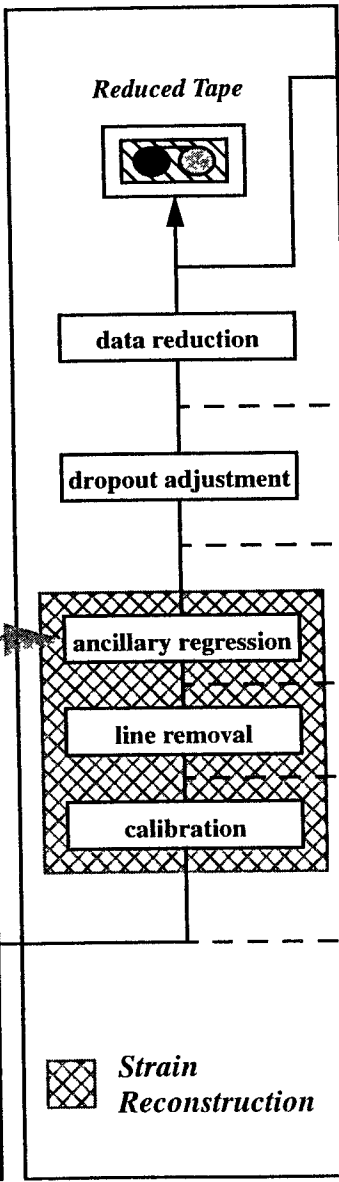
Of these the first two can be addressed with straight forward methods. The third requires an additional 5 parameters to model making the parameter space too large to search. The fourth can be neglected if observation times are kept well under one year and frequencies are under 1 kHz. Based on these a significant amount of study and modeling have gone into the correcting the detected signal for Doppler shifts and spindown. The other complications are neglected due to their inherent difficulties.

Data Flow Diagram for Periodic Sources

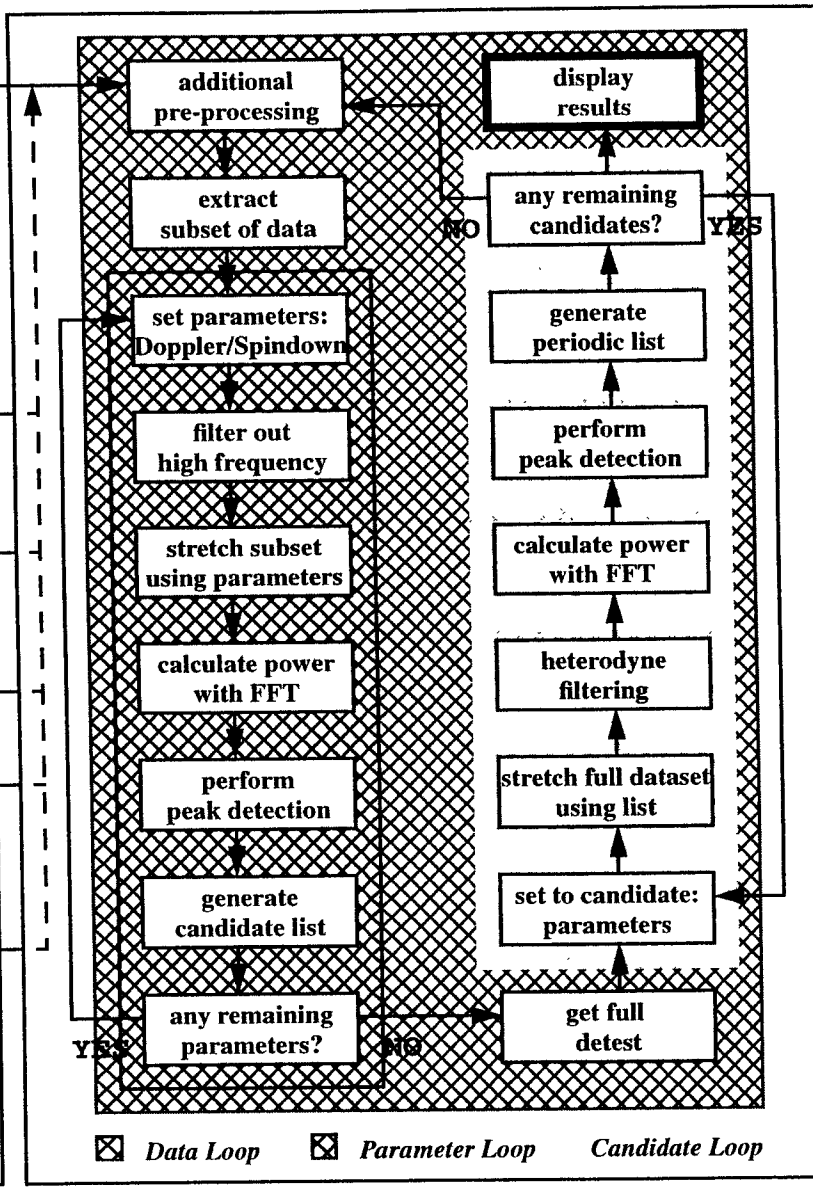
Data Acquisition



Data Processing



Periodic Source Data Analysis



Compute Model for Periodic Sources

Using a technique based on differential geometry similar to the technique used to determine the number of templates needed in the binary inspiral data analysis, the number of sets of parameters or “patches” required to search the whole sky with 0, 1, or 2 spin down parameters is given by

$$N_{patches} \equiv \text{Max} \left\{ \left[\left(\frac{f_o}{1\text{kHz}} \right)^{s+2} \left(\frac{40\text{yrs}}{\tau} \right)^{\frac{s+1}{2}} \cdot \left(\frac{0.3}{\mu_{max}} \right)^{\frac{s+2}{2}} \right] \cdot F_s(T) \right\}$$

where μ_{max} is the mismatch between signal and patch and T is the integration time in days and the

$$F_0(T) = 6.9 \times 10^3 T^2 + 3.0 T^5$$

$$F_1(T) = \frac{1.9 \times 10^8 \cdot T^8 + 5.0 \times 10^4 \cdot T^{11}}{4.7 + T^6}$$

$$F_2(T) = \frac{2.2 \times 10^7 \cdot T^{14}}{56.0 + T^9}$$

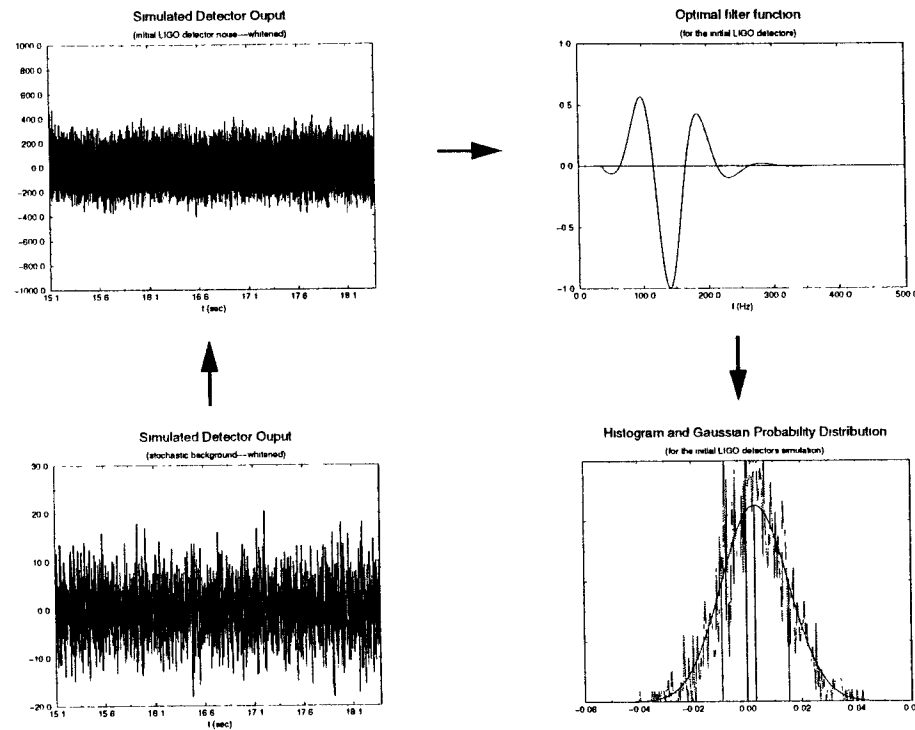
functions F are given above. The computational requirements are driven by the number of patches and the floating point operations for the FFT (neglecting the correct for the Doppler shift and thresholding). Taken together, the computer power needed to keep up with the data for one detector is

$$P_{pulsar} = 6 \cdot f_{max} \cdot N_{patches} \cdot \left[\log_2(2 \cdot f_{max} \cdot T) + \frac{1}{2} \right]$$

When values consistent with current understanding of pulsars are used in these expressions, the compute requirement exceeds 10^{+15} FLOPS! With a teraflops computer analysis one can do becomes:

- 18 days of data could be coherently searched for gravitational wave frequencies $f < 200$ Hz and minimal spindown ages $\tau > 1000$ years (reasonable data lengths for expected signal strengths)
- 0.8 days of data could be coherently searched for gravitational wave frequencies $f < 1\text{kHz}$ and minimal spindown ages as low as 40 years (the more interesting case)
- Directed search at known supernova remnants, galactic center, etc. increase observation times by order 10 (only).

Stochastic Background Simulation

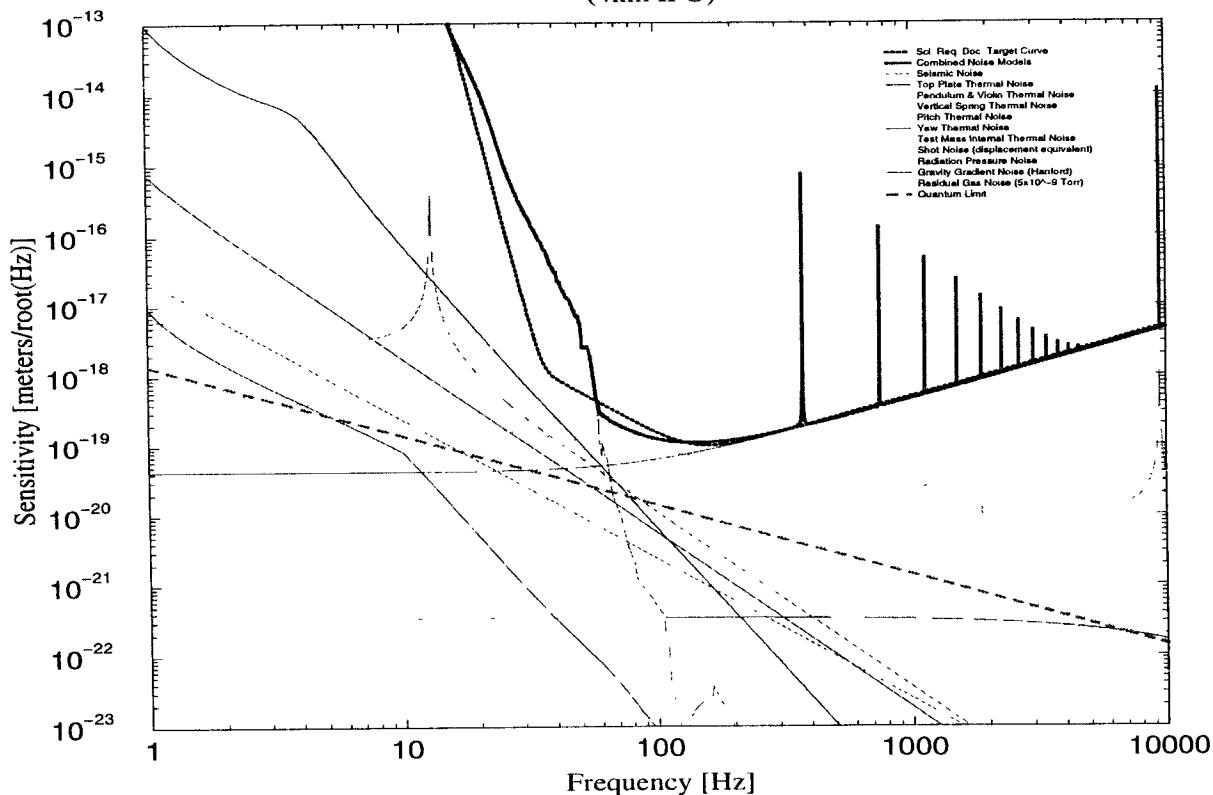


Bruce Allen and Joe Romano have carried out studies of stochastic back-ground analysis of LIGO data. The method is computationally simple as LIGO data analysis goes, and involves the correlation of data from two different interferometers. An optimal filter is constructed which accounts for the differences in arrival times and orientations for the two interferometers. This filter is shown on the top right for the LIGO Hanford, WA and Livingston, LA detector pair. The analysis combines simulated stochastic signals with simulated initial LIGO detector noise through the optimal filter to calculate the signal to noise ratio from the stochastic background. The simulations shown here finds an (SNR) of 7.937 corresponding to an energy density Ω_0 of 1.955×10^{-4} with a 95% detection confidence. The bottom right figure shows the measured cross correlation signal values against the Gaussian fit.

Modeled LIGO Noise Floor

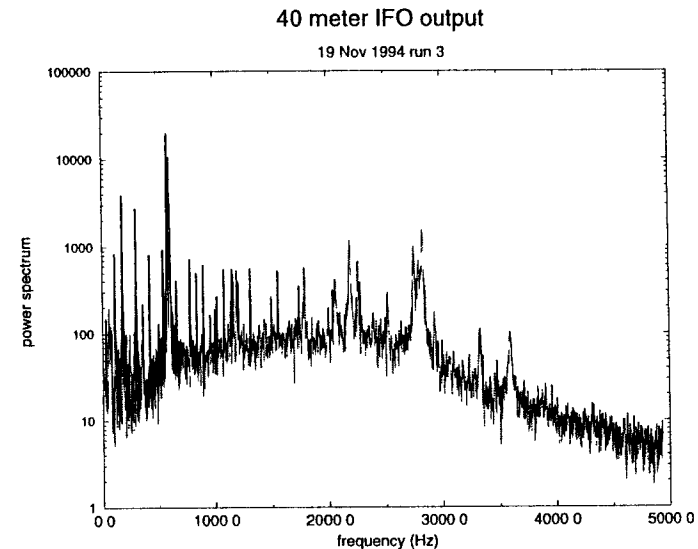
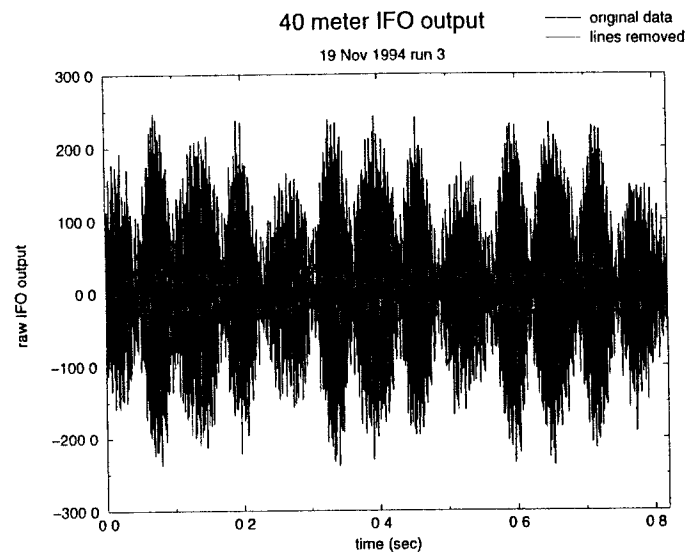
Initial LIGO Noise Curves

(4km IFO)



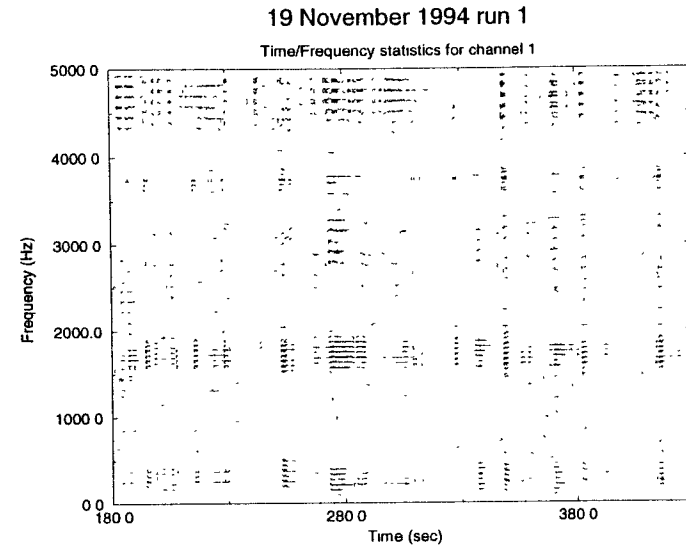
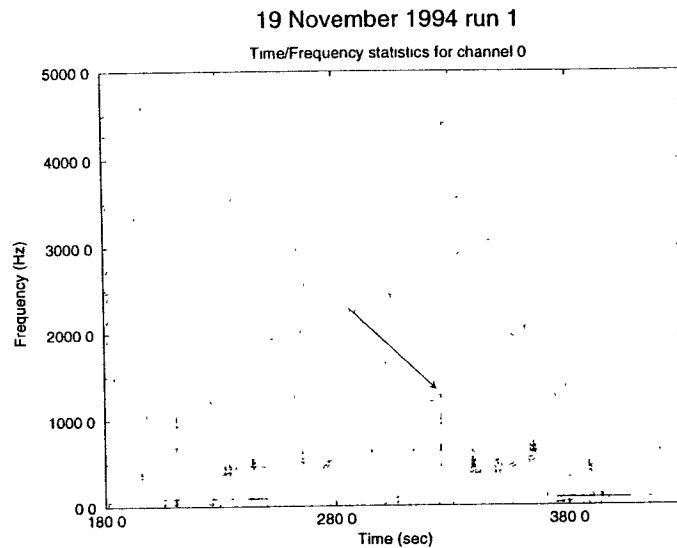
The sensitivity of LIGO to gravitational waves is limited by the noise sources in the detector. The signal output from the initial LIGO interferometers will span four orders of magnitude over the frequency band of interest as a result of the colored noise floor. Gravitational waves from anticipated sources will only occasionally have signal to noise ratios detectable above this noise floor.

Line Removal using Multi-Taper Methods



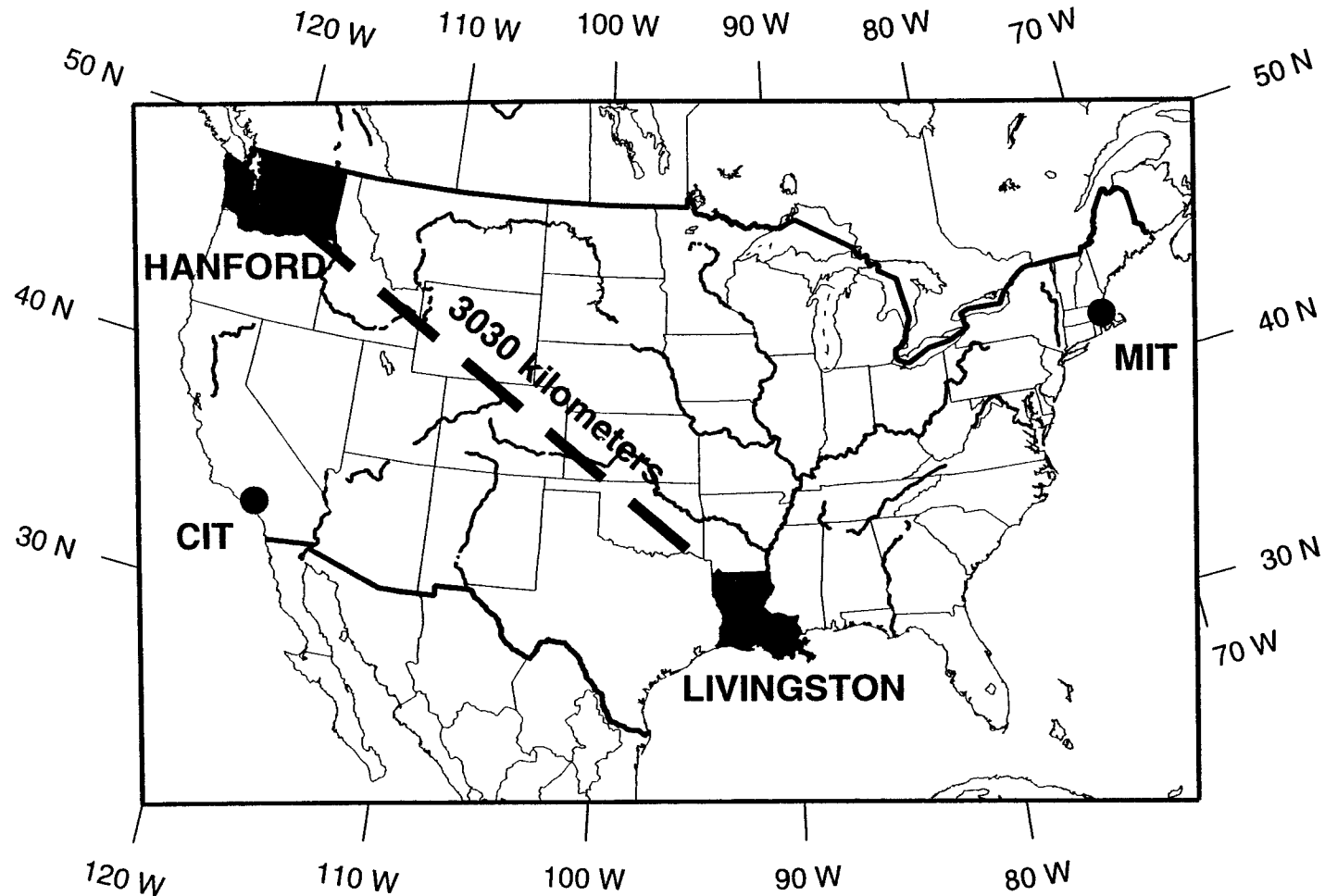
LIGO data will possess a multitude of narrow line resonances found in the interferometer's noise floor. These lines are highly predictable and thus easily removed from the signal. The figures above illustrate the ability of the multi-taper method for removing these types of resonances. The figure on the left shows the raw signal of the 40 meter proto-type interferometer at Caltech in black. The signal is processed using the multi-taper method found in the GRASP software package developed by Bruce Allen. The results are shown in red. On the right is the frequency representation of the signal showing the narrow lines (39 in total) which were removed. These lines are associated with harmonics of the 60 Hertz line frequencies and thermal noise resonances in the suspension system. A simulation where by a binary inspiral signal was added to real 40 meter data demonstrated that this method improves signal to noise by 30%, equivalent to an 80% increase in the volume of the universe observable by the interferometer.

Time Frequency Analysis Methods



The figures above demonstrate an application of time-frequency analysis methods, used here for diagnostics. This particular method uses an auto-regressive averaging technique to derive a mean power spectrum with an exponential-decay time constant of 10 seconds. The current power spectrum is calculated and compared to the mean spectrum. If the difference exceeds a specified threshold, the time-frequency pixel is highlighted. The figure on the left is of the gravitational wave signal on the 40 meter proto-type interferometer. The arrow indicates the appearance of an instrumental signature. The figure on the right is for the magnetometer, one of the ancillary channels acquired at the 40 meter lab. These time-frequency methods have proven very useful in instrument diagnostics and are expected to be important to data analysis. Other time-frequency methods currently being explored include Gabor transforms and wavelets analysis.

Primary Sites for LIGO Wide Area Network



LIGO networks will communicate data between the two sites in Hanford, Washington and Livingston Parish, Louisiana, as well as the joint developing institutions of California Institute of Technology and Massachusetts Institute of Technology. LIGO is currently studying technologies and options for implementing this wide area network.

Dynamic Models of Fabry-Perot Cavities

David Redding^{*}, Martin Regehr[†], Lisa Sievers[‡]

February 28, 1997

Abstract

Longitudinal mirror motions affect the fields circulating in high-finesse Fabry-Perot cavities in complex, time-dependent ways. These effects must be accounted for in the design of high-bandwidth cavity length controllers. Nonlinear time-domain models are presented, which are used to design and test lock-acquisition controllers. Once locked, linear small-amplitude transfer functions provide an adequate model of the cavity signals. Analytic and numerical methods of computing transfer functions are described. Performance examples are provided.

Introduction

Changes in the distance between the mirrors of a high-finesse Fabry-Perot cavity can be measured to extraordinary precision through synchronous detection. This technique is used in various proposed methods for the broadband detection of gravitational radiation (Ref. 1). Fabry-Perot cavities used as gravity wave detector prototypes have demonstrated measurement precision of 10^{-18} m/ $\sqrt{\text{Hz}}$ at 200 Hz.

Successful operation of a Fabry-Perot cavity at this level of performance requires passive and active isolation of the optics from ambient seismic disturbances. In the Caltech LIGO interferometers, the mirrors are hung from pendulum suspensions mounted on dynamically isolated platforms. The suspension system isolates the mirrors from seismically driven displacements at frequencies well above the pendulum resonant frequencies (common resonant frequency is 1 Hz). This passive isolation stage is augmented by lateral and longitudinal active mirror position and angle control systems. In this paper, we derive mathematical models for the longitudinal response of the cavity fields, assuming the cavity to be well aligned in angle.

The Pound-Drever-Hall (PDH) radio-frequency modulation technique (Ref. 2) provides signals for high-bandwidth mirror controls that “lock” the cavity length to the stabilized laser resonant length. As sketched in Fig. 1, the laser light is RF phase modulated before it enters the cavity. The light returning back towards the laser is detected and synchronously demodulated. The in-phase demodulated signal is proportional to the phase of the light at the carrier frequency, provided the cavity is within a fringe-width of resonance. This signal is then used by the control system to lock the cavity on resonance.

The control system must work in 2 operational modes. Initially the cavity will be out of resonance, with relatively large mirror velocities. During this initialization phase, the “Lock Acquisition” controller captures a fringe as it sweeps by, establishing the desired

* Member of Technical Staff, Jet Propulsion Laboratory, California Institute of Technology

† Graduate Student, LIGO Project, California Institute of Technology.

‡ Senior Scientist, LIGO Project, California Institute of Technology.

resonance condition. Once the cavity is in resonance, very precise displacement measurements can be taken during “Operations Mode.”

The control problem is complicated by the fact that the cavity response is not memoryless. The detected field at any instant in time is a function of the cavity geometry and source phase at previous times, due to the long dwell time of the light in the cavity. Accurate knowledge of the dynamic response of the cavity is required in order to devise stable, high performance controls.

This paper presents models that accurately depict the dynamical response of Fabry-Perot cavities. We derive numerical time-domain models that are valid over both large and small motions of the mirrors. These are required for testing Lock Acquisition Mode controls. As we show, the model results closely match experimental data. An application of this modeling approach in the design of acquisition controllers is described in Ref. 3.

We also present analytic and numerical linear frequency-response models. Though valid only for small motions, these are very useful in the design of controls for Operations Mode, where the cavity length is kept within half of a fringe width of resonance. The frequency-response models are derived using two independent approaches. The first approach linearizes the difference equations developed for the time-domain model about the cavity resonant condition. The linearized equations are then Laplace-transformed to obtain analytic transfer functions of error signal to laser source phase and mirror motions. The second approach treats the laser source phase and mirror motions as audio-frequency modulators, yielding numerical transfer functions that match the derived analytic expressions.

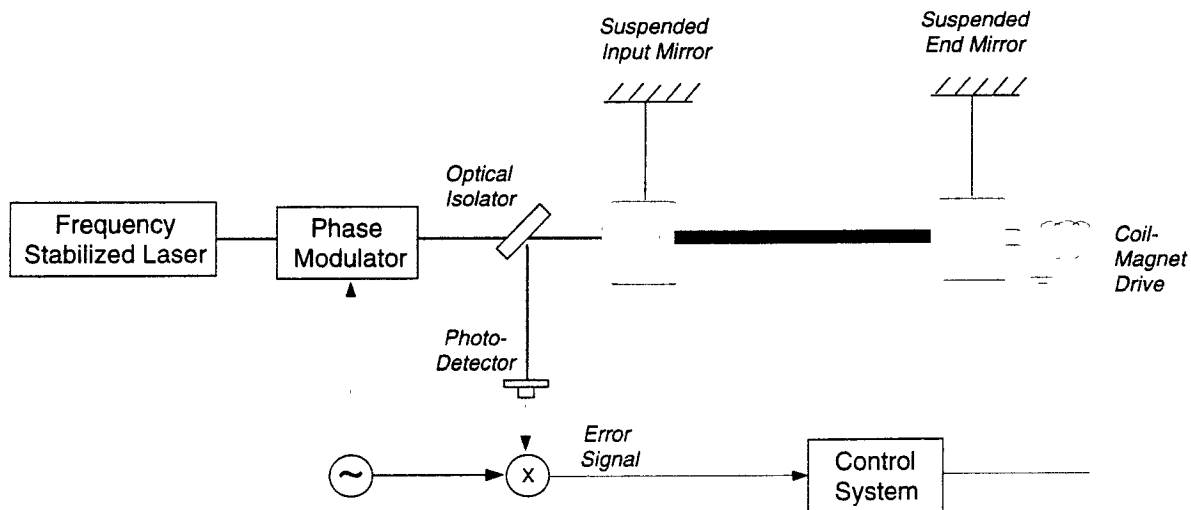


Figure 1. Fabry-Perot cavity and error signal generation.

Notation

In this paper we signify the complex transverse-electric field using the letter E . The point where the field is evaluated is indicated by a 2-letter subscript, as in E_{Aa} . The first subscript refers to the element in the beam train (here, to mirror A). The field is evaluated at an inertially-fixed point in the vicinity of the element, rather than on the

moving surface of the element. The second subscript refers to the direction of the field: *a* to the field entering from the left; *b* to the field departing to the right; *c* to the field entering from the right; and *d* to the field departing to the left, as illustrated in Fig. 2.

When the cavity is illuminated by light at multiple frequencies, such as by the carrier and upper and lower sidebands that result from modulation of the source, an additional numeric superscript is used to signify the component of the field produced by illumination at each frequency. Thus E_{Aa0} denotes the input field at mirror A due to illumination at the carrier frequency, and E_{Aa1} and E_{Aa-1} denote the corresponding upper and lower sideband fields, respectively.

Properties of elements are identified using a single subscript, such as T_A and R_A for intensity transmittance and reflectance for mirror A.

Finally, this work ignores transverse effects, such as mirror or beam tilt or beamwalk. The cavity is assumed to remain aligned in angle and to sustain only the TEM₀₀ mode.

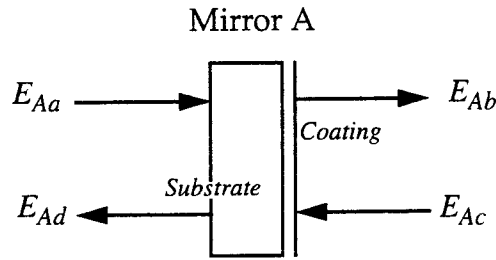


Figure 2. Fields at a mirror.

Cavity Field Equations for a Single Frequency Source

The fields affected by a single stationary cavity mirror (mirror A) are illustrated in Fig. 3. For light of a single frequency travelling from left to right, the incident field is E_{Aa} and the transmitted field is E_{Ab} . For light traveling from right to left the incident field is E_{Ac} and the transmitted field is E_{Ad} . The transmitted fields sum reflected and transmitted parts of the 2 incident fields, as:

$$E_{Ab} = t_A E_{Aa} + r_A E_{Ac} \quad (\text{EQ 1})$$

$$E_{Ad} = t_A E_{Ac} - r_A E_{Aa} \quad (\text{EQ 2})$$

Here r_A and t_A are the amplitude reflectance and transmittance, respectively, of the mirror. They are derived from the intensity reflectance and transmittance R_A and T_A :

$$r_A = \sqrt{R_A} \quad (\text{EQ 3})$$

$$t_A = \sqrt{T_A} \quad (\text{EQ 4})$$

The power budget for each cavity mirror is such that:

$$R_A + T_A + A = 1 \quad (\text{EQ 5})$$

where A is the power loss due to absorption and scattering (if A is a polarizing beam splitter used as an optical isolator, both R_A and T_A will be equal to $1 - A/2$). The sign used

for the amplitude reflectance depends on whether the reflection is internal or external. Following the Fresnel equations (Ref. 4), the negative value is used for light directly incident on the coated side of the mirror, and the positive value is used for light that comes through the substrate.

If the mirror moves from its nominal inertially-fixed position (which it will do as an arbitrary function $\delta(t)$ of time), it imparts a phase shift on the reflected fields proportional to twice its displacement. Taking this into account, a more general expression of the fields at mirror A is

$$E_{Ab}(t) = t_A E_{Aa}(t) - r_A e^{2jk\delta_A(t)} E_{Ac}(t) \quad (\text{EQ 6})$$

$$E_{Ad}(t) = t_A E_{Ac}(t) + r_A e^{-2jk\delta_A(t)} E_{Aa}(t) \quad (\text{EQ 7})$$

The fields within a cavity consisting of 2 mirrors and a source are illustrated In Fig.3. The equations describing the fields are generated by applying Eqs. 6 and 7 to mirrors A and B, and by adding 2 additional equations defining the propagation between the 2 mirrors. For mirror B, assuming there is no illumination entering the back of the cavity ($E_{Bc} = 0$):

$$E_{Bb}(t) = t_B E_{Ba}(t) \quad (\text{EQ 8})$$

$$E_{Bd}(t) = -r_B e^{-2jk\delta_B(t)} E_{Ba}(t) \quad (\text{EQ 9})$$

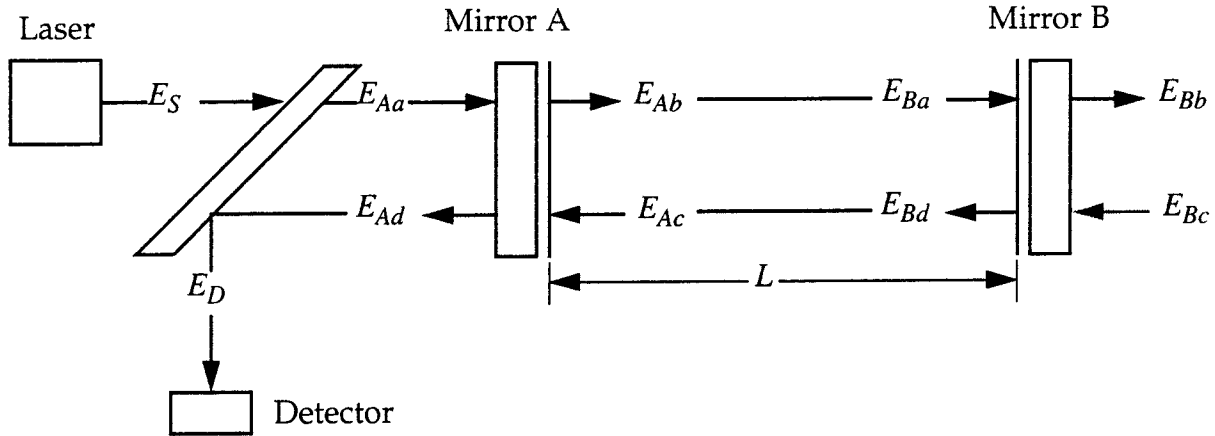


Figure 3. Fields in a Fabry-Perot interferometer.

The propagation over the distance L between the mirrors is:

$$E_{Ba}(t) = e^{-jkL} E_{Ab}(t - \tau) \quad (\text{EQ 10})$$

$$E_{Ac}(t) = e^{-jkL} E_{Bd}(t - \tau) \quad (\text{EQ 11})$$

Here τ is the one-way light time between the 2 mirrors.

The input to the cavity comes from the laser source field, which can vary in phase and amplitude. Neglecting the distance between the source and the front mirror:

$$E_{Aa}(t) = t_{BS} E_S(t) \quad (\text{EQ 12})$$

The field at the detector (neglecting the distance between the front mirror and the detector):

$$E_D(t) = r_{BS}E_{Ad}(t) \quad (\text{EQ 13})$$

The fields of primary interest are the circulating field E_{Ab} and the detector field E_D , from which the detected signal is derived. Substituting among Eqs. 6-13, these can be expressed in terms of the source field and mirror displacement parameters. The field circulating in the cavity, sampled near the front mirror, is:

$$E_{Ab}(t) = t_A t_{BS} E_S(t) + g(t) E_{Ab}(t - 2\tau) \quad (\text{EQ 14})$$

The "round trip gain," $g(t)$ is defined:

$$g(t) = r_A r_B e^{-2jk[L + \delta_B(t - \tau) - \delta_A(t)]} \quad (\text{EQ 15})$$

The field at the detector:

$$E_D(t) = r_A r_{BS} e^{-2jk\delta_A(t)} E_S(t) - t_A r_{BS} r_B e^{-2jk[L + \delta_B(t - \tau)]} E_{Ab}(t - 2\tau) \quad (\text{EQ 16})$$

Static Response for a Single Frequency Source

In a static cavity, there is no variation in mirror position or source amplitude:

$$E_{Ab}(t) = E_{Ab}(t - 2\tau) \equiv E_{Ab} \quad (\text{EQ 17})$$

$$E_S(t) = E_S(t - 2\tau) \equiv E_S \quad (\text{EQ 18})$$

$$\delta_A(t) = \delta_A(t - 2\tau) \equiv \delta_A \quad (\text{EQ 19})$$

$$\delta_B(t - \tau) = \delta_B(t - 3\tau) \equiv \delta_B \quad (\text{EQ 20})$$

Substituting Eqs. 17-20 into Eq. 14 and simplifying, the static-cavity circulating field is:

$$E_{Ab} = \frac{t_A t_{BS} E_S}{1 - r_A r_B e^{-2jk(L + \delta_B - \delta_A)}} \quad (\text{EQ 21})$$

Similarly, the detector field is:

$$E_D = \left[r_A r_{BS} e^{-2jk\delta_A} - \frac{t_A^2 t_{BS} r_{BS} r_B e^{-2jk[L + \delta_B]}}{1 - r_A r_B e^{-2jk(L + \delta_B - \delta_A)}} \right] E_S \quad (\text{EQ 22})$$

These are standard results appearing in textbooks (e.g., Ref. 5).

Time Response for a Single Frequency Source

In a dynamically-varying cavity, the source and mirror states will change as arbitrary functions of time. The output of the cavity at a time t is computed from the cavity field difference equations (Eqs. 14-16), given the (single-frequency) source field at time t , the cavity mirror displacements at time t (mirror A) and $t - \tau$ (mirror B), and the circulating field at time $t - 2\tau$. Of course, the circulating field at time $t - 2\tau$ is a function of the source

at time $t - 2\tau$, cavity mirror displacements at time $t - 2\tau$ and $t - 3\tau$, and the circulating field at time $t - 4\tau$, which is itself a function of the circulating field at time $t - 4\tau$, cavity mirror displacements at time $t - 4\tau$ and $t - 5\tau$, and the circulating field at time $t - 6\tau$, and so on (see Fig. 4).

This recursive sequence continues back in time until the cavity was first turned on. As a practical matter, though, it is not always necessary to go that far back in time. There is a finite number of beams (n_{beams}) that must be summed to achieve a specific level of accuracy in the calculation of the circulating field, as illustrated in Fig. 4. If the cavity geometry is fixed at the resonance, which is the most sensitive condition, the circulating field can be written:

$$E_{Ab} = \frac{t_A t_{BS} E_S}{1 - r_A r_B} = t_A t_{BS} E_S \left[\sum_{i=1}^n (r_A r_B)^i + \frac{(r_A r_B)^{n+1}}{1 - r_A r_B} \right] \quad (\text{EQ 23})$$

Here n is the number of beams explicitly summed. The normalized error due to summing a finite number of beams is ϵ , where:

$$\epsilon = \frac{t_A t_{BS} E_S \frac{(r_A r_B)^{n+1}}{1 - r_A r_B}}{E_{Ab}} = (r_A r_B)^{n+1} \quad (\text{EQ 24})$$

The error level ϵ can be specified (e.g., 0.1% of the full resonant circulating field). The minimum number of summed beams n_{beams} that gives residual error less than ϵ is:

$$n_{beams} = \log_{r_A r_B} (\epsilon - \epsilon r_A r_B) \quad (\text{EQ 25})$$

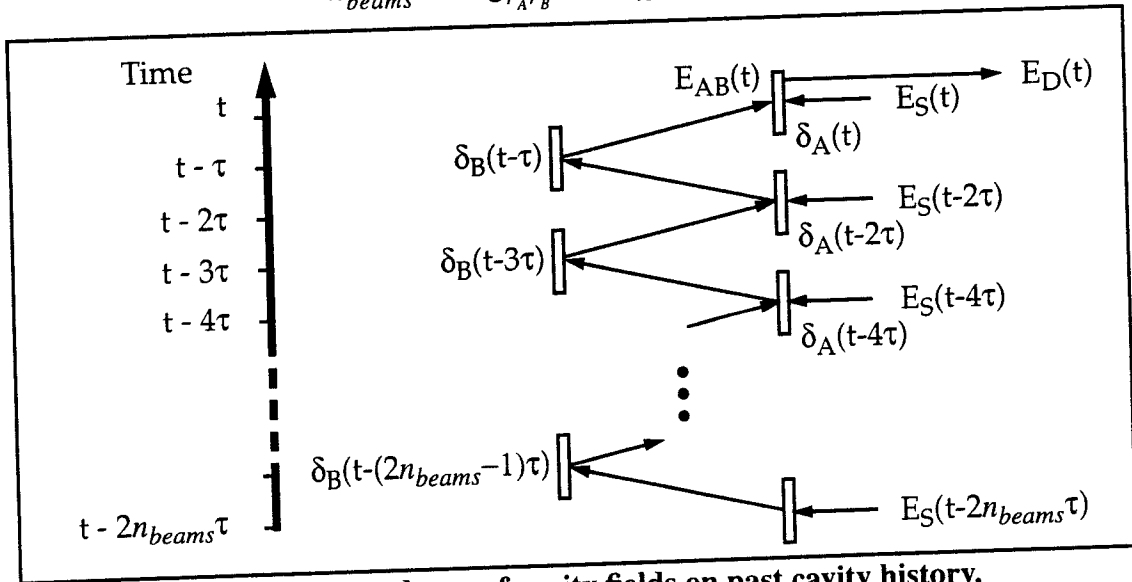


Figure 4. Dependence of cavity fields on past cavity history.

Assuming that the one-way cavity light time τ remains constant (this is usually true to better than 1 part in 10^{10}), the full computation for the circulating field can be written:

$$\begin{aligned}
E_{Ab}(t) = & t_A t_{BS} E_S(t) + g(t)(t_A t_{BS} E_S(t - 2\tau) + \\
& g(t - 2\tau)(t_A t_{BS} E_S(t - 4\tau) + \\
& g(t - 4\tau)(\dots(t_A t_{BS} E_S(t - (2(n - 1)\tau)) + \\
& g(t - 2n\tau)(t_A t_{BS} E_S(t - 2n\tau))\dots))
\end{aligned}
\tag{EQ 26}$$

A simple algorithm that realizes this calculation as part of a time simulation is summarized in pseudocode in Fig. 5.

```

EAb = tA*Es                                ! Initial circulating field
for time = 0 to t by 2*tau,                 ! Begin simulation time loop
  call dynamics (delA,delB,ES,time)        ! Compute cavity geometry
  g = rA*rB*exp(-2*j*k*(L + delB - delA) ! Compute round-trip cavity gain
  EAb = tBS*tA*Es + g*EAb                  ! Update circulating field
  if (mod(time,dtprint)=0),
    call print (EAb,delA,delB,dLs,time) ! Print state at times of interest
  end;
end;                                         ! End simulation time loop

```

Figure 5. Cavity simulation algorithm for time scales less than $n_{beams}\tau$.

The computational effort required by this algorithm per one-way light time τ is quite small. It is a good approach for high-finesse cavities driven by high-bandwidth controllers, where the time interval of interest (dt_{print}) is less than $n_{beams}\tau$.

The algorithm of Fig. 5 may not be the fastest for modeling lower-finesse cavities, or low-bandwidth controls. For cases where the shortest time interval of interest is longer than $n_{beams}\tau$, it is more efficient to reorder the calculation. Equation 26 is rewritten:

$$E_{Ab}(t) = t_A t_{BS} \left[E_S(t) + \sum_{n=1}^{n_{beams}} \left(\prod_{i=0}^n g(t - 2i\tau) \right) E_S(t - 2n\tau) \right]
\tag{EQ 27}$$

This approach limits the number of beams that must be evaluated to n_{beams} . The algorithm of Fig. 6. illustrates its implementation in pseudocode.

```

for time = 0 to t by dtprint,               ! Begin simulation time loop
  call dynamics (delA,delB,Es,time)        ! Compute cavity geometry
  gprod = 1                                ! Initialize running gain product
  EAb = tBS*tA*Es                          ! Initialize circulating field sum
  for n = 1 to nbeams                       ! Loop to evaluate sum
    loopTime = time - 2*n*tau              ! loopTime runs backwards from time
    call dynamics (delA,delB,Es,loopTime) ! Compute cavity geometry
    g = rA*rB*exp(-2*j*k*(L + delB - delA) ! Compute round-trip cavity gain
    gprod = g*gprod                         ! Update running product
    EAb = EAb + gprod*tBS*tA*ES           ! Update circulating field sum
  end;
  call print (EAb,delA,delB,dLs,time)      ! Print state at times of interest
end;                                         ! End simulation time loop

```

Figure 6. Cavity simulation algorithm for time scales greater than $n_{beams}\tau$.

Equation 27 can be viewed as a Green's function solution for the cavity fields. The product in parentheses is the impulse response of the circulating field at time t to the source field at the time $t - 2n\tau$. The sum is then the convolution of the impulse response with the source field at all relevant past times (all n less than n_{beams}). This ordering of the calculation is also used in later sections, in the derivation of transfer functions.

The models of Eqs. 26 and 27 neglect second-order effects of deviations from the nominal one-way light time τ . These occur when the mirrors are displaced from their nominal positions ($\delta \neq 0$), so that the beams arrive at the mirrors at slightly different times than assumed by the model. For mirror displacements of a few wavelengths, this time-of-arrival error is about 10^{-16} sec per traversal of the cavity. In very high-finesse cavities, this might grow to about 10^{-12} sec total after many bounces. The neglected beam phase is equal to this time-of-arrival error times the velocity of the mirror, which is typically less than a few wavelengths per second for Lock Acquisition (much less in Operation Mode). The ratio of this worst-case error to the width of the fringe is about 1 ppm for a cavity with a finesse of 15,000, and much smaller for lower-finesse cavities and/or smaller velocities. This level of error is usually negligible.

Approximate Differential Equation Form for the Cavity Field Equations

The cavity field difference equations can be directly evaluated, following Eqs. 26 and 27, as has just been described. In some cases, however, it may be more convenient to use a differential equation form for the cavity fields. From Eqs. 14 and 15:

$$\frac{E_{Ab}(t + 2\tau) - E_{Ab}(t)}{2\tau} = \frac{1}{2\tau}(t_A t_{BS} E_S(t + 2\tau) + r_A r_B e^{-2jk[\delta_B(t + \tau) - \delta_A(t - \tau)]} E_{Ab}(t)) \quad (\text{EQ 28})$$

Approximating the left hand side as a derivative, and assuming that E_S and E_{Ab} change only slightly over any interval 2τ :

$$\frac{dE_{Ab}}{dt} = \frac{1}{2\tau}(t_A t_{BS} E_S(t) + (r_A r_B e^{-2jk[\delta_B(t + \tau) - \delta_A(t - \tau)]} - 1)E_{Ab}(t)) \quad (\text{EQ 29})$$

This equation can be integrated to find the circulating field at any particular time and frequency. Equation 16 can then be applied to obtain the detector field.

Equation 29 turns out to be the simplest of a sequence of differential equations derivable using Pade approximants, which are rational function representations of the time delay. Higher-order forms, which are more accurate, can be derived following Ref. 6. Solutions computed using Eq. 29 deviate from the exact results in conditions where the cavity fields are changing rapidly; in these cases, higher-order approximants are preferred if a differential equation form is required.

Time Response Example: Single Frequency Source

Figure 7 shows the carrier field intensity in a Fabry-Perot cavity as the input mirror (Mirror A) sweeps through the resonance condition (which occurs at $\delta = 0$). The full dynamic response of the cavity, computed by integrating Eq. 14, is shown as the solid

line. The static response, which neglects the dynamics of the cavity, as per Eq. 21, is shown as the dashed line.

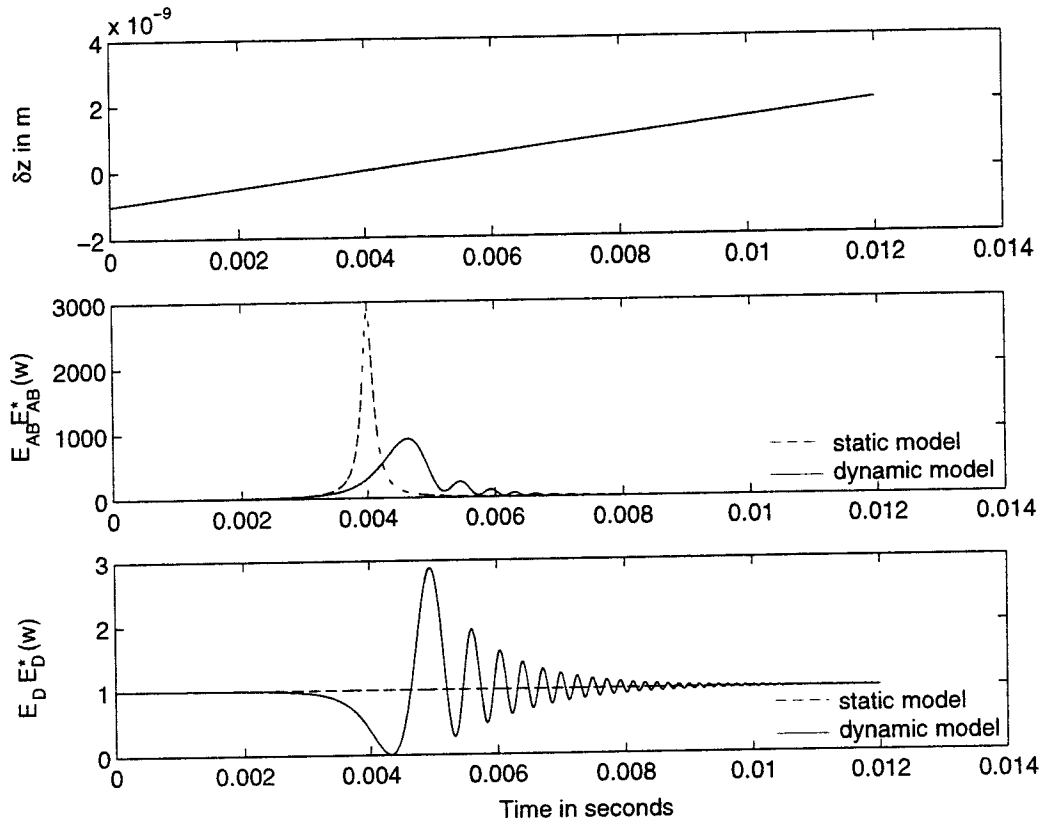


Figure 7. Field intensities as cavity goes through resonance.

As shown in Fig. 7, the passage of the mirror through the resonance condition causes a bolt of high amplitude light to build up in the cavity. After the cavity passes through the fringe, this light dissipates gradually, while bouncing from mirror to mirror. The frequency of the light is shifted higher with each successive bounce, creating a Doppler “chirp.” The parameters defining this example are listed in Table 1. The width of the resonant fringe is 0.11 nanometers, about 0.02% of the wavelength. The lock acquisition controller must stabilize the mirror over a time period much shorter than the duration of the “chirp” signal (see Ref. 3).

Table 1: Example parameters for 40-meter interferometer.

Parameter	Value	Parameter	Value
RA	0.998604	Wavelength	0.5145 μm
RB	1	Mirror A velocity	0.25 $\mu\text{m}/\text{sec}$
Length	40 m	Finesse	4500

Demodulated Cavity Phase Signals

Radio-frequency phase modulation and synchronous detection provides a means of creating signals that are proportional to the phase of the reflected field, provided that the cavity is near resonance. Phase modulation is implemented using a Pockels cell in the beam immediately prior to the cavity (Fig. 1). The (radio) frequency f_{mod} of the modulation is chosen to put the resulting sidebands out-of-resonance in the cavity to reduce noise from the dynamics of the sidebands in the cavity.

For small modulation depth Γ and frequency $f_{mod} = \omega_{mod}/2\pi$, the field after the modulator (the cavity source field) is written in terms of Bessel functions as (Ref. 5):

$$E_S(t) = E_{laser}(t)(J_0(\Gamma) + J_1(\Gamma)e^{j\omega_{mod}t} - J_1(\Gamma)e^{-j\omega_{mod}t})e^{j\omega_0 t} \quad (\text{EQ 30})$$

Here the frequency of the illumination is $f_0 = \omega_0/2\pi = c/\lambda_0$. The source field can be rewritten as the sum of 3 independent fields of slightly different color:

$$E_S(t) = E_{S0}(t)e^{j\omega_0 t} + E_{S1}(t)e^{j\omega_1 t} - E_{S-1}(t)e^{-j\omega_{-1} t} \quad (\text{EQ 31})$$

The carrier and sideband source fields are:

$$E_{S0}(t) = E_{laser}(t)J_0(\Gamma)e^{j\omega_0 t} \quad (\text{EQ 32})$$

$$E_{S1}(t) = E_{laser}(t)J_1(\Gamma)e^{j\omega_1 t} \quad (\text{EQ 33})$$

$$E_{S-1}(t) = -E_{laser}(t)J_1(\Gamma)e^{j\omega_{-1} t} \quad (\text{EQ 34})$$

The carrier wavelength is the source laser wavelength, and the upper and lower sidebands have slightly longer and shorter wavelengths, respectively. For the upper sideband:

$$\lambda_1 = 2\pi c/(\omega_0 - \omega_{mod}) = (2\pi c)/\omega_1 \quad (\text{EQ 35})$$

For the lower sideband:

$$\lambda_{-1} = 2\pi c/(\omega_0 + \omega_{mod}) = (2\pi c)/\omega_{-1} \quad (\text{EQ 36})$$

The nominal operational condition of the cavity puts the carrier in resonance in the cavity by making the length L_{nom} an integer multiple of half the carrier wavelength:

$$L_{nom} = n(\lambda_0/2) \quad (\text{EQ 37})$$

for some n . The ideal modulation frequency is then chosen to put the sidebands out of resonance with the carrier, by making the modulation wavelength close to an integer factor n_{mod} of $4L_{nom}$. It is not chosen to be exactly anti-resonant or the second order sidebands would be perfectly resonant in the arm cavity too; a situation to be avoided. The effective phase of each sideband is then shifted approximately $\pm 90^\circ$ per round-trip of the cavity, relative to the carrier. Relative to the other sideband, the shift is 180° . When $L = L_{nom}$ the carrier is resonant, and the sidebands are close to an anti-resonant state. The sidebands are also equal in amplitude and of opposite sign, so they cancel even though

the modulation is not not precisely anti-resonant. Ideal modulation occurs at frequencies that satisfy:

$$f_{mod} = (c/\lambda_{mod}) \cong n_{mod}(c/(4L)) \quad (\text{EQ 38})$$

The choice of integer n_{mod} determines the particular modulation frequency. For long cavities a relatively large number may be desirable to reduce the effects of $1/f$ noise in the detection.

The detector field of the cavity at a time t can be computed separately for each frequency component, by application of Eqs. 14 and 16 to the source fields of Eqs. 32-34. The total detector field is simply the sum of the detector fields at each frequency:

$$E_D(t) = E_{D0}(t)e^{j\omega_0 t} + E_{D1}(t)e^{j\omega_1 t} - E_{D-1}(t)e^{-j\omega_{-1} t} \quad (\text{EQ 39})$$

The detector intensity is the modulus squared of the field of Eq. 39. It includes terms at DC and frequencies f_{mod} , $2f_{mod}$ and higher harmonics. The error signal for the control system is the output of the demodulator: the components of the detector intensity synchronous with the modulation signal at the modulation frequency f_{mod} . With sinusoidal modulation, the demodulated in-phase signal I_{demod} is:

$$I_{In} = 2\text{Imag}(E_{D0}(t)(E_{D-1}^*(t) - E_{D1}^*(t))) \quad (\text{EQ 40})$$

The quadrature-phase signal I_{quad} is:

$$I_{Quad} = 2\text{Real}(E_{D0}(t)(E_{D-1}^*(t) + E_{D1}^*(t))) \quad (\text{EQ 41})$$

Time Response Examples: Cavity Phase Signals

Two examples are shown in this section. The first continues the example of Fig. 7. Figure 8 shows the demodulated in-phase and quadrature phase signals detected at the input mirror for the cavity defined in Table 1. Modulation frequency was 12.5 MHz, which puts the sidebands in an antiresonant condition in the cavity as per Eq. 37.

The second example compares simulated and actual response for the LIGO 40 m interferometer (Ref. 1). This interferometer provides an experimental testbed for development of gravity wave detectors. In the configuration we ran, the interferometer is made up of two orthogonal suspended 40 m Fabry-Perot cavities. Both cavities have a finesse of 15000 with an approximate storage time (amplitude half life) of 0.338 milliseconds. The main function of one of the cavities is to provide a reference for stabilizing the laser frequency to approximately 10^{-6} hz/sqrt(hz). We used the second cavity to measure the optical response to mirror motions. The interferometer and signal extraction scheme is shown in Fig. 1. Time traces were taken of the in-phase demodulated reflected light as the cavity length swung freely through resonance; one such is shown in Fig. 9.

To compare the experimental data with model data we fit two parameters: the relative velocity of the cavity test masses; and the absolute amplitude of the field incident on the photodetector. This is necessary as we have no independent means of measuring these

parameters. Figure 9 compares model and experimental response for a typical case, showing good agreement.

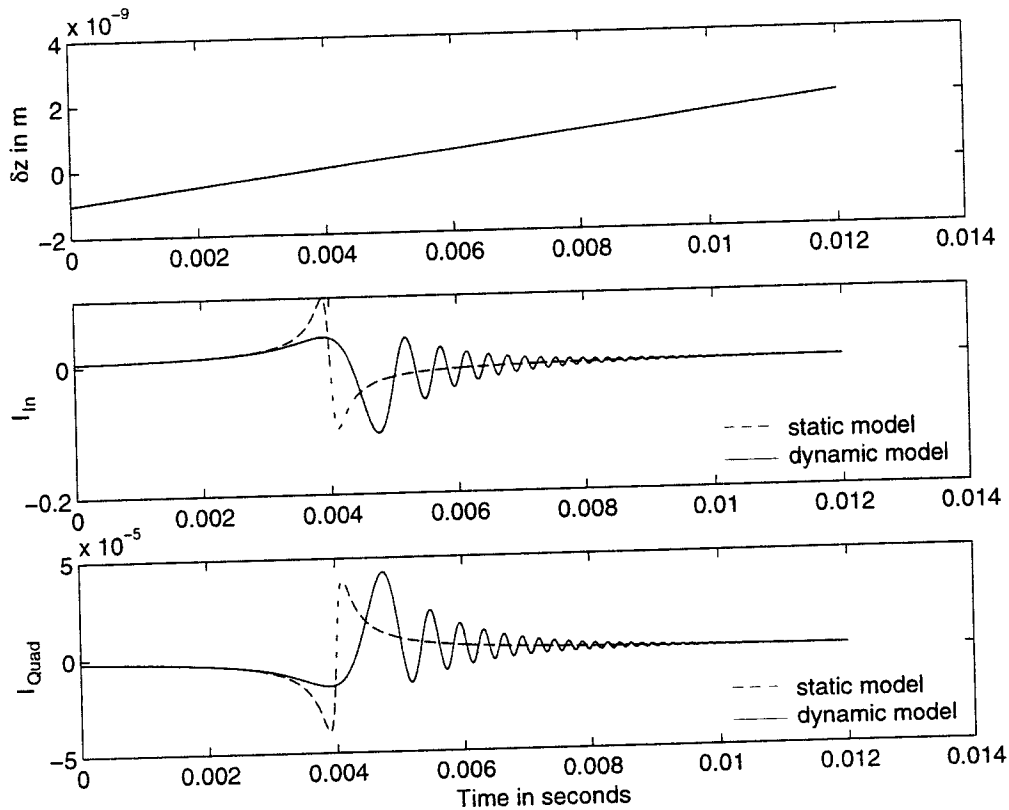


Figure 8. Constant velocity sweep showing signals at input mirror detector.

Frequency Response of Interferometer on Resonance

In order to use a Fabry-Perot interferometer as a Gravity Wave Detector, the length of the interferometer has to be controlled so that the carrier field in the cavity resonates (i.e. the relative position between the mirrors is kept at $n\lambda_0/2$) for long periods of time. When the interferometer is close to the resonant state the interferometer can be modeled as a simple linear system. A linear model is important for two reasons: 1) it provides a predictive model for how gravity wave strain drives the error signal and 2) it provides a simple transfer function model that can be used for control system design.

We can obtain transfer functions for small motions of the cavity mirrors and source phase about the resonant condition in 3 distinct ways. The first approach, described in this section, reduces the solution of the in-phase demodulated signal (Eq. 40) to the case of small disturbances, and then takes the Laplace transform to obtain cavity transfer functions in closed form. The second approach, which is described in a later section, takes the point of view that the cavity mirrors are audio-frequency phase modulators, and sets up a numerical method for computing the frequency response directly. The third approach is simply to exercise the full nonlinear time-domain model in a series of simulated sine sweeps, recording amplitude and phase response to build up a complete

transfer function. This method provides a useful cross-check of the time-domain and frequency-domain models. These 3 methods produce identical results.

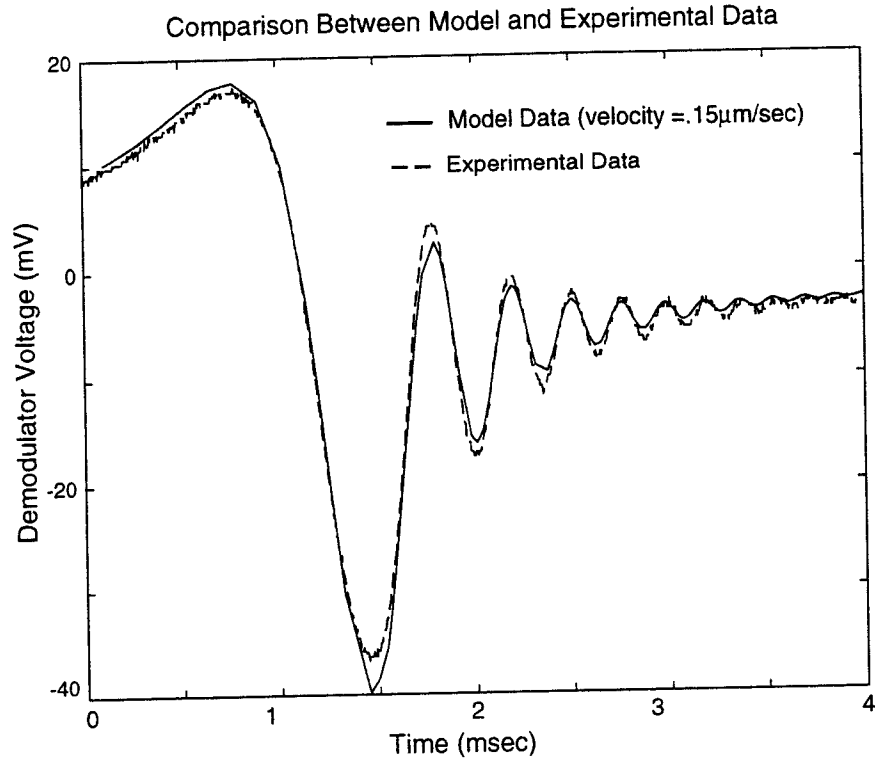


Figure 9. Measured and predicted demodulator voltage: constant velocity sweep.

The first approach for deriving transfer functions, assumes that the cavity is near its ideal configuration, so that the carrier is resonant and the sidebands are essentially anti-resonant. The cavity gain factors for the carrier and sidebands (Eq. 15) become:

$$g_0(t) = r_A r_B e^{-2jk[\delta_B(t-\tau) - \delta_A(t)]} \quad (\text{EQ 42})$$

$$g_1(t) = g_{-1}(t) = -r_A r_B e^{-2jk[\delta_B(t-\tau) - \delta_A(t)]} \quad (\text{EQ 43})$$

where δ_A and δ_B are mirror displacements of mirror A and B, respectively. Assume also that the magnitude of the laser illumination is constant. The source field is then written (for the carrier):

$$E_{s0}(t) = E_{s0} e^{-jk\delta_s} \quad (\text{EQ 44})$$

Carrier source amplitude E_{s0} is a constant; similar expressions obtain for the sidebands. To further simplify the equations, we introduce a cumulative beam phase parameter Δ_n , where:

$$\Delta_n(t) = 2 \sum_{i=1}^n \delta_B(t - (2i-1)\tau) - 2 \sum_{i=1}^n \delta_A(t - 2i\tau) + \delta_s(t - 2n\tau) \quad (\text{EQ 45})$$

We also introduce 2 cavity reflectance parameters R_g and R_r :

$$R_g = r_A r_B \quad (\text{EQ 46})$$

$$R_r = \frac{t_A^2 t_{BS} r_{BS}}{r_A} \quad (\text{EQ 47})$$

Substituting and simplifying, the detected carrier field becomes:

$$E_{D0}(t) = \left[r_A e^{-jk(2\delta_A(t) + \delta_s(t))} + R_r \sum_{n=1}^{n_{beams}} [R_g^n e^{-jk\Delta_n(t)}] \right] E_{s0} \quad (\text{EQ 48})$$

Similarly, the difference of the detected sideband fields becomes:

$$E_{D-1}(t) - E_{D1}(t) = 2 \left[r_A e^{-jk(2\delta_A(t) + \delta_s(t))} + R_r \sum_{n=1}^{n_{beams}} [(-R_g)^n e^{-jk\Delta_n(t)}] \right] E_{s1} \quad (\text{EQ 49})$$

Multiplying the carrier and sideband terms to obtain the demodulated in-phase signal (Eq. 40):

$$\begin{aligned} I_{In}(t) = 4E_{s0}E_{s1} \text{Imag} & \left(r_A^2 - r_A^2 R_r^2 \sum_{n=1}^{n_{beams}} [R_g^n e^{-jk(\Delta_n(t) - 2\delta_A(t) - \delta_s(t))}] \right. \\ & \left. - r_A^2 R_r^2 \sum_{n=1}^{n_{beams}} [(-R_g)^n e^{-jk(\Delta_n(t) - 2\delta_A(t) - \delta_s(t))}] \right. \\ & \left. + R_r^4 \left[\sum_{n=1}^{n_{beams}} R_g^n e^{-jk\Delta_n(t)} \right] \left[\sum_{n=1}^{n_{beams}} (-R_g)^n e^{jk\Delta_n(t)} \right] \right) \quad (\text{EQ 50}) \end{aligned}$$

Near resonance, the phasor exponentials can be replaced with the first 2 terms in a power series expansion:

$$\begin{aligned} I_{In}(t) = 4E_{s0}E_{s1} \text{Imag} & \left(r_A^2 - r_A^2 R_r^2 \sum_{n=1}^{n_{beams}} [R_g^n (1 - jk(\Delta_n(t) - 2\delta_A(t) - \delta_s(t)))] \right. \\ & \left. - r_A^2 R_r^2 \sum_{n=1}^{n_{beams}} [(-R_g)^n (1 - jk(\Delta_n(t) - 2\delta_A(t) - \delta_s(t)))] \right. \\ & \left. + R_r^4 \left[\sum_{n=1}^{n_{beams}} R_g^n (1 - jk(\Delta_n(t))) \right] \left[\sum_{n=1}^{n_{beams}} (-R_g)^n (1 - jk(\Delta_n(t))) \right] \right) \quad (\text{EQ 51}) \end{aligned}$$

Constant terms can be extracted from the sums, and some sums can be closed using the binomial theorem. The result is:

$$\begin{aligned}
I_{In}(t) = & 4E_{s0}E_{s1} \left(-R_r^2 \left[\frac{R_g}{1-R_g} (2\delta_A(t) + \delta_s(t)) + \sum_{n=1}^{n_{beams}} [R_g^n \Delta_n(t)] \right] \right. \\
& - R_r^2 \left[\frac{R_g}{1+R_g} (2\delta_A(t) + \delta_s(t)) - \sum_{n=1}^{n_{beams}} [(-R_g)^n \Delta_n(t)] \right] \\
& \left. + R_r^4 \left[\frac{R_g}{1-R_g} \sum_{n=1}^{n_{beams}} (-R_g)^n \Delta_n(t) + \frac{R_g}{1+R_g} \sum_{n=1}^{n_{beams}} R_g^n \Delta_n(t) \right] \right) \quad (EQ 52)
\end{aligned}$$

This expression can be put back in terms of the source phase and mirror position states by substituting for the cumulative beam phase parameter Δ_n from Eq. 45:

$$\Delta_n(s) = 2 \sum_{i=1}^n \delta_B(s) e^{-(2i-1)\tau s} - 2 \sum_{i=1}^n \delta_A(s) e^{-2i\tau s} + \delta_s(s) e^{-2n\tau s} \quad (EQ 53)$$

$$\begin{aligned}
I_{In}(t) = & 4E_{s0}E_{s1} \left(-R_r^2 \left[\frac{2R_g}{1-R_g} \delta_s(t) - \sum_{n=1}^{\infty} R_g^n \delta_s(t-2n\tau) + \sum_{n=1}^{\infty} (-R_g)^n \delta_s(t-2n\tau) \right] \right. \\
& + R_r^4 \left[\frac{R_g}{1-R_g} \sum_{n=1}^{\infty} (-R_g)^n \delta_s(t-2n\tau) + \frac{R_g}{1+R_g} \sum_{n=1}^{\infty} R_g^n \delta_s(t-2n\tau) \right] \\
& - 2R_r^2 \left[\frac{2R_g}{1-R_g} \delta_A(t) - \sum_{n=2}^{\infty} R_g^n \sum_{i=1}^{n-1} \delta_A(t-2i\tau) + \sum_{n=2}^{\infty} (-R_g)^n \sum_{i=1}^{n-1} \delta_A(t-2i\tau) \right] \\
& - 2R_r^4 \left[\frac{R_g}{1-R_g} \sum_{n=2}^{\infty} (-R_g)^n \sum_{i=1}^{n-1} \delta_A(t-2i\tau) + \frac{R_g}{1+R_g} \sum_{n=2}^{\infty} R_g^n \sum_{i=1}^{n-1} \delta_A(t-2i\tau) \right] \\
& + R_r^2 \left[\sum_{n=1}^{\infty} R_g^n \sum_{i=1}^n \delta_B(t-(2i-1)\tau) - \sum_{n=1}^{\infty} (-R_g)^n \sum_{i=1}^n \delta_B(t-(2i-1)\tau) \right] \\
& \left. + 2R_r^4 \left[\frac{R_g}{1-R_g} \sum_{n=1}^{\infty} (-R_g)^n \delta_B(t-(2i-1)\tau) + \frac{R_g}{1+R_g} \sum_{n=1}^{\infty} R_g^n \delta_B(t-(2i-1)\tau) \right] \right) \quad (EQ 54)
\end{aligned}$$

The transfer functions of the demodulated in-phase signals are obtained from this expression by taking the Laplace transform, closing the sums and simplifying. The transfer function from source phase to in-phase demodulated signal is:

$$\begin{aligned}
\frac{I_{In}(s)}{\delta_s} = & 4kE_{s0}E_{s1} \left(\frac{-2R_g}{1-R_g^2} + \left(1 - t_A^2 r_A^2 \frac{R_g}{1-R_g} \right) \frac{R_g e^{-2\tau s}}{1+R_g e^{-2\tau s}} \right. \\
& \left. + \left(1 + t_A^2 r_A^2 \frac{R_g}{1+R_g} \right) \frac{R_g e^{-2\tau s}}{1-R_g e^{-2\tau s}} \right) \quad (EQ 55)
\end{aligned}$$

At DC ($s=0$), this transfer function is zero. The transfer function from mirror A displacement to in-phase demodulated signal is:

$$I_{In}(s) = 8kE_{s0}E_{s1} \left(\frac{-2R_g}{1-R_g^2} + \left(\frac{-1}{1+R_g} + t_A^2 r_A^2 \frac{R_g}{1-R_g^2} \right) \frac{R_g e^{-2\tau s}}{1+R_g e^{-2\tau s}} \right) + \left(\frac{1}{1-R_g} + t_A^2 r_A^2 \frac{R_g}{1-R_g^2} \right) \frac{R_g e^{-2\tau s}}{1-R_g e^{-2\tau s}} \quad (\text{EQ 56})$$

The transfer function from mirror B to in-phase demodulated signal is:

$$\frac{I_{In}}{\delta_B}(s) = 8kE_{s0}E_{s1} \left(\left(\frac{1}{1+R_g} - t_A^2 r_A^2 \frac{R_g}{1-R_g^2} \right) \frac{R_g e^{-\tau s}}{1+R_g e^{-2\tau s}} - \left(\frac{1}{1-R_g} + t_A^2 r_A^2 \frac{R_g}{1-R_g^2} \right) \frac{R_g e^{-\tau s}}{1-R_g e^{-2\tau s}} \right) \quad (\text{EQ 57})$$

Frequency Response Example

A very long-baseline interferometer, typical of the lengths used for LIGO gravity-wave detection, provides an example to illustrate frequency response characteristics. Interferometer parameters are summarized in Table 2. Figure 10 shows the transfer function from source phase to in-phase demodulated voltage. There is a zero at DC, indicating that low-frequency changes in the source phase have little or no effect on the in-phase signal. The gain increases with frequency, saturating above 90 dB for frequencies above the cavity pole at 92.4 Hz. There are sharp zeros in the amplitude response at frequencies that are multiples of half the cavity free spectral range. These occur when the excitation becomes synchronous or anti-synchronous with the carrier light circulating in the cavity, aliasing the DC condition (0 gain) in the first case, and killing the leaked light contribution to the detector field in the second.

Table 2: Example parameters for 4 km interferometer.

Parameter	Value	Parameter	Value
RA	0.9699	Finesse	410
RB	0.9998	Free Spectral Range	37.5 kHz
Length	4,000 m	Cavity pole frequency	92.4 Hz
Wavelength	0.5145 μm	Fringe width	2.5 nm

The transfer functions from motion of mirrors A and B to in-phase demodulated voltage are shown in Figs. 11 and 12, respectively. The amplitude response is identical for both mirrors. DC gain is 136 dB. Gain is flat vs. frequency up to the cavity pole, where it rolls off slowly. At high frequencies, there are peaks in the amplitude response occurring at

multiples of the cavity free spectral range, where the mirror motion is synchronous with the light circulating in the cavity. This effectively aliases the DC condition, so the peaks recover the DC gain value. There are also very narrow zeros at odd multiples of half the free spectral range, where the excitation is anti-synchronous with the circulating carrier field (and synchronous with the sideband fields). Although the amplitude response of the two transfer functions is identical, the phase response is different. The difference is exactly a time delay whose time constant is the one-way light travel time in the cavity. It should be obvious that the response from moving mirror B relative to moving mirror A is phase delayed by this characteristic time constant.

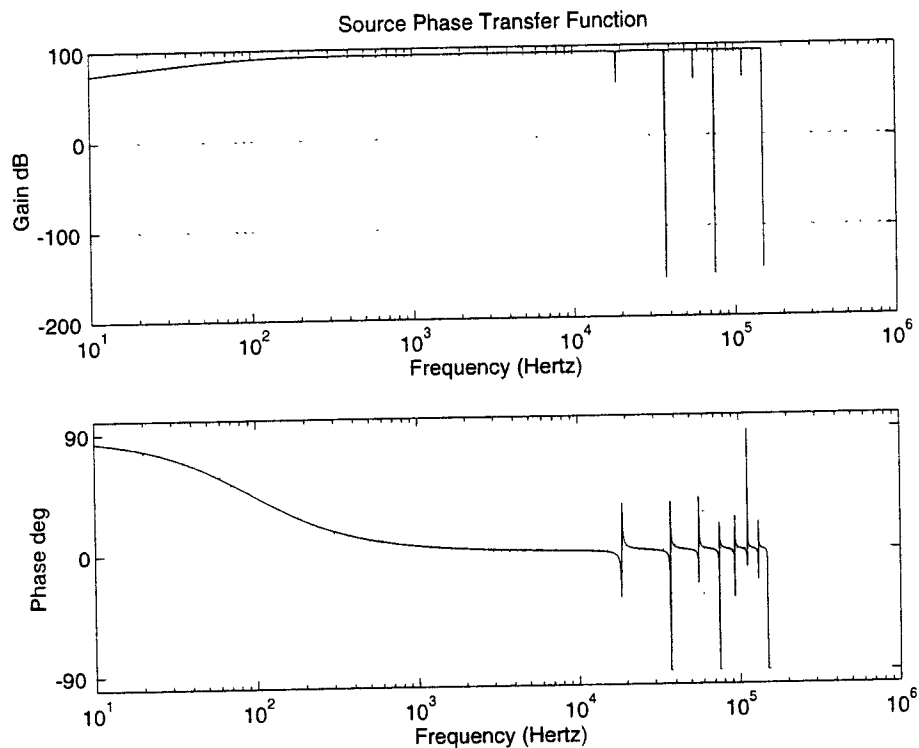


Figure 10. Source phase transfer function example.

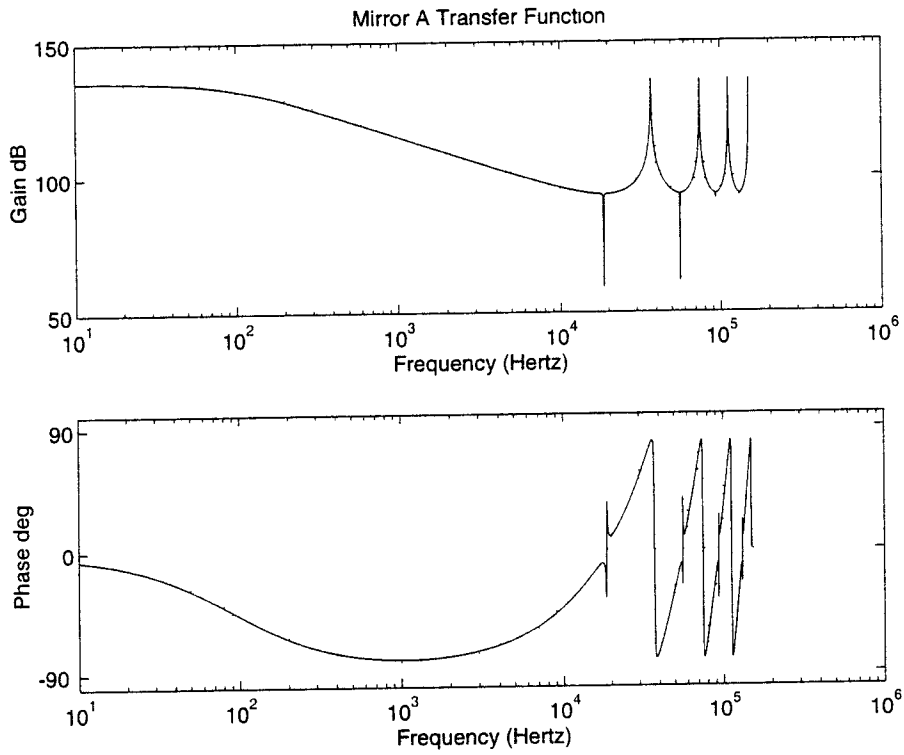


Figure 11. Mirror A transfer function example.

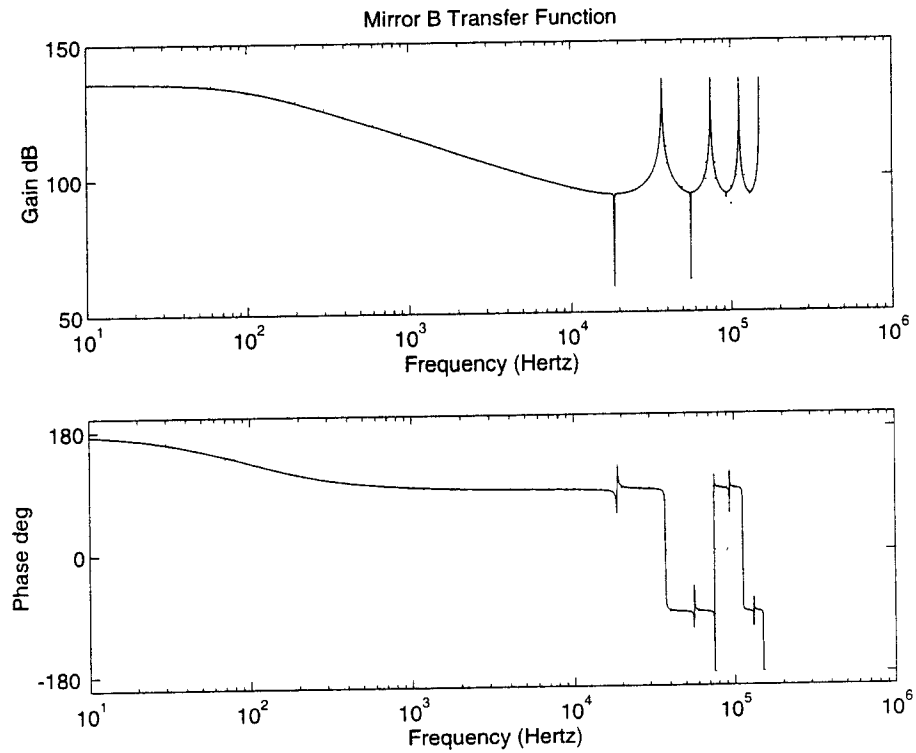


Figure 12. Mirror B transfer function example.

Cavity Transfer Functions in Rational Form

These transfer functions can be further simplified by eliminating certain sideband terms (which do not affect the response significantly) and replacing the time-delay exponentials ($e^{-2\tau s}$) with a rational approximation. The resulting rational transfer functions provide a good match to the exact form over the main frequencies of interest. They offer a convenient form for control design.

The time delay can be approximated as a truncated infinite series, derived by picking a form for the solution, expanding it out in MacLaurin series, and matching coefficients of terms of like order to the series expansion of $e^{-2\tau s}$. We picked a form that matches the high-frequency response well. The result is:

$$e^{-2\tau s} = \frac{(s - \sigma)(s - (\sigma \pm j\omega))(s - (\sigma \pm 2j\omega)) \dots}{(s + \sigma)(s + (\sigma \pm j\omega))(s + (\sigma \pm 2j\omega)) \dots} \quad (\text{EQ 58})$$

Here (in Hz.):

$$\sigma = \frac{\pi}{2\tau} \quad (\text{EQ 59})$$

$$\omega = \frac{\pi}{\tau} \quad (\text{EQ 60})$$

Experience suggests that, in truncating the series, one should carry all terms up to twice the highest frequency of interest. The rational transfer functions in normalized form are (where $\alpha = -\log(r_A r_B) / (2\tau)$):

$$\frac{I_{In}(s)}{\delta_A} = \frac{(s + \sigma) \prod_{n=1}^{\infty} (s + \sigma + jn\omega) \prod_{n=1}^{\infty} (s + \sigma - jn\omega)}{(s + \alpha) \prod_{n=1}^{\infty} (s + \alpha + j2\omega) \prod_{n=1}^{\infty} (s + \alpha - j2\omega)} \quad (\text{EQ 61})$$

$$\frac{I_{In}(s)}{\delta_B} = \frac{I_{In}(s)}{\delta_A} \frac{(s - 2\sigma) \prod_{n=1}^{\infty} (s - 2\sigma + j2(2n-1)\omega) \prod_{n=1}^{\infty} (s + 2\sigma - j2(2n-1)\omega)}{(s + 2\sigma) \prod_{n=1}^{\infty} (s + 2\sigma + j2(2n-1)\omega) \prod_{n=1}^{\infty} (s + 2\sigma - j2(2n-1)\omega)} \quad (\text{EQ 62})$$

The first few poles and zeros of these transfer functions are sketched in Fig. 13.

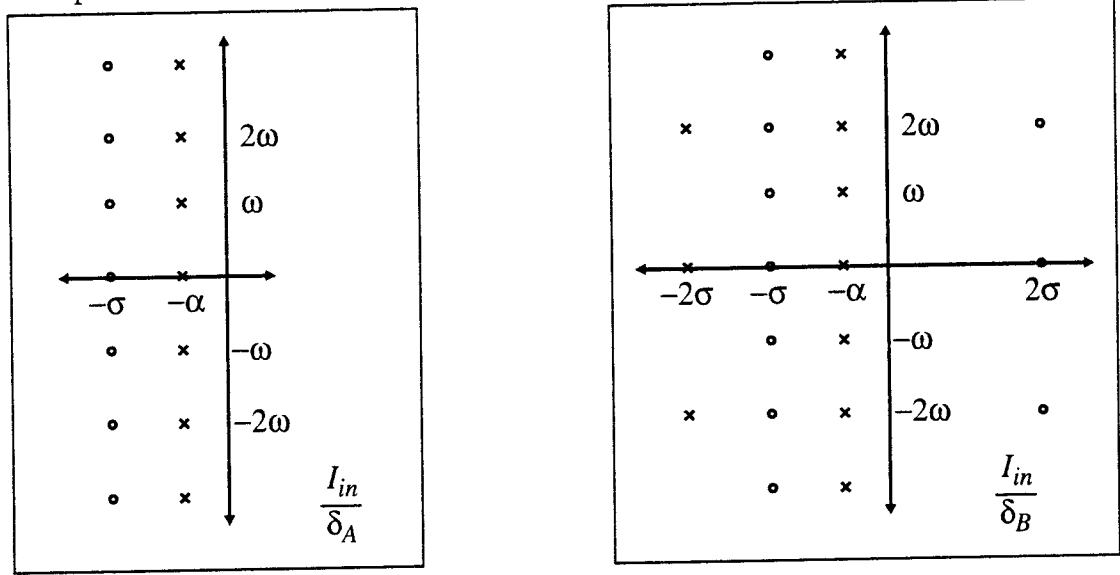


Figure 13. Roots of the cavity mirror transfer functions (rational approximation).

Frequency Response of Cavity Phase Signals by a Frequency Domain Method

This section presents a second method for computing the same transfer functions. Here we take the point of view that moving mirrors act as audio-frequency phase modulators that impart audio sidebands on the reflected fields. This approach has the advantage of being easily generalized to a wide variety of interferometer configurations. It is elaborated in more detail in Ref. 7. Others have also pursued this approach (e.g., Ref. 8).

Consider (for example) mirror B to be moving with small amplitude X at frequency ω_B in an otherwise stationary cavity:

$$\delta_B(t) = X \cos \omega t = \text{Real}(X e^{i\omega_B t}) \quad (\text{EQ 63})$$

The mirror motion frequency ω_B is in the audio band, as opposed to the RF frequencies ω_{mod} used in the PDH detection ($\omega_B \ll \omega_{mod}$). The light reflected from the mirror is then phase modulated. From Eq. 9:

$$E_{Bd}(t) = -r_B (1 - jkX e^{j\omega_B t} + jkX e^{-j\omega_B t}) E_{Ba}(t) \quad (\text{EQ 64})$$

Here we have used $J_0(2kX) \approx 1$ for the carrier term and $J_1(2kX) \approx j$ for the sidebands where J_0 and J_1 are the zeroth and first order Bessel functions. The total field is the sum of the fields at each frequency (carrier and sidebands).

At this point it becomes convenient to modify our notation by adding a second numeric subscript to the field variables to index the mirror audio sidebands. For example, E_{Bd1-1} indicates the component of the field at the upper RF (first subscript) and lower audio (second subscript) sideband frequencies. Using this notation, the total field incident on mirror B is written:

$$E_{Ba} = \sum_{u=-1}^1 \sum_{v=-1}^1 E_{Bauv} e^{-i(u\omega_{mod} + v\omega_B)t} \quad (\text{EQ 65})$$

Discarding terms quadratic in X , the light reflected by mirror B is:

$$E_{Bd} = -r_B \sum_{u=-1}^1 \left(E_{Bau0} e^{-iu\omega_{mod}t} + \sum_{v=-1,1} (E_{Bauv} + ikXE_{Bau0}) e^{-i(u\omega_{mod} + v\omega_B)t} \right) \quad (\text{EQ 66})$$

The source field at the audio sideband frequencies is zero. The detected field can be solved from Eqs. 1 to 13 while substituting Eq. 65 for Eq. 9. The demodulated signal is then computed from the modulus squared of the detected field following Eq.. Only terms at frequencies $\omega_B + \omega_{mod}$ and $\omega_B - \omega_{mod}$ are of interest. With sinusoidal modulation, the in-phase response is:

$$I_{In} = 2\text{Real} \left\{ \sum_{u=-1}^0 \sum_{v=-1}^0 (E_{Bauv}^* E_{Ba(u+1)(v+1)} + E_{Bau(v+1)} E_{Ba(u+1)v}^*) \right\} \quad (\text{EQ 67})$$

The quadrature phase response is:

$$I_{Quad} = 2\text{Real} \left\{ \sum_{u=-1}^0 \sum_{v=-1}^0 (E_{Bauv}^* E_{Ba(u+1)(v+1)} - E_{Bau(v+1)} E_{Ba(u+1)v}^*) \right\} \quad (\text{EQ 68})$$

These expressions are functions of the mirror B motion frequency. They are in fact the transfer functions from mirror B motion to detected in-phase and quadrature-phase signals, for comparison with those derived earlier. A similar analysis leads to transfer functions for motion of mirror A and source phase; the methodology is easily extended to other interferometer configurations as well.

Conclusions

The models presented here capture the longitudinal dynamics of the light circulating in well-aligned Fabry-Perot cavities, for large or small displacements of mirrors or source phase. The models provide useful tools for the design of high-bandwidth cavity length controls. They are also useful for computing the influence of laser phase and mirror seismic noise effects on the noise performance of cavity length measurements. The same basic modeling approach can be extended to encompass more complex interferometer configurations, higher-order modes, and different modulation schemes.

Acknowledgements

The authors wish to thank Stan Whitcomb, Hiro Yamamoto and Jordan Camp of Caltech for their contributions to this work. Thanks also to Rai Weiss of MIT for useful discussions.

References

1. A. Abramovici et al, *Science*, Vol. 256, pp. 281-284, April 17, 1992.

2. R. Drever, J. Hall, F. Kowalski, J. Hough, G. Ford, A. Munley and H. Ward, "Laser Phase and Frequency Stabilization Using an Optical Resonator," *Applied Physics B*, Vol. 31, pgs. 97-105, 1983.
3. J. Camp, L. Sievers, R. Bork and J. Heefner, "Guided Lock Acquisition in a Suspended Fabry-Perot Cavity," *Optics Letters*, Vol. 20, No. 24, pp. 2463-2465, Dec 15, 1995.
4. M. Born and E. Wolfe, Principles of Optics, Pergamon Press, 1987.
5. A. Siegman, Lasers, University Science Books, 1986.
6. G. Franklin, J. Powell and A. Emami-Naeini, *Feedback Control of Dynamic Systems*, Addison-Wesley, 1994.
7. M. Regher, Signal Extraction and Control for an Interferometric Gravitational Wave Detector, Ph.D. Thesis, California Institute of Technology, Pasadena, California, 1995.
8. R. Weiss, personal communication.

LASER INTERFEROMETER GRAVITATIONAL WAVE OBSERVATORY
 - LIGO -
 CALIFORNIA INSTITUTE OF TECHNOLOGY
 MASSACHUSETTS INSTITUTE OF TECHNOLOGY

Document Type	LIGO-T970051-00 - R	2-6-97
NPRO frequency stabilization		
Rich Abbott, James Mason, and Rick Savage		

Distribution of this draft:

This is an internal working note
 of the LIGO Project.

California Institute of Technology
LIGO Project - MS 51-33
Pasadena CA 91125
 Phone (818) 395-2129
 Fax (818) 304-9834
 E-mail: info@ligo.caltech.edu

Massachusetts Institute of Technology
LIGO Project - MS 20B-145
Cambridge, MA 01239
 Phone (617) 253-4824
 Fax (617) 253-7014
 E-mail: info@ligo.mit.edu

WWW: <http://www.ligo.caltech.edu/>

1 ABSTRACT

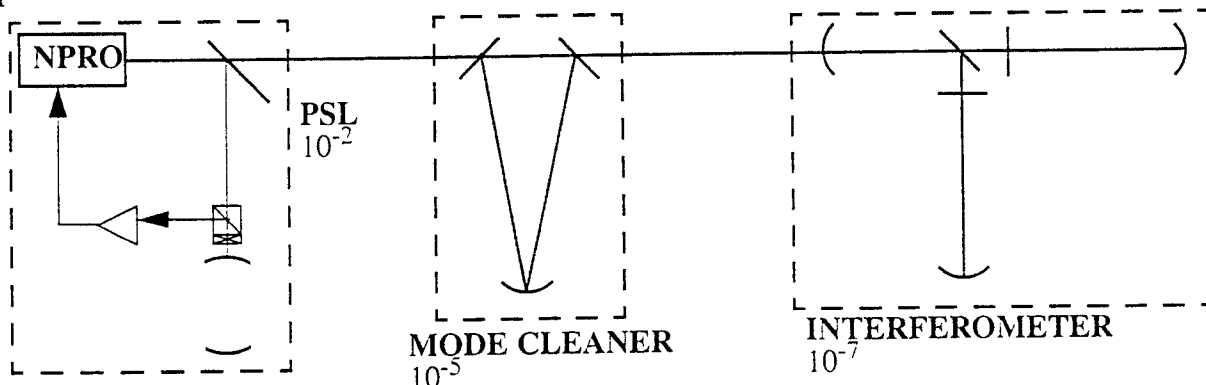
As a first step in the process in switching to Nd:YAG lasers in LIGO, frequency stabilization techniques were applied to a Lightwave model 126 Nd:YAG 1064 nm 700 mW laser. This has two main motivations. First is that the proposed 10 W laser under development for LIGO by Lightwave uses the Model 126 laser as a master oscillator in a MOPA (master oscillator/power amplifier) configuration, and as such will be the point at which frequency corrections are applied in the 10 W version. The second motivation is simply to develop a 1064 nm light source for various experiments while the 10 W version is still being developed, such as the PNI IR conversion.

In this document, a description of the system is outlined, the design of the servos is detailed, and a procedure for obtaining lock using a fixed length reference cavity is described. This system can readily provide stabilization to the level of $10 \text{ mHz}/\sqrt{\text{Hz}}$ from 10 Hz to $\sim 10 \text{ kHz}$. Lock is also quite robust, with lock being kept for time periods of at least 24 hours on a regular basis.

2 CONCEPTUAL DESIGN

2.1. Outline of an interferometer

LIGO proposes to measure strains due to gravitational radiation on the order of $10^{-23}/\sqrt{\text{Hz}}$. An interferometer is to be used by essentially comparing the phase history of light down one arm of the interferometer with the phase history of the light that travelled down the second arm of the interferometer. If there is any mismatch to the lengths of the arms, it can be seen that phase noise, or equivalently, frequency noise, would be a source of noise in the signal, by the relation $\delta f \ll (\delta l)/l \cdot f \cdot (1 - \text{CMRR})$, CMRR being the common mode rejection ratio. In order for LIGO to measure the proposed strains, frequency fluctuations will need to be kept below $10^{-7} \text{ Hz}/\sqrt{\text{Hz}}$ in the interferometer in the bandwidth of interest, assuming a CMRR of 99%. Since the proposed Nd:YAG laser has a frequency noise level typically about $100 \text{ Hz}/\sqrt{\text{Hz}}$ at 100 Hz, it's obvious that some frequency stabilization will need to be done to the laser. This level of suppression is a bit beyond the abilities of a single control loop, so one way to do this is to provide suppression in stages. The first stage of this is called the PSL (Pre-stabilized laser). This supplies approximately 80 dB at 100 Hz. Next is the mode cleaner, after which the laser light should be about $10^{-5} \text{ Hz}/\sqrt{\text{Hz}}$. The common mode servo of the interferometer locks the laser light to the interferometer, and will provide the additional attenuation.



The above diagram gives a rough outline of how a LIGO-like system could be laid out. Not shown in the above diagram are feedback paths from the interferometer and the mode cleaner back to the PSL. The details of how the servo topology for frequency noise in LIGO will be laid out is yet to be finalized.

2.2. Requirements

For this first version of the NPRO PSL, refer to document “NPRO-PSL Design Requirements” (LIGO T960082-00-D) for requirements. Initial requirements of $1 \text{ mHz}/\sqrt{\text{Hz}}$ were relaxed while testing was going on to $10 \text{ mHz}/\sqrt{\text{Hz}}$ from approximately 10 Hz to 10 kHz. This calls for a servo gain of at least 46 dB at 10 kHz, and a gain of about 106 dB at 10 Hz. Also two feedaround paths were to be supplied, to allow direct frequency control to be applied from the mode cleaner and the interferometer. The reference cavity to be used would be a fixed length cavity made of two mirrors optically contacted to a ULE fused silica spacer. In order to have some ability to shift the frequency of the output beam from that of the reference cavity, a double-passed AOM would be used in the PSL stabilization path to shift the frequency of the light $2f_{\text{AOM}} \pm f_{\text{Tuning}}$, where f_{Tuning} is $\pm 5 \text{ MHz}$, determined by the requirement to keep the laser locked to both the reference and some external cavity.

3 SYSTEM LAYOUT

The proposed topology for frequency stabilization of the PSL is specified in the document, “NPRO-PSL Conceptual Design” (LIGO T960089-00-D).

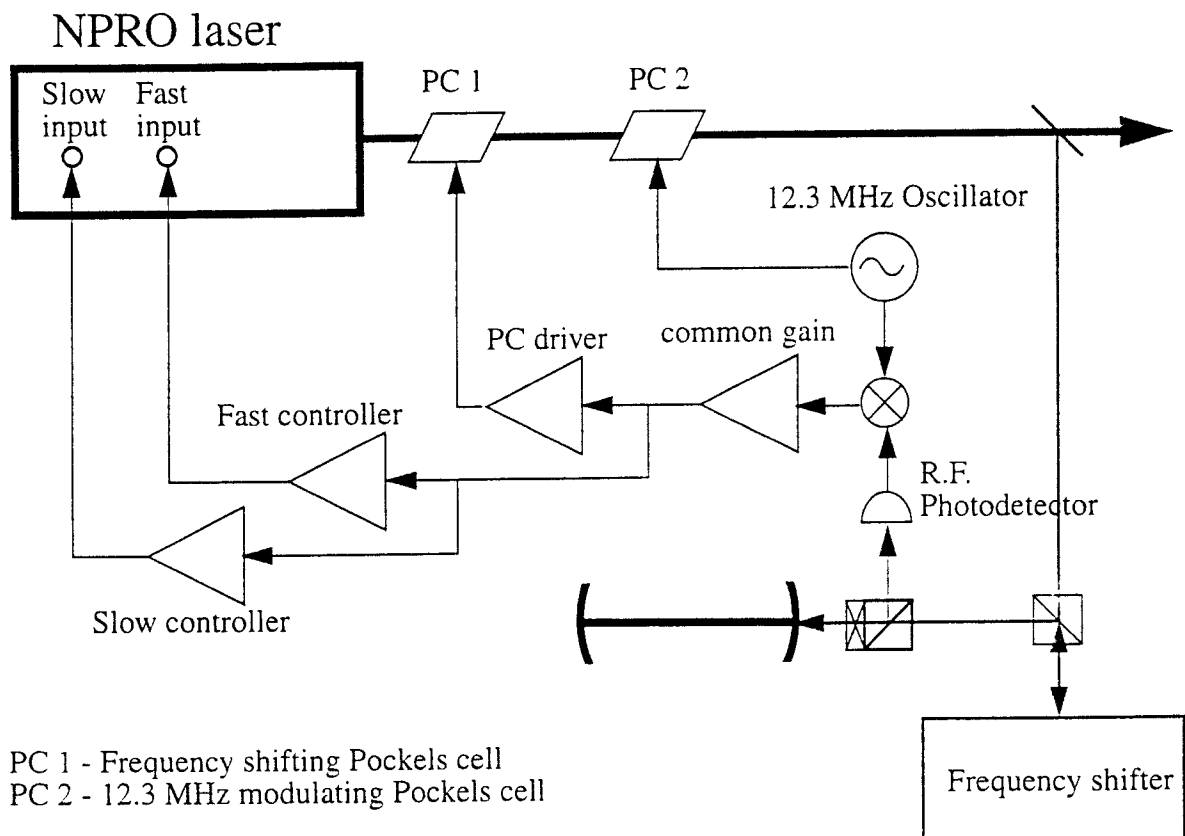
The Model 126 NPRO laser comes with two frequency correction actuators built in. The “slow” controller consists of a thermoelectric cooler, which sets the temperature of the NPRO crystal. This has two effects, to change the physical size of the resonator cavity and to change the index of refraction of the crystal. Lightwave reports that the change Δn of the crystal has a much larger effect than the change in the size Δl . This input has a usable bandwidth of about 0.1 to 1 Hz. The gain is approximately 3-4 GHz/V, with a range of $\pm 10 \text{ V}$. The “fast” controller consists of a piezo bonded to the resonator crystal. Voltage applied to it stresses the crystal, inducing changes in frequency. The bandwidth of this path is nominally limited by the internal resonances of the piezo, which begin around 200 kHz. The gain here is approximately 4 MHz/V, with a range of $\pm 50 \text{ V}$. Both inputs give a positive change in frequency for a positive voltage. The free running frequency noise of the laser is approximately $(2 \times 10^4/f) \text{ Hz}/\sqrt{\text{Hz}}$ from 10 to 10 kHz.

The reference cavity is a ULE fused silica spacer, 20 cm in length, with mirrors optically contacted to each end. The mirror transmissions are 300 ppm, with losses $< 30 \text{ ppm}$. This gives a finesse of ~ 10000 , and a bandwidth of about 75 kHz. The temperature induced resonant frequency change is $\sim 150 \text{ MHz}/^\circ \text{C}$. The light is to be locked to this cavity using the Pound-Drever-Hall reflection locking technique, using sidebands at 12.3 MHz. The cavity is suspended in a vacuum chamber at 10^{-7} torr by two loops of wire from a 3 layer seismic isolation stack.

Since the cavity has no length adjustment, a double passed AOM is used to shift the frequency of the output laser light from that of the reference cavity. Double passing the 1st order diffracted beam output of the AOM, the light is shifted by twice the drive frequency of the AOM. This fre-

quency is a nominal 80 MHz \pm 5 MHz. This gives a tuning range of \pm 10 MHz, which was chosen after analysis of data from the 40m interferometer and the 12m triangular mode cleaner.

The stabilization servo would need about 46 dB of gain at 10 kHz, but the fast piezos probably don't have a usable bandwidth much more than 20 kHz due to their resonances. This makes it necessary to utilize an external phase correcting Pockels cell to extend the bandwidth of the servo so it can be stable. The Pockels cell used is a New Focus model 4004 broadband Pockels cell, with a specified modulation depth of 15 mrad/V.



The diagram above lays out the general design of the NPRO PSL. The other Pockels cell in the diagram is the 12.3 MHz Pockels cell, a New Focus 4003 resonant Pockels cell. The 12.3 MHz oscillator and amplifier are existing modules. The photodiode is an existing RF photodetector, using a tuned tank circuit at 12.3 MHz, modified for 1064 nm with either a YAG444 or a 220A photodiode.

4 SERVO DESIGN

Servo design requires some modeling, into which physical parameters need to be put. Measurements were made of the various actuators to build the model.

4.1. Actuators and existing gains

4.1.1. Slow actuator

The slow actuator frequency response was measured by locking the laser to a Coherent optical spectrum analyzer in transmission. The slow input was driven and the transfer function from the slow input to the locking error signal was taken. The closed loop gain was divided out, giving the frequency response of the actuator. This is shown in Figure 1 (All figures are collected at the end of this document). A simple model for this response is a 3-pole roll off at 0.2 Hz, with a DC gain of 3 GHz/V.

4.1.2. Fast actuator

Nominally, the piezo of the fast actuator should have a relatively flat frequency response out to the mechanical resonances of the piezo. A measurement of this was made by locking the laser to the reference cavity with low gain and bandwidth (< 1 kHz). Above the servo bandwidth, then, the signal out of the demodulator is essentially an open loop measurement of the frequency noise. The fast piezo was driven above the unity gain of the servo, and a transfer function was measured from this input to the demodulator out. Figure 2 shows a 10-100 kHz span of this measurement. Included in the dynamics of this measurement is the cavity pole, which shows up at 35 kHz. Subtracting the cavity pole results in a flat response at least to 100 kHz. Of note are the features around 30 kHz, 60-70 kHz, and above 90 kHz. These are consistent with parallel, or parasitic resonances, most likely of the structure the piezo is mounted on. A measurement was made to higher frequencies, also. Piezo resonances were found around 250 kHz, above which the response was not coherent. The gain of the piezo was determined by driving the piezo open loop with a triangle wave generator. The amplitude was high enough to scan through the carrier and both sidebands. A photodiode monitored the transmitted light through the cavity, and an oscilloscope was used to determine the amount of voltage needed to scan from sideband to carrier, then carrier to the next sideband. Several measurements were averaged to give 4.1 MHz/V.

4.1.3. Pockels cell

The Pockels cell response was measured in the same fashion. The laser was locked with low gain and bandwidth (~2 kHz). The Pockels cell was driven, and the transfer function from the Pockels cell to the demodulator output was measured. Figure 3 shows this transfer function, with the cavity pole, the demodulator gain, and the zero of the Pockels cell divided out. The measured gain of the Pockels cell is 19 mrad/V.

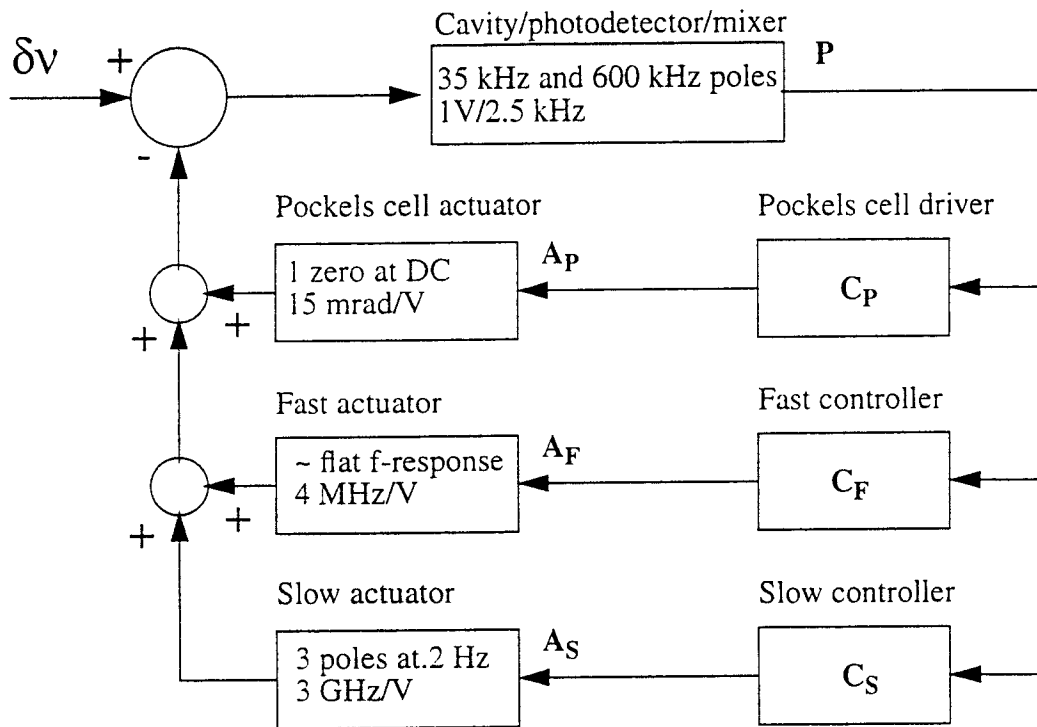
4.1.4. Demodulator gain

The “demodulator gain” refers to the voltage out of the mixer due to a frequency fluctuation about the point of resonance. This can be estimated using a relatively simple analytical model. The power incident on the photodiode which contains the signal proportional to frequency fluctuations goes as $Re\{E_0 \cdot (E_{+1} + E_{-1})^*\}$, where E_0 , E_{+1} , and E_{-1} are the carrier and sideband fields reflected from the cavity. Using 85% photodiode efficiency, a known impedance of 8000 Ω in the tank circuit of the R.F. photodiodes, and a 6 dB insertion loss into the mixers, a demodulator gain of

about 1 V/2.5 kHz is arrived at. In reality, the actual gain will probably be lower, due to imperfect modematching, etc. However, this number is sufficient to use in a model.

4.2. Controller design

A block diagram of the controller is shown below. Each of the actuator loops needs to be used in parallel with the other 2. The rule for parallel open loop gains is that the open loop looks like the frequency response of the particular loop which dominates in gain. In this case, we expect to see the slow loop dominate below .1 Hz, the fast loop to dominate up to about 20 kHz, and the Pockels cell to dominate out to the bandwidth of the servo.



4.2.1. Slow controller

The main purpose of the slow controller is to provide DC control of the laser. That is, for long term drifts due to variations in temperature of the laser, the reference cavity, etc., the slow actuator, with a possible tuning range of about 600 GHz, is used. Since the reference cavity has no length control, and a free spectral range of 750 MHz, DC fluctuations are most easily controlled using the slow actuator. This is most effectively done by using an integrator in the slow controller. For practical purposes, this controller needs a “switch” that turns the integrator off, which is done by moving the pole from DC to some finite frequency, in our case 0.05 Hz. This is useful to short the integrator if any offsets have been integrated, and allows for faster time responses of the slow controller in this mode. Since acquiring lock would also be very difficult with the integrator on, the shorted integrator is referred to as “acquisition mode”. This loop should have a bandwidth of approximately 0.1 Hz, due to the poles at 0.2 Hz in the actuator.

The range of the slow controller would in principle need to be within one free spectral range of the cavity, or 750 MHz, which corresponds to about 200 mV in the slow actuator. Standard op-amps will have plenty voltage output to tune over many free spectral ranges, so the dynamic range of this controller would not be a problem.

At the upper end of the slow bandwidth, 0.1 Hz, we have no specific frequency noise requirement, but the requirement at 10 Hz of $10 \text{ mHz}/\sqrt{\text{Hz}}$ might suggest a level of $100 \text{ mHz}/\sqrt{\text{Hz}}$ at 0.1 Hz. Based on a conservative 1V/10 kHz mixer output, this corresponds to an input referred electronics noise of $\sim 1 \mu\text{V}/\sqrt{\text{Hz}}$, which is pretty trivial.

4.2.2. Fast controller

The fast path will be responsible for the frequency noise suppression in the bandwidth of interest. The main design requirement is that the servo has enough gain, and has low enough noise. Given a $1/f$ free running noise spectrum, then the controller needs to be at least $1/f$. A 2 pole controller was designed, mostly because it was simple enough to do. A third pole was added to help roll off the response at higher frequencies, in response to the presence of piezo resonances in the 200's of kHz. A zero was added to improve the phase of the fast loop at the point where control is handed over to the Pockels cell. So, the fast controller has poles at 10, 100, and 10000 Hz, and a zero at 500 Hz. The nominal gain at DC is about 10^6 .

Given the free running frequency noise quoted in section 3.1, and assuming this is reasonably good down to .1 Hz, integrating this power gives about $2 \times 10^6 \text{ Hz}_{\text{RMS}}$ from .1 to 10000 Hz. Working back from the fast actuator, this corresponds to about $0.5 \text{ V}_{\text{RMS}}$, which is not a problem for controller or actuator.

The noise of this servo must be small, at least a factor of 10 below the frequency noise goal. Using $1 \text{ mHz}/\sqrt{\text{Hz}}$, and the demodulator gain, we specified an input referred noise of $300 \text{ nV}/\sqrt{\text{Hz}}$, which is also fairly simple, as long as the gain of this loop is kept in the early stages of the electronics.

4.2.3. Pockels cell driver

The main purpose of the Pockels cell path is to extend the bandwidth of the overall loop gain, so that there can be $\sim 46 \text{ dB}$ of gain at 10 kHz. There are several factors that motivate the shape of this loop. Drive voltages to a frequency correcting Pockels cell typically are rather high. In order to keep this number as low as possible, the loop is ac-coupled with 2 zeros at DC. This puts the phase of the loop $+270$ degrees. At the point where the Pockels cell loop gain equals the fast loop gain, however, stability considerations dictate that the difference in phase of the two loops needs to be less than 180 degrees. Since the fast loop has phase close to -180 , several poles need to be incorporated in the Pockels cell path to bring the phase to an acceptable level. Zeros are also incorporated in the controller to account for the cavity pole and the photodiode pole. To this end, the Pockels cell controller has two zeros at 0 Hz, one at 50kHz, and one at 1MHz. A pole is put at 1 kHz, and 3 more at 5 kHz. Gain is adjusted to cross the fast loop gain around 20 kHz.

As mentioned before, the two zeros in the Pockels cell path are included to reduce the amount of rms contribution from frequency noise out of the band dominated by the Pockels cell. A model of the loop was put together in Matlab, the transfer function was calculated from frequency noise to the voltage into the Pockels cell. Multiplied by the frequency noise of the laser, and integrated, the

total rms to the Pockels cell is about 1-2 V_{RMS} . This allows the Pockels cell controller to be made using standard op-amps, which simplifies the problem somewhat.

Noise consideration are similar to the slow controller in that the bandwidth dominated by this controller is out of the specified frequency range for control.

4.2.4. Additional features

In addition to the poles and zeros and voltage requirements for each of the three loops above, other features of note are included in the design. First, a feedaround input, as required in the conceptual design document, is incorporated into the early stages of the amplifier. This is simply to be a unity gain buffer. Also, to simplify the amount of cabling, the mixer is included on board, along with notch filters for the modulation frequency and its first two harmonics. The slow path also includes a buffered input at the end of its path in order to sum an external DC voltage offset. As mentioned in the conceptual design document, this is necessary for lock acquisition. A DC bias is applied to the slow input in order to coarsely tune the laser to the resonant frequency of the reference cavity. Once the laser is close to the cavity frequency, lock can be acquired and the integrator in the slow path can be used to maintain the proper bias to the slow controller to keep the laser at that frequency. Also included are test inputs and outputs to measure transfer functions, and monitor outputs are on each of the servo path outputs. Since this is a 3 degree of freedom system, 3 gain controls are included. Since the Pockels cell path goes to high bandwidth where phase delays can have significant effect, the placement of the 3 gain stages are an overall gain stage, and one each in the slow and fast paths, leaving out any direct gain control in the Pockels cell path. Switches are included to switch off the slow controller, to switch between “acquisition” and “integration” mode in the slow controller, and to switch to a test input after the mixer output for diagnostic purposes.

A schematic of the controller along with a list of the front panel features and labels is included at the end of this document.

4.3. Modeling results and predictions

4.3.1. Loop gain and expected residual frequency noise

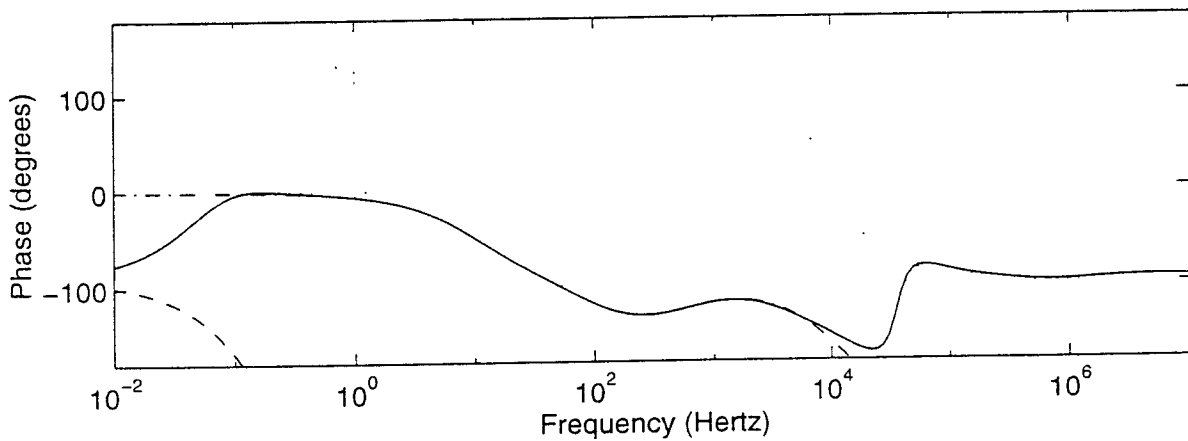
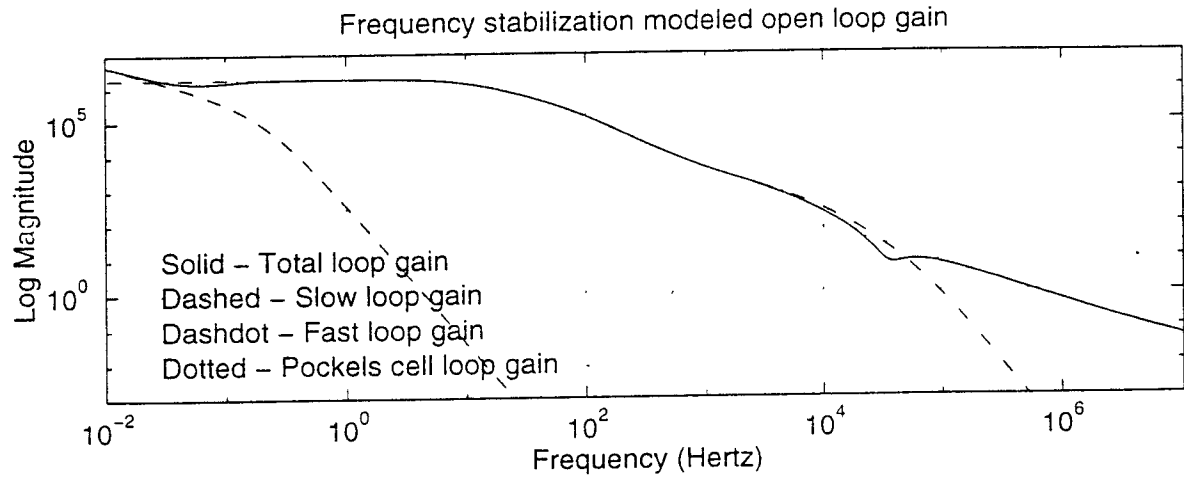
As mentioned in section 4.2.3, a model of this control loop was built in Matlab, using the measured parameters of the system and the proposed control electronics, as laid out in the diagram above. The paradigm consisted of *.m files which contained the frequency response of each of the blocks in the diagram in section 4.2. A master file called these transfer functions and multiplied them in the appropriate fashion to generate whatever transfer function was required. The resulting open loop gain is given by the following equation, and shown in the following figure. The C's, P's and A's are defined as in the block diagram in section 4.2. Calculating the residual frequency

$$L_{OL} = P \cdot (C_S A_S + C_F A_F + C_P A_P)$$

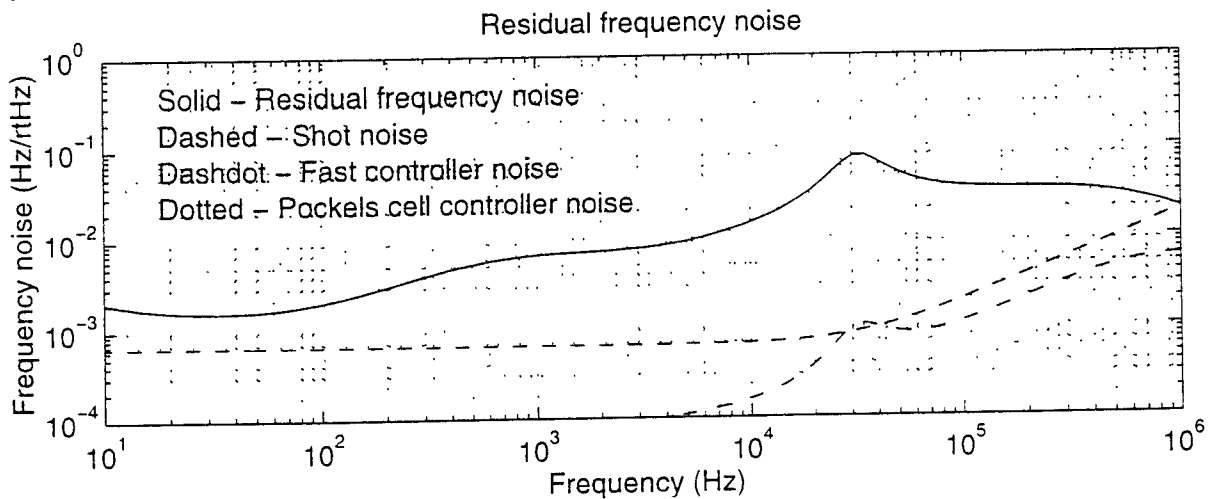
noise requires the closed loop gain, shown below, multiplied by the open loop frequency noise

spectrum. Based on this transfer function, and assuming a frequency noise spectrum like that

$$L_{CL} = \frac{1}{1 + L_{OL}}$$



stated in section 3.1, this results in a residual frequency noise spectrum shown in the following figure.



4.3.2. Limiting noise sources

4.3.2.1 Shot noise

The frequency detection method is a process dependent on sensitivity to optical power, in other words, it counts photons. A fundamental noise source with this sort of detection is shot noise, which essentially goes as \sqrt{N} , where N is the number of photons detected. Detailed calculations have derived formulas for the shot noise sensitivity of this detection method, given as

$$\frac{S}{N}(f) = \vartheta_{FSR} \sqrt{\frac{e}{\sigma}} \cdot \frac{\sqrt{3|E_+|^2 + E_{DC}^2}}{2\pi E_2 E_+} \cdot \frac{(1 - r_a r_b)^2}{T_a r_b} \cdot \sqrt{1 + \left(\frac{2\pi f}{\omega_c}\right)^2}$$

Definitions for the various parameters are found by referring to either “Shot Noise in a Recycled Unbalanced LIGO” by Torrey Lyons and Martin Regehr, or “Calculations for the Shot Noise in the Recycled 40m” by Malik Rahkmanov. Given the appropriate parameters for the optical configuration, the level of shot noise is shown on the previous figure.

4.3.2.2 Electronic noise

The designed electronics were modeled in Cadence to predict their transfer functions, and estimate their noise outputs. Cadence is a sophisticated program which takes into account real properties of op-amps, phase delays in circuits, etc. From the output referred noise predicted by the Cadence model, transfer functions were derived from the output of the controllers to the frequency error point to estimate the contribution to frequency noise due to noise in the electronics. The figure above containing the residual frequency noise also contains the level of noise contributions from both the fast and Pockels cell controllers.

5 PERFORMANCE

5.1. Measured transfer functions and noise

Figures 4 and 5 show measured transfer functions of the fast and pockels cell controllers. These all agree with the modeled transfer functions to reasonable levels of accuracy. Figures 6 to 8 show measured output referred noises of each of the controller electronics. These also agree remarkably well with the Cadence model prediction.

5.2. Locked laser measurements

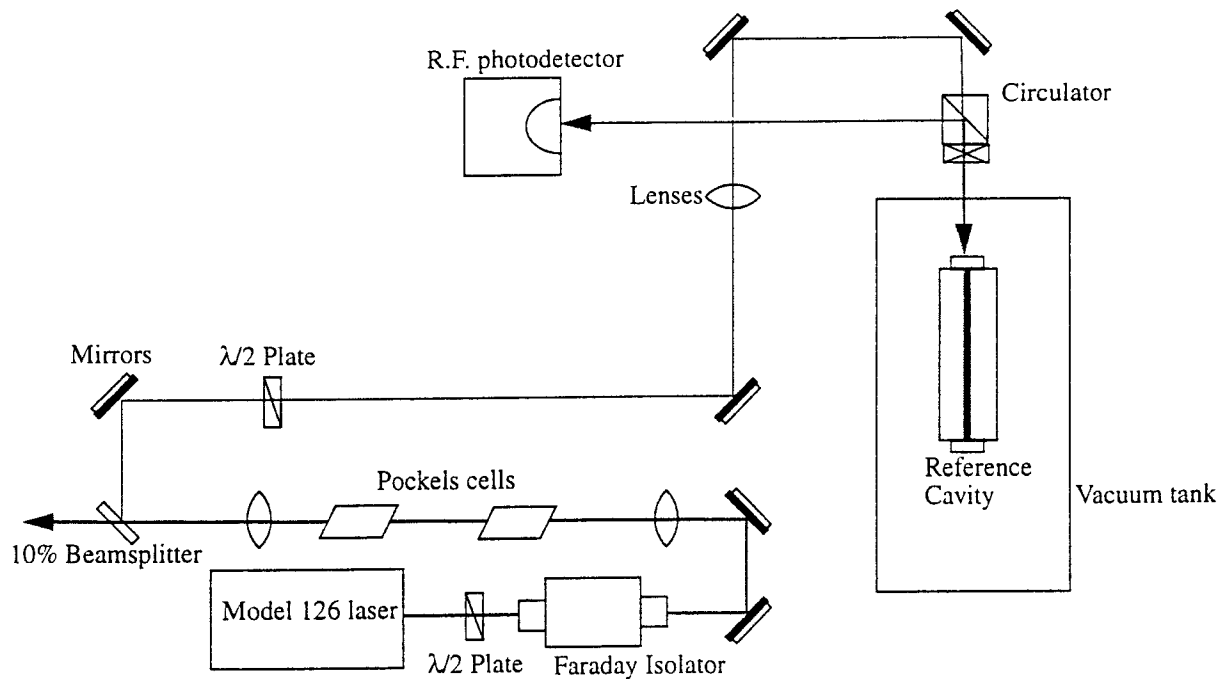
Figure 9 shows an in-loop (and hence lower bound) measurement of the residual frequency noise. The following figures, 10 and 11, shows measurements of the open loop gain for this particular measurement, over different bandwidths. Of note is that the frequency noise requirements have mostly been met within the bandwidth of interest as measured inside the loop. Although the figure shows $10 \text{ mHz}/\sqrt{\text{Hz}}$ only to 7 kHz, obtaining this level at 10 kHz was not difficult, however, it entailed increasing the gain of the fast loop, which causes the bump at 30 kHz to grow. This is a result of the relative phase of the fast and Pockels cell paths at the crossover point, which gets worse at higher frequency. Agreement between this and the predicted residual frequency noise is

very good. However, some problems show up in the measurement of the loop gain, most notably the amount of phase available at unity gain. The model prediction shows that there should be plenty of phase at unity gain, and bandwidth shouldn't be limited at all by this consideration. The measurement on the other hand indicates that the phase drops considerably in the 100 kHz band, and that phase margin goes to 0 at about 600 kHz. The fact that the phase is decreasing in the fashion that it does tends to suggest that phase delays are accumulating in the Pockels cell path. The measurement of the pockels cell controller supports this, and modeling phase delay produces a loop gain which agrees with the measurement.

6 OPERATION

6.1. Setup

The figure below lays out our optical table and elements.



The first $\lambda/2$ plate is used to rotate the polarization of the light from vertical to 45 degrees for insertion into the Faraday isolator (measured insertion of 93%). The light leaving the isolator is then polarized perpendicular to the table. The first lens is used to focus the light to a waist position between the two Pockels cells. The measured spot size at 5 cm from the laser is $\sim .2$ mm, and the waist positioned between the Pockels cells is nominally .1 mm. The first Pockels cell is the broadband frequency correcting Pockels cell, and the second is used to impose the 12.3 MHz modulation. This was driven at ~ 6 V_{p-p} resulting in a modulation of $\sim \Gamma = .75$. The next lens is used in conjunction with the 3rd lens for modematching. A 10% window is used to pick off a portion of the light for frequency stabilization. Since the laser is outputting about 600 mW, and we really only would like about 10 mW input to the cavity, the second $\lambda/2$ plate is used in conjunction with the circulator's polarizing beamsplitter to dump the rest of the light. This obviously is not optimal

for use in an interferometer, however it suited this particular setup. The circulator is a polarizing beamsplitter with an optically contacted $\lambda/4$ plate. This causes the light reflected from the cavity to be reflected by the polarizing beamsplitter, not transmitted. This light is then detected by an R.F. photodetector, which has a tuned resonant circuit to maximally transmit power at 12.3 MHz. The vacuum tank was kept at 10^{-7} torr using a Vac-Ion pump. Inside the vacuum, the reference cavity was hung from small springs mounted on posts. Two small copper vanes were hung from the cavity close to two sets of 4 magnets in a quadrupolar configuration for eddy current damping of the two swinging modes of the suspended cavity. The supports for the cavity are mounted on an isolation system made up of 3 plates with RTV silicone springs between them. Not shown but also used was an infrared camera, placed at the far end of the vacuum tank in order to see the light transmitted when the cavity was on resonance. Also not shown is an optical spectrum analyzer, which has another 10% pick off just before the RF photodiode. Note that the frequency shifter was not incorporated into this layout, because time did not allow.

6.2. Alignment

Typical alignment procedure involved first passing the light through the Faraday isolator. This was done using an infrared photo card, and eyeballing the position of the beam approximately to the center of the F.I. apertures. The alignment was done by shifting the position and tilt of the F.I.. The next alignment was the first lens, which simply involved positioning the lens such that the beam passed through the center of the lens, by marking the position of the beam without the lens at the other end of the table, and bringing the position of the beam back to the same place once the lens was installed. Next, in order to align the beam through the 2 mm apertures of the Pockels cell, a negative lens was used to blow the beam up so it was approximately 2 cm in diameter on a beam block. The position of the front aperture for each Pockels cell was adjusted by finding where the beam clipped the aperture on each side, then centering the aperture in between these points. Then the positions of the rear apertures were dithered to minimize the distortion to the beam as viewed in the expanded spot. The next two lenses were also centered, and placed according to calculations to mode match into the cavity. Alignment into the cavity was performed first by roughly eyeballing the light to the center of the input cavity mirror, using the final two mirrors in the optical path. Then a function generator was used to dither the frequency of the laser over a large range in the slow actuator (by at least one free spectral range), while the camera which looked at the output of the cavity was monitored. Once modes began flashing in the cavity, adjustments were made based on the strength of the modes, to begin optimizing for lower order modes. Once a TEM_{00} mode was found, a slow DC offset was applied to the slow actuator to bring the laser close to the frequency of the 00 mode, and the function generator drove the fast actuator (the time scales of the slow actuator were irritatingly slow). Then, the alignment attempted to maximize the output of the 00 mode through the cavity. For reference, irises were placed in the optical path and centered on the beam for future alignment.

Some "electrical" alignment is also done. First, the phase of the local oscillator applied to the mixer needs to be set. Since the phase shifter has, at the smallest, 10 degree divisions, this was done by eye. The 00 mode was found, and the function generator used to dither the fast input of the NPRO. The output of the mixer was viewed on an oscilloscope set to trigger as the laser went through resonance. The phase was adjusted to maximize the symmetry of the demodulator output, verified by setting the phase to the "wrong" phase and confirming the symmetry in that output.

Also, the electronics comes with the ability to tune out any voltage offset out of the mixer. This was done by looking at the MIXROUT output through a SR560 and a gain of about 100, low passed at .03 Hz. The pot, located inside the NIM module, was tuned such that the DMM read about 1 mV, after the bias of the SR560 was tuned out, which seemed to be about as good as could be done.

6.3. Nominal settings

A set of parameters was developed as indications of the state of the system. Nominal values for these parameters were worked out to insure repeatability of results. These are listed in the table below.

Modulation voltage	2.5 V _{Peak}
Modulation depth	.75
Cavity input power	10 mW
Visibility	80-90%
Laser power	600 mW
Vacuum pressure	10 ⁻⁷ torr
RFPD V _{DC} (out of lock)	-130 mV
RFPD V _{DC} (locked)	-48 mV

Table 1: Nominal parameters for NPRO laser

6.4. Lock acquisition

The process used to acquire lock in these experiments was not automated. Gains in all loops are turned to 0, the slow loop is left open, and the integrator is switched off to keep from integrating up any offsets in the path. The slow actuator is ramped in the slow DC input using the Calibrators DC voltage supply until the 00 mode is found, usually by watching the camera which is looking at the transmitted cavity light. Once the mode is found, the gain in the fast path is turned up slightly. If the laser is very close to resonating, the laser will usually lock right away. If not, the slow actuator must be used to tune the laser closer to the right frequency, with the fast gain small, maybe about 0.1, and the common gain at minimum. The reason that the fast gain must be kept low is that when the laser needs to tune through the point where the sidebands are resonant, the servo has the wrong sign, and a large voltage builds up in the fast path as the slow DC tries to push against the fast gain of the servo. When the slow finally manages to exceed the ability of the fast loop to keep away from the sideband resonance, the fast voltage drops to zero and the laser frequency shifts very rapidly through the carrier and the other sideband, to the tuned point of the slow DC. However, with low fast gain, it's easy to tune via the slow DC close to resonance, then turning up the fast gain usually will lock the laser immediately. At this point, the fast gain needs to be increased to about 0.5 to 1.0 before the common gain can be turned up. This sets the crossover between the fast loop and Pockels cell at approximately the right place in the 20 kHz region. Then

the common gain can be turned up to approximately 0.6 or 0.7. This brings the loop very close to the maximum gain possible, limited by the loss of phase margin at 600 kHz. If the MIXROUT output is being monitored on an oscilloscope, this is evident by the output voltage beginning to grow as the gain is increased. This is not due to a noisier laser, but rather unity gain oscillations at around 500 kHz. At this point, the slow loop is turned on, and the slow mode is switched from acquisition to integration. The gain of the slow loop can be turned up to about 0.3 or 0.4 before oscillations begin to develop.

Re-acquisition once lock is lost is a similar process. The first thing that needs to be done fairly quickly is the integrator must be switched off. Also the gains must be turned down in the same way as acquiring lock the first time. If the slow DC bias is still hooked up and supplying the DC voltage which brought the laser roughly to resonance, frequently all that's needed is to wait until the laser relaxes and returns to equilibrium. Loosing lock typically causes the laser to shift its frequency somewhat, and requires about a half a minute to relax. Once close to resonance, again, the fast gain is turned up, then the common gain. However, if the laser frequency set by the slow DC bias has drifted relative to the cavity sufficiently, the laser will not return to the point where the fast loop can acquire. At this point, the slow DC bias voltage must be scanned again to find the resonance. This typically is not far away, though, so radical shifts in voltage should not be required.

6.5. Problems

Below is a list of problems and other notes concerning frequency stabilization of the NPRO, both understood and not understood.

- When the common gain is turned up too high, although not high enough to lose lock, occasionally 2 spikes in the frequency spectrum show up around 3 and 5 kHz. The origin of this is unknown, however it's suspected that a stage in the pockels cell path may be saturating. The pockels cell path has very high gain, which peaks at about 4 kHz, and the first pass at these electronics had bad saturation problems in the pockels cell path (not on the output, however).
- Concerning the use of the power adjust input for power stabilization. There is a very strong coupling between the power adjust input and frequency noise. Figure 12 shows a transfer function between the power adjust input and frequency noise output. This measurement was made with the built in "noise eater" off, however with the noise eater on, this trace goes down maybe only 10 dB. It was made by driving the power adjust and looking at the voltage out of the demodulator. The cavity pole and the loop gain have been divided out, as well as the frequency to voltage gain of the demodulator. This coupling is both good and bad. The good is that stabilizing the power output of the laser diodes does help the frequency stabilization, which tends to suggest that a large amount of frequency noise comes from intensity fluctuations of the laser diodes. The bad is that stabilizing the laser light at some point far down the optical path may introduce noise into the laser diode in order to correct for artificial intensity fluctuations (i.e., fluctuations due to beam jitter through a mode cleaner, parasitic interferometers). This in turn will make the frequency stabilization worse.
- Changing the common gain of the servo while the integrator is on seems to occasionally cause problems, that is the slow path seems to want to begin oscillating. Not understood.

- The slow monitor output monitors the output of the slow controller before the slow DC bias is summed.
- Fast monitor offsets. The laser, once locked using the fast and Pockels cell, can be tuned using the slow DC bias until the DC offset out of the fast controller is nulled. Turning the slow controller on in acquisition mode will not typically change this, that is the slow controller will hold the DC laser frequency close enough to resonance such that the fast path will have no DC offset (over short time scales). However, turning the integrator on will typically shift the fast offset to a couple volts. The origin of this is uncertain, but could be consistent with mV offsets in the slow path. Changing the gain of the slow controller affects this offset, also. For long time scales, though, it's favorable to use the integrator, since it will keep this offset constant, whereas in acquisition mode, there isn't enough gain to adequately track the long term variations in the laser temperature and the cavity fluctuations.

7 FIGURES

Figure 1 : Slow actuator frequency response

Figure 2 : Fast actuator frequency response

Figure 3 : Pockels cell frequency response, with $i\omega$ divided out

Figure 4 : Fast controller transfer function

Figure 5 : Pockels cell transfer function

Figure 6 : Slow controller output noise (input 50Ω terminated)

Figure 7 : Fast controller output noise

Figure 8 : Pockels cell controller output noise

Figure 9 : Residual frequency noise

Figure 10 : Measured loop gain, 100 kHz bandwidth

Figure 11 : Measured loop gain, 1 MHz bandwidth

Figure 12 : Power adjust to frequency transfer function

29 MARCH 96 14:10

Response of "SLOW" NPRO Input

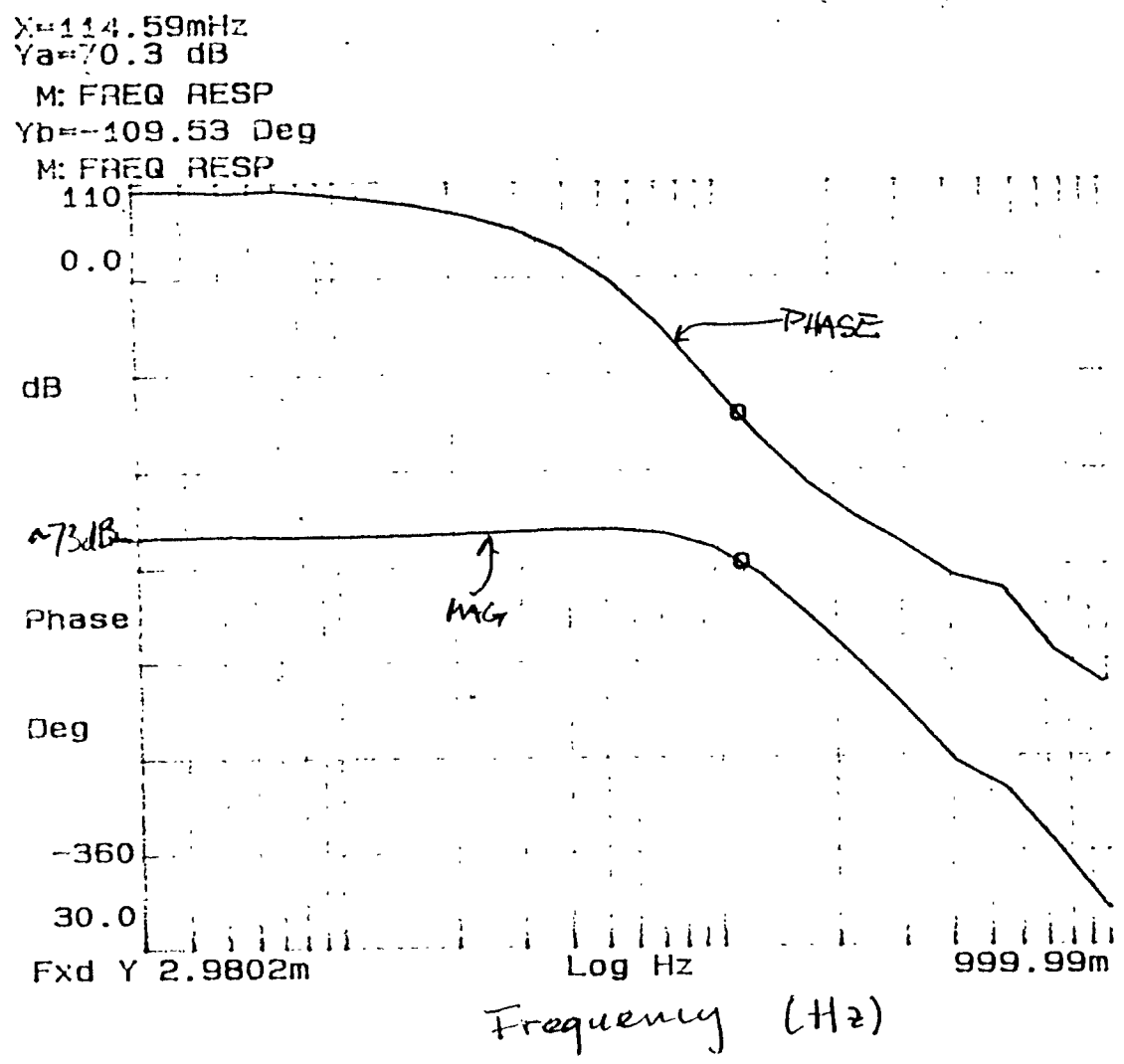


FIGURE 1

$3dB \sim 4 \cdot 10^3$
 $\Rightarrow 43 Hz/V$

The magnitude for this plot is obtained by multiplying the measured one by:

$\times 100$ (since $\div 100$ monitor was actually measured)
 $\times \frac{300 MHz}{86V}$ TROPOL tuning constant (measured)

Drive voltage to slow input
 $35 mV_{peak} \div 2 \div 30$
 $\approx \underline{.6 mV_{peak}}$

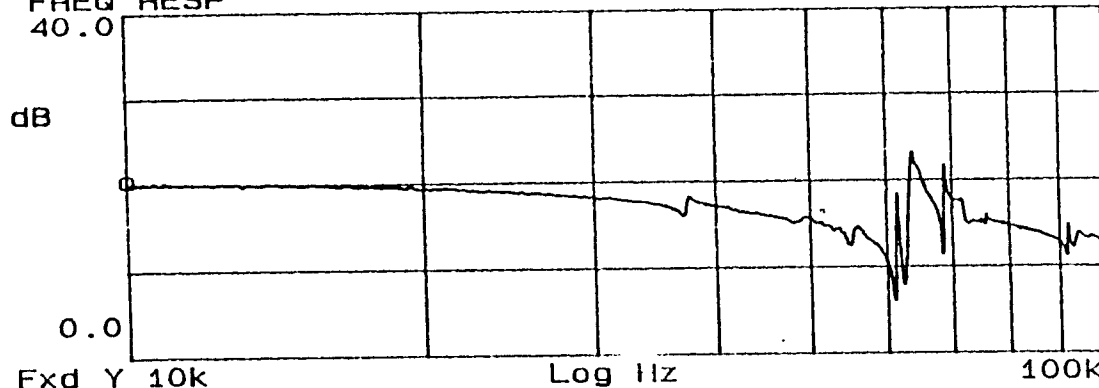
File: PSL/Slowin

10/16/96 16:00
JEM

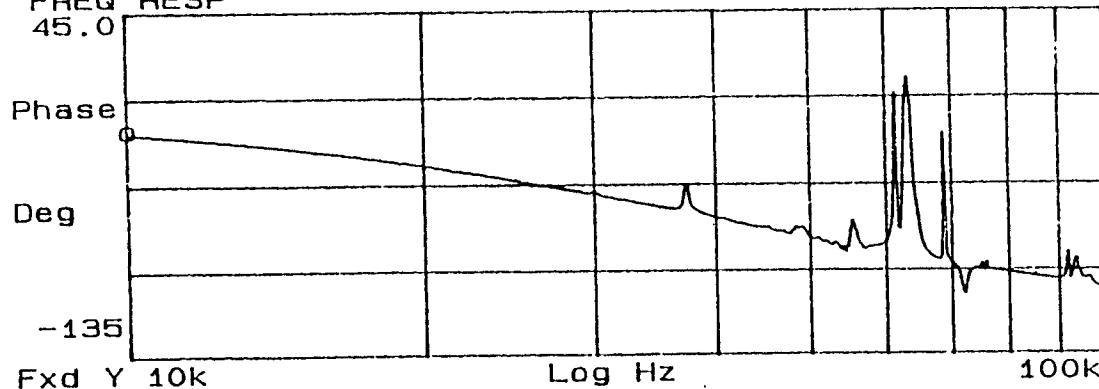
"1016FPNT"
COHERENCE SAVED
AS 1016FPTC

FAST PLANT (ACTUATOR/CAVITY/PHOTODIODE)

X=10kHz
Ya=20.2353 dB
FREQ RESP
40.0



Fxd Y 10k
Yb=-17.719 Deg
FREQ RESP
45.0



PROVIDED THAT THIS IS
ESSENTIALLY AN OPEN
LOOP MEASUREMENT, AND
THAT WE EXPECT NO
POLES/ZEROS < 10kHz,
THIS GIVES THE DELAY
BUT $V \rightarrow$ FREQUENCY CONVERTS
OF $\sim 400 \text{ kHz/V}$

FIGURE 2

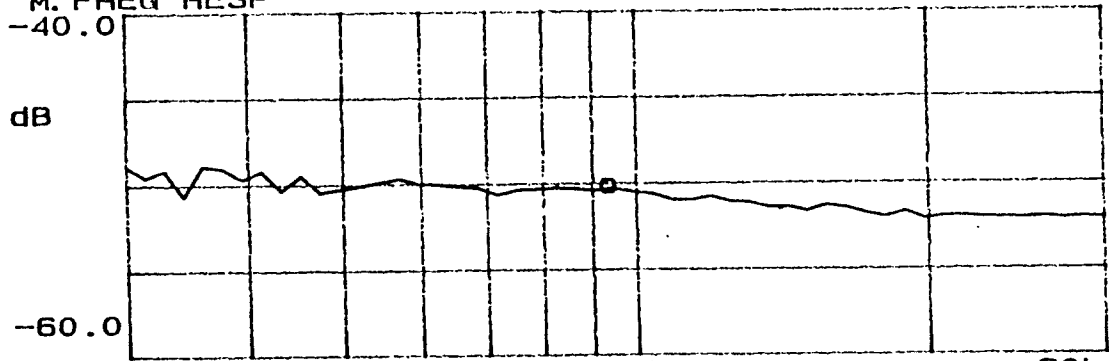
12/17/96

JEM

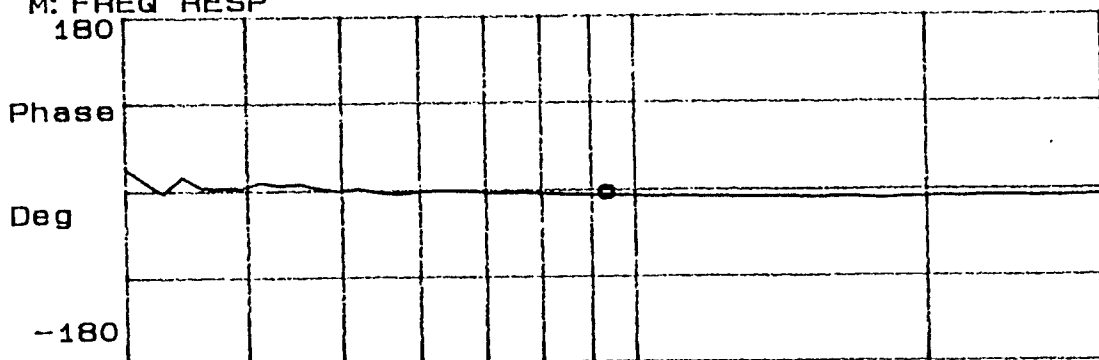
POCKELS CELL ACTUATOR GAIN

$$\frac{V_{\text{DEMOD OUT}}}{V_{\text{POCKELS CELL}}} \text{ TRANSFER FUNCTION } \times \underbrace{33.7 \text{ kHz/V}}_{\text{DEMOD OUT CONVERSION}} \times \underbrace{\frac{2\pi \times 35000}{s + 2\pi \times 35000}}_{\text{CAVITY POLE}} \times \underbrace{\frac{1}{i\omega}}_{\frac{1}{s}}$$

X=9.3513kHz
 Ya=-50.283 dB
 M: FREQ RESP



Fxd Y 3k
 Yb=-5.1992 Deg
 M: FREQ RESP



ROUGHLY -50dB = 32 mRad/V
 x 2π = 20 mRad/V
 @ 30 kHz, -52dB ⇒ 16 mRad/V

FIGURE 3

FAST CONTROLLER TRANSFER FUNCTION
 COMMON GAIN - 0.65 FAST GAIN - 1

1/30/91
 JCM.

NETWORK

A: REF	B: REF	○ MKR	3 981.072 Hz
80.00	180.0	T/R	4.25477 dB
[dB]	[deg]	θ	60.8732 deg

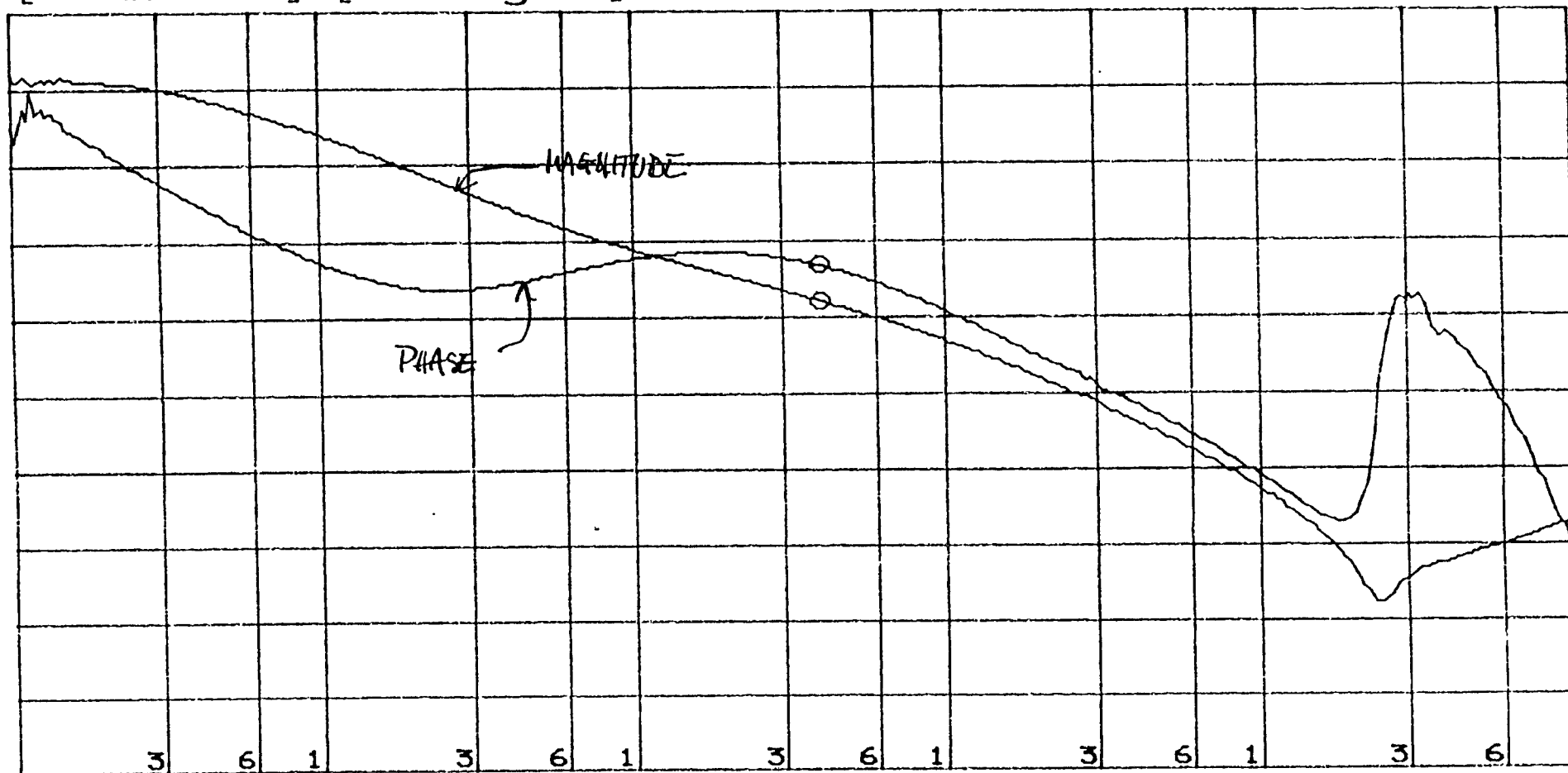


FIGURE 4

DIV	DIV	START	10.000 Hz
20.00	36.00	STOP	1 000 000.000 Hz
RBW: 10 Hz	ST: 3.62 min	RANGE: R=-10, T=	20dBm

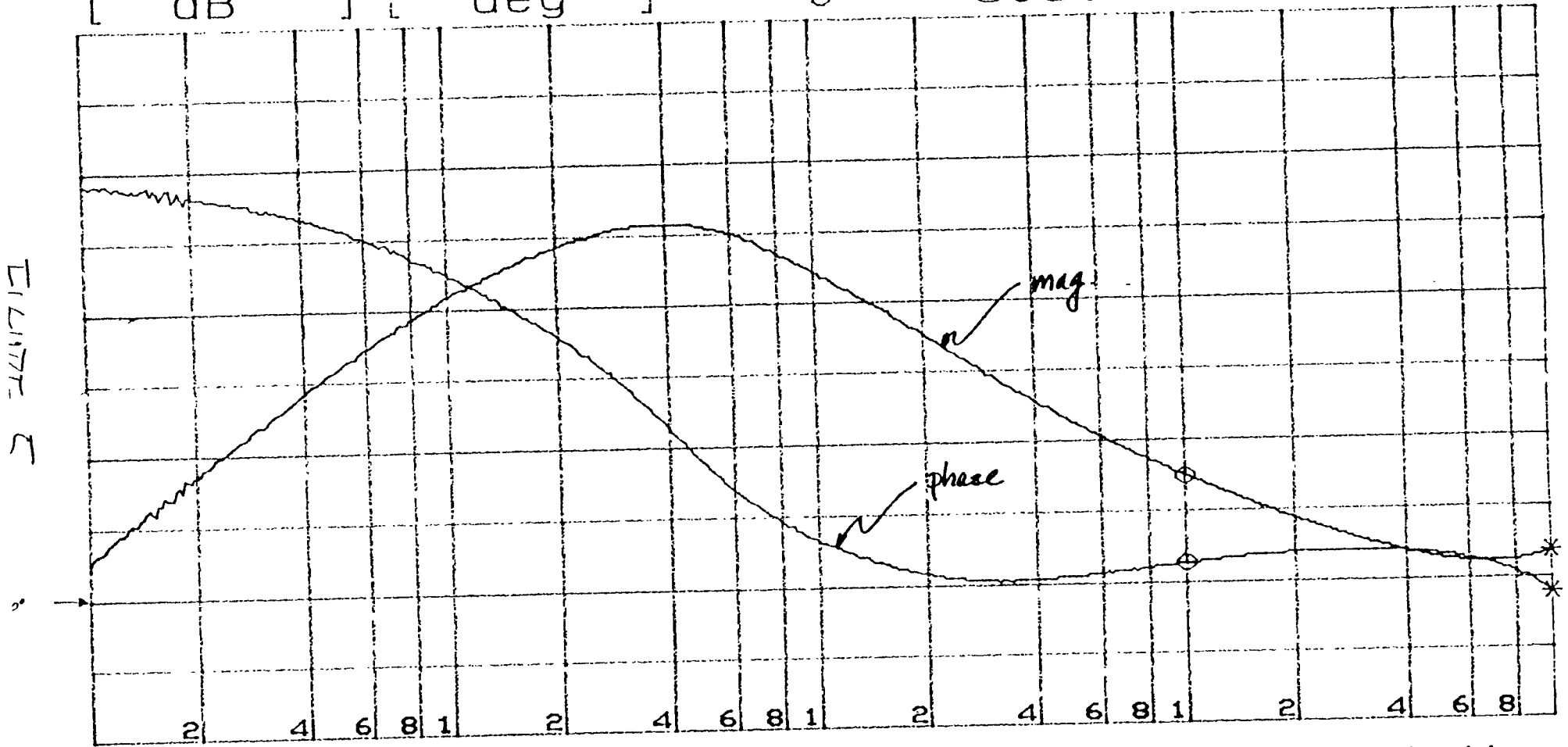
FREQ STAB. SERVO ELECT. MCS. "INT1" TO "PCOUT"

21 JAN 77 RA.
1447

PLOT RE-TAKEN (THIS PLOT IS CORRECT.) WITH HIGH Z PROBE ON NWA "T" PORT.

NETWORK

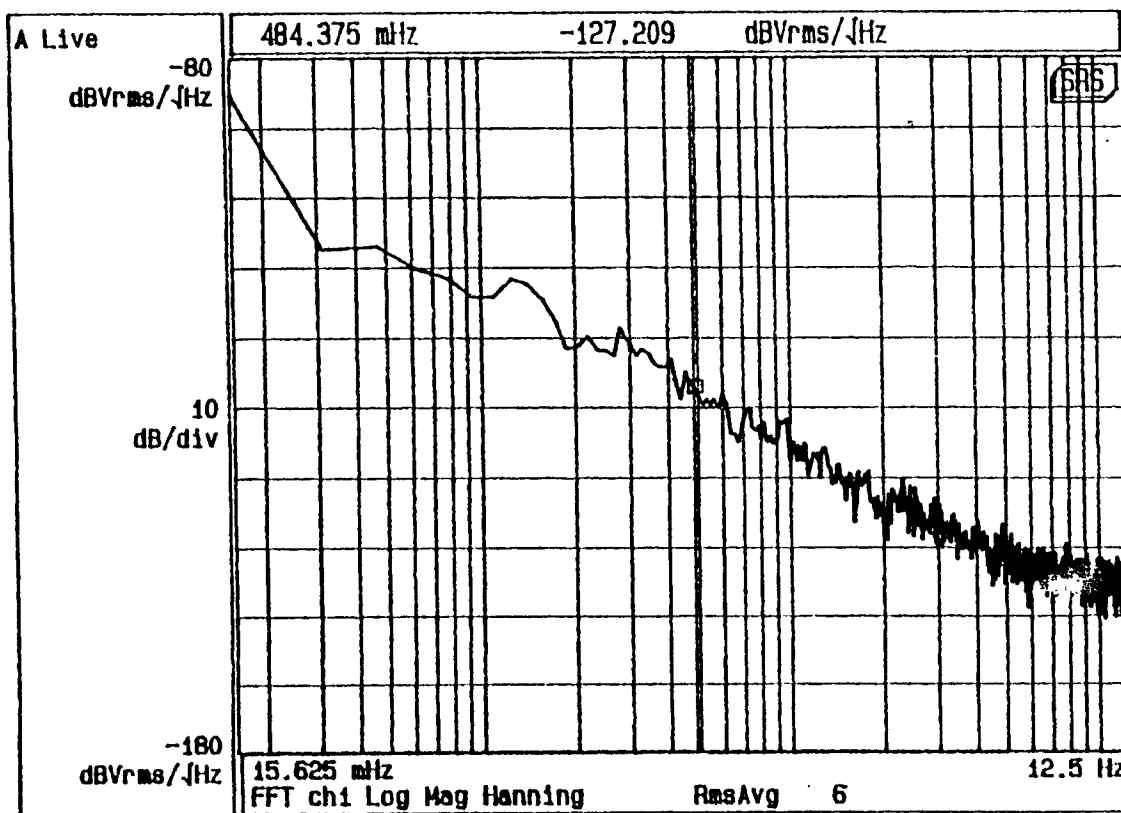
A: REF	B: REF	* MKR	1 000 000.000 Hz
110.0	100.0	T/R	33.8060 dB
[dB]	[deg]	θ	-309.999 deg



DIV	DIV	START	100.000 Hz
10.00	50.00	STOP	1 000 000.000 Hz
RBW: 100 Hz	ST: 40.2	sec	RANGE: R= 0, T= 20dBm

1/26/97 JEM

OUTPUT REFERRED NOISE OF THE SLOW CONTROLLER



INPUT 60Ω TERMINATED

COMMON GAIN 0.65

SLOW GAIN 0.35

1/26/97 18:11:02

FIGURE 6

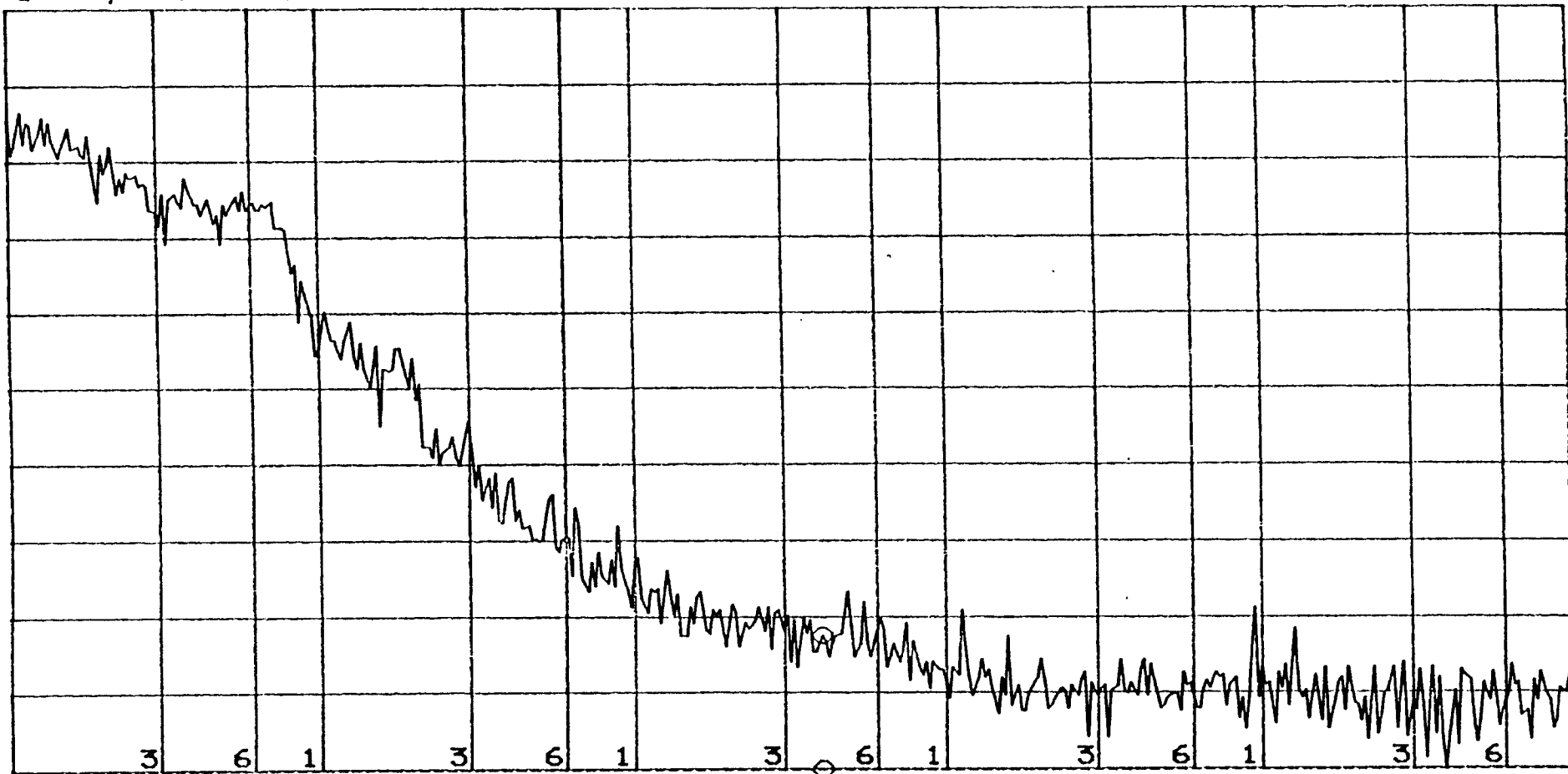
OUTPUT REFERRED NOISE = THE FAST CONTROLLED
 INPUT 50Ω TERMINATED COMMON GAIN - 0.65 FAST GAIN - 1.0

1176/97
 JEM

SPECTRUM

A: REF B: REF ○ MKR 3 981.072 Hz
 60.00 -10.00 MAG -22.4445 dBμV/Hz
 [dBμV/Hz] [] MAG

LEVEL 7



DIV DIV START 10.000 Hz
 10.00 10.00 STOP 1 000 000.000 Hz
 RBW: 30 Hz ST: 3.13 min RANGE: R=-20, T=-20dBm

OUTPUT REFERRED NOISE OF THE POKKELS CELL CONTROLLER

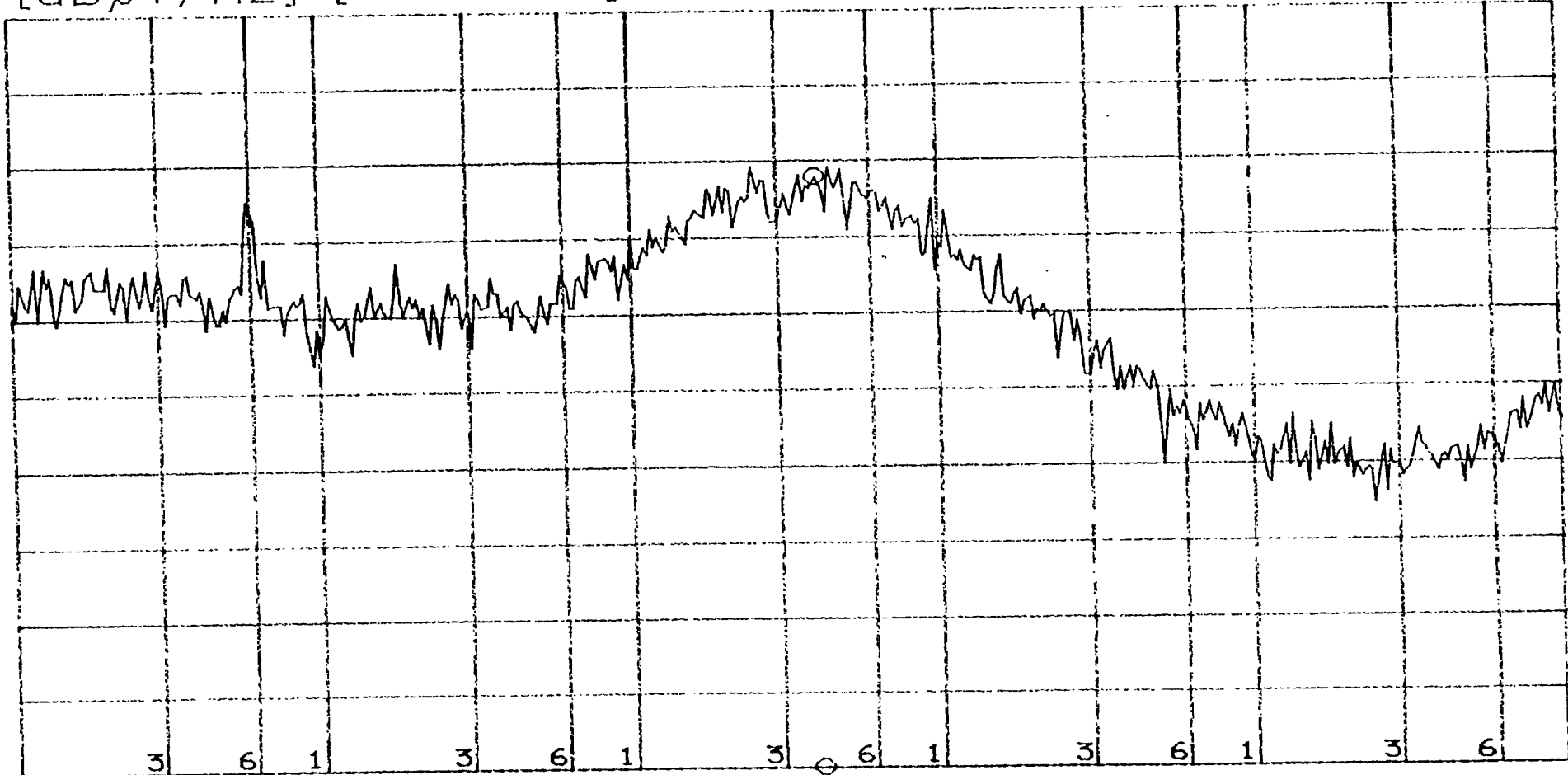
4/7/91
JEM

INPUT 50Ω TERMINATED COMMON GAIN-0.65

SPECTRUM

A: REF	B: REF	○ MKR	3 981.072 Hz
60.00	-10.00	MAG	37.9227 dBμV/Hz
[dBμV/Hz]	[]	MAG	

FIGURE 8



DIV	DIV	START	10.000 Hz
10.00	10.00	STOP	1 000 000.000 Hz
RBW:	30 Hz	ST: 3.13 min	RANGE: R=-20, T=-20dBm

12/2/76
JEH

FREQUENCY NOISE MEASUREMENT (IN-LOOP)

SLOW 0.2 USES 5.8 kHz/V
FAST 1.0
COMMON 0.8

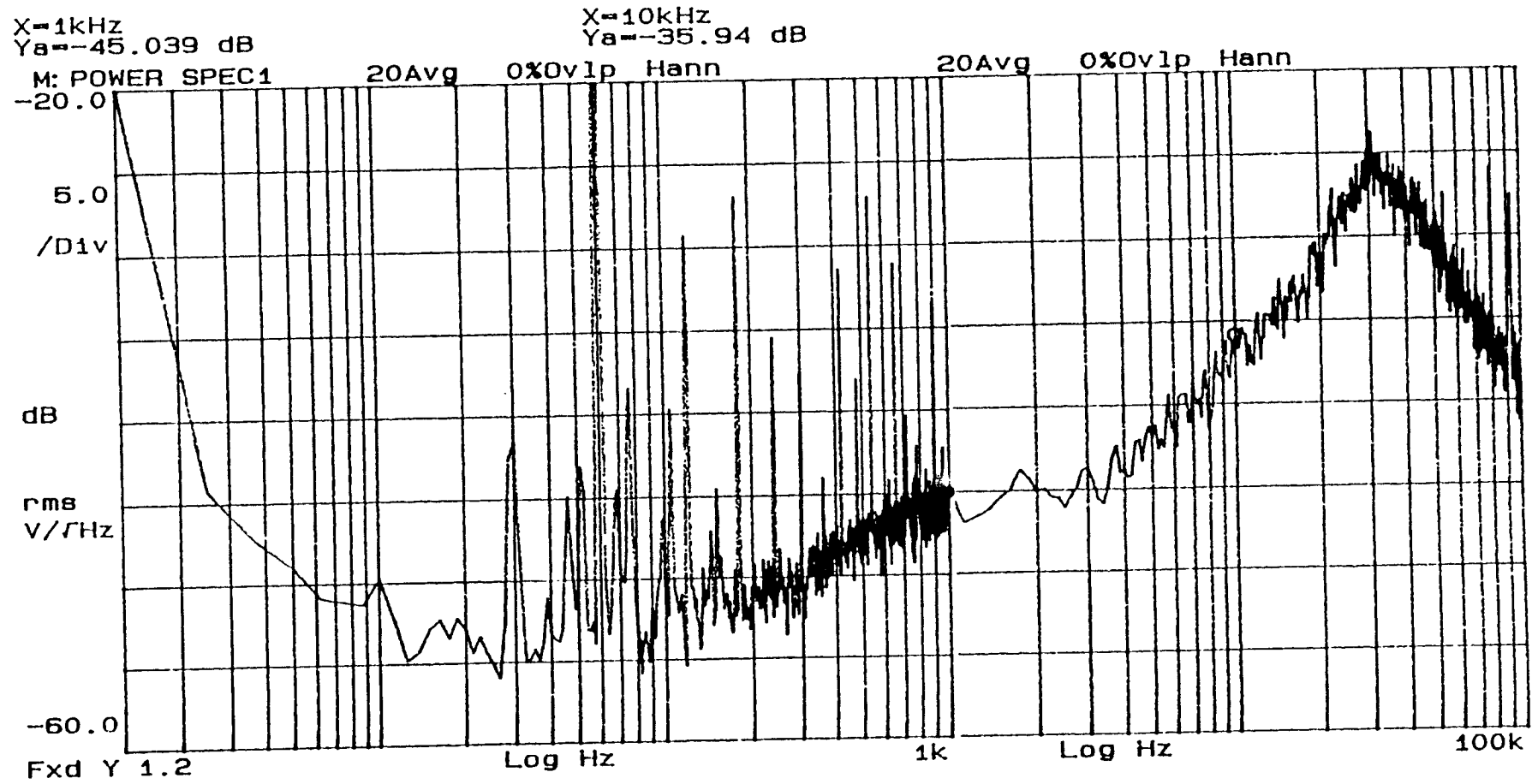


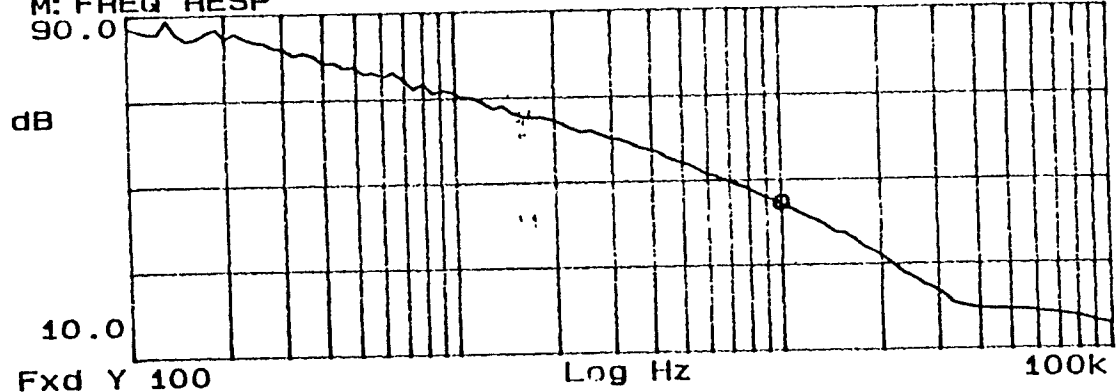
FIGURE 9

COMPOSITE OF THE 100 kHz &
1 kHz SPAN, FILES
1231PSM1 & 1231PSM1

12/31/96
JEM
"1231LG1"

FULL LOOP GAIN MEASUREMENT

X=10.058kHz
Ya=44.5394 dB
M: FREQ RESP



SLOW-OFF
FAST - 1
COM - 0.8

12.3MHz - 6.06Vpp
RPD V_{DC} - -49.1mV_{DC}
SLOWIN V_{DC} - -198.4mV
10mV TO THE CAVITY

Fxd Y 100
Yb=-147.23 Deg
M: FREQ RESP

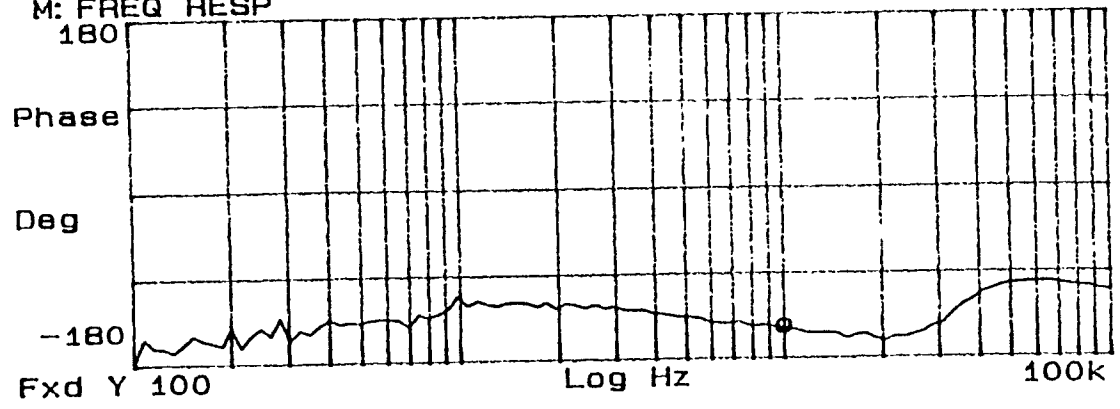


FIGURE 10

FREQUENCY STABILIZATION LOOP IN MEAS.

$\Gamma = 10$
 $H = 0.8$
 ~10mW LIGHT TO CAVITY,
 $\Gamma = 75$, VISIBILITY ~83%

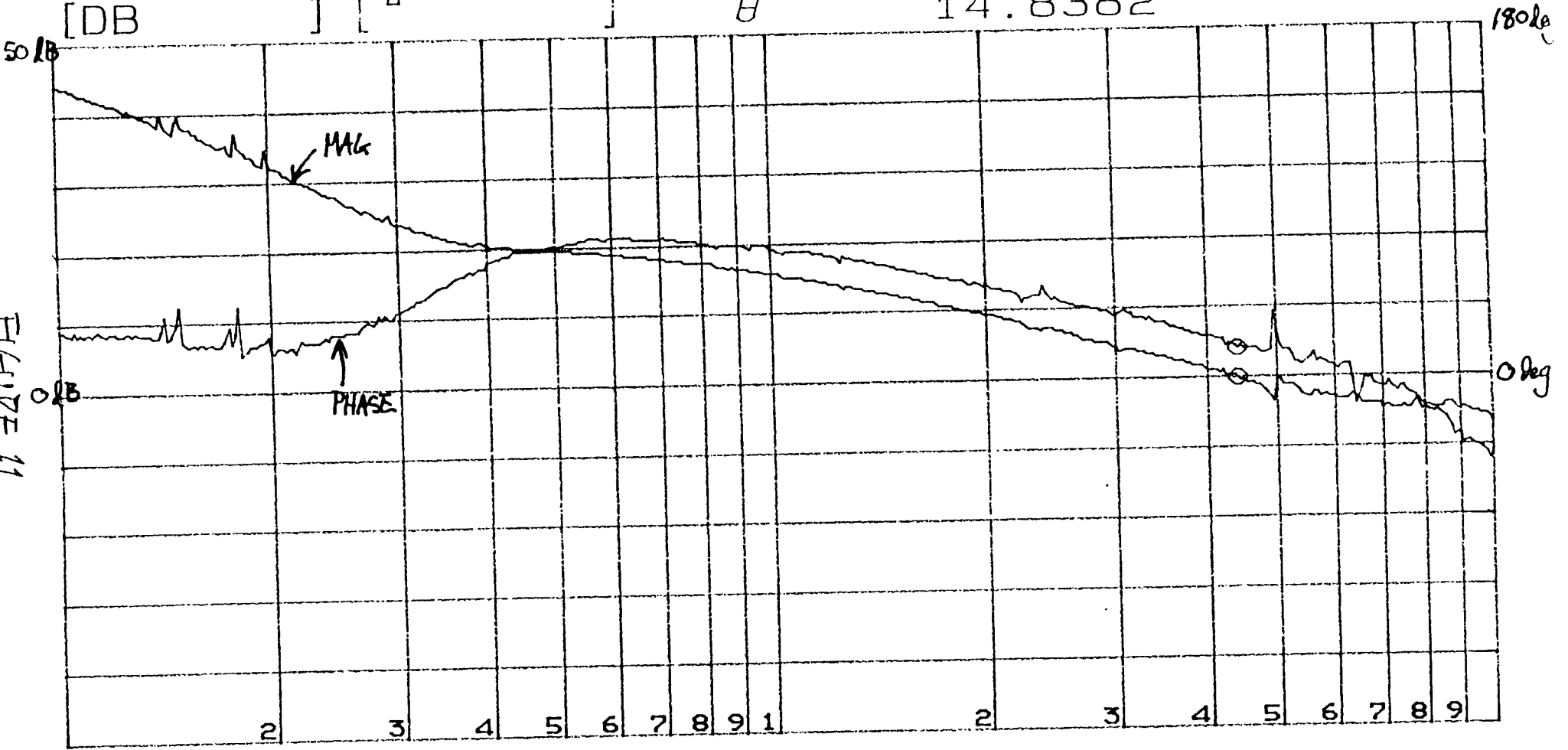
NETWORK
 A: REF
 50.00
 [DB]

Math
 B: REF
 180.0
 []

MKR
 MAG
 θ

441 570.447 Hz
 -158.841m DB
 14.8382

FIGURE 11

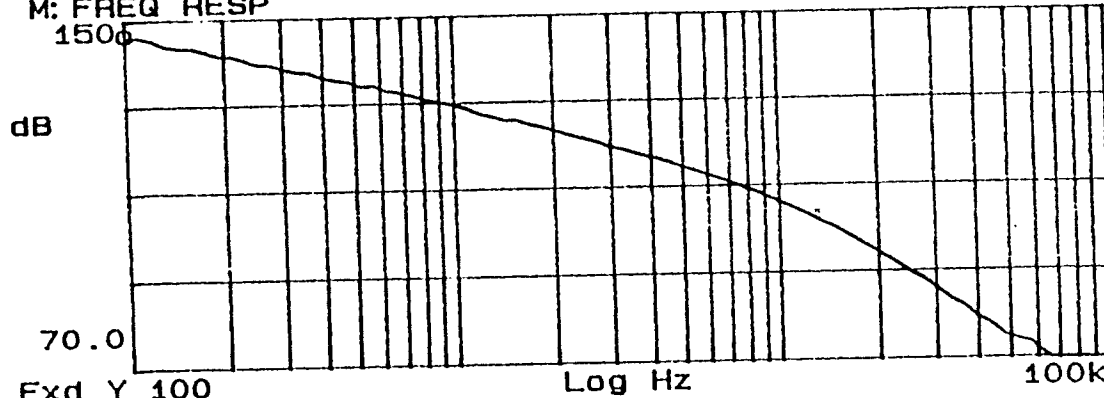


DIV 10.00 DIV 36.00 START 10 000.000 Hz
 STOP 1 000 000.000 Hz
 RBW: 30 Hz ST: 1.70 min RANGE: R= 0, T= 0dBm

1/5/97 JEM

'POWER ADJUST' TO FREQUENCY NOISE TRANSFER FUNCTION

X=100 Hz
Ya=146.35 dB
M: FREQ RESP



Fxd Y 100
Yb=-64.371 Deg
M: FREQ RESP

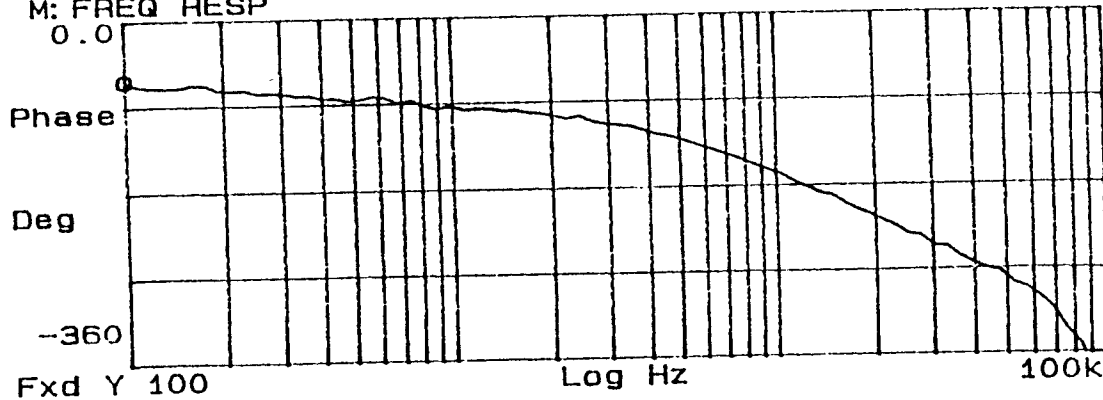


FIGURE 12

NOISE EATER - OFF

~~COMMON~~

LASER LOCKED,

COMMON GAIN - 0

FAST GAIN - 0

POCKETS CELL DISCONNECTED

INPUT - POWER ADJUST
OUTPUT - PCTI

THIS PLOT IS:

$$\frac{\text{PCTI}}{\text{POWER ADJUST}} \times \frac{5800 \text{ Hz}}{V} \times \frac{1}{\text{C.L.}} \times \frac{1}{\text{CIV. POL.}}$$

↑
CLOSED LOOP GAIN.

$\frac{\text{PCTI}}{\text{PWR ADJ.}} \Rightarrow \text{13PRTF3}$

THIS PLOT $\Rightarrow \text{13PRTF4}$

Front Panel Features For NPRO Servo Electronics.

1. **SLOWMON**: Buffered monitoring point for the output of the slow loop.
2. **FASTTO**: Output of fast loop test amplifier (U13).
3. **FASTTI**: Input to fast loop test amplifier (U13).
4. **SLOW ADJ**: Slow loop gain adjust pot.
5. **FAST ADJ**: Fast loop gain adjust pot.
6. **FASTOUT**: Output of the fast loop (U7).
7. **MIXROUT**: Output of the first stage after the mixer (U8), through a 1K resistor. This results in a gain of 5.2dB from that at the plane of the mixer itself.
8. **PCTO**: Pockels cell test output (U12).
9. **SLOW DC**: DC adjustment input for the slow loop. This input is used in initial locking to align laser frequency to the desired value in preparation for lock acquisition.
10. **FASTMON**: Buffered monitoring point for output of the fast loop.
11. **PCOUT**: Output of the pockels cell loop.
12. **FEEDIN**: Feed around input.
13. **MAINTI**: Used for overall closed loop transfer function measurement. Input to U4.
14. **PCMON**: Buffered monitoring point for output of the pockels cell loop.
15. **SLOWOUT**: Output of the slow loop (U25).
16. **MAINTO**: Output used in conjunction with MAINTI for closed loop transfer function verification. Output of U18.
17. **INTI**: Test input that when the RFSW is in the "ON" position, allows for injection of signals at the output of the mixer. Used for aligning the traps among other things.
18. **AQ/SLAQ**: Switch to go between integrator (SLAQ) mode and reduced gain mode (AQ) for the slow loop. Used during lock acquisition.
19. **CLOSE/SLOW LOOP**: Switch used to close the feedback path (CLOSE) for the slow loop electronics. The switch should be closed during normal locked operation. When the loop loses lock, the loop must be taken to the downward position to remove feedback to the slow actuator.
20. **ON/RFSW**: Switch used to select between INTI (ON) and normal mixer feedback path (U9A).
21. **INADJ**: Adjustment of the overall electronics gain or common gain. This will change the gain of all paths simultaneously.
22. **RF**: Input from the RF Photodiode.
23. **LO**: Local Oscillator input from reference phase shifter. Nominal level of 9 V P-P or 23 dBm.

OPTICS DEVELOPMENT FOR LIGO

Stanley WHITCOMB*, GariLynn BILLINGSLEY, John CARRI, Alex GOLOVITSER, Doug JUNGWIRTH, William KELLS, and Hiro YAMAMOTO
LIGO Project, M/S 51-33, California Institute of Technology, Pasadena CA 91125 USA

and

Brett BOCHNER, Yaron HEFETZ†, Partha SAHA, and Rainer WEISS
LIGO Project, Massachusetts Institute of Technology, Room 20 B 145, 18 Vassar Street, Cambridge, MA 02139 USA

ABSTRACT

The large optical components (the test masses, beamsplitters, and recycling mirrors) represent one of the most challenging aspects for large gravitational wave interferometers. The requirements for the LIGO optical components have been derived using a computer model of the interferometer which uses an FFT-based optical propagation code. This model includes the surface figure of all optical components, the homogeneity of the substrates, an allowance for losses due to scattering and absorption in the optical coatings, and the carrier and sideband modulation/detection technique. To meet these requirements, LIGO has undertaken a program to work with industry to evaluate and improve current fabrication capabilities. Full-size LIGO test masses have been polished and measured for microroughness and surface figure. Evaluation of these optics show that it is possible to polish and measure optic substrates with surface figures accurate to < 1 nm over spatial scales from 0.2 mm to 10 cm. To measure coating uniformity, LIGO has developed a technique using measurements of the reflectivity of specially-designed two-layer coatings to extract the thicknesses of the individual layers with a precision of $\sim 0.02\%$ (rms). This paper summarizes the requirements for LIGO optics that have been derived, results from the polishing development, and preliminary data on the large-scale uniformity of ion-beam-sputtered coatings.

1. Introduction

The large optical components represent one of the most challenging aspects for large gravitational wave interferometers. The large optical components ("Core Optics") in a LIGO interferometer¹ (see Figure 1) consist of four test masses (two end mirrors and two input mirrors), a beamsplitter, and a recycling mirror. The total number required for the three initial LIGO interferometers is 20, 6 each for the Washington and Louisiana 4 km interferometers and 8 for the Washington 2 km interferometer (the 2 km interferometer also includes 2 folding mirrors which must meet requirements similar to those of the recycling mirror). In addition, a number of spares are required to insure against possible damage during the fabrication and installation processes. Because of the long time required for their fabrication, these spares must be procured along with the main optics.

The LIGO Core Optics will be made from high purity fused silica. They will

*This paper was presented at the TAMA Workshop for the LIGO Project by S.E. Whitcomb.

†Current affiliation: Elscint, Nuclear Medicine Division, Haifa, Israel

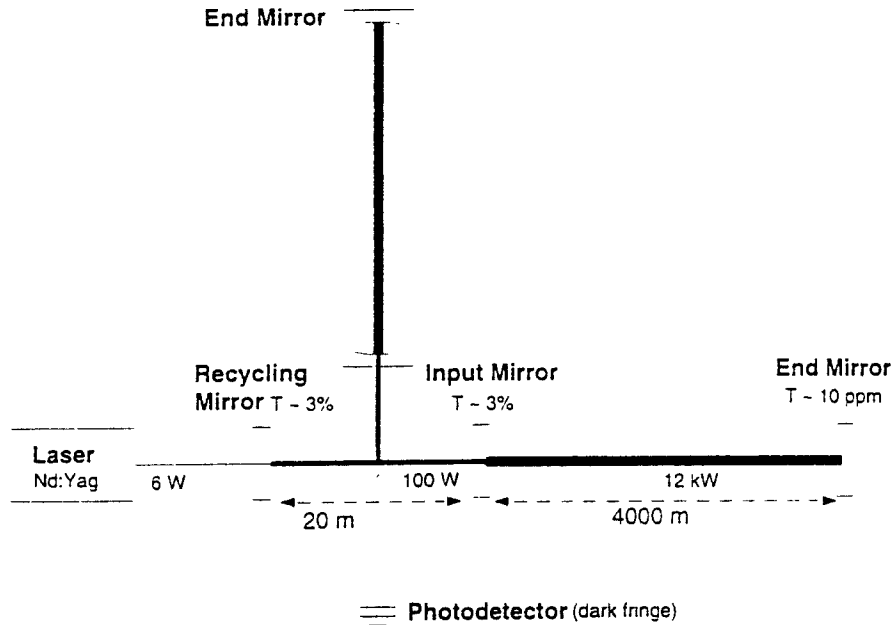


Figure 1: A schematic diagram of a LIGO interferometer showing the Core Optics.

be 25 cm in diameter \times 10 cm thick (except the beamsplitter which will be \sim 4 cm thick). Beams fill some of the optics, with approximately 1 part per million (ppm) of the total intensity lost outside the mirror. All optics have enhanced reflectivity 1064 nm coatings on one surface and anti-reflective (AR) coatings on the second surface. Their principal performance requirements include:

- | | |
|---|---|
| < 50 ppm loss per surface | \Rightarrow Limit loss of resonant stored energy: minimize shot noise |
| Surface figure errors to scatter negligible power from TEM_{00} | \Rightarrow Best dark fringe |
| High mechanical Q
($Q > few \times 10^6$) | \Rightarrow Minimize thermal noise |
| Low bulk (< 5 ppm/cm) and coating (< 2 ppm) absorption | \Rightarrow Limit effect of thermal lensing on power and dark fringe contrast |

2. Defining the Optics Requirements

The primary tool for investigating the effects of different optical parameters on the LIGO interferometer sensitivity is a computer model of a full recycled Michelson interferometer with Fabry-Perot arms.²⁻⁵ This computer model is based on original code provided to LIGO by Jean-Yves Vinet and Patrice Hello of the VIRGO Project.⁶ This computer model uses an FFT-based optical propagation code. It includes the surface figure of all optical components (either real or simulated maps of the surface errors) and the optical pathlength difference (OPD) maps of substrates for the input mirror and beamsplitter. It solves for both the carrier and the

Table 1: partial listing of requirements for the LIGO Core Optics

Physical Quantity	Test Mass		Beam splitter	Recycling Mirror
	End	Input		
Diameter of optic (cm)	25	25	25	25
Thickness of optic (cm)	10	10	4	10
1 ppm intensity dia. (cm)	24	19.1	30.2 ^a	19.2
Lowest internal mode (kHz)	6.79	6.79	3.58	6.79
Mass of optic (kg)	10.7	10.7	4.2	10.7
Nominal surface 1 radius of curvature (m) and g factor	7400 $g_2 = 0.46$	14571 $g_1 = 0.72$	inf	9998 $g = 0.98$
Tolerance on radius of curvature (m)	absolute: ± 220 matching: ± 111	-1000. +145	> -720 km convex. > 200 km concave	-100. +500

^aFor these 45° angle of incidence optics, this is the smallest diameter circle centered on the optic face which is everywhere outside of the 1 ppm intensity field.

modulation sidebands, and combines them to realistically model the demodulated gravitational wave signal. Important features of the code include its adaptation to a supercomputer⁴ and development of a fast convergence algorithm,³ enabling full recycled interferometers to be modeled rapidly. It has been tested in a variety of limiting cases against a semianalytic modal model that was developed independently.

This model has been used to develop a set of requirements for the LIGO Core Optics. These requirements include the size of the optics (to ensure that diffractive losses are not too large), surface figure, scatter losses, and tolerances on radii of curvature. Some of these requirements are summarized in Table 1.

3. Optics Development Program (“Pathfinder”)

To ensure that LIGO can obtain suitable optics for its initial detectors, an optics development program (called “Pathfinder”) has been underway for some time. The purposes of this program were to evaluate the state of the art in optical fabrication and metrology, to initiate work to further the state of the art where needed, and to identify companies with the ability to fabricate the LIGO Core Optics. The main steps in this program were:

- Purchase and evaluate fused silica blanks (5/94)
- Best effort polishing of substrates (8/95-4/96)
- Independent substrate metrology (4/96-8/96)

- Coating uniformity development (7/95-ongoing)
- Coated optic metrology (expected in early 1997)

Industrial partners were engaged in all phases of this effort. Data from the Pathfinder are analyzed in the LIGO computer model to assess the performance of the optics against the requirements.

4. Substrate Material Results

The Pathfinder program began in 1994 with the ordering of a number of large fused silica blanks to be fabricated into finished components. These blanks were specified to have bulk index of refraction variations $\delta n \leq 5 \times 10^{-7}$ through the 10 cm thickness. The order was placed with Corning and other specifications were consistent with their specifications for OAA Grade 7940 fused silica. Optical homogeneity maps were provided with each Pathfinder fused silica blank and these were evaluated using FFT model. These analyses indicate sufficient homogeneity that optical distortions due to transmission through the beamsplitter and input mirror substrates would not degrade the optical performance of the initial LIGO interferometers.

Mechanical Q 's for the five lowest-frequency internal vibrational modes were measured on one of the Pathfinder substrates after polishing.⁷ For these modes, the average Q was $> 5 \times 10^6$. These values meet the requirements for the initial LIGO interferometers.

In late 1995, the LIGO project made a decision to switch from using visible Argon ion lasers to using Nd:YAG lasers operating at 1064 nm. This change made the Corning fused silica unsuitable in one way. The large dependence of the index of refraction with temperature dn/dT in fused silica requires very low absorption to avoid thermal lensing of transmitted beams in the beamsplitter and input mirrors. Measurements by the VIRGO project⁸ have shown a correlation between 1064 nm absorption and OH concentration. Typical high purity fused silica contains 500-1000 parts per million (ppm) OH giving 10-20 ppm/cm absorption, which is too high for the input mirrors and beamsplitters. Fortunately, the VIRGO project has determined that Heraeus has a process which yields fused silica with ~ 200 ppm OH (~ 5 ppm/cm absorption). In the initial LIGO interferometers, the low absorption of the Heraeus substrate material is only critical for input mirrors and beamsplitters where the laser light is increased by the recycling cavity.

Orders for approximately 40 blanks were placed in 1996, with delivery scheduled for 1997. Heraeus was selected for input mirrors and beamsplitters and Corning for all others. The total number of blanks ordered allows for both spare finished optics and for any problems during the fabrication process.

5. Core Optics Polishing Demonstration

The Core Optics polishing demonstration was carried out through best effort polishing and metrology of full-size substrates. Three companies participated in this

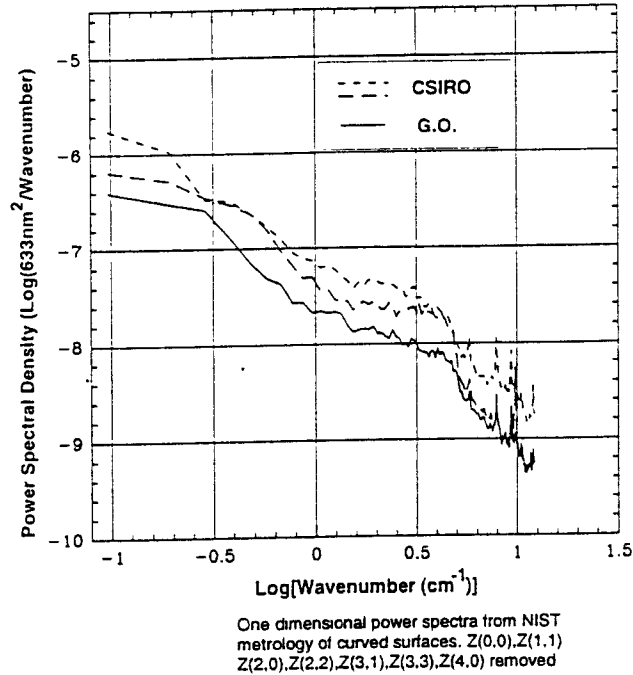


Figure 2: Comparisons of the power spectra of the deviations from the perfect figure of the CSIRO and GO pathfinder substrates as measured by NIST.

effort: Commonwealth Scientific and Industrial Research Organization (CSIRO), General Optics (GO), and Hughes-Danbury Optical Systems (HDOS). Each of these companies polished full size substrates with characteristics typical of the LIGO Core Optics. The specification called for the optics to be polished concave on one side with a radius of curvature of 6000 m and flat on other side.

The requirements for these polishing efforts were derived using the FFT optical model for the LIGO interferometers and tailored to the known capabilities of different classes of polishers. For CSIRO and HDOS, the primary goal was to demonstrate "mid scale" surface figure errors (after removing focus error and astigmatism) < 0.8 nm rms over the central 8 cm diameter; a second requirement was to achieve simultaneously a microroughness < 0.4 nm rms. For GO, the requirements were a surface figure error $< \lambda/20$ with a microroughness of < 0.1 nm.

To provide a consistent comparison of the figure errors in the polished substrates, independent metrology was performed by Chris Evans, Robert Parks, and Paul Sullivan at the National Institute of Standards and Technology (NIST). The technique used involved multiply redundant measurements on an existing 633 nm phase shifting interferometer, analyzed to give absolute metrology at the subnanometer level. With care, measurements at < 1 nm level proved possible. Reproducible features were seen and consistent intercomparisons demonstrated at this level. The instrument used gave information on spatial scales from its full aperture (15 cm) down to 3mm. Figure 2 shows power spectral densities of the figure errors for the GO and CSIRO substrates derived from these measurements. The HDOS results were

Table 2: Comparison of microroughness of polished substrates as measured by REO (using a Micromap instrument with a 20X objective).

Polisher	Serial Number/ Surface	Microroughness (\AA) (Ave. 5 Locations)
CSIRO ($< 4 \text{ \AA}$ reqt.)	006/Curved	3.6
	006/Flat	2.8
	002/Curved	2.7
	002/Flat	3.1
GO ($< 1 \text{ \AA}$ reqt.)	005/Curved	0.85
	005/Flat	0.88

overall comparable to those for CSIRO.

The most important conclusion from Figure 2 is that polished surfaces with rms deviation (after removing focus and astigmatism) $< 1 \text{ nm}$ over $\sim 20 \text{ cm}$ diameter are achievable! In some cases, apparent deviations $\sim 0.5 \text{ nm}$ were measured.

To evaluate the microroughness of the various substrates, comparative surface roughness measurements were made at Research Electro-Optics (REO). Table 2 shows the result of these measurements. Microroughness contributes to large-angle scattering, and thus is particularly important for the test masses where the light intensity is greatest. Again, the HDOS results were comparable to those for CSIRO.

Based on the Pathfinder results and on competitive proposals, GO and CSIRO have been selected to polish the LIGO Core Optics.

6. Coating Uniformity Development

In developing coating uniformity, the LIGO project has collaborated with Research Electro Optics (REO). The goal of this effort is to scale REO's low-loss ion-beam-sputtered coating technology to LIGO diameters. Preliminary work has focussed on developing the techniques needed to quickly measure coating thickness variations over both long and short spatial scales and optimizing the coating process.

The technique developed for measuring coating uniformity⁹ involves mapping the reflectivity of specially-designed two-layer AR coatings (see Figure 3). Near the reflectivity minimum, the reflectivity depends on the interference of the fields from the three interfaces in a two layer stack and is thus a strong function of the thickness of the two layers. By mapping the reflectivity at different angles of incidence and polarizations, one can derive maps of individual coating layers by fitting the observed reflectance maps through a least-squares minimization process. A standard set of measurements consists of six maps at 2 polarizations and 3 different angles of incidence.

The AR coating design which was selected for initial testing is the design shown

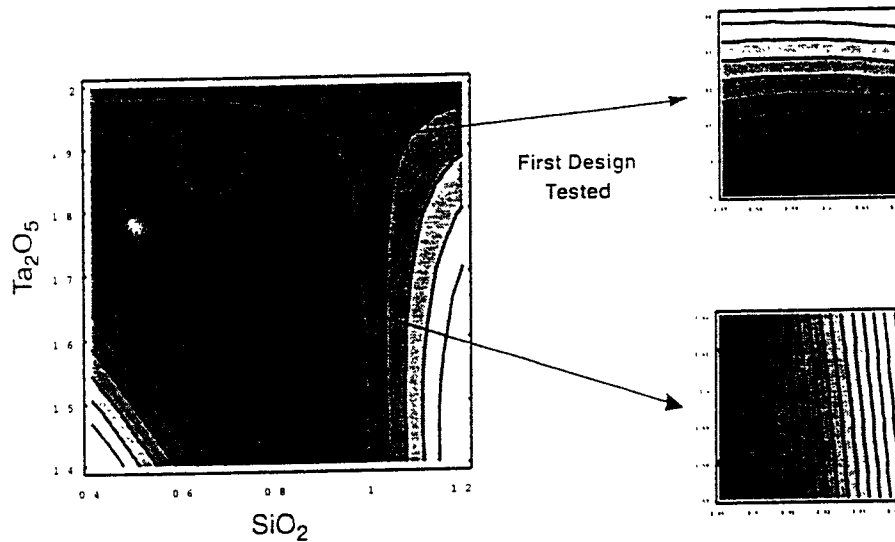


Figure 3: A contour map of the reflectivity of a two layer stack highlighting designs with predominant sensitivity to Ta_2O_5 (top right) and to SiO_2 (bottom) thickness.

in the top right of Figure 3. This coating is primarily sensitive to the thickness of the Ta_2O_5 layer. A 24 cm diameter test piece was coated with this design. Reflectance measurements were made with the apparatus shown in Figure 4. Typical reflectance scan data show good reproducibility ($< 0.2\%$); because of the steep dependence of reflectance on layer thickness this permits the thickness variations of the Ta_2O_5 layer to be determined with a precision of $\sim 0.02\%$. One advantage of this technique is that it is insensitive to the surface figure of the underlying substrate, thus permitting multiple iterations in the coating chamber with easily obtainable, inexpensive substrates.

After a complete set of measurements is performed, individual maps of thicknesses for the two layers are determined by a least squares minimization process. This minimization takes into account known instrumental effects and uncertainties. For the initial test coating, maps of the thickness of the SiO_2 and Ta_2O_5 layers are shown in Figure 5.

To evaluate this coating against our requirements, we fit the maps in Figure 5 with Zernike polynomials up to tenth order. Residual deviations from the fits are consistent with measurement errors indicating that the fine structure observed in Figure 5 is dominated by noise in the measurements and therefore not a real property of the coating. These layer maps are then stacked in a coherent way to synthesize a predicted phase map for a HR coating. (The coherent stacking assumes that the observed structure is systematic and represents a worst case assumption about how the individual layer stack.) The predicted map produced in this fashion is shown in Figure 6.

The map in Figure 6 was then tested in the FFT optical model to assess its suitability in a LIGO interferometer. The shot-noise limited sensitivity for an in-

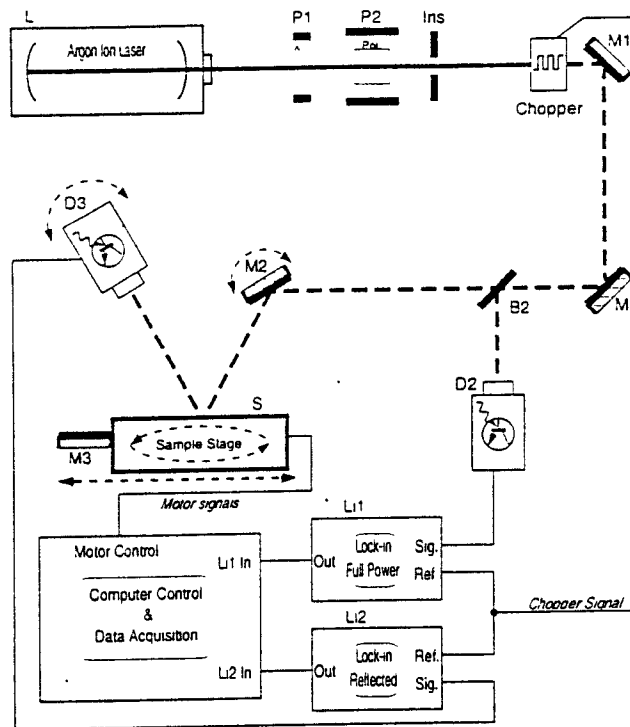


Figure 4: A schematic diagram of the apparatus used to test coating uniformity. A chopped Argon ion laser is used to illuminate the AR test piece which is mounted on the sample stage. Photodetectors D2 and D3 are used to measure the incident and reflected power respectively. The signals are synchronously detected and recorded by a computer which controls the motion of the motorized stage to map the reflectivity automatically. A quarter wave plate and polarizer are used to control the polarization of the incident light and the angle incidence can be adjusted by mirror M2.

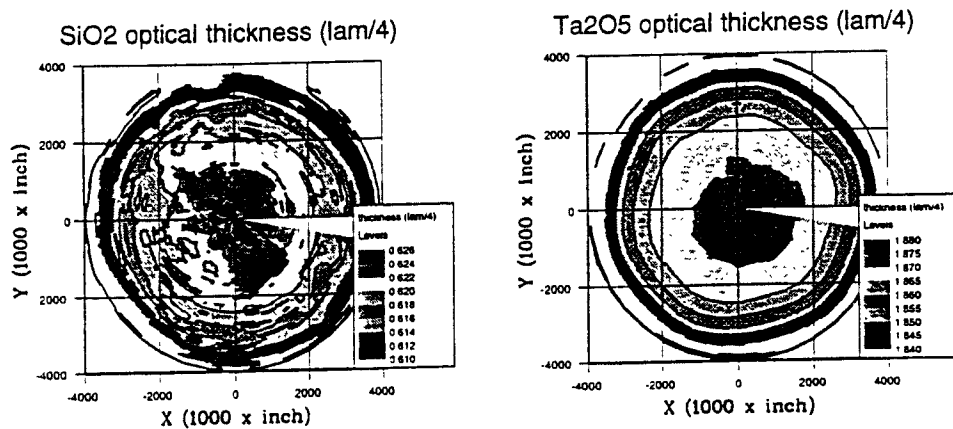


Figure 5: Maps of the thickness of the SiO_2 and Ta_2O_5 layers of the test coating. The smoother appearance of the Ta_2O_5 map is due in part to the fact that this map was made for a Ta_2O_5 -sensitive coating, and thus noise in the measurement affects the derived Ta_2O_5 thickness less than that of the SiO_2 .

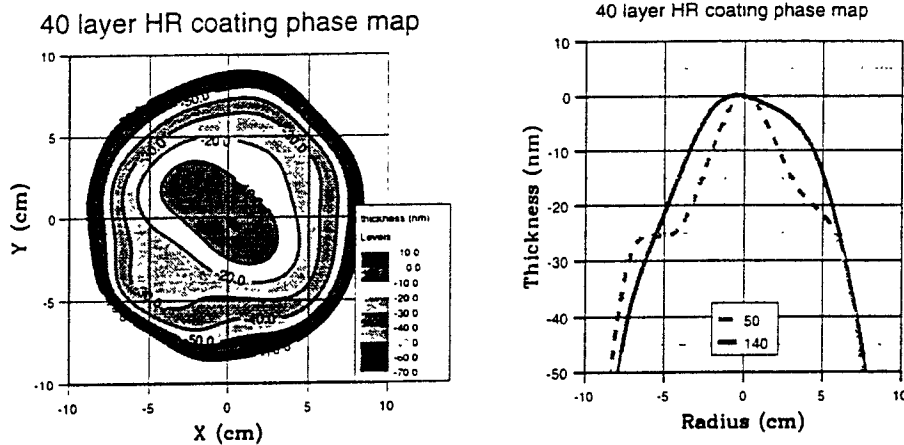


Figure 6: A simulated map of a 40 layer high reflector (HR) stack constructed from the individual layer maps from Figure 5. The graph at the right shows cuts through the map at two different angles.

interferometer with this surface profile used for end mirrors (and a similar one used for input mirrors) is compared with a standard configuration in which all of the mirrors have surface figures derived from maps of bare polished substrates in Table 3. Two measures of interferometer performance are compared in the table: the recycling factor and the shot noise limit to sensitivity at 100 Hz. These runs show some loss in sensitivity due to the coating non-uniformity, but the relatively modest degradation indicates that the coating non-uniformities are not too far from the required level.

The next steps in developing improved coating uniformity are beginning immediately. REO is making adjustments to their coating chamber and masking to reduce curvature. Once these are completed, they will make two new test AR coating runs, one identical to the coating tested above and one designed for high sensitivity to the SiO_2 thickness. If these are satisfactory then the Pathfinder optics will be coated with HR coatings (at 633 nm). These will then be measured at NIST to confirm scaling from single layers to HR coatings.

Note: After this paper was presented at the Workshop, another iteration of the coating uniformity development was completed by REO, and the preliminary analysis of test data indicate that the uniformity has been improved by approximately a factor of 5 over the central 20 cm diameter region, and that the SiO_2 layer is similar, but not identical, to the Ta_2O_5 layer.¹⁰

7. Summary

The Pathfinder program to develop the optics for LIGO is nearing its conclusion. It has enabled us to put in place the tools and techniques (both experimental and analytical) to evaluate optics against the LIGO requirements. The capabilities of

Table 3: Very preliminary estimates of the effect of coating nonuniformities on interferometer sensitivity.

Run Conditions	Surface Figure (\AA rms)	Recycling Factor	$h(100\text{Hz})$ ($\times 10^{-23}\text{Hz}^{1/2}$)
Standard Configuration: Measured substrate OPD's Surface phase maps based on polished substrates	0.8	52	1.39
Standard Configuration, except 40 Layer HR substituted on End Mirror	3.8 (ETM)	17	2.14
Standard Configuration, except 16 Layer HR substituted on Input Mirror	1.9 (ITM)	33	1.73
Standard Configuration, except End and Input Mirror substituted	3.8 (ETM) 1.9 (ITM)	15	2.52

industry to manufacture substrate material and to polish the substrates appear to be adequate for initial LIGO interferometers. The main ongoing activity is the development of coating uniformity. Preliminary coating uniformity data are promising, and further improvements and testing are expected within the next few months. Procurement of the LIGO substrates and their polishing are underway.

Acknowledgements

We thank our colleagues on the LIGO Project who have contributed in many ways to the work described here. We also thank Jean-Yves Vinet and Patrice Hello for the code which formed the basis of the FFT optical model of the LIGO interferometers. This work is supported by the National Science Foundation under Cooperative Agreement PHY-9210038.

References

1. A. Abramovici, et al. *Science* **256** (1992) 325-333.
2. H. Yamamoto, in *Proceedings of the TAMA Workshop on Gravitational Wave Detection*, ed. K. Tsubono (Universal Academic Press, Tokyo, 1997).
3. P. Saha, submitted to *J. Opt. Soc. Amer.* (1997).
4. B. Bochner, Ph. D. Thesis, Massachusetts Institute of Technology, in preparation.
5. B. Bochner, to be submitted to *Phys. Rev. D* (in preparation).
6. J. Vinet, P. Hello, C. N. Man, and A. Brillet, *J. Phys. I France* **2** (1992) 1287.
7. J. Carri, Ph. D. Thesis, California Institute of Technology, in preparation.

8. B. Y. Baures and C. N. Man. *Optical Materials* **2** (1993) 241.
9. A. Golovitser, D. Jungwirth, and H. Yamamoto. to be submitted to *Appl. Opt.* (in preparation).
10. G. Billingsley, A. Golovitser, D. Jungwirth, W. Kells, R. Lalezari, S. Whitcomb, and H. Yamamoto. to be submitted to *Opt. Letters* (in preparation).

LASER INTERFEROMETER GRAVITATIONAL WAVE OBSERVATORY
 - LIGO -
 CALIFORNIA INSTITUTE OF TECHNOLOGY
 MASSACHUSETTS INSTITUTE OF TECHNOLOGY

Document Type	LIGO-T960168-A - E	10/18/96
Measurement of coating layer thickness		
Hiroaki Yamamoto		

Distribution of this document:

LIGO science

This is an internal working note
 of the LIGO Project.

California Institute of Technology
LIGO Project - MS 51-33
Pasadena CA 91125
 Phone (818) 395-2129
 Fax (818) 304-9834
 E-mail: info@ligo.caltech.edu

Massachusetts Institute of Technology
LIGO Project - MS 20B-145
Cambridge, MA 01239
 Phone (617) 253-4824
 Fax (617) 253-7014
 E-mail: info@ligo.mit.edu

WWW: <http://www.ligo.caltech.edu/>

1 INTRODUCTION

In order to achieve the required performance of LIGO, the phase disturbance caused by aberrations of the core optics mirrors must be very small ($\sim \lambda/800$ rms). In order to study the uniformity of coatings of LIGO core optics, LIGO requested Research Electro-Optics, Inc. (REO) to make a special two layer AR (antireflection) coating, using SiO_2 and Ta_2O_5 on a SiO_2 substrate. This note summarizes the analysis of this optic with the AR coating.

From the measurements of reflectance with different polarizations and incidence angles, the thickness of SiO_2 (ΔSiO_2) and that of Ta_2O_5 ($\Delta\text{Ta}_2\text{O}_5$) were calculated over a area within 4 inch radius. Both layers become thinner as the radius increases. The effect is 0.1% at 2 inch radius for the Ta_2O_5 layer and 0.4% for the SiO_2 layer. The $\Delta\text{Ta}_2\text{O}_5$ variation is smooth with no spatial high frequency components. The ΔSiO_2 distribution shows high frequency components, which are comparable to measurement errors.

Assuming a dual-accordion structure (see below) for the global variation of thickness, a phase map was predicted for a HR (high reflectance) coating of an input test mass (ITM, 16 layers) and end test mass (ETM, 40 layers coating). The RMS of the phase variation after subtracting the tilt and curvature was $\lambda/560$ for ITM and $\lambda/270$ for ETM within 4.5 cm radius.

2 DESIGN OF THE AR COATING

The AR coating was designed so that the reflectance is primarily sensitive to the $\Delta\text{Ta}_2\text{O}_5$. Figure 1 shows contour plots of the reflectance at the Ar^+ laser wavelength (λ_{Ar} is 514.5 nm) at normal incidence. The spacing of contour lines in (b) and (c) is 500 ppm.

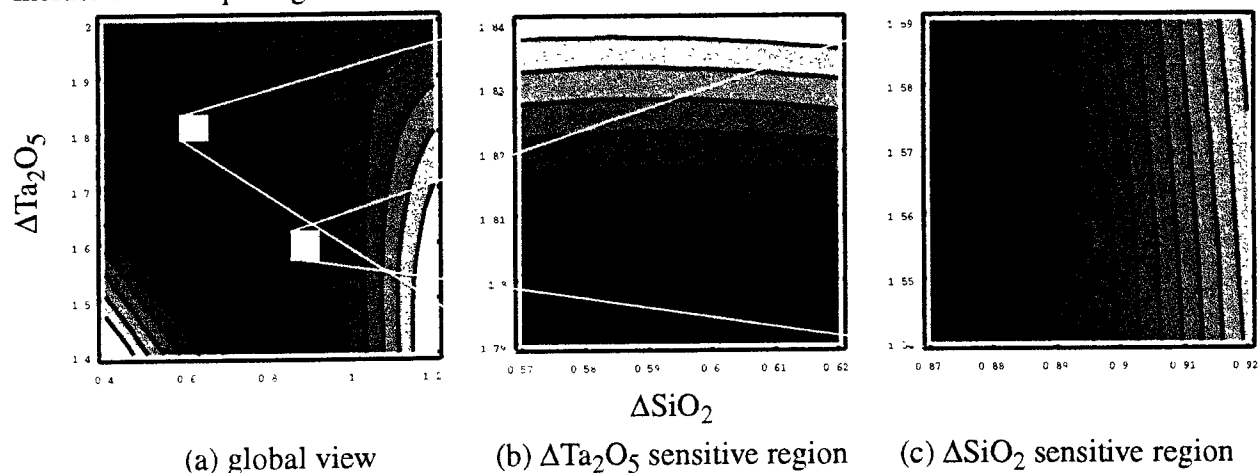


Figure 1: Reflectance of Ar laser at normal incidence

The axes are optical thickness (physical thickness times refractive index) of each of the two materials in units of $\lambda_{\text{Ar}}/4$. Figure 1 (b) is an expanded view where the reflectance is sensitive to $\Delta\text{Ta}_2\text{O}_5$ and (c) is that sensitive to ΔSiO_2 . The design coating thickness of the analyzed optic was $\Delta\text{SiO}_2 = 0.597$ and $\Delta\text{Ta}_2\text{O}_5 = 1.820$. The best fit values deduced from measurements are slightly different from these specification. The discrepancy appears to come from that the refractive

indexes used in the analysis were not exactly the same those achieved in the coating. This does not affect the uniformity study. A discussion is given in Appendix 1 about the criteria to select the thickness of layers.

3 MEASUREMENT

For the calculation of the two coating layer thicknesses, 6 power reflectance measurements were performed using the Ar⁺ laser, 3 incidence angles (12°, 45° and 60°) and both S and P polarization for each angle. These measurements were needed to obtain the necessary accuracy. For each measurement, a map was made along radial scans every 10°, at 0.04 inch radial spacing. All the points were measured twice, the second one following the first set without modifying the setup. In other words, scans were performed for angles from 0° to 710°. The parameters of the measurement set are summarized in the following table.

Table 1: Reflectance measurement parameters

Data set	P12	S12	P45	S45	P60	S60
Resolution (Eq. 1)	0.0018	0.0012	0.0018	0.0020	0.0015	0.0014
Polarization	P	S	P	S	P	S
Incident Angle	12°		45°		60°	
Radius (inch)	4	4	4	4	4	2.4

All the data sets, except S60, show reasonably smooth behavior out to 4 inch radius and all data within 4 inch radius were used in the following analysis. The S60 data show very noisy structure at the peripheral region, possibly caused by dusts on the optic, and only data within 2.4 inch radius were used.

The resolution of the reflectance measurement was determined by comparing the reflectances of the same point in the first and second scan, i.e., the resolution in the above table is defined as

$$\sqrt{2} \cdot \frac{R(\theta + 360, r) - R(\theta, r)}{R(\theta + 360, r) + R(\theta, r)} \quad \text{Eq. 1}$$

where $R(\theta, r)$ is the reflectance at angle θ and radius r .

The polarizations, incidence angles and overall normalizations are determined in the analysis explained below.

4 ANTIREFLECTION COATING

The detailed description of the antireflection coating may be found in “Thin film optical filters” by H. A. Macleod (published by Adam Hilger Ltd). The formula for the two layer coating is given in Eq. 2. In this equation, n_r is the refractive index, d_r is the physical thickness, θ_r is the angle in the material r , and material 0 stands for the air, S for the SiO₂ layer, T for the Ta₂O₅ layer, and m

$$\begin{bmatrix} B \\ C \end{bmatrix} = \begin{bmatrix} \cos \delta_S & \frac{i \sin \delta_S}{\eta_S} \\ i \eta_S \sin \delta_S & \cos \delta_S \end{bmatrix} \cdot \begin{bmatrix} \cos \delta_T & \frac{i \sin \delta_T}{\eta_T} \\ i \eta_T \sin \delta_T & \cos \delta_T \end{bmatrix} \cdot \begin{bmatrix} 1 \\ \eta_m \end{bmatrix}$$

$$Y = \frac{C}{B}$$

$$R = \left(\frac{\eta_0 - Y}{\eta_0 + Y} \right) \cdot \left(\frac{\eta_0 - Y}{\eta_0 + Y} \right)^* \quad \text{Eq. 2}$$

$$\delta_r = \frac{2\pi n_r d_r \cos \theta_r}{\lambda}$$

$$\eta_r = n_r \cos \theta_r \quad \text{for S polarization}$$

$$\eta_r = n_r / \cos \theta_r \quad \text{for P polarization}$$

$$n_r \sin \theta_r = n_m \sin \theta_m$$

stands for the substrate SiO₂. In this analysis, the following refractive indices are used and assumed to be constant: $n_S = 1.4598$, $n_T = 2.1021$ and $n_m = 1.4578$.

The reflectance is a function of thicknesses, incidence angles and the polarization of the laser. Eq. 2 is the formula for the perfect S (electric field vector is parallel to the surface plane) and P polarization (magnetic field parallel to surface plane). When the field vector is not parallel to the surface, the reflectance is given by weighted sum of the reflectances for the S and P polarized cases:

$$R(\Theta_{pol}) = R_S \cdot \cos^2 \Theta_{pol} + R_P \cdot \sin^2 \Theta_{pol} \quad \text{Eq. 3}$$

5 THICKNESS CALCULATION

There are 12 reflectance measurements for the same spot at angle θ and radius r : three angles, two polarizations and two scans, 0° to 350° and 360° to 710°. Two sets of measurements (6 in the first scan and 6 in the second scan) were analyzed separately, and the difference was taken as indicative of systematic error. For each spot, the two thicknesses of layers were calculated by minimizing the following quantity using the minimization program MINUIT ("MINUIT - Function Minimization and Error Analysis", by F. James, CERN Program Library entry D506):

$$\sum_I \left\{ \left(\frac{R_I(\theta, r)}{\left((1 + \delta_I) \Re(\Delta SiO_2, \Delta Ta_2O_5, \Theta_{inc}, \Theta_{pol}) - 1 \right)} \right)^2 + \left(\frac{\Theta_{inc} - \overline{\Theta_{inc}}}{\epsilon_\Theta} \right)^2 \right\} \quad \text{Eq. 4}$$

In this equation, I represents the data set, P12, S12, P45, S45, P60 and S60 and $R_I(\theta, r)$ is the reflectance measured at the point θ, r and ϵ_I is the resolution defined in Eq. 1. $\Re(\Delta SiO_2, \Delta Ta_2O_5, \Theta_{inc}, \Theta_{pol})$ is the reflectance calculated using Eq. 2 and Eq. 3, where Θ_{inc} is the incidence angle at

the surface. The second term forces the incidence angle to be distributed around an average incident angle, $\overline{\Theta}_{inc}$, for the pairs of measurements, 12P and 12S, 45P and 45S and 60P and 60S.

Table 2 summarizes the unknowns which were fitted.

Table 2: Free Parameters in the minimization

Unknown	Meaning	Comment
ΔSiO_2	thickness of SiO_2 layer	one parameter for each spot
$\Delta\text{Ta}_2\text{O}_5$	thickness of Ta_2O_5 layer	one parameter for each spot
δ_I	overall normalization	one parameter for each set
Θ_{inc}	incident angle	one parameter along each radial direction for each data set
$\overline{\Theta}_{inc}$	average incident angle	one parameter for the pair of angles, 12P&S, 45P&S, 60P&S
Θ_{pol}	polarization	one parameter for each set

The calibration process introduces overall uncertainties of the order of 1% in power. The incidence angle has two uncertainties. The accuracy of the incident direction setup is of the order of 0.5° . In addition to this uncertainty, there are various sources which can change the direction of the incidence angle, such as a change of orientation of the plate holding the optic due to the bearing motion. The accuracy of the polarization angle setup, determined by maximizing or minimizing the measured power, is of the order of 1° . With this size of possible polarization admixture, the contamination of the two polarizations could possibly affect only P45 and P60.

The details of the minimization process and some of the results are given in Appendix 2.

The error in the extracted thicknesses was estimated by combining factors listed in the following table. MINUIT error is calculated after all iterations were done by fixing all other parameters. The comparison of the first set (angle 0° - 350°) and the second set (360° - 710°) gives an estimation of

Table 3: Error estimation contribution (unit is $\lambda/4$)

	ΔSiO_2	$\Delta\text{Ta}_2\text{O}_5$
thickness at $r=0$ (center)	0.624	1.872
MINUIT fit error	2.6×10^{-4}	0.9×10^{-4}
Set 0° - 350° vs. Set 360° - 710°	3.5×10^{-4}	1.6×10^{-4}

Table 3: Error estimation contribution (unit is $\lambda/4$)

Convergence of repetition	1×10^{-4}	0.2×10^{-4}
Random error	5.5×10^{-4}	1.3×10^{-4}
Combined	10×10^{-3}	3.1×10^{-4}

the reproducibility of the measurement, including the change of environment during tests. A comparison of the results of different iteration levels gives an error estimation on how the minimization as a whole works. There is a time dependent systematic error which is not yet understood. This is estimated from the variation of the thickness at $r = 0$ calculated along different directions. The combined error was calculated by taking the quadrature sum of the first three errors and the random error was added linearly to it.

The variation of the layer thickness must be less than 0.02% to satisfy the $\lambda/800$ requirement when accordion structure is assumed (“Multi thin layer coating modeling”, by H. Yamamoto, LIGO-T950008-A). The resolution of $\Delta\text{Ta}_2\text{O}_5$ is good enough to test this variation, but that of ΔSiO_2 is factor 10 worse than this requirement.

6 RESULTS - THICKNESS

The fit results are shown in the following figures. Figure 3 shows the contour plot of the two layers. As can be seen from this figure, the Ta_2O_5 layer is smooth and cylindrically symmetric, but the SiO_2 layer appears rough. To see this more quantitatively, the distributions of thickness along two diameters are shown in Figure 3. (a-1) and (b-1) show the thickness (solid line) and the 10th order Zernike polynomial fit (dashed line) and (a-2) and (b-2) show the residuals between measured thickness and the polynomial fit. From (a-1) and (b-1), again it is clear that the Ta_2O_5 layer is more smooth and symmetric, while the SiO_2 layer appears rough and asymmetric.

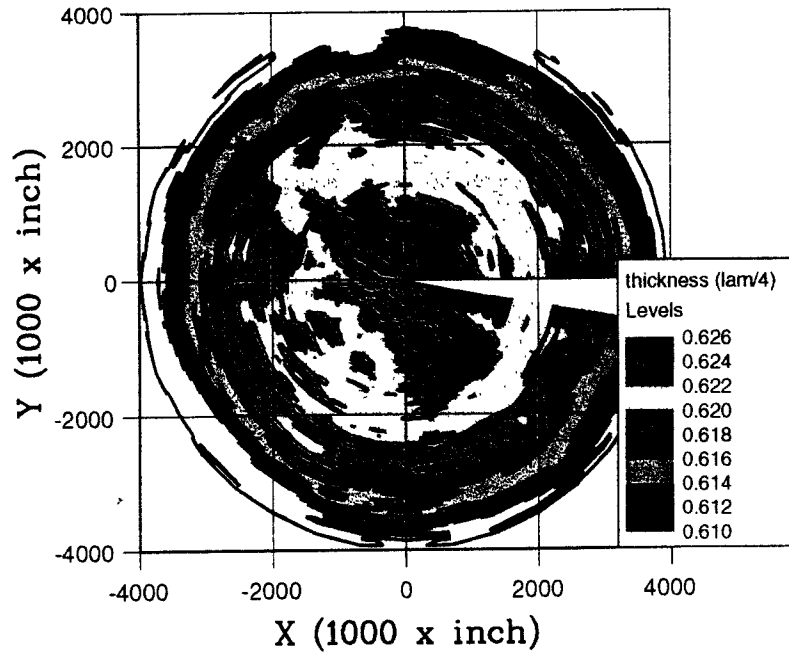
The standard deviation of the difference of the measured thickness from the polynomial fit ((a-2) and (b-2)) was 1.8×10^{-4} for the Ta_2O_5 layer and was 10.7×10^{-4} for the SiO_2 layer. Both are of comparable magnitude to the respective systematic uncertainties for each layer.

7 PHASEMAP

From the thickness variation measurements, a phase map for the LIGO HR mirror was calculated from the Zernike fit to the data assuming the dual accordion model (low frequency components of thickness variations accumulate linearly, “Multi thin layer coating modeling”, by H. Yamamoto, LIGO-T950008-A). The phase map and cross sections along two diameters are shown in Figure 4. The phase map is given in nanometers. The RMS and P-V in the central 4.5 cm radius area, after subtracting tilt and curvature, was 4.0 nm ($\lambda/130$) and 17.8 nm for the 40 layer mirror, and 1.9 nm ($\lambda/270$) and 8.4 nm for the 16 layer mirror.

(a)

SiO₂ optical thickness (λm/4)



(b)

Ta₂O₅ optical thickness (λm/4)

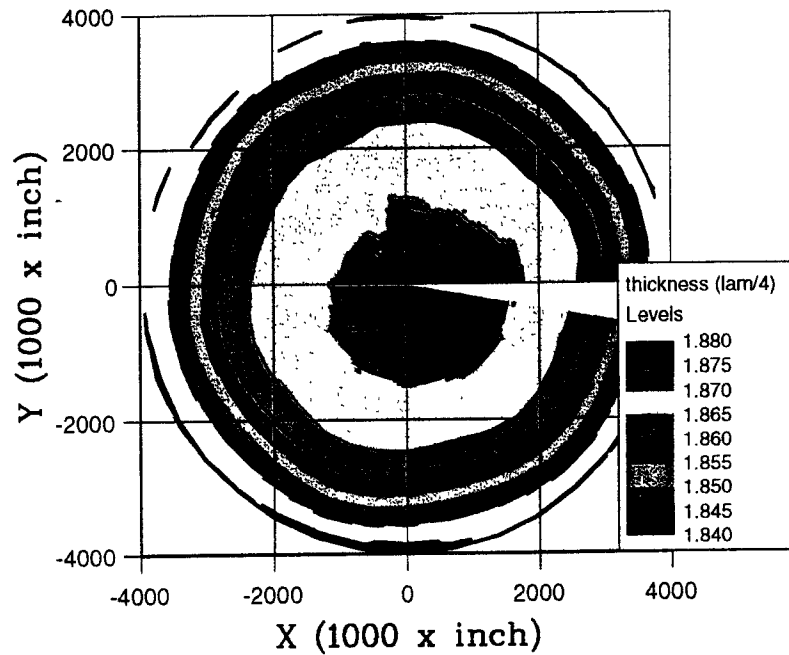


Figure 2: Contour Plot of layer thickness

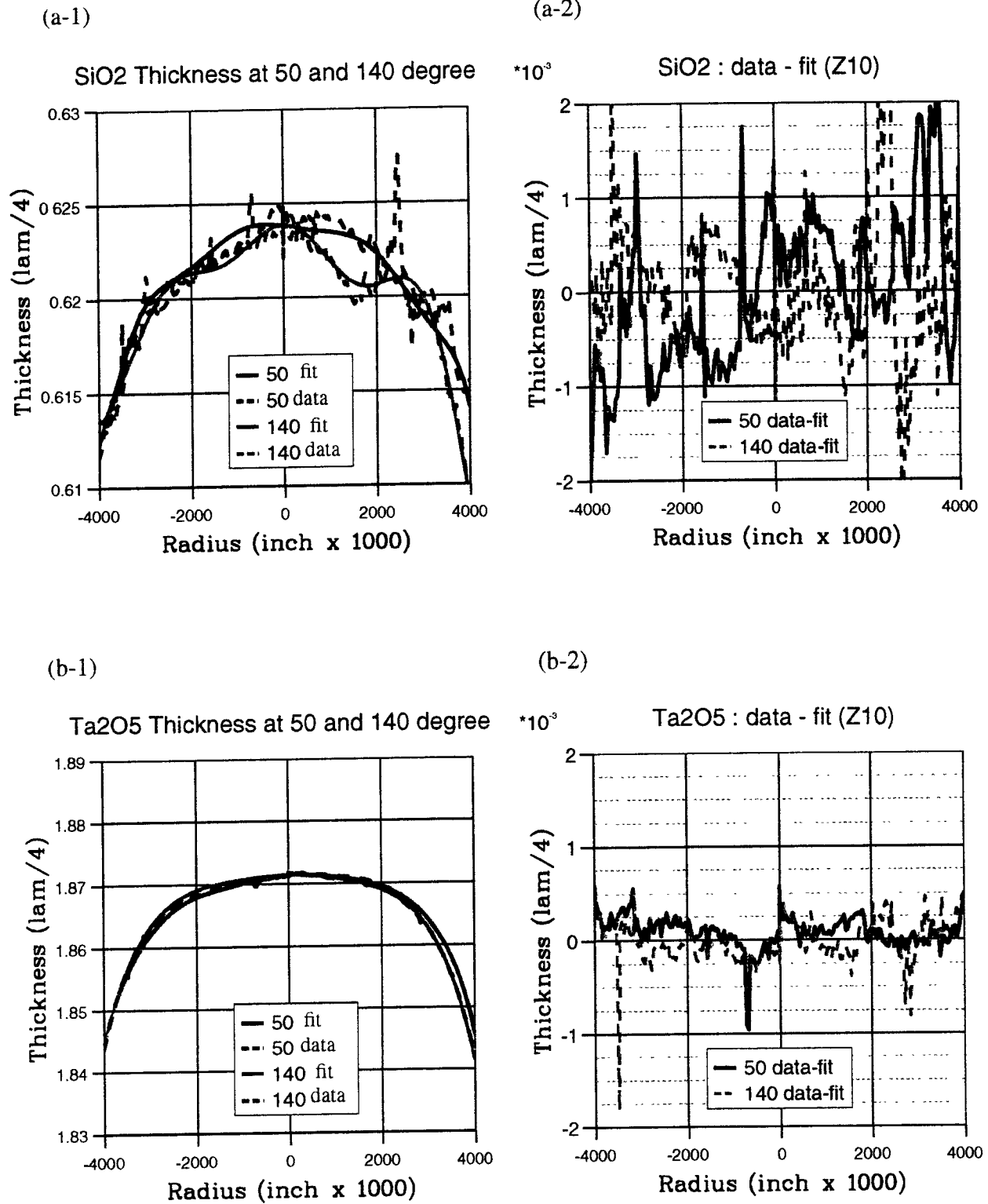
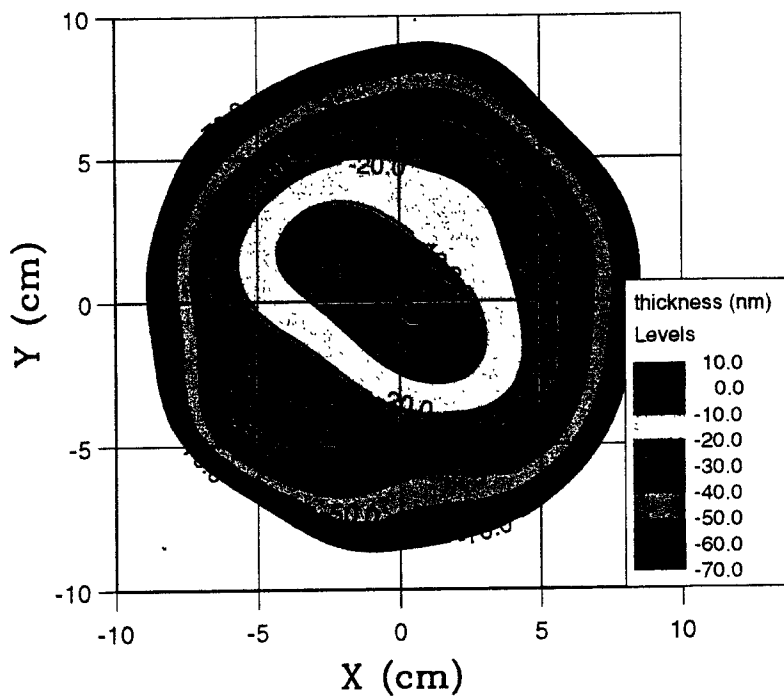


Figure 3: Thickness cross section

(a) 40 layer HR coating phase map



(b) 40 layer HR coating phase map

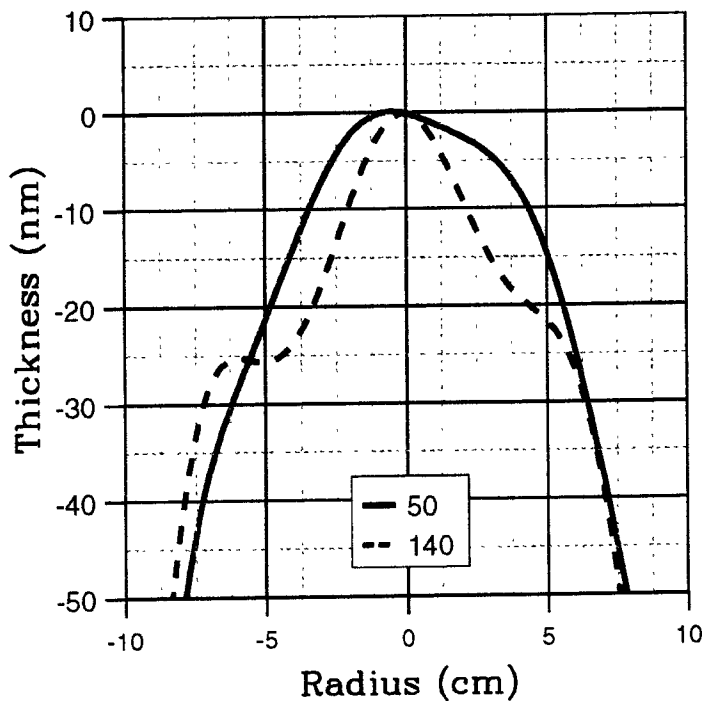


Figure 4: 40 layer HR mirror phasemap

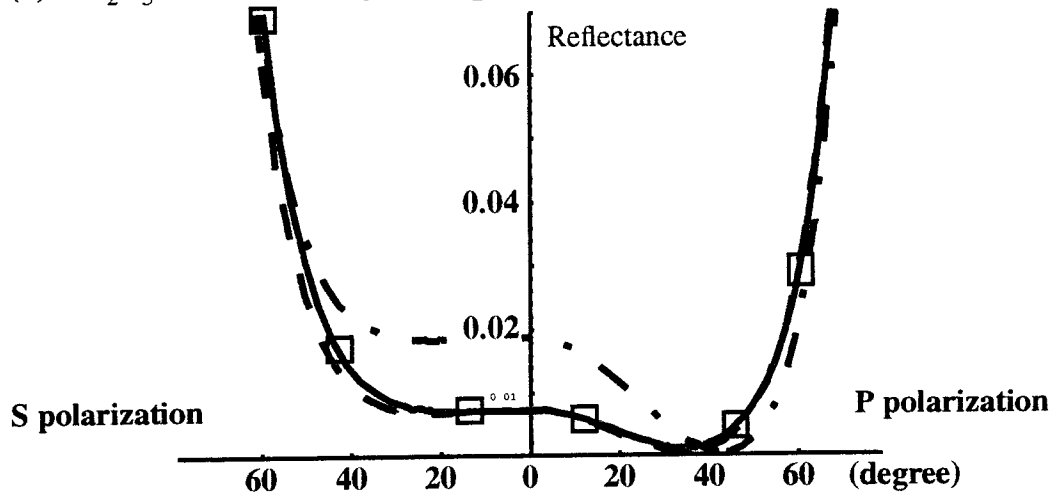
8 CONCLUSIONS

A noninterferometric method was developed to measure the coating layer thickness very accurately using special AR coatings. This is useful to predict the coating qualities of LIGO optics. Using a reasonable model relating one layer thickness to the entire HR coating, the phase maps of the input and output test masses were created. The rms of the variation of the phase map shows that the coating analyzed here is not good enough to meet the LIGO requirements. The analysis result was informed to REO to improve the coating for the next AR coatings.

APPENDIX 1 OPTIMAL THICKNESS

The thicknesses of the two coating layers were chosen so that the correlation of the two layers would not degrade the accuracy of each layer. Intuitively speaking, a point was chosen in Figure 1 (a) where the contour (equi-reflectance line) is horizontal (insensitive to ΔSiO_2) or vertical (insensitive to $\Delta\text{Ta}_2\text{O}_5$). In this appendix, further discussion is give about the choice and the thickness and incident angles of the layer.

(a) $\Delta\text{Ta}_2\text{O}_5$ sensitive coating ($\Delta\text{SiO}_2=0.597, \Delta\text{Ta}_2\text{O}_5=1.820$)



(b) ΔSiO_2 sensitive coating ($\Delta\text{SiO}_2=0.882, \Delta\text{Ta}_2\text{O}_5=1.560$)

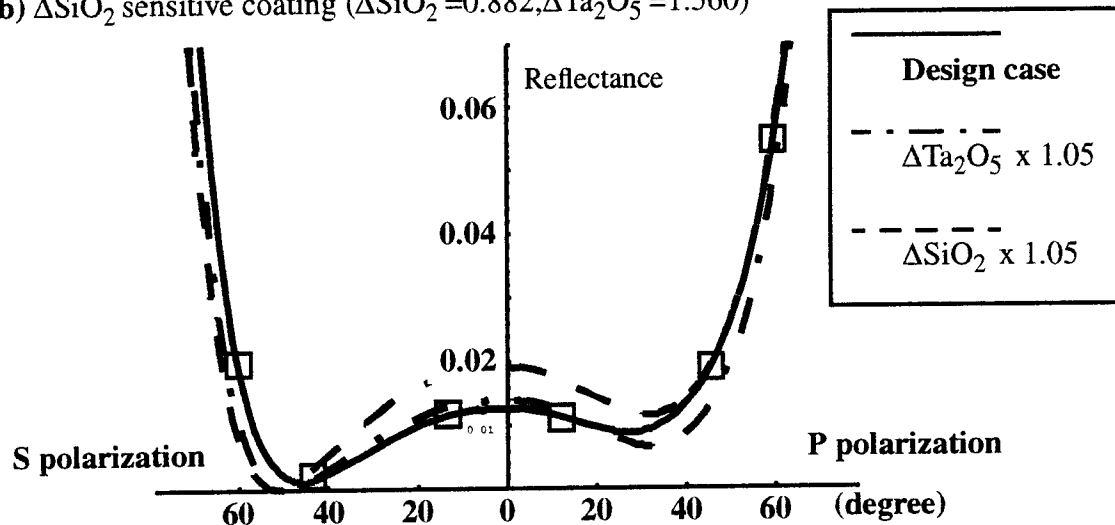


Figure 5: Incident angle and polarization dependence of Reflectance

Figure 5 shows the reflectance as a function of the incident angle for P and S polarized field. The right hand side of the reflectance axis represents the angle for the P polarization and the left for the S polarization. Figure (a) is a plot for the coating analyzed in this note. It was designed for the better measurement of $\Delta\text{Ta}_2\text{O}_5$. In this plot, the solid line is the reflectance with the designed thickness, $\Delta\text{SiO}_2=0.597$ and $\Delta\text{Ta}_2\text{O}_5=1.820$. The dashed line is that with the ΔSiO_2 5% thicker than

the design value and the dash-dotted line is that with $\Delta\text{Ta}_2\text{O}_5$ 5% thicker. Figure (b) is the case designed for the precise measurement of ΔSiO_2 .

As is seen from these plots, the reflectance is very sensitive to one of the thicknesses in some regions, while it is sensitive to the other in other regions. This is because the contour of the reflectance, Figure 1, changes as the incident angle and the polarization changes. The following quantity can characterize the sensitivity of the reflectance to the change of thickness.

$$\Xi_m = \frac{\delta\Xi_m}{\delta R} = \xi \cdot \frac{\delta_m}{\epsilon_R}$$

$$\delta\Xi_m = \frac{dR}{d\Delta_m} \cdot \delta\Delta_m, \quad \delta\Delta_m = \delta_m \cdot \Delta_m, \quad \delta R = R \cdot \epsilon_R \quad \text{Eq. 5}$$

$$\xi = \frac{dR}{d\Delta_m} \cdot \frac{\Delta_m}{R}$$

In this equation, R is the reflectance and Δ_m is the thickness of a material. The sensitivity of the reflectance to the change of the thickness is given by the ratio of $\delta\Xi_m$ and δR , where $\delta\Xi_m$ is the change of the reflectance when the thickness changed by $\delta\Delta_m$, and δR is the resolution of the reflectance. If Ξ_m is more than several times larger than 1, the change is observable, otherwise, the change is consistent with the resolution. The resolution δR was found to be roughly proportional to the reflectance, i.e., ϵ_R is around 0.1% for a wide range of the reflectance value, and fractional thickness change, $\delta_m = \delta\Delta_m/\Delta_m$, is the direct concern. E.g., if ξ is 10, the thickness can be measured to the accuracy of the order of 0.01%. This is a very crude argument, and the final accuracy depends on the details of the analysis, but ξ is a good measure of the sensitivity.

The following table shows the sensitivities for the two sets of coatings.

Table 4: Sensitivity ξ

angle (degree)	polar- ization	$\Delta\text{Ta}_2\text{O}_5$ sensitive coating ($\Delta\text{SiO}_2=0.597, \Delta\text{Ta}_2\text{O}_5=1.820$)		ΔSiO_2 sensitive coating ($\Delta\text{SiO}_2=0.882, \Delta\text{Ta}_2\text{O}_5=1.560$)	
		$\xi(\text{SiO}_2)$	$\xi(\text{Ta}_2\text{O}_5)$	$\xi(\text{SiO}_2)$	$\xi(\text{Ta}_2\text{O}_5)$
12	P	0.3	8.3	9.2	0.002
	S	0.3	7.7	9.8	0.5
45	P	3.6	8.5	2×10^{-4}	3.7
	S	3.9	0.2	10	26
60	P	0.4	1.8	0.2	1.4
	S	2.7	1.1	13	7.1

APPENDIX 2 MINIMIZATION PROCESS

In this appendix, the details of the minimization process is described. The minimization process goes as follows:

1. finding Θ_{inc} for 12P, 45P and 60P
 - Fix all but ΔSiO_2 , $\Delta\text{Ta}_2\text{O}_5$ and Θ_{inc} for 12P, 45P and 60P
 - repeat minimization along one radial direction
 - calculate the average of each Θ_{inc} as the improved estimation
 - repeat this for all 36 directions
2. finding Θ_{inc} for 12S, 45S and 60S
 - Fix all but ΔSiO_2 , $\Delta\text{Ta}_2\text{O}_5$ and Θ_{inc} for 12S, 45S and 60S
 - do the same as process 1
3. finding δ_{I} for 12P, 45P and 60P
 - Fix all but ΔSiO_2 , $\Delta\text{Ta}_2\text{O}_5$ and δ_{I} for 12P, 45P and 60P
 - repeat minimization for all points
 - calculate the average of each δ_{I} as the improved estimation
4. finding δ_{I} for 12S, 45S and 60S
 - Fix all but ΔSiO_2 , $\Delta\text{Ta}_2\text{O}_5$ and δ_{I} for 12S, 45S and 60S
 - do the same as process 3
5. finding Θ_{pol} for 45P and 60P
 - Fix all but ΔSiO_2 , $\Delta\text{Ta}_2\text{O}_5$ and Θ_{pol} for 45P and 60P
 - do the same as process 3
6. finding ΔSiO_2 and $\Delta\text{Ta}_2\text{O}_5$
 - Fix all but ΔSiO_2 and $\Delta\text{Ta}_2\text{O}_5$
 - do minimization for all points

These processes are repeated 50 times to obtain the final results. In the above description, “fix” means to use the best estimation, e.g., in the 9th iteration, the result of 8th iteration is used. Separate minimization of P and S cases (process 1 and 2, and process 3 and 4) was needed because the convergence of parameters for S polarization was slower than those for P. Polarization angles Θ_{pol} were fixed to be 0 for 12P, 12S, 45S and 60S, because the effect was estimated to be less than 0.1%. All steps except 6 (“finding ΔSiO_2 and $\Delta\text{Ta}_2\text{O}_5$ ”) were done using points within 2.4 inch, and all points were used for step 6.

The parameters from this minimization is summarized in Table 5.

There are strong correlations between some of these parameters, which did not converge in the iteration process. The polarization angles were very uncertain. The current measurement accuracy

Table 5: Minimization result of parameters

Data set	P12	S12	P45	S45	P60	S60
δ_I	-0.004	0.001	0.044	-0.001	0.0003	-0.006
$\overline{\Theta}_{inc}$	11.7°		44.8°		60.9°	
Θ_{pol}	0	0	2.6°	0	5°	0

prohibited resolving these correlated uncertainties. Fortunately, the thickness itself converged well.

APPENDIX 3 ZERNIKE FIT OF THICKNESS

The following are the coefficients of the Zernike polynomial fit to ΔSiO_2 and $\Delta\text{Ta}_2\text{O}_5$ up to 10th order. The thickness is measured in units of $\lambda_{Ar}/4$. The Zernike polynomial are normalized as

$$\int_0^{12\pi} \int_0^1 |Z_n^m|^2 \rho d\rho d\theta = \pi \quad \text{Eq. 6}$$

The table NMInd is a Zernike polynomial index list corresponding to the coefficient tables, and one can calculate the thickness at (x,y) by the following formula, where x and y are measured in inch, $R_0 = 4$ inch and the formula is valid within 4 inch radius.

$$\sum_{i=0}^{65} \text{Coeff}[i] \cdot Z_{NMInd[i][0]}^{NMInd[i][1]} \left(\frac{x}{R_0}, \frac{y}{R_0} \right) \quad \text{Eq. 7}$$

```
double SiO2_Coeff[66] = {
  0.619012333388677,    0.000156265256488991, -0.000321980508092953,
-0.00282296170517754, -5.45320688098129e-05, -0.000113109158825177,
-2.85105721321284e-06, -8.80101932312538e-05,  2.9598739602242e-05,
  0.000212361124239879, -0.000518557632835147,  0.000113234537531658,
  8.74435184086548e-06,  3.90019171145128e-05, -5.03929076840117e-05,
  0.000143903003883856,  2.01517221627806e-05, -0.000108288208956386,
  6.82451773115462e-05,  6.5136127527658e-05, -3.09191750504923e-05,
-0.000246797186879683, -7.2103215671994e-05, -0.000206920126111847,
  0.000168681160547177, -0.000102589224995085,  0.000111273096576501,
  0.000103575857393477,  2.29627121299996e-05,  8.75439746061231e-06,
-4.52373718872082e-05,  5.88837812809871e-05, -8.07940881455159e-05,
-0.000116593389391504, -9.24495766488402e-06, -1.83923068516447e-05,
  0.000125511532789133, -1.74555022680888e-05,  0.000142484444093809,
-6.87640939986527e-05,  2.24743437208803e-05, -5.42896540159113e-05,
```

LIGO-T960168-A

```

    2.02222730868513e-05, -2.30151081119354e-05, 4.66781195941343e-07,
-0.000125612172644031, 4.09379677793508e-05, 5.80209319577049e-05,
-3.0593070762432e-05, 4.51455778790111e-05, -9.9363258727246e-05,
 9.83868225054161e-05, 7.92701341978037e-06, 8.70374959132922e-05,
-0.000105229968529457, -2.71582354047475e-05, -1.96598965836745e-06,
-8.63135418964949e-05, 1.6419884695572e-05, -2.36712468095223e-05,
-1.68854004719202e-05, -2.67479447340342e-05, 4.42619138459018e-05,
-8.56649909808693e-05, -0.000136297682436168, -2.12339569178882e-06
    };

double Ta205_Coeff[66] = {
    1.86234598256416, 0.000697474830465895, -0.00031057222570545,
-0.00735367528389809, 6.22282310027014e-05, 0.000220082793750541,
 3.07495427456881e-05, 0.00012965451246771, 0.000157264008411776,
-2.79873729618476e-05, -0.00208875048827788, -3.71466754583935e-05,
-4.6255600715418e-05, 2.47188798382459e-05, 5.53105055257562e-05,
 4.77074990926081e-06, 1.12829385936055e-05, -3.20585051803876e-05,
 3.32643822739324e-05, -4.54505334234589e-05, 0.000122583562132193,
-0.000346744528526219, 1.12069618453088e-05, -3.66174628906737e-06,
-1.32769724216994e-06, -1.92368957532105e-05, 6.68566311214454e-05,
 0.000526667028466874, -1.37092992069054e-05, 3.78744131761632e-05,
 9.5279303609876e-06, -2.03822868063874e-05, -1.97506491783682e-05,
-3.91736900159534e-05, 6.35108305215154e-05, -4.34210192884159e-05,
-3.29524509797853e-05, 9.51865611105489e-06, 1.66297773030175e-05,
-1.74231651459414e-06, 4.68859974450932e-06, -5.83544913795732e-06,
-0.000107470210581129, 1.47631267322353e-05, 3.10872316314558e-05,
-9.82525051039489e-06, -2.63889138162706e-05, -1.57729791157443e-05,
 9.40114084173473e-06, 1.33093452867471e-05, 3.06647317939234e-05,
-1.33372697391081e-05, -7.40492733684629e-06, -3.32453400247268e-05,
 4.25031402438399e-05, -6.30133623123188e-05, 4.8638856544958e-06,
 2.0844279851528e-05, 6.10102849397591e-06, -1.24495435847617e-05,
-1.79849472948392e-05, 2.07653328411359e-05, -1.05790051972946e-05,
-1.1894692629988e-05, 5.43609418574919e-07, -6.46133195583986e-05
    };

int NMInd[66][2] = {
    0, 0, 1, 1, 1, -1, 2, 0, 2, 2, 2, -2,
 3, 1, 3, -1, 3, 3, 3, -3, 4, 0, 4, 2, 4, -2, 4, 4, 4, -4,
 5, 1, 5, -1, 5, 3, 5, -3, 5, 5, 5, -5,
 6, 0, 6, 2, 6, -2, 6, 4, 6, -4, 6, 6, 6, -6,
 7, 1, 7, -1, 7, 3, 7, -3, 7, 5, 7, -5, 7, 7, 7, -7,
 8, 0, 8, 2, 8, -2, 8, 4, 8, -4, 8, 6, 8, -6, 8, 8, 8, -8,

```

LIGO-T960168-A

```
9, 1, 9, -1, 9, 3, 9, -3, 9, 5, 9, -5, 9, 7, 9, -7, 9, 9, 9, -9,  
10, 0, 10, 2, 10, -2, 10, 4, 10, -4, 10, 6, 10, -6,  
10, 8, 10, -8, 10, 10, 10, -10  
};
```


PDR/CDR DESIGN REVIEW DOCUMENT

Tim Thompson, William Miller, and Eric Ponslet

February 18, 1997

Abstract

This document provides an overview of the SEI preliminary design for the BSC and HAM systems. The SEI systems are under design for the LIGO Project, sponsored by the National Science Foundation. The work is focused in four areas; LIGO Stack Development, BSC Design and Fabrication, HAM Design and Fabrication, and BSC/HAM External Support and Actuator System. This report documents the preliminary design of the BSC and HAM stacks and supports, and the conceptual design of the actuator systems and their external supports.

HYTEC Inc.

110 Eastgate Dr., Ste 100

Los Alamos, NM 87544

(505) 662-0080 / Fax (505) 662-5179

LIGO  **PROJECT**

Table of Contents

1. EXECUTIVE SUMMARY.....	7
2. INTRODUCTION.....	8
2.1 SEI SYSTEM DESCRIPTION AND REQUIREMENTS	8
2.2 SYSTEM INTEGRATION AND SYSTEM TESTING	11
3. BSC DESIGN AND FABRICATION	14
3.1.1 Component Description.....	14
3.1.2 Support Structure Description ^[6]	14
3.1.3 Isolation Stack Description ^[5,7]	17
3.1.3.1 Leg Description ^[7]	18
3.1.3.2 Downtube and Optics Table Description ^[5]	18
3.2 STRUCTURAL ANALYSIS	19
3.2.1 Support Structure ^[6]	19
3.2.2 Downtube and Optics Table ^[5]	19
3.3 FABRICATION COSTS	20
3.4 1ST ARTICLE PERFORMANCE EVALUATION AND TEST.....	21
3.5 ASSEMBLY AND STAGING.....	21
3.5.1 Fixturing and Tooling Required.....	21
4. HAM DESIGN AND FABRICATION.....	22
4.1 COMPONENT DESCRIPTION	22
4.1.1 Support Structure ^[12]	23
4.1.2 Isolation Stack Description ^[13]	24
4.2 HAM FABRICATION COSTS.....	25
4.3 1ST ARTICLE PERFORMANCE EVALUATION AND TEST.....	26
4.4 ASSEMBLY AND STAGING.....	26
4.4.1 Fixturing and Tooling Required.....	26
5. EXTERNAL SUPPORTS AND ACTUATOR SYSTEMS, CDR.....	27

5.1 REQUIREMENTS	27
5.2 DESIGN OPTIONS	27
5.2.1 Coarse Actuator	27
5.2.2 Fine Actuator	28
5.3 CONCEPTUAL DESIGN CONFIGURATION	28
5.3.1 Coarse Actuators	29
5.3.1.1 Coarse Actuators UX, UY, RZ	30
5.3.1.2 Coarse Actuator UZ	31
5.3.2 Fine Actuator	31
5.4 COARSE/FINE ACTUATOR TESTS	32
5.4.1 Coarse Actuator Tests	32
5.4.2 Fine Actuator Tests	33
6. DAMPED METAL SPRING DEVELOPMENT^[4,14]	34
6.1 INTRODUCTION	34
6.2 METAL SPRING CONCEPTS	34
6.3 DEVELOPMENT AND TEST RESULTS	35
6.3.1 Coil Spring	35
6.3.2 Leaf Spring	37
6.4 FUTURE PROTOTYPING AND DEVELOPMENT PLANS	38
6.4.1 Prototype qualification tests	38
6.4.2 Damped Spring Pre-Production Process Qualification	38
6.4.3 Metal Spring Decision	38
7. LIGO SEISMIC ISOLATION PERFORMANCE	39
7.1 REQUIREMENTS	39
7.2 SEISMIC ISOLATION PREDICTIONS	39
7.2.1 Introduction	39
7.2.2 Simulation results for BSC stacks	40
7.2.3 Simulation results for HAM stacks	41
8. PROGRAM PLANS	42
8.1 LIGO STACK DEVELOPMENT	42

8.2 LIGO BSC DESIGN/FABRICATION	42
8.3 LIGO HAM DESIGN/FABRICATION.....	43
8.4 BSC AND HAM EXTERNAL SUPPORTS AND ACTUATORS	43
8.5 SUMMARY.....	43
8.6 HAM/BSC DELIVERY AND ASSEMBLY SCHEDULE	43
9. REFERENCES.....	45
10. ATTACHEMENTS.....	47
10.1 REPORTS	47
10.2 TECHNICAL SPECIFICATIONS	47
10.3 ASSEMBLY DRAWINGS	47
10.4 COST ESTIMATES.....	47
10.5 WEIGHT BREAKDOWNS	48

List of Figures

Figure 1. BSC Assembly.....	9
Figure 2. HAM Assembly.....	9
Figure 3. BSC SEI Layout.....	14
Figure 4. BSC Support Structure.....	15
Figure 5. BSC SEI Support Structure Overall Dimensions.....	16
Figure 6. BSC Downtube/Optics Table and Stack Assembly.....	17
Figure 7. BSC SIS Stack Layout Options; Coil, Leaf, and Viton Springs.....	18
Figure 8. HAM SEI Layout.....	22
Figure 9. HAM Support Structure.....	23
Figure 10. HAM SEI Support Structure Overall Dimensions.....	24
Figure 11. HAM Isolation Stack Layout (Viton Spring Stack Shown).....	25
Figure 12. Coarse and Fine Actuator Assembly.....	28
Figure 13. Coarse X/Y - Actuator Assembly.....	30
Figure 14. Coarse Actuator Assembly - UZ.....	31
Figure 15. Fine Actuator Assembly - UX.....	32
Figure 16. Coil spring concept.....	35
Figure 17. Leaf spring concept.....	35
Figure 18. Coil Spring Prototype. The seats are temporary epoxy resin versions.....	36
Figure 19. Axial Loss Factors. Measured by free decay on four damped coil prototypes (DC00, 01, 02, and 03) compared to analytical prediction.....	36
Figure 20. Leaf Spring Prototype. Photograph on right shows beryllium copper parts before assembly (viscoelastic material not shown).....	37
Figure 21. Leaf Spring Prototype Being Deformed in MTS Testing Machine.....	37
Figure 22. Spectrum of residual test mass motion for BSC stacks. Approximate support dynamics is included. The green curve shows total residual seismic noise while the black and blue curves show individual contributions from horizontal and vertical floor noise, respectively.....	40
Figure 23. Horizontal Transmissibilities of HAM Stacks. Support dynamics is not included.....	41

List of Tables

Table 1. Top Level requirements of the BSC	10
Table 2. Top Level requirements of the HAM.....	11
Table 3 Testing requirements for the BSC and HAM.....	13
Table 4. BSC 1 st Article Costs	20
Table 5. BSC Production Article Costs.....	20
Table 6. HAM 1 st Article Costs	25
Table 7. HAM Production Article Costs.....	26
Table 8. Top Level Requirements of the HAM	40
Table 9. BSC Stack Design with VITON Springs	41

1. EXECUTIVE SUMMARY

HYTEC is designing the seismic isolation system (SEI) for the BSC and HAM components used in the LIGO project. Considerable progress has been made on the mechanical design for both stacks. Preliminary fabrication drawings have been completed for all hardware. The drawings have been sent to vendors to obtain preliminary pricing information. Our near term objective is to complete the fabrication drawings early in order to permit construction of 1st article hardware. Our program plan calls for fabrication to begin June 1997 and assembly of the 1st article of BSC and HAM hardware to commence November 1997. Hardware testing will begin by November of this year.

Initial development tests with the damped metal spring concepts have produced quite promising results. Both static and dynamic tests have been completed with the coil spring. The leaf spring has not been tested to the same extent as the coil spring, so at this stage its loss factor has not been completely defined. Loss factors recovered by simple pendulum tests on the coil spring agreed with our expectations. Results obtained on a 6 DOF layer test also agreed fairly well with the pendulum tests, although much needs to still be learned about the damping in terms of construction attributes. Our present activities center on improving the coil quality by optimizing the aluminum core pieces. As an alternate spring concept, the leaf spring has proven to be a worthwhile investment. Its dimensional quality has been quite good, and the fabrication processing may be more straight forward than the coil spring. Damped metal springs offer significant performance advantages and will provide substantially better isolation than the previously used Viton spring concept.

We have revised the program activities to allow for 1st article testing of the major system elements. Production schedule estimates provided by our vendors indicate we could produce 1st article hardware, conduct evaluation tests, and still make contractual delivery of the balance of hardware. This new schedule information provided a clear opportunity to lower overall program risk. By prototyping, mistakes in fabrication can be avoided, and/or design problems can be quickly isolated and corrected. Another benefit in this re-planning effort is to advance the delivery of hardware to Hanford. Early hardware deliveries at Hanford will prove instrumental in bringing the experiment on line in timely fashion. We also benefit by being able to concurrently design all handling fixtures, and evaluate their adequacy during the 1st article tests.

Schedules have been modified to bring the actuator design to FDR in time to dovetail with the installation schedules of the remaining seismic hardware at Hanford. This will allow us to install the support structure and actuator hardware at the point in time when it should logically be installed thus eliminating the step of retrofitting the hardware as was originally planned.

In summary, the design of the SEI system is on schedule with a solid plan for resolving technical concerns and getting prototype hardware in the users hands earlier than originally planned. In addition, the modified plan for the development of the SEI will reduce the programmatic risk to LIGO.

2. INTRODUCTION

HYTEC's responsibilities for the LIGO program include the execution of four major elements that comprise the seismic isolation (SEI) program plan. The four elements include the LIGO Stack development, BSC Design/Fab, HAM Design/Fab, and the External Support and Actuator Design/Fab. This document reviews the progress made to date in preparation for the PDR of the BSC/HAM stack and support structures, and CDR of the actuator system.

Several key milestones have been introduced to insure that the progress is consistent with final hardware delivery to Hanford starting in May of 1998.

Key technical elements of the BSC and HAM SEI include the use of a damped metal spring to achieve the stated passive isolation performance requirements. A damped metal spring concept is under development and the predicted performance is substantially enhanced, thus lowering the seismic-to-thermal noise cross-over point from 90Hz with Viton springs to less than 35 Hz. The second key area in the SEI system is the development of the actuators and external support structure.

2.1 SEI SYSTEM DESCRIPTION AND REQUIREMENTS

HYTEC is responsible for the design of all the hardware shown in Figures 1 and 2 for the BSC and HAM (with the exception of the vacuum chambers). A total of 15 BSC's and 18 HAM's will be built for the Washington and Louisiana facilities. A top level summary of the key design requirements for the two system is shown in Tables 1 and 2. The design requirements for the Actuator System are shown in attachment HYTEC-TS-LIGO-02. The design goals, simply stated, are to produce a system that provides passive vibration isolation for gravity wave measurements on the LIGO system.

To meet these objectives an isolation system was conceived that utilizes a series of mechanical filters made from springs and heavy masses. A passive four layer stack and three layer stack are used in the BSC and HAM respectively to effectively attenuate the anticipated floor vibration spectrum. An on-line (fine) actuator system is required to attenuate motions from micro-seismic disturbances at a frequency of 1/6 Hz, in addition to diurnal ground motions resulting from earth tides. A coarse alignment system is periodically needed to bring the system into alignment

Figure 1 shows the key components of the BSC system. The components have to meet the design requirements shown in Table 1. To accomplish this task the system can be broken into several key areas that will be referred to in this document. The key elements are the "Stack Assembly", the "Actuator System", and the "Support Structure". These three elements are functionally integrated together to form the BSC and HAM SEI.

The BSC Stack is composed of the downtube, optics table, and the mass and spring elements. The HAM stack does not utilize a downtube, its optic table is lower than the beamline (ref. Fig. 2). The Actuator Systems are composed of the coarse and fine actuators, and the active isolation system (e.g. STACIS 2000), if one is used. The support structure interfaces the two previous systems together and is comprised of the cross beams, the support beams, the piers, and the ancillary hardware that ties these components together.

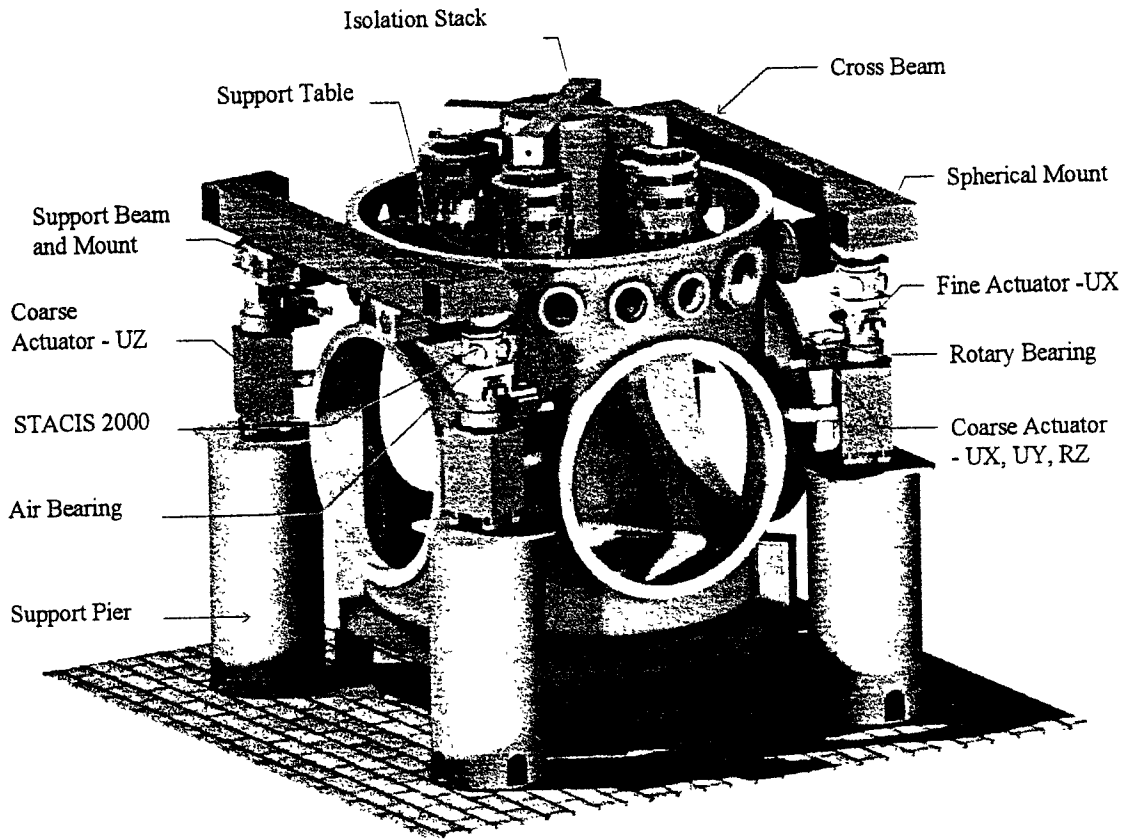


Figure 1. BSC Assembly.

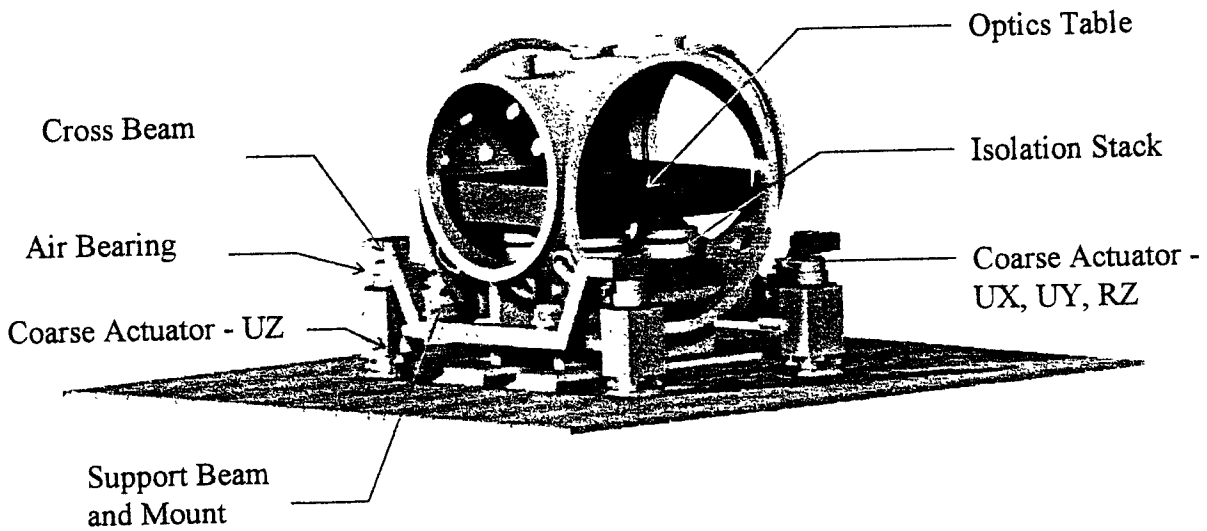


Figure 2. HAM Assembly.

Figure 2 shows the HAM components. The performance of the HAM chambers is not as stringent as the BSC. Nonetheless, its performance is still quite good in terms of general isolation systems. The Ham has a lower weight, and needs only a coarse actuator system. The design approach is to employ the actuator system developed for the BSC on the HAM. This will reduce the development time for the actuator system.

Requirement	Status	Reference(s)	Remarks
Seismic Isolation / Resonances / Noise / Drift			
test mass PSD, X direction	close (metal spgs)	7	Viton stack violates requirement
horizontal transmissibility	close (metal spgs)	7	Viton stack violates requirement
vertical transmissibility	satisfied (metal spgs)	7	Viton stack violates requirement
lock acquisition	close (metal spgs)	7	Viton stack satisfies requirement
lock maintenance	satisfied (all spgs)	7	
mass element resonances	satisfied	5	nat. freq. > 500 Hz
spring resonances	satisfied	4	will be checked through testing
downtube resonances	satisfied	5	
support assembly resonances	acceptable	6	
downtube static stresses & buckling	OK	5	
support assy static stresses & buckling	OK	5	Al. Alloy selection & treatment under research
downtube creaking / relaxation	TBD		
downtube thermal noise			
stack drift	TBD	9	to be tested (spq alone & complete stack)
Geometry			
optics table diameter	satisfied	5, LIG12001 sheet 1	
optics table to beam line separation	satisfied	LIG10000 sheet 1	
Coarse Actuators			
X, Y, Z, rotation static ranges	OK		
backlash / noise / creak	TBD		Z stage is marginal at this weight
load capacity	to be looked at	12	Z-stage will be revised for increased shear stiffness
stiffness	to be improved		
accuracy / repeatability	OK		
status feedback / error checking	OK		
Fine Actuators			
X dynamic range	TBD		testing will look at dynamic range vs frequency
smoothness / noise	TBD		testing will resolve
stiffness	OK		
accuracy / repeatability	OK		
status feedback / error checking			
Environmental			
vacuum compatibility (components inside chamber)	OK		process control approach for large structures and springs
Earthquake safety : stack	TBD		stack to be tested under static equivalent loads
Earthquake safety : support assembly	satisfied	6	structural integrity verified (pseudo-static FEM analysis)
Earthquake safety : actuators	TBD		to be checked via FEM analysis & testing
bake-out conditions	TBD		metal springs would have to be removed
Vacuum Bellows (Support Beams)			
axial / shear / twist ranges	TBD	8, 22	bellows will be prototyped and tested
fatigue life	TBD	8, 22	
leak rate	TBD	8, 22	
Others			
maintenance	TBD		fixtures and procedures TBD via BSC prototype
cabling	TBD		

Table 1. Top Level requirements of the BSC

Requirement	Status	Reference(s)	Remarks
Seismic Isolation / Resonances / Noise / Drift			
horizontal transmissibility	satisfied	13	
lock acquisition	close (metal springs)	13	
lock maintenance	satisfied	13	natural frequency > 500 Hz
mass element resonances	satisfied		
spring resonances	satisfied	4	
optics table resonances	satisfied	11	
support assembly resonances	satisfied	12, 13	
optics table static stresses & buckling	verified	11	
support assy static stresses & buckling	verified	12	
optics table creaking / relaxation	TBD		Al. Alloy selection & treatment under research
optics table thermal noise	satisfied	11	
stack drift	TBD	9	to be tested (springs alone & complete stack)
Geometry			
optics table dimensions	satisfied	11, LIG24011 sheet 1	
optics table to beam line separation	satisfied	LIG20001 sheet 1	
Coarse Actuators			
X, Y, Z, rotation static ranges	OK		
backlash / noise / creak	TBD		Z stage is marginal at this weight
load capacity	to be looked at		Z-stage will be revised for increased shear stiffness
stiffness	to be improved	12	
accuracy / repeatability	OK		
status feedback / error checking	OK		
Environmental			
vacuum compatibility (components inside chamber)	TBD		process control approach for large structures and springs
Earthquake safety : stack	TBD		stack to be tested under static equivalent loads
Earthquake safety : support assembly	satisfied	12	structural integrity verified (pseudo static FEM analysis)
Earthquake safety : actuators	TBD		to be checked via FEM analysis & testing
bake-out conditions	TBD		metal springs would have to be removed
Vacuum Bellows (Support Beams)			
axial / shear / twist ranges	TBD	10, 22	similar bellows (BSC) will be prototyped and tested
fatigue life	TBD	10, 22	"
leak rate	TBD	10, 22	"
Others			
assembly / maintenance	TBD		fixtures & procedures TBD via BSC prototype
cabling	TBD		

Table 2. Top Level requirements of the HAM

2.2 SYSTEM INTEGRATION AND SYSTEM TESTING

The system assembly, integration and testing is key to overall success of LIGO. This testing is an important aspect of proving a system of this magnitude can be made to work successfully at a cost that remains within the scope of the program. Table 3 shows the required development and test objectives that have been outlined for both the BSC and HAM.

The four elements that are involved in the development/prototype, and testing phase are:

1. Assembly and Check-Out (e.g. Fit-Check) of All the Hardware (BSC/HAM).

Partially at the vendor

Final at HYTEC and Hanford

2. External Support and Actuator Assembly Prototype Evaluation (BSC).

3. Design, Development, and Testing of the Assembly/Alignment/Maintenance Fixtures (BSC/HAM).

4. End-to-End System Performance Measurements.

Major/Critical Task	Minimum Hardware Required	Testing Equipment and/or Conditions Required	Highly Interactive with Design & Analysis?
1st ARTICLE ASSEMBLY AND CHECK-OUT			
Interface & Fit Debugging, all BSC/HAM components	piers, actuators, support structure, stack, table/downtube	-	yes
Design evaluation of Safety / Alignment / lifting Pin system (stacks)	All Stack Components	-	yes
SINGLE PIER ACTUATOR PROTOTYPE & DEVELOPMENT			
Software testing & debugging (interfaces, functionality)	1 actuator set	standard electronic meas. equipment.	yes
Hardware & Software safety stops	1 actuator set	-	yes
Functional simulation of range of motions	1 actuator set	-	yes
4- PIER ACTUATOR SYSTEM PROTOTYPE & DEVELOPMENT			
Coordination accuracy	4 piers & actuator systems	position sensors	yes
Software testing & debugging (coordination)	4 piers & actuator systems	position sensors	yes
Stiffness Estimations	4 piers & actuator systems + support structure	displacement sensors	yes
Immunity to binding	4 piers & actuator systems + support structure + mass of stack	accelerometers, load cells, motion sensors	yes
Actuator Smoothness	4 piers & actuator systems + support structure + mass of stack	accelerometers, motion sensors	somewhat
Actuator Accuracy / repeatability (coarse)	4 piers & actuator systems + support structure + mass of stack	3 D position measurement system	yes
ASSEMBLY / ALIGNMENT / MAINTENANCE FIXTURES AND PROCEDURES			
Spring positioning and indexing tools	All Stack Components, support platform	-	yes
Spring unload/ maintenance/ replacement, accuracy of stack repositioning	support structure and stack	-	yes
Bellows replacement	4 piers & actuator systems + support structure + mass of stack	-	yes
Stack insertion	All Stack Components, support platform	-	yes
Pier-to-Pier Alignment	Piers	-	yes
Actuator Assy-to-Actuator Assy Alignment	Piers and Actuators	-	yes
Actuator component replacement	4 piers & actuator systems + support structure + mass of stack	-	yes
PERFORMANCE EVALUATION AND TESTING			
Stack stability/Drift (coarse)	All Stack Components	dial indicator displacement	no
Stack stability / Drift (fine)	All Stack Components	sensors	no
Stack Q's (rough)	All Stack Components	accelerometers	possible
Stack Q's (fine, low amplitude)	All Stack Components	ultra-sensitive motion sensors	no
Actuator Accuracy / repeatability (fine)	4 piers & actuator systems + support structure + mass of stack	3 D position measurement system	no
Stack transmissibility	All Stack Components	Vacuum, ultra-sensitive motion	no

Thermal noise, creak , etc.	complete SEI system (piers, actuators, support, stack)	sensors Vacuum, ultra-sensitive motion sensors	no
Stack safety under earthquake conditions (static)	All stack components	-	yes

Table 3 Testing requirements for the BSC and HAM.

3. BSC DESIGN AND FABRICATION

3.1.1 Component Description

Figure 3 shows BSC components currently under design at HYTEC. The support structure consists of a support platform, 2 support beams, and 2 cross beams. The support platform provides support for the BSC seismic isolation stack. The support beams penetrate the BSC chamber, and hold the support platform. The support beam penetration is sealed by a welded diaphragm bellows (4 required). Cross beams on the outside of the chamber connect the ends of the support beams and interface with the coarse and fine actuators.

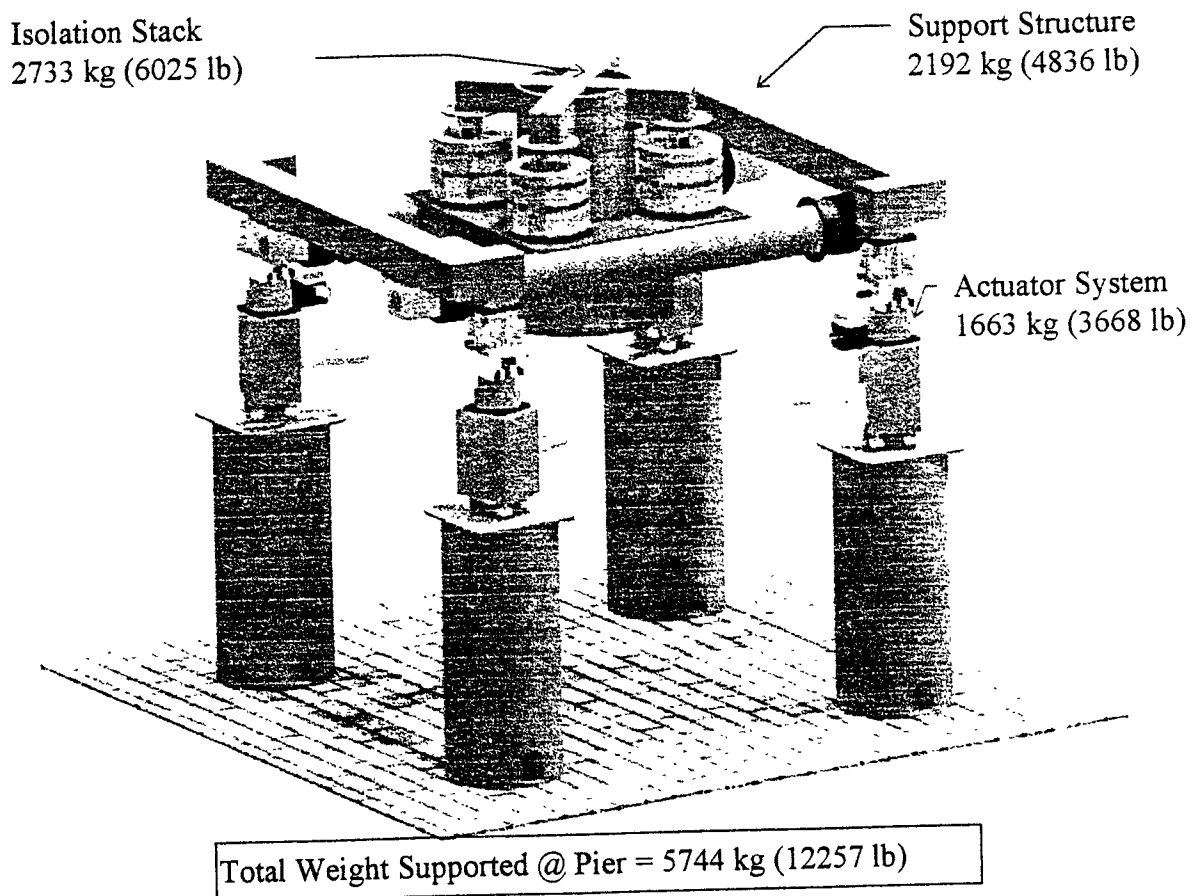


Figure 3. BSC SEI Layout.

3.1.2 Support Structure Description^[6]

The support structure is comprised of the following components, the cross beam, the support beam, and the support table as shown in Figure 4. The materials and weight of each component can be seen in the figure. A description of this design and associated analysis is available in Reference 6.

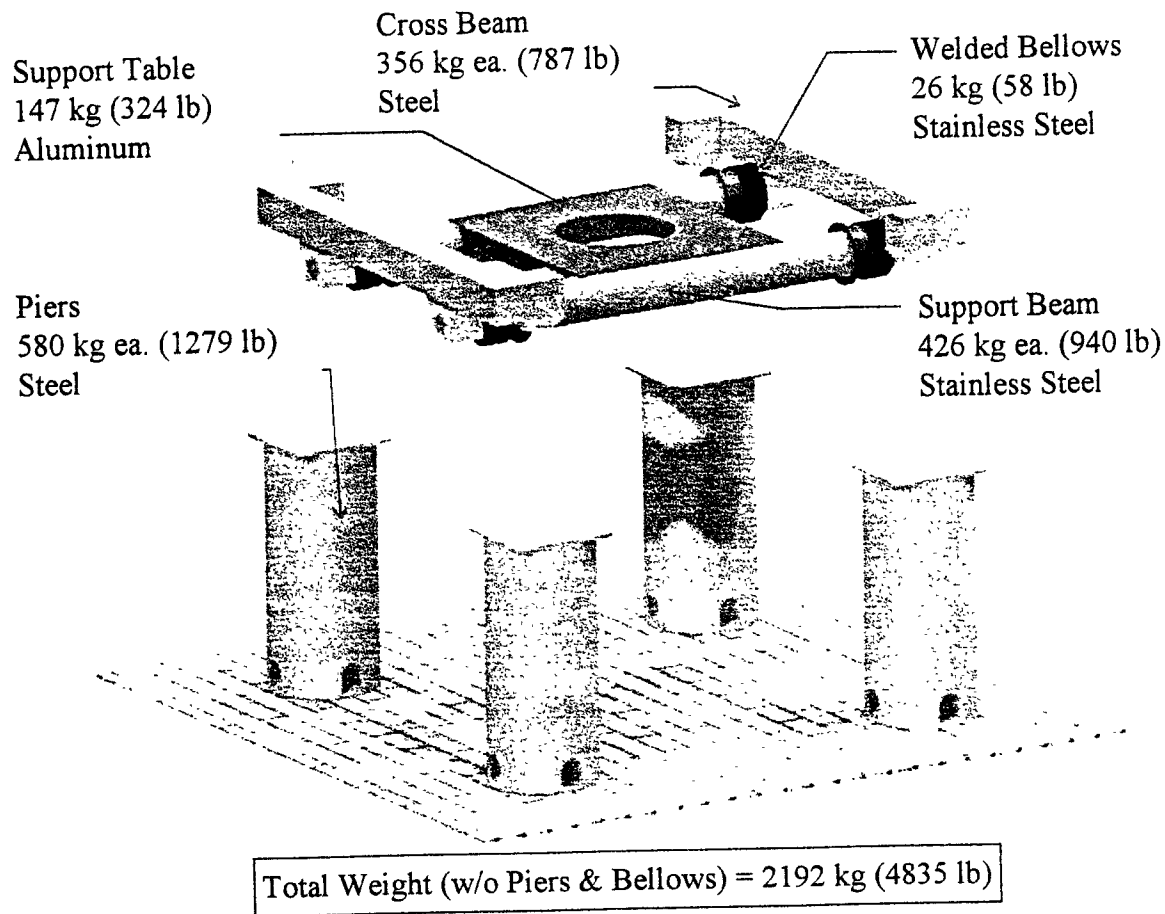


Figure 4. BSC Support Structure.

Overall dimensions of the support structure are shown in Figure 5. The support platform is a welded aluminum sandwich structure with a 12.7 mm (.5") thick upper face, a 9.5 mm (.375") lower face, and a grid of 6.4 mm (.25") rib plates for the core. Aluminum is used to minimize weight at the center of the support beam span.

The support beams are made of stainless steel tubing 305 mm (12") in diameter with a wall of 13 mm (.5"). Solid stainless steel plugs with a diameter of 140 mm (5.5"), are welded to the tube at each end. The plugs incorporate a knife edge and tapped holes to seal and mount the custom flange that is welded to one end of the bellows. These plugs rest in solid steel V-blocks bolted to the cross beams.

The cross beams are built up from standard square steel tubing, 254 x 13 mm (10" x .5").

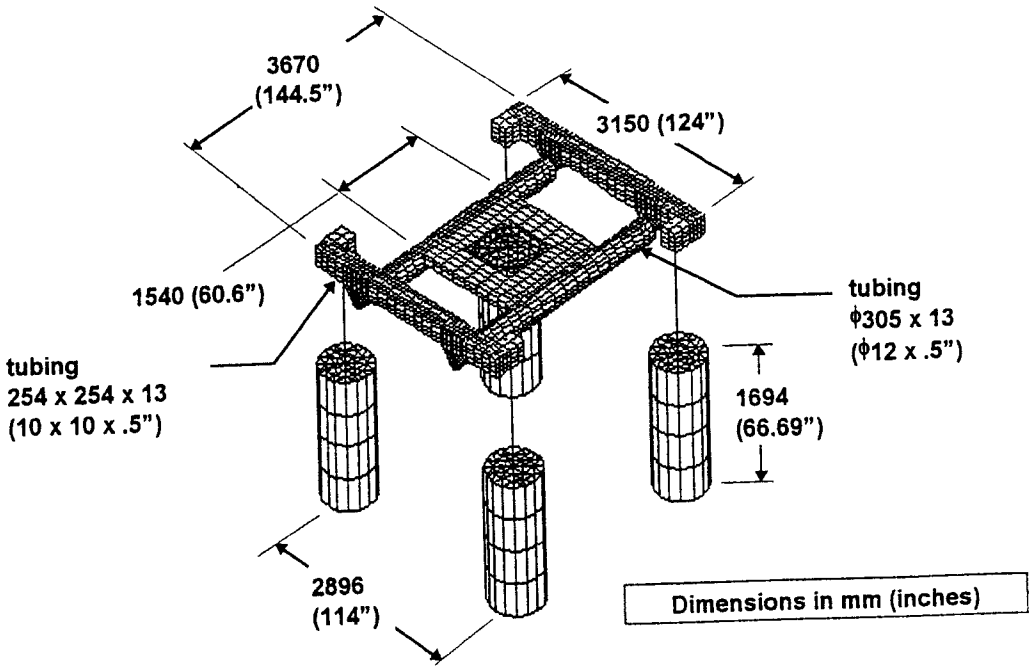


Figure 5. BSC SEI Support Structure Overall Dimensions

3.1.3 Isolation Stack Description^[5,7]

The BSC stack is comprised of the leg elements and the downtube structure as shown in Figure 6. The test mass is suspended by a wire pendulum from the optics table. The stack has 4 legs symmetrically arranged around the downtube. Each leg is composed of 4 stages of spring/mass filters; the masses of each leg element and the number of springs in each layer have been optimized^[2,3] to maximize isolation around 35 Hz (isolation requirements are most stringent at that frequency).

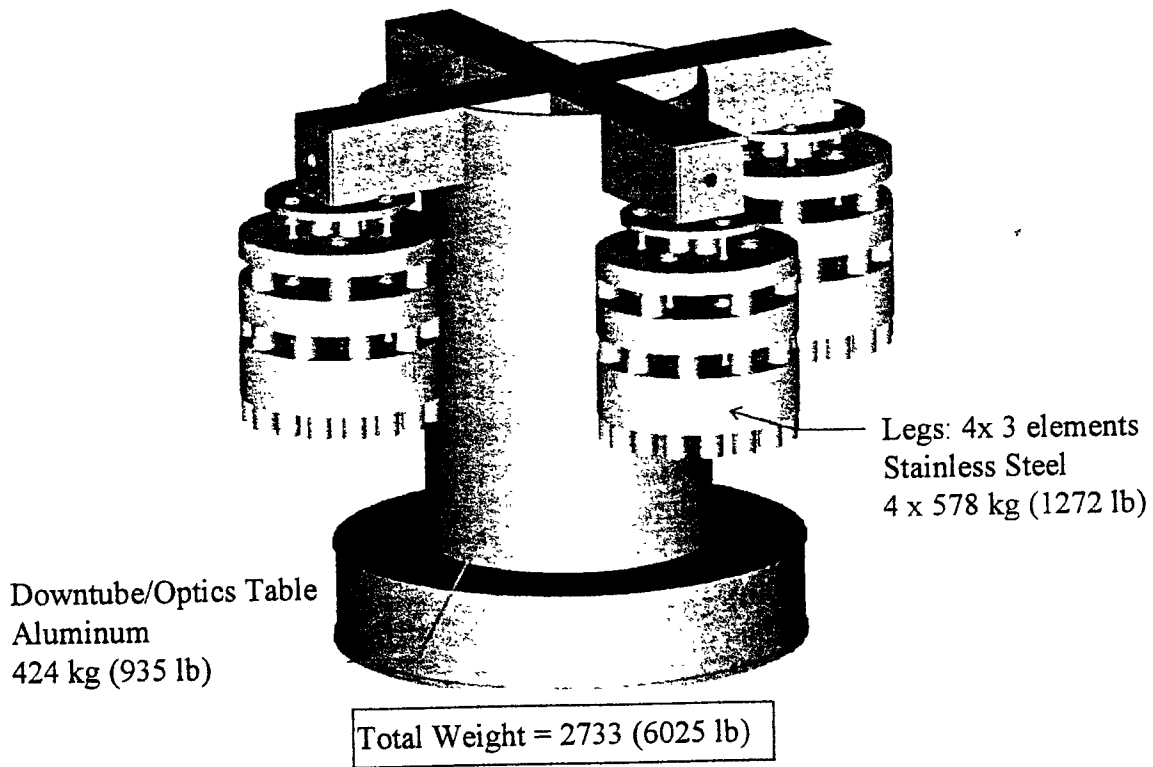


Figure 6. BSC Downtube/Optics Table and Stack Assembly.

3.1.3.1 Leg Description^[7]

Each BSC stack leg is comprised of 4 layers of springs/mass filters and associated alignment/lifting/safety pins for a complete assembly. The pins serve as lifting devices that automatically unload every layer of springs when the downtube is lifted. This allows for convenient maintenance of the springs and enables their removal in the event of a bakeout operation. The same pins also provide self-centering of the leg elements when the stack is reloaded and protect from complete collapse of the stack in the case of an earthquake or other off-normal condition. Shown in Figure 7 are the three spring options under consideration for the BSC. The current baseline is the coil spring stack. The Viton system is designed so that it can be substituted without any re-machining of the leg elements or downtube. All three stacks have the same total height under load, outside diameter, weight and use the same leg elements. In the case of the Viton stack, an extra layer of springs was added to compensate for their much shorter length compared to metal springs. The only modifications required to switch from Viton to coil springs are the machining of a set of safety/alignment/lifting pins.

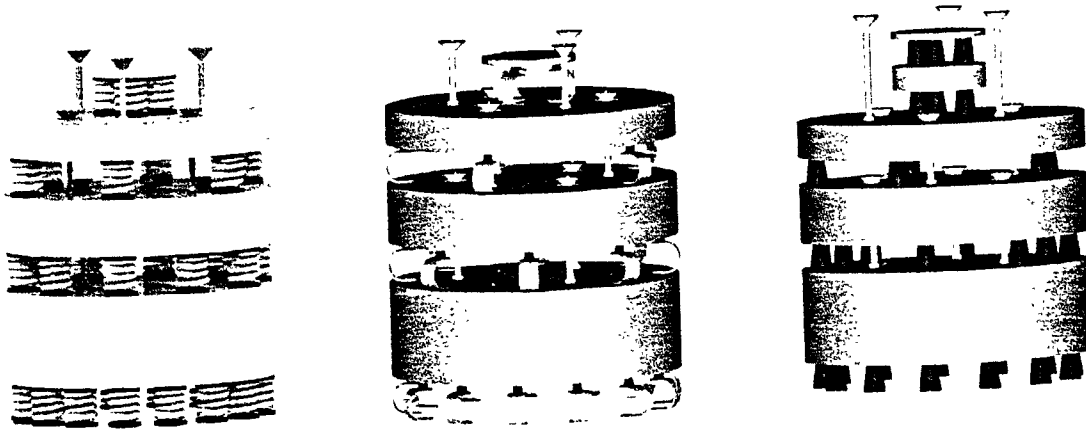


Figure 7. BSC SIS Stack Layout Options; Coil, Leaf, and Viton Springs.

3.1.3.2 Downtube and Optics Table Description^[5]

The isolation stack's other major critical element are the downtube/optics table (Figure 5). We have chosen an Aluminum alloy (5086) and conventional stress relief procedures used on large optical structures¹. We will continue to investigate this topic before committing to pre-production fabrication. The requirements for the process is that the structure must remain quiescent during operation.

¹ ANTARES Laser Fusion Program, Los Alamos National Laboratory

3.2 STRUCTURAL ANALYSIS

3.2.1 Support Structure^[6]

The structural analysis of the BSC has been completed for the geometry described above. The results are summarized in the BSC Support Assembly Analysis Report^[6].

The structure was analyzed for fundamental frequencies, the stresses and deflection under gravitational loading conditions, and under pseudo-static earthquake loading conditions. A buckling solution was included to assure the support structure is stable under the heavy load.

The results of the analysis confirmed that the design is fundamentally sound. Static stresses and deflections are small. In addition, the buckling calculation showed ample margin of safety. These results are not unexpected since this is a stiffness driven design.

There was an area uncovered in the analysis that will require further study. The issue is the stiffness of the actuator z-stage support structure. This current conceptual design is not stiff enough to meet our design goals for fundamental frequency of the structure. This Z-Stage's stiffness resulted in significantly lowering the fundamental frequency. The stiffness of this stage will be further addressed after the PDR/CDR

3.2.2 Downtube and Optics Table^[5]

Structural analysis of the downtube structure is reported in reference 5.

The structure was checked for natural frequencies, and stresses and buckling under gravitational loads. As expected for a stiffness driven design, static stresses are minimal. Buckling solutions show wide margins of safety for local panel buckling.

Estimates of thermal noise induced vibrations^[15] were also calculated and show a very wide margin of safety.

3.3 FABRICATION COSTS

Fabrication costs for all components are listed in Attachment 1 of the cost section. The total hardware program cost are now estimated to be \$4.44 M for the 15 assemblies. This cost includes the 1st article prototype hardware that will be assembled in Los Alamos. The estimates that we have secured from the vendors **do not** currently include all the costs expected for processing high vacuum hardware. Our best estimate of this additional cost is \$391,700 for both the BSC and HAM².

<i>Item</i>	<i>unit</i>	<i>\$/unit</i>	<i>qty/BSC</i>	<i>total systems</i>	<i>total</i>
Stack Assembly	BSC	137172	1	1	137,172
Support Structures	BSC	62758	1	1	62,758
Bellows	ea.	9000	4	1	36,000
Coarse Actuator System	BSC	77037	1	1	77,037
Fine Actuator System	BSC	50048	1	1	50,048
Electronics, Packaging and Integration	BSC	54344	1	1	54344
TOTAL					417,359

Table 4. BSC 1st Article Costs.

<i>Item</i>	<i>unit</i>	<i>\$/unit</i>	<i>qty/BSC</i>	<i>total systems</i>	<i>total</i>
Stack Assembly	BSC	108056	1	14	1,512,784
Support Structures	BSC	41824	1	14	585,536
Bellows	ea.	4869	4	14	272,664
Coarse Actuator System	BSC	66219	1	14	927,066
Fine Actuator System	BSC	42576	1	5	212,880
Electronics, Packaging and Integration	BSC	36607	1	14	512498
Cleaning, Shipping, Stress Relief	BSC	191700	1	1	191700
TOTAL					4,215,128

Table 5. BSC Production Article Costs.

² Miscellaneous Production Costs - HYTEC-LIGO-COST-03

Hardware costs for the 15 BSC units is \$ 4,632,487 **including** our best estimate of cleaning, stress relieving, and shipping the hardware. The uncertainty of these additional costs is high. HYTEC is pursuing additional vendor comments and quotes to the LIGO specifications that will lower this uncertainty.

3.4 1ST ARTICLE PERFORMANCE EVALUATION AND TEST

In a build-to-cost environment, such as LIGO, it is important to take steps to lower risk, and to proceed with production when confident that integration issues have been resolved. A case in point is demonstration of the actuator system, fine and coarse, when assembled and integrated with the stack support system. Another area is the need to validate structural interfaces (like between the support beams and the cross beams) where we have concern about residual strain. This phase of testing and evaluation will be structured to address these issues. Table 3 shows the "Performance and Evaluation and Testing" expected for the BSC.

3.5 ASSEMBLY AND STAGING

Table 3 describes the planned development and performance testing that should be conducted on the BSC hardware. Of primary importance to this effort is what is called "1st Article Assembly and Check-Out". This phase will give the engineers and designers and opportunity to fix or improve the design, to lower cost, and to improve the procedure for assembling the hardware.

3.5.1 Fixturing and Tooling Required

Although we have not fully developed the required tooling necessary to pull the BSC together, we fully realize that this is a significant undertaking in itself. We have indicated areas of tooling and fixturing we know will have to be designed in attachment HYTEC-LIGO-COST-04. The costing reflects an estimate of the tooling and assembly fixture costs. These numbers are quite preliminary and should be considered in that light.

4. HAM DESIGN AND FABRICATION

4.1 COMPONENT DESCRIPTION

The HAM support assembly, shown in Figure 8, consists of a support platform, 2 support beams, and 2 cross beams. The seismic isolation stack rests on the support platform. The support beams penetrate the HAM chamber and are sealed by 4 welded diaphragm bellows (not shown). Cross beams on the outside of the chamber connect the ends of the support beams and interface with the coarse actuators.

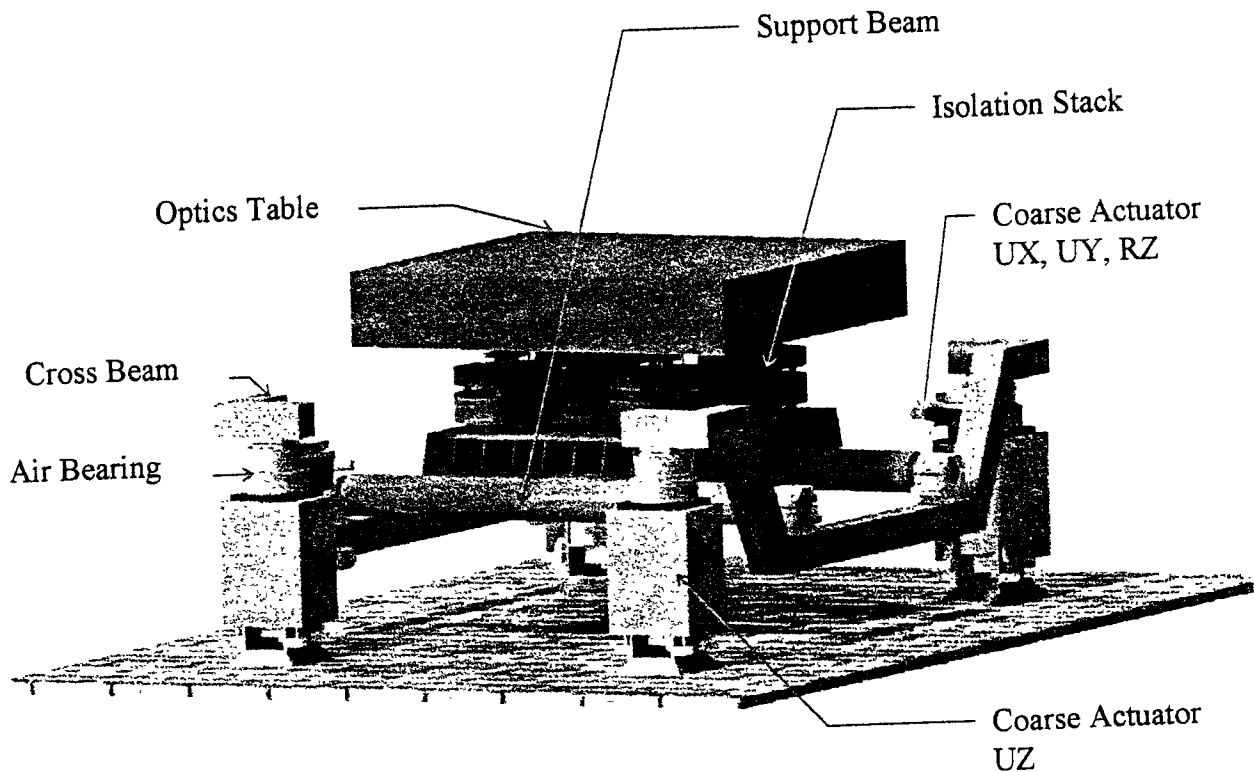


Figure 8. HAM SEI Layout

4.1.1 Support Structure^[12]

The support structure used in the HAM is shown in Figure 9. The structure is similar in concept to that of the BSC.

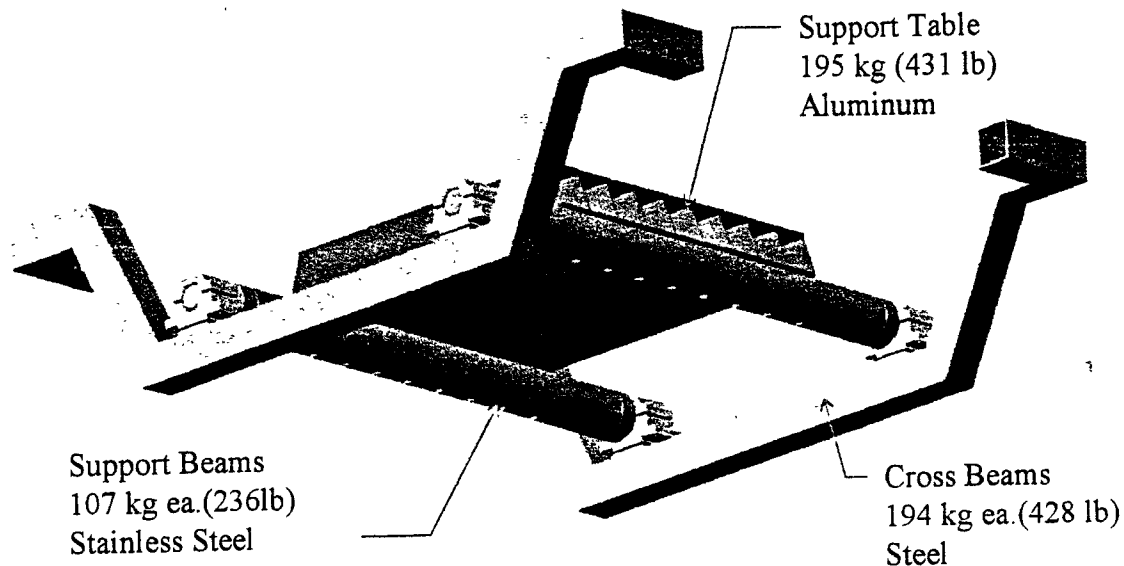


Figure 9. HAM Support Structure

Overall dimensions of the HAM support structure are shown in Fig. 10. The support platform is a welded aluminum structure with a 19.1 mm (.75") thick upper face, a 12.7 mm (.5") thick lower face, and 9 parallel stiffeners 6.4 mm (.25") thick. Aluminum is used to minimize weight at the center of the support beam span.

The support beams are made of stainless steel tubing 191 mm (7.5") in diameter with a wall thickness of 6.4 mm (.25"). Solid stainless steel plugs with a diameter of 114 mm (4.5"), are welded to the tube at each end. The plugs incorporate a knife edge and tapped holes to seal and mount the custom flange that is welded to one end of the bellows. The support beams are anchored to the cross beams by heavy V-block attachments. Low carbon steel square tubing 152 x 152 x 9.5 mm (6 x 6 x .375") form the crossbeams that carry the load to the actuators.

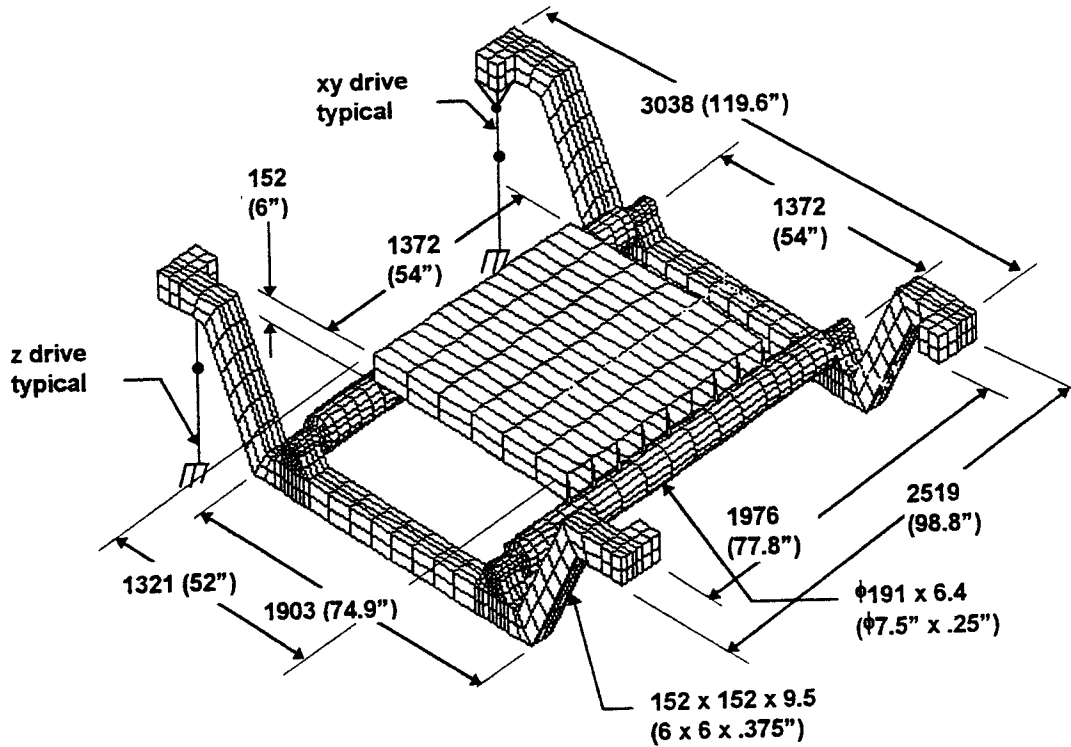


Figure 10. HAM SEI Support Structure Overall Dimensions

4.1.2 Isolation Stack Description^[13]

Like for the BSC, the HAM isolation stack is composed of 4 legs. Each leg is a series assembly of mechanical springs/mass filters. Because the isolation requirements for the HAM^[15] are much less severe than for the BSC, the number of stages was reduced to 3.

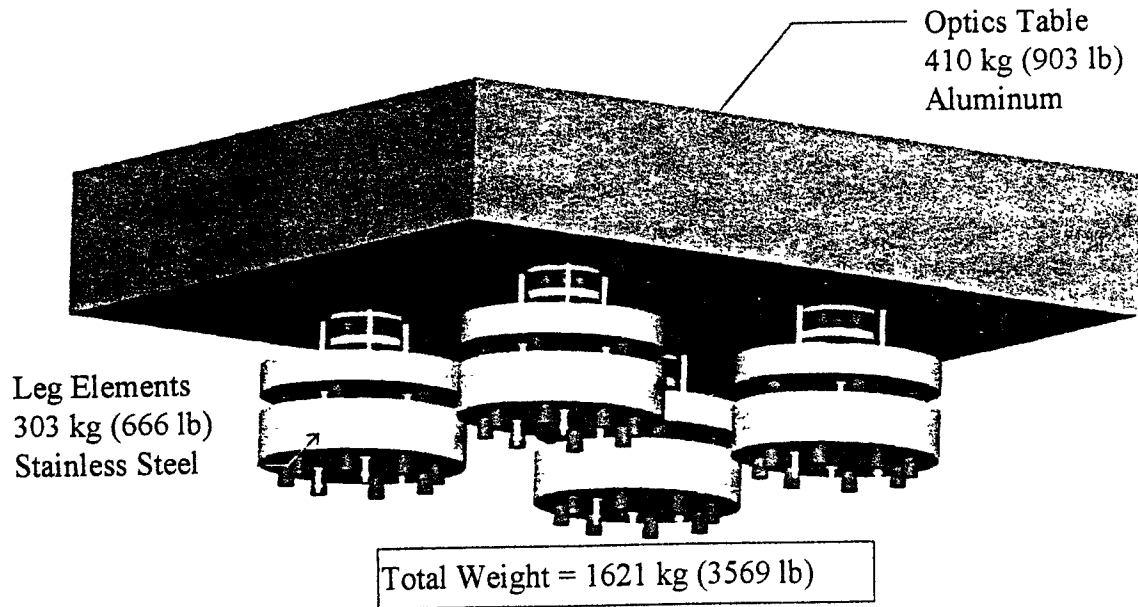


Figure 11. HAM Isolation Stack Layout (Viton Spring Stack Shown)

4.2 HAM FABRICATION COSTS

The fabrication costs of the HAM SEI components are listed in Attachment 1. The hardware costs are now estimated to be \$4.20 M for the 18 assemblies. This cost includes the three sets of 1st article hardware that will be assembled and checked at Hanford. The estimates that we have secured from the vendors do not currently include our best estimate of the expected processing high vacuum hardware.

<i>Item</i>	<i>unit</i>	<i>\$/unit</i>	<i>qty/HAM</i>	<i>total systems</i>	<i>total</i>
Stack Assembly	HAM	92356	1	3	277,068
Support Structures	HAM	34490	1	3	103,470
Bellows	ea.	8000	4	3	96,000
Coarse Actuator System	HAM	81187	1	3	243,561
Electronics, Packaging and Integration	HAM	40420	1	3	121260
TOTAL					841,359

Table 6. HAM 1st Article Costs.

<i>Item</i>	<i>unit</i>	<i>\$/unit</i>	<i>qty/BSC</i>	<i>total systems</i>	<i>total</i>
Stack Assembly	HAM	69707	1	15	1,045,605
External Support Structures	HAM	30090	1	15	451,350
Bellows	ea.	4200	4	15	252,000
Coarse Actuator System	HAM	75945	1	15	1,139,175
Electronics, Packaging and Integration	HAM	31420	1	15	471300
Cleaning, Shipping, Stress Relief	HAM	200000	1	1	200000
TOTAL					3,559,430

Table 7. HAM Production Article Costs

Hardware cost for the 18 HAM units is \$4,400,789, **including** the estimated cost of cleaning, stress relieving, and shipping the hardware. The uncertainty of these additional costs is high. HYTEC is pursuing additional vendor comments and quotes to the LIGO specifications that will lower this uncertainty. These stringent processing parameters will effect the hardware costs.

4.3 1ST ARTICLE PERFORMANCE EVALUATION AND TEST

In a build to cost environment, such as LIGO, it is important to take steps to lower risk, and then to proceed with production when confident that integration issues have been resolved. A case in point is demonstration of the actuator system, fine and coarse, when assembled and integrated with the stack support system. Another area is the need to validate structural interfaces (like between the support beams and the cross beams) where we have concern about residual strain. Table 3 shows the "Performance and Evaluation and Testing" expected for the HAM.

4.4 ASSEMBLY AND STAGING

Table 3 also lists the planned development tests and additional performance testing that should be conducted on the HAM hardware. Of primary importance to this effort is what is called "1st Article Assembly and Check-Out". This will give the engineers and designers and opportunity to fix or improve the design to lower cost and improve the performance of the hardware.

4.4.1 Fixturing and Tooling Required

Although we have not fully developed the required tooling necessary to pull the HAM together, we fully realize that this is a significant undertaking in itself. We have indicated what areas of tooling and fixturing we know will have to be designed in attachment HYTEC-LIGO-COST-04. The costing is quite preliminary and should be considered in this light.

5. EXTERNAL SUPPORTS AND ACTUATOR SYSTEMS, CDR

5.1 REQUIREMENTS

The requirements for the design of the external supports and actuator system are broken into two categories (for the coarse and fine actuator systems) that are listed in attachment HYTEC-TS-LIGO-02. These requirements are still being evolved, but will be frozen after CDR.

The coarse actuator system has to move the support platform in four degrees of freedom: along the beamline (UX), transverse to the beamline in the horizontal plane (UY), transverse in the vertical plane (UZ), and rotation about the vertical centerline axis (RZ). These motions are made when the LIGO system is off-line. Accuracy normally would not be an, but precise motion of the platform is required to allow movement in a synchronized fashion. In this manner we are able to avoid binding in the four independent actuators.

The fine actuator system has to move the platform with very high resolution in the beamline direction (UX). The fine actuator must operate smoothly while the laser is in a locked mode. It therefore must possess several critical features. The system must be able to move the entire mass of the BSC in a smooth, vibration free manner. In addition, the system must have a high stiffness to meet our system isolation goals.

5.2 DESIGN OPTIONS

The conceptual design of the external support and actuator system flowed from the set of requirements needed to satisfy alignment and positioning of the platforms during set-up and operation of the machine. The concept shown in Figure 12 is a point design to meet the stated design requirements. The actuator system that will be deployed for the HAM will use the identical design as for the BSC.

Because of the tight schedule of the external support and actuator design it was imperative to choose a path, review the possible alternatives and then select a point design to pursue. This design is by no means static, in fact it has changed dramatically as a result of recent analysis.

5.2.1 Coarse Actuator

The design approach is to use commercially available components in a custom mechanical design. The options that we looked at were derivatives of what we currently have shown in SEI layout in Figure 3.

The time scale between movements the HAM and BSC platforms is long, on order one month. The required range of motion is only $\pm 1/2$ cm. Therefore the motion demands on the system are quite straight forward except for two elements; the load of the entire stack (approximately 14,000 lb), and the stringent coordination of moving the entire platform without binding .

5.2.2 Fine Actuator

Piezoelectric translators are electrically controllable positioning elements which function according to the "Piezoelectric Effect". They directly convert electrical energy into linear motion without the use of gears or rotating parts. PZT systems can produce high forces with a dynamic range of 120 microns at 1/6 Hz.

Piezoelectric translators can perform superfine positioning from nanometers to millimeters with exceptionally high accuracy. They offer the advantage of having high positioning accuracy, no backlash, high stiffness, high load capability, no wearing parts, high efficiency, and fast response. There is a possibility that 120 microns is not sufficient to correct for the Earth's tides. Currently, our best estimate is that PZTs will provide enough range of motion for LIGO.

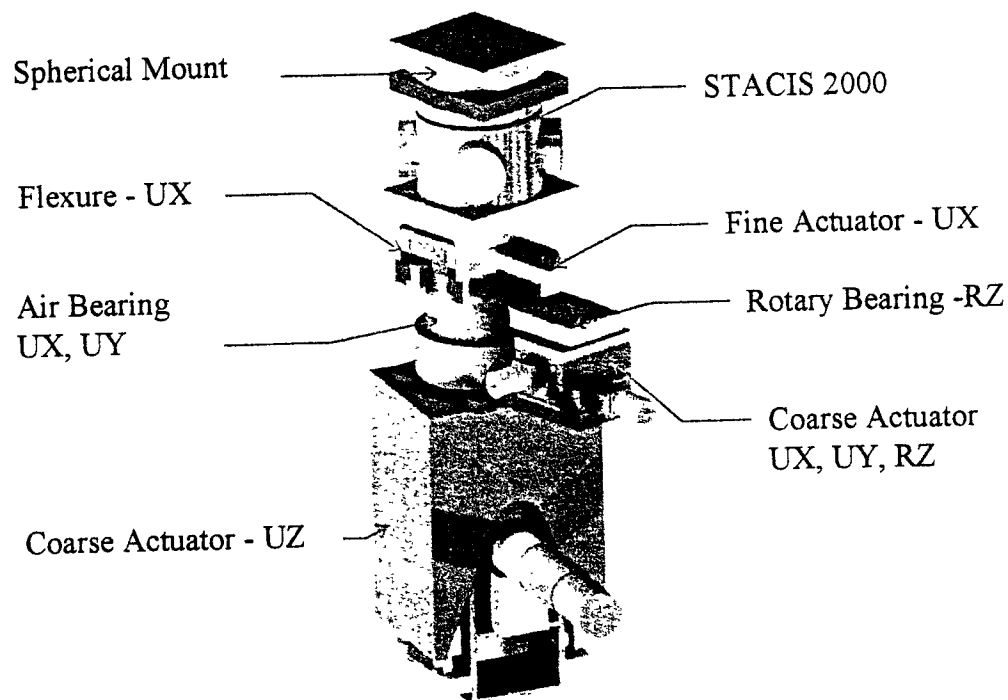


Figure 12. Coarse and Fine Actuator Assembly

5.3 CONCEPTUAL DESIGN CONFIGURATION

Shown in Figure 12 are the elements in the actuator system, including an active isolation element, STACIS 2000. The current baseline shows the STACIS 2000 in the layout, however it is only shown as a place holder and is not included in our costing. The system will be replaced with an Aluminum block in the initial installation of the hardware. The present design is configured to allow easy retrofitting of the STACIS system.

A component identification of the actuator assembly starting at the bottom is: a coarse Z actuator for lifting the platform, a coarse X/Y actuator for providing UX, UY, and RZ motions to the platform, in parallel to the X/Y actuator is shown an air bearing for carrying the gravity loads for the X/Y stage, above the X/Y stage is the fine X actuator assembly, and above the fine X actuator system is the active isolation system (future use). The cross beam mechanical mounts are shown on top for clarity of the interface.

The angular twist (Figure 12) between the Z and X/Y stages is a result of the tight packaging constraint around both the BSC and HAM that will not permit them to be mounted square to one another.

The vertical location of each element came from dynamic simulations that indicated the need to get the STACIS active isolator as close as possible to the cross beams, thus reducing the effective moment arm, and increasing the system fundamental frequencies. This is also advantageous from a noise stand point since the STACIS can reduce the cultural noise from the actuators.

An important design feature is the use of an air bearing. This allows us to carry the heavy gravity loads of the isolation system through the air bearing and not through the X/Y actuator stage.

The electronic control system is made easier by only driving the two opposing corners on each platform. This results in not requiring special electronic hardware that would be required to invert the direction bit ($x1 = -x2$) and the switch axis' ($x1 = y1$) if all four corners are driven. This is a result of using a single controller to synchronize the electronic signal to the actuators. Two corners being driven only requires the direction ($x1 = -x2$) to be inverted. An added benefit is not needing to have a synchronous signal for all corners, again improving our concern with binding of the actuators.

5.3.1 Coarse Actuators

The coarse actuator system is made of two separate sub-assemblies as shown in Figures 13 and 14.

Dynamic loads created from moving the platform during coarse operation are quite small. The baseline design has only two corners actuated (Figure 3) in the X/Y plane. This solution offers several advantages. The cost of the system is lower, and it is a simpler to debug the motion control. Also, the serious issue of potential binding during movement is mitigated when actuating only two corners of the system.

The design of the current system provides 4 degrees of motions, UX, UY, UZ, RZ. These motions are accomplished by actuators, the in the X, Y, and Z planes. The X and Y actuator can be moved in synchronized motion to give the UX, and UY motion. They can also be moved asynchronously to give a rotation about the Z axis. The components shown were selected to meet the design goals. The range of motion in the X, Y, and Z is small only requiring +/- 1/2 cm.

Most commercial actuators offer a greater range of travel than required. The additional capability does not go unused since the actuator system can be used as an alignment tool negating the need for shimming the column elements into position.

5.3.1.1 Coarse Actuators UX, UY, RZ

The coarse actuators used in the X and Y direction are commercial off the shelf units (see cost sheets for details). The selection of these units was based on the need for accuracy and repeatability during operation. The driven slides use cross rollers to minimize errors during the movement. Accuracy of motion is key to our success since both actuators have to move precisely in order to work without the system binding up. The slides utilize precision ground cross roller ways, and precision grade ball screws.

The actuators selected have a travel of 100 mm (4"), with a positional accuracy over the length of travel of 8 microns (32 mils). The slides will be cross-mounted at the factory for a precise normality in the X/Y plane.

High resolution DC microstepping motor and controller are used. Stepping motors offer a low cost solution, and are very rugged and reliable. They fail safe, and require no maintenance. They are ideal for the infrequent use of the coarse actuators.

An important design feature in the coarse actuator system is the use of an air bearing. This allows us to carry the heavy gravity loads of the isolation system through the air bearing and not through the X/Y actuator stage. This substantially lowers the system cost by allowing us to use actuators that are sized to *move* the load and not sized to *carry* the load, an important distinction.

As can be seen in Figure 13 we also have a rotary bearing that is mounted between the X/Y actuator stages and the air bearing. This is required to allow for the relative rotations that occur when the platform rotates about the Z axis.

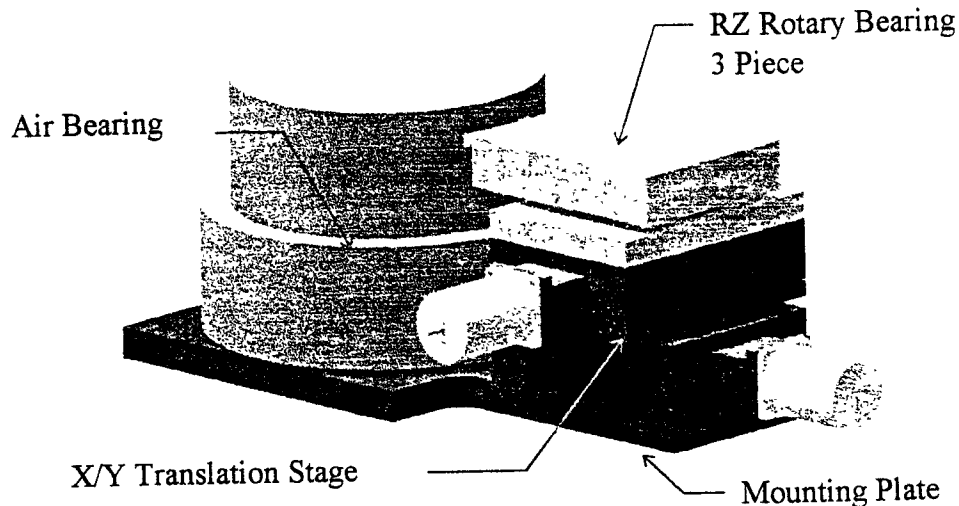


Figure 13. Coarse X/Y - Actuator Assembly.

5.3.1.2 Coarse Actuator UZ

For applications that do not require high velocities the use of gear heads offer two advantages. First, the resolution is increased by a factor of the gear ratio. Second, the torque is multiplied by the gear ratio, so that even low power motors can move heavy loads. This was the premise behind the Z actuator. Since these systems operate under a continuous gravity load backlash is not a concern.

The coarse actuator used in Z-direction is a commercial off the shelf unit (see cost sheets for details). The selection of this unit was driven by the high operational load it must move. The actuator stage selected can carry over 4100 lbs for a total lift capacity of 16,400 lb.

The unit selected will provide 100 mm (4") of travel. This much travel is not required but it will allow us the flexibility to eliminate shimming the four corners.

To carry the high load a ball screw configuration was preferred over an acme screw. This requires the use an electro-mechanical brake to prevent back-driving of the system. Ball screws also provide a more efficient and smoother operation.

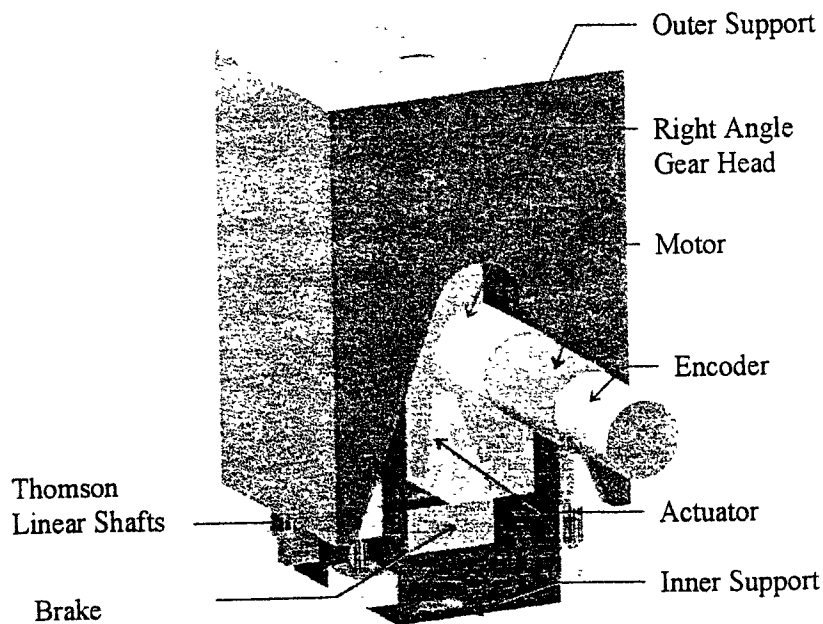


Figure 14. Coarse Actuator Assembly - UZ

5.3.2 Fine Actuator

The fine actuator sub-assembly is shown in Figure 15. This actuator is responsible for the precision motions required in the six end and mid-station BSC systems to keep the laser locked during operation. The original design would operate this system slowly, only being used to take out the earth tides, i.e. diurnal motions. However, the use of a PZT system will enable its use for the correction of ground motions associated with micro-seismic disturbances up to 1/6 Hz.

The support platforms can be moved with extremely high resolution. This high resolution, and the high motive force available in a PZT stack allow the stack to undergo a push (or pull) efficiently. The maximum range for the PZT stack is 120 microns under low frequency conditions (< 1/6 Hz).

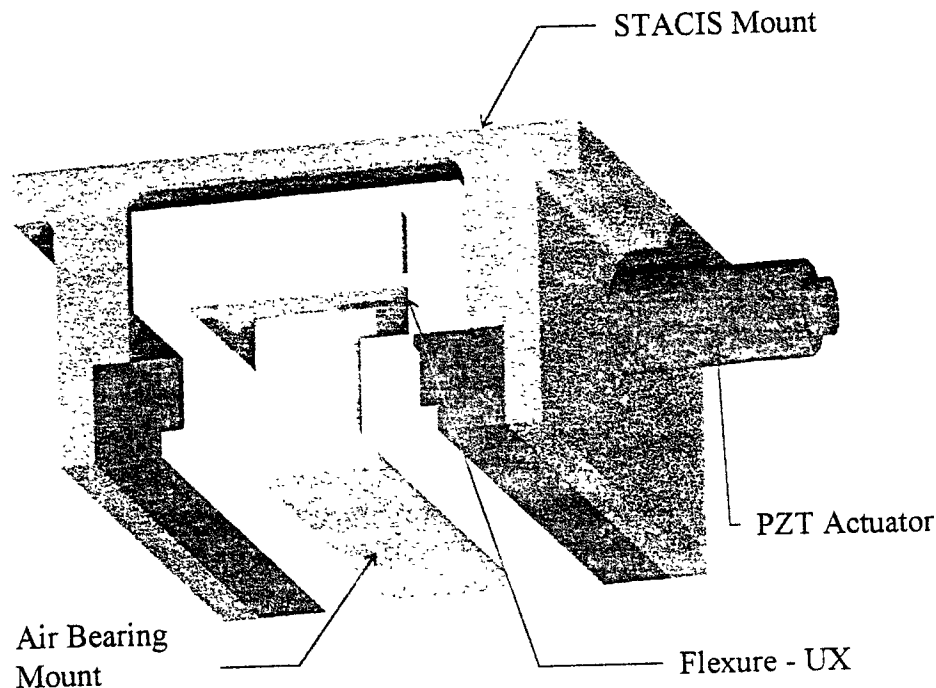


Figure 15. Fine Actuator Assembly - UX

5.4 COARSE/FINE ACTUATOR TESTS

The actuator testing that will be undertaken is shown in Table 3. The testing is broken into three major phases. The first will only involve one set of actuators (i.e. a single pier) that will be used to get the software controls written for the actuators and to simulate the functional motions of the system. There will be no testing to validate the system integration aspects. Phase 2 will involve building a full system test of the coarse actuators. This test is meant to debug the systems integration aspects of the actuator. It will require a full set of components on the BSC. Phase 3 of testing will be to bring the fine actuator components on line. This phase will require a concerted effort to validate the system resolution and stability requirements.

5.4.1 Coarse Actuator Tests

Phase 1 testing will commence by July 1997 and will be focused on understanding the basic actuator issues and idiosyncrasies. The testing will consume about 6 weeks of time and will address all software and interface electronics issues.

Phase 2 of the external actuator testing is to assemble the full system, and to operate the system under realistic conditions. We anticipate that the key issue here is the synchronization of motion between the actuators in such a way that the system does not bind. The binding of the system is a real concern since the hardware is quite stiff by design and has little compliance to allow for errors in motion profiles. Tests will be performed with the bellows loads acting on the components to simulate any conflict in range of motion or binding.

5.4.2 Fine Actuator Tests

The fine actuator tests are summarized in Table 3. The testing of the fine actuator system will involve insuring the operation is smooth and has the range of motion required. Some of the testing will require simply capacitance measuring equipment to verify the operation as advertised.

6. DAMPED METAL SPRING DEVELOPMENT^[4,14]

6.1 INTRODUCTION

Because BSC stacks designed around the solid Viton rubber spring cannot achieve the required level of seismic isolation (they violate requirements by factors of more than 2000 in the 10 to 100 Hz range, see section 3.1 and references 2 and 7) a considerable amount of effort was dedicated to the design and development of damped metal spring concepts.

The main objective for those designs is to achieve a large ratio of static load capacity to dynamic stiffness: the larger this ratio, the better the attenuation of seismic noise through the stack. The other primary requirement is that the springs must provide some damping to the low frequency resonances of the stack. Our understanding of that requirement has evolved over time from early requirements for 10% loss factor at frequencies below 30 Hz^[3] to more realistic expectations of about 3% at 10 Hz^[4] and finally to a more important requirement of a minimum of about 1.4% loss at the frequency of the lowest stack resonance (1.2 Hz typical). This last limit is related to difficulties in designing the SUS control systems for stacks with large quality factors (Q). Unfortunately, the viscoelastic materials used in our metal spring concepts show a very steep decrease in loss at low frequency, making this requirement challenging.

Additional requirements include creep limitations, creak noise, internal resonances, acoustic transmission, and vacuum compatibility.

Two metal spring concepts have been designed, developed, and partially tested at this time. Both designs lead to BSC isolation stacks with wide band isolation performance dramatically improved as compared to a Viton stack (see section 7 and references 4 and 7). Test results obtained so far are extremely encouraging and confirm the validity of the spring concepts. Performance targets defined by analysis appear to be met. However, manufacturing processes are still in need of refinement to achieve repeatable performance and minimize fabrication costs. Because of the huge performance benefit to be gained from the use of metal springs and the schedule risks associated with final qualification of either concept, the only reasonable approach from this point is to pursue development of both concepts in parallel until it is determined which option leads to the best performance and the lowest cost. As an additional risk reduction measure, we are designing fully compatible Viton spring stacks^[7] that can be used as last minute fall-back solutions in case neither metal spring proved successful.

6.2 METAL SPRING CONCEPTS

The two metal spring concepts are referred to as the *coil* and the *leaf* springs. Both concepts use a form of constrained layer damping. They are illustrated in Figures 16 and 17. Detailed descriptions are available in reference 4.

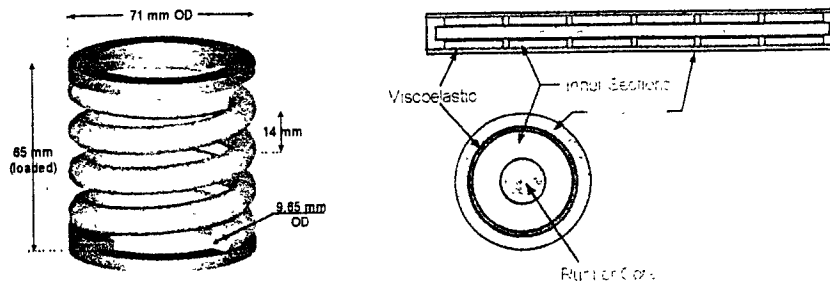


Figure 16. Coil spring concept

The coil spring is made from a “wire” with a multi-layer tubular cross section. The outer phosphor bronze tube is the load bearing component. Inside that tube is a discontinuous tubular aluminum core separated from the outside tube by a layer of viscoelastic damping material. The inside rubber core is there only to facilitate assembly. Compression of the coil results in twist deformations of the outside tube and shear in the damping layer which in turn produces damping. The proportions of the cross section, geometry of the coil, and lengths of the aluminum core sections were all numerically optimized based on a closed form analytical model^[4]. The resulting design maximizes isolation performance while providing the necessary amount of damping. Details of the analysis and optimization can be found in reference 4. The ends of the phosphor bronze tube are sealed with a welded phosphor bronze cap to produce an all metal, vacuum tight envelope. To provide interface with the leg elements, the coil rests in two molded Viton seats. These seats are also intended to prevent transmission of acoustic disturbances through the spring.

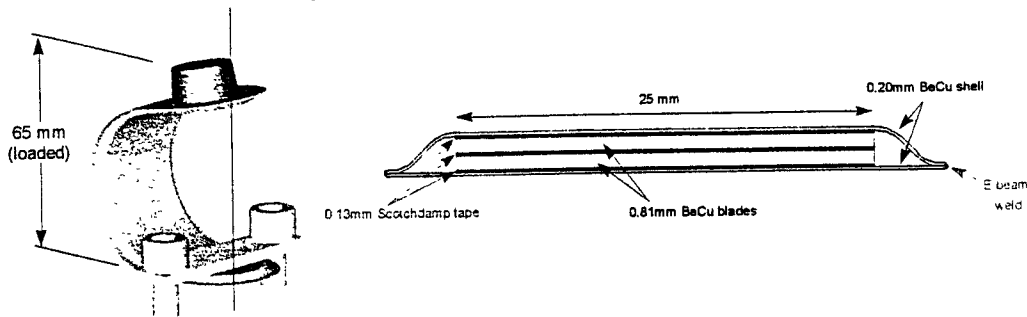


Figure 17. Leaf spring concept

The leaf spring is a more classical constrained layer blade, curved in the shape of a “C”. The blade is composed of 4 layers of beryllium copper separated by 3 layers of viscoelastic material. The thin outer layers are welded together around the edges to form a vacuum tight envelope sealing the inside structure. Compression of the spring produces bending of the multi-layer cross section and creates large shear strains in the damping layers. The lower end of the “C” is clamped to its base while the upper end is fitted with a Viton tip that receives the load. The Viton tip should also prevent transmission of acoustic disturbances.

6.3 DEVELOPMENT AND TEST RESULTS

6.3.1 Coil Spring

This design obviously poses a few problems in terms of manufacturing process. Significant effort was invested in resolving those difficulties and has resulted in successful production of 4 damped coil prototypes. One of those is shown in Figure 18 together with a longitudinal cross-section.

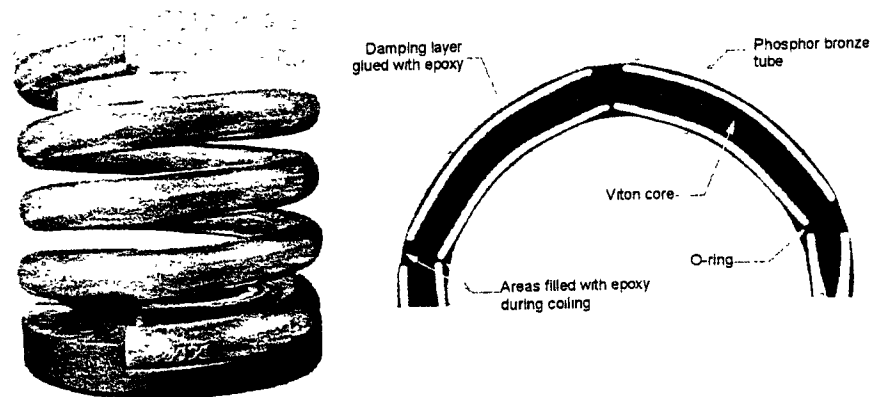


Figure 18. Coil Spring Prototype. The seats are temporary epoxy resin versions.

Those prototype have been tested for static load capacity, fatigue, stiffness, and loss factor. All experimental results are in reasonable agreement with analytical predictions and are meeting performance targets. Figure 19 shows measured axial loss factors at various frequencies and compares them to analytical predictions. Note that the analytical curve only predicts damping due to the internal structure of the spring (i.e. shear in the damping layer) and does not account for any other possible sources of energy dissipation.

Complete descriptions of all tests performed to date on those springs can be found in reference 14.

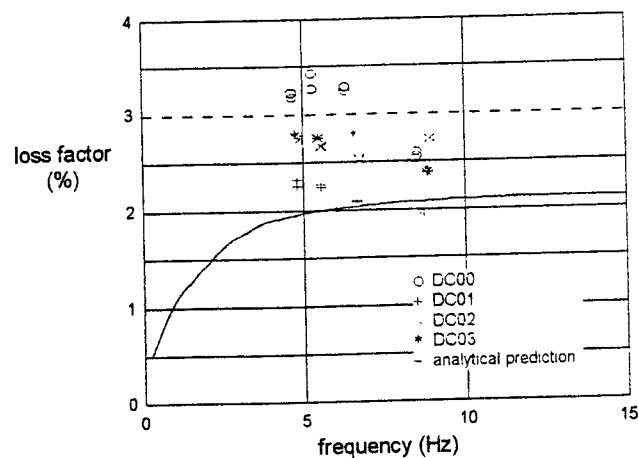


Figure 19. Axial Loss Factors. Measured by free decay on four damped coil prototypes (DC00, 01, 02, and 03) compared to analytical prediction.

Clearly, some work remains to be done to improve the repeatability of spring properties. Also, because of the importance of damping at low frequency (1 Hz) for achieving lock, more testing will have to be performed at lower frequencies. A test fixture is currently being designed to allow such testing.

6.3.2 Leaf Spring

After spending some time resolving difficulties with stamping operations, we have assembled and E-beam welded 4 leaf spring prototypes. Figure 20 shows the beryllium copper parts before assembly and a completed prototype.

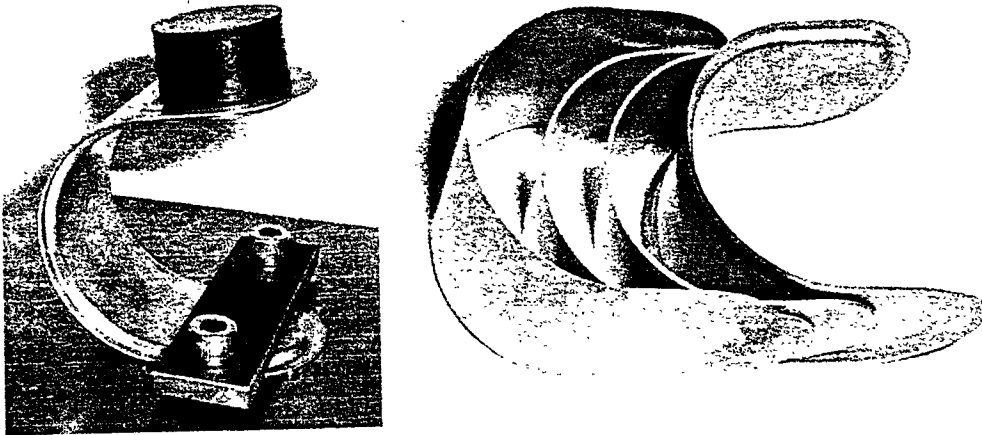


Figure 20. Leaf Spring Prototype. Photograph on right shows beryllium copper parts before assembly (viscoelastic material not shown).

One of those prototypes has been tested for axial load capacity. The results are encouraging and in good agreement with model predictions. The spring could not be destroyed, even at relatively large deflections (Figure 21). No dynamic testing has yet been performed.

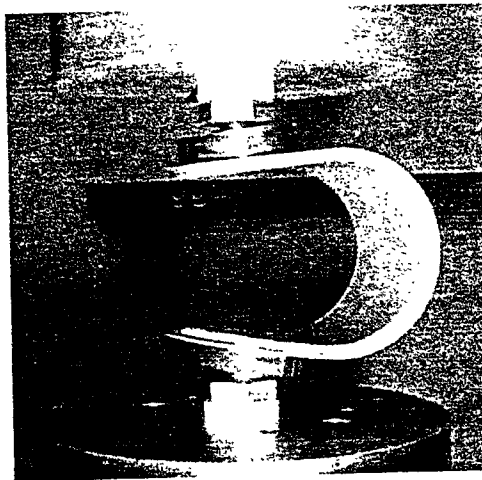


Figure 21. Leaf Spring Prototype Being Deformed in MTS Testing Machine.

6.4 FUTURE PROTOTYPING AND DEVELOPMENT PLANS

The damped metal springs are a key element in the design of satisfactory seismic isolation systems for LIGO. As such, a great deal of testing will be performed to further validate the engineering, and fabrication processes. We are anticipating to carry both spring designs forward until which time one spring concept can be selected without risk of compromising the programs milestones. We feel that to down select a spring concept prematurely would create significant schedule risk. The spring concepts are novel enough that their development presents substantial risk; developing both concepts in parallel minimizes the risk of schedule delays in the event of problems with the primary concept.

6.4.1 Prototype qualification tests

In addition to completing static and dynamic evaluations, a number of tests will be conducted on coil and leaf spring prototypes^[9].

- Creep: initial creep testing will be performed on single springs or single stage stacks. Full creep and asymmetry checks are planned as part of the BSC and HAM first article testing.
- Creak: very low energy creaking noises will be difficult to detect with conventional instrumentation. Reference 9 contains a suggestion to attempt such testing using a suspended single stage platform setup.
- Vacuum Compatibility: the springs will be tested for outgassing, possibly using a tracer gas. Because the springs have a completely welded metal envelope, we do not anticipate difficulties in this area.
- Acoustic Transmission: a test setup has been suggested in reference 9; because both springs have at least one Viton interface, we anticipate that acoustic transmission will not be a problem.

6.4.2 Damped Spring Pre-Production Process Qualification

Assuming the springs pass their qualification tests in the prototype development phase, it will be necessary to quickly move to manufacturing of a pre-production quantity to evaluate the repeatability of the fabrication process. Testing of those springs should also help define appropriate QA testing for production units.

6.4.3 Metal Spring Decision

In view of the great performance incentive and the existence of a fully compatible Viton stack design that can be used as a last minute fall back position, we recommend delaying final decision as to pursue or not pursue fabrication of metal springs until just before committing to full production of the SIS hardware. If necessary, first article hardware can even be retrofitted with Viton springs at minimal expense (fabrication of new sets of alignment/safety pins) in case the stack prototype encounters unexpected problems.

7. LIGO SEISMIC ISOLATION PERFORMANCE

7.1 REQUIREMENTS

The primary requirement for the design of the isolation stacks is that they must provide sufficient wide-band horizontal and vertical isolation from floor-borne seismic noise to satisfy the LIGO science requirement^[15].

Limitations in the dynamic range of the test mass/mirror actuators and control systems also impose limits on the RMS motion of the test masses/mirrors in response to seismic noise. These limits lead to the definition of lock acquisition and lock maintenance requirements^[15]. These requirements are dominated by low frequency noise, in particular the micro-seismic peak and the first couple stack resonances.

7.2 SEISMIC ISOLATION PREDICTIONS

7.2.1 Introduction

Three interchangeable stacks have been developed for both the BSC and the HAM SEI. These stacks use the Viton, coil, or leaf springs presented in the previous section. Through careful optimization of the mass and stiffness distributions in the stacks^[2,3] and the design of specialized metal springs (section 6), two of those stacks (metal coil or leaf springs) come very close to satisfying broad band isolation requirements. In contrast, the Viton stack violates those requirements by more than 3 orders of magnitude.

All stacks were analyzed for isolation performance using a specially designed 3D rigid body analysis code^[1] (in MATLAB) which was instrumental in allowing fast design iterations and optimization of the stack configurations. Frequency dependent spring stiffnesses and loss factors are used throughout the simulations. The effects of support assembly compliance and stack imperfections were also studied as described in reference 7. The results show that performance is fairly insensitive to minor imperfections and asymmetries in the stacks. Also, in some cases, support flexibility was shown to significantly degrade performance in the 15 to 35 Hz range and provided valuable guidance for the design of the support and actuator systems.

Lock acquisition and maintenance figures of merit were also evaluated^[7, 13]. Stack design only has a weak influence on those requirements: they are dominated by transmission of the 1/6 Hz micro-seismic peak which cannot be attenuated with passive stacks. However, there is some contribution from the first few resonances of the stacks, especially when the quality factor (Q) of those resonances is high. Simulations have shown that, for that reason, the metal spring stacks are more critical for lock acquisition than a Viton stack and pointed to possible difficulties due to the higher Q of those stacks. Careful redesign of the SUS control systems is expected to accommodate stack with Q's of 75 or less; this value is now adopted as an additional design goal for the metal spring stacks and also moderates the importance of achieving a lock acquisition figure around 1 $\mu\text{m}/\text{sec}$.

7.2.2 Simulation results for BSC stacks

Predicted spectra of test mass motions for the BSC stacks are shown in Figure 22 and compared to the science requirement. Note the vast performance improvement when going from Viton springs to metal springs. The figure also separates individual contributions from horizontal and vertical floor noise components and show that direct transmission of horizontal noise dominates at low frequencies while conversion of vertical floor noise takes more importance at higher frequencies.

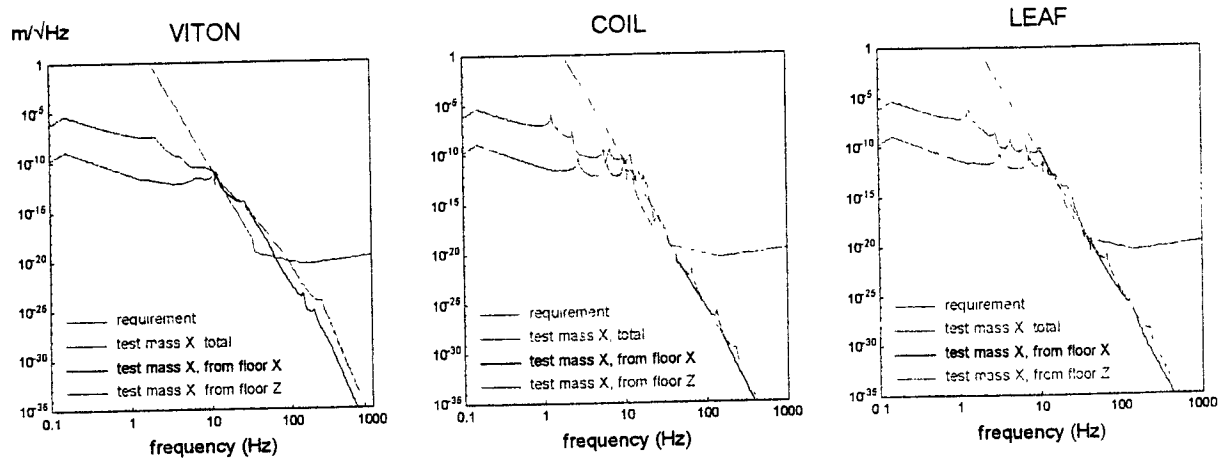


Figure 22. Spectrum of residual test mass motion for BSC stacks. Approximate support dynamics is included. The green curve shows total residual seismic noise while the black and blue curves show individual contributions from horizontal and vertical floor noise, respectively.

Lock acquisition and maintenance figures of merit are summarized in Table 8. It should be pointed out that all simulations of metal spring stacks have been performed with the most pessimistic estimates of spring loss factors. Because of this, the figures of merit for lock listed in the table are also pessimistic.

		Viton	Coil	Leaf
Lock acquisition:	$V_{RMS} \sim 1 \mu\text{m}/\text{sec}^*$	1.25	2.50	1.88
Lock maintenance:	$\chi_{RMS} \leq 2.7 \mu\text{m}$	2.12	2.45	2.27

* See note in section 2.2.1

Table 8. Top Level Requirements of the HAM

Model descriptions and detailed simulation results can be found in reference 7.

7.2.3 Simulation results for HAM stacks

Simulation results for the three compatible HAM stacks are summarized in Figure 23. Because no explicit requirement on recycling mirror residual noise was imposed on the design, the figure shows horizontal transmissibilities of the stack (there is no explicit requirement on vertical transmissibility either). Note that in this case, all 3 stack satisfy the isolation requirements with comparable margins.

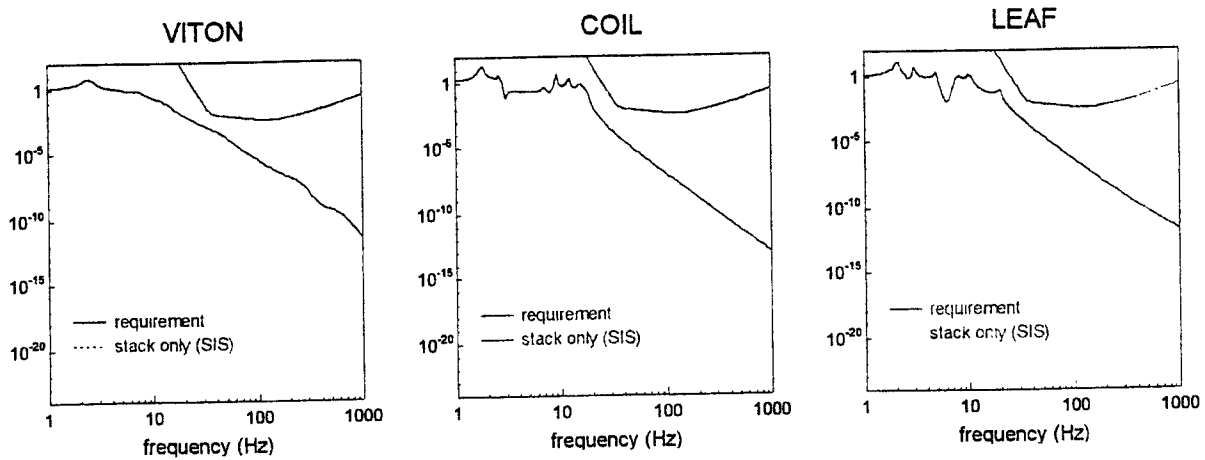


Figure 23. Horizontal Transmissibilities of HAM Stacks. Support dynamics is not included.

Table 9 summarizes the lock acquisition and maintenance requirements for the HAM and the BSC stacks, respectively.

		Viton	Coil	Leaf
Lock acquisition:	$V_{RMS} \sim 1 \mu\text{m}/\text{sec}$	1.21	1.94	1.42
Lock maintenance:	$\chi_{RMS} \leq 2.7 \mu\text{m}$	2.10	2.51	2.29

* See note in section 2.2.1

Table 9. BSC Stack Design with VITON Springs

Model descriptions and detailed simulation results can be found in reference 13.

8. PROGRAM PLANS

The revised program activities allow for 1st article testing of the major system elements prior to the final production order. Production schedule estimates provided by our vendors indicated we could produce 1st article hardware, conduct evaluation tests, and still make contractual delivery of the balance of hardware. This new information provided a clear opportunity to lower overall program risk. By prototyping, mistakes in fabrication can be avoided, and/or design problems can be quickly isolated and corrected. Another benefit in this re-planning effort was to advance the delivery of hardware to Hanford. Early hardware deliveries at Hanford will prove instrumental in bringing the experiment on line in a timely fashion. We also benefit by being able to concurrently design all handling fixtures, and evaluate their adequacy during the 1st article tests.

Schedules have been shifted to bring the actuator design to FDR in time to dovetail with the installation schedules of the remaining seismic hardware at Hanford. This will allow us to install the support structure and actuator hardware at the point in time when it should logically be installed, thus eliminating the step of retrofitting the hardware as was originally planned.

In summary, the design of the SEI system is on schedule with a robust plan for resolving technical concerns and getting prototype hardware in the users hands earlier than originally planned. The re-plan for the development of the SEI will reduce the programmatic risk to LIGO.

8.1 LIGO STACK DEVELOPMENT

Considerable progress has been made in this program element. The damped metal spring effort is tasked under this category. Initial tests with the damped coiled spring have been quite encouraging, and construction of the damped leaf spring is underway. Resources currently contained in this task element cover the development test phase for the springs and updating of the SIS performance predictions as relevant spring design characteristics become available. In anticipation of successfully completing the spring development, we propose to build a quantity of pre-production springs to provide for a qualification and QA test phase. These qualification tests will demonstrate that the final fabrication processes derived from the development tests will produce reliable and consistent spring behavior.

8.2 LIGO BSC DESIGN/FABRICATION

The BSC/HAM FDR scheduled for 7/28/96 has been advanced to 7/7/96 to coincide with our re-plan schedule for the external supports/actuators PDR. The main focus for the BSC/HAM FDR will be to release the P.O. for procuring the 1st article hardware. This 1st article hardware will be assembled with the external supports and actuators, both coarse and fine. Component and system tests will be performed.

In this program element, effort will be expended to complete a full prototype test on the BSC. The increased efforts include: the prototype development, the prototype testing, and increased support in the manufacturing liaison needed for the final production hardware.

8.3 LIGO HAM DESIGN/FABRICATION

The focus of this re-plan will be to deliver 1st article hardware to Hanford by November of 1997. This will allow the assembly and fit-check operation to begin. In addition, LIGO technicians will gain valuable experience with the stack assembly and fit-check on a much earlier time frame at Hanford.

8.4 BSC AND HAM EXTERNAL SUPPORTS AND ACTUATORS

We have made excellent progress so far on the design of an actuator system to meet the overall requirements for LIGO. HYTEC believes that a much more robust design can be delivered to Cal Tech by including a thorough 1st article testing phase. This testing phase will begin in November of 1997.

The BSC fine and coarse actuators are stacked one on another, and some structural dynamic coupling may exist between the two systems. Unexpected movements in the coarse actuator elements, i.e., strain relief, stiction etc., during fine actuator operation may be unlikely, but an extremely serious occurrence. Consequently, we would not propose entering into production of these elements without thorough prototype testing of both the fine and coarse systems. Otherwise, retrofitting of the modified actuator system could prove quite expensive in downtime, as well as in component costs.

8.5 SUMMARY

The re-plan effort will allow us to certify the system off-line prior to installation at the facilities. In addition, the replication of this hardware to produce the 33 systems provides strong motivation to get it right the first time. The actuator system is on the critical path and any slip in its development will impact the program at a far greater cost. HYTEC feels that by improving the scheduled delivery of the actuator systems to coincide with the BSC/HAM assembly will reduce the cost of having to retrofit the actuator subsystems.

We have arranged the schedules to bring the actuator design to a final design state, prior to submitting the BSC for final design review. We recommend adjusting the times for the FDR for actuator designs to allow time to complete the prototype testing. In spite of the delay shown in the final FDR we have improve the overall construction schedule substantially.

8.6 HAM/BSC DELIVERY AND ASSEMBLY SCHEDULE

The dates shown below are our latest estimates of delivery times for the first units to be installed at Hanford. These dates coincide with the installation of other key components at Hanford.

11/4/97 - Deliver 1st article HAM1 to Hanford with actuators

11/4/97 - Deliver 1st article BSC1 to HYTEC

4/1/98 - Deliver Actuator Supports For HAM 2,3

5/1/98 - Update and deliver Production HAM1 to Hanford

- 5/18/98 - Deliver Production Unit HAM2 to Hanford
- 6/1/98 - Deliver Production Unit HAM3 to Hanford
- 6/7/98 - 6/22/98 Initial Alignment Set-Up for the Input Optics
- 6/24/98 - 8/24/98 Install Input Optics Laser Lock Mode Cleaner
- 7/1/98 - Deliver Piers BSC 1,2,3
- 8/17/98 - Deliver BSC1 (Production Unit 1)
- 10/1/98 - Deliver BSC2 (Production Unit 2)
- 10/1/98 - Deliver HAM1,2,3 Actuators
- 10/15/98 - Deliver HAM4 All Components
- 10/15/98 - Deliver BSC3 (Production Unit 3)

9. REFERENCES

1. E. Ponslet, *Isolation Stack Modeling*, HYTEC Inc., Los Alamos, NM, document HYTEC-TN-LIGO-01, January 23, 1996.
2. E. Ponslet, *Isolation Stacks Preliminary Design Methodology*, HYTEC Inc., Los Alamos, NM, document HYTEC-TN-LIGO-02, February 21, 1996.
3. E. Ponslet, *BSC Stack Design Trend Study*, HYTEC Inc., Los Alamos, NM, document HYTEC-TN-LIGO-03, March 1st, 1996.
4. E. Ponslet, *Design of Vacuum Compatible Damped Metal Springs for Passive Isolation of The LIGO Detectors*, HYTEC Inc., Los Alamos, NM, document HYTEC-TN-LIGO-04a (revision a), January 1997.
5. E. Ponslet and B. Weinstein, *BSC Downtube Structure - Mechanical Design and Analysis*, HYTEC Inc., Los Alamos, NM, document HYTEC-TN-LIGO-05a (revision a), January 1997.
6. B. Weinstein, *BSC Support Assembly - Analytical Design*, HYTEC Inc., Los Alamos, NM, document HYTEC-TN-LIGO-06a (revision a), January 1997.
7. E. Ponslet, *BSC Seismic Isolation - Projected Performance Update*, HYTEC Inc., Los Alamos, NM, document HYTEC-TN-LIGO-07a (revision a), January 1997.
8. E. Ponslet and B. Weinstein, *Determination of Deflection Requirements for BSC Support Beam Bellows*, HYTEC Inc., document HYTEC-TN-LIGO-08a (revision a), January 1997.
9. E. Ponslet, *LIGO Coil Springs - Test Plan*, HYTEC Inc., Los Alamos, NM, document HYTEC-TN-LIGO-09, November 1996.
10. E. Ponslet and B. Weinstein, *Deflection Requirements for HAM Support Beam Bellows*, HYTEC Inc., document HYTEC-TN-LIGO-10a (revision a), January 1997.
11. E. Ponslet and B. Weinstein, *HAM Optics Table - Mechanical Design and Analysis*, HYTEC Inc., Los Alamos, NM, document HYTEC-TN-LIGO-11 (revision a), January 1997.
12. B. Weinstein, *HAM Support Assembly - Analytical Design*, HYTEC Inc., Los Alamos, NM, document HYTEC-TN-LIGO-12, January 1997.
13. E. Ponslet, *HAM Seismic Isolation - Projected Performance Update*, HYTEC Inc., Los Alamos, NM, document HYTEC-TN-LIGO-13, January 1997.
14. E. Ponslet, *LIGO Coil Spring - Test Report*, HYTEC Inc., Los Alamos, NM, document HYTEC-TN-LIGO-14, February 1997.
15. F. Raab and N. Solomonson, *Seismic Isolation Design Requirements Document* (draft and early corrections), LIGO draft document LIGO-T960065-02-D, California Institute of Technology and Massachusetts Institute of Technology, April 15, 1996.
16. F. Raab, *Seismic Isolation Conceptual Design*, LIGO document LIGO-T960066-00-D, California Institute of Technology and Massachusetts Institute of Technology, April 15, 1996.

17. F. Raab, *Thermal Noise Requirements for HAM Seismic Isolation*, LIGO draft document LIGO-T960188-00-D, California Institute of Technology and Massachusetts Institute of Technology, January 7, 1997.
18. W. Young, *LIGO Vacuum Compatibility, Cleaning Methods, and Qualification Procedures*, LIGO draft document LIGO-T960022-03-E, California Institute of Technology and Massachusetts Institute of Technology, January 14, 1997.
19. W. Young, *LIGO Vacuum Compatible Materials List*, LIGO document LIGO-T960050-A-E, California Institute of Technology and Massachusetts Institute of Technology, July 8, 1996.
20. *Specification for the LIGO Vacuum Equipment*, LIGO document LIGO-E940002-02-V, Revision 2, California Institute of Technology, September 1995.
21. D. Coyne, *Specification Guidance for Seismic Component Cleaning, Baking, and Shipping Preparation*, LIGO document LIGO-L97061-00-D, California Institute of Technology, February 10, 1997.
22. *BSC Support Beam Bellows Prototype - Fabrication Requirements and Test Plan*, HYTEC Inc., document HYTEC-TS-LIGO-01, January 1997.

10. ATTACHEMENTS

10.1 REPORTS

- HYTEC-TN-LIGO-01
- HYTEC-TN-LIGO-02
- HYTEC-TN-LIGO-03
- HYTEC-TN-LIGO-04a
- HYTEC-TN-LIGO-05a
- HYTEC-TN-LIGO-06a
- HYTEC-TN-LIGO-07a
- HYTEC-TN-LIGO-08a
- HYTEC-TN-LIGO-09
- HYTEC-TN-LIGO-10a
- HYTEC-TN-LIGO-11
- HYTEC-TN-LIGO-12
- HYTEC-TN-LIGO-13
- HYTEC-TN-LIGO-14

10.2 TECHNICAL SPECIFICATIONS

- HYTEC-TS-LIGO-01
- HYTEC-TS-LIGO-02

10.3 ASSEMBLY DRAWINGS

- LIG-10000
- LIG-13000
- LIG-12001
- LIG-12002
- LIG-11002
- LIG-11003
- LIG-11004
- LIG-11005
- LIG-20001
- LIG-24011
- LIG-25000

10.4 COST ESTIMATES

- HYTEC-COST-LIGO-01
- HYTEC-COST-LIGO-02
- HYTEC-COST-LIGO-03
- HYTEC-COST-LIGO-04

10.5 WEIGHT BREAKDOWNS

- HYTEC-WT-LIGO-01
- HYTEC-WT-LIGO-02

MEASUREMENT OF THE ALIGNMENT SENSITIVITY OF A POWER-RECYCLED MICHELSON INTERFEROMETER WITH FABRY-PEROT ARM CAVITIES

NERGIS MAVALVALA¹, DANIEL SIGG² AND DAVID SHOEMAKER

DEPARTMENT OF PHYSICS AND CENTER FOR SPACE RESEARCH,
MASSACHUSETTS INSTITUTE OF TECHNOLOGY, CAMBRIDGE, MA 02139

MARCH 18, 1997

DRAFT

ABSTRACT

Long baseline interferometric gravitational wave detectors, currently under construction (LIGO, VIRGO, GEO600 and TAMA), call for an automatic alignment system independent of the local reference frames of the interferometer mirrors to maintain their high displacement sensitivity. We develop an alignment sensing scheme for all angular degrees of freedom based on a multiple-frequency spatial mode sampling technique. The alignment sensitivity of a table-top scale power recycled Michelson interferometer with Fabry-Perot arm cavities is measured and the *wavefront sensor* signals are used to implement the first angular servo control of a LIGO-like interferometer. Within the experimental errors of about $\pm 20\%$, good agreement is found between the measured alignment sensitivity and theoretical calculations.

KEYWORDS

Gravitational-wave observatories, laser interferometer, automatic alignment, LIGO.

-
1. Phone: (818) 395-3130; Fax: (818) 304-9834; E-mail: nergis@ligo.caltech.edu.
 2. Phone: (617) 258-8295; Fax: (617) 253-7014; E-mail: sigg@tristan.mit.edu.

1 INTRODUCTION

The gravitational radiation [1] emitted by astrophysical sources such as coalescing neutron star or black hole binaries can be strong enough to be measured by highly sensitive earth-based detectors [2]. Presently, four international collaborations (LIGO [3], VIRGO [4], GEO600 [5] and TAMA300 [6]) are constructing long baseline laser interferometers with the objective of opening a new observation window to the universe.

The detectors currently planned for the Laser Interferometer Gravitational-wave Observatory (LIGO) [7] are modified versions of a simple Michelson interferometer (see Fig. 1). They

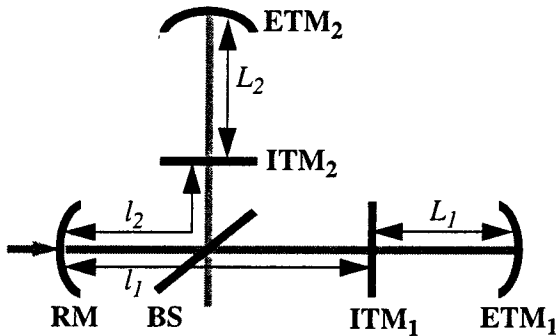


Figure 1: Schematic optical layout of an interferometric gravitational wave detector.

include Fabry-Perot arm cavities to yield a storage time in the arms comparable to the gravitational wave period and a partially transmitting power-recycling mirror in the input beam path to increase the light power incident on the beamsplitter (with the differential port of the Michelson interferometer held on a dark fringe [8]). To maintain maximum detection sensitivity for gravitational waves the angular alignment of the interferometer mirrors relative to the incoming TEM_{00} laser beam has to be better than of the order of 10^{-8} rad r.m.s. per degree of freedom during operation [9].

Misalignment can affect the gravitational wave sensitivity either by allowing unwanted light power to leak out of the differential Michelson port and thereby increasing the shot noise, or by lowering the stored light power in the arm cavities and

thereby decreasing the signal induced by a gravitational wave. The necessary angular alignment of 10^{-8} rad r.m.s. is about an order of magnitude lower than the stability of a local reference frame in a time interval of several minutes and over the 4 km arm length in LIGO [9]. Consequently, an interferometric alignment sensing and control scheme which makes only reference to the optical system axes is essential.

Measuring angular misalignments in a resonant optical cavity by heterodyne detection of off-axis spatial modes was first proposed and demonstrated by Anderson and Sampas [10]. They added phase modulation sidebands at the off-axis mode frequency to the input laser beam (carrier) and measured their asymmetric transmission through the cavity when the mirrors were misaligned relative to the input beam direction. Based on an idea proposed by Drever [11], Morrison et al. [12] extended this idea to off-resonance phase modulation sidebands and used the spatial asymmetries of the amplitude modulation light in reflection of a resonant optical cavity to determine the angular misalignment. This method has the advantage that if the cavity length is held on resonance for the carrier light frequency using the Pound-Drever-Hall reflection locking technique [13],[14], no additional sidebands are required to sense the deviations from perfect alignment.

To analyze more complex optical configurations we have developed a mathematical formalism [15] which is powerful enough to accurately predict the effects of misalignments in coupled-cavity systems, such as LIGO. This formalism describes misaligned mirrors and free space propagation as operators acting on the eigenmodes of the perfectly aligned system and treats distortion effects as perturbations. Operators representing complicated optical systems are then recursively built upon simpler ones, allowing a straightforward generalization to arbitrarily complex resonant optical configurations. Based on calculations done with this mathematical tool we have significantly advanced our understanding of alignment effects in long baseline laser interferometers [9]. Indeed, it has been pivotal in deriving the requirements for angular alignment for LIGO and it is the primary

design tool for a feasible wavefront sensing scheme which has distinct discriminants for misalignments of all angular degrees of freedom.

In this paper we report the results of a table-top experiment implementing an optical configuration closely resembling the LIGO one, that is, a power recycled Michelson interferometer with Fabry-Perot arm cavities [16]. The alignment sensitivity for all interferometer mirrors is measured with an absolute precision of about $\pm 20\%$. The experimental values are found to be in good agreement with the theoretical predictions, firmly establishing the wavefront sensing technique and the mathematical model used to calculate the interferometer sensitivity to alignment. Finally, the wavefront sensing signals are decomposed into individual mirror misalignment angles in real time and feedback loops have been closed on all angular degrees of freedom, yielding the first power recycled Michelson interferometer with Fabry-Perot arm cavities utilizing a complete automatic alignment system with all angular degrees of freedom under closed loop control.

2 THEORY

Referring to Fig. 1, we can count twelve angular degrees of freedom in the interferometer: the yaw and pitch angles of the end test masses (ETMs), the input test masses (ITMs), the power recycling mirror (RM) and the beamsplitter (BS). The orientation of the beamsplitter, however, is not an independent degree of freedom since its misalignment can always be compensated by adjusting ETM_2 and ITM_2 . This leaves ten independent angular degrees of freedom which are to be determined by wavefront sensors (WFS): By spatially sampling the left-right and the top-bottom asymmetry of amplitude modulated light at the sideband frequencies, the detection ports of the length photodetectors are also used to sense the angular alignment of the interferometer. When the differential port of the Michelson is operated on a dark fringe, it is sensitive to differential length changes, whereas the reflected beam is sensitive to common length changes. Similarly, a wavefront sensor at the dark port mostly sees differential misalignments and a wavefront sensor in reflection

can be used to detect common misalignments. One important difference between length and alignment sensing is the additional Guoy phase shift acquired by higher-order spatial modes due to free space propagation. This makes it possible to distinguish alignment signals produced in different phases — signals due to misalignments of the front and rear mirrors of a cavity, for example — by adjusting the distance between the detection port and the wavefront sensor. In practice, a telescope which allows for simultaneous adjustment of the Guoy phase shift and the spot size is used.

To first order, the signal detected by the i -th wavefront sensor can be written as:

$$WFS_i = 2J_0(\Gamma_i)J_1(\Gamma_i)P f_i \times \sum_j A_{ij} \Theta_j \cos(\eta_i - \eta_{ij}) \cos(\Omega_i t + \phi_{ij}) \quad (1)$$

where the sum is taken over all j angular degrees of freedom. J_0 and J_1 are the Bessel functions, Γ_i are the modulation indices, P is the input laser power, f_i is the fraction of power at the port which is diverted to the i -th photodetector, A_{ij} is the alignment sensitivity matrix, Θ_j is the misalignment angle of the j -th degree of freedom, η_i is the Guoy phase shift between the detection port and the detector, η_{ij} is the intrinsic Guoy phase shift of the signal, Ω_i is the modulation frequency and ϕ_{ij} is the intrinsic RF phase shift of the signal. The predicted values of the alignment sensitivity matrix of the table-top experiment are listed in Table 1 for a particular choice of Guoy and RF phase shifts. *An important feature is its non-singular character which makes it possible to clearly separate the individual mirror angles.*

PORT	PHASES		ANGULAR DEGREES OF FREEDOM				
	ϕ_{ii}	η_i	RM	ITM ₁	ITM ₂	ETM ₁	ETM ₂
WFS ₁	0°	152°	-2.59	0.34	0.43	0	0
WFS ₂	0°	92°	-1.42	0.76	0.78	0	0
WFS ₃	90°	168°	-0.67	-2.77	2.98	0	0
WFS ₄	90°	80°	-1.01	14.8	-12.1	15.5	-12.6
WFS ₅	0°	87°	-2.05	3.65	3.67	3.74	3.77
WFS ₆	0°	140°	-20.7	32.4	32.8	30.4	30.8

Table 1: Calculated alignment sensitivity matrix for the experimental parameters described in the text.

3 EXPERIMENTAL TECHNIQUE

A schematic overview of the table-top experiment is shown in Fig. 2. Referring to the naming conventions of Fig. 1, the end test masses (ETMs) are high reflectors, while the power reflectivity of cavities. After adjusting the differential Michelson length to give a dark fringe at the differential port, the heterodyne reflection locking technique is used with photodetector LS_4 at a pick-off of the recycling cavity to sense deviations from resonance for the common arm cavity length $L_1 + L_2$. To sense differential degrees of freedom a macroscopic path length difference (Schnupp asymmetry) of 0.384 m is added to the differential Michelson length [18]. Consequently, the differential port of the Michelson interferometer is not dark for the sidebands and photodetector LS_3 is mainly sensitive to the differential arm cavity length $L_2 - L_1$.

It is possible to control all longitudinal degrees of freedom with just one pair of sidebands [19], if a gain hierarchy is implemented in the servo control to separate the recycling cavity length from the common arm cavity length. For this experiment we added a separate subcarrier which is only resonant in the recycling cavity and, therefore, yields more robust error signals [20]. To operate the subcarrier on a dark fringe it is frequency shifted by 391.6 MHz (putting one full additional wavelength round trip in the longer Michelson arm). The

each input test mass (ITM) is 0.97 and that of the recycling mirror (RM) is 0.90. Mirror losses in the prototype are measured to be about 25 parts per million (ppm) per reflective surface for the super-polished ETMs and ITMs and 1000 ppm for the RM. A pellicle pick-off in the recycling cavity and imperfect contrast at the beamsplitter introduce an additional loss of 5% in the recycling cavity, leading to a recycling gain of ~ 7 for the main carrier.

The macroscopic arm cavity lengths are $L_1 \approx L_2 \approx 0.575$ m and the length of the recycling cavity is $l_C = (l_1 + l_2)/2 \approx 3.83$ m. These three longitudinal degrees of freedom are microscopically adjusted to maintain the cavity resonance conditions for the main carrier light, that is, the round-trip phase of the light has to be a multiple of 2π [17]. Phase modulation sidebands at a frequency of ± 58.5 Mhz are imposed on the carrier input laser light. The frequency of the sidebands was chosen to be resonant in the recycling cavity, but not resonant in the arm subcarrier has its own sets of sidebands and since none of these frequencies resonate in the arm cavities, they provide an independent means of controlling the recycling cavity and the differential Michelson lengths. One pair of subcarrier sidebands at 39.2 Mhz is resonant in the recycling cavity; this signal is detected by photodetector LS_2 at the dark port and is used to control the differential Michelson length. The other pair of sidebands at 32.3 MHz is not resonant in the recycling cavity and does not couple to the interferometer; this signal is detected by LS_1 in reflection and is used to control the recycling cavity length.

The laser source is a frequency and power stabilized Ar^+ CW laser with a wavelength of $\lambda = 514.5$ nm. Typical output power is 250 mW and frequency noise levels of $0.4 \text{ Hz}/\sqrt{\text{Hz}}$ in the 20 to 40 kHz band are achieved. After generating the frequency-shifted subcarrier with a double-passed acousto-optic modulator and impressing phase modulation sidebands with Pockels cells, the laser light is launched into a fiber which serves as a spatial mode filter.

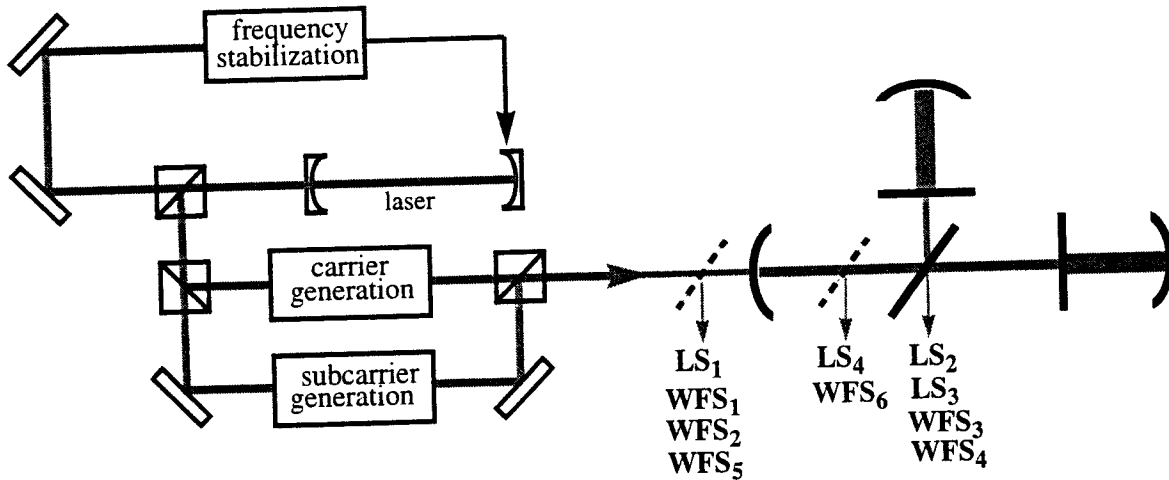


Figure 2: Overview of the experiment with length sensors (LS_i) and alignment sensors (WFS_i) shown.

The length sensing detectors comprise of monolithic photodiodes followed by a tuned circuit, an RF amplifier, and a mixer with low-pass filtering to achieve a low noise down-conversion of the length error signal at the modulation frequency. The error signals are fed back to PZT actuators controlling the axial position of the interferometer mirrors. Each longitudinal degree of freedom is controlled by two PZT actuators: one with a small bandwidth ($\sim 100\text{Hz}$), but a large dynamic range ($\sim 2\mu\text{m}$) and the other with a small dynamic range ($\sim 200\text{nm}$), but a large bandwidth ($\sim 20\text{kHz}$). Since the interferometer is operated in air with minimal seismic or acoustic isolation, high bandwidth and large dynamic range are crucial for a reliable length lock.

The wavefront sensors are electronically very similar to the length sensors, but use a quadrant photocell with four read-out channels. Their signals are digitized by analog-to-digital converters and read into a VME-based computer system. Digital-to-analog converters are used to drive angular PZT actuators which tilt the interferometer mirrors about both the horizontal and vertical axes. An independent calibrated pointing system (a set of optical levers) is implemented to accurately measure the absolute tilt angles of each mirror.

At the differential Michelson port, WFS_3 senses the demodulated signal at the frequency of the resonant sidebands of the subcarrier to determine primarily differential misalignments of the ITMs, while the WFS_4 signal, demodulated at the carrier sideband frequency, is most sensitive to a linear combination of differential ITM and differential ETM misalignment (see Table 1). WFS_1 and WFS_2 are placed in reflection and are using the subcarrier with its non resonant sidebands to measure both common ITM and RM misalignments. WFS_5 is using the carrier and its sidebands to sense a combination of common ETM, common ITM and RM misalignments. Together, they are able to discriminate all angular degrees of freedom. (WFS_6 is colinear with WFS_5 and acts as a consistency check.)

A measurement of the alignment sensitivity matrix is then performed as follows: the calculated values of the sensitivity matrix are used to digitally close the angular feedback loops with a low bandwidth ($\sim 1\text{ Hz}$) thus bringing the interferometer into a known (optimal) alignment state (see Fig. 3). Then each angular degree of freedom is dithered at a different frequency well above the bandwidth of the angular servos and the data from the wavefront sensors and the pointing system are collected and stored to disk for off-line analysis.

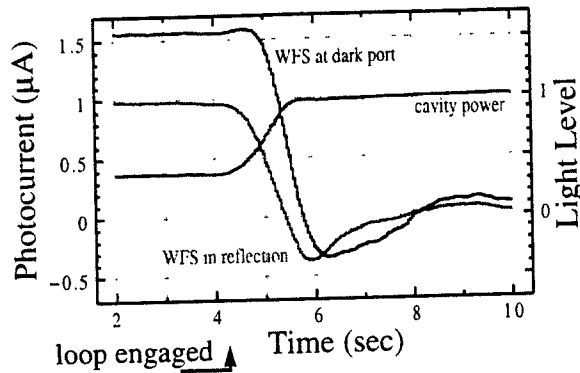


Figure 3: Closed loop alignment control. The power in the recycling cavity is maximized when the alignment loops are engaged.

Fig. 4 shows the amplitude spectral density of a measured time series of the pointing system measuring the yaw misalignment of the RM and of WFS_1 measuring horizontal alignment signals. Clearly present is the peak at 40Hz, the dither

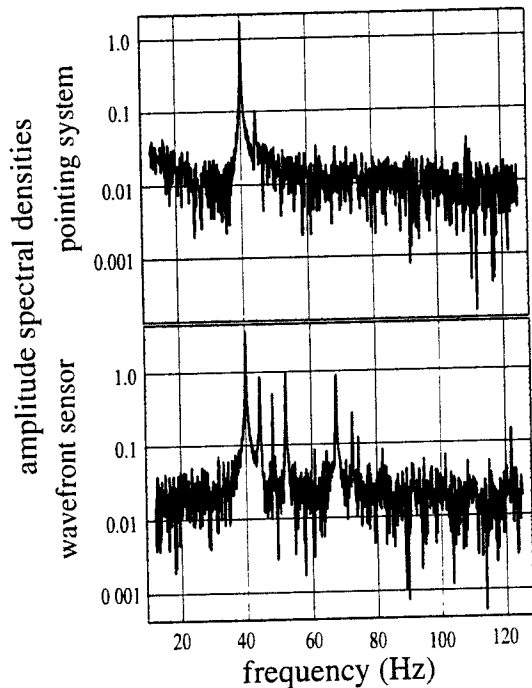


Figure 4: Fourier spectrum of pointing system signal for horizontal misalignments of the RM and the corresponding signal on WFS_1 . The peak at 40 Hz is due to horizontal misalignment of the recycling mirror, RM_x ; RM_y appears at 44 Hz; ITM_{1y} at 48 Hz; ITM_{1x} at 52 Hz; ETM_{1y} at 56 Hz; ETM_{2y} at 59 Hz; ETM_{1x} at 63 Hz; ITM_{2x} at 67 Hz; ITM_{2y} at 72 Hz; and ETM_{2x} at 76 Hz.

frequency for horizontal RM misalignment. The smaller peak at 44Hz is due to the vertical dither of the RM. WFS_1 is nominally placed to be most sensitive to RM misalignments and, indeed, the strongest signal appears at 40Hz. As is to be expected, signals at the horizontal dither frequency of ITM_1 and ITM_2 — 52Hz and 67Hz, respectively — are also pronounced. We note that the vertical dither at 44Hz appears stronger in the wavefront sensor spectrum than in the one of the pointing system. This effect is too large to be explained solely by the uncertainty of the detector orientation. In fact, a rather large (and unwanted) beam ellipticity is observed on WFS_1 and WFS_2 , leading to corrections of opposite signs for the horizontal and the vertical alignment signals. To decrease the uncertainty induced by this effect, horizontal and vertical alignment signals corresponding to the same mirror are averaged.

By determining the signal amplitude due to each angular degree of freedom in each wavefront sensor and pointing system spectrum and by taking into account the light power hitting the wavefront sensors, their quantum efficiency and their transimpedance gain, we directly calculate each element of the alignment sensitivity matrix.

4 RESULTS

Matrix elements which are predicted to be very small do indeed correspond to insignificant signals on the wavefront sensors. The dominant elements of the alignment sensitivity matrix are shown in Fig. 5; they are scaled to give unity if the measured values are identical to the predicted ones. The error bars arise from uncertainties in the power built up in the recycling cavity (6% – 24%, depending on the matrix element), the Guoy phase shift in the telescopes (~1% for on-diagonal elements and 5% – 20% for off-diagonal elements), the transimpedance gains of the wavefront sensors (5% – 10%), the absolute light power incident on each detector (6%), the modulation indices (5% – 10%) and the calibration of the pointing system (10%). The statistical errors are small, typically below 3%. Since these errors are independent of each other they are added in quadrature; resulting

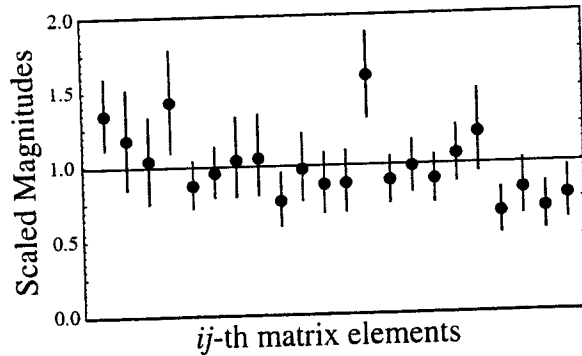


Figure 5: Dominant elements of the measured alignment sensitivity matrix. The measurements are scaled to the predicted values of Table 1, which are normalized to 1.0.

in about 20% total error for the matrix elements plotted in Fig. 5.

The quantitative agreement between the modal predictions and the measurement, evinced in Fig. 5, is a strong validation of the model. Furthermore, we have proven that a complete set of alignment signals can be experimentally determined in a complex resonant optical system with sufficient precision to enable an automatic alignment system.

With this confirmation of our model, we have studied the effects of misalignment in the LIGO detector using the modal model in the small angle regime. We find that the interferometer mirrors must be aligned to within $\sim 10^{-8}$ rad r.m.s. per degree of freedom with respect to the incoming laser beam if the gravitational wave sensitivity of the detector is to be compromised by less than 0.5% due to misalignment [9]. Based on the wavefront sensing scheme described above, we have designed an automatic alignment system for LIGO [16], [9]. One important characteristic of the LIGO interferometer is that due to the disparity in the lengths of the recycling and the arm cavities, the recycling cavity is nearly degenerate, that is, higher-order spatial modes are also resonant. This requires the addition of a non-resonant sideband pair to the main carrier light in order to distinguish RM and common ITM misalignments. We calculate that the detection noise due to photon counting statistics is in the range of 10^{-15} to 10^{-14} rad/ $\sqrt{\text{Hz}}$ and is thus negligible compared to

the required alignment tolerance of 10^{-8} rad r.m.s. per degree of freedom. Alignment fluctuations induced by thermal noise are of order 5×10^{-18} rad/ $\sqrt{\text{Hz}}$ at 100Hz [9] and are only relevant for the servo design, since the controller noise has to be below this limit.

Summarizing, we conclude that the wavefront sensing technique is well understood, both theoretically and experimentally, and that this technique is feasible for closed loop servo control of complex resonant optical interferometers.

We thank our colleagues on the LIGO project who helped us in many ways carrying out this experiment and gave us many useful suggestions and comments. This work is supported by NSF grant PHY-9210038. One of us (D.S.) was partially supported by the Swiss National Science Foundation.

REFERENCES

- [1] See, for example, K.S. Thorne, *Gravitational radiation*, in 300 Years of Gravitation, S.W. Hawking and W. Israel (eds.), Cambridge University Press (Cambridge, 1987), 330.
- [2] R. Weiss, *Quarterly progress report of the research laboratory of electronics of the Massachusetts Institute of Technology*, **105**, 54 (1972).
- [3] F.J. Raab, *The LIGO project: progress and prospects*, in First Edoardo Amaldi conference on gravitational wave experiments, E. Coccia, G. Pixella and F. Ronga (eds.), World Scientific (Singapore, 1995), 70–85.
- [4] A. Giazotto, *The VIRGO experiment: status of the art*, *ibid.*, 86–99.
- [5] K. Danzmann, *GEO600 — a 600 m laser interferometric gravitational wave antenna*, *ibid.*, 100–111.
- [6] K. Tsubono, *300 m laser interferometric gravitational wave detector (TAMA300) in Japan*, *ibid.*, 112–114.

- [7] A. Abramovici, W.E. Althouse, R.W.P. Drever, Y. Gürsel, S. Kawamura, F.J. Raab, D. Shoemaker, L. Sievers, R.E. Spero, K.S. Thorne, R.E. Vogt, R. Weiss, S.E. Whitcomb and M.E. Zucker, *LIGO: the Laser Interferometer Gravitational-wave Observatory*, Science **256**, 325–333 (1992).
- [8] See, for example, R.W.P. Drever, in *Gravitational Radiation*, N. Deruelle and T. Piran (eds.), North Holland (Dordrecht, 1992), 320; D. Schnier, J. Mizuno, G. Heinzel, H. Lück, A. Rüdiger, R. Schilling, M. Schrepel, W. Winkler and K. Danzmann, *Power recycling in the Garching 30 m prototype interferometer for gravitational-wave detection*, Phys. Lett. **A225**, 210-216 (1997).
- [9] P. Fritschel, G. Gonzáles, N. Mavalvala, D. Shoemaker, D. Sigg and M. Zucker, *Alignment of a long baseline gravitational wave interferometer*, in preparation.
- [10] D.Z. Anderson, *Alignment of resonant optical cavities*, Appl. Opt. **23**, 2944–2949 (1984).
N. Sampas and D.Z. Anderson, *Stabilization of laser beam alignment to an optical resonator by heterodyne detection of off-axis modes*, Appl. Opt. **29**, 394–403 (1990).
- [11] R.W.P. Drever, Department of Physics, California Institute of Technology, Pasadena, USA, private communication (1984).
- [12] E. Morrison, B.J. Meers, D.I. Robertson, and H. Ward, *Experimental demonstration of an automatic alignment system for optical interferometers*, Appl. Opt. **33**, 5037–5040 (1994).
E. Morrison, B.J. Meers, D.I. Robertson, and H. Ward, *Automatic alignment of optical interferometers*, Appl. Opt. **33**, 5041–5049 (1994).
- [13] A. Schenzle, R. DeVoe and G. Brewer, *Phase-modulation laser spectroscopy*, Phys. Rev. **A25**, 2606–2621 (1982).
- [14] R.W.P. Drever, J.L. Hall, F.V. Kowalski, J. Hough, G.M. Ford, A.J. Munley and H. Ward, *Laser phase and frequency stabilization using an optical resonator*, Appl. Phys. **B31**, 97–105 (1983).
- [15] Y. Hefetz, N. Mavalvala and D. Sigg, *Principles of calculating alignment signals in complex optical interferometers*, accepted by J. Opt. Soc. Am. **B** (1996).
- [16] N. Mavalvala, *Alignment issues in laser interferometric gravitational-wave detectors*, Ph. D. dissertation, (Massachusetts Institute of Technology, Cambridge, MA, 1997).
- [17] See, for example, A.E. Siegman, *Lasers*, University Science (Mill Valley CA, 1986).
- [18] L. Schnupp, Max Planck Institute for Quantum Optics, Garching, Germany, private communication (1986).
- [19] M.W. Regehr, F.J. Raab, and S.E. Whitcomb, *Demonstration of a power-recycled Michelson interferometer with Fabry-Perot arms by frontal modulation*, Appl. Opt. **20**, 1507–1509 (1995).
- [20] J.A. Giaime, *Studies of laser interferometric design and a vibration isolation system for interferometric gravitational wave detectors*, Ph. D. dissertation, (Massachusetts Institute of Technology, Cambridge, MA, 1995).

LASER INTERFEROMETER GRAVITATIONAL WAVE OBSERVATORY
- LIGO -

CALIFORNIA INSTITUTE OF TECHNOLOGY
MASSACHUSETTS INSTITUTE OF TECHNOLOGY

Document Type	LIGO-T970062-00 - Cxx	2/18/97
ASC CDS Conceptual Design		
Jay Heefner		

Distribution of this draft:

This is an internal working note
of the LIGO Project.

California Institute of Technology
LIGO Project - MS 51-33
Pasadena CA 91125
Phone (818) 395-2129
Fax (818) 304-9834
E-mail: info@ligo.caltech.edu

Massachusetts Institute of Technology
LIGO Project - MS 20B-145
Cambridge, MA 01239
Phone (617) 253-4824
Fax (617) 253-7014
E-mail: info@ligo.mit.edu

WWW: <http://www.ligo.caltech.edu/>

1 INTRODUCTION

1.1. Document Organization

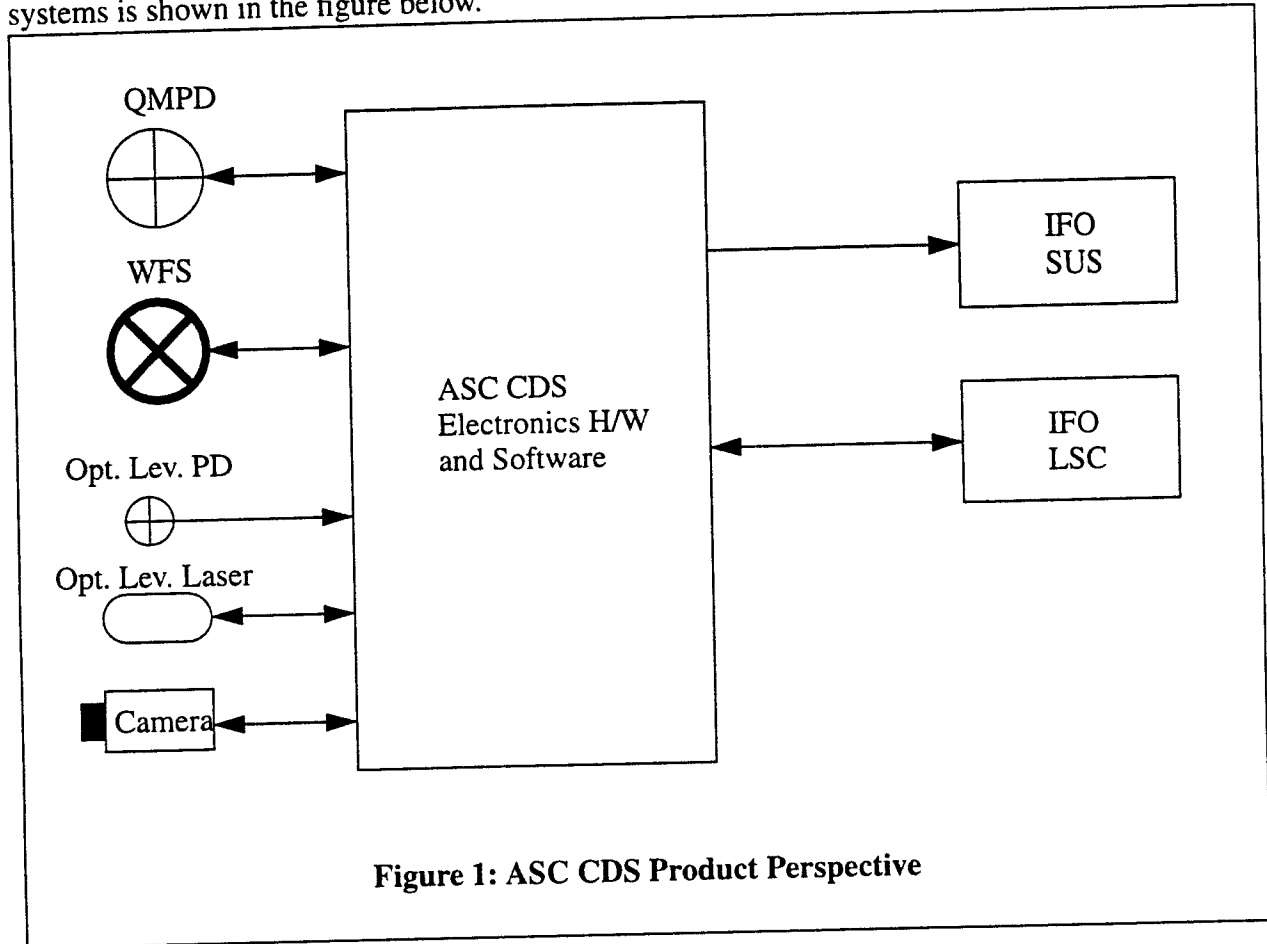
This document describes the ASC CDS conceptual design and was produced as a result of the ASC CDS DRD (LIGO T970061). The conceptual design presented shows how the ASC CDS system for one interferometer at the Washington site could be organized. The design for the second interferometer and the Louisiana site would be similar. The complete designs for the Washington and Louisiana sites will be developed during the preliminary design.

The document is organized as follows:

- Section 2: Wavefront Processing Unit Design provides a description of the systems that would be used to provide to implement the wavefront processing subsystem.
- Section 3: Quadrant Monitor Processing Unit Design provides a description of the systems that would be used to implement the quadrant monitor photodiode subsystem.
- Section 4: Optical Lever Design provides a description of the systems that would be used to implement the optical lever subsystem.
- Section 5: Camera System Design provides a description of the systems that would be used to implement the video camera subsystem.
- Section 6: ASC CDS System Level Design provides a description of the systems that would be used to provide higher level processing and functionality. Typically information from each of the ASC CDS subsystems (wavefront sensors, quadrant monitor photodiodes, optical levers and cameras) is collected and processed at this level.
- Section 7: ASC CDS Prototype Setup provides a brief description of the prototype test setup that will be used to verify the ASC and ASC CDS designs. This prototype test setup is more fully described in D. Sigg's document (LIGO T970TBD).

1.2. System Overview

A block diagram showing the ASC CDS system in relation to the ASC system and other LIGO systems is shown in the figure below.



The figure below shows the functional layout of the ASC CDS system with respect to the LIGO optical layout.

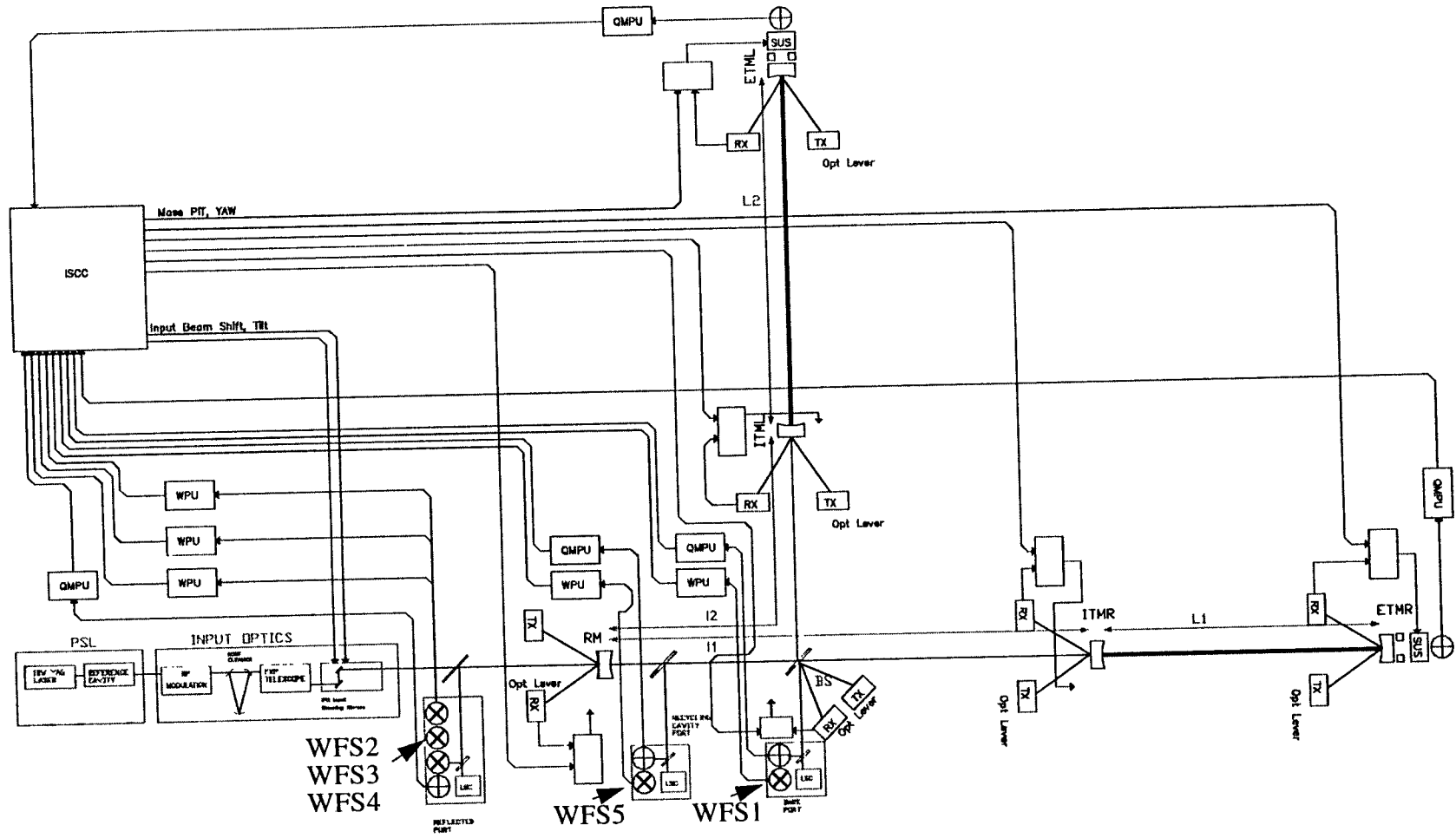


Figure 2: ASC CDS Functional Layout

1.3. Acronyms

- ADC- Analog to Digital Converter
- ASC- Alignment Sensing and Control
- BSC- Beam Splitter Chamber
- CDS- Control and Data System
- CPU- Central Processing Unit
- DAQ- LIGO CDS Data Acquisition
- EPICS- Experimental Physics Industrial Control System
- ETM- End Test Mass
- F/O- Fiber Optic
- HAM- Horizontal Access Module
- IFO- Interferometer
- IOO- Input/Output Optics
- ITM- Input Test Mass
- LA- Louisiana Site
- LIGO- Laser Interferometer Gravitational-wave Observatory
- LPF- Low Pass Filter
- LSC- Length Sensing and Control
- LVEA- Laser Vacuum and Equipment Area
- MUX- Multiplexer
- QMPD- Quadrant Monitor Photodiode
- QMPU- Quadrant Monitor Processing Unit
- SUS- Suspension System
- TBD- To Be Determined
- VEA- Vacuum Equipment Area
- WA- Washington Site
- WFS- Wavefront Sensor
- WPU- Wavefront Processing Unit

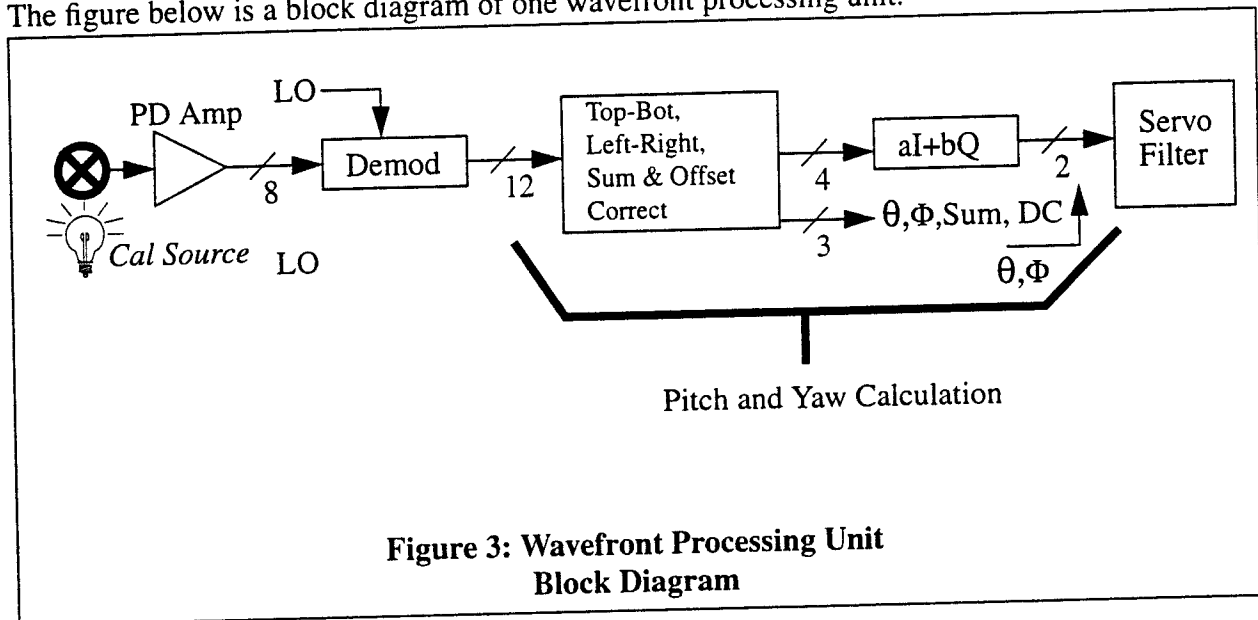
2 WAVEFRONT PROCESSING UNIT DESIGN

Wavefront sensor photodiodes are located on common ASC/LSC optical tables in the LVEA. The rough placement of the optical tables is depicted in Figure 2: ASC CDS Functional Layout. The table below lists the location of each sensor.

Table 1: WFS Number vs. Location

<i>WFS Number</i>	<i>Location</i>
1	ASC/LSC Dark Port Optical Table
2	ASC/LSC Reflected Port Optical Table
3	ASC/LSC Reflected Port Optical Table
4	ASC/LSC Reflected Port Optical Table
5	ASC/LSC Recycling Cavity Pick-Off Optical Table

The figure below is a block diagram of one wavefront processing unit.



As can be seen from the figure the WPU consists of the following parts:

- Photodiode amplifier
- Demodulator Module
- Pitch and Yaw Calculation
- Servo Filtering
- Motorized Mirror, Calibration Source and Shutter Control (not shown)

Filtered pitch and yaw data from the WPU is passed to the basis transformation described in the ASC CDS system level section.

2.1. Photodiode Amplifier Design

It is currently envisioned that the photodiode amplifier design that was used for the FMI WFS prototype testing will be modified and used for the LIGO photodiode amplifiers. During the preliminary design phase the design will be modified to match the LIGO ASC CDS requirements. The design will be tested using an ASC prototype setup.

The current design meets most of the requirements outlined in the ASC CDS DRD but some changes may be required. These changes include:

- Retuning of front end tank circuit and traps to LIGO frequencies.
- Transimpedance (Gain) changes to meet LIGO requirements.
- Addition of operator selectable gain changes.
- Circuit packaging changes to meet LIGO CDS design specifications and standards.

2.2. Demodulator Design

It is currently envisioned that the demodulator design (LIGO D950TBD) that was used for the FMI WFS prototype testing will be modified and used for the LIGO demodulators. During the preliminary design phase the design will be modified to match the LIGO ASC CDS requirements. The design will be tested using an ASC prototype setup.

The current design meets most of the requirements outlined in the ASC CDS DRD but some changes may be required. These changes include:

- Gain changes to match LIGO requirements.
- IF filter tailoring to match demodulator output to WPU ADC inputs. (This filtering may be used as a combination anti-alias and whitening filter.)
- Addition of operator selectable gain changes.
- Circuit packaging changes to meet LIGO CDS design specifications and standards.

2.3. Pitch and Yaw Processing and Filtering Section Design

The figure below is a block diagram of the pitch and yaw processing and servo filtering section for the demodulated outputs from the demodulator module.

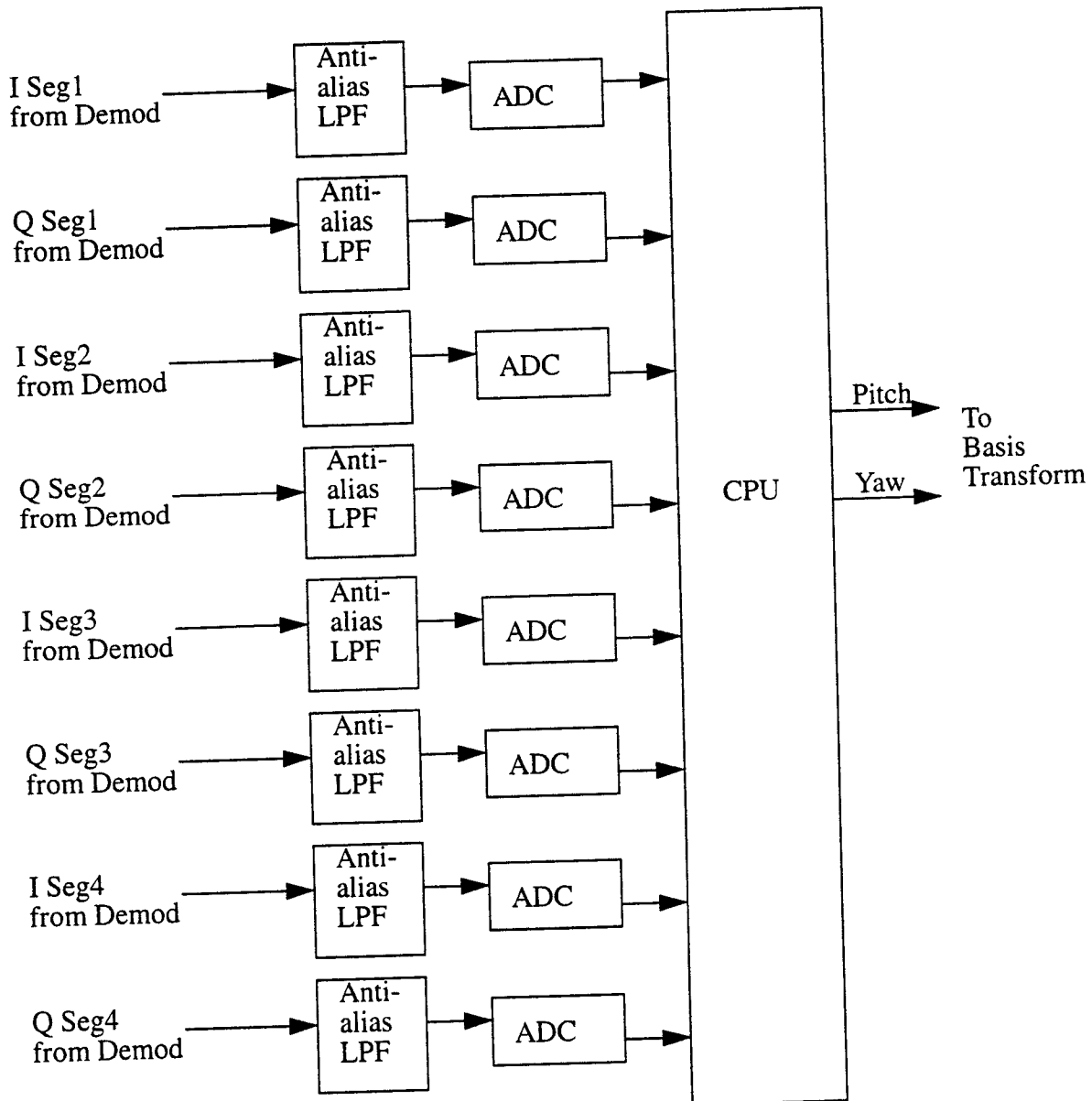


Figure 4: Pitch and Yaw Processing and Filtering Section Block Diagram for One WPU

The ADCs shown in the figure are one channel each of a VMIC model 3123, 16 bit, 32 channel module located in the ASC VME crate in the LVEA. The sampling rate for the ADCs will be 10 Ksamples/second. Testing done within the CDS group and data sheets obtained from the manufacturer show that the input referred noise for the VMIC 3123 will be less than $(10\mu V)/(\sqrt{Hz})$

when the input voltage range is set to +/- 10 volts, which is less than the required $(100\mu V)/(\sqrt{Hz})$.

The CPU is a Heurikon model baja 4700 VME processor in the ASC CDS VME crate in the LVEA. Data from the ADCs is passed to the CPU via the VME backplane. Initial calculations and estimates show that the baja 4700 processor operating under the VxWorks operating system should be adequate to perform the processing for at least 2 WPU's. Testing during the preliminary design phase will verify these estimates.

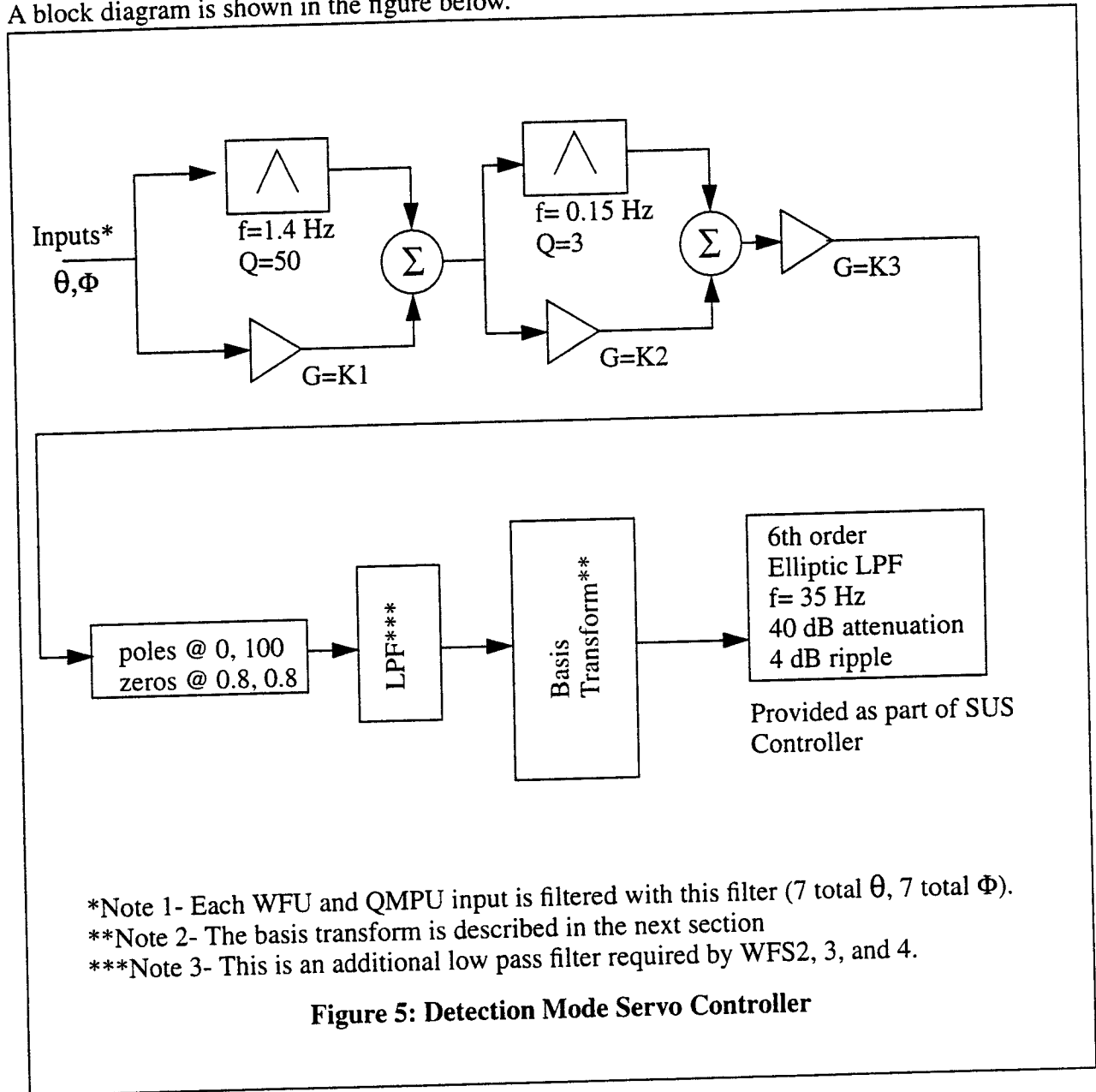
The block diagram and components for monitoring the DC outputs from the demodulator module will be similar to the figure shown above, with the exception that the ADCs will be model TBD, multi-channel, 16 bit ADC modules sampling at 10 (TBR) samples per second.

The table below is a list of the signals to be acquired and processed by each WPU.

Table 2: WPU Signals and Sampling Rates

<i>Signal</i>	<i>Sample Rate (samples/sec)</i>
I segment 1	10 K
Q segment 1	10 K
I segment 2	10 K
Q segment 2	10 K
I segment 3	10 K
Q segment 3	10 K
I segment 4	10 K
Q segment 4	10 K
DC segment 1	10
DC segment 2	10
DC segment 3	10
DC segment 4	10
TOTAL PER WPU	Fast (10K) Channels = 8 Slow (10) Channels = 4

The pitch and yaw calculations and the servo filtering will be as specified in the ASC CDS DRD. A block diagram is shown in the figure below.



2.4. Motorized Mirror and Shutter Control

Each WPU will have motorized mirrors and shutters that must be controlled by the operator. The motorized mirror and shutter controls will be provided using VME analog input, output and binary input and output modules and EPICS software running on a CPU such as the Motorola MVME162-333.

2.5. Calibration Procedures

As the system designs and requirements are refined during the preliminary design phase, the on and off line calibration procedures will be developed.

3 QUADRANT MONITOR PROCESSING UNIT DESIGN

Quadrant monitor sensor photodiodes are located on optical tables in the LVEA and VEAs. The rough placement of the optical tables is depicted in Figure 2: ASC CDS Functional Layout. Photodiodes in the LVEA are located on the same optical tables as the LSC and wavefront photodiodes.

3.1. Photodiode Amplifier Design

A four quadrant photodiode amplifier will be developed to meet the requirements outlined in the ASC CDS DRD. The QMPD requirements versus operating mode are repeated in the table below.

Table 3: QMPD Requirements vs. Operational Modes

<i>I/O State</i>	<i>Transimpedance gain (each element)</i>	<i>Output Noise Density (f > 30 Hz)</i>	<i>Bandwidth (3 dB)</i>
2. Recycled Michelson	10 Mohm	N/A	>100 Hz
3. Recycled Michelson + one arm	10 Mohm/250 Kohm	N/A	>100 Hz
4. Detection Mode	500 ohm	$(20nV)/(\sqrt{Hz})$	> 1 KHz

Gain selection will be operator controlled and be in nominal 6 dB and 20 dB steps from 500 ohms to 10 Mohms. The output filtering may be tailored to perform the anti-aliasing and whitening required before the QMPU ADC shown in Figure 6: Pitch and Yaw Processing and Filtering Section Block Diagram for One QMPU.

3.2. Pitch and Yaw Processing and Filtering Section Design

The figure below is a block diagram of the pitch and yaw processing and servo filtering section for the QMPD outputs from the photodiode amplifier.

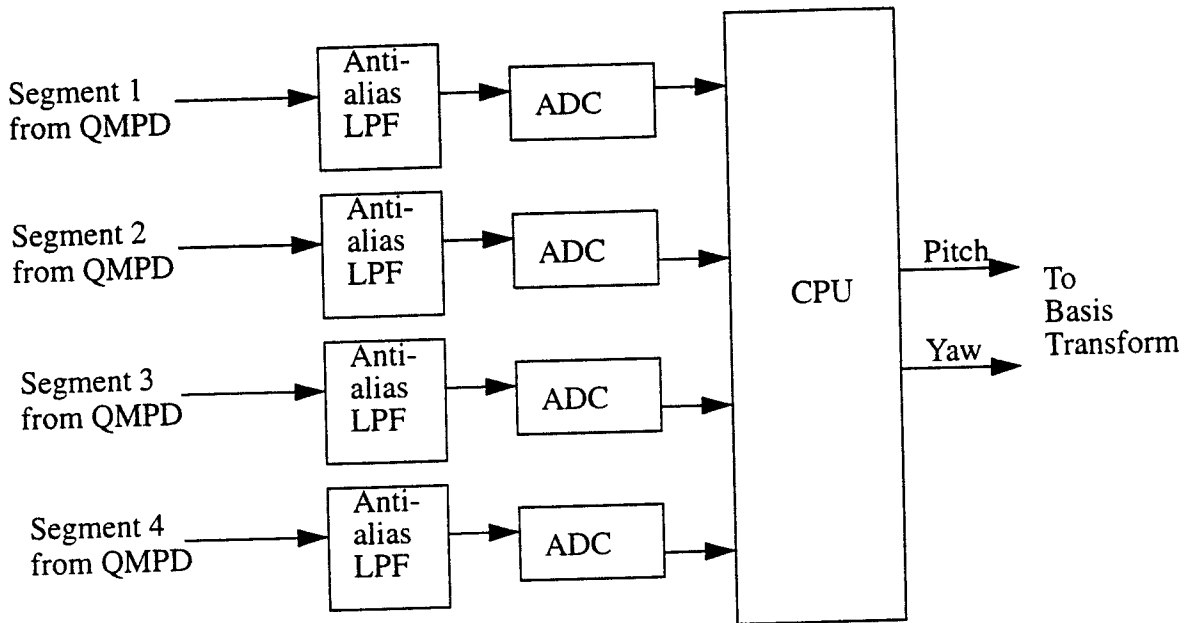


Figure 6: Pitch and Yaw Processing and Filtering Section Block Diagram for One QMPU

The ADCs shown in the figure are one channel each of a VMIC model 3123, 16 bit, 32 channel module located in the ASC VME crate in the LVEA. The sampling rate for the ADCs will be 10 Ksamples/second. Testing done within the CDS group and data sheets obtained from the manufacturer show that the input referred noise for the VMIC 3123 will be less than $(10\mu V)/(\sqrt{Hz})$ when the input voltage range is set to +/- 10 volts, which is less than the required $(100\mu V)/(\sqrt{Hz})$.

The CPU is a Heurikon model baja 4700 VME processor in the ASC CDS VME crate in the LVEA. Data from the ADCs is passed to the CPU via the VME backplane. Initial calculations and estimates show that the baja 4700 processor operating under the VxWorks operating system should be adequate to perform the processing for more than one QMPU. Testing during the preliminary design phase will verify these estimates.

The pitch and yaw calculations and the servo filtering will be as specified in the ASC CDS DRD.

The pitch, yaw and sum calculation is shown in the following equations,

$$Y_{Position} = \frac{K_{Top}(Top - Top_{offset}) - K_{Bottom}(Bot - Bot_{offset})}{Sum}$$

$$X_{Position} = \frac{K_{Left}(Left - Left_{offset}) - K_{Right}(Right - Right_{offset})}{Sum}$$

$$Sum = (K_{Top}Top) + (K_{Bot}Bot) + (K_{Left}Left) + (K_{Right}Right) - \sum_{Top}^{Right} offsets$$

where the offsets for each channel are obtained during a calibration procedure in which the beam to quad photodiode is blocked and the offset voltage for each channel is measured and stored for use in the calculations listed above. The gain constants are obtained during a calibration procedure in which the quad photodiode is uniformly illuminated and the output of each channel is measured. The relative gain for each channel is then calculated once the offsets are subtracted.

The filtering function will be the same as for the WPU data shown in Figure 5: Detection Mode Servo Controller.

4 OPTICAL LEVER DESIGN

A block diagram of a typical optical lever is shown in the figure below.

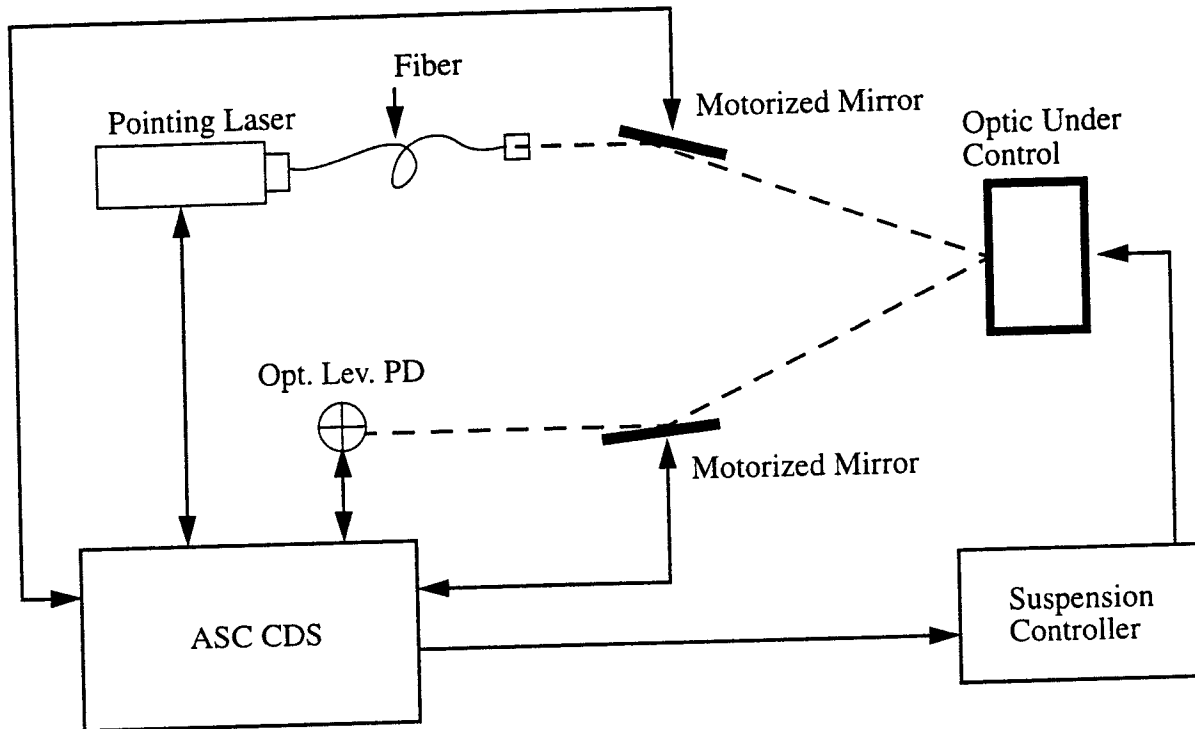


Figure 7: Optical Lever Block Diagram

Optical levers are located on the following optics:

- Recycling Mirror
- Beam Splitter
- X Arm ITM
- Y Arm ITM
- X Arm ETM
- Y Arm ETM
- 2 Folding Mirrors for 2 Km IFO

4.1. Photodiode Amplifier Design

A four quadrant photodiode amplifier will be developed to meet the requirements outlined in the ASC CDS DRD. This amplifier will be similar in design to the amplifiers that are currently used on the 40 meter and Phase Noise Interferometers. The specifications for the amplifier are:

- Gain: 1000 ohms
- Frequency Response: > 1KHz
- Input Referred Noise: $< 6 \times 10^{-12} \frac{\text{A}}{\sqrt{\text{Hz}}}$ for frequencies > 40 Hz

4.2. Optical Lever Control and Monitoring Design

The figure below is a block diagram of a typical optical lever receiver.

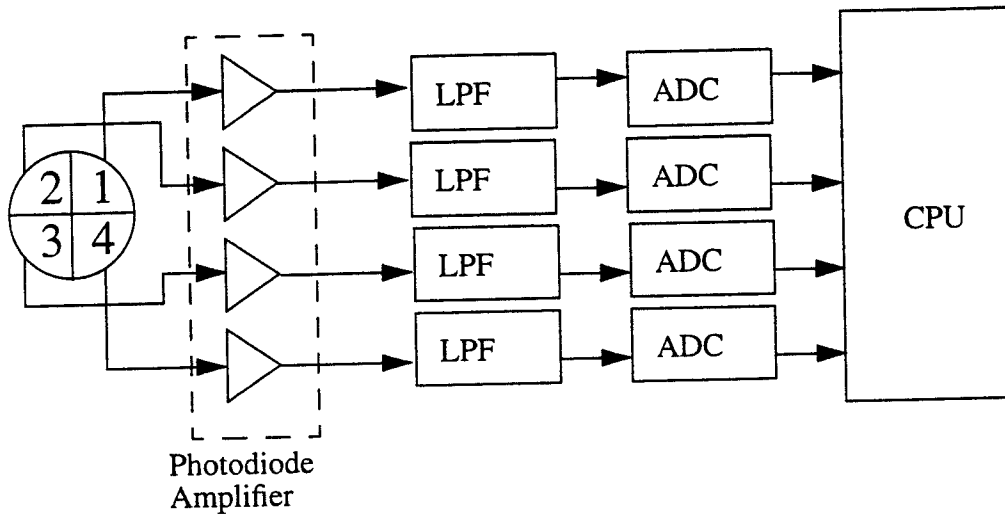


Figure 8: Optical Lever Receiver Block Diagram

Motorized mirrors and the pointing lasers (see Figure 7: Optical Lever Block Diagram) will be controlled via analog input and output and binary input and output modules in the ASC CDS VME crates.

The X and Y position and Sum calculations including the offset and gain adjustments described in the ASC CDS DRD will be performed in software.

The ADCs shown in the figure will be multiple channel, 16-bit VME modules. The CPU will be a Motorola MVME162.

5 CAMERA SYSTEM DESIGN

The nominal placement of cameras for one interferometer at the Washington site is shown in the table below.

Table 4: Nominal Camera Locations for One WA IFO

<i>Location</i>	<i>Number of Cameras</i>	<i>Nominal Viewing</i>
LVEA; at BSC1	2-4	interior of BSC1
LVEA; at BSC2	2-4	interior of BSC2
LVEA; at BSC3	2-4	interior of BSC3
End Station; X Arm/Y Arm	2-4/2-4	interior of BSC9/BSC10
LVEA; at BSC1	1	surface of Y-arm ITM
LVEA; at BSC2	1	surface of beamsplitter
LVEA; at BSC3	1	surface of X-arm ITM
End Station; X Arm/Y Arm	1/1	surface of X-arm/Y-arm ETM
LVEA; at HAM3	1	surface of recycling mirror
LVEA; at HAM2	1	surface of MC mirror
LVEA; at HAM1	1	surface of MC mirror
ISC Table; Rec Cav sample	1	recycling cavity beam
ISC Table; Anti-symmetric port	1	Anti-symmetric beam
ISC Table; Reflected port	1	Reflected beam
ISC Table; ETM transmission, X/Y Arm	1/1	X/Y Arm ETM transmitted beam
ISC Mode Cleaner Table	1	MC transmitted beam

The figure below is a block diagram of how the ASC camera video outputs can be displayed on operator screens. The AVA-300 is a multimedia encoder that will interface as many as six cameras to a 155 Mbps ATM link. Any operator console running the SVA software can then view the out-

put of any camera (each console can view a different camera output). Both the AVA-300 and the SVA software are available from Nemesys Research Ltd. (A subsidiary of Fore Systems Inc.).

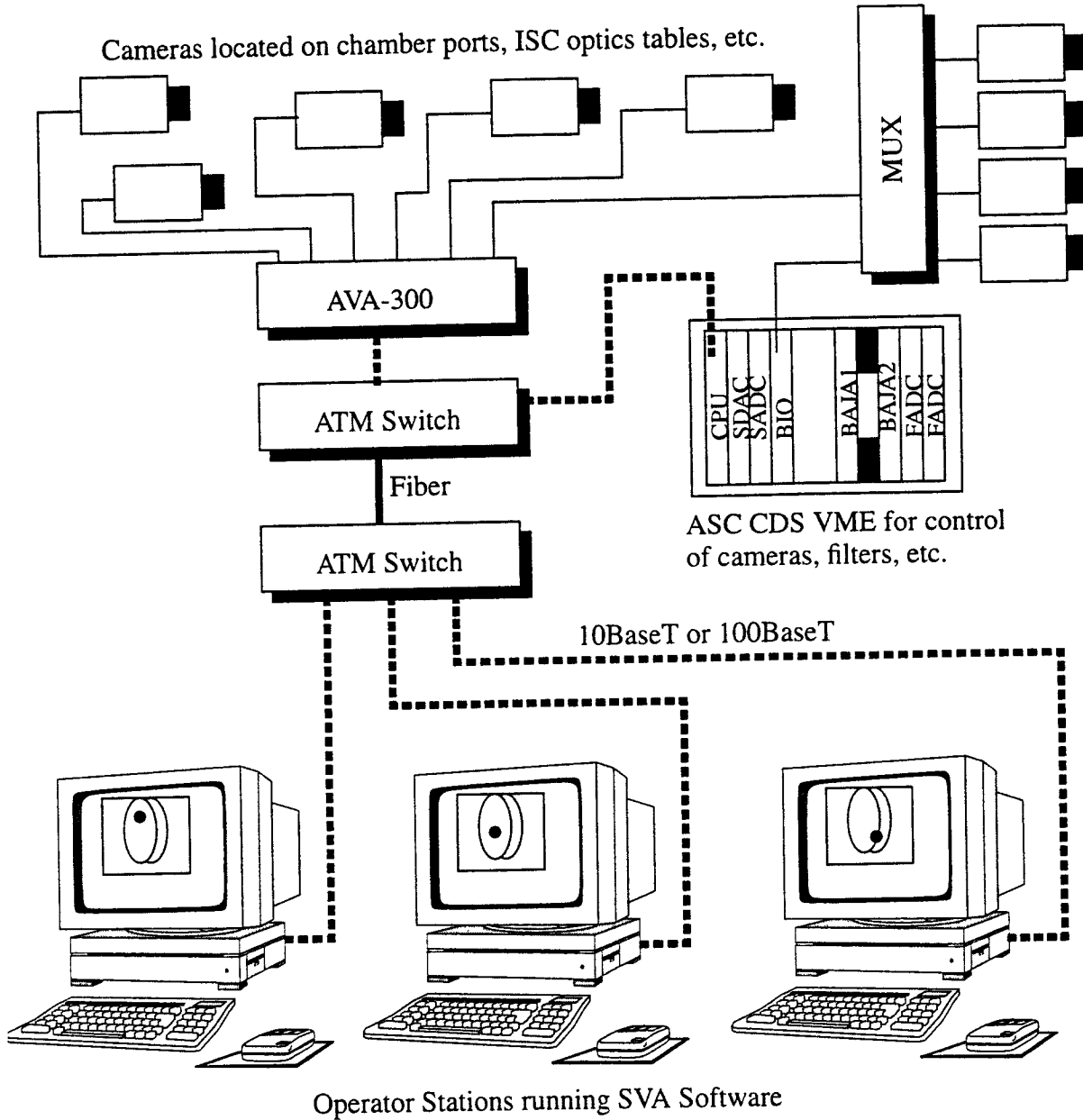


Figure 9: ASC CDS Camera Connections

Each AVA-300 will handle as many as six video inputs. One AVA-300 would be placed in each building. The six inputs would be adequate for the mid and end station buildings, but the LVEA has many more than six cameras. Cameras in the LVEA will be run through multiplexers prior to connection to the AVA-300 unit as shown on the right hand side of the figure. The multiplexers will be controlled by the operator via binary output modules in the ASC CDS VME crates.

Images on the operator consoles will then be captured using tools such as “snapshot” available on the workstation.

Camera controls such as panning, zooming IR filters and test mass illuminators will be provided using VME analog input, output and binary input and output modules and EPICS software running on a CPU such as the Motorola MVME162-333.

6 ASC CDS SYSTEM LEVEL DESIGN

6.1. Design Description

The figure below is a block diagram wavefront sensor and quadrant monitor portions of the ASC CDS system. Blocks within the shaded region are part of the system level design. Other blocks are described in the sections that follow.

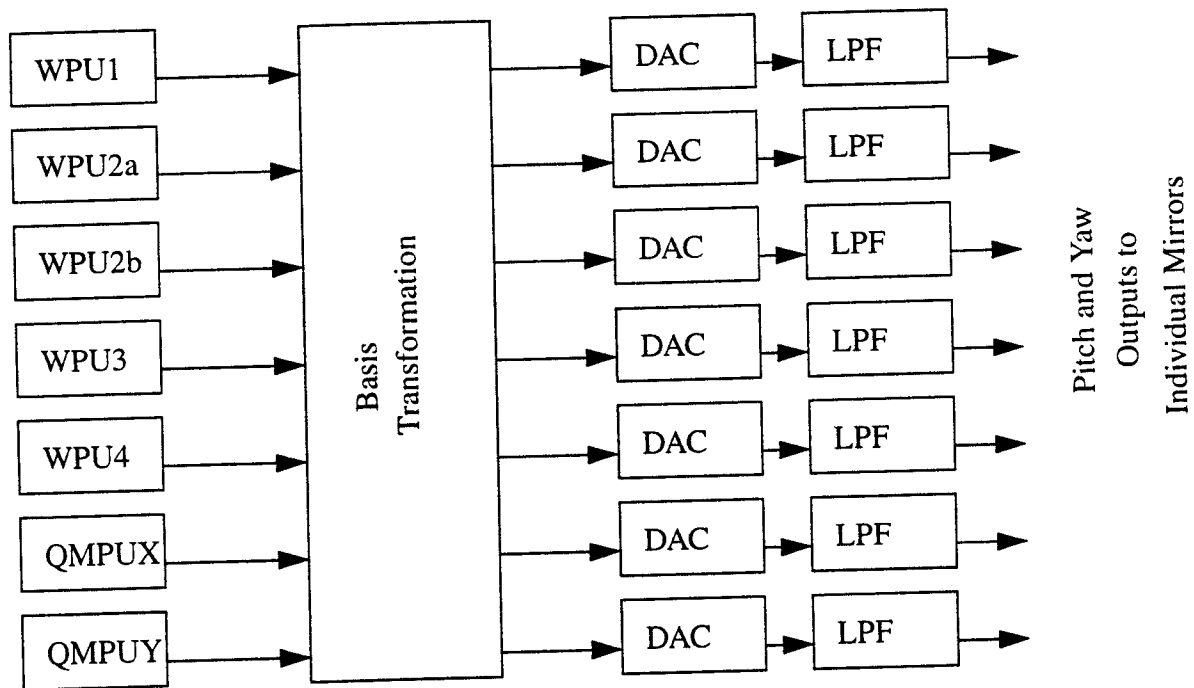


Figure 10: WFS and QMPD Block Diagram

The basis transformation is a 7x7 matrix conversion of the pitch and yaw information from the WPU's and QMPUs. The basis transformation matrix is depicted in the following equations,

$$\begin{bmatrix} \Theta_{WFS1} \\ \Theta_{WFS2} \\ \Theta_{WFS3} \\ \Theta_{WFS4} \\ \Theta_{WFS5} \\ \Theta_{QMPU1} \\ \Theta_{QMPU2} \end{bmatrix} \times \begin{bmatrix} a_{11} & a_{12} & a_{13} & a_{14} & a_{15} & a_{16} & a_{17} \\ a_{21} & a_{22} & a_{23} & a_{24} & a_{25} & a_{26} & a_{27} \\ a_{31} & a_{32} & a_{33} & a_{34} & a_{35} & a_{36} & a_{37} \\ a_{41} & a_{42} & a_{43} & a_{44} & a_{45} & a_{46} & a_{47} \\ a_{51} & a_{52} & a_{53} & a_{54} & a_{55} & a_{56} & a_{57} \\ a_{61} & a_{62} & a_{63} & a_{64} & a_{65} & a_{66} & a_{67} \\ a_{71} & a_{72} & a_{73} & a_{74} & a_{75} & a_{76} & a_{77} \end{bmatrix} = \begin{bmatrix} \Theta_{ITM1} \\ \Theta_{ETM1} \\ \Theta_{ITM2} \\ \Theta_{ETM2} \\ \Theta_{RM} \\ \Theta_{BS} \\ \Theta_{IB} \end{bmatrix}$$

$$\begin{bmatrix} \Phi_{WFS1} \\ \Phi_{WFS2} \\ \Phi_{WFS3} \\ \Phi_{WFS4} \\ \Phi_{WFS5} \\ \Phi_{QMPU1} \\ \Phi_{QMPU2} \end{bmatrix} \times \begin{bmatrix} b_{11} & b_{12} & b_{13} & b_{14} & b_{15} & b_{16} & b_{17} \\ b_{21} & b_{22} & b_{23} & b_{24} & b_{25} & b_{26} & b_{27} \\ b_{31} & b_{32} & b_{33} & b_{34} & b_{35} & b_{36} & b_{37} \\ b_{41} & b_{42} & b_{43} & b_{44} & b_{45} & b_{46} & b_{47} \\ b_{51} & b_{52} & b_{53} & b_{54} & b_{55} & b_{56} & b_{57} \\ b_{61} & b_{62} & b_{63} & b_{64} & b_{65} & b_{66} & b_{67} \\ b_{71} & b_{72} & b_{73} & b_{74} & b_{75} & b_{76} & b_{77} \end{bmatrix} = \begin{bmatrix} \Phi_{ITM1} \\ \Phi_{ETM1} \\ \Phi_{ITM2} \\ \Phi_{ETM2} \\ \Phi_{RM} \\ \Phi_{BS} \\ \Phi_{IB} \end{bmatrix}$$

where ITM= input test mass, ETM= end test mass, RM= recycling mirror, BS= beam splitter, and IB= input beam.

The conversion matrix elements are TBD. This conversion will be done in a CPU designated as the ISCC (ISC Computer, Figure 2: ASC CDS Functional Layout). This CPU will be a Heurikon Model Baja 4700 located in the ASC VME crate in the LVEA near HAM 2. Data from each of the WPU's will be passed via Reflective Memory. Data from the QMPUs (located in VME crates in the end station VEA) will also be passed via Reflective Memory.

The DACs shown in the figure will be located in VME crates near the suspension controller controlling each of the optics under control. These DACs will be 16 bit PMC module DACs, model TBD. The output sample rate will be 10 Ksamples/second. Data is passed from the ISCC VME crate to DAC VME crates via Reflective Memory.

The low pass filters will be 6th order 35 Hz, 4 dB ripple, 60 dB stopband attenuation filters implemented in hardware inside the suspension controller. The interface will be as described in the ASC CDS DRD.

6.2. System Layout

The block diagram in Figure 11: ASC CDS System Layout for One IFO shows how the ASC CDS

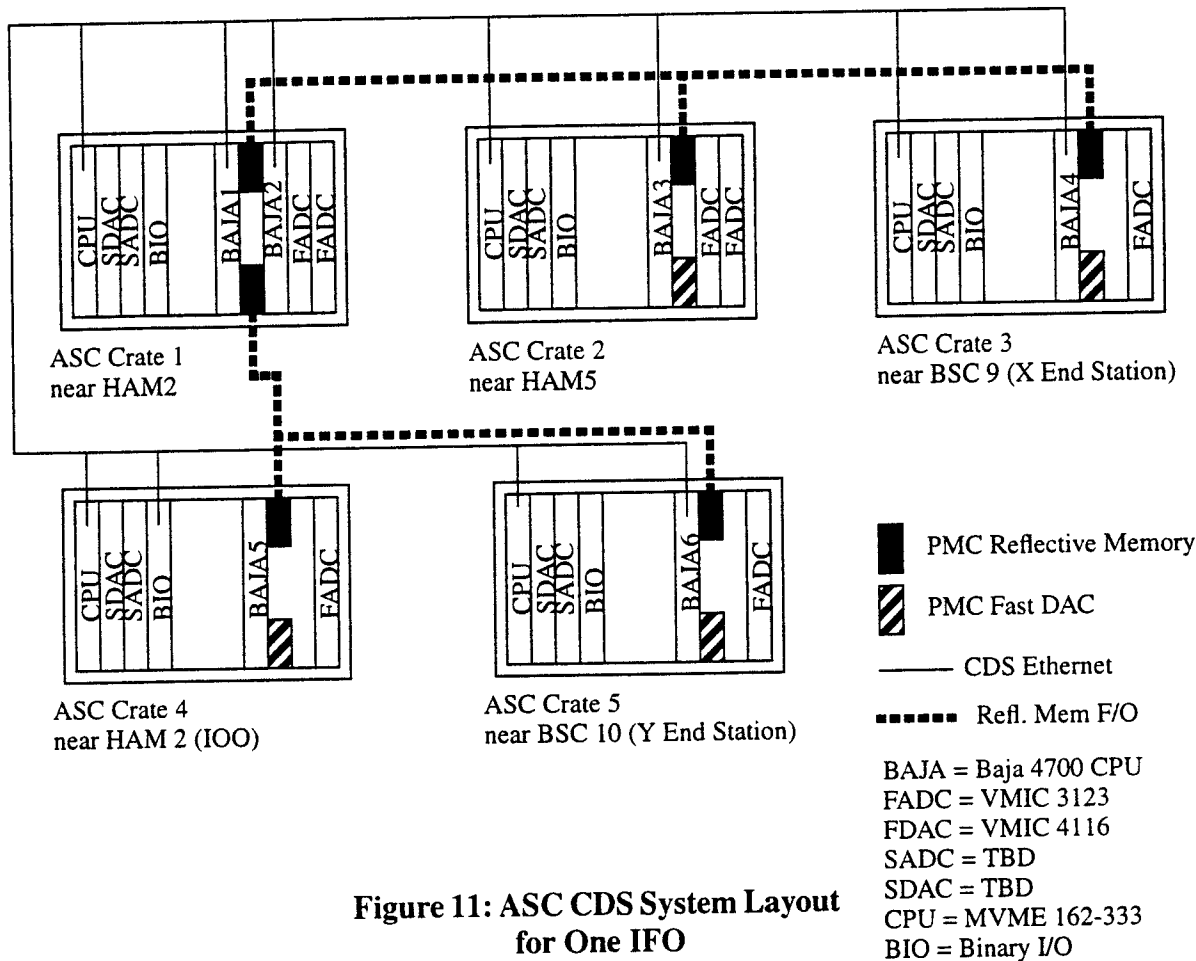


Figure 11: ASC CDS System Layout for One IFO

system can be configured to meet the requirements outlined ASC CDS DRD.

The processor assignments are as follows:

- BAJA1 - WPU and QMPU basis transformation and output angle calculation and WPU 2 functions.
- BAJA2 - WPU 3 and WPU 4 functions.
- BAJA3 - WPU 5 functions and control of DAC for X and Y Arm ITM angle outputs.
- BAJA4 - X Arm QMPU functions and control of DAC for X Arm ETM angle outputs.
- BAJA5 - WPU 1 functions and control of DAC for Input Beam, Recycling Mirror and Beam Splitter angle outputs.
- BAJA6 - Y Arm QMPU functions and control of DAC for Y Arm ETM angle outputs.

The PMC reflective memory modules are Systran model H-AS-DPMCN reflective memory modules plugged into one PMC slot of the Baja 4700 processor.

The PMC Fast DAC modules are TBD model TBD multi-channel, 16-bit DAC modules plugged into one PMC slot of the Baja 4700 processor.

The CPU, SDAC (slow DAC), SADC (slow ADC) and BIO (binary input/output) modules are standard VME modules available from commercial manufacturers. The SDAC and SADC modules will be multi-channel, 16 bit modules. These modules will be used to control and monitor motorized mirrors, optical levers, cameras, shutters, etc. located near each of the VME crates. Typically the motorized mirrors and DC readbacks from a particular WFS or QMPD will be assigned to the VME crate that houses the WPU processor for that particular unit.

6.3. System Software

Two types of software will be developed for the ASC CDS system. The first type of software is the typical EPICS based slow control and monitoring software that is currently be developed for other LIGO systems and currently in use on the 40 meter interferometer.

The second type of software that will be developed is the high speed signal processing software that is required by the WPUs, QMPUs and ISCC. This software will be modeled using the Alta Group SPW software currently in use by the CDS group. The code will be written in the C programming language and compiled for operation on the Baja 4700 processor running under the VxWorks operating system. EPICS channel access will be used to provide network connection and communications between the processor and other CDS systems such as operator consoles, servers and other processors.

Operator interfaces, backup and restore functions and alarm handlers will be developed using the standard LIGO CDS tools.

6.4. ASC CDS Modes of Operation

The ASC CDS system hardware and software will be designed to support the various modes of operation described in the ASC PDD and the ASC CDS DRD. These modes of operation include:

- Initial Alignment Mode -
 - Optical Lever Zero Setting
 - Initial Beam Direction Zero
- Transition to Acquisition Alignment Mode -
 - Unlocked Recycled Michelson
 - Resonating Short Michelson (state 2)
 - Recycled Michelson and One Arm Locked (State 3)
- Detection Mode
 - Establish Center of Rotation for Masses
 - Detection Mode Hold

For the most part the various modes of operation put no requirements on the system design that are not required for the Detection Mode or “normal” of operation of the system. The different modes only require that individual pieces of the system be operational during the commissioning

phase of the interferometer. The installation and commissioning schedule for the ASC CDS system will be adjusted to ensure support of each mode of operation as it is required.

7 ASC CDS PROTOTYPE SETUP

A combined ASC and ASC CDS prototype test setup will be developed during the preliminary design phase. This prototype will include:

- A suspended optic and suspension controller,
- a laser source,
- at least one WFS and WPU, including motorized mirrors,
- at least one QMPD and QMPU,
- the ISCC,
- at least one camera and video display system,
- at least one optical lever.

This test setup is fully described in D. Sigg's document (LIGO T970TBD). A block diagram of the proposed setup from this document is included below for reference.

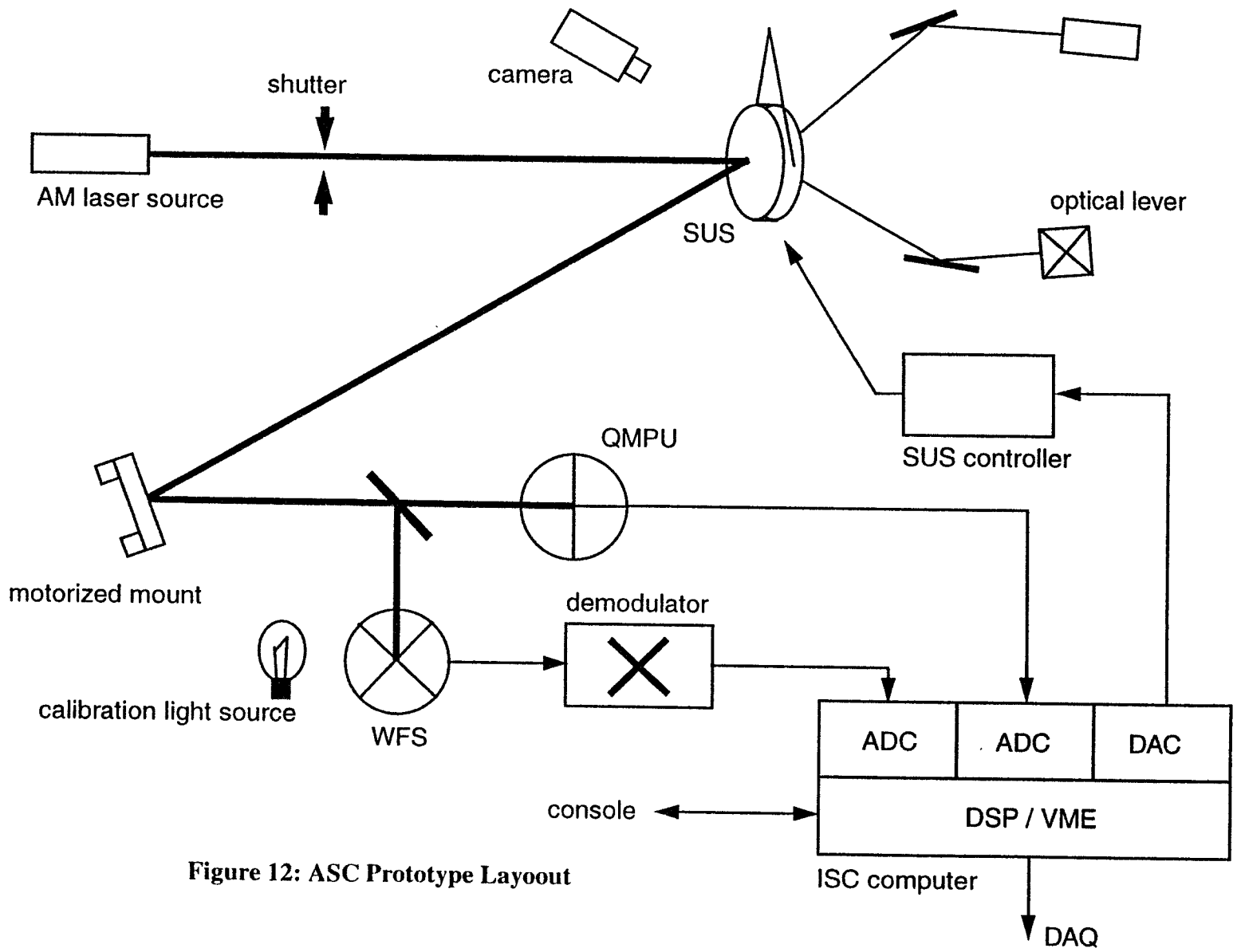


Figure 12: ASC Prototype Layout